UNIVERSITÉ DE STRASBOURG

ÉCOLE DOCTORALE DES SCIENCES CHIMIQUES

Institut Charles Sadron, UPR22 – CNRS

THÈSE présentée par :

Christian Camilo CARMONA VARGAS

soutenue le : **27 septembre 2022**

pour obtenir le grade de : **Docteur de l'Université de Strasbourg**

Discipline/ Spécialité : Chimie moléculaire et Supramoléculaire

Synthèse et couplage de rotaxanes [*c*2] bistables pour la fabrication de matériaux stimulables

THÈSE dirigée par :

Dr. GIUSEPPONE Nicolas	Professeur, Université de Strasbourg
Dr. MOULIN Émilie	Directeur de Recherche, CNRS

RAPPORTEURS :

Dr. DE BO Guillaume	Professeur, Université de Manchester
Dr. HASENKNOPF Bernold	Professeur, Université Pierre et Marie Curie–Paris 6

Quiero dedicar este trabajo a mi madre Marjorie Vargas Anacona y a mi abuela Ismaelina Anacona Mamian, porque ellas siempre me han apoyado, creído y confiado en mí, pero sobre todo por inculcarme que la educación y el conocimiento son los tesoros más importantes en este mundo.

Je voudrais dédier ce travail à ma mère Marjorie Vargas Anacona et à ma grand-mère Ismaelina Anacona Mamian, parce qu'elles ont toujours fait confiance en moi, elles m'ont toujours soutenu et cru en moi, mais surtout pour m'inculquer que l'éducation et le savoir sont les trésors plus importants dans ce monde.

I want to dedicate this work to my mother Marjorie Vargas Anacona and to my grandmother Ismaelina Anacona, because they have always supported me, believed, and trusted on me, but overall, for inculcate me that education and knowledge are the most important treasures in this world.

Table of contents

"Your first draft does not define you as a writer.

Neither does your second, third or twenty -seventh draft.

What matters is how you grow and develop and hone your creativity and form over the time.

We are all work in progress"

— Prof. Jen Heemstra (2022)

Washington University in St. Louis

Acknowledgments

When I decided to embark on the PhD journey, I knocked on a few doors and one day I had the chance to get a replied message from Professor Nicolas Giuseppone, who I would like to thank for giving me the opportunity to carry out my PhD studies in his research group. I would like to extend my thanks to my co-director, Dr. Émilie Moulin, for all her scientific support from the beginning to the end of this doctoral thesis. Thank you both for having trusted me and given me the opportunity to work on cutting-edge research projects from where I have learned a lot in the field of synthetic molecular machines. Finally, these acknowledgements would not be written now without the financial support of the grant awarded to me by the Fondation pour la Recherche en Chimie and the Solvay Excellence Programme 2017-2018.

Importantly, I want to thank my previous advisors Prof. Manuel N. Chaur, Prof. Luz Marina Jaramillo and Prof. Kleber T. de Oliveira. Working under your supervision helped me to be here, as well as the recommendation letters you kindly gave me for my PhD application. I will always be thankful with you.

I also want to thank Madame Odile Lemblé for being always very kind, and available to help me filling all the documents to prepare my arrival to the Institut Charles Sadron and to Strasbourg. Merci beaucoup.

Then, I thank Marie-Celine Samy-Arlaye for all the great efforts that she makes to support the research projects in the lab like purchasing the chemical reagents and solvents, keeping working the precious UPLC-MS and drying solvent machine, and so on. Thank you, a lot, for standing my jokes, my good and my bad mood (sometimes) almost every day in the laboratory during my period in SAMS group. Je voudrais te dire merci beaucoup aussi pour m'aider à apprendre le français, je crois que je n'ai pu pas avoir un meilleur cours de français que t'entendre m'engueuler tous les jours. Tu vas me manquer.

During the last two years as PhD student, I enjoyed a lot working with Dr. Damien Dattler, who I want to thank for the synthetic organic tricks that he taught me, and for all his intellectual contributions that helped me a lot with the Chapter 4 of this thesis. Damien, tu es très intelligent est un grand scientifique, j'espère un jour tu deviens le big boss de la pharma en Suisse ou en France. Sinon, ce n'est pas grave non plus, au moins j'espère qu'un jour on pourra jouer au foot pour te montrer mes compétences sur le terrain. Also, I want to thank Dr. Chuan Gao for all his support as office colleague. Despite we did not have a common research project, you are a good scientist and a smart guy who helped to reflect when my reactions were not working at all, that was very important for me. My best wishes for him in China.

Then, I want to thank Odile Gavat for her efforts and her collaborations during the last few months with the gram-scale synthesis of the optimised synthetic routes of the MAGNIFY project. Merci beaucoup. I also thank Prof. Éric Buhler for his help in the analysis and interpretation of scattering experiments.

As a member of the SAMS research group, I had the opportunity to meet many people that contributed in one way or another to my well-being, or to my personal and professional growth, and I cannot thank all of them individually. Therefore, I thank Alexis Perrot, Andreas Vargas Jentzsch, Melodie Galerne, Nicolas Capit, Flavio Picini, Joakim Heiser, Raphael Pauchet, Whenzi Wang, Lara Faour, Vasyl Chumachenko, Shoichi Tokunaga, Alessandro Cavasso, Dania Daou, Philippe Schiel, Thiebault Chavez, Nathan Aknine, Andres Andrade, Teodor Cucuiet, Lorenzo Marradi, Axel Pinabiaux, Andrei Goloux.

As a member of the Institut Charles Sadron, I met people from other research teams that have contributed to my well-being always with a smile, or with small but enjoyable talks. Thus, I thank Svetlana Samokhvalova (SvetLoca), Jean Muller, Capucine Loth, Eulalie Lafarge, Leandro Jacomine, Dario Barreto Reino de Almeida, Ana Garcia. I wish a successful personal and professional future to all of them.

My time at the Institut Charles Sadron was also possible thanks to the administrative staff, specially to Nadia Barkani, Jean-Marc, Virginie Oberlé, Estelle Brunette. I also thank Catherine Foussat and Laurance Ostwald from the characterisation platform. I extend my acknowledgments to Jean-Marc Strub from the Laboratoire de Spectrometrie de Masse BioOrganique (LSMBO) for his kindness and patience with the numerous samples I gave to him for high resolution mass spectrometry. Merci beaucoup Jean-Marc.

A PhD thesis is a road that you should not walk alone, because when things do not work, you need something more than academy and the lab to stand for, and for me, that is family and friends, who are the family that we have the opportunity to choose. Therefore, I want to thank friends who were by my side in a presential or virtual manner during this time: Felipe Wasem Klein, my dear Brazilian friend that at the beginning of my PhD made my time easier at the ICS when I did not speak any French word. Muito obrigado meu caro pela tua companhia ao longo do meu doutorado, a tua amizade é muito especial. Yuvna Ramnarain, your kindness, and your support at the beginning of my arrival to Strasbourg were very important for me. Thank you for being by my side despite my very bad jokes. Maria Jesus Aguilera Roldan, thank you for receiving me every day in the lab with a smile. Tú fuiste esa chispa latina que le faltaba a mi día a día en el trabajo y con quien he tenido momentos muy agradables. Thanks for everything.

Special thanks to Gabriel Santiago Martinez, a very smart guy, good scientist, and my dear friend who made my days way more easier during the last two years of my PhD. Antes no tenía con quien hablar en español, luego llegó mi hora preferida, la del almuerzo. Nathaly Ortiz Peña, a very smart, strong woman

and scientist that I know since more than ten years, but who has been very close to me since I arrived in Strasbourg. Soy un afortunado por contar con tu amistad, tu cariño y tu presencia. Alejandro Guerrero, in spite of the distance you are always by my side amigo, you introduced me to the organic chemistry world. Gracias por ese apoyo incondicional tanto profesional como personal. Wenziz Manuel, one of the kindest people I have met and a very smart guy. You gave me the first bicycle to come to the lab, and your French parties helped a lot to learn French. Gracias por tu amistad y por todo el cariño, y el servicio técnico en bicicletas que me has brindado. Gracias por llevarme a conocer otros paisajes. Finally, I thank my friends and colleagues Juan David Villada, Juan Camilo Barona, Paola Benavides, Andrea Naranjo, Melissa Cabrera, which in spite of the continental distance you have also offered me your support. Gracias!

Strasbourg is a very international city, however, being around of Latin American people have contributed tremendously to my happiness in Strasbourg. Therefore, I want to thank Jennifer Tatiana Durant Vesga for her friendship, love, and confidence. Mi Tati, gracias por alimentarme, por sacarme a pasear cuando éramos un par de mesdames, y por estar siempre pendiente de mí. Juan Sebastian Aguirre Araque, thanks for being my partner of bad jokes to Victor. Tu compañía alegró mucho mi estadía aquí. Es una pena que tengas que partir a Grenoble, pero allá iré a molestarte por una cervecirri. Craig James Hudson, the funniest flatmate I have had in my life. Sharing the apartment with you was just amazing. I appreciated a lot all your lessons about football, the history of Wales and your company. Finally, Paula C. Stefi, Jhon Valmen, Paloma Garzon, Luciana Castillo, the Latin crew which I have danced, laughed, hiked, cooked, cried, being drunk, etc. Thanks a lot for taking my mind out of the lab when I needed.

Some people say that happiness is just in front of our door and that you just need to let it enter. That is exactly what happened when Laura Márquez Malia opened the door of the apartment at 8, Rue de l'Argonne, one year ago. Tu compañía, tu cariño y tu amor han sido un complemento excepcional a mi vida. Estos últimos meses han sido estresantes, pero me siento afortunado de compartir mis días a tu lado.

I would not be here without all the support of my family, especially my mom Marjorie Vargas Anacona, my grandmother Ismaelina Anacona Mamian, my uncle Victor Hugo Riveros, and my uncle Edison Carmona Acevedo Despite the huge distance that separate us, I know you have always been by my side with your strong support, as you always have been since I was a child. A pesar de la distancia continental que nos separa, yo sé que han estado a mi lado, apoyándome enormemente como siempre lo han hecho.

Finally, I want to thank Prof. Bernold Hasenknopf and Prof. Guillaume De Bo for kindly accepting to examine this work. I hope you enjoy the reading, and we can have a fruitful discussion soon.

Résumé

Les systèmes biologiques reposent sur une machinerie complexe, en perpétuel mouvement et qui veille au bon fonctionnement de nos fonctions vitales. La plupart des processus biologiques qui ont lieu dans les systèmes vivants impliquent des machines et des moteurs biomoléculaires complexes à base de protéines.[1] Par exemple, le transport de cargos le long des filaments de microtubules des cellules eucaryotes par le moteur protéique myosine, la synthèse des protéines par le moteur moléculaire du ribosome et le fonctionnement de nos muscles sont autant d'événements biologiques impliquant des machines moléculaires.

Considérons le fonctionnement des tissus musculaires, l'unité de base des muscles, appelée sarcomère, est constituée de moteurs à myosine, alimentés chimiquement par l'adénosine triphosphate (ATP), qui tirent sur les filaments d'actine et réduisent collectivement la taille micrométrique du sarcomère. L'organisation hiérarchique de ces unités forme des myofibrilles, qui s'assemblent en fibres musculaires plus grandes capables de produire une action macroscopique à partir de machines biomoléculaires nanoscopiques. Cette amplification du mouvement moléculaire de nanomachines biomoléculaires à des échelles de taille plus élevées a récemment attiré l'attention des chimistes capables de synthétiser des machines moléculaires artificielles.[2] En effet, par analogie avec les systèmes biologiques, ces unités individuelles pourraient être capables d'intégrer le mouvement à des échelles de taille supérieures. Cette intégration du mouvement moléculaire pourrait conduire à la formation de matériaux sensibles aux stimuli et capables d'accomplir des tâches de manière bien définie et contrôlée.

En 2000, les travaux pionniers du Prof. Sauvage et de ses collègues ont ouvert la voie à la synthèse de muscles moléculaires artificiels.[3] Dans ce travail, la contraction chimiquement induite d'une molécule mécaniquement entrelacée (MIM de l'anglais : *Mechanically Interlocked Molecules*) appelée rotaxane de chaîne de marguerite (en anglais [*c*2]*daisy chain rotaxane*) a généré une réduction de la taille de la molécule d'environ 22% de sa longueur initiale, une variation proche de ce qui est observé dans les sarcomères. Cependant, le mouvement d'une seule unité contractile ne permet pas l'obtention d'un mouvement à des échelles de longueur élevées. Les chimistes ont alors envisagé d'exploiter les propriétés d'actuation de ce type de machines moléculaires au sein de polymères.[4,5] En 2012, notre équipe a décrit le premier exemple d'amplification du mouvement moléculaire au sein de polymères métallo-supramoléculaires de rotaxanes de type [*c*2]daisy chains.[6] Le mouvement induit par le pH au niveau moléculaire a généré une contraction globale de la chaîne polymère à l'échelle microscopique.

Notre groupe a développé divers systèmes auto-assemblés et ordonnés capables d'amplifier le mouvement moléculaire aux échelles micrométriques et macroscopiques. En 2017, nous avons également décrit le premier matériau polymère contractile à base de machines moléculaires.[7] Malgré ces avancées, certains défis comme, par exemple, un changement de propriétés du matériau à l'échelle macroscopique voire des applications précises de ses matériaux contractiles, restent encore à être relevés. Le travail de recherche effectué durant mon doctorat a consisté en l'obtention des matériaux mous stimulables basés sur des rotaxanes de type [*c*2]daisy chains et dont les mouvements à l'échelle moléculaire conduisent à une réponse macroscopique. Pour cela, nous avons envisagé 1) une approche visant à développer de nouveaux matériaux cristaux-liquides dont les propriétés macroscopiques pourraient varier en fonction de l'état contractile de la [*c*2]daisy chain et 2) la formation de polymères dont la mise en œuvre pourrait permettre l'obtention de matériaux utiles à la robotique.

I. Actionnement moléculaire déclenché par le pH d'un « [c2]daisy chain » liquide-cristallin

Les systèmes liquide-cristallins (LC) sont de bons candidats pour traduire les mouvements moléculaires orientés générés par l'actionnement de machines moléculaires, car ils combinent les propriétés fluides des liquides et la propriété anisotrope des cristaux, offrant un environnement dynamique aux MIMs. Par exemple, l'équipe du Prof. Kato, en collaboration avec le groupe du Prof. Stoddart,[8] ont décrit la formation d'un [2]rotaxane redox actif présentant des propriétés LC (Figure I). Cette molécule présente une mésophase smectique A dans une gamme de températures comprises entre 10 et 150 °C. L'application d'un potentiel redox au film LC correspondant conduit à un changement de couleur,[9] qui correspond au mouvement du macrocycle sur l'axe. Cependant, aucun changement de la phase LC n'a été observé lors de ce mouvement.

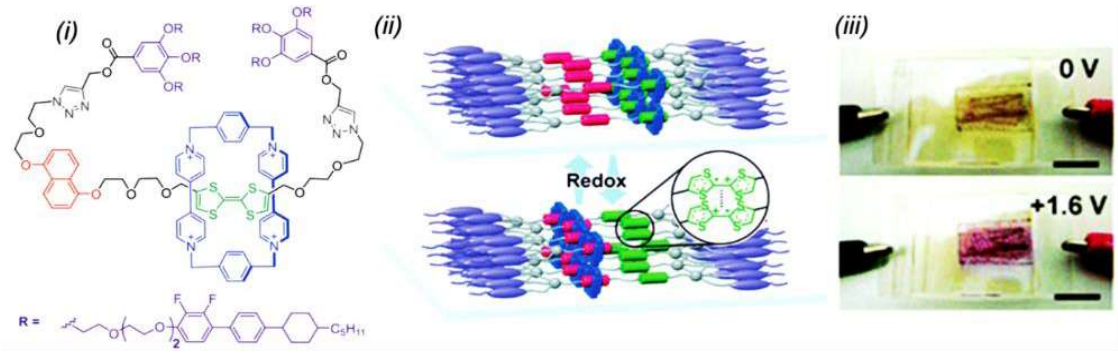

Figure I. i) Structure chimique du [2]rotaxane bistable liquide-cristallin décrit par l'équipe de Stoddart.[8] **ii**) Représentation schématique du film correspondant sur la surface d'une électrode et de son actionnement par stimulation redox; **iii**) Images d'une cellule électrochimique constituée de ce film LC avant et après application d'un potentiel redox.[9]

A notre connaissance, la plupart des matériaux LC impliquant des machines moléculaires consistent en la combinaison d'une matrice cristal liquide avec des (poly-)rotaxanes. Il n'existe pas d'exemples impliquant l'utilisation de rotaxanes de type [*c*2]daisy chains dans des phases LC, ni même une transition de phase lors de l'activation de la liaison mécanique. Dans le cadre de ce travail, nous avons conçu, synthétisé et caractérisé un rotaxane de type [*c*2]daisy chain incorporant des bouts de chaînes mésogènes. Nous avons étudié par différentes techniques de caractérisation les possibles changements de phase à l'échelle macroscopique sous l'influence de l'actuation de la liaison mécanique.

Tout d'abord, la synthèse du composé [*c*2]daisy chain **20** nécessite l'obtention de deux molécules clés : le mésogène **18** et le rotaxane de type pseudo[*c*2]daisy chain **9**,[II] dont la synthèse a déjà été décrite par notre équipe. La synthèse du mésogène **18** a été réalisée en sept étapes (Schéma I). Une réaction de couplage croisé de Suzuki-Miyaura entre le 1-iodo-4-(4-pentylcyclohexyl)benzène (**11**) et l'acide boronique **10**, deux composés commerciaux, en présence de tétrakis(triphénylphosphine)palladium(0) dans une quantité catalytique, suivie d'un clivage de l'éther éthylique en utilisant du tribromure de bore permet l'obtention du composé **12** avec une excellent rendement sur les deux étapes. La fonction phénol est alkylée avec le composé **13** pour conduire au composé **14** qui a ensuite été utilisé pour alkyler le gallate de méthyle. L'ester **15** est alors réduit en alcool avec l'hydrure de lithium et d'aluminium, puis converti en chlorure benzylique qui subit enfin une réaction de substitution nucléophile par l'azidure de sodium pour conduire au mésogène **18** (Schéma I).

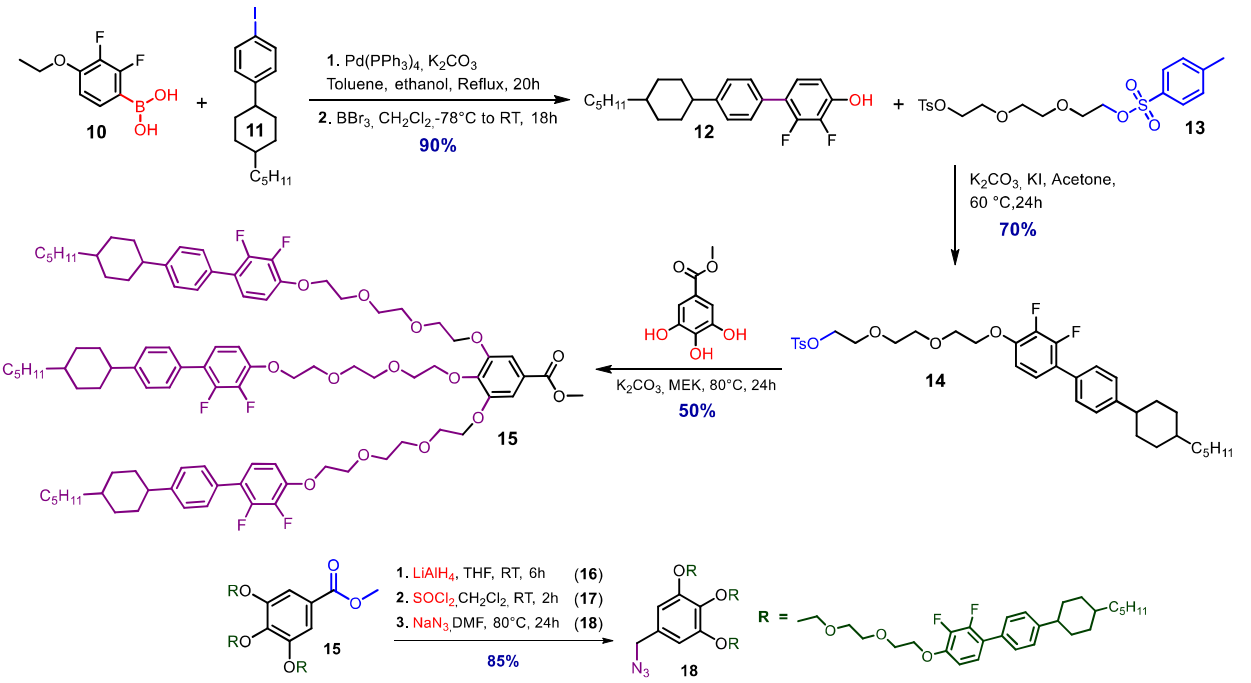

Schéma I. Synthèse du mésogène **18** à partir des composés **9** et **10** commerciaux.

Le dérivé azide **18** et le rotaxane de type pseudo[*c*2]daisy chain **9** sont ensuite couplés par une réaction de cycloaddition de Huisgen selon un protocole déjà utilisé au laboratoire puis les groupements triazoles sont alkylés par l'iodure de méthyle pour conduire au composé **20** avec un bon rendement (Schéma II).

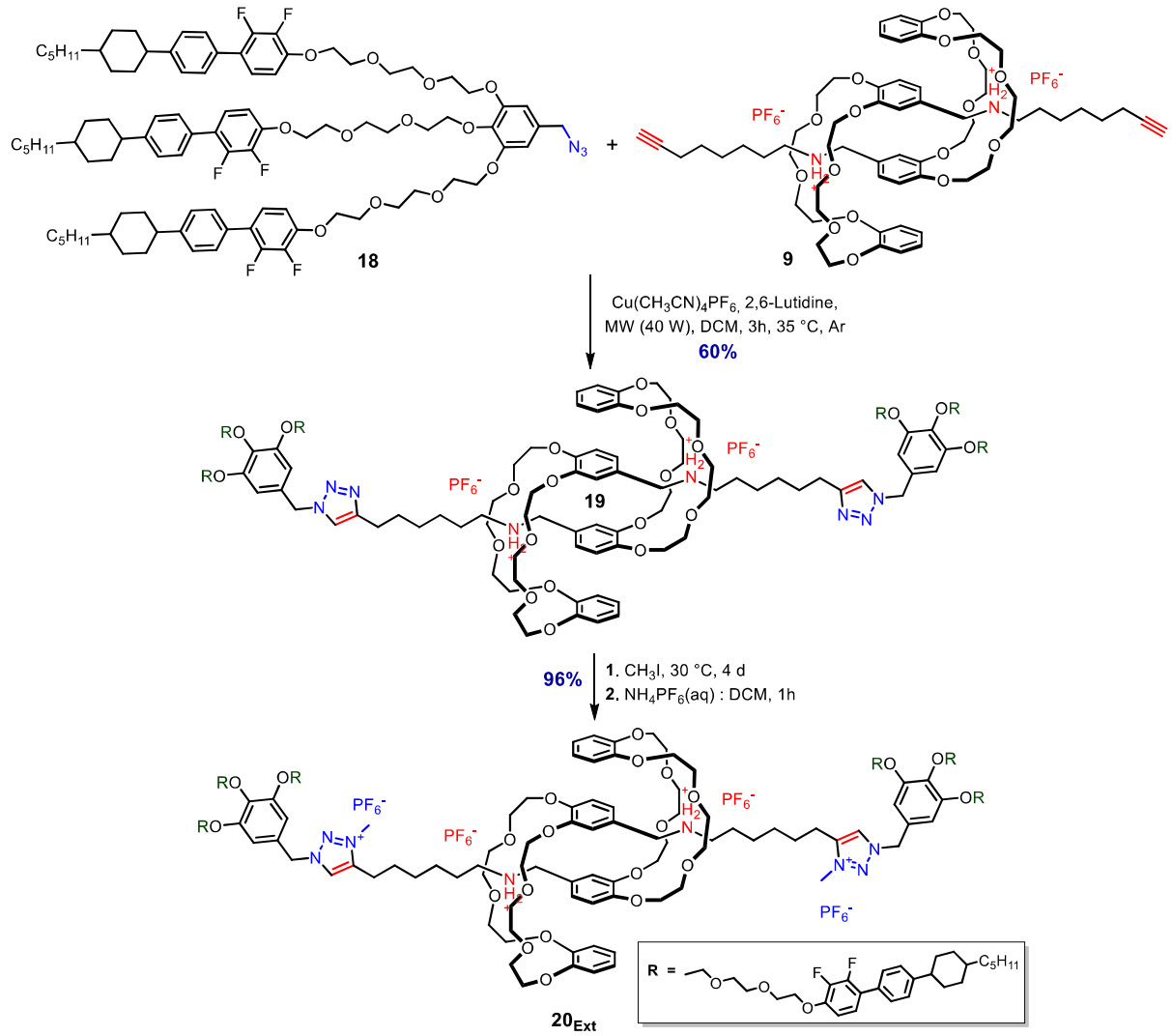

Schéma II. Voie de synthèse permettant l'obtention du rotaxane **18** à partir du mésogène **17** et du rotaxane **8**.

L'actuation moléculaire de la [*c*2]daisy chain **20** a été démontrée par déprotonation/protonation de la station ammonium. Le mouvement à l'échelle moléculaire du composé $\mathbf{20}_{\mathbf{Ext}}$ sous l'influence du pH a été caractérisé par spectroscopie RMN (Figure II). Il se caractérise par un déplacement à haut champ du proton du triazole (en bleu), des protons des noyaux aromatiques de l'éther couronne (cerclés en rouge) et la disparition du signal du CH_2 situé entre le triazole et le motif acide gallique (en vert). D'autre part, les résultats préliminaires obtenus à partir des expériences DOSY indiquent que la taille de rotaxane contracté $\mathbf{20}_{\mathbf{Cont}}$ est environ trois fois plus petite que celle de $\mathbf{20}_{\mathbf{Ext}}$, ce qui est en accord avec ce que nous attendions.

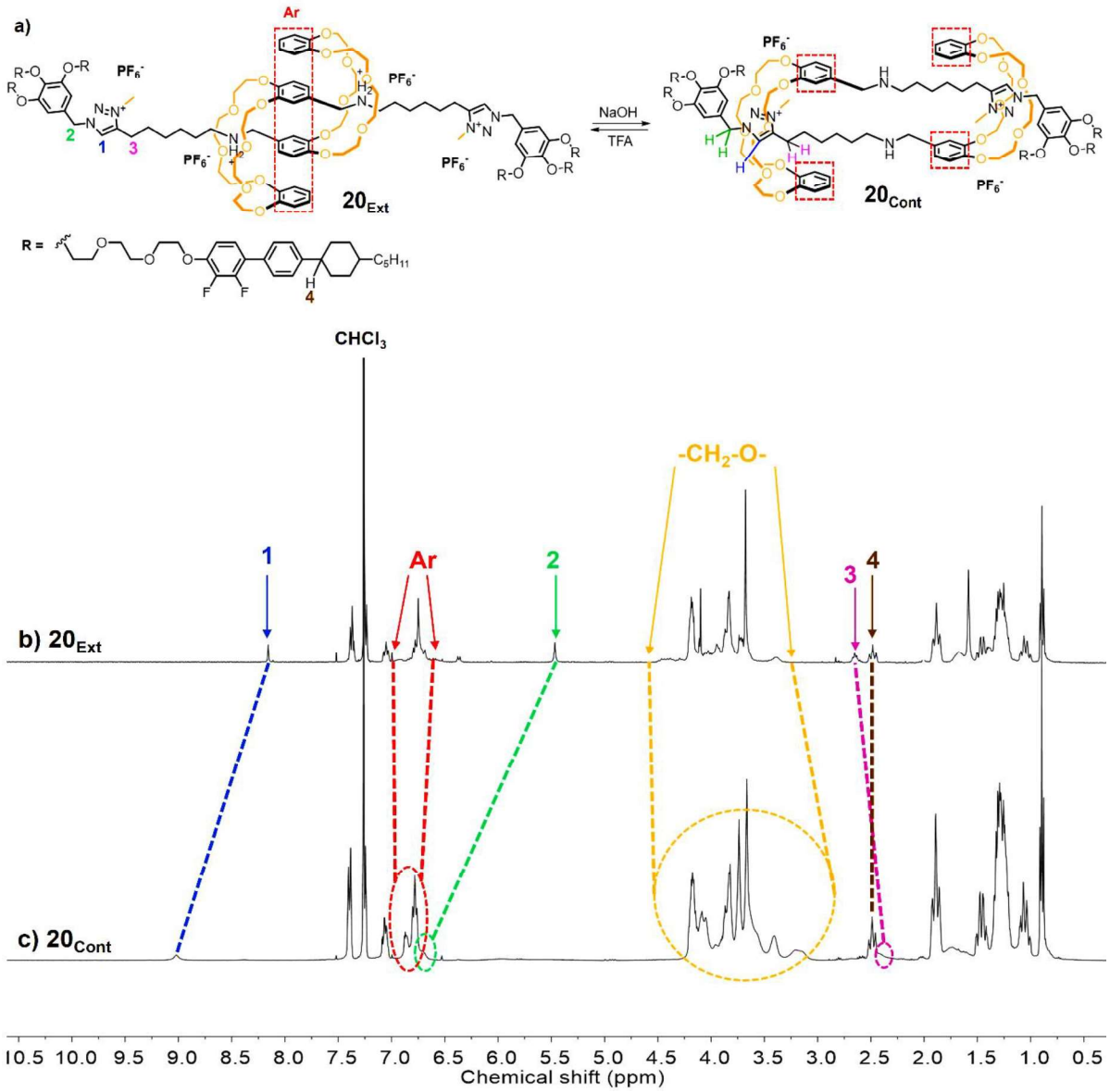

Figure II. Spectres de RMN ^{1}H des composés **20**$_{Ext}$ et **20**$_{Cont}$ en $CDCl_3$ à 25 °C (400 MHz).

Des mesures d'analyse thermogravimétrique indiquent une bonne stabilité thermique avec une température de décomposition à 240 °C pour **20**$_{Ext}$ et à 270 °C pour **20**$_{Cont}$ (ces températures sont déterminées pour une perte de poids de 5%). Des analyses de calorimétrie à balayage différentiel combinées (Figure III) à de l'imagerie par microscopie en lumière polarisée démontrent une température de transition de phase plus faible pour le système contracté par rapport à l'étendu (165 °C for **20**$_{Ext}$ vs 150 °C for 20$_{Cont}$). En outre, les images POM ont montré des textures liquides cristallines dans la gamme de températures mentionnée. Des expériences SAXS ont été réalisées et ont montrées une distribution de pics typique d'une phase LC de type smectic A (SmA) pour les deux états (contractés et étendus).

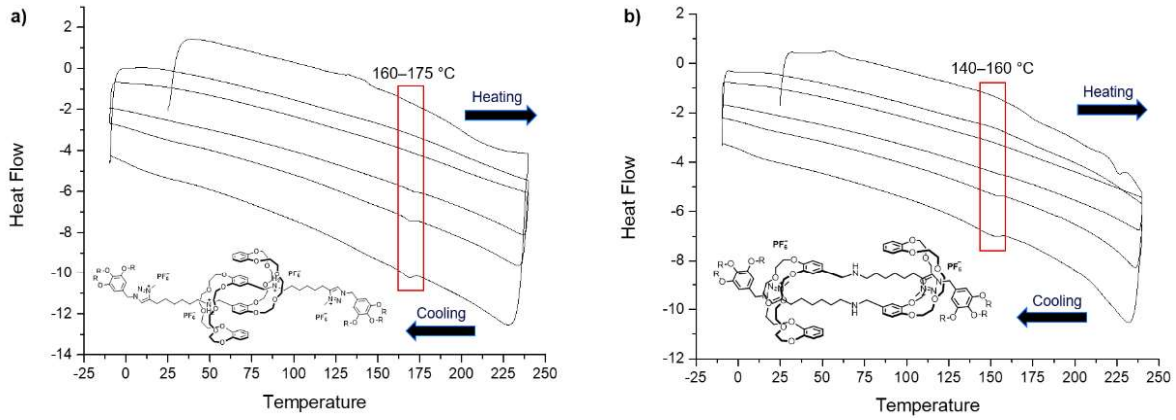

Figure III. Analyse DSC **a)** du composé $\mathbf{20}_{\mathbf{Ext}}$ montrant une transition de phase entre 160 et 175 °C et **b)** du composé $\mathbf{20}_{\mathbf{Cont}}$ montrant une transition de phase entre 140 et 160 °C.

II. Intégration du mouvement moléculaire au sein de polymères constitués de rotaxanes de type[*c*2]daisy chain redox actifs

Les travaux réalisés dans notre équipe au cours des dix dernières années ont mis en jeu des [*c*2]daisy chains stimulables par le pH. Dans le cadre d'un projet européen collaboratif H2020-FET-OPEN, qui vise à développer de nouveaux matériaux pour la robotique impliquant des machines moléculaires, nous avons développé des [*c*2]daisy chains stimulables électrochimiquement. Pour des raisons de diffusion des résultats dans le cadre de ce projet, nous ne décrivons que la synthèse et la caractérisation des polymères obtenus et non leur mise en œuvre pour conduire à de nouveaux matériaux pour la robotique. Le travail de synthèse a été réalisé en étroite collaboration avec l'équipe du Prof. Credi à l'université de Bologne.

L'objectif de mon travail visait à développer la synthèse de la [*c*2]daisy chain $\mathbf{30}_{\mathbf{Ext}}$. Pour cela, plusieurs approches ont été envisagées (Figure IV). Tout d'abord, une voie convergente visant à attacher de manière covalente le stoppeur contenant déjà le motif polymérisable à la [*c*2]daisy chain a été adoptée. Cependant, cette stratégie de synthèse se limite à l'obtention du produit final portant un groupement protecteur qui évite la polymérisation. De plus, des problèmes liés à la purification et la montée en échelle de cette stratégie ont été observés. Par conséquent, une voie linéaire alternative a été proposée, consistant à lier dans un premier temps le stoppeur contenant les stations moléculaires pour les macrocycles à la pseudo[*c*2]daisy chain, puis à utiliser un groupement fonctionnel présent sur le stoppeur pour effectuer une fonctionnalisation tardive de la [*c*2]daisy chain. Cette voie de synthèse nous a permis d'obtenir des [*c*2]daisy chains fonctionnalisées par des groupements uréidopyrimidinones (UPy) en bouts de chaînes et des polymères covalents de type polyurées. Les dérivés incorporant des groupements UPy ont présenté des problèmes de solubilité dans des

solvants non concurrents pour les liaisons hydrogène, ce qui n'a pas permis l'obtention de polymères supramoléculaires. Cependant, les polyurées ont pu être obtenues selon la voie de synthèse décrite ci-après (Schéma IV).

Le composé **19** disponible commercialement a été *O*-alkylé avec le l,6-dibromohexane pour conduire au composé **20** qui réagit ensuite avec l'azidure de sodium pour former le composé **21** qui a ensuite été converti en l'acide carboxylique **22** par une réaction de saponification. Un couplage peptidique avec l'éthylène diamine mono-protégée permet l'obtention du composé **23** qui est ensuite couplé par réaction de cycloaddition de Huisgen à un composé bromoalcyne de deux tailles différentes (C4 et C9) pour conduire aux composés **24**.

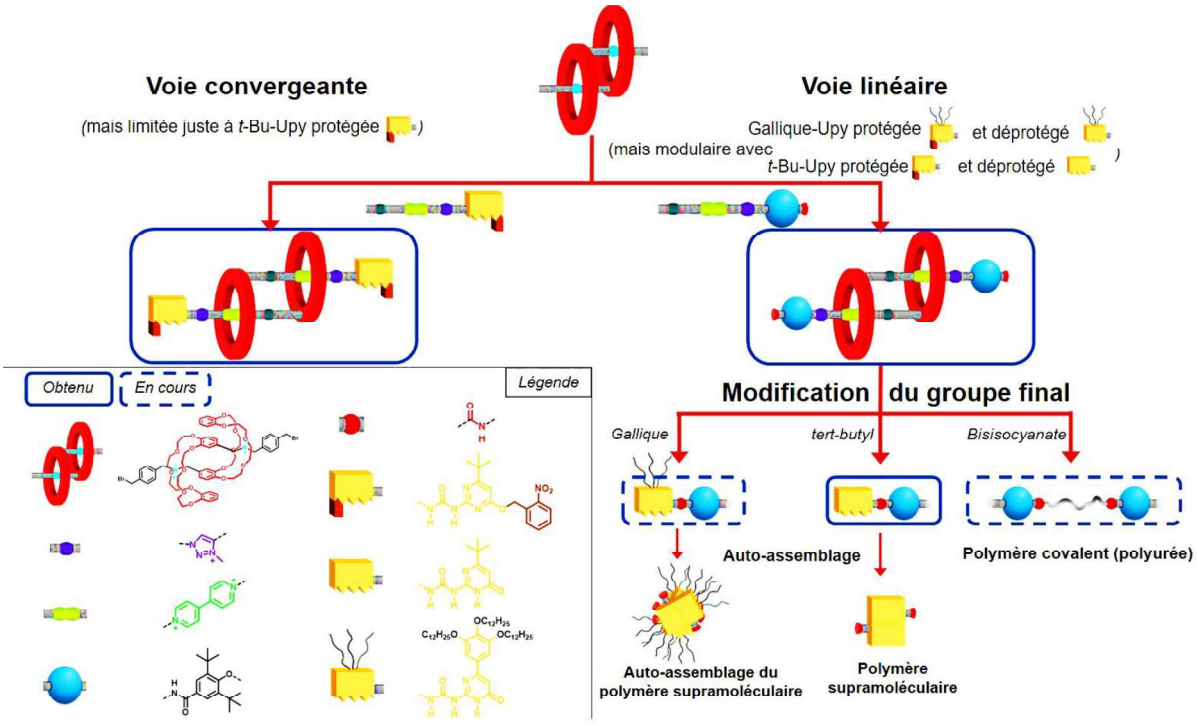

Figure IV. Approches synthétiques pour obtenir des polymères à base de rotaxanes bistables sensibles à des potentiels redox.

Les dérivés triazole obtenus sont ensuite méthylés pour donner les composés triazolium **25** qui sont ensuite mis en présence du 4,4'-bipyridine pour conduire aux composés **26** avec de bons rendements. Ce composé est alors couplé à la pseudo[*c*2]daisy chain **27** synthétisée par le groupe du Prof. Credi de l'université de Bologne. Ayant obtenu la [*c*2]daisy chain **28**, il convenait ensuite de bloquer la station ammonium afin de pouvoir actionner électrochimiquement la daisy chain. Une réaction d'acétylation suivie d'une déprotection du groupe NH en conditions acides permet l'obtention des monomères **30** de la [*c*2]daisy

chain. Après déprotection des groupements Boc terminaux, ces monomères peuvent être engagés dans une réaction de polyaddition avec le diisocyanate de méthylène diphénylène (MDI) pour conduire aux polyurées **31**.

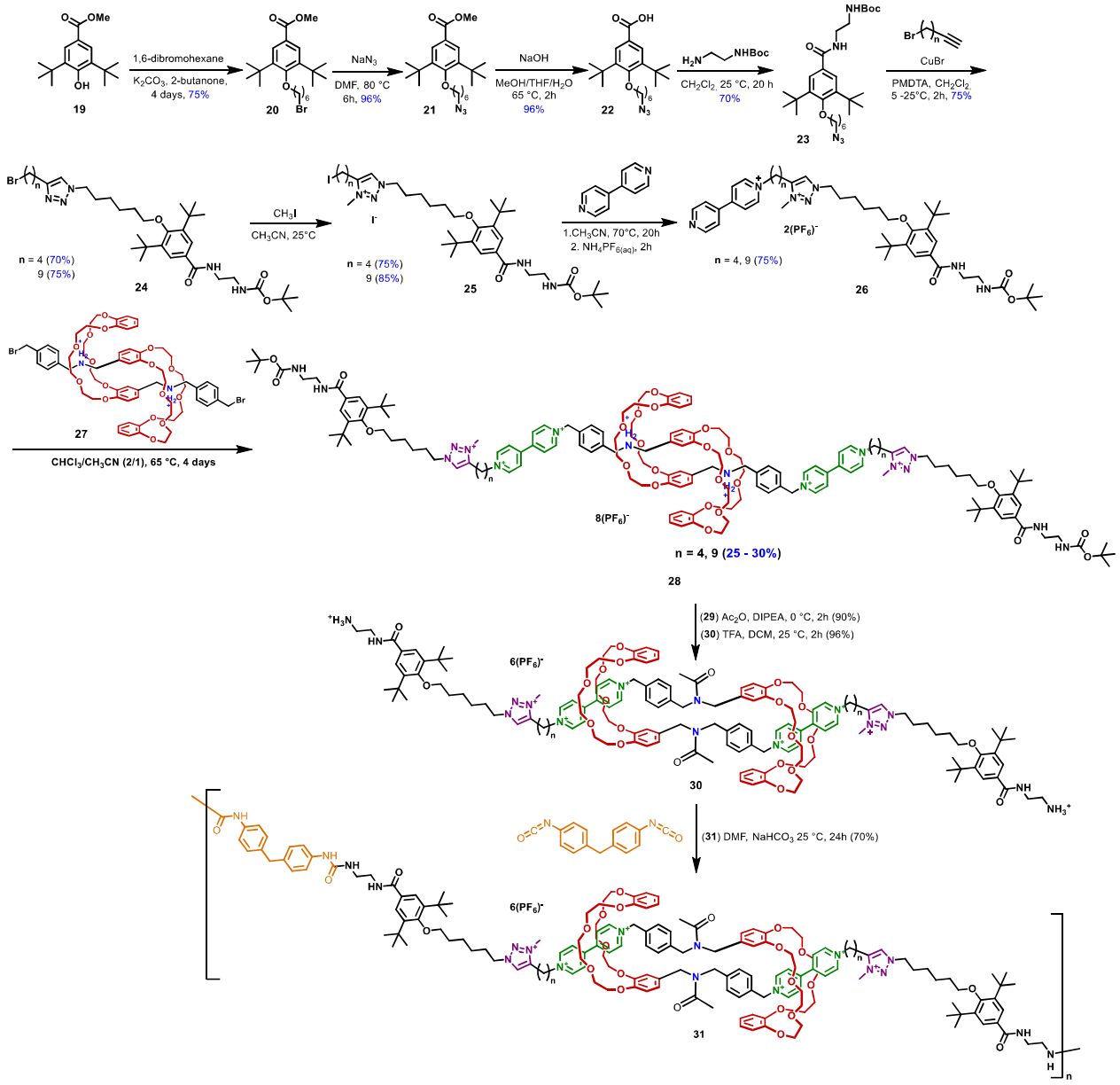

Schéma 4. Voie de synthèse permettant l'obtention du polymère **31** à partir du stoppeur **28** et du composé **27**.

La caractérisation par chromatographie d'exclusion stérique des polymères obtenus a permis de déterminer une masse moléculaire en nombre (Mn) de 203.000 g/mol pour le polymère de chaîne C9. Ces polymères ont été étudiés par voltampérométrie cyclique (VC) et voltampérométrie différentielle à impulsions pour déterminer les potentiels redox des stations bipyridinium et triazolium lors de la

commutation électrochimique (Figure V). La VC a permis de déterminer que les deux processus de réduction du bipyridinium se situent autour de -0.48 et -0.76 V. Le comportement observé dans les voltammogrammes est en accord avec celui observé pour les monomères de rotaxane de type [*c*2]daisy chain, indiquant que les macrocycles entourent initialement la station bipy mais une fois qu'ils sont sur la station triazolium, les potentiels de réduction de cette station sont affectés. Le processus de réduction du triazolium a été observé à environ -2.0 V vs SCE par voltammétrie à impulsion différentielle.

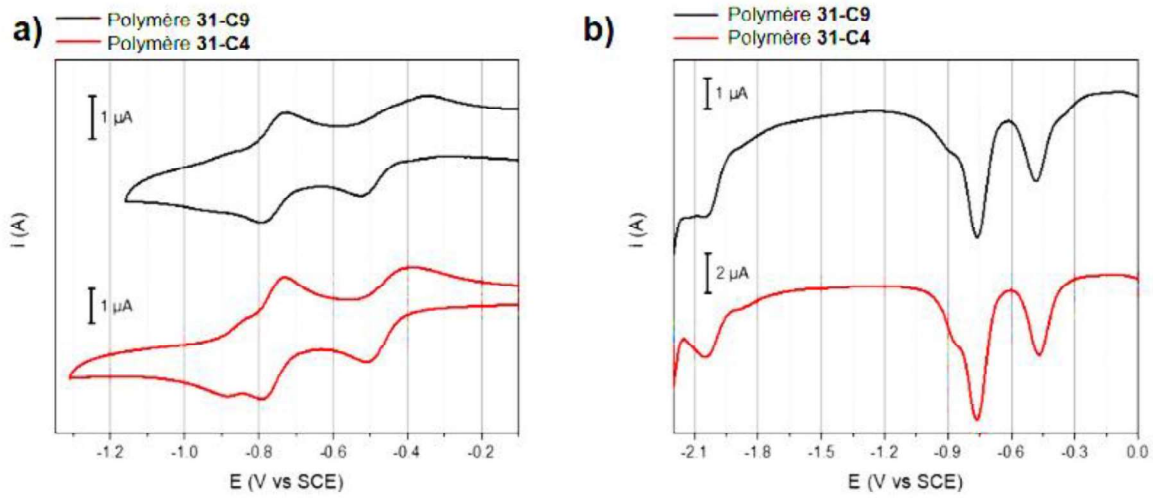

Figure V. a) Voltamogramme cyclique pour les polymères **31-C9** et **31-C4**. b) Voltamogramme à impulsion différentielle pour les polymères **31-C9** et **31-C4**. Conditions : DMF / perchlorate de tétraéthylammonium, 25 °C, électrode de travail en carbone vitreux, vitesse de balayage CV : 50 mV/s, taux de balayage DPV : 20 mV/s.

Afin de prouver l'actionnement réversible du polymère, nous avons réalisé des expériences de diffusion de neutrons sur une solution à 0,5 %m dans le DMSO. Ces expériences, qui requièrent une analyse complète afin d'extraire des données quantitatives telles que la densité de masse linéaire, la taille de la section, la longueur du polymère etc., ont montré que le processus d'actionnement se produit en donnant lieu à différentes conformations des chaînes de polymère et que le processus contractile est réversible.

III. Conclusions

Le premier objectif de cette thèse visait à obtenir un rotaxane de type [*c*2]daisy chain liquide-cristallin et d'étudier l'effet de l'actionnement de la liaison mécanique sur ce comportement LC. Les études DSC menées sur le composé synthétisé montrent une diminution de la température de transition de phase pour l'état contracté par rapport à l'état étendu, et les images obtenues par microscopie en lumière polarisée montrent des textures cristallines liquides pendant le processus de refroidissement entre 170°C et 140°C. Les

expériences de diffusion des rayons X aux petits angles réalisées sur les composés étendus et contractés ont montrées les paramètres d'ordre d'une mésophase de type SmA pour chacun des composés et donc de conclure quant à la possibilité d'un changement de phase par mouvement de la liaison mécanique.

Le deuxième objectif visait à concevoir, synthétiser et caractériser un matériau polymère basé sur des unités de type [*c*2]daisy chain pour de possibles applications dans le domaine de la robotique. Deux polyurées sensibles au stimulus électrochimique ont été synthétisées à l'échelle de plusieurs grammes et la réversibilité de leur actionnement par un stimulus électrochimique a été démontrée par voltammétrie cyclique. Ces polymères sont désormais entre les mains de chimistes des matériaux à l'université de Bologne pour leur mise en œuvre afin d'obtenir des matériaux polymères qui pourraient être utilisé pour la robotique. Une étape importante consistera à vérifier le bon actionnement électrochimique des rotaxanes de type [*c*2]daisy chain dans le matériau en vrac pour conduire à un phénomène d'actuation à l'échelle macroscopique.

Références

[1] K. Kinbara, T. Aida, *Chem. Rev* **2005**, *105*, 1377.

[2] E. Moulin, L. Faour, C. C. Carmona-Vargas, N. Giuseppone, *Adv. Mater.* **2020**, *32*, 1906036.

[3] M. C. Jimenez, C. Dietrich-buchecker, J. Sauvage, *Angew Chem Int Ed* **2000**, *39*, 3284.

[4] L. Fang, M. Hmadeh, J. Wu, M. A. Olson, J. M. Spruell, A. Trabolsi, Y. Yang, M. Elhabiri, J. F. Stoddart, *J. Am. Chem. Soc.* **2009**, *131*, 7126.

[5] P. G. Clark, M. W. Day, R. H. Grubbs, *J. Am. Chem. Soc.* **2009**, *131*, 13631.

[6] G. Du, E. Moulin, N. Jouault, E. Buhler, N. Giuseppone, *Angew. Chemie - Int. Ed.* **2012**, *51*, 12504.

[7] A. Goujon, T. Lang, G. Mariani, E. Moulin, G. Fuks, J. Raya, E. Buhler, N. Giuseppone, *J. Am. Chem. Soc.* **2017**, *139*, 14825.

[8] I. Aprahamian, T. Yasuda, T. Ikeda, S. Saha, W. R. Dichtel, K. Isoda, T. Kato, J. F. Stoddart, *Angew. Chemie - Int. Ed.* **2007**, *46*, 4675.

[9] T. Yasuda, K. Tanabe, T. Tsuji, K. K. Coti, I. Aprahamian, J. F. Stoddart, T. Kato, *Chem. Commun.* **2010**, *46*, 1224.

List of figures, schemes, and tables

Chapter 1.

Chapter 3.

Chapter 4.

Chapter 1.

Chapter 2.

Chapter 3.

Chapter 3.

List of units, symbols, and abbreviations

°C	degree Celsius
%	percent
μm	micrometre
Å	Ångstrom
Boc	*tert*-butoxycarbonyl
bs	broad singlet
ESI	Electrospray Ionization
g	gram
HR-MS	High-Resolution Mass Spectrometry
imH	imidazole
M	$mol \cdot L^{-1}$
MALDI	Matrix-Assisted Laser Desorption Ionization
MEK	methyl ethyl ketone
ppm	parts per million
TLC	Thin Layer Chromatography
R*g*	radius of gyration
UPLC	Ultra-Performance Liquid Chromatography

General introduction

In the past few decades, most of the technological advances and developments have been achieved through multidisciplinary research. One of the most interdisciplinary branches of science is supramolecular chemistry, which is focused on understanding and controlling the way in which molecules communicate with each other by non-covalent interactions. This emergent research area has played a key role in several fields, allowing the construction of molecular architectures with potential applications in areas ranging from biology and medicine to physics and nanotechnologies.

Non-covalent interactions like hydrogen bonding, π-π stacking, coordination bonds, among others are at the core of supramolecular chemistry. For instance, the latter served to form a template for the generation of the mechanical bond in an efficient way. The conception of this 'new' type of bond (already present in Nature) has allowed scientists to design and bring to reality molecular structures with diverse topologies, like mechanically interlocked molecules. The pioneering works of Prof. Jean-Pierre Sauvage and Prof. Fraser Stoddart in the decade of 80s and 90s as well as their tremendous contributions to this field were awarded with the 2016 Nobel Prize in Chemistry, for the development of synthetic molecular machines, most specifically for setting the roots for the design and construction of mechanically active molecular catenanes and rotaxanes respectively. These stimuli-responsive molecules can undergo circumrotational and translational motion of large amplitudes that can be harnessed to carry out functional tasks.

In the last two decades, materials science has witnessed a technological revolution with the hand of chemical, physical, biological sciences, and the support of engineering to face some challenges in regenerative medicine, human-machine interfaces, robotics, among others. Actuating soft materials based on synthetic molecular machines have a great potential to be part of it. Therefore, investigations towards the integration of stimuli-sensitive organic molecules like mechanically interlocked molecules, in advanced responsive is a scientific challenge of interest. In that direction, several research groups (including us) have invested many efforts to couple molecular machines with one another and with their environment to extract their collective (nanometric) motion at higher length scales, and possibly up to the macroscopic scale. However, to go further with such molecular machines and extract optimized macroscopic actuations, one should precisely control their spatial 3D organisation over very long distances. For instance, the incorporation of mechanically interlocked molecules in soft materials like liquid crystals has been envisioned, including a few examples regarding liquid-crystalline [2]catenanes and [2]rotaxanes but, to the best of our

knowledge, no study was found in the literature relating the controlled movement of the mechanical bond with a mechanical modification of the liquid crystal organisation.

In other attempts to amplify the motion of molecular machines at macroscopic scales, [*c*2]daisy chain units, which are bistable doubly threatened dimers of rotaxanes were introduced into polymer chains to harness their collective motion within the individual polymer chains and by bundling these polymer chains together in polymer films of gels. However, so far, the long range organisation of these polymers into highly aligned and oriented structures that mimic natural muscles could not be achieved, precluding their optimal use in advanced applications where robustness and resilience are required, for instance, soft robotics.

This thesis manuscript contains four chapters: the first one is dedicated to the state of the art of the literature reported in a condensed manner and including the concepts and most representative examples in the field that can serve the reader to understand the context of the present work. The second chapter describes the synthetic pathway followed to obtain a [*c*2]daisy chain rotaxane with potential liquid-crystalline properties. This system was analysed by NMR spectroscopy, differential scanning calorimetry, polarised optical microscopy and small-angle X-ray scattering to investigate the effect of the pH-triggered contraction event that takes place at the nanoscopic scale, in how it relates to the mesoscopic properties of the material.

Chapters 3 and 4 are mostly dedicated to the design and synthesis of [*c*2]daisy chain rotaxane monomers to be involved in covalent and supramolecular polymerisations. Chapter 3 is more particularly related to the synthesis of pH-switchable [*c*2]daisy chain rotaxane monomers, containing free hydroxyl groups at the extremities and describes our attempts to obtain polyurethanes by reaction with diisocyanates of different chemical nature. Chapter 4 addresses most of the synthetic approaches that were designed to obtain redox-responsive poly[*c*2]daisy chain rotaxanes monomers, which were used for polymerisation and further electrospinning intro fibres. It is important to mention that the work presented in this last chapter was performed in the frame of the MAGNIFY FET-open collaborative project, a consortium composed by four research institutions: the University of Groningen, the University of Bologna (UNIBO), the National Research Centre in Italy (CNR) and us, the Centre National de la Recherche Scientifique (CNRS).

Finally, we end this manuscript with a general overview of the results obtained and a consideration of the next steps to follow as possible future directions in order to contribute to the advancement of the field of artificial molecular machines.

Chapter 1

Molecular Machines and Amplification of the Mechanical Motion

Molecular machines are molecular assemblies composed of a certain number of molecular components that convert, upon external stimulation, an energy input (chemical, thermal, electrical, etc.) into mechanical energy, or vice versa, to carry out a determined task or work by directional molecular motion.[1] These nanomachines are divided into two categories: molecular switches and molecular motors. They can be either natural-occurring or artificial molecular systems. In the next section, we discuss some molecular machines found in biological systems and a very short explanation about their functioning principle.

1.1. Biomolecular machines: a natural source of inspiration

Complex molecular machines have been identified in the cellular media accomplishing crucial tasks for the correct functioning of living systems. They include RNA and DNA polymerases as well as ribosomes[2] just to name a few, which are all fundamental for life. Enzymatic systems carry out specific functions through their mechanical motions fuelled either by solar energy, in the case of the photosynthetic systems, or by chemical energy using adenosine triphosphate (ATP). ATP synthase is one of the ubiquitous biological machines that produces the chemical fuel of life. It is a unidirectional rotary motor made of two main domains (F_0 and F_1) each operating in a different mechanism. The F_0 motor is embedded in the lipid bilayer membrane and its rotation is driven by a flux of ions passing through the hosting membrane, causing in turn the rotation of gamma unit into the F_1 enzymatic unit. This rotation generates mechanical deformations of the F_1 catalytic domain and the subsequent production of ATP from adenosine diphosphate (ADP) and inorganic phosphorus (Figure 1.1a).[3,4] The production of ATP from phosphorylation of ADP is an energetically unfavourable step, which is made possible by the ATP synthase because a proton gradient is generated by a series of redox processes that take place in the mitochondrial membrane, using a number of complex protein pumps.[5] The proton flux across the inner membrane of mitochondria creates the necessary driving force to produce ATP by making the overall process exergonic.[6]

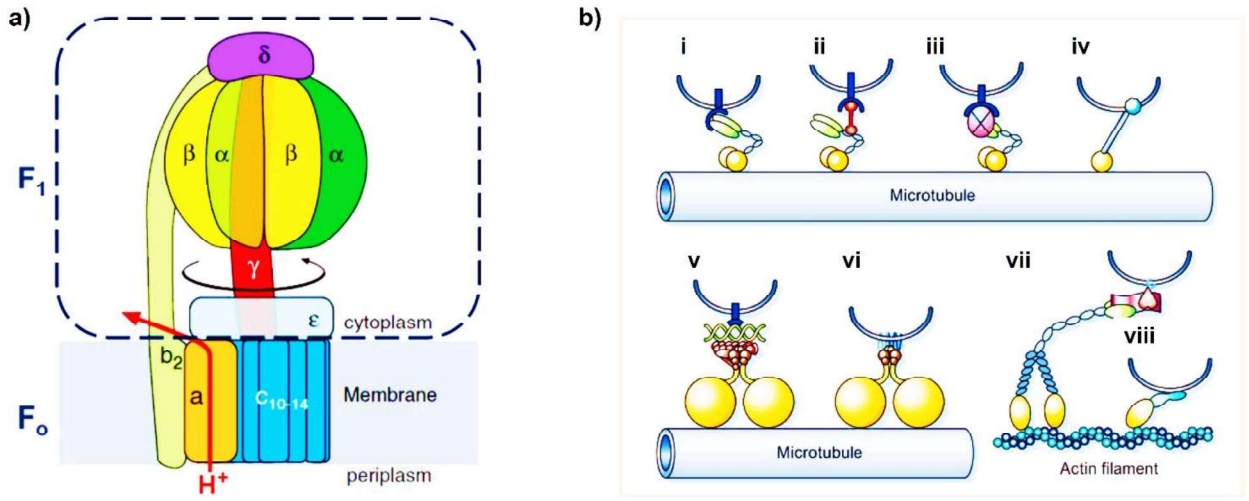

Figure 1.1. (**a**) Schematic representation showing the relative rotation of the biomolecular rotor of the ATP and the flow direction of the proton ions. Adapted from reference [4]. (**b**) Types of transport-cargo biomolecular motors: **a-d** kinesins: interaction between a transmembrane receptor (blue) and kinesin light and heavy chains; **e-f** dyneins: interaction between cytoplasmic dyneins and an integral membrane protein; g-h myosin: Interaction of the tail domain of myosin V and I with actin. Adapted from reference[5].

Molecular mechanical motions can also be used to move cellular objects, such as transporting cargo along microtubule filaments of eukaryotic cells (in the case of kinesins and dyneins) or to move on the actin filaments, which is the case of the myosins in skeletal muscles (Figure 1.1b). In particular, understanding the properties of biological muscles that generate and amplify controlled movements across length scales may inspire the conception of functional smart materials based on artificial molecular machines.

Skeletal muscles are organs present in vertebrate animals that are attached to the bones of the skeleton by collagen fibres forming tendons. They undergo billions of work cycles and possess high conformability with strain above ~20%,[7] being able to self-heal depending on the type of suffered damage. Additionally, natural muscles provide excellent mechanical stability, high output power of 323 W kg^{-1}, and convert biochemical energy into mechanical motion with 40% efficiency.[8] At the nanoscopic level, when muscles cells are excited by motor neurons, calcium ions interact with a thin filament composed by the actin protein and two regulatory proteins called troponin and tropomyosin. Ca^{2+} ions bind to troponin, making the tropomyosin protein rotate and creating exposed sites on the actin filament for the myosin heads to bind. In turn, myosin heads rotate by pulling on the actin filaments towards the centre of the A-band of the sarcomere, the basic unit of the muscles, resulting in a muscle contraction driven by a force generated by ATP hydrolysis.[9]

Figure 1.2. (**a**) Directional conformational change done by the ATP hydrolysis, which generates a stroke of about 10 nm by the lever arm. Such movement pulls on the myosin tail, which in turn is attached to the thick filament of the myosin. Then, a relative movement of the myosin and actin filaments is induced. (**b**) Actin-myosin complex.

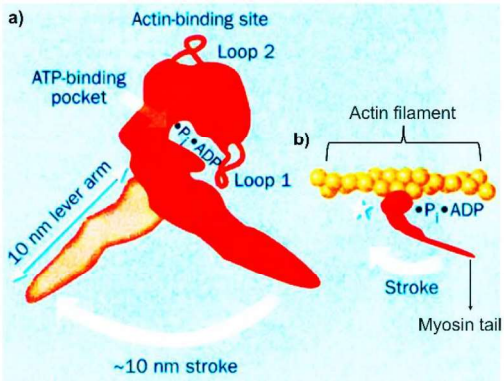

Panel adapted from reference[10].

Initially, ATP binds to a globular head domain of the myosin motor, causing a dissociation from the actin filament. Then, ATP is hydrolysed into ADP and inorganic phosphorus (P_i) and subsequent conformational changes lead to a release of Pi. This event triggers a large conformational change that generates a step motion of around 10 nm thanks to the working stroke performed by the lever arm, an α-helix bound to the head of the myosin that acts as mechanical amplifier by a swinging motion[11] (Figure 1.2).

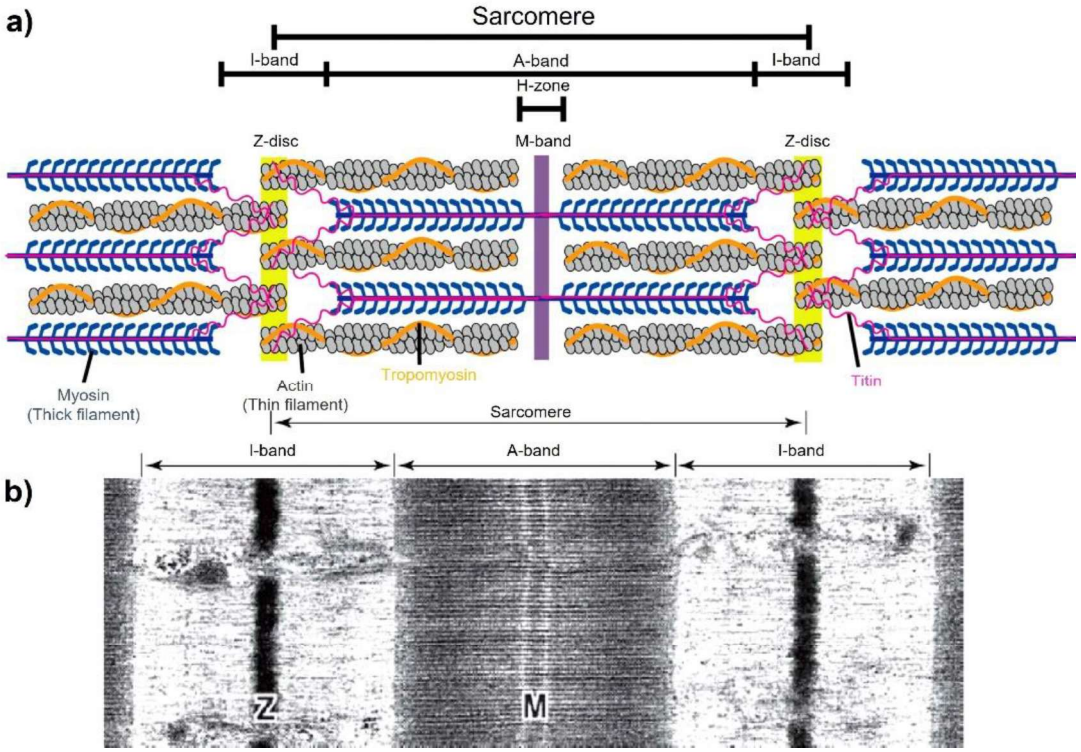

Figure 1.3. The sarcomere is the basic unit of contraction comprised of various components: (**a**) Lateral boundaries of the sarcomere are protein-dense **Z-discs**. **I-bands** are referred to the region on either side of the Z-discs and they are not in contact with the myosin thick filaments. The **A band** comprises the region along the entire length of the myosin thick filaments and the **M-band** is at the centre of the A-band (the **H-zone**) where myosin and actin do not interact. (**b**) Electron micrograph of a skeletal muscle sarcomere. Adapted from reference[12].

Such muscle contraction results from the enzymatically generated pivoting movement of approximately 10 nm of the myosin's light chain domain, which acts as a lever arm.[10] The translation caused by this pivoting motion of the lever arm generates a gliding between the myosin protein motor and actin filaments (Figure 1.2).[13] The high workload and power of the muscles come from the dense packing of these protein filaments into sarcomeres, the functional and contractile unit of biological muscles. Longitudinally repeated units form bundles of sarcomeres which in turn form myofibrils, fuelled by ATP provided by the mitochondria, creating a set of fibres with a diameter ranging 5-100 μm connected in parallel (Figure 1.3).[14,15] Such hierarchical organisation of the muscle fibres allow biological muscles to reversibly contract by 50% in isolated environments and 30% in natural movements, achieving an actuation from the micrometric scale of the sarcomeres, up to the macroscopic scale of a running leg for instance.[9] The knowledge of the biophysical principles of these enzymes and protein motors, especially the ones present in our muscles,[16] have served as source of inspiration to the emerging field of artificial molecular machines (AMM).

1.2. Artificial Molecular Machines (AMMs)

Since ancient times, Nature has been the most important and reliable source of inspiration for philosophers and thinkers,[17] artists,[18] writers,[19] and of course for scientists.[20] As briefly described in the previous section, biomolecular machines are a fundamental part of living systems since they run numerous tasks and are involved in many energetically demanding processes that would not be possible if they were not present. The structural complexity of biomachines is the result of billions of years along the way of evolution of life, which has allowed overcoming the major limitations in the cellular medium including spatial and temporal specificity for binding events, as well as catalytic activations of reaction networks.

Such constraints are reduced in artificial molecular systems, which can also perform precise motion and continuous work on their environment. Synthetic organic chemistry has appeared to serve as a useful tool to close the gap between the naturally occurring systems at the nanoscopic scale and the artificial systems, through enabling the fine chemical synthesis of diverse artificial molecular machines (AMMs).[21] Such AMMs must convert an energy input into a mechanical output, and one of the best candidates to carry out such function are the mechanically interlocked molecules (MIMs) like catenanes and rotaxanes owing to their motional dynamic nature. In addition to the development of modern approaches in synthetic organic chemistry such as template synthesis,[22] self-sorting,[23] or dynamic combinatorial chemistry,[24] the emergence of mechanically interlocked molecular machines started with the emergence of the mechanical bond, an interaction beyond the classical chemical bond.

1.2.1. The mechanical bond: from chemical to physical bond.

A chemical bond is the result of the interaction of two or more atoms, leading to the formation of what we know as molecules.[25] The formation of this set of aggregates is driven by attractive forces that involve "sharing" of electrons (covalent bonds), or by electrostatic interactions (ionic bonds) among the atoms present in the majority of molecular entities (Figure 1.4a).

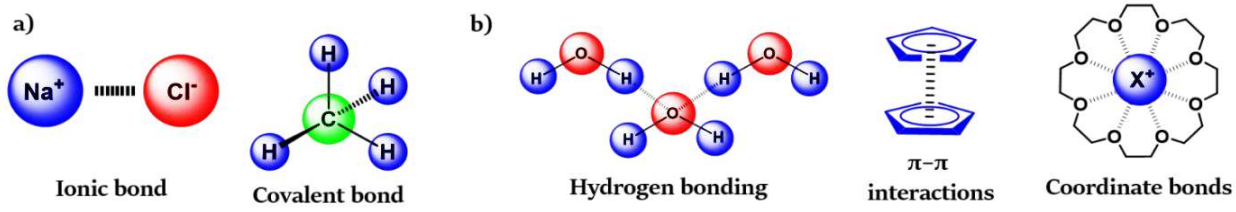

Figure 1.4. Types of chemical bonds: **a)** Ionic and covalent interactions. **b)** Supramolecular interactions.

In the 1970s, a new type of chemistry governed by non-covalent interactions such as coordinate bonds, hydrogen bonding and π-π interactions (Figure 1.4b), allowed the formation of higher-order molecular assemblies (supramolecules) through molecular recognition processes, giving birth to the supramolecular chemistry, defined by the Nobel laureate Jean-Marie Lehn as 'the chemistry beyond the molecule'.[26]

During the late 80's, host-guest interactions boosted the formation of numerous metal complexes between crown ethers (flat macrocycles),[27,28] cryptands (3D macrocycles) and *N*-heterocyclic ligands with cations.[29] Around the same time, Prof. J-P Sauvage and his team were focused on inorganic photosensitizers using Cu(I) complexes with phenanthroline derivative ligands (Scheme 1.1a). The obtained tri-dimensional structure of such metal complex (in fact, a pseudo-catenane) paved the road towards the construction of a new type of bond, a physical one; called the mechanical bond (Scheme 1.1b).[30]

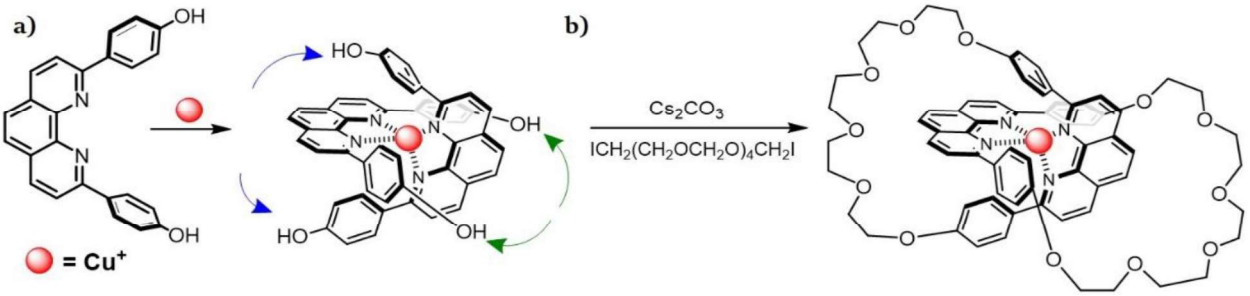

Scheme 1. 1. a) Formation of the pseudo[2]catenane by copper complexation of two phenanthroline derivative ligands. **b)** Formation of the metallic [2]catenane structure by O-alkylation reaction using copper as template to favour ring closing.

Scheme 1.1a shows the template-directed strategy involving metal ion coordination and the extremities of each ligand which reacts with diiodopentaethylene glycol under basic conditions using caesium ion as template to favour the ring closing, generating a metallocatenane with 42% yield (Scheme 1.1b). Once the metal cation is removed, the two macrocycles retained the interlocked structure which nowadays is known as the mechanical bond (Figure 1.5).[31] This contemporary variant of bond consists in the physical union of two or more well defined molecular entities. Conversely to the typical covalent or ionic bonds in which the attraction and sharing of electrons is involved, in the mechanical interaction, repulsive forces prevent the intersection of chemical bonds.[32] Therefore, the mechanical bond can be understood as the union of two or more components in such an interlocked manner that they cannot be separated unless by breaking chemical bonds between the molecular entities.[33] Such way to connect molecules have been used to create Mechanically Interlocked Molecules (MIMs) like for instance, catenanes,[34] rotaxanes,[36] but also molecular knots[35] (Figure 1.5).

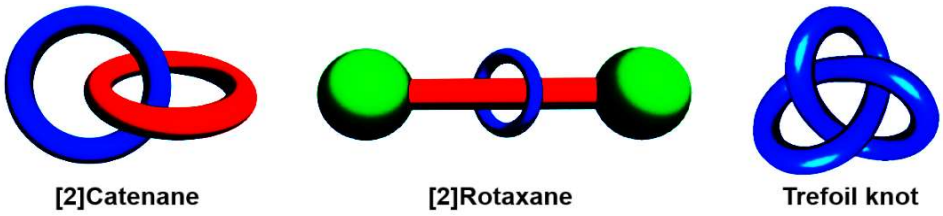

Figure 1.5. Examples of Mechanically Interlocked Molecules (MIMs) and topological knots.

As shown in Scheme 1.1, the chemical information provided by the chelating nature and denticity of the ligand, and the coordination number of the metal cation, lead to the formation of molecular recognition units or "stations" in MIMs. Complementary recognition sites well located in the components are crucial for an efficient preparation of, not only catenanes, but also other molecules with an interlocked topology. Such molecular stations led to the development of switchable artificial molecular machines. The individual components of these molecules can be constrained to undergo back and forth movements (molecular shuttling) in a controlled and directed fashion upon external stimulation (chemical or physical).[37] As a result, large amplitude mechanical motions performed by these tiny machines can be harnessed in different fields, ranging from chemical sensing[38] to information storage devices.[39]

Once the isolated switchable MIMs return to their initial stage, the backward motion of the mobile components cancels any work done during the initial forward motion. This is precisely what differentiate molecular switches from molecular motors, since the latter move their components in a non-reversible way influencing the surroundings as a function of their spatial trajectory. Conversely, switches can only alternate

between two states namely ON/OFF or *cis*/*trans* (*E*/*Z*) to name a few. This bibliographic introduction will focus only on the actuation of mechanically interlocked molecules such as [*n*]rotaxanes and [*c*n]rotaxanes acting as molecular switches, which are at the core of my PhD project. In addition, the use of molecular motors as chiral molecular switches in self-assembled systems will be described later in the manuscript.

1.2.2. [*n*]Rotaxanes

Firstly, it is important to know what the word rotaxane means. It originates from two Latin words *rota* (which means wheel) and *axis* (for axle), since it is composed by rings or macrocycles, and a linear axle that threads such macrocycle or "wheel".[33] The prefix [*n*] indicates the number of compartments forming the rotaxane, for example, a [2]rotaxane is made of one axle and one ring. Bulky end-capping groups are covalently attached to the axle serving as stoppers and preventing the slide out of the ring without breaking covalent bonds.

The first approach reported towards the synthesis of this molecular topology using non-covalent interactions was carried out in 1991[40] by the research team of Nobel laureate Prof. Stoddart. At that time, a [2]rotaxane was obtained containing an axle with two identical (degenerated) hydroquinone molecular stations that served as non-covalent template to favour the ring closing of a cyclobis(paraquat-p-phenylene) ($CBPQT^{4+}$) unit by mostly C-H···O and π donor-accepting interactions (Figure 1.6). Different signals observed in NMR studies showed that the ring alternated its position between the two hydroquinone units, simply driven by Brownian motion.

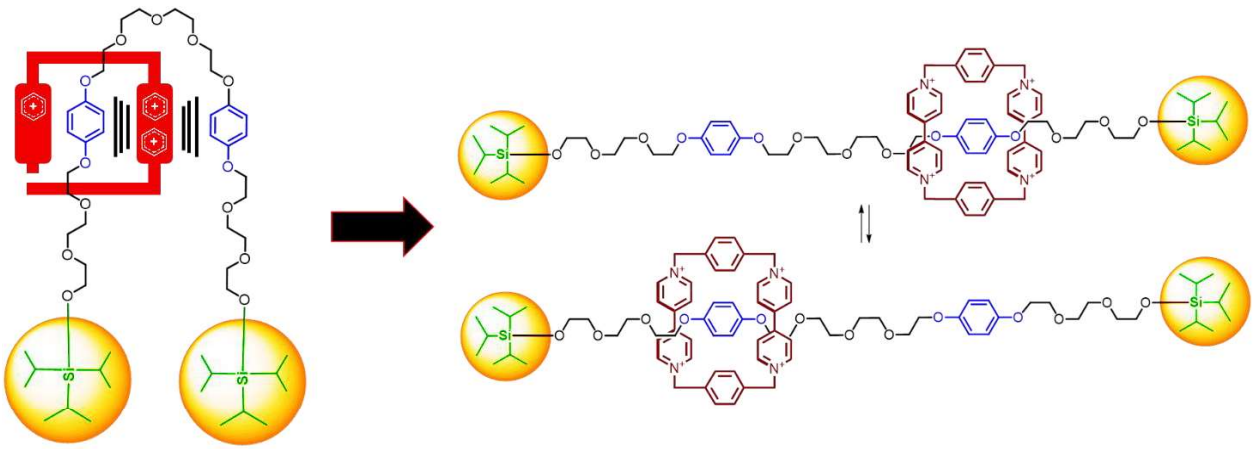

Figure 1.6. First example of a [2]rotaxane obtained by Stoddart and co-workers.[40] The non-covalent bonding interactions between the hydroquinone moieties and the positively charged bipyridinium units serve as template for ring closing.

This proof of concept was one of the milestones that motivated scientists to break the symmetry of the system by introducing of two different stations on the thread, with the objective of using different external stimuli (chemical and electrochemical) to trigger the molecular motion of the ring in a controlled manner. In 1994, control of a chemically-driven molecular shuttling was achieved with a [2]rotaxane, in which the axle contained the pH-sensitive benzidine unit and the π-donor electron bisphenol, while maintaining the electron accepting tetracyclophane.[41] NMR studies confirmed that the ring spent more than 80% of the time on the electron donating benzidine unit. Formation of the secondary ammonium groups by protonation of the NH group made the ring moving towards the bisphenol unit with a ratio of 98/2 as consequence of electrostatic repulsion. As a matter of fact, this work demonstrated that the combination of mechanical bonds with molecular stations having different affinities lead to internal motions of larger amplitudes[42] than those produced by configurational *cis*/*trans* isomerisation of double bonds.

In addition, other type of macrocycles have been used to construct pH-triggered [2]rotaxanes besides $CBPQT^{4+}$. This is the case for crown ethers, which possess great affinity to form coordination complexes with ammonium groups, as Prof. Stoddart and co-workers demonstrated using of the host ability of dibenzo[24]crown-8 ether (DB24C8) with secondary ammonium groups as guests, in order to create a molecular recognition couple.[43,44] Hydrogen bonding and electrostatic dipole-dipole interactions between the ammonium centre and the precise arrangement of the ligating oxygen atoms are the roots of this supramolecular self-assembly. Scheme 1.2 shows a [2]rotaxane based on an axle containing a 4,4'-bypyridinium moiety bearing a 3,5-diisopropylbenzyl fragment as bulky stopper and a $-CH_2NH_2^+CH_2-$ fragment encircled by the DB24C8 macrocycle with an adjacent anthracenyl group serving also as stopper.

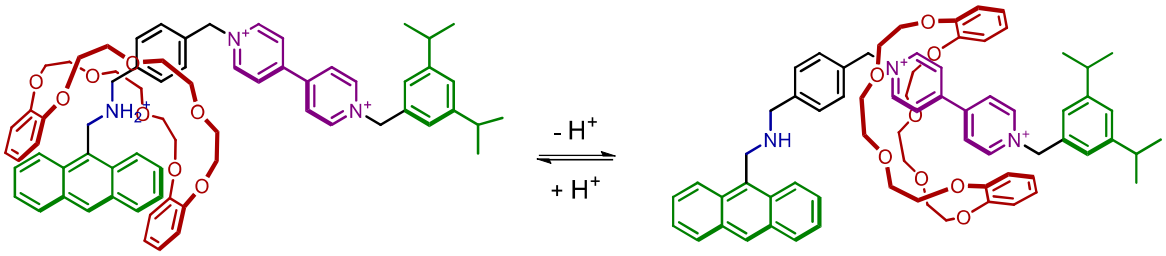

Scheme 1.2. pH-induced mechanical shuttling of a [2]rotaxane containing a crown ether as "wheel".

Upon deprotonation of the ammonium station, the macrocycle moves away toward the electron deficient 4,4'-bipyridinium unit, while the molecular actuation can be reversed by protonation of the secondary amine. Besides controlling the motion of the ring, the electronic properties of the molecule could be tuned by an efficient mechanical switching. The emission of the anthracene moiety is quenched in the deprotonated state by electron transfer from the free amino group but enhanced in the protonated state due to the protection

exerted by the DB24C8 against the dicationic bipy moiety. This precludes a quencher effect of the bipyridinium fragment on the excited state of the anthracene moiety.[45]

The construction of these molecular shuttles, along with the exploitation of the non-covalent interactions in the field of supramolecular chemistry, opened the door towards the design of new molecular topologies. In particular, this led to the creation of functional compartments that could be used to construct molecular machines that are able to accomplish complex tasks upon chemical or physical stimulation. Once it was established that disubstituted ammonium cations interact with the internal cavity of the DB24C8 macrocyclic ring in a threaded manner[44], the discrete and interwoven supramolecular architectures emerged.

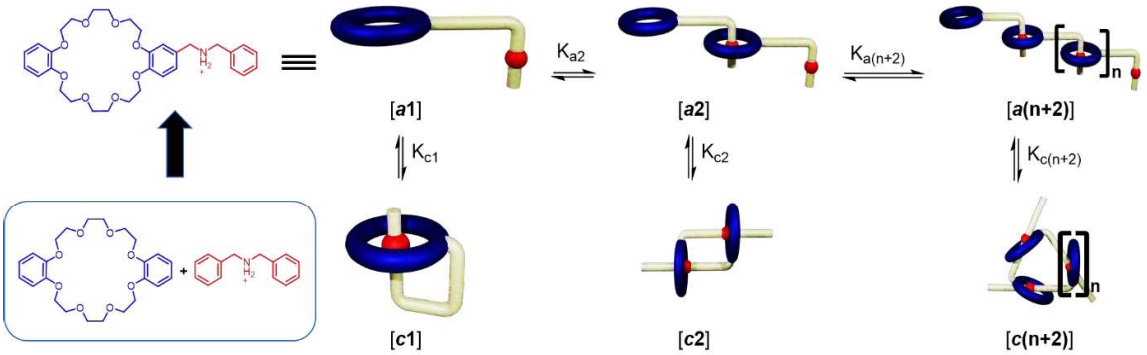

Figure 1.7. Cyclic and acyclic structures formed by the self-complementary structure [*a*1]. Adapted from reference[46].

In fact, covalent binding of this crown ether with a secondary protonated amine gave rise to a self-complementary structure which has the ability to self-assemble into linear, cyclic, or daisy chain structures (Figure 1.7). In particular, the next section and this thesis as a whole focus on [*c*2]daisy chain rotaxane structures and their sliding molecular motion.

1.2.3. [*c*2]Daisy chains: First steps towards artificial molecular muscles

The beauty of the natural occurring and synchronous movement of the actin-myosin filaments[47] described previously in Section 1.1 has probable been the source of inspiration for the Nobel laureate Prof. Sauvage and co-workers.[48] In 2000, they carried out the design and synthesis of the first prototype of an artificial molecular muscle. Inspired by the sliding movement of the actin and myosin natural filaments, a double-threaded structure with two recognition sites was obtained based on a [*c*2]daisy chain structure initially described by Stoddart *et. al*.[49] In fact, such topology name was attributed due to the similarity to garlands assembled by repeated threading of the stem of one flower through a hole in the stem of another one, with the flower heads precluding the structural disassembly.[50]

In this case, the presence of Cu(I) ions induced in metal-coordination bonding played a key role as gathering and threading centre. The monomer was designed in a way of having a chelating unit able to coordinate the copper ions in both the ring and the tethered rod-shape axle, conferring it a "hermaphroditic" character[51] (Scheme 1.3). Molecular modelling studies revealed that such interlocked structure was not able to form a self-threaded complex such as [*c*1], due to the rigidity of the rod shape aromatic axle and the short CH_2 linker. This two interpenetrated rotaxane metal complexes opened the door towards the synthesis of molecular muscles.

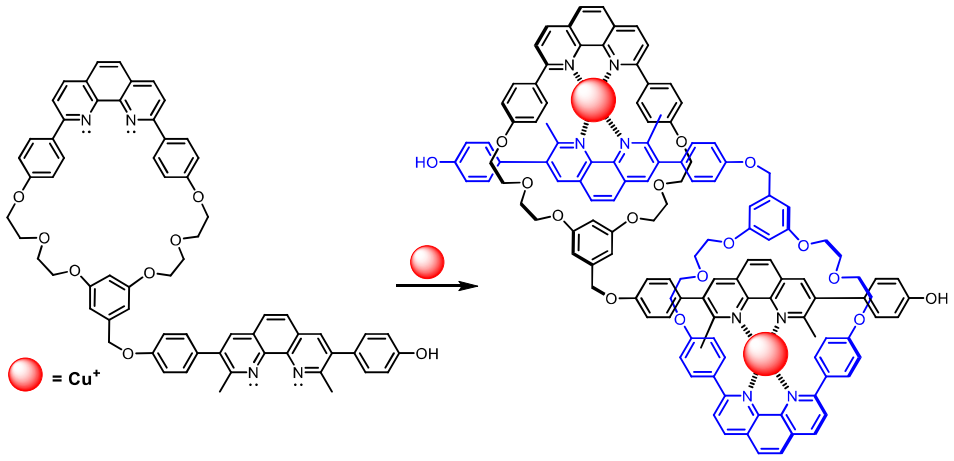

Scheme 1.3. Molecular structure of the double threading process induced by CuI ions between two hermaphrodite ligands.

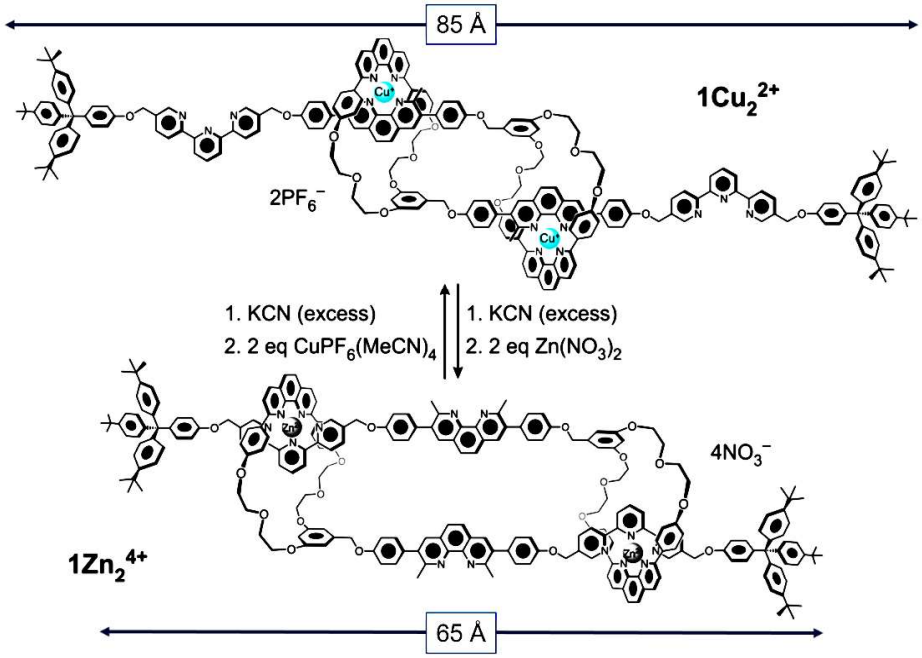

Figure 1.8. First prototype of an artificial molecular muscle based on a [c2]daisy chain structure. The mechanical actuation is driven by transition metal ion exchange. Adapted from reference[52].

Besides the phenanthroline coordinating moieties present in the macrocycles, the axle of the [*c*2]daisy chain contained two terpyridine units. Such a combination provides the advantage of using two different metal cations as chemical stimulus (Figure 1.8). At the initial state, Cu(I) are complexed by the phenanthroline units rendering an extended conformation to the molecule. After demetalation using cyanide ions and subsequent addition of zinc(II) ions, a sliding of the two components of the [*c*2]daisy chain occurs in order to form zinc(II) complexes between the phenanthroline and terpyridine ligands due to the higher coordination number of Zn(II). The chemically-induced motion, leads to a longitudinal reduction of the size of the molecule of about 22% compared to its original state and the formation of a contracted state, similar to what is observed in the sarcomeres of muscular tissues (Figure 1.8).[48]

However, this molecular actuation driven by metal ion exchange is poorly reversible and leads to the generation of significant amount of cyanide waste. Therefore, the metal-induced switching was replaced by systems sensitive to pH changes. In 2008, the teams of Stoddart and Coutrot reported independently pH-switchable [*c*2]daisy chains. Both systems were based on a DB24C8 crown ether initially sitting on a secondary ammonium group. However, upon deprotonation, in the case of Stoddart's work, the macrocycles sit on a bipyridinium station (Scheme 1.4a),[53] while in Coutrot's work the macrocycles sit on a triazolium ring with two mannosidic groups acting as stoppers (Scheme 4c).[54]

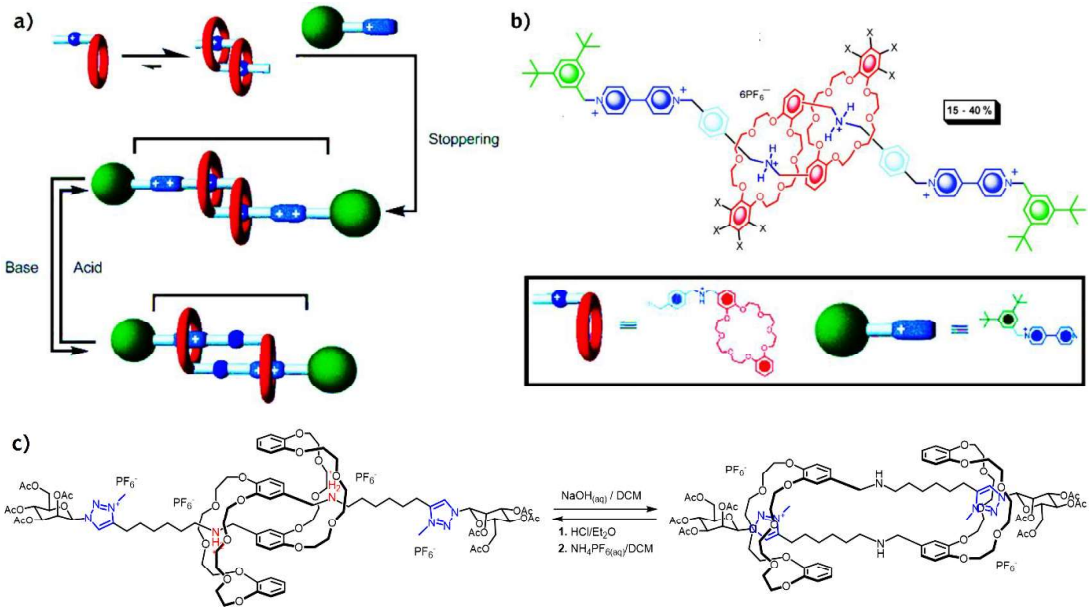

Scheme 1.4. a) Schematic representation of the pH-triggered mechanical motion of a [*c*2]daisy chain rotaxane. The first step consists in the self-assembly of the complementary macrocycle followed by an end-capping reaction. **b)** Chemical structure of a [*c*2]daisy chain structure using bipyridinium as molecular stations for the crown ether macrocycles. **c)** Mechanical actuation of a [*c*2]daisy chain structure using triazolium rings as molecular stations for the crown ethers.

In both cases, a reduction in the size of the molecule of about 29% as a result of the deprotonation of the ammonium station provides the molecule in the contracted state. The shuttling is reversed to the extended form at low pH due to the higher affinity of the crown ether for the secondary ammonium compared to the triazolium or the bipyridinium stations. In Coutrot's work, the mannosyl stoppers were introduced together with the second station by a click chemistry approach. This strategy has been useful to obtain other [*c*2]daisy chains,[55] including unsymmetrical ones.[56] Besides chemically-induced actuating systems, other external stimuli have been used to actuate [*c*2]daisy chain systems. Light has been used as source of energy to actuate [*c*2]daisy chain rotaxanes,[57] as well as solvent polarity[58] and redox potentials. For instance, in 2014, Stoddart and co-workers reported the one-pot synthesis of electrochemically bistable [*c*2]daisy chain rotaxane switches based on the tetracationic cyclophane CBPQT4^{+} as macrocyclic ring, and a redox responsive axle containing a bipyridinium unit and the electron donor 1,5-dioxynaphthalene (DNP).[59] Click chemistry was crucial for covalently coupling the axle to the macrocycle and for stoppering kinetically the self-complementary assemblies formed in solution (Figure 1.9).

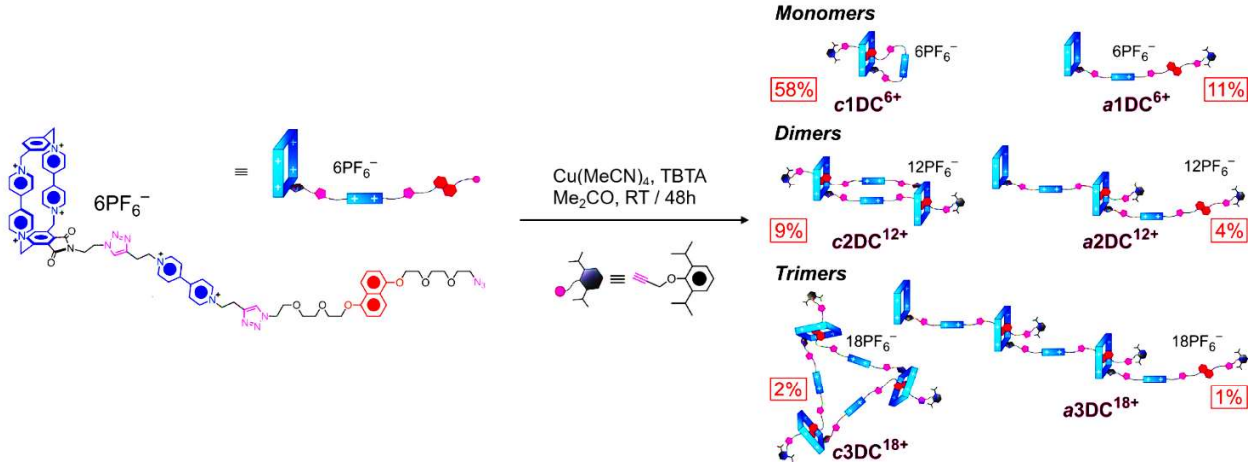

Figure 1.9. Various redox-active molecular daisy chains obtained by stoppering through click chemistry. Adapted from reference[59].

Except from the acyclic versions of daisy chains formed, cyclic voltammetry experiments showed an electrochemical contraction/extension event in the cyclic daisy chains. Such mechanical movement along the molecular length of the axle is of particular interest due to the similarity to sliding of the muscle like contraction. In fact, such contractile event has been observed not only in one dimension but also in multidimensional spaces as exhibited by higher order [*c*3] and [*c*4]daisy chain systems. Chiu and co-workers designed threads featuring urea and bipyridine recognition motifs linked to a complementary macrocycle containing a pyridine unit. Varying the length of the linker allowed the formation of trimeric and tetrameric

structures through chelation of Zn(II) ions by both the bipyridine and the pyridine moiety.[60] The urea stations were introduced in the presence of a bulky isocyanate which avoid the slipping out of the rings, once the Zn(II) ions were removed by a competing ligand. In the case of the trimeric species, such demetalation caused a mechanical actuation of the macrocycles towards the urea sites, switching from a stretched to a contracted triangular geometry. Alternatively, the tetramers switched between a contracted 2D square planar geometry and a stretched 3D tetrahedron.

More recently, Stoddart and co-workers found an efficient strategy based on radical and anionic templates to synthesise in high yields (>90%) [*c*3]daisy chain rotaxanes exhibiting electrochemical switching between a relaxed macrocycle and a trisarm-shaped conformation (Figure 1.10).[61] These results open the door towards muscle-like (sliding) movements in higher dimensions based on cyclic daisy chains, an attractive characteristic that can be useful in the creation of stimuli-responsive materials.[46]

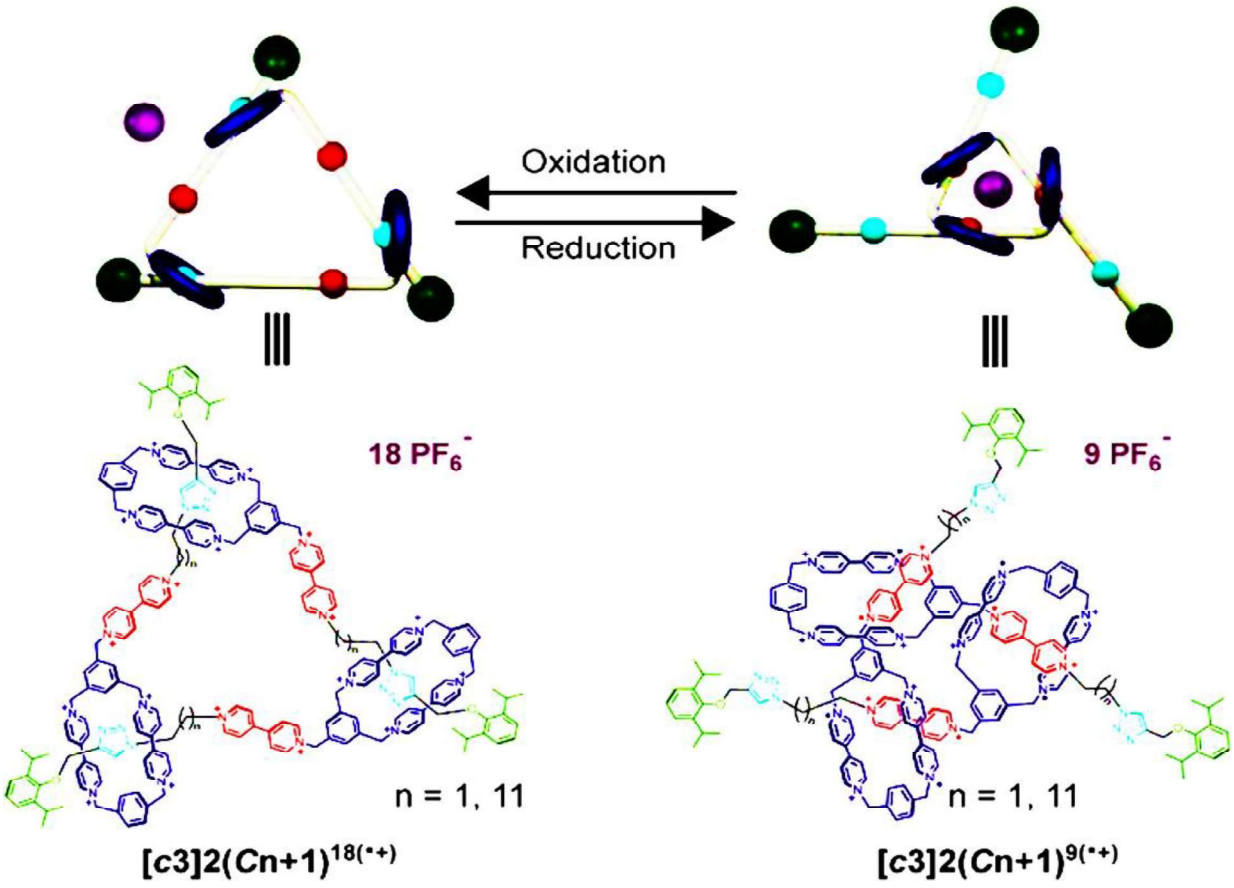

Figure 1.10. Reversible electrochemical actuation between a relaxed macrocycle [*c*3]2(Cn+1)$^{18(\bullet+)}$ and its star shaped counterpart [*c*3]2(Cn+1)$^{9(\bullet+)}$. Adapted from reference[46].

Changes of topology upon mechanical actuation of MIMs have been achieved using a [*c*2]daisy chain unit inserted in polycaprolactone polymer chains, decorated at the extremities with urethane bonds obtained upon reaction with 3,5-dimethylphenyl isocyanate. Carbamates served as molecular stations for the macrocyclic crown ethers once the ammonium stations are locked by acetylation with acetic anhydride. This cause a sliding motion which in turn changes the topology of the polymer from a linear geometry to a macrocyclic one.[62]

So far, we have described the relevance of the chemical structure and the type of external stimuli used to obtain artificial molecular muscles based on [*c*2]daisy chain rotaxanes consisting of only one contractile unit. Nevertheless, in order to harness the nanoscopic contraction/extension event and transfer it hierarchically to the micro- and macroscale as occurs in sarcomeres, it was necessary to design synthetic molecular machines capable to undergo collective mechanical motion to generate changes in properties at higher length scales, a topic that will be treated in the next section.

1.3. Amplification of molecular motion from molecular machines

The amplification of molecular motion generated from the actuation of molecular machines is of great interest to scientists and engineers in the field of materials science. They have harnessed collective motion to design and construct smart materials and soft actuators governed by nanoscale motions that can be amplified to microscopic and macroscopic length scales.[63] Different approaches have been envisioned to achieve such motions at higher length scales, including the introduction of molecular machines in bulky and robust materials such as polymers, and self-assembled dynamical systems such as mesophases.

In the following sections, most of the strategies and obtained results reported in the literature on the collective motion exerted by mechanically interlocked molecular machines are presented. Examples of polymeric materials and condensed matter phases based on or containing switchable mechanically interlocked molecules and light-driven chiral motors used as molecular switches are described.

1.3.1. Collective motion from [*c*2]daisy chains based polymers

The molecular movement that takes place inside the sarcomeres, the basic unit of muscles, has served as source of inspiration of synthetic chemists interested in the design of robust systems that can amplify mechanical molecular motion in a synchronised and hierarchical manner. The first efforts invested in attaining this goal were performed by the group of Kaneda in 2006.[64] They reported the oligomerisation (up to pentamers) of [*c*2]daisy chain rotaxanes based on fully methylated α-cyclodextrins bearing a

photoactive axle containing an amide motif. Polymerisation of the interlocked structure occurred through a nucleophilic substitution reaction between this amide and dibenzyl bromide. Initially, the azo bond is on the *E* (*trans*) configuration, then, upon light stimulation at 366 nm, the cyclodextrin units moved away from the azobenzene motifs, which adopt a *Z* (*cis*) configuration. Several configurational isomers were observed by NMR spectroscopy, meaning that not all the azobenzene motifs were converted to the *Z* state. Thus, a more effective strategy was needed to overcome the constraints of low degree of polymerisation and yields, as well as incomplete contraction of the oligomers.

Three years later and in parallel, the research groups of Prof. Stoddart and Prof. Grubbs independently reported the synthesis of pH-switchable [*c*2]daisy chain covalent polymers by an end-capping strategy using the Cu(I)-catalysed azide/alkyne cycloaddition (CuAAC) reaction. Stoddart's system DB24C8 crown ether able to bind either the secondary ammonium groups or bipyridinium stations present on the axle, which has two bulky stoppers containing an alkyne moiety at each extremities.[65]

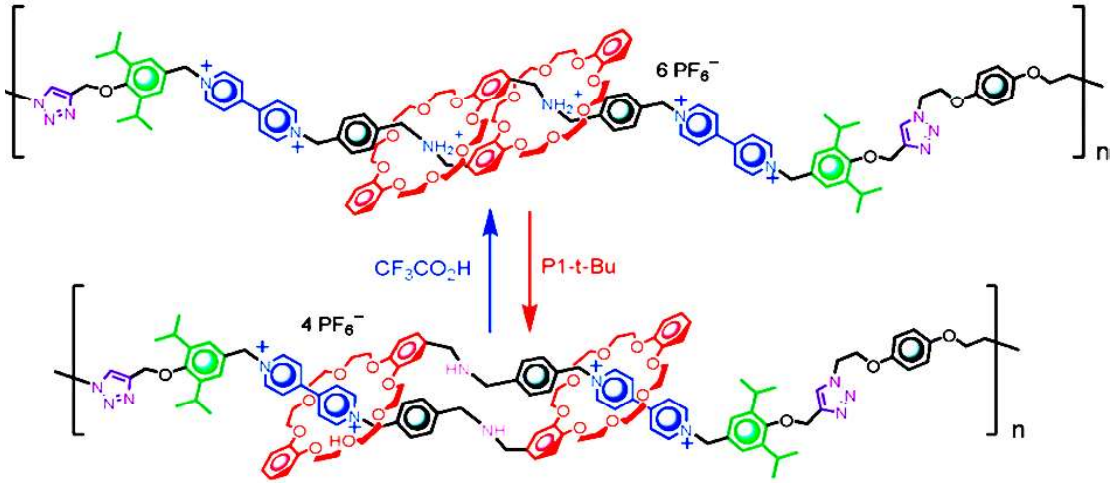

Scheme 1.5. pH actuation of poly[*c*2]daisy chain rotaxanes obtained by CuAAC reaction. Adapted from reference[65].

The bis-alkyne terminated [*c*2]daisy chain was subjected to step-growth polymerisation with a bis-azide derivative providing a linear polymer composed of approximately 11 repeating units (Scheme 1.5). The reversible pH-triggered switching of the oligomers was demonstrated by ^{1}H NMR spectroscopy and cyclic voltammetry. Despite the small size of the polymer and the lack of amplification of the molecular motion, this work opened the door towards the development of stimuli-responsive contractile polymers.

On the other side, Grubbs and co-workers considered for another synthetic approach to obtain [*c*2]daisy chain architectures.[66] First, a macromer was designed and synthesized containing a host based on two polyether chains attached to an aromatic ring, which in turn was bound to a secondary ammonium group

through a biphenyl rigid linker. The ammonium group was in turn linked to a stopper that was functionalised with an alkyl chain having a terminal hydroxyl group. Unlike Stoddart's work in which the interlocked structure is obtained by an end-capping reaction, this strategy developed by the group of Grubbs's is based on a dynamic ring-closing metathesis (RCM) reaction. Here, the polyether chains encircle the secondary ammonium unit in a self-assembled structure favouring the proximity of the terminal double bonds in order to react with the olefin metathesis catalyst, affording the [*c*2]daisy chain in high yields (Scheme 1.6).

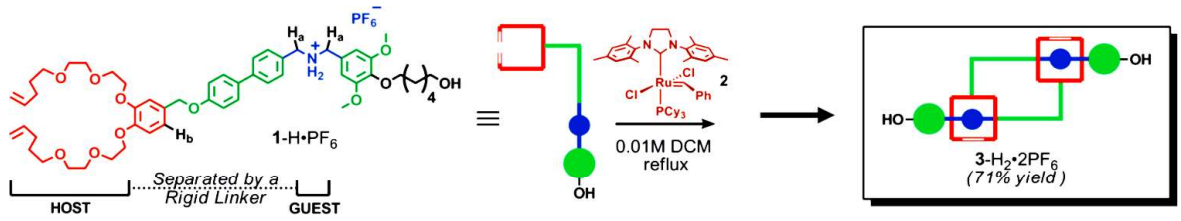

Scheme 1.6. Synthesis of the [*c*2]daisy chain rotaxane obtained by Grubbs and co-workers by ring closing metathesis. Adapted from reference[66].

The terminal alcohol was crucial for polymer synthesis, since it was converted to an azide group (Scheme 1.7a) to carry out a step-growth polymerisation by click chemistry reaction with 1,4-ethynylbenzene (Scheme 1.7b (*i*)). The obtained polymer was composed of main chains with approximately 22 repeating units (Scheme 1.7b (*iii*)), twice the size of the polymer obtained by Stoddart's team. The extended state of the polymer chains was not obtained after deprotonation of the ammonium station as in previously mentioned cases, likely due to π-π stacking interactions between the biphenyl substituents (Scheme 1.7b (*ii*)).

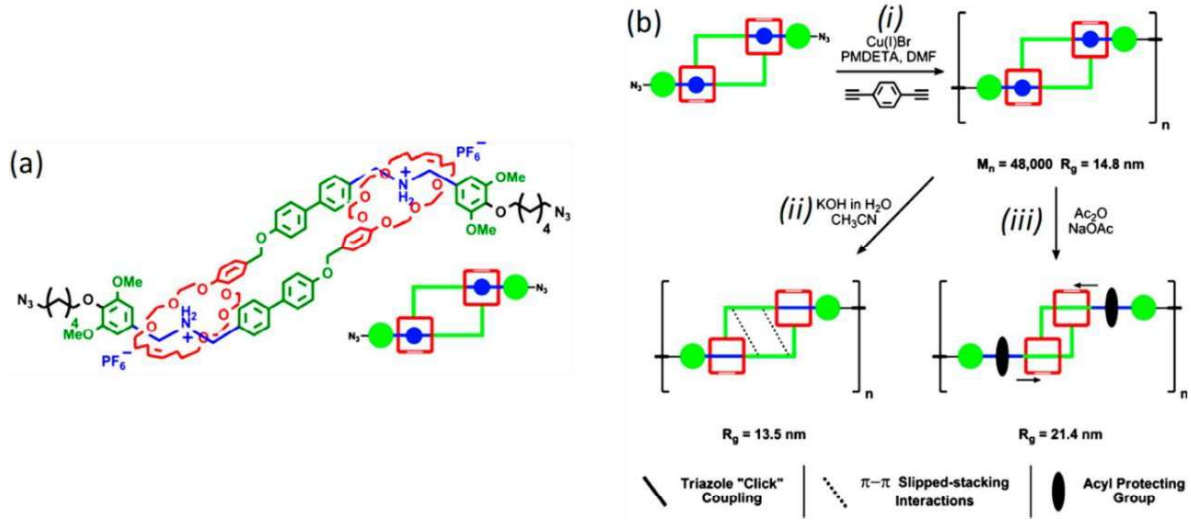

Scheme 1.7. a) Chemical structure of the [*c*2]daisy chain rotaxane monomer decorated with azide groups at the extremities. **b)** (***i***) Step-growth polymerisation of the monomer with 1,4-diethynylbenzene and actuation of the polymer using (***ii***) basic media or (***iii***) acetic anhydride to block irreversibly the ammonium station. Adapted from reference[66].

However, acylation of the secondary ammonium group increased the bulkiness in the region, forcing the displacement of the macrocycles over the biphenyl units, leading to a polymer in the extended state with an increase in the hydrodynamic radius up to 48%. The sizes of poly[*c*2]daisy chain rotaxanes obtained by the groups of Grubbs and Stoddart were still not enough to amplify the molecular motion of individual molecular machines to higher length scales. These results challenged scientists rapidly to look for other strategies to obtain linear polymers with higher degrees of polymerisation.

In 2012, Giuseppone and co-workers reported for the first time the amplification of the molecular motion from the nano- to the micrometric scale in a single-chain polymer based on pH-switchable [*c*2]daisy chain units obtained by metallosupramolecular polymerisation.[67] The [*c*2]daisy chain rotaxane monomers contain DB24C8 macrocycles as hosts of the ammonium stations, and of the triazolium stations, as well as two terpyridine moieties at the extremities for polymerisation (Figure 1.11a). The terpyridine were coupled to the pseudo[c2]daisy chain rotaxane by click reaction, thus allowing the formation of the second station, and playing the role of stoppers.

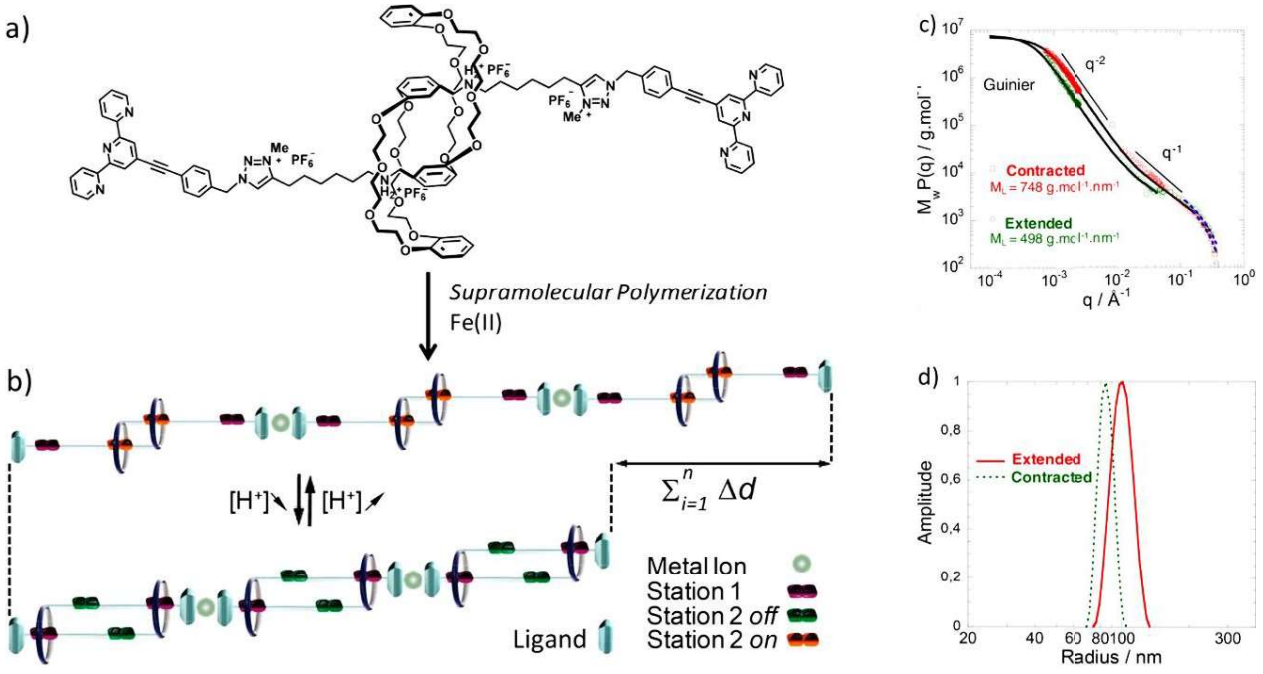

Figure 1.11. a) Chemical structure of the [*c*2]daisy chain monomer containing terpyridine units at the extremities conceived and synthesised by Giuseppone and co-workers. **b)** Schematic representation of the acid-base actuation of single chain metallosupramolecular poly[*c*2]daisy chains using Fe(II) ions. **c)** Light and neutron scattering curves of Fe^{II} poly[*c*2]daisy chains in both extended and contracted states exhibiting the different values of linear mass density M_L. **d)** Light scattering experiments showing the difference in hydrodynamic radius confirming the actuation at the microscopic scale. Adapted from references[67,68].

Additionally, and most importantly, the terpyridine units act as ligands to carry out a metallosupramolecular polymerisation with Zn(II) and Fe(II) ions (Figure 1.11b). Results obtained from light (DLS and SLS) and neutron (SANS) scattering experiments allowed to determine a high degree of polymerisation (~2900 units) for the iron-based polymers, as well as the shape and size change of the single wormlike polymer chains after acid-base stimulation (Figure 1.11c-d). The length of the single worm-like polymer chains in the contracted state was estimated to be around 9.37 μm and 15.86 μm after the acid-induced extension, causing a global change in the contour length of the polymer chains as result of the local change in the linear mass density of the polymer, confirming the overall contractile motion. This work represented a breakthrough report about the amplification of a nanoscopic motion by four orders of magnitude, proving the achievement of the integration of molecular motion across several length scales.

On the other side, taking as model the metallosupramolecular approach proposed by the Prof. Giuseppone's team, a solvent switchable poly[*c*2]daisy chain based on pillar[5]arenes was obtained by the group of Prof. Huang and co-workers.[69] Herein, the contractile event was studied by dynamic light scattering (DLS) observing an increase of the radius of gyration (R_g) in chloroform when DMSO was progressively added to the solution. In that case, molecules remained in the contracted state when they are in a low polarity solvent, and then the extension takes place once the polarity of the medium increases. Despite the achievement of the contraction/extension, solvent-dependent systems cannot be used in practical applications since they require progressive dilution and the concentration affect the size of the objects.

So far, it has been demonstrated that the collective motion of individual [*c*2]daisy chain units embedded in polymers can cause a global change of the single-chain polymers at the microscopic scale, following a biomimetic approach of what happens inside the sarcomere. Nonetheless, beyond the mechanical actuation of the molecular machines, bundling and orienting single polymer chains was still an important challenge. Therefore, in order to have access to efficient macroscopic responses, it is necessary to achieve a hierarchical organisation of single-chain polymers into higher scale structures like sarcomeres do in myofibrils, which in turn interact laterally to be packed in bundles of larger and stiffer muscular fibres, leading to macroscopic actuation with high workload.

In 2016, Giuseppone and co-workers set to the task of obtaining bundles of single chain polymers. They were prepared through the hydrogen-bonding supramolecular copolymerisation between [*c*2]daisy chain rotaxane monomers bearing 2,6-diacetylaminopyridine fragments as stoppers and a complementary bis-uracil terminated hydrophobic linker (Figure 1.12a).[70] In the extended state, the formation of micrometric entangled fibres arising from lateral π-π stacking and van der Waals interactions of mainly the bis-uracil

linker was observed. Upon pH stimulation, notable morphological differences between the contracted and extended states were observed by microscopy (TEM and AFM). The morphology of the bundled fibres changed to coffee-grain shape in the contracted form due to the rigidity adopted by the polymer chains. This rigidity destabilises the lateral hydrogen-bonding interactions by steric hindrance leading to a shortening of the polymer chains (Figure 1.12b).

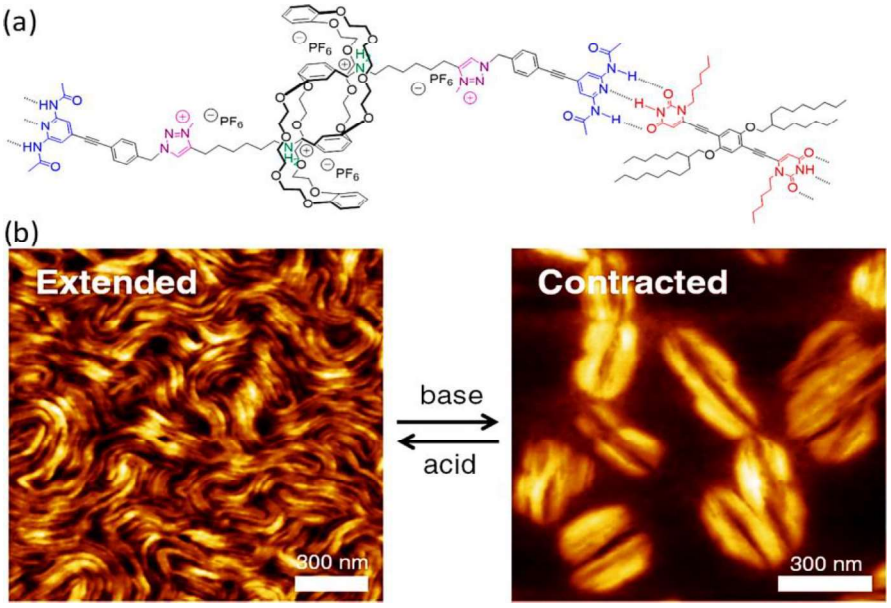

Figure 1.12. a) Chemical structure of the [*c*2]daisy chain rotaxane monomer functionalised with 2,6-diamidopyridine groups used as stoppers and the complementary bis-uracil linker in order to form hydrogen-bonded supramolecular polymers. **b)** AFM images of both the extended and contracted states displaying clear morphological changes. Adapted from references[68,70].

The possibility of obtaining bundles of fibres in an organised fashion from pH-switchable [*c*2]daisy chain copolymers at the mesoscale, motivated even more research about the impact of this nanomechanical motion in other type of hydrogen-bonded supramolecular polymers. Specially, the synthesis of a more resilient material that could maintain its physical integrity after actuation.

In 2017, the same group reported bistable [*c*2]daisy chain rotaxane polymers capped with two 2-ureido-4-[1*H*]-pyrimidinone (Upy) derivatives protected with a photolabile group (Figure 1.13a).[71] UV-light irradiation triggered the removal of the *o*-nitrobenzyl group, allowing polymerization through the Upy units and the subsequent formation of physical reticulated gels in the extended state due to π-π stacking and hydrogen-bond interactions (Figure 1.13b(*i*)). In fact, these hydrogen-bonded motifs have been widely exploited for the formation of supramolecular polymers due to the very high association constant of

dimerization in non-polar solvents like chloroform and toluene.[72] After deprotonation of the ammonium station with triethylamine, the polymer contracts causing a pH-modulated gel-sol transition, a behaviour that is explained by a partial depolymerisation caused by the proximity of the DB24C8 macrocycles to the Upy units (Figure 1.13b(i*i*)). Such vicinity affected the dimerization of Upy motifs, decreasing the association constant value and precluding the physical reticulation. Besides, it leads to the formation of single chain polymers of about 22 monomers according to the results obtained by SANS and SAXS. Interestingly, the gel-sol transition can be reversed by adding hydrochloric acid in diethyl ether, thus returning to the protonated and extended state (Figure 1.13b(i*i*)).

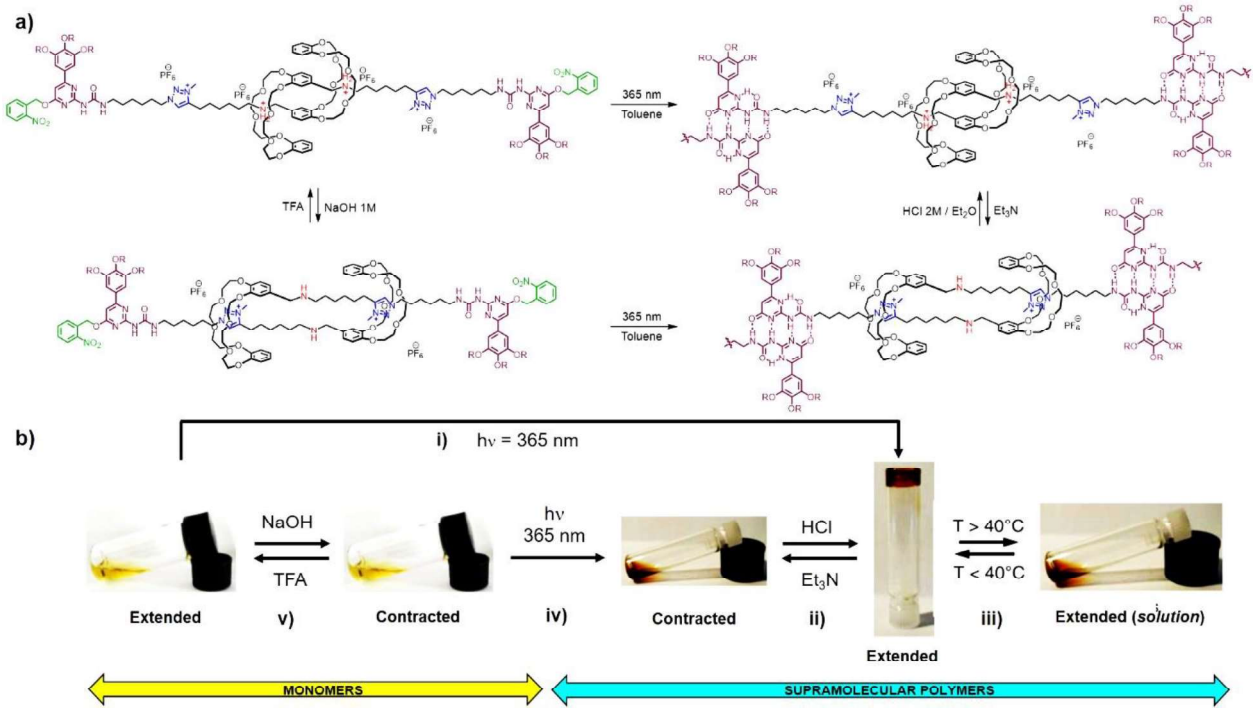

Figure 1.13. a) Chemical structures of the [*c*2]daisy chain rotaxanes in both, extended and contracted states (left). Photochemical triggered supramolecular polymerisation in toluene based on self-complementary ureidopyrimidinone (Upy) stoppers (right). **b)** Reversible sol-gel transitions of monomers obtained upon (***i***) polymerisation (***ii***) chemical actuation and (***iii***) heating. Adapted from references[71,73].

The three previously described research works show the impact at higher scales of the collective motion of [*c*2]daisy chain units in supramolecular polymeric materials. However, the mechanical integrity of materials was compromised in all cases upon actuation. Therefore, the gap between a mechanical actuation and resilience of the materials had to be addressed from another approach. In 2016, Harada and co-workers carried out the preparation of photoresponsive covalent polymeric gels (hydro and xerogels) based on [*c*2]daisy chains rotaxanes using cyclodextrin as hosts threaded by azobenzenes as recognition motifs (Figure

1.14a (*i*)).[74] The photochemical *trans*-*cis* isomerisation of the azo bond by UV light irradiation led to the contracted state, which could be reversed to the initial state by visible light irradiation. Thin pieces of [*c*2]daisy chain hydrogel (Figure 1.14a (*iv*)) and xerogel (Figure 1.14a (*v*)) were clipped, suspended and irradiated independently with UV-light. The pieces bended toward the light source in hours and seconds respectively, without remarkable alteration of the materials. Interestingly, despite not achieving reversible motion of the xerogel with visible light irradiation, this material was used to lift a 100 mg object.

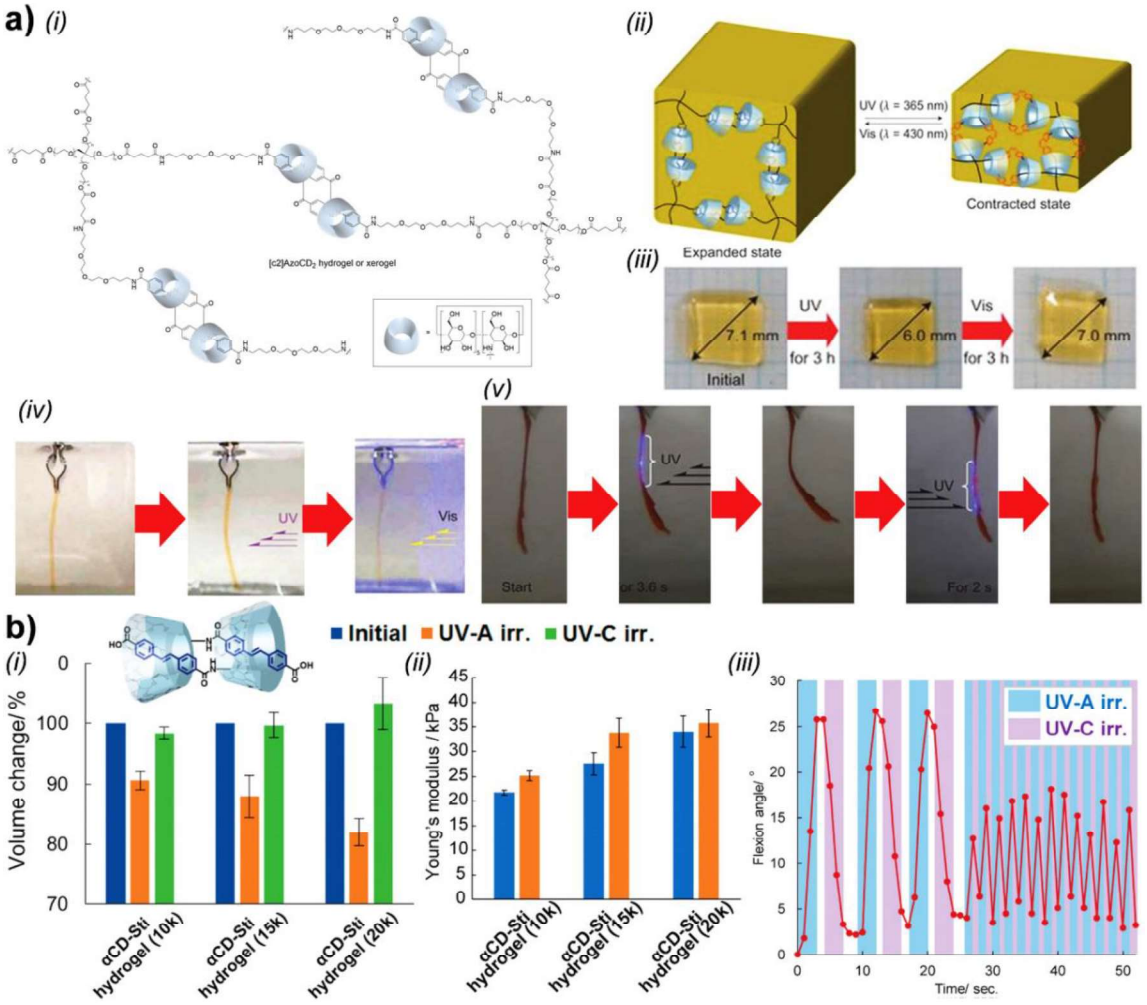

Figure 1.14. a) (***i***) Chemical structure of the covalent poly[*c*2]daisy chain rotaxanes based on α-cyclodextrins. (***ii***) Schematic representation of the contractile behaviour of the gels under UV and Visible light irradiation. (***iii***).Pictures of a small portion of the material upon actuation: (***iv***) Hydrogel and (*v*) xerogel under light irradiation. **b**) Changes in (***i***) volume and (***ii***) Young's modulus as function of PEG size connecters of a hydrogel similar to (**a-*i***) but made with stilbene instead of azobenzene as photoactive units. (***iii***) Evolution of the flexion angle of a xerogel upon sequential UV light irradiation. Adapted from reference[73].

A more efficient example similar to the covalent approach of [*c*2]daisy chain polymers based on cyclodextrin was carried out by the same group. Azobenzene was changed for the stilbene motif which requires using mainly UV light to perform the contractile motion (Figure 1.14b).[75] These hydrogels actuated faster than those based on azobenzene (30 seconds vs 3 hours) owing to the higher photoisomerization reaction rate and quantum yield of the stilbene (Figure 1.14b(*iii*)). The [*c*2]daisy chain units were connected by four polymeric arms of PEG units whose molecular weight was varied to study the effect on the mechanical actuation. It was found that the higher the molecular weight of the connectors, the higher the volume change upon photochemical contraction (Figure 1.14b(*i*)). Following with a covalent approach, in 2017, Giuseppone and co-workers reported the design, synthesis and characterisation of branched covalent polymers based on pH-switchable [*c*2]daisy chain rotaxanes as contractile units. The click polymerisation allowed to obtain chemically reticulated gels using ditopic and tritopic linkers (Figure 1.15a, top).[76] The nanoscopic actuation taking place in the chemically cross-linked network is translated to a reversible contraction/extension of the swollen chemical gels by around 40% of the initial macroscopic volume (Figure 1.15a, bottom).

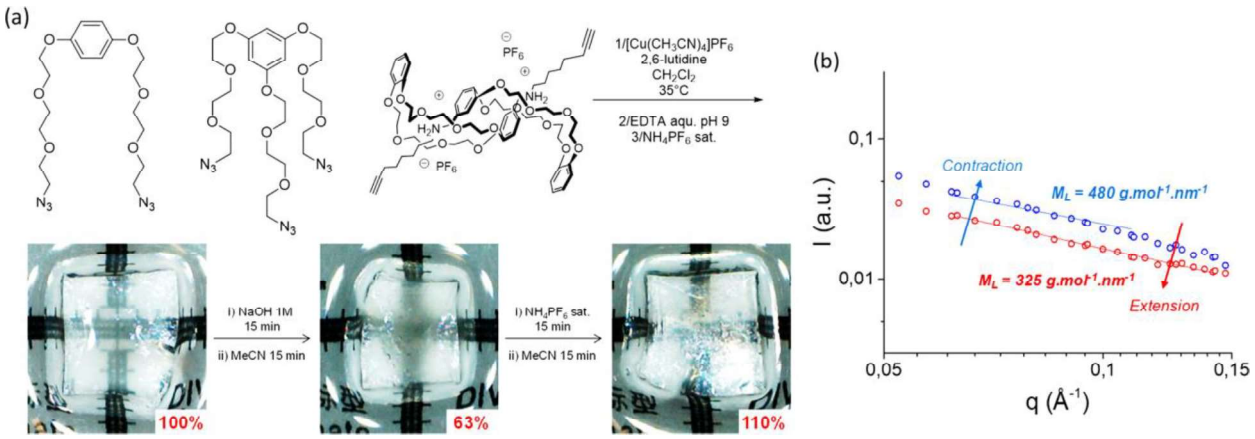

Figure 1.15. a) Chemical structure of azide linkers and the pseudo[*c*2]daisy chain rotaxane used to prepare the chemical gels, which show a noticeable volume change upon actuation. **b)** Neutron scattering curves showing remarkable differences in linear mass density values, indicating a macroscopic contraction as result of the collective motion of [*c*2]daisy chain rotaxane units. Adapted from reference[68].

Neutron scattering experiments helped determining that the local motion of the polymer chains was the responsible for the macroscopic actuation of the gels. This is explained by an increase of approximately 50% in the linear mass density of the polymer chains after the contraction movement (Figure 1.15b). However, fibre manufacturing of polymer gels is complicated due to the three-dimensional network structure resulting from the chemical crosslinking. Moreover, it is important to remember that the formation of fibrillar

materials is required in order to have bundles of hierarchically organised systems, which can lead towards amplification of nanoscopic actuations with major efficiency as in our muscles.

The previous example shows materials with robustness and resilience since there were no signals of degradation after several switching cycles, thus demonstrating that macroscopic changes even observed with the naked eye can be achieved by the collective motion of [*c*2]daisy chain rotaxane units. Nevertheless, polymeric materials are not the only systems that can translate the nanoscopic mechanical actuation of molecular machines to higher length scales. Functional and 3D soft materials like vesicles, or liquid crystals, which possess molecular dynamics and phase orders have been exploited to amplify the nano-motions.

1.3.2. Motion amplification in self-assembled 3D materials

In Nature, the formation of many biological substances is driven by the spontaneous complex 3D self-assembly of molecular entities. In artificial systems, processes are not so different. Bottom-up fabrication of 3D functional materials follow a supramolecular assembly approach in a hierarchical fashion. It has been possible to obtain mechanically interlocked molecules with self-assembling properties by combining mechanically active building blocks with ordering units. Their mechanical actuation can be amplified up to the macroscopic scale by collective motion of the individual molecular machines.[77]

The molecular shuttling of switchable rotaxanes can be used to carry out modifications of supramolecular structures by mechanical motion, and characteristics like shape and volume of the materials are affected upon synchronised mechanical actuations. In 2010, a collaborative work between the groups of Chen and Chui led to obtain a [2]rotaxane exhibiting gelation properties (Figure 1.16).

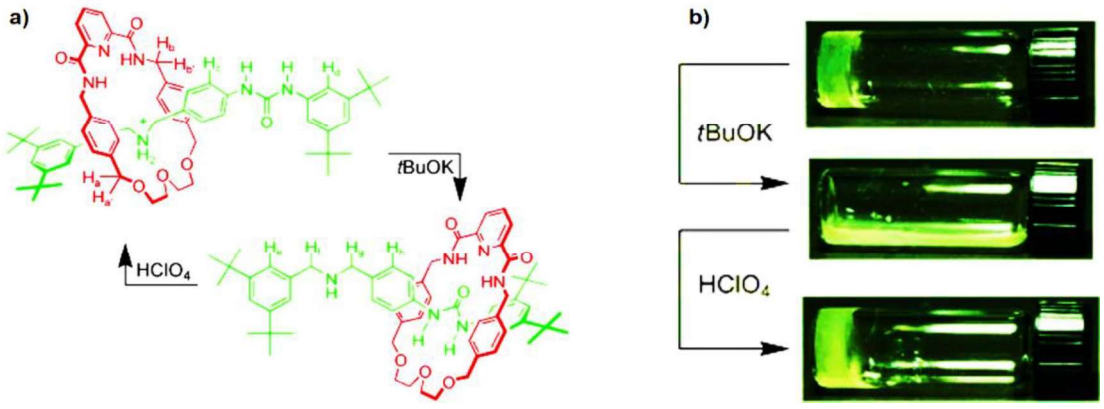

Figure 1. 16. a) Switching of the [2]rotaxane featuring urea fragments responsible for the gelation properties. **b)** Reversible sol-gel transitions of the [2]rotaxane upon addition of *t*-BuOK in 1-pentanol and subsequent addition of aqueous $HClO_4$. Adapted from reference [78].

The molecular machine is composed of a macrocycle encircling a secondary ammonium station located on an axle also containing a urea motif. The latter acts as second station and is responsible for the gelation properties of the molecule by intermolecular hydrogen bonding.[79] Upon deprotonation, the macrocycle moved away towards the urea fragment, inhibiting the hydrogen bonding interactions and disrupting the network of bundled fibres and the origin of the gel state. A similar behaviour was observed in a more recent work led by Chung and co-workers, in which the reversible molecular switching of amphiphilic [2]rotaxanes led to a sol-gel transition behaviour in organic solvents.[80] The amphiphiles composed by calix[4]arenes as macrocyclic hosts initially resides on the secondary ammonium station of the axle, which possesses additionally an urea station as in the previous example. One of the extremities of the amphiphilic-interlocked machines bear a tetraphenylethyelene moiety, which is known for exhibiting aggregation-induced emission. Such fragment plays an important role in the formation of pH-responsive dumbbell-shape crosslinked gelation networks owing to the intermolecular π-π stacking of the aromatic cores and van-der Waals interactions of the macrocyclic hosts. Additionally, SEM images show a 3D arrangement of the molecules in nanospheres, which are disrupted in basic media generating a change in the morphology of the 3D material towards hollow nanospheres.

Such morphological changes of 3D self-assembled materials were observed also by Qu and co-workers through the acid-base actuation of an amphiphilic [2]rotaxane.[81] In this work, the crown ether acting as wheel was decorated with two *O*-alkylated gallic ester derivative, shuttling between a secondary ammonium station and a positively charged triazolium ring. Such movement generated changes in the self-assembly behaviour between the hydrophobic and the hydrophilic blocks, leading to mesoscopic differences as observed by TEM. In the protonated state, the [2]rotaxane self-assembles in spherical vesicles, while in the deprotonated state, worm-like micelles are formed (Figure 1.17).

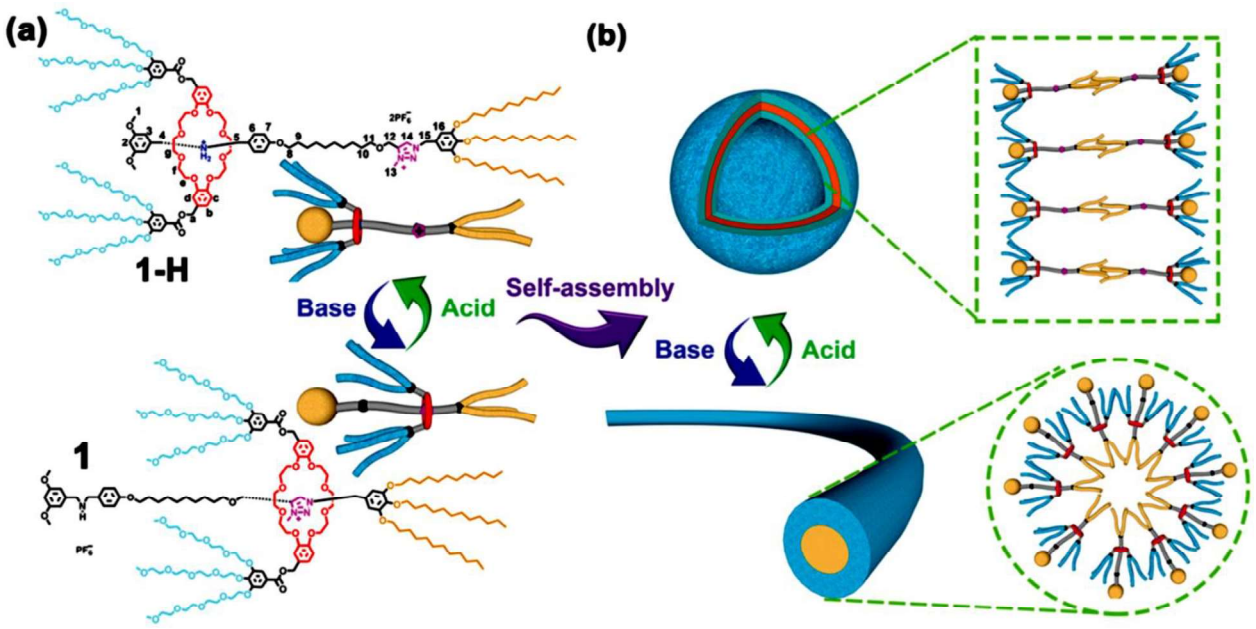

Figure 1.17. a) Chemical structure of the amphiphilic [2]rotaxane and its acid-base actuation. **b)** Formation of vesicles and worm-like micelles by self-assembly of the [2]rotaxane in the protonated and deprotonated states respectively. Adapted from reference[81].

Another kind of soft materials used to express the amplification of the molecular motion are liquid crystalline matrices. Liquid crystals (LCs) belong to an intermediate state of matter between isotropic liquids and crystalline solids (Figure 1.18a). As the name suggests, they combine the fluid-like properties of liquids and the anisotropic property of crystals.[82] Typically, their structure contains a mesogen, which is responsible for inducing the liquid-crystalline behaviour. LC molecules can generate intermediate (meso-) phases by intermolecular interactions, providing a lower orientational or positional order compared with a crystalline solid but higher compared to liquids. Contrary to the molecules in the regular liquid state, mesogens possess anisotropic shapes which tend to promote their alignment along a common axle known as the director. For example, calamitic mesogens have an elongated and rod-like molecular structure, while discotic ones have a disk-like shape (Figure 1.18b-c).

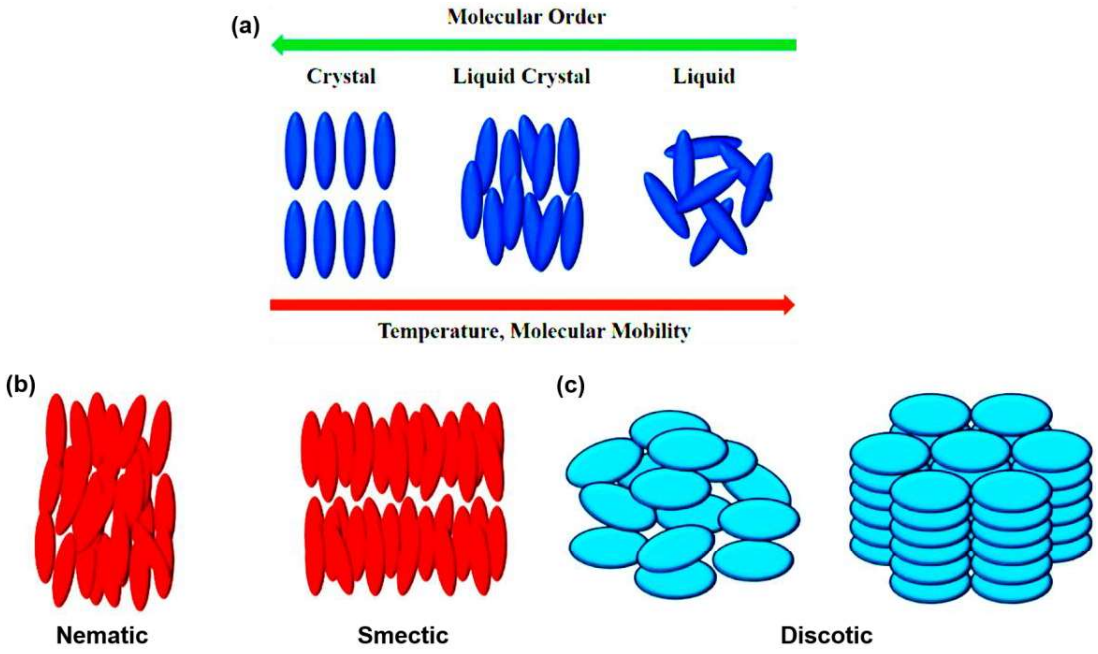

Figure 1.18. a) Organisation of a material with an elongated shape in the different states of matter. **b-c)** Schematic representation of the thermotropic LC phases of **b)** rod-like and **c)** discotic shapes. Adapted from reference[82].

LCs are divided principally into two main categories: lyotropic and thermotropic. In the first case, a mesophase is obtained by dissolving the amphiphilic compound in a suitable solvent and at a certain concentration. On the other side, in the thermotropic LCs the formation of the mesophase does not require a solvent and occurs as a function of the temperature variation. Additionally, there are many subcategories of liquid crystalline phases depending on the order of the mesogens dictated by the director vector. For example, in nematic mesophases the vectors are oriented in the same direction with molecules aligned parallel to each other but with some degree of freedom. In smectic phases, the centres of mass of the molecules are located in well-arranged layers, having a well-defined thickness, but the molecular axis is perpendicular to the lamellar planes. The simplest smectic phase is the smectic A (SmA) phase, where each layer has a short-range order and the ability to slide over each other like layers inside graphite. Due to their dynamic nature, liquid-crystalline materials have been coupled mainly to photoactive compounds like molecular switches and motors.[83]

Several examples of molecular motors acting as switchable dopants in LC matrices have been reported up to date. They have facilitated the light induced reorganisation of the mesophases, allowing the formation of light-responsive liquid crystalline materials exhibiting changes in properties at the macroscopic scale.[84]

1.3.2.1. Amplification from molecular motors as chiroptical switches

In 2006, Feringa and co-workers incorporated a second generation molecular motor as dopant in a E7 liquid-crystalline matrix, achieving full tuning of the reflection wavelengths of the LC film throughout the visible spectrum (Figure 1.19a).[85] This work opened the door towards the incorporation of molecular machines in liquid crystals aiming to exert control over the optical properties of these smart materials.

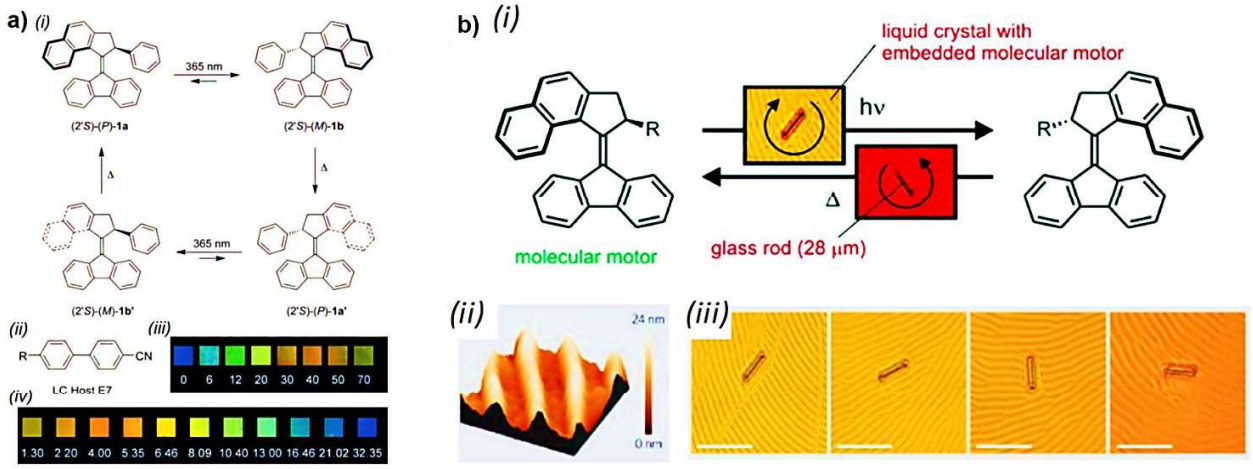

Figure 1.19. a) (***i***) Chemical structure and unidirectional rotary cycle of a second-generation molecular motor. (***ii***) Chemical structure of the mesogen E7 host as mixture of four compounds. (***iii-iv***) Gradual colour change in function of the time of a liquid-crystalline film made of E7 and doped with the molecular motor. **b)** (***i***) Schematic representation of the rotation of a micrometric glass rod at the surface of a liquid-crystalline film doped with a molecular motor upon light irradiation. (***ii***) AFM image of the LC film surface (15µm^2). Rotation of the glass rod on the LC film under UV light irradiation. Adapted from reference[86].

The same year, the same group used the twisting power of the molecular motor to obtain a macroscopic change beyond the optical regime. Feringa and co-workers doped an unidirectionally cholesteric liquid crystalline film with the same second-generation molecular motor, exhibiting a polygonal fingerprint texture (Figure 1.19b).[87] Optical microscopy allowed observing that such texture reorganises in a clockwise fashion under light irradiation at 365 nm and to the opposite direction once the light source is removed. Additionally, the surface of the LC film has reliefs of 20 nm height that are affected by the rotation generated by the photochemical isomerisation and thermal helix inversion processes undergone by the molecular motor. Such reorganisation of the relief generates a torque that was harnessed to rotate a micrometric glass rod placed on the top of the doped LC film (Figure 1.19b (*ii-iii*)).

Along the same lines, Feringa and co-workers functionalised a modified version of the second-generation molecular motor used in the previous example, with the LC polymer poly-(*n*)-hexylisocyanate (PHIC). The goal was to amplify the induced chirality of the macromolecular system to the supramolecular level in a lyotropic LC phase.[88] The helical conformation of the PHIC can be fully switched under UV light irradiation from the initial *M* helical conformation with the chiroptical switch at the (2'*S*)-(*P*) state to the *P* helical conformation of the (2'*S*)-(*M*) state of the switch. In addition, this conformational change can be reversed under visible light irradiation at 480 nm (Figure 1.20(*i*)). The authors used this chiroptical effect to dope a LC with 30% w/w of the functionalised molecular motor (2'*S*)-(*P*)-m-PHIC.[89]

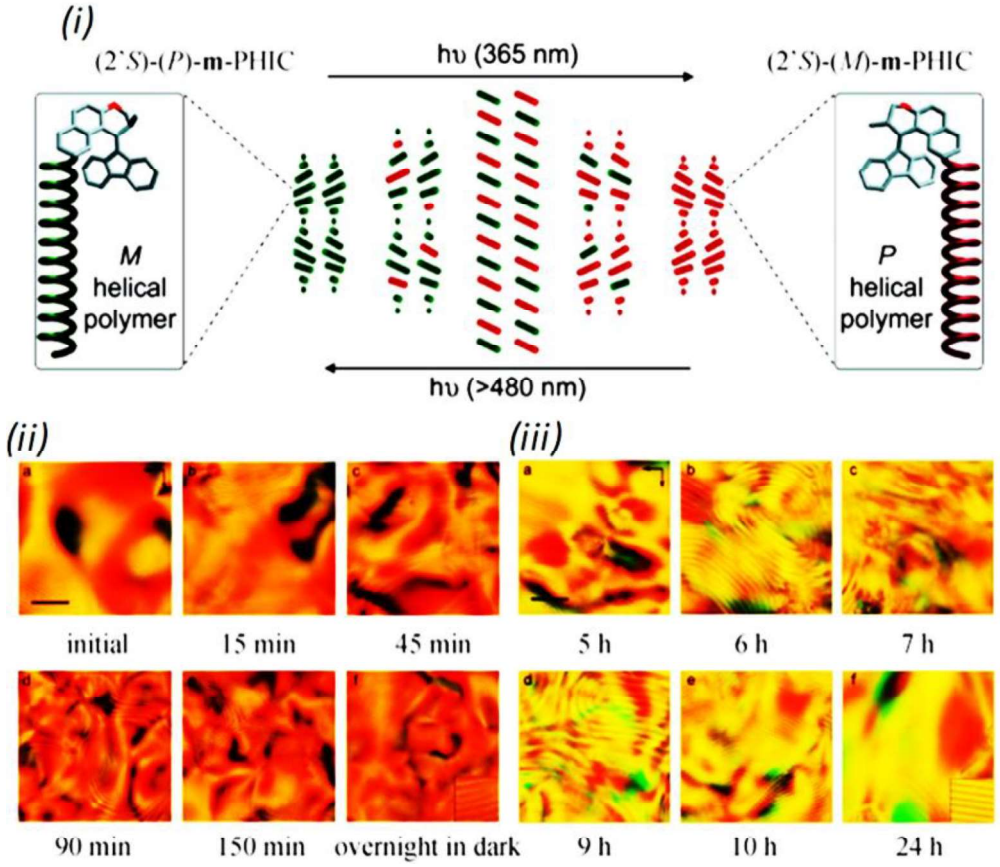

Figure 1.20. (***i***) Schematic representation of the UV-Vis induced inversion of the preferred helical twist of a polymer functionalised with a molecular motor acting as chiroptical molecular switch. (2'S)-(*P*)-m-PHIC induces a *M* helical twist of the polymer chain. Photochromic switch under UV irradiation yielding (2'S)-(*M*)-m-PHIC and inducing a *P* helicity of the polymer. Irradiation with visible light reverts the system to (2'S)-(*P*)-m-PHIC with a *M* helicity of the polymer. (***ii***) Micrographs of a thin film of (2'S)-(*P*)-m-PHIC in toluene at various times of UV irradiation. After 150 min, a photostationary state (PSS) mixture is obtained that consists of a large excess of (2'S)-(*M*)-m-PHIC. (***iii***) Optical micrographs of a thin film of (2'S)-(*M*)-m-PHIC in toluene at various times of UV irradiation. After 24 h, a PSS mixture of a large excess of (2'S)-(*P*)-m-PHIC is obtained. Adapted from reference[68].

After 45 min of irradiation, a racemic mixture of the *P* and *M* polymers was present in the LC films, which caused vanishing of the cholesteric lines (Figure 1.20(*ii*) top). However, prolonging irradiation time (up to 150 min) allowed the recovery of the cholesteric texture due to the formation of the *M* helical polymers as predominant species (Figure 1.20(*ii*) bottom). On the other hand, a similar behaviour was observed when (2'*S*)-(*M*)-PHIC was subjected to UV light irradiation. Although longer irradiation times were needed to obtain the *P* helical polymer as predominant species (Figure 1.20(*iii*)). In any case, both systems proved to be fully reversible in the dark due to the thermal reorganisation of the system.[89] The aforementioned examples have served to demonstrate that the motion performed by molecular motors as switchable chiral dopants can be transmitted to higher length scales in these self-assembled and ordered materials. The large amplitude motion undergone by switchable mechanically interlocked molecules represents an interesting approach for molecular amplification.

1.3.2.2. Amplification from Mechanically Interlocked Molecules (MIMs)

Mechanically Interlocked Molecules have been introduced in bulk and ordered systems leading to materials with emerging properties. Liquid-crystalline (LC) systems are good candidates to support and translate the oriented molecular motions generated by the actuation of mechanically interlocked molecules. For instance, in 2007, Sauvage and co-workers reported for the first time the formation of a [2]catenane exhibiting a liquid-crystalline behaviour (Figure 1.21 (*i*)).[90]

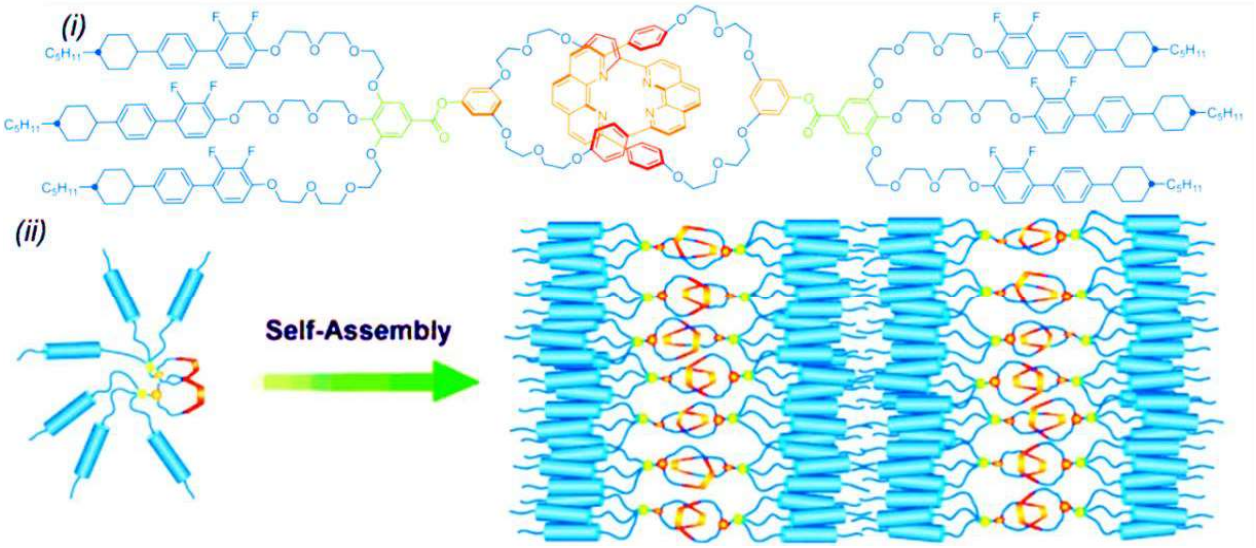

Figure 1.21. (***i***) Chemical structure of the liquid-crystalline [2]catenane. (***ii***) Hierarchical self-assembly of the [2]rotaxane into a Smectic A-type packing. Adapted from reference[90].

The functionalisation of a previous formed Cu^{I} metal complex with a mesogen derived from the gallic methyl ester gave rise to the metallic liquid crystalline [2]catenane. Free [2]catenane (Figure 1.21(*i*)) was formed after demetalation using cyanide ions. Both compounds, the metal complex and the free catenane were analysed by TGA, DSC and POM, observing the formation of smectic mesophases at 147 and 117 °C respectively, as result of a layered arrangement of the mesogens (Figure 1.21(*ii*)).

In parallel to the work of Prof. Sauvage, Kato's research team in collaboration with the research group of Prof. Stoddart reported for the first time the formation of a bistable [2]rotaxane showing LC characteristics.[91] The molecular structure can be divided in three parts: the first one consists in an axle containing two recognition sites; one tetrathiafulvalene (TTF) working as a redox active station, and the 1,5-dioxynapthalene (DNP) acting as a π-donor station. The second part, corresponds to the π-electron deficient macrocycle cyclobis(paraquat-*p*-phenylene) known as $CBPQT^{4+}$ which surrounds the axle. The third part consists in attaching at the extremities of the axle the same mesogenic fragments used in the [2]catenane work, this time acting as stoppers and also inducing the liquid-crystalline properties (Figure 1.22(*i-ii*)).

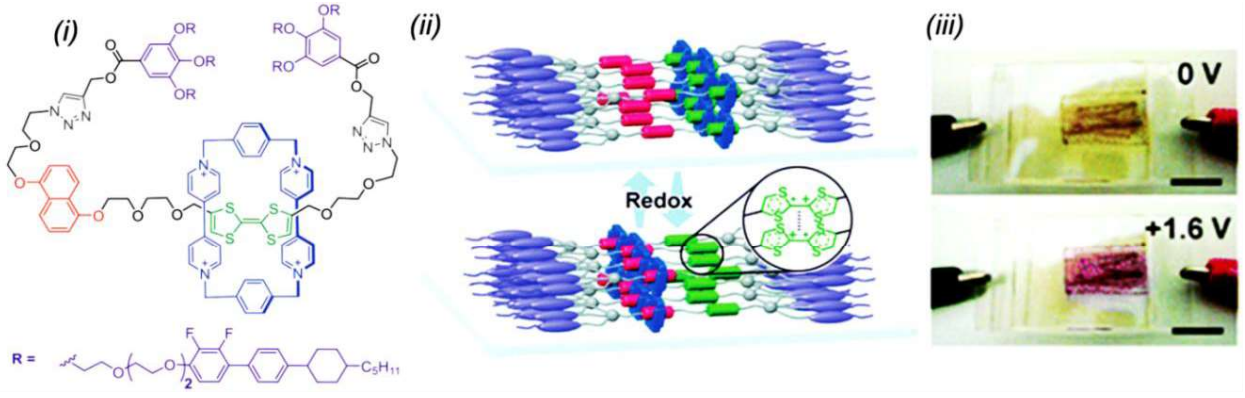

Figure 1.22. (***i***) Chemical structure of a liquid-crystalline [2]rotaxane. (***ii***) Schematic representation of the electrochemical shuttling of a [2]rotaxane. (***iii***) An electrochemical cell containing a LC film upon application of a redox potential. Adapted from reference[92].

Microscopy and scattering experiments showed that this compound exhibited a smectic A mesophase in a wide range of temperatures (10 – 150 °C). Moreover, reversible shuttling of the macrocycle in the LC state was carried out by electrochemical means and confirmed by cyclic voltammetry. This feature was used to construct an electrochromic cell with LC films deposited over ITO, a colour transition from brown to pink as a result of the formation of radical-cation species by oxidation of the TTF could be observed by naked eyes. Such redox event generated the shuttling of the ring towards the DNP unit, and the formation of the

charge-transfer complex between the $CBPQT^{4+}$ and the DNP (Figure 1.22(*iii*)).[92] This is one of the first example of a macroscopic change of a physical property, as a result of a redox driven nanoscale movement.

One of the current challenges in the field of artificial molecular machines concerns the amplification of the molecular motion towards higher length scales in a controlled manner. So far, and to the best of our knowledge, there are no examples in the literature describing mesophases based on [*c*2]daisy chain, nor even their phase transition upon actuation of the mechanical bond. Therefore, the following sections will be dedicated to the design and synthetic work carried out to obtain a [*c*2]daisy chain rotaxane bearing a mesogen in the structure as stopper. The pH change was used as an external stimulus to trigger the sliding motion of the macrocycles in the [*c*2]daisy chain rotaxanes, and a possible change in the liquid-crystalline phase.

References

[1] M. Baroncini, L. Casimiro, C. de Vet, J. Groppi, S. Silvi, A. Credi, *ChemistryOpen* **2018**, *7*, 169.

[2] A. Spirin, *FEBS Lett.* **2002**, *514*, 2.

[3] V. Almendro-vedia, P. Natale, D. Valdivieso, M. P. Lillo, J. L. Aragones, I. Lopez-Montero, *Arch. Biochem. Biophys.* **2021**, *708*, 108939.

[4] G. Oster, H. Wang, *Mol. Mot.* **2004**, 205.

[5] M. Schliwa, G. Woehlke, *Nature* **2003**, *422*, 759.

[6] P. Neupane, S. Bhuju, N. Thapa, H. K. Bhattarai, *Biomol. Concepts* **2019**, *10*, 1.

[7] J. D. W. Madden, N. A. Vandesteeg, P. A. Anquetil, P. G. A. Madden, A. Takshi, R. Z. Pytel, S. R. Lafontaine, P. A. Wieringa, I. W. Hunter, *IEEE J. Ocean. Eng.* **2004**, *29*, 706.

[8] R. H. Baughman, *Science* **2005**, *308*, 63.

[9] D. R. Higueras-Ruiz, K. Nishikawa, H. Feigenbaum, M. Shafer, *Bioinspiration and Biomimetics* **2022**, *17*, DOI 10.1088/1748-3190/ac3adf.

[10] J. A. Spudich, *Nature* **1994**, *372*, 515.

[11] J. A. Spudich, *Nat. Rev. Mol. Cell Biol.* **2001**, *2*, 387.

[12] C. A. Henderson, C. G. Gomez, S. M. Novak, L. Mi-Mi, C. C. Gregorio, *Compr. Physiol.* **2017**, *7*, 891.

[13] K. Kitamura, M. Tokunaga, A. H. Iwane, T. Yanagida, *Nature* **1999**, *397*, 129.

[14] H. Huxley, J. Hanson, *Nature* **1954**, *173*, 973.

[15] A. F. Huxley, R. Niedergerke, *Nature* **1954**, *173*, 971.

[16] M. Clarke, *Nat. Rev. Mol. Cell Biol.* **2008**, *9*, DOI 10.1038/nrm2581.

[17] A. Gare, *Philosophies* **2018**, *3*, 33.

[18] C. Heinrich, O. Westheider, M. Philipp, *Claude Monet: The Truth of Nature*, Prestel, **2019**.

[19] R. Macfarlane, *Nature* **2013**, *498*, 166.

[20] G. Karageorgis, S. Warriner, *Nat. Chem.* **2014**, *6*, 841.

[21] V. Balzani, A. Credi, F. M. Raymo, J. F. Stoddart, *Angew. Chem. Int. Ed.* **2000**, *39*, 3348.

[22] J. D. Crowley, S. M. Goldup, A. L. Lee, D. A. Leigh, R. T. Mc Burney, *Chem. Soc. Rev.* **2009**, *38*, 1530.

[23] Z. He, W. Jiang, C. A. Schalley, *Chem. Soc. Rev.* **2015**, *44*, 779.

[24] B. Rasmussen, A. Sørensen, S. R. Beeren, M. Pittelkow, *Chem. Rev.* **2006**, *106*, 3652.

[25] L. Pauling, *J. Am. Chem. Soc.* **1931**, *53*, 1367.

[26] J. Lehn, *Angew Chem Int Ed Engl* **1988**, *27*, 89.

[27] C. J. Pedersen, *Angew. Chemie Int. Ed. English* **1988**, *27*, 1021.

[28] F. De Jong, D. N. Reinhoudt, *Adv. Phys. Org. Chem.* **1980**, *17*, 279.

[29] D.J. Cram, *Angew. Chemie Int. Ed. English* **1988**, *27*, 1009.

[30] C. O. Dietrich-Buchecker, J.-P. Sauvage, *Tetrahedron Lett.* **1983**, *24*, 5095.

[31] M. Cesario, C. O. Dietrich-Buchecker, J. Guilhem, C. Pascard, J.-P. Sauvage, *J. Chem. Soc. Chem. Commun.* **1985**, 244.

[32] J. F. Stoddart, *Angew Chem Int Ed Engl* **2017**, *56*, 11094.

[33] C. J. Bruns, J. F. Stoddart, in *Nat. Mech. Bond*, **2016**, pp. 3–54.

[34] H. Y. Au-Yeung, Y. Deng, *Chem. Sci.* **2022**, *13*, 3315.

[35] S. D. P. Fielden, D. A. Leigh, S. L. Woltering, *Angew Chem Int Ed* **2017**, *56*, 11166.

[36] S. Nygaard, K. C. Leung, I. Aprahamian, T. Ikeda, S. Saha, B. W. Laursen, S. Kim, S. W. Hansen, P. C. Stein, A. H. Flood, J. F. Stoddart, J. O. Jeppesen, A. V Hilgard, L. Angeles, V. Uni, V. Uni, V. Ø. Københa, *J. Am. Chem. Soc.* **2007**, *129*, 960.

[37] C. Dietrich-Buchecker, M. C. Jimenez-Molero, V. Sartor, J.-P. Sauvage, *Pure Appl. Chem.* **2003**, *75*, 1383.

[38] M. J. Langton, P. D. Beer, *Acc. Chem. Res.* **2014**, *47*, 1935.

[39] J. E. Green, J. W. Choi, A. Boukai, Y. Bunimovich, E. Johnston-Halperin, E. DeIonno, Y. Luo, B. a Sheriff, K. Xu, Y. S. Shin, H.-R. Tseng, J. F. Stoddart, J. R. Heath, *Nature* **2007**, *445*, 414.

[40] P. L. Anelli, N. Spencer, J. F. Stoddart, *J. Am. Chem. Soc.* **1991**, *113*, 5131.

[41] R. A. Bissell, E. Córdova, A. E. Kaifer, J. F. Stoddart, *Nature* **1994**, *369*, 133.

[42] E. M. Perez, D. T. F. Dryden, D. A. Leigh, G. Teobaldi, F. Zerbetto, *J. Am. Chem. Soc.* **2004**, *126*, 12210.

[43] P. T. Glink, C. Schiavo, J. F. Stoddart, D. J. Williams, *Chem. Commun.* **1996**, *13*, 1483.

[44] P. R. Ashton, P. J. Campbell, P. T. Glink, D. Philp, N. Spencer, J. F. Stoddart, E. J. T. Chrystal, S. Menzer, D. J. Williams, P. A. Tasker, *Angew. Chemie Int. Ed. English* **1995**, *34*, 1865.

[45] P. R. Ashton, R. Ballardini, V. Balzani, I. Baxter, A. Credi, M. C. T. Fyfe, M. T. Gandolfi, M. Go, A. Piersanti, N. Spencer, J. F. Stoddart, M. Venturi, A. J. P. White, D. J. Williams, I. Frae-cnr, V. Gobetti, D. Chimica, G. Ciamician, V. Uni, V. Selmi, I. College, S. Kensington, L. Sw, *J. Am. Chem. Soc.* **1998**, *120*, 11932.

[46] C. C. Carmona-Vargas, N. Giuseppone, *Chem* **2021**, *7*, 11.

[47] R. Cooke, *J. Gen. Physiol.* **2004**, *123*, 643.

[48] M. C. Jimenez, C. Dietrich-buchecker, J. Sauvage, *Angew Chem Int Ed* **2000**, *39*, 3284.

[49] P. R. Ashton, I. Baxter, S. J. Cantrill, M. C. T. Fyfe, P. T. Glink, J. F. Stoddart, A. J. P. White, D. J. Williams, *Angew Chem Int Ed* **1998**, *37*, 1294.

[50] J. Rotzler, M. Mayor, *Chem. Soc. Rev.* **2013**, *42*, 44.

[51] M. C. Jimenez, C. Dietrich-buchecker, J.-P. Sauvage, A. De cian, *Angew Chem Int Ed* **2000**, *39*, 1295.

[52] C. J. Bruns, J. F. Stoddart, *Acc. Chem. Res.* **2014**, *47*, 2186.

[53] J. Wu, K. C. F. Leung, D. Benítez, J. Y. Han, S. J. Cantrill, L. Fang, J. F. Stoddart, *Angew. Chemie - Int. Ed.* **2008**, *47*, 7470.

[54] F. Coutrot, C. Romuald, E. Busseron, *Org. Lett.* **2008**, *10*, 3741.

[55] F. Coutrot, *ChemistryOpen* **2015**, *4*, 556.

[56] A. Wolf, J. J. Cid, E. Moulin, F. Niess, G. Du, A. Goujon, E. Busseron, A. Ruff, S. Ludwigs, N. Giuseppone, *European J. Org. Chem.* **2019**, *2019*, 3421.

[57] R. E. Dawson, S. F. Lincoln, C. J. Easton, *Chem. Commun.* **2008**, 3980.

[58] S. Tsukagoshi, A. Miyawaki, Y. Takashima, H. Yamaguchi, A. Harada, *Org. Lett.* **2007**, *9*, 1053.

[59] C. J. Bruns, M. Frasconi, J. Iehl, K. J. Hartlieb, S. T. Schneebeli, C. Cheng, S. I. Stupp, J. F. Stoddart, *J. Am. Chem. Soc.* **2014**, *136*, 4714.

[60] J. Chang, S. Tseng, C. Lai, Y. Liu, S. Peng, S. Chiu, *Nat. Chem.* **2017**, *9*, 128.

[61] K. Cai, B. Cui, G. C. Schatz, X. Li, J. F. Stoddart, K. Cai, B. Cui, B. Song, H. Wang, Y. Qiu, L. O. Jones, W. Liu, Y. Shi, S. Vemuri, D. Shen, T. Jiao, L. Zhang, H. Wu, H. Chen, Y. Jiao, *Chem* **2021**, *7*, 174.

[62] D. Aoki, G. Aibara, S. Uchida, T. Takata, *J. Am. Chem. Soc.* **2017**, *139*, 6791.

[63] A. Perrot, E. Moulin, N. Giuseppone, *Trends Chem.* **2021**, *3*, 926.

[64] S. Tsuda, Y. Aso, T. Kaneda, *Chem. Commun.* **2006**, 3072.

[65] L. Fang, M. Hmadeh, J. Wu, M. A. Olson, J. M. Spruell, A. Trabolsi, Y. Yang, M. Elhabiri, J. F. Stoddart, *J. Am. Chem. Soc.* **2009**, *131*, 7126.

[66] P. G. Clark, M. W. Day, R. H. Grubbs, *J. Am. Chem. Soc.* **2009**, *131*, 13631.

[67] G. Du, E. Moulin, N. Jouault, E. Buhler, N. Giuseppone, *Angew. Chemie - Int. Ed.* **2012**, *51*, 12504.

[68] D. Dattler, G. Fuks, J. Heiser, E. Moulin, A. Perrot, X. Yao, N. Giuseppone, *Chem. Rev.* **2020**, *120*, 310.

[69] L. Gao, Z. Zhang, B. Zheng, F. Huang, *Polym. Chem.* **2014**, *5*, 5734.

[70] A. Goujon, G. Du, E. Moulin, G. Fuks, M. Maaloum, E. Buhler, N. Giuseppone, *Angew. Chemie - Int. Ed.* **2016**, *55*, 703.

[71] A. Goujon, G. Mariani, T. Lang, E. Moulin, M. Rawiso, E. Buhler, N. Giuseppone, *J. Am. Chem. Soc.* **2017**, *139*, 4923.

[72] R. P. Sijbesma, M. H. P. Van Genderen, E. W. Meijer, R. V February, *J. Am. Chem. Soc.* **2000**, *122*, 7487.

[73] E. Moulin, L. Faour, C. C. Carmona-Vargas, N. Giuseppone, *Adv. Mater.* **2020**, *32*, 1906036.

[74] K. Iwaso, Y. Takashima, A. Harada, *Nat. Chem.* **2016**, *8*, 625.

[75] S. Ikejiri, Y. Takashima, M. Osaki, H. Yamaguchi, A. Harada, *J. Am. Chem. Soc.* **2018**, *140*, 17308.

[76] A. Goujon, T. Lang, G. Mariani, E. Moulin, G. Fuks, J. Raya, E. Buhler, N. Giuseppone, *J. Am. Chem. Soc.* **2017**, *139*, 14825.

[77] Y. L. Zhao, I. Aprahamian, A. Trabolsi, N. Erina, J. F. Stoddart, *J. Am. Chem. Soc.* **2008**, *130*, 6348.

[78] S. Y. Hsueh, C. T. Kuo, T. W. Lu, C. C. Lai, Y. H. Liu, H. F. Hsu, S. M. Peng, C. H. Chen, S. H. Chiu, *Angew. Chemie - Int. Ed.* **2010**, *49*, 9170.

[79] S. Y. Hsueh, C. T. Kuo, T. W. Lu, C. C. Lai, Y. H. Liu, H. F. Hsu, S. M. Peng, C. H. Chen, S. H. Chiu, *Angew. Chemie - Int. Ed.* **2010**, *49*, 9170.

[80] R. Arumugaperumal, P. Raghunath, M. C. Lin, W. S. Chung, *Chem. Mater.* **2018**, *30*, 7221.

[81] Z. Q. Cao, Y. C. Wang, A. H. Zou, G. London, Q. Zhang, C. Gao, D. H. Qu, *Chem. Commun.* **2017**, *53*, 8683.

[82] H. K. Bisoyi, Q. Li, *Chem. Rev.* **2022**, *122*, 4887.

[83] Y. Wang, Q. Li, *Adv. Mater.* **2012**, *24*, 1926.

[84] R. A. van Delden, N. Koumura, N. Harada, B. L. Feringa, *Proc. Natl. Acad. Sci.* **2002**, *99*, 4945.

[85] R. Eelkema, B. L. Feringa, *Chem. An Asian J.* **2006**, *1*, 367.

[86] Q. Li, J. T. Foy, J. R. Colard-Itté, A. Goujon, D. Dattler, G. Fuks, E. Moulin, N. Giuseppone, *Tetrahedron* **2017**, *73*, 4874.

[87] J. Vicario, N. Katsonis, B. S. Ramon, C. W. M. Bastiaanset, D. J. Broer, B. L. Feringa, *Nature* **2006**, *440*, 163.

[88] D. Pijper, B. L. Feringa, *Angew. Chemie - Int. Ed.* **2007**, *46*, 3693.

[89] D. Pijper, M. G. M. Jongejan, A. Meetsma, B. L. Feringa, *J. Am. Chem. Soc.* **2008**, *130*, 4541.

[90] E. D. Baranoff, J. Voignier, T. Yasuda, V. Heitz, J. P. Sauvage, T. Kato, *Angew. Chemie - Int. Ed.* **2007**, *46*, 4680.

[91] I. Aprahamian, T. Yasuda, T. Ikeda, S. Saha, W. R. Dichtel, K. Isoda, T. Kato, J. F. Stoddart, *Angew. Chemie - Int. Ed.* **2007**, *46*, 4675.

[92] T. Yasuda, K. Tanabe, T. Tsuji, K. K. Coti, I. Aprahamian, J. F. Stoddart, T. Kato, *Chem. Commun.* **2010**, *46*, 1224.

Chapter 2
pH-induced actuation of a liquid-crystalline [*c*2]daisy chain rotaxane

I thank Dr. Doru Constantin and Guillaume Fleith for their help in the interpretation of the SAXS data. I also thank Dr. Shoichi Tokunaga for taking the POM images.

As exposed in Chapter 1, amplifying the nanoscopic motion of artificial molecular machines, requires their integration into responsive materials like polymers or liquid crystalline systems. In that sense, the strategy addressed in this chapter relies on the combination of interlocked nature of a [*c*2]daisy chain rotaxane structure with a fork-like shape mesogen, in order to study the effect of the pH-triggered mechanical actuation of such switchable mechanically interlocked structure over the liquid crystalline behaviour.

3,4,5-*O*-alkylated aromatic ring derived from the gallic methyl ester is a well-known dendritic mesogen that induce liquid-crystalline properties, when covalently bound to non-mesogenic functional molecules, for instance, catenanes[1] and rotaxanes.[2] For the formation of liquid crystals based on [*c*2]daisy chain rotaxanes, we designed the interlocked structure **20**$_{Ext}$, incorporating the gallic azide derivative **18** as end-capping units.

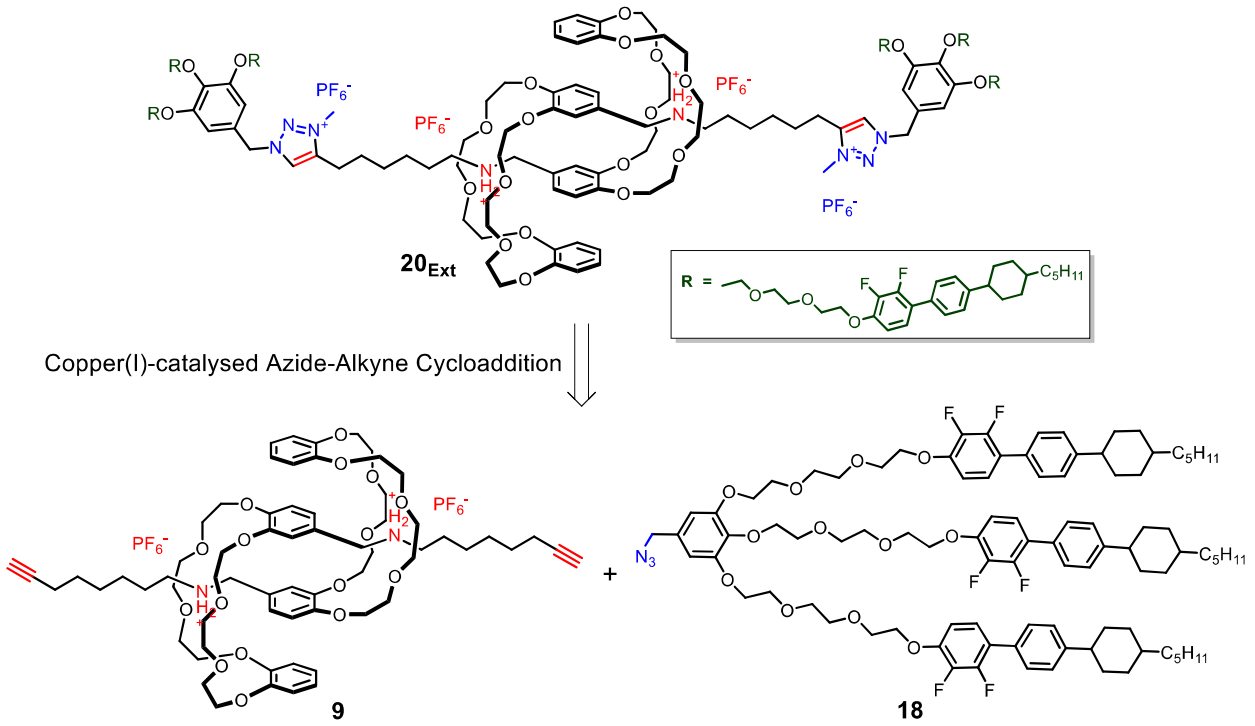

Scheme 2.1. Key retrosynthetic step towards **20**$_{Ext}$.

The main step towards **20**$_{Ext}$ consists of a Copper(I)-catalysed Azide-Alkyne Cycloaddition (CuAAC) between pseudo[*c*2]daisy chain rotaxane **9** and mesogen **18** (Scheme 2.1). The mesogen **18** has a fork-like structure, which favours the induction of liquid crystalline properties[1] and the decreasing of phase transitions temperatures due to its fluoro-substituents.[3] This dendritic molecule contains rigid cores composed of 2,3-difluoro-4'-(4-pentylcyclohexyl)-biphenyl fragments, which are covalently attached to the phenyl moiety of the benzyl azide derivative through a flexible spacer based on a triethylene oxide chain.

On the other side, the pseudo[*c*2]daisy chain rotaxane **9** has been widely used in the formation of [*c*2]daisy chain rotaxanes due to the good stability of its interlocked structure, which is maintained by the high affinity of the crown ether macrocycle DB24C8 for the *N*-benzylammonium group.

2.1. Synthesis of the pseudo[*c*2]daisy chain rotaxane 9

Given the interlocked structure of pseudo[*c*2]daisy chain rotaxane **9** (Scheme 2.1), we followed the retrosynthetic approach shown in Scheme 2.2 for being the shortest one. Considering the strong affinity of the crown ether macrocycle for ammonium groups,[4] and to favour the self-assembly process, it was necessary the secondary *N*-benzyl amine group of the structure **8**. The latter (**8**) was obtained from reductive amination of a previously formed imine by condensation reaction. Rupture of the C-N benzylic bond indicated on structure **8** led to the key building blocks **6** and **3**.

Substrate **6** was retrosynthetically doubly cut at the indicated ether bonds to unravel the intermediate **5**, (appropriately modified to tosyl moieties representing the required leaving groups) and the commercially available 4-formylcatechol. Finally, removal of the tosyl activating groups led to structure **4**, which was doubly cut at the C-O ether bonds adjacent to the benzyl ring and traced the origins of this intermediate to the key commercially available building blocks catechol and 2-(2-(2-chloroethoxy)ethoxy)ethan-1-ol. On the other hand, we envisioned substrate **3** as arising retrosynthetically from deprotection of compound **2**, which in turn, was the product of a modified Mitsunobu reaction with alcohol **1**. Although, compound **1** is commercially available, it was more worthy to prepare it from the cheaper constitutional isomer oct-5-yn-1-ol.

Having decided upon the pathway towards **9** by the retrosynthetic analysis shown in Scheme 2.2, we set to the task of synthesizing each of the precursors required to obtain the pseudo[*c*2]daisy chain rotaxane **9**.

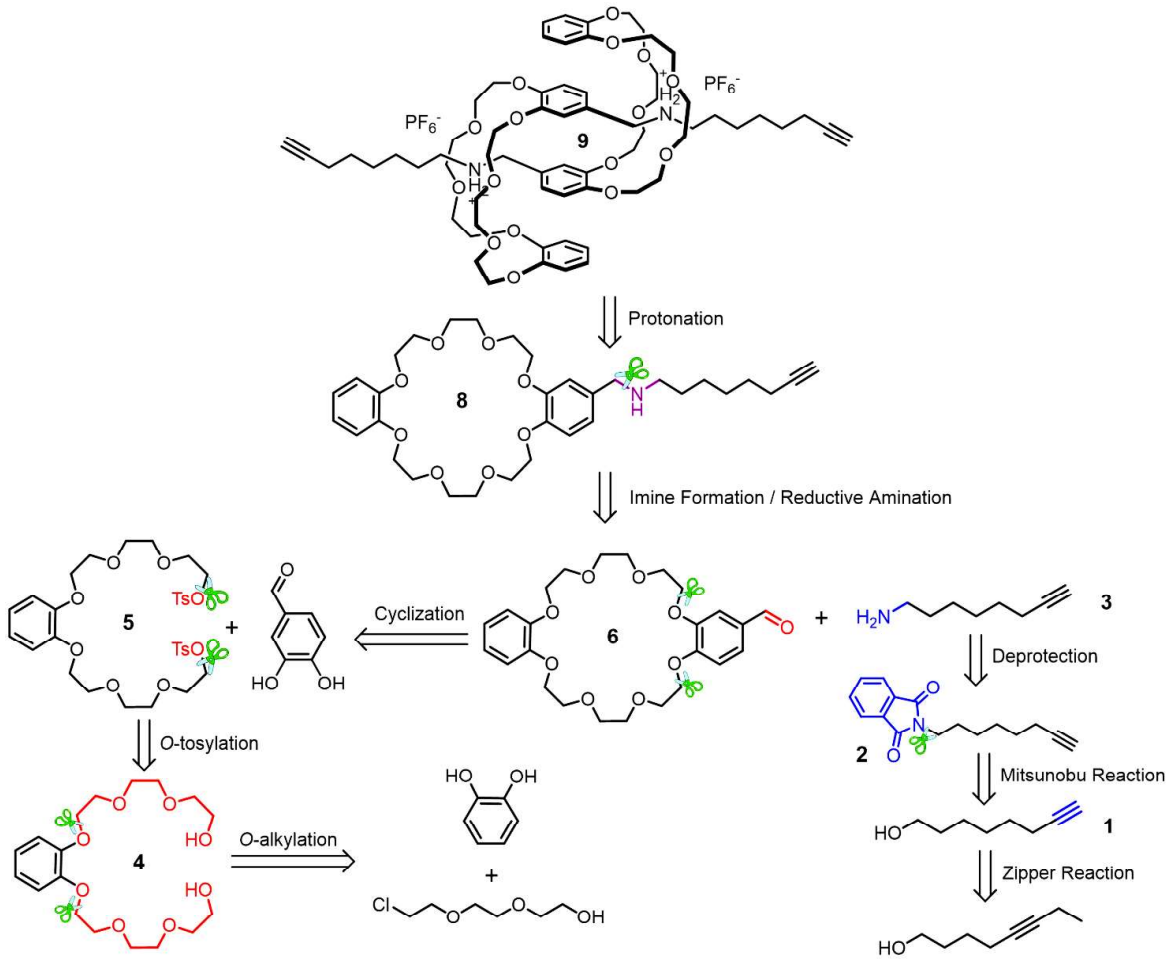

Scheme 2.2. Retrosynthetic analysis of compound **9**.

All compounds described in this chapter were characterised by ^{1}H and ^{13}C NMR spectroscopy and mass spectrometry (see experimental section for protocols and Annexes A for NMR spectra).

2.1.1. 8-aminooct-1-yne (3)

Primary amine **3** was obtained in three synthetic steps: The commercially available 3-octyn-1-ol was subjected to an acetylenic zipper isomerisation reaction[5] in the presence of a strong base generated *in situ* between sodium hydride and ethylenediamine. This base produces a contra-thermodynamic isomerisation and rapid migration of the internal triple bond to the end of the carbon chain leading to alcohol **1** in 80% yield. After purification, this compound was subsequently converted to the phthalimide derivative **2** using a Mitsunobu reaction,[6] in presence of triphenylphosphine and diisopropyl azodicarboxylate (DIAD). This azodicarboxylate is more frequently used compared to the more common diethyl azodicarboxylate (DEAD),[7] as it is more hindered, and thus less likely to generate hydrazide products.

Finally, compound **2** was subjected to Gabriel synthesis[8] deprotection conditions using an aqueous solution of hydrazine in methanol, in order to obtain the primary free amine **3** in 70% yield. (Scheme 2.3). It is important to mention that this is a shorter synthetic strategy to prepare amine **3**, in comparison with previous reports on the literature,[9] since it avoids the synthesis and purification of a haloalkyne by Appel's reaction.[10]

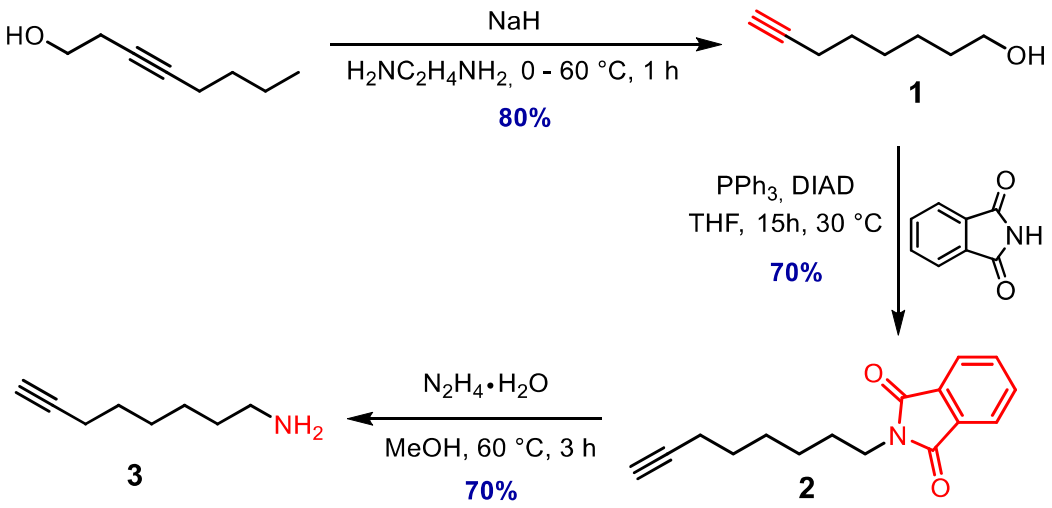

Scheme 2.3. Synthesis of amine **3**.

2.1.2. Formyl-DB24C8 (6)

Macrocycle **6** was prepared following the procedure reported by Takata and co-workers[11] (Scheme 2.4). Starting from commercially available catechol, *O*-alkylation reaction of the phenolic derivative yielded compound **4**, which was subjected without further purification to tosylation reaction of the free hydroxyl groups affording compound **5** in 75% yield. Then, the synthesis of dibenzo crown ether **6** involved bistosylate **5** and 4-formylcatechol. The ability of the polyether chain to coordinate caesium cations (4 equivalents),[12] in order to approach both reactive ends under diluted conditions, favours the formation of the macrocycle over undesired products like oligomers.

Here, it is worthy to mention the effect of the used solvent on the reaction yield. Several experiments were carried out in anhydrous DMF following the methodology reported in 2001 by Stoddart and co-workers,[13] obtaining compound **6** with very low yields (<20%). However, once the solvent was changed to anhydrous THF, the reaction time and yield were highly improved.

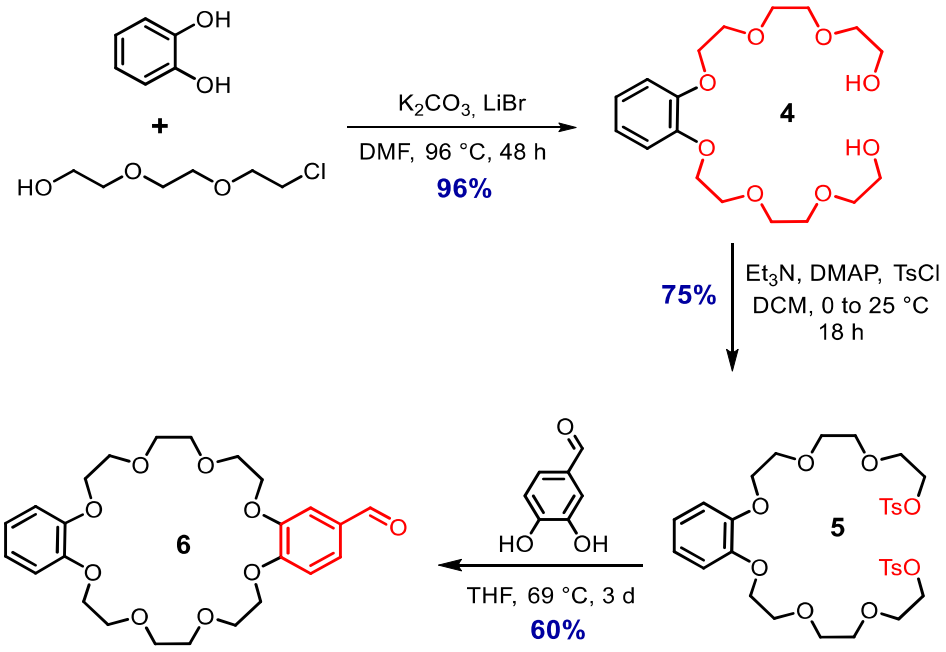

Scheme 2.4. Synthesis of compound **6**.

A hypothesis to explain this enhancement could be the fact that the templation reaction could be more favoured by stabilisation of the coordination complex formed between the donating oxygen atoms of the crown ether and the caesium cation provided by the THF. After optimisation, macrocycle **6** was obtained at the gram scale (8.0 g), with 59% yield after three days of reaction at 69 °C and purification by column chromatography (Scheme 2.4). With this compound in hands, the next step was to carry out the condensation reaction with the primary amine described on Scheme 2.2.

2.1.3. Self-assembly of the amine 9

Aldehyde **6** and amine **3** were reacted in boiling toluene to form imine **7**, which was obtained in quantitative yield after one day of reaction. A Dean-Stark trap was used to remove the water produced by the dehydration of the hemiaminal formed as intermediate, in this way shifting the equilibrium towards the reaction products.[14] Reductive amination of the previously synthesized imine **7** was carried out in anhydrous methanol using sodium borohydride to yield secondary amine **8** in 70% overall yield (Scheme 2.5). This amine was protonated with a 2 M solution of hydrochloric acid in diethyl ether, and washed with a saturated aqueous solution of ammonium hexafluorophosphate for a counterion exchange, affording the assembled pseudo[*c*2]daisy chain rotaxane **9** (Scheme 2.5). It is important to note that the self-assembly of compound **8** should be carried out in hydrogen bond promoting solvents, to allow the oxygen atoms of the macrocycle

to interact with the ammonium group through hydrogen bonding interactions. In fact, compound **9** is one of the main building blocks of the target [*c*2]daisy chain rotaxanes that will be described along this manuscript.

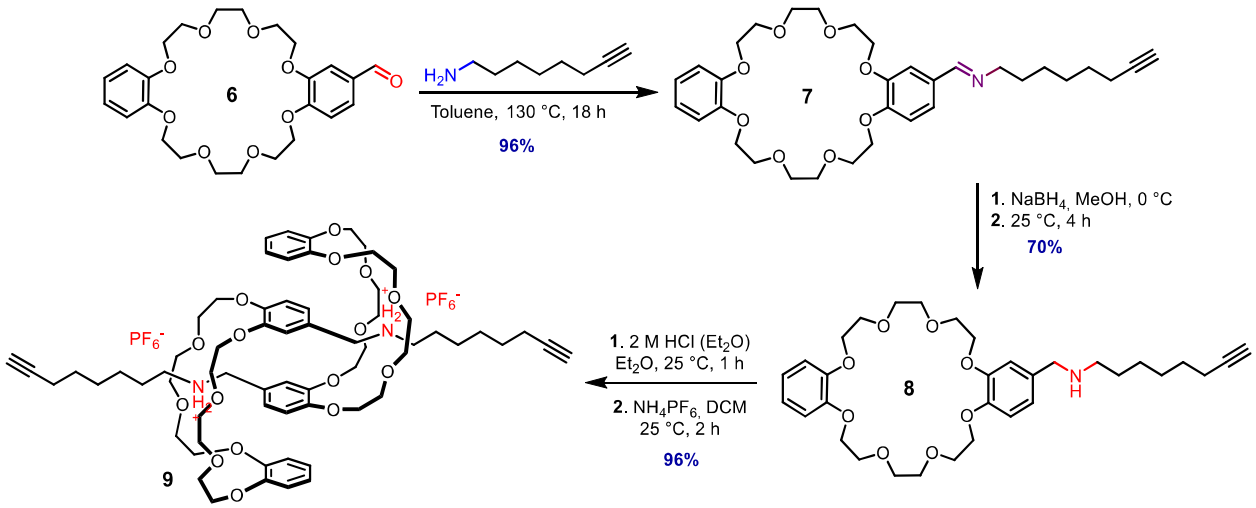

Scheme 2.5. Synthesis of pseudo[*c*2]daisy chain rotaxane **9**.

2.2. Synthesis of the mesogen 18

The synthesis of mesogen **18** was carried out in seven steps. First, a Suzuki-Miyaura cross-coupling reaction between commercially available 1-iodo-4-(4-pentylcyclohexyl)benzene (**11**) and boronic acid **11**[15] was carried out using *tetrakis*(triphenylphosphine)palladium(0) as catalyst affording compound **12** in 90% yield. The coupling was carried out under mild conditions, as well as under heterogeneous conditions using aqueous and an environmentally friendly solvents (Water/Ethanol) and toluene.[16]

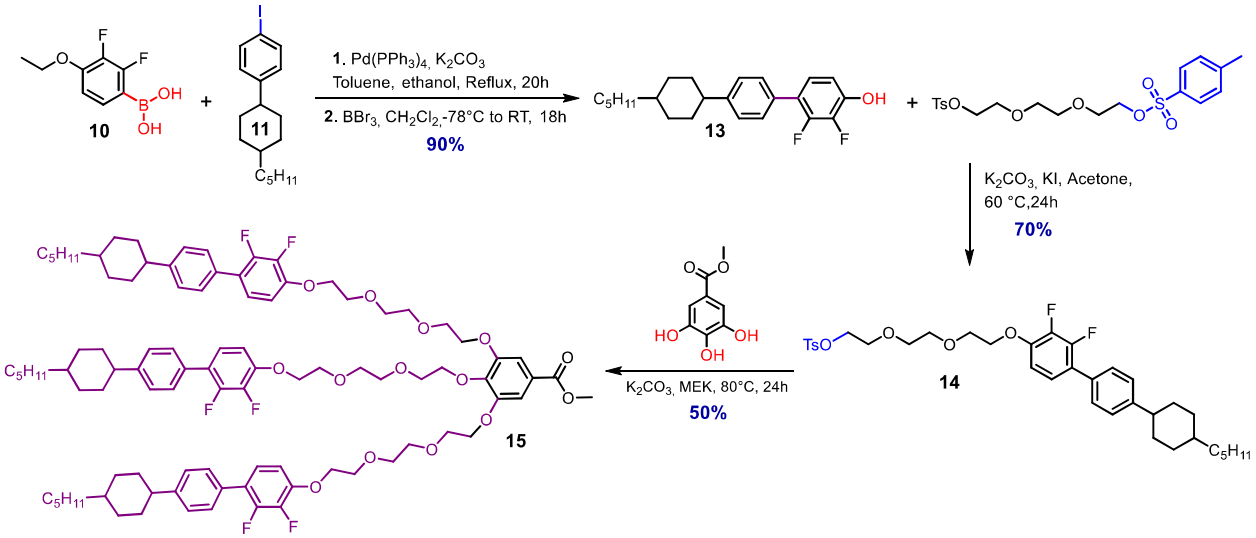

Scheme 2.6. Synthesis of the mesogen **15**. MEK = methyl ethyl ketone

The cross-coupled compound was subjected to an ether cleavage using boron tribromide, using a 1:1 stoichiometric ratio with the ethers,[17] resulting in near quantitative conversion to phenol **13**. *O*-alkylation of the phenolic group with a bistosylate derivative led to compound **14** that was used to alkylate the methyl gallate, to reach compound **15** in moderate yields (Scheme 2.6).

The *O*-alkylated ester **15** was reduced to the alcohol **16** with lithium aluminium hydride, and subsequently converted to benzylic chloride **17**. Then, this compound was reacted with sodium azide in DMF to obtain mesogen **18** (Scheme 2.7). The ^{1}H NMR spectra of compounds **15–18** are very similar (see Annexes A), therefore we decided that is more pertinent just to describe the ^{1}H NMR spectrum of compound **18** (Figure 2.1).

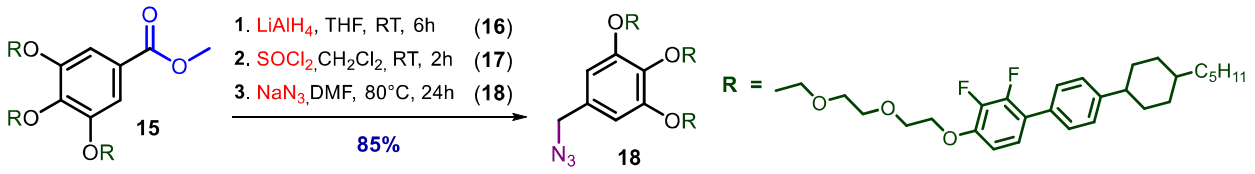

Scheme 2.7. Synthesis of the azide mesogen **18**.

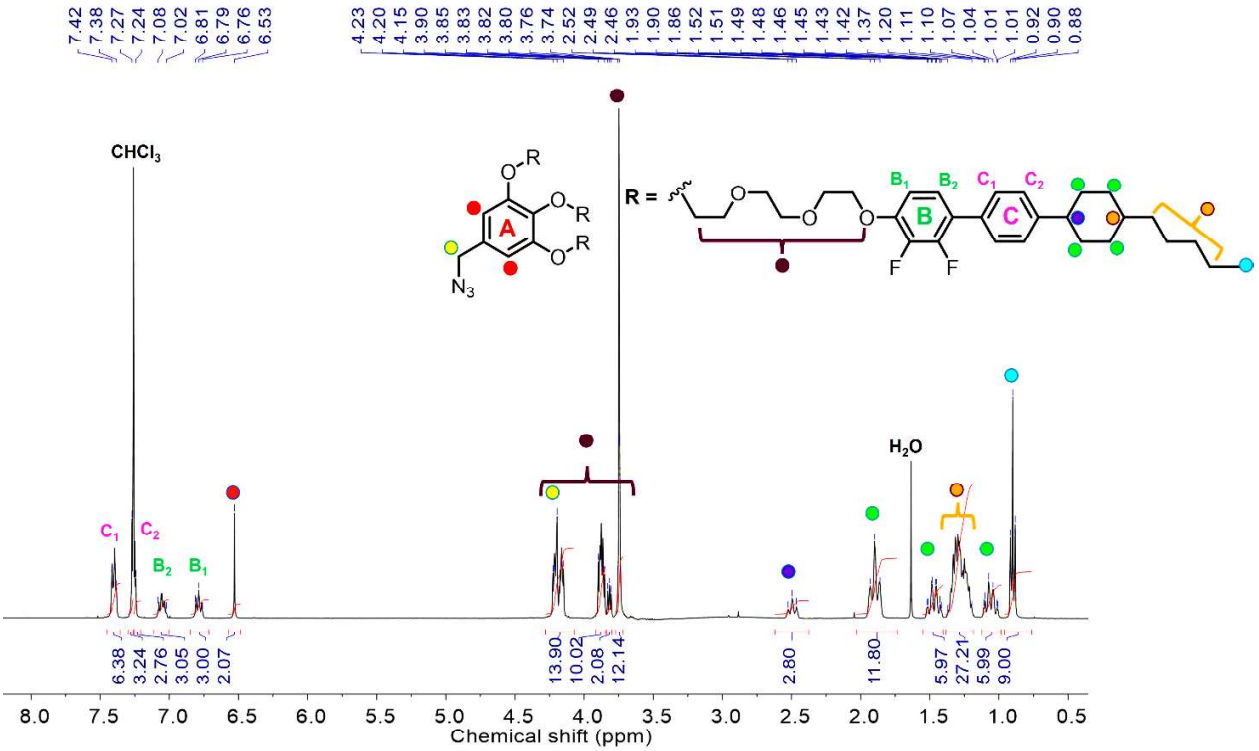

Figure 2.1. ^{1}H NMR of compound **18** in $CDCl_3$ at 25 °C (400 MHz).

Two sets of multiplets between 7.45 and 7.20 ppm are observed for H_{C1} and H_{C2}. Compared to proton C1, the chemical shift proton C2 is at higher field due to the electron-donating effect of the cyclohexyl substituent. The same inductive effect was observed for protons B2 which are located at lower field (7.05 ppm) than protons B1 (6.79 ppm), due to the electron-donating effect caused by the polyether substituent at the *ortho* position with respect to it. The multiplet at 2.49 ppm (purple spot) corresponds to the proton of the cyclohexyl substituent adjacent to the aromatic ring C, that makes it shifting towards downfield. The remaining protons (green and orange spots) of the aliphatic substituents, as well as the triplet that corresponds to the methyl group (cyan spot) of the alkyl tail are at upfield as expected. Furthermore, the CH_2 protons of the polyether chains are located between 4.3 and 3.4 ppm, a pattern of signals that is also exhibited for compounds **15–17**. Indeed, these signals usually were not affected during the synthetic sequences carried out with compounds **15–17**.

On the other side, the singlet at 6.53 ppm that corresponds to the protons of the aromatic ring A barely shifts towards downfield in the ^{1}H NMR spectra of compounds **16** and **17** (see Annexes A). Additionally, the signal that corresponds to the benzylic protons (yellow spot) is masked in the region between 4.23 – 4.15 ppm. Compared to compound **18**, these protons undergo noticeable shifts toward downfield in compounds **16** and **17** due to the higher electronegativity of the oxygen and chlorine atoms respectively.

2.3. Synthesis and characterisation of the [*c*2]daisy chain rotaxane $\mathbf{20_{Ext}}$

Azide derivative **18** and pseudo[*c*2]daisy chain rotaxane **9**, were coupled through a Copper(I)-catalysed Azide-Alkyne Cycloaddition (CuAAC) "click reaction" using a procedure initially reported by Coutrot and co-workers[9] and optimised in our laboratory (Scheme 2.8). Pure compound **19** was obtained in 60% yield after column chromatography. Then, compound $\mathbf{20_{Ext}}$ was quantitatively accessible through a *N*-methylation of the triazole rings, in the presence of a large excess of methyl iodide at room temperature over four days. The molecular actuation of the [*c*2]daisy chain $\mathbf{20_{Ext}}$ was assessed by ^{1}H NMR experiments upon deprotonation/protonation of the ammonium station. Figure 2.2 displays the ^{1}H NMR spectra of both states with all the expected set of signals.

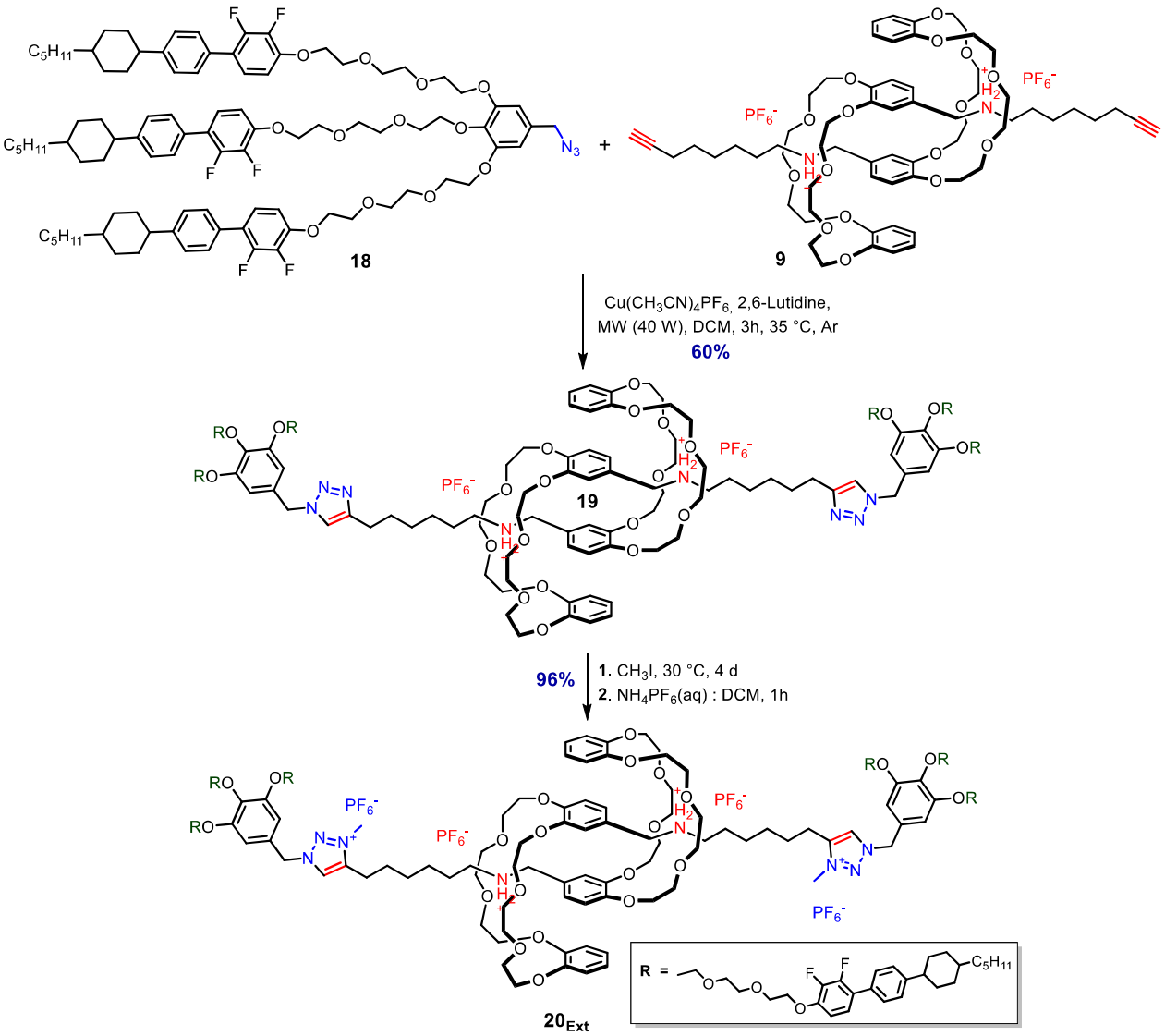

Scheme 2.8. Synthesis of the [*c*2]daisy chain rotaxane **20**$_{Ext}$.

In order to probe the contraction/extension event of [*c*2]daisy chain rotaxane by NMR spectroscopy, it was necessary first to elucidate the chemical structure of **20**$_{Ext}$ by determination of the key ^{1}H signals. A large set of broad signals from 7.20 to 6.20 ppm is observed, corresponding to protons H_{Ar} of the DB24C8, due to the proximity and interaction of such protons with the ones from the threaded macrocycle by π-π stacking (Figure 2.2b). Additionally, the possible formation of interlocked stereoisomers which accounts for the unsymmetrical substitution of the DB24C8 ring,[13,18] and the difference in magnetic chemical environment contribute to make this region complicated.

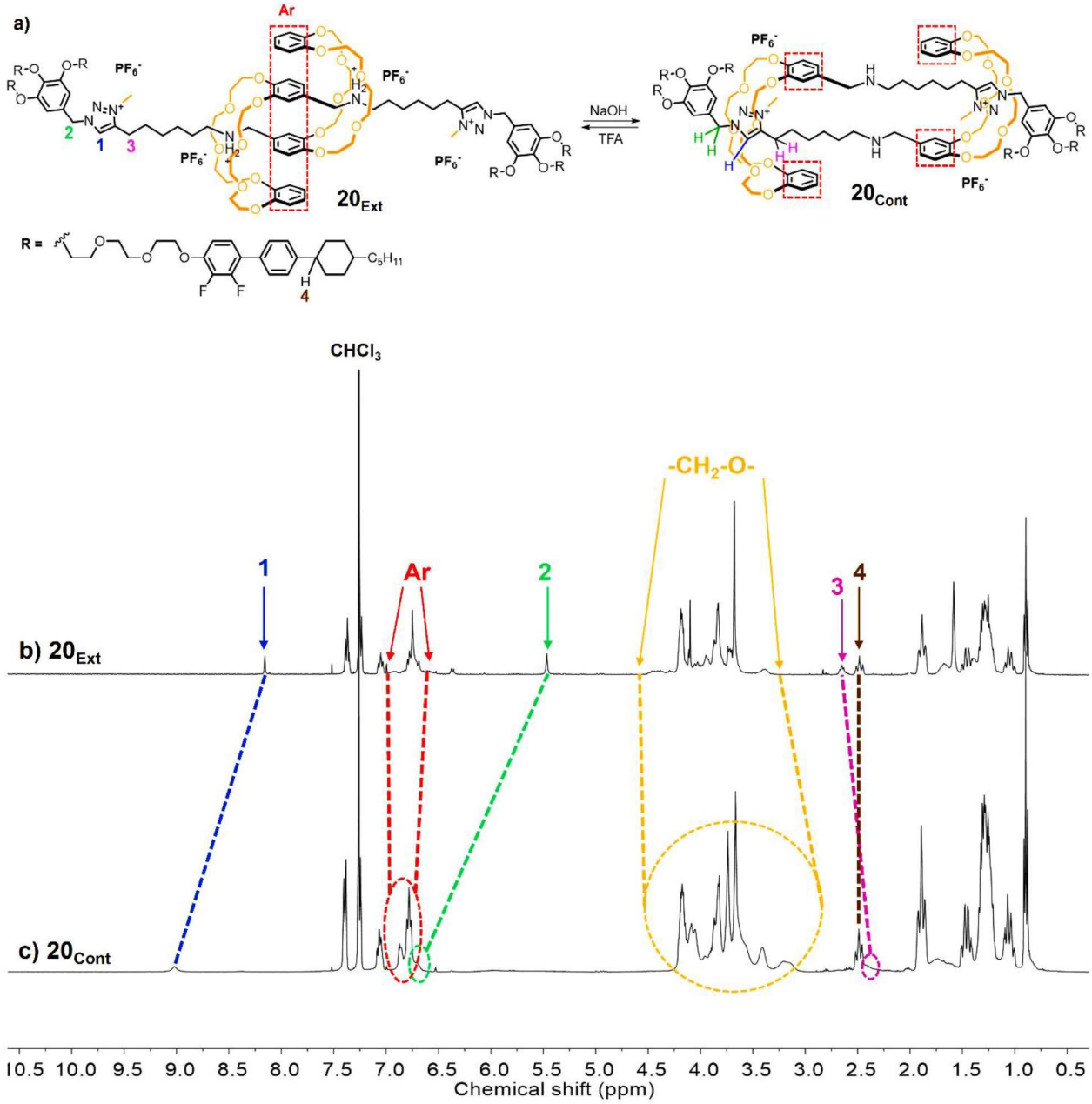

Figure 2.2. (**a**) pH-triggered contraction/extension event of **20**$_{Ext}$. (**b**) ^{1}H NMR spectra of **20**$_{Ext}$ and (**c**) **20**$_{Cont}$ in $CDCl_3$.

However, a slight shift of these protons towards downfield, as well as sharper peaks are observed for the contracted state **20**$_{Cont}$ (Figure 2.2c), most likely due to the loss of π-π interactions. Furthermore, remarkable differences in the chemical shifts of the vinylic proton of the triazolium rings occur between the extended and the contracted states. For **20**$_{Ext}$, proton H_1 (in blue) appears as singlet at 8.10 ppm, however, upon addition of an aqueous solution of sodium hydroxide contraction of the molecule occurs, leading to an appreciable shifting of this signal towards downfield (9.10 ppm). This fact suggests the existence of hydrogen bonding

interactions between this proton and the oxygens of the crown ether. These observations are in agreement with what was observed for other [*c*2]daisy chain molecules.[9,19] Interestingly, the signal corresponding to the benzylic protons H_2 (in green) that appears as a singlet at 5.5 ppm in compound **20**$_{\mathbf{Ext}}$, moves towards the aromatic region between 6.70 and 6.50 ppm in the contracted state. This shifting could be explained by an electron-withdrawing effect from the triazolium ring, which in turn, is interacting with the electron-demanding crown ether.

On the other side, protons H_3 (pink) adjacent to the triazolium ring appears at 2.8 ppm for **20**$_{\mathbf{Ext}}$. This signal moves towards upfield for **20**$_{\mathbf{Cont}}$ appearing at 2.4 ppm, next to the triplet that corresponds to proton H_4 (brown). Such shifting is an indication of the shielding effect exerted by the magnetic field of the aromatic rings, which are sandwiching these protons. Additionally, we can also observe a slight shifting of the methylene protons (CH_2-O) of the crown ether macrocycle towards upfield, due to a weaker interaction with the triazolium station, in turn, less electron demanding compared to the strong hydrogen bonding interaction with the secondary ammonium station. Finally, we observed that protons that correspond to the aromatic rings, the polyether chains, and the alkyl substituents of the mesogen maintain almost the same chemical shifts independently whether the molecule is in the contracted or extended state.

We also used ^{1}H diffusion-ordered spectroscopy (DOSY) to confirm the contraction/extension event on compound **20** in $CDCl_3$ (Figure 2.3). DOSY NMR is a 2D-NMR experiment in which one dimension represents ^{1}H NMR chemical shifts while the second dimension resolves species according to their diffusion properties, therefore, this technique is also called non-invasive chromatography.[20] DOSY provides quantitative information about the diffusion behaviour of molecular species through the diffusion coefficient determined by the Stokes-Einstein equation:

$$D = \frac{\kappa T}{6\pi\eta R_H} \tag{2.1}$$

Here, κ is the Boltzmann constant, T is the temperature, η is the viscosity of the liquid and R_H is the hydrodynamic radius of molecules.[21]

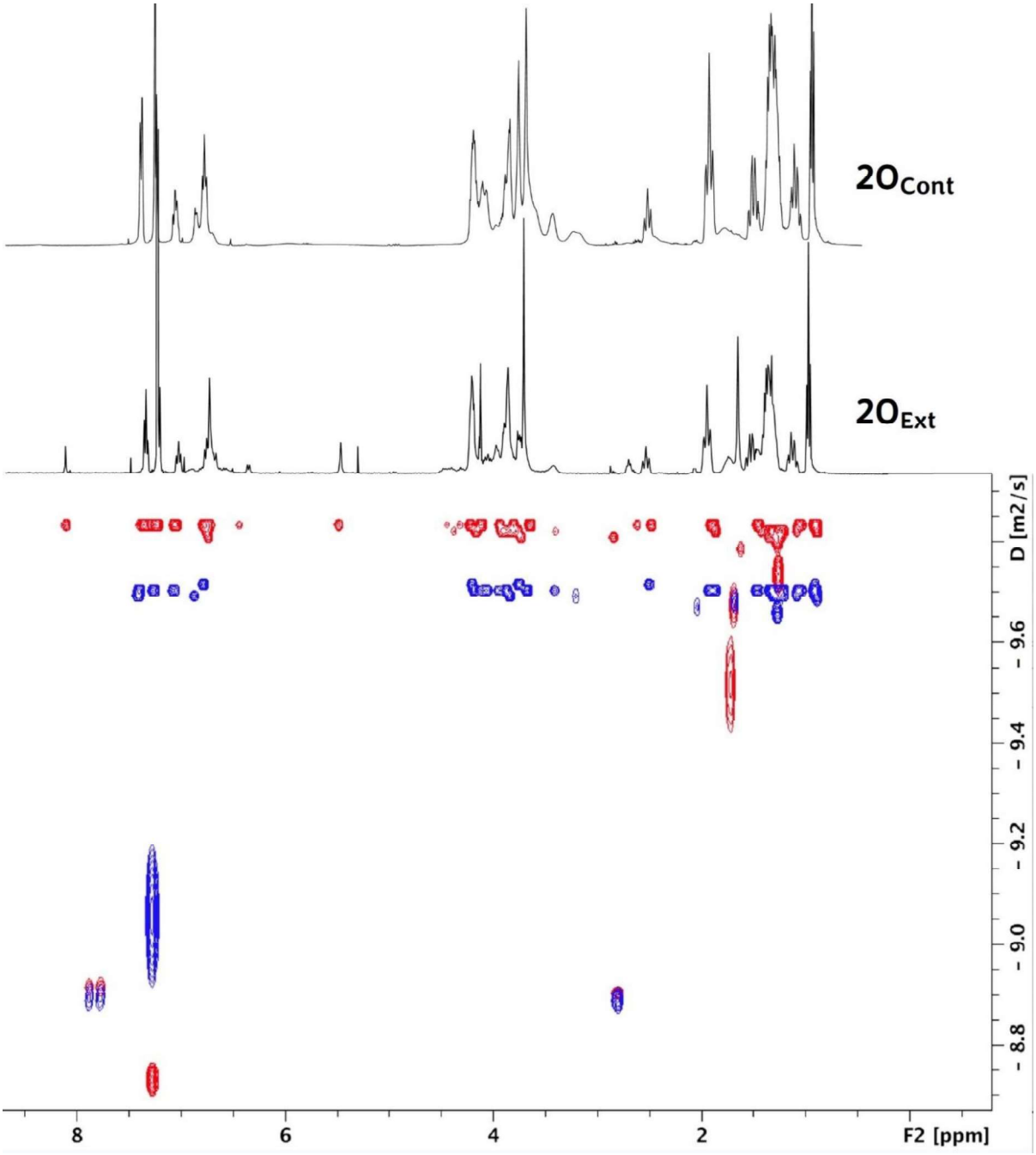

Figure 2.3. DOSY NMR spectra of $\mathbf{20_{Ext}}$ (red) and $\mathbf{20_{Cont}}$ (blue) recorded in $CDCl_3$ at 26 °C (600 MHz).

The diffusion coefficient (D) is very sensitive to size and shape of molecular species, thus, with this data in hands, it is possible to obtain information about the hydrodynamic radii (R_H) of the molecules by using equation 1.1.[22] For $\mathbf{20_{Ext}}$, $D = 1.40 \times 10^{-10}$ $m^2 \cdot s^{-1}$, lower in comparison with $D = 1.90 \times 10^{-10}$ $m^2 \cdot s^{-1}$ for $\mathbf{20_{Cont}}$. These values correspond to $R_H = 2.80$ nm and $R_H = 2.07$ nm for $\mathbf{20_{Ext}}$ and $\mathbf{20_{Cont}}$ respectively, which are consistent with the pH-triggered contraction.

We then carried out thermogravimetric analysis (TGA) to know the thermal stability of the [*c*2]daisy chain rotaxanes (Figure 2.4), before studying their mesomorphic properties. All interlocked compounds (**19**–**20**) displayed good thermal stability with a decomposition temperature of 300, 240 and 270 °C for **19**, **20**$_{Ext}$ and **20**$_{Cont}$ calculated at 5% weight loss, respectively.

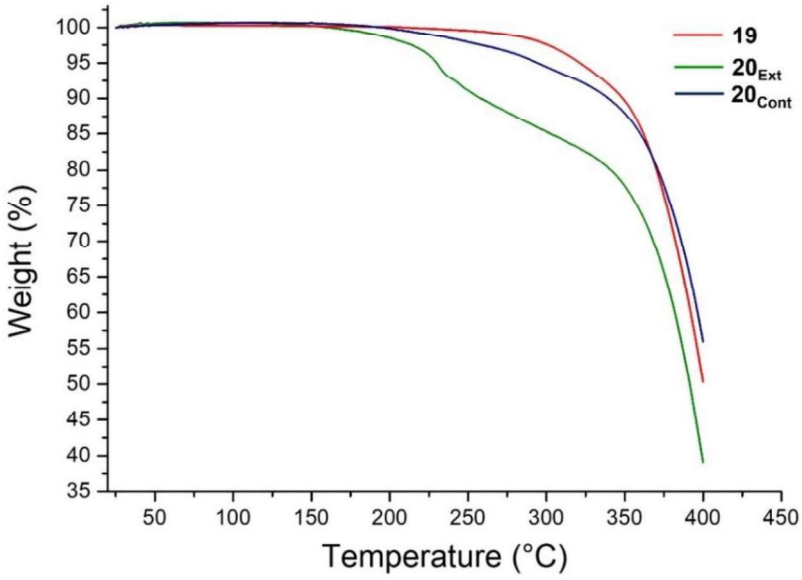

Figure 2.4. TGA thermograms of **19**, **20**$_{Ext}$ and **20**$_{Cont}$ obtained a heating rate of 5 °C/min in nitrogen.

Differential scanning calorimetry analyses (DSC) were carried out to examine the potential thermotropic behaviour of compounds **20**$_{Ext}$ and **20**$_{Cont}$ (Figure 2.5). This thermal analysis was combined with variable temperature polarised optical microscopy (POM) images (Figure 2.6). For **20**$_{Ext}$, upon cooling a small exotherm can be observed as a broad peak between 175 and 165 °C.

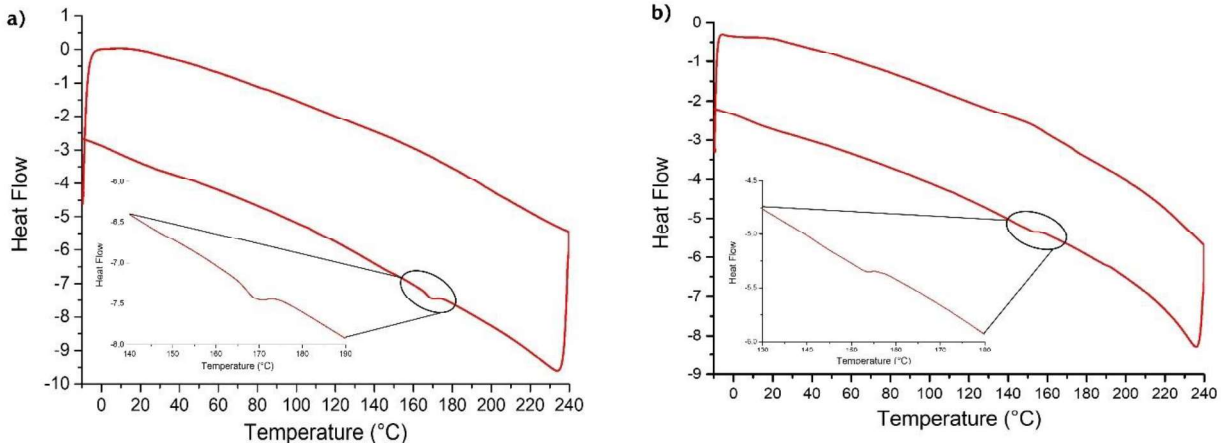

Figure 2.5. DSC thermograms of **20**$_{Ext}$ (**a**) and **20**$_{Cont}$ (**b**) obtained at cooling rate of 5 °C/min under nitrogen.

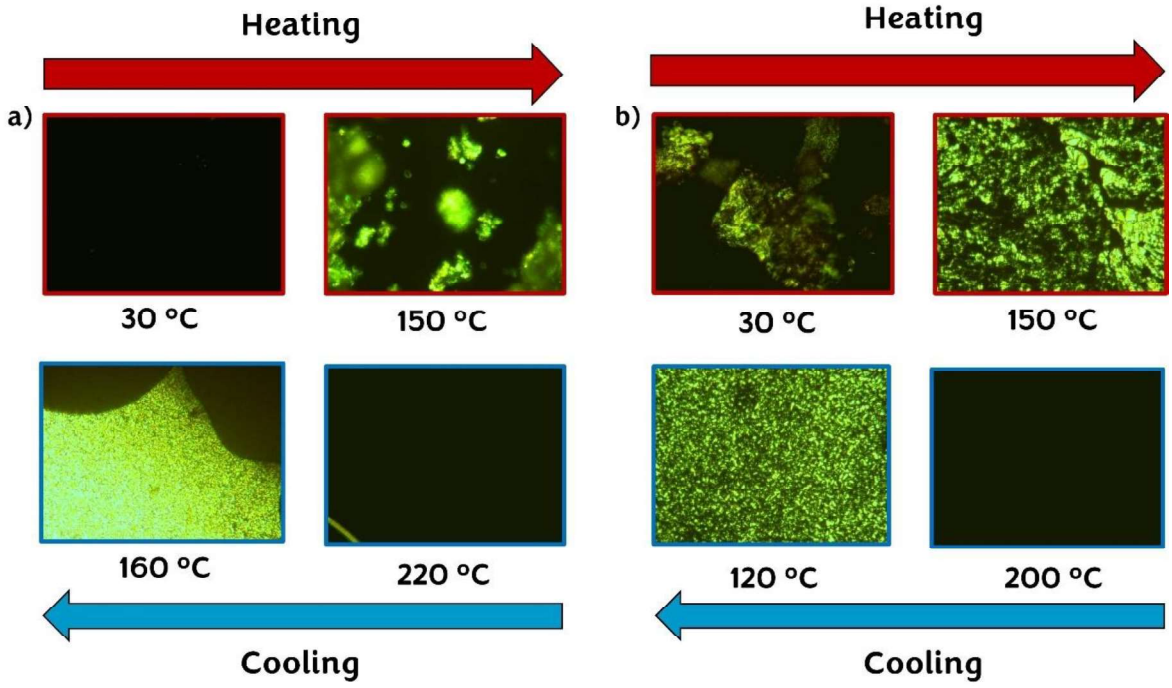

Figure 2.6. Photomicrographs for [*c*2]daisy chain rotaxanes (**a**) **20**$_{Ext}$ and (**b**) **20**$_{Cont}$ in the isotropic and SmA phase.

In conjunction with polarised optical microscopy images, the exotherm are coherent with a liquid-crystal ↔ isotropic phase transition (Figure 2.6a). For **20**$_{Ext}$, nothing is observed at the initial state (30 °C). However, at 150 °C, there are some brilliant spots that indicate a small anisotropic ordering. Finally at 220 °C, the compound reaches its isotropic phase and thus, a dark image is obtained. Upon cooling down the sample from the isotropic state, a liquid crystalline texture was observed at 160 °C.

The DSC thermogram for **20**$_{Cont}$ was essentially like the one of **20**$_{Ext}$, displaying a shift towards lower temperatures of the phase transition occurring between 150 and 160 °C. Similarly, for **20**$_{Cont}$ POM images demonstrate that such range of temperatures correspond to a liquid-crystal ↔ isotropic phase transition (Figure 2.6b). Interestingly, at the initial state, **20**$_{Cont}$ presents some anisotropic behaviour which is observed at 30 °C. At 150 °C, a liquid crystalline fan texture was observed and at 200 °C the system became completely isotropic. When cooling down, a liquid crystalline texture was observed around 120 °C, which indicates that **20**$_{Cont}$ exhibit LC behaviour at temperatures lower than the ones detected by DSC.

It is important to mention that other systems[23] containing the same or a similar fork-like shape mesogen exhibit DSC thermograms with similar behaviour and very low intensities of the phase transitions. For instance, in the liquid crystalline [2]rotaxane developed initially by Stoddart and co-workers,[2] the phase transitions were barely seen by DSC experiments.

To further identify the LC phases, small angle X-ray scattering (SAXS) experiments were carried out for [*c*2]daisy chain rotaxanes in both extended and contracted states. Besides the interlayer distance, Figure 2.7 shows that both compounds **20**$_{\mathbf{Ext}}$ and **20**$_{\mathbf{Cont}}$ exhibit identical SAXS profiles and WAXS patterns. In the small-angle region, three reflections are visible in a ratio 1:2:3 which were indexed as (100), (200), and (300) for both systems (Figure 2.7 a-b).

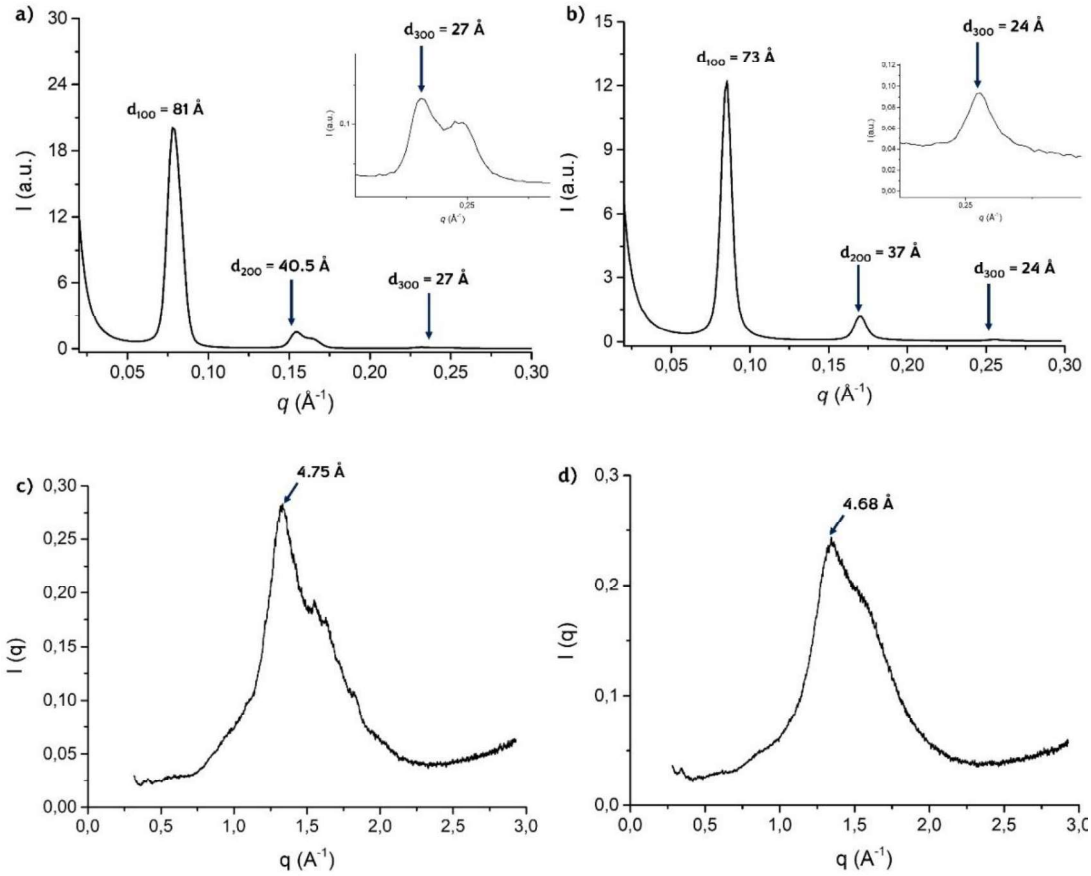

Figure 2.7. SAXS and WAXS plots for (**a, c**) **20**$_{\mathbf{Ext}}$ and (**b, d**)**20**$_{\mathbf{Cont}}$ at 25 °C.

This diffraction pattern is typical for a lamellar-like molecular arrangement Smectic A (SmA) phase geometries with alternate layers of the mesogenic cores densely packed by π-π stacking and van der Waals interactions, and the [*c*2]daisy chain units at the middle. The SAXS profile for **20**$_{\mathbf{Ext}}$ displays other two peaks adjacent to the reflection d_{200} and d_{300}, which can be attributed to the perpendicular organisation of the molecules inside the layers. The smectic layer length d is obtained from the position of the first peak by means of the Bragg relation:

$$d = \frac{2\pi}{q} \tag{2.2}$$

Figure 2.8 displays a schematic representation of the layer spacing and local packing found for **20$_{Ext}$** (81 Å) at 25 °C, which is bigger than that of **20Cont** (73 Å). This observation suggests that **20$_{Cont}$** forms a smaller organised structure, which agrees with the molecular contraction carried out by deprotonation.

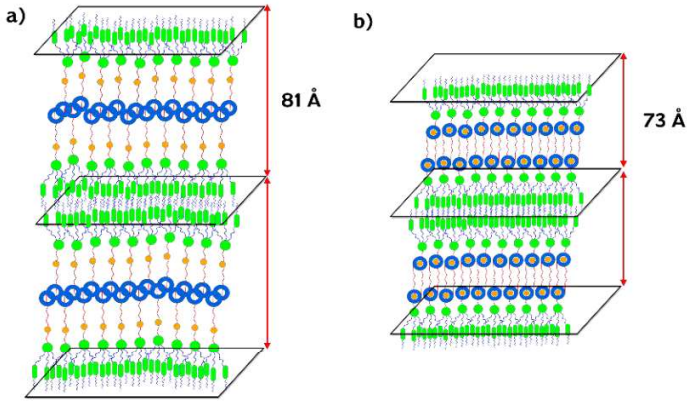

Figure 2. 8. Schematic representation of a hypothetical organisation of (**a**) **20$_{Ext}$** and (b) **20$_{Cont}$** at 25 °C.

Temperature-dependent SAXS and WAXS experiments were carried out to confirm the smectic phase observed by POM (Figure 2.9).

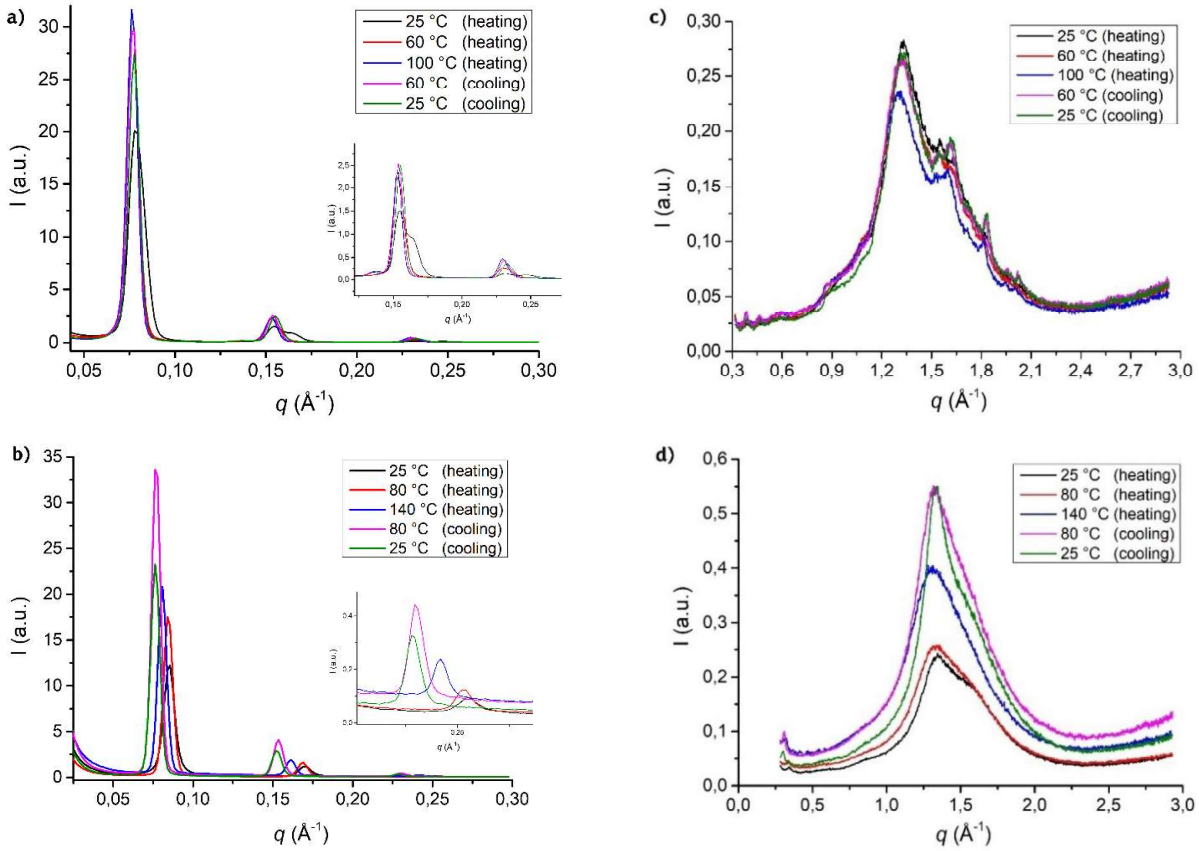

Figure 2.9. SAXS and WAXS plots for (**a, c**) **20$_{Ext}$** and (**b, d**)**20$_{Cont}$** at different temperatures.

For **20**$_{Ext}$, we found small changes in the layer thickness 100 °C, probably due to an amplitude motion of the mesogenic units attached to the interlocked crown macrocycles, and the permanent shifting of reflections at d = 37 Å and 25 Å towards higher values of q. We can attribute this behaviour as an internal reorganisation of the molecules inside the layers of the SmA phase. Upon cooling at 25 °C, all the peaks reset to their initial values. For **20**$_{Cont}$, we found dramatic changes in the position of the peaks of the SAXS plot upon heating and cooling. We observed a non-reversible transition and an increase of the interlayer spacing with values very similar to **20**$_{Ext}$. The same behaviour is observed for WAXS peaks, however, upon cooling, the peak at 25 °C resets to its initial position. So far, these results suggests that high temperatures destabilise the LC phase of **20**$_{Cont}$, which deserve further and more controlled SAXS experiments to get better insights behind this behaviour.

2.4. Conclusions

In this part, we have designed, synthesized and characterised a pH-responsive bistable [*c*2]daisy chain rotaxane (**20**) containing fork-like dendritic end-capping stoppers that induce a liquid-crystalline behaviour. The synthetic route proposed that led to compound **20** involved 18 synthetic steps, which were carried out in most of the cases with moderate to high yields, except for the *O*-alkylation reaction of the gallic methyl ester. Despite this reaction has been already described, we could not reproduce the yields (~90%) reported on the literature.

Nevertheless, we were able to carry out the key step of the synthetic route, the coupling between the dendritic mesogen **18** and the interlocked structure of the pseudo[*c*2]daisy chain **9**. Click chemistry reaction and subsequent *N*-methylation reaction led us to obtain our [*c*2]daisy chain rotaxane **20** in its extended state (**20Ext**). Upon deprotonation of **20**$_{Ext}$, a shortening of the molecular size was achieved due to the sliding motion of the DB24C8 macrocycles towards the triazolium station, (which was confirmed by (^{1}H and DOSY NMR experiments), leading to compound **20**$_{Cont}$.

The results already obtained from POM images, DSC analyses and SAXS and WAXS profiles are in line with our original objective as they highlight a 15°C temperature change of the Smectic A mesophase formation between the extended and contracted forms of the rotaxane. This shows that around 175°C, the rotaxane can switch from LC to isotropic state depending on the station linked by the macrocycles. To finalize this work in the form of a publication, some refinements of the scattering data as well as a more advanced molecular modelling are currently ongoing in order to have a precise structural view relating the conformation of the molecular machine with the observed liquid-crystal structure.

References

[1] E. D. Baranoff, J. Voignier, T. Yasuda, V. Heitz, J. P. Sauvage, T. Kato, *Angew. Chemie - Int. Ed.* **2007**, *46*, 4680.

[2] I. Aprahamian, T. Yasuda, T. Ikeda, S. Saha, W. R. Dichtel, K. Isoda, T. Kato, J. F. Stoddart, *Angew. Chemie - Int. Ed.* **2007**, *46*, 4675.

[3] M. Yoshio, T. Mukai, M. Yoshizawa, H. Ohno, T. Kato, *J. Am. Chem. Soc.* **2003**, *125*, 3196.

[4] F. Coutrot, E. Busseron, *Chem. - A Eur. J.* **2008**, *14*, 4784.

[5] C. A. Brown, A. Yamashita, *J. Am. Chem. Soc.* **1975**, *97*, 891.

[6] M. A. Walker, *J. Org. Chem.* **1995**, *60*, 5352.

[7] O. Mitsunobu, *Synthesis (Stuttg).* **1981**, *1*, 1.

[8] M. S. Gibson, R. W. Bradshaw, *Angew. Chem. Int. Ed.* **1968**, *7*, 919.

[9] F. Coutrot, C. Romuald, E. Busseron, *Org. Lett.* **2008**, *10*, 3741.

[10] R. Appel, *Angew. Chem. Int. Ed.* **1975**, *14*, 801.

[11] T. Sato, T. Takata, *Polym. J.* **2009**, *41*, 470.

[12] A. Ostrowicki, E. Koepp, F. Vögtle, *Top. Curr. Chem.* **1992**, *161*, 37.

[13] S. J. Cantrill, G. J. Youn, J. F. Stoddart, D. J. Williams, *J. Org. Chem.* **2001**, *66*, 6857.

[14] M. E. Belowich, J. F. Stoddart, *Chem. Soc. Rev.* **2012**, *41*, 2003.

[15] Y. Wang, C. P. Cabry, M. Xiao, L. Male, S. J. Cowling, D. W. Bruce, J. Shi, W. Zhu, E. Baranoff, *Chem. - A Eur. J.* **2016**, *22*, 1618.

[16] A. Suzuki, *Angew. Chem. Int. Ed.* **2011**, *50*, 6722.

[17] T. M. Kosak, H. A. Conrad, A. L. Korich, R. L. Lord, *European J. Org. Chem.* **2015**, 7460.

[18] L. Fang, M. Hmadeh, J. Wu, M. A. Olson, J. M. Spruell, A. Trabolsi, Y. Yang, M. Elhabiri, J. F. Stoddart, *J. Am. Chem. Soc.* **2009**, *131*, 7126.

[19] A. Wolf, J. J. Cid, E. Moulin, F. Niess, G. Du, A. Goujon, E. Busseron, A. Ruff, S. Ludwigs, N. Giuseppone, *European J. Org. Chem.* **2019**, *2019*, 3421.

[20] C. S. Johnson Jr, *Prog. Nucl. Magn. Reson. Spectrosc.* **1999**, *34*, 203.

[21] W. Ge, J. H. Zhang, C. M. Pedersen, T. Zhao, F. Yue, C. Chen, P. Wang, Y. Wang, Y. Qiao, *ACS*

Sustain. Chem. Eng. **2016**, *4*, 1193.

[22] P. S. Pregosin, P. G. A. Kumar, I. Ferna, *Chem. Rev.* **2005**, *105*, 2977.

[23] G. Yin, X. Li, H. Peng, H. Yang, *J. Am. Chem. Soc.* **2020**, *142*, 6285.

Chapter 3
Preparation of polyurethanes based on bistable [*c*2]daisy chain rotaxanes

As discussed previously, the amplification of molecular motion can be achieved in soft matter systems like liquid crystals, characterised by intermolecular interactions and local organisational order. However, the motion carried out by single mechanically interlocked molecules, more specifically, by [*c*2]daisy chain rotaxanes, can be potentially translated to the macroscopic scale through their introduction within polymer materials. So far, some examples on the literature have demonstrated that it is possible to obtain a macroscopic response in polymeric systems from the mechanical actuation of individual units, as long as their collective motions are synchronised. In order to build contractile materials based on [*c*2]daisy chains polymers, directionality and hierarchical organisation of the polymer chains is very important. These characteristics would allow the formation of stiffer fibres that can self-assemble as myofibrils do when they are laterally packed to form muscular fibres.

In that sense, polyurethanes (PUs) are good candidates to achieve such molecular ordering due to the strong hydrogen bonding between the urethane bonds of the polymer chains. PUs are mostly synthesised via polycondensation reaction (Scheme 3.1) between polyols (OH groups) and polyisocyanates (N=C=O groups),[1] as reported by Otto Bayer and his co-workers in 1937.[2]

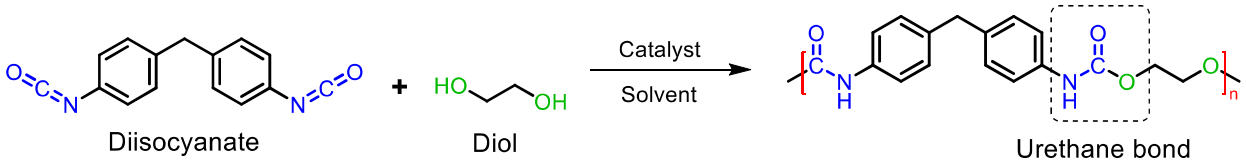

Scheme 3.1. Classical route to synthesize polyurethanes.

Scheme 3.1 shows the reaction between an aromatic diisocyanate and an aliphatic diol. However, the great variety of commercially available polyols and polyisocyanates renders versatility to the formation of polyurethane based materials. The uses and applications of these materials are based on their structure-property relationships. For instance, PUs containing aromatic rings from diols of low molecular weight are often used for the production of rigid foams due to their high endurance and breathability.[3]

PUs are an important class of thermoplastic elastomers,[4] endowed with malleable properties which make them easy to process and to recycle.[5] The mechanical properties of thermoplastic polyurethanes (TPU's) are related to the hard and soft segments content of the material. The elastic modulus, the hardness and strength of the materials are related with the hard segments, whereas the elasticity, the elongation and the temperature resistance depend on the chemical structure of the soft segments.

TPUs find applications ranging from self-healing and shape memory materials[6] to materials for soft robotics,[7] because of their versatile mechanical performance properties, owing to the multiple combinations between hard and soft segments. For example, they have found applications in 3D printing of soft robotic systems, as flexure hinges for tendon-driven soft prosthetic fingers.[8] TPU filaments can also be used for biomedical applications[9] and stretchable electronics, where needs for elongations of up to 700% are required.

Urethane bonds have also been considered for the polymerisation of rotaxane units at the end of the 20th century. In 1993, Gibson and co-workers carried out the synthesis of elastomeric poly(urethane rotaxanes) based on the template-synthesis approach reported by Stoddart (see Chapter 1, Section 1.2.2.). Solubilities of the polymer were improved with the interlocked molecules when compared with the parent backbone. More recently, Takata and co-workers reported the synthesis of elastomeric PUs containing rotaxane units, from a [2]rotaxane diol with a hydroxyl group in each wheel and axle component. They found that introduction of mechanically interlocked units enhanced the toughness of the material compared to the model polyurethane.[10]

To the best of our knowledge, there are no reports on poly[*c*2]daisy chains containing urethane bonds. Considering the wide spectrum of applications of polyurethane chemistry, the robustness and the versatility of the mechanical properties of these materials, we were interested into carry out the polymerisation of bistable [*c*2]daisy chain rotaxanes as monomer diols, with different diisocyanates. Therefore, the following sections concern the synthesis of [*c*2]daisy chain rotaxane monomers capable of forming polyurethanes once in contact with diisocyanates.

3.1. Synthesis of the [*c*2]daisy chain rotaxane 25

The first synthetic strategy targeted compound **25** whose retrosynthesis is depicted on Scheme 3.2. To obtain such an interlocked structure, it was necessary to protect the primary hydroxyl groups to avoid side reactions during the *N*-methylation reaction on substrate **23**. We envisioned the synthesis of substrate **23** arising retrosynthetically from pseudo[*c*2]daisy chain rotaxane **9** (see section 2.1) and azide derivative **22**, by doubly cutting the C-N bonds of the triazole rings formed by the copper(I) catalysed 1,3-dipolar cycloaddition.

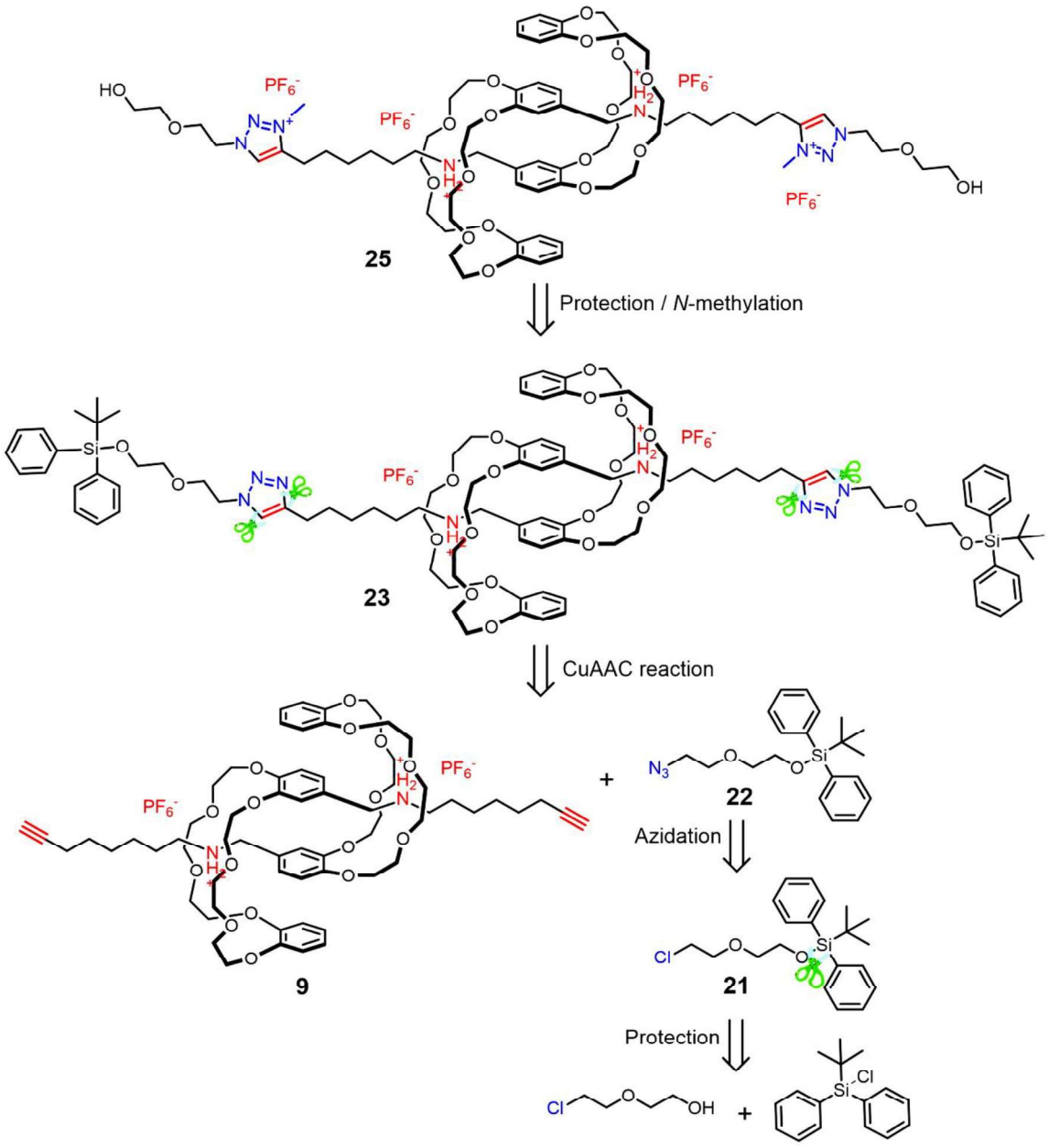

Scheme 3.2. Retrosynthesis of compound **25**.

Replacing the azide group of key intermediate **22** by the chlorine one took us to substrate **21**, which can be cut at the silyl ether bond to unravel the origins of this intermediate to the commercially available *tert*-butyldiphenylsilyl chloride and 2-(2-chloroethoxy)ethan-1-ol. Having decided upon the pathway towards **25** by the retrosynthetic analysis shown in Scheme 3.2, and taking into account that pseudo[*c*2]daisy chain **9** was already synthesized, we set to the task of synthesizing the precursors required to obtain compound **22**. It is important to highlight that all compounds described in this chapter were characterised by ^{1}H and ^{13}C NMR spectroscopy (see experimental section for protocols and Annexes A for NMR spectra).

3.1.1. Synthesis of [*c*2]daisy chain rotaxane 23

2-(2-Chloroethoxy)ethanol was subjected to an *O*-protection with *tert*-butyl(chloro)diphenylsilane (TBDPSCl)[11] leading to compound **21** in high yields. Then, the chlorine atom was substituted by an azide group using sodium azide, affording compound **22** in high yields. Finally, compounds **9** and **22** were coupled using a Copper(I)-catalysed Azide-Alkyne Cycloaddition reaction, providing compound **23** in 70% yield.

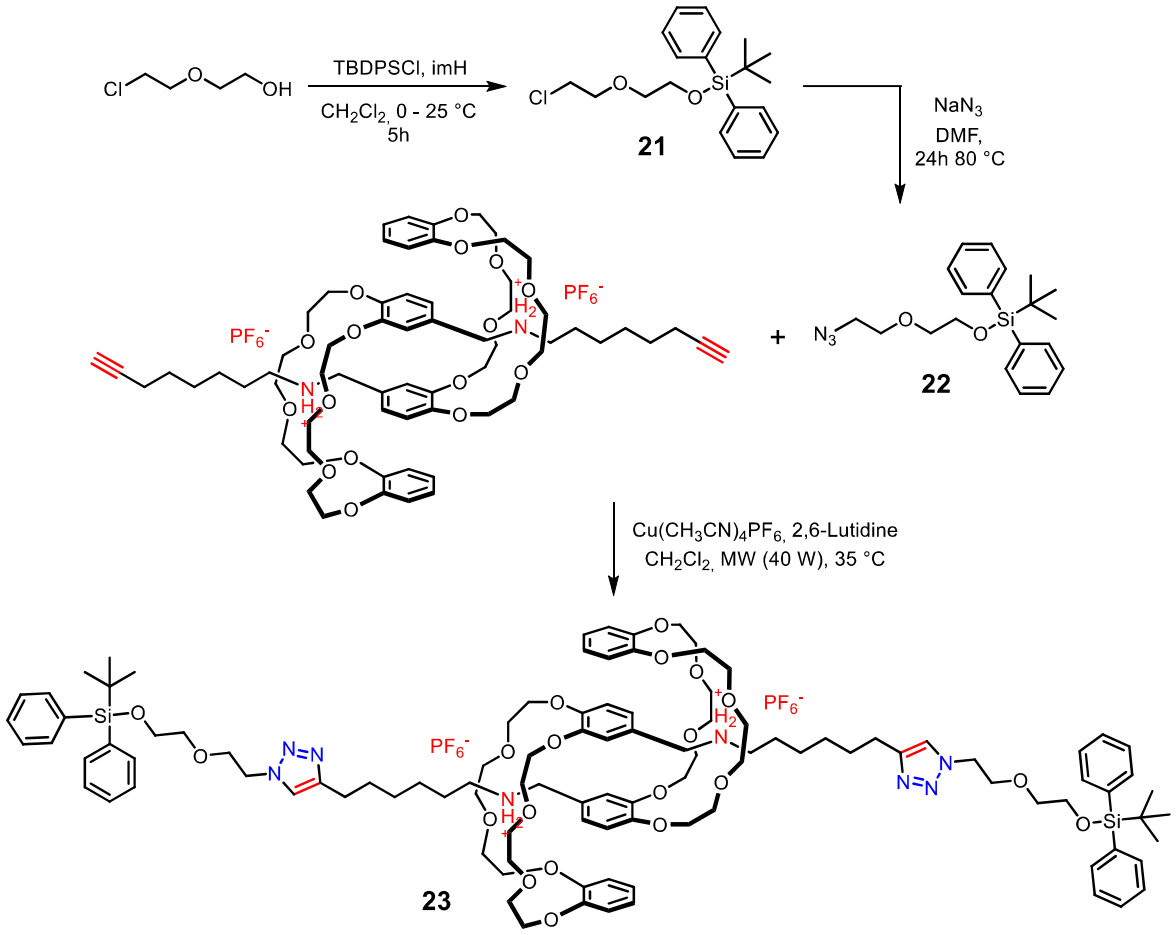

Scheme 3.3. Synthesis of compound **23**. imH = Imidazole, MW = Microwave heating.

The following steps consisted in the methylation of the triazole rings, in order to form the second station for the crown ether, as it was done for the [*c*2]daisy chain rotaxane prepared in Chapter 2. This was done as usual, using an excess of methyl iodide and at room temperature to avoid any side methylation reaction, leading to compound **24** in quantitative yield. With this compound in hands, we considered the deprotection of the terminal hydroxyl groups with a little excess of a tetrabutylammonium fluoride (TBAF) solution in THF for one hour (Scheme 3.4). However, this reaction led to dethreading of the [*c*2]daisy chain **24** and subsequent deprotection of hydroxyl groups observed by ^{1}H NMR spectroscopy (Figure 3.1a) and MALDI mass spectrometry (Figure 3.1b)

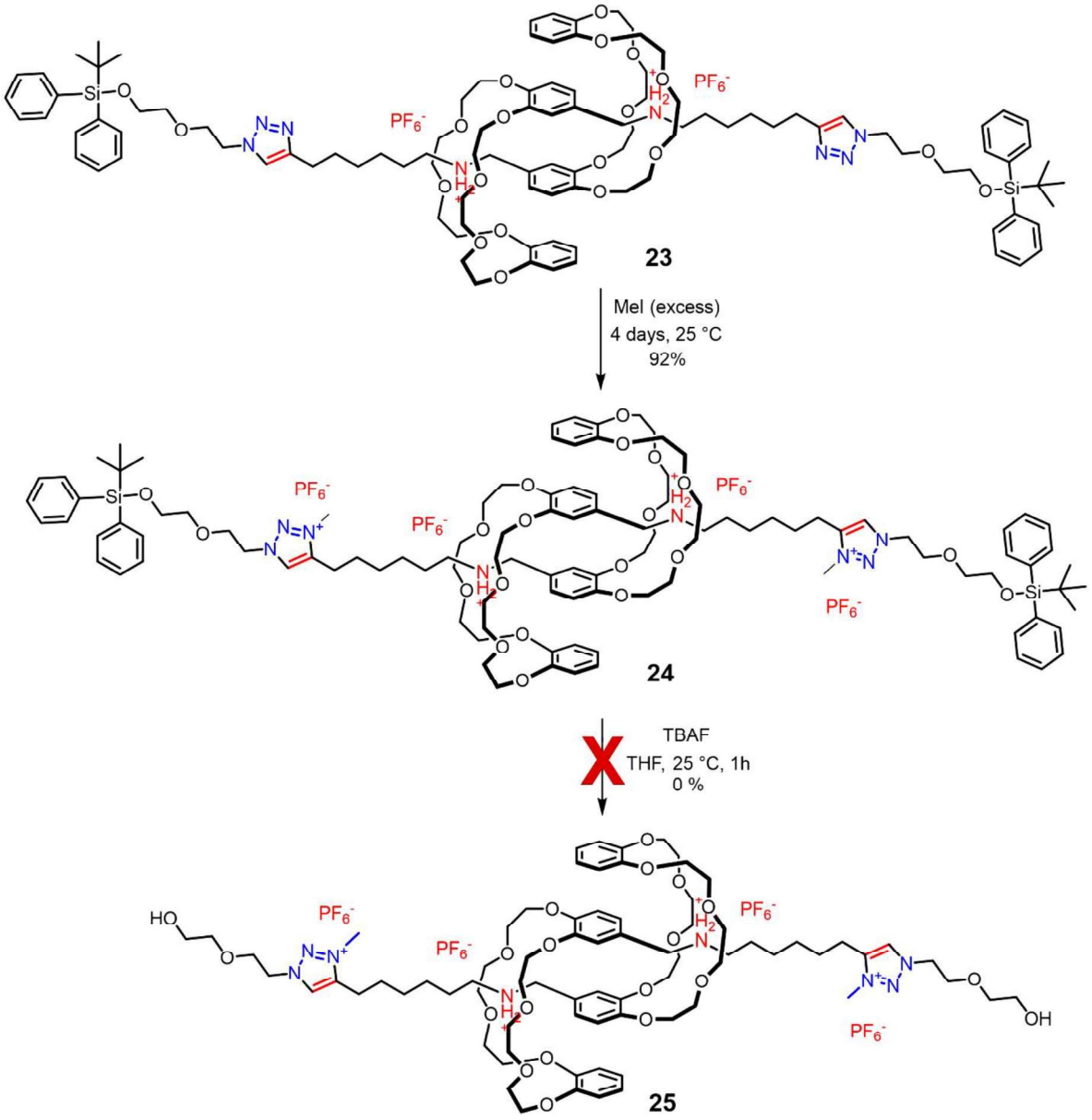

Scheme 3.4. Synthetic route to obtain compound **25**.

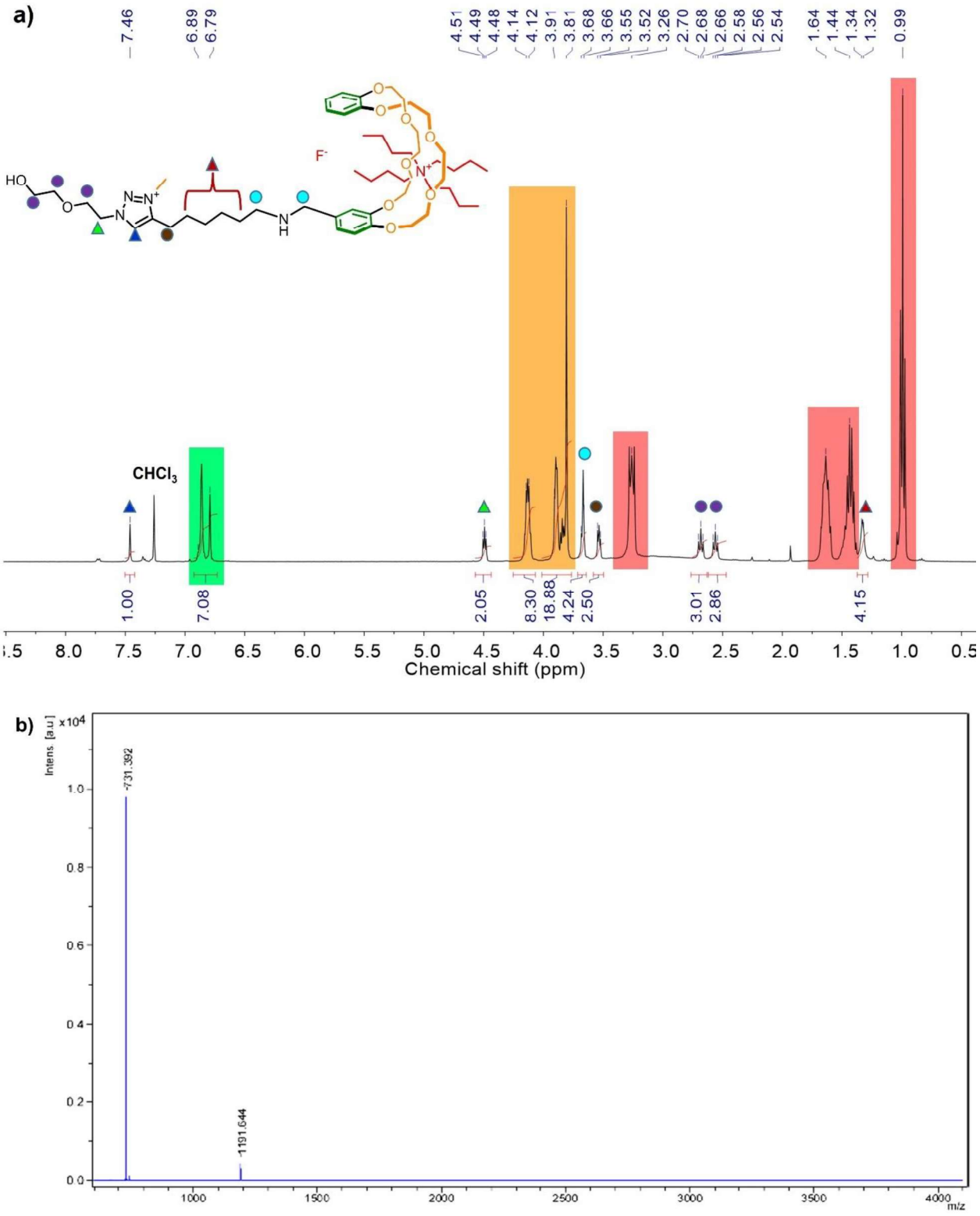

Figure 3.1. (**a**) ^{1}H NMR spectrum in $CDCl_3$ at 25 °C and (**b**) MALDI mass spectrum of the unthreaded compound obtained after treating compound **24** with a 1 M THF solution of TBAF.

In our case, we believe that fluoride ions from TBAF played two roles; one is related to the deprotection of the OH group by removing the silyl stopper, and the other one consists in weakening the host-guest interaction between the ammonium station and the crown ether of the macrocyclic ring, a behaviour that has been already demonstrated on the literature.[12] Figure 3.2a shows a clear ^{1}H NMR spectrum of the unthreaded compound with all the expected signals. The region between 4.25 and 3.75 ppm (highlighted in light orange) corresponds to the methylene protons of the crown ether macrocycle. This region is usually very complex to analyse for [*c*2]daisy chain rotaxane structures, exhibiting broad signals due to the interlocked nature of the molecule. However, in the ^{1}H NMR spectrum the signals are well defined, giving an indication that the obtained compound was not the threaded one.

In addition, multiplets highlighted in light red at 3.25, 1.64 and 1.44 ppm, and the triplet at 0.99 ppm correspond to the signals for the tetrabutylammonium cation, which could probably interact with the crown ether macrocycle and therefore favour the dethreading process. Furthermore, the MALDI spectrum displays an intense peak at m/z = 731.392 (Figure 3.2b), which corresponds to the molecular ion peak of the individual molecule confirming the unthreaded structure. Although fluoride ions can boost such dethreading, this can be avoided by the presence of a bulky stopper that can prevent such slippage process.[13]

3.2. Synthesis of the *O*-alkylated aldehyde 26

Taking in consideration the aforementioned observations, we considered the synthesis of an azide derivative containing a hydroxyl group that could allow the synthesis of the urethane bonds, and a bulky structure to avoid slippage of the macrocycle. We first considered the use of commercially available 3,5-di-*tert*-butyl-4-hydroxybenzaldehyde and its alkylation with bromoalcohol derivatives (Scheme 3.5).

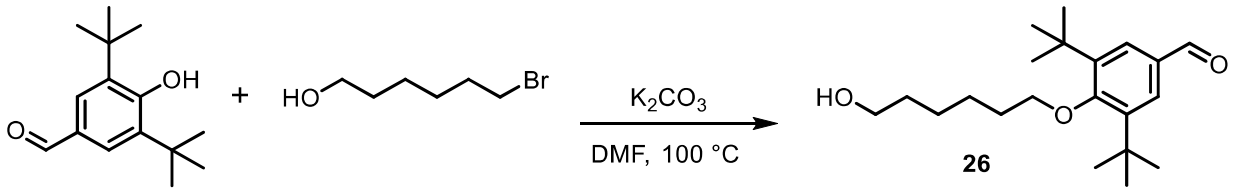

Scheme 3.5. Synthetic route towards compound **26**.

Several attempts were carried out to obtain compound **26**, since varying the number of alcohol and base equivalents, the temperature, the time, and the source of heating (hot plate and microwave irradiation). However, it was not possible to obtain this compound in yields higher than 10 or 15%. Table 3.1 summarises some of the most representative attempts carried out towards the obtaining of compound **26**.

Run	Alcohol equivalents	Base Equivalents	Temperature (° C)	Time (h)	Heating	Yield (%)
1	2	2	80	8	Conventional	Not found
2	2	2	80	48	Conventional	Traces
3	2	4	80	48	Conventional	Traces
4	2	2	80	4	Microwave	Traces
5	2	2	100	24	Microwave	Traces
6	2	4	80	24	Microwave	5–10
7	2	4	100	24	Microwave	10-15
8	4	4	100	24	Microwave	10-15

Table 3.1. *O*-alkylation conditions tested towards the synthesis of compound **26**.

Entries 1–3 involved the use of conventional heating varying the reaction times and the number of equivalents of potassium carbonate. In the three cases, the compound was obtained either in traces or not obtained. Then, we considered the use of a more homogeneous way of heating by using microwave irradiation. Conditions of entries 4 and 5 allowed us to obtain compound **26** one more time in traces, despite the use of microwave heating, longer reaction times and a small increase of the reaction temperature.

In order to force the formation of the phenolate ion, we increased the number of equivalents of potassium carbonate, while maintaining the reaction time up to 24 hours. Conditions of entries 6 and 7 allowed us to obtain **26** in 15% yield maximum after purification by column chromatography. Also, we increased the number of equivalents of 6-bromohexanol, (Entry 8) while maintaining the excess of potassium carbonate. However, we obtained the same results as with an equimolar amount of alcohol with respect to the phenol derivate. In addition, it is important to mention that we tried other conditions that are not included in Table 3.1. Considering, the steric hindrance around the phenol group, we decided to use of a smaller base like sodium hydride. Several attempts were carried out in different solvents (dimethylformamide, tetrahydrofuran, acetonitrile), however, the starting material did not show any reaction. Also, the reaction solvent was changed while keeping the use of potassium carbonate. Dry solvents like methyl ethyl ketone or 2-butanone, and acetonitrile were tested without obtaining any positive result. These results prompted us to look for another building block.

3.3. Synthesis of the *O*-silyl protected azide 31

Other bulky aromatic fragments besides 3,5-di-*tert*-butylbenzene have been employed as stoppers in the synthesis of rotaxanes to preclude dethreading processes. Substituents like 3,5-dimethylbenzene[14] and 3,5-dimethoxybenzene[15] are bulky enough to prevent the slippage of macrocyclic hosts. Therefore, as a question of molecular size, we decided to use commercially available 3,5-dimethoxy-4-hydroxybenzaldehyde (also known as syringaldehyde) as building block to obtain a bulky azide derivative containing in its structure a hydroxyl functional group. Scheme 3.6 describes the synthetic route towards the synthesis of *O*-silyl protected azide **31**.

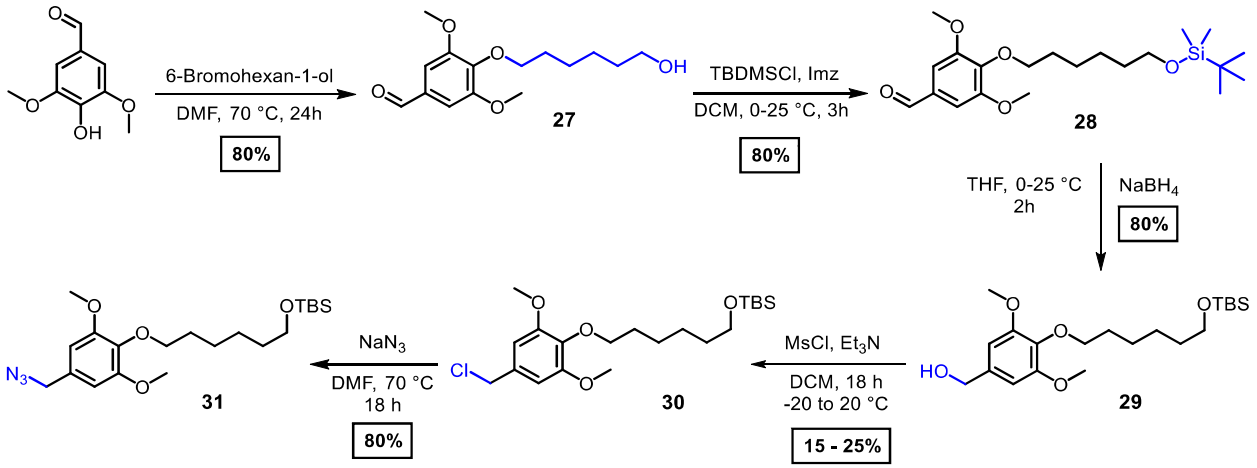

Scheme 3.6. Synthetic pathway to obtain compound **31**.

Syringaldehyde was subjected to classical conditions of *O*-alkylation reaction using potassium carbonate as base to form the phenolate ion. Such nucleophile will substitute the bromine atom of 6-bromohexan-1-ol leading to compound **27** in high yields after purification by column chromatography. Then, the free hydroxyl group was protected with *tert*-butyldimethylsilyl chloride to avoid side products in further reactions. This protecting group was chosen due to the lability against acid solutions, in order to avoid using tetrabutylammonium fluoride as deprotecting agent, due to the reasons mentioned before in Section 3.1.

Compound **28** was obtained in high yields and short times under classic mild conditions for this type of *O*-protection.[16] It is important to mention the key role played by imidazole in this organic transformation, which act as catalyst binding to the silyl compound and displacing the chlorine atom.[17] Then, the OH group binds to the silicon and cause the release of the imidazole, which act as base neutralising the hydrochloric acid formed *in situ*.

In addition, low temperatures at the beginning of the reaction are important not only because of the exothermic nature of this reaction, but also to make the imidazolium salt precipitate in aprotic/apolar solvents like chloroform or dichloromethane, shifting the equilibrium of the reaction towards the desired products.

One of the advantages of the *tert*-butyldimethylsilyl group is its chemical stability against reducing agents like sodium borohydride ($NaBH_4$). Therefore, compound **29** was obtained in high yields after reduction of the aldehyde functional group by using $NaBH_4$ under argon atmosphere, in THF dry and at low temperature. During the work-up of the reaction, the addition of aqueous ammonium chloride was needed to destroy the borate compound formed between the reducing agent and the substrate.

Having alcohol **29** in hands, the next step consisted in converting the benzylic OH group in a good leaving group. Therefore, **29** was subjected to a series of mesylation conditions, but most of the trials resulted in the chlorinated product **30** with low yields, ranging from 15 to 25%. Thin layer chromatography monitoring displayed several spots, suggesting that some decomposition of the starting material occurred. In fact, some of the side products were isolated, such as the benzylic alcohol derivative bearing the deprotected OH group attached to the alkyl tail, and the chlorinated compound also with the deprotected OH group (Scheme 3.7).

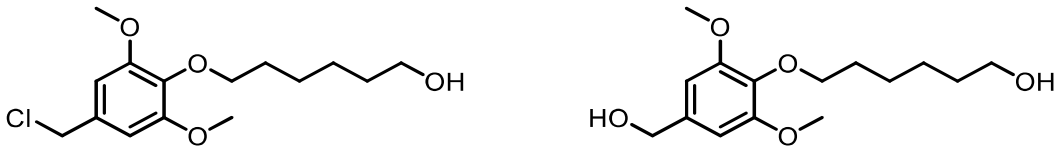

Scheme 3.7. Chemical structures of the isolated side products from the crude mesylation reaction.

We think that elimination of the silyl protecting group occurs due to the *in situ* formation of hydrochloric acid which is strong enough to promote its release. Actually, this behaviour could also explain the insertion of the chlorine atom to the benzylic carbon, instead of the mesyl group. If the reaction medium is acid enough to protonate the benzylic OH group, release of water can occur, promoting the formation of a benzylic carbocation and the subsequent insertion of the chloride ion. It is worthy to mention that we tried to form the tosyl derivative, but the reaction followed the same tendency of decomposition and chlorination in low yields. Although chlorinated compound **30** was not the expected product, it was successfully reacted with sodium azide in dry *N*,*N*-dimethylformamide at 80 °C, to afford compound **31** in good yields.

3.4. Synthesis of the [*c*2]daisy chain rotaxane 34$_{Ext}$

We then coupled azide **31** with pseudo[*c*2]daisy chain rotaxane **9** by a Copper(I)-catalysed Azide-Alkyne Cycloaddition reaction, in order to obtain [*c*2]daisy chain rotaxane **32** (Scheme 3.8).

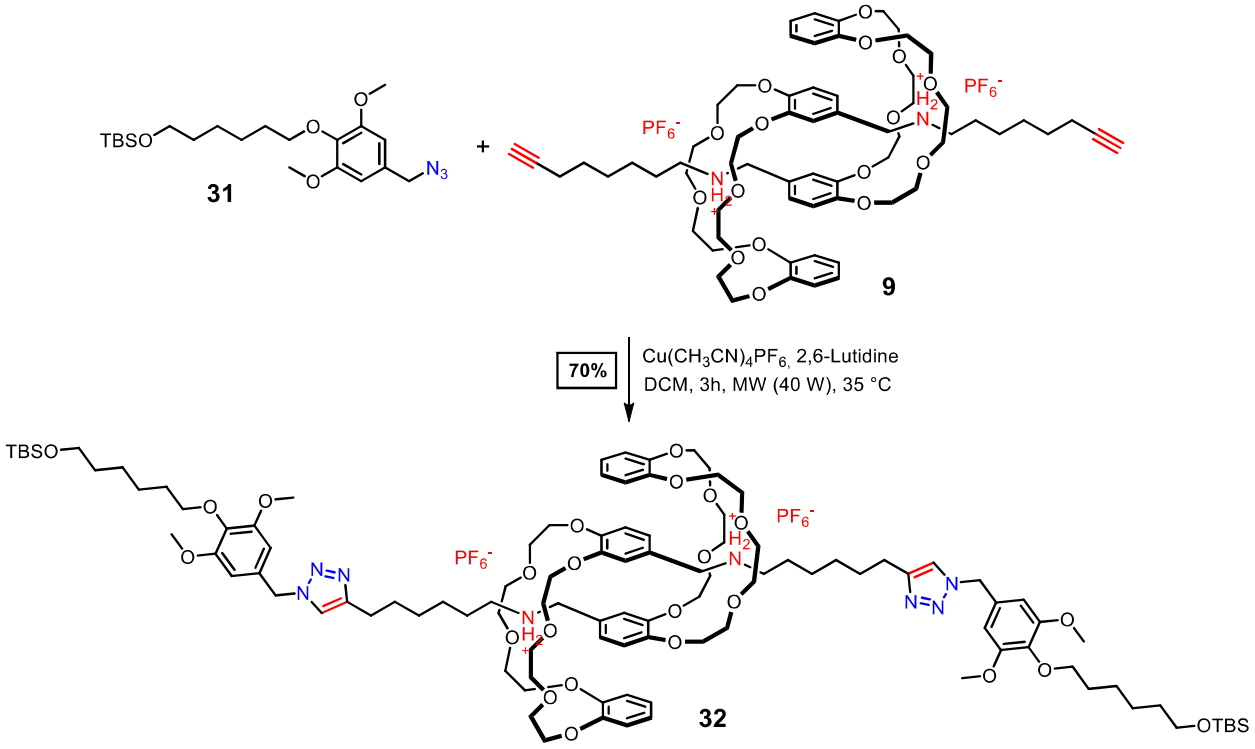

Scheme 3.8. Synthetic step to obtain compound **32**.

The ^{1}H NMR spectrum of **32** (Figure 3.2) displays all the expected signals, in particular the vinylic proton signal of the triazole H_1 at 7.38 ppm. Between 7.00 and 6.50 ppm, we can find broad multiplets that correspond to the aromatic protons for both the crown ether macrocycle and the aromatic ring adjacent to the triazole. Singlet at 5.42 ppm corresponds to the benzylic protons H_2. The region between 4.50 and 3.50 ppm encompasses the CH_2 protons of the crown ether macrocycle, as well as the CH_2 adjacent to the oxygens in the alkyl chain substituent of the aromatic ring Ar. The methoxy groups at positions 3 and 5 of the aromatic ring Ar, and the CH_2 next to the ammonium group are also masked in this complex region of the spectrum. The signal at 2.62 ppm corresponds to the protons H_3 due to the proximity to the triazole ring. At high field of the spectrum can be seen the proton signals corresponding to the CH_2 of the alkyl chains as a set of multiplets between 1.75 and 1.30 ppm (gathered in a red bracket). Finally, the signals of the *tert*-butyl and dimethyl aliphatic protons attached to the silyl protecting groups are located at 0.88 ppm and 0.04 ppm respectively.

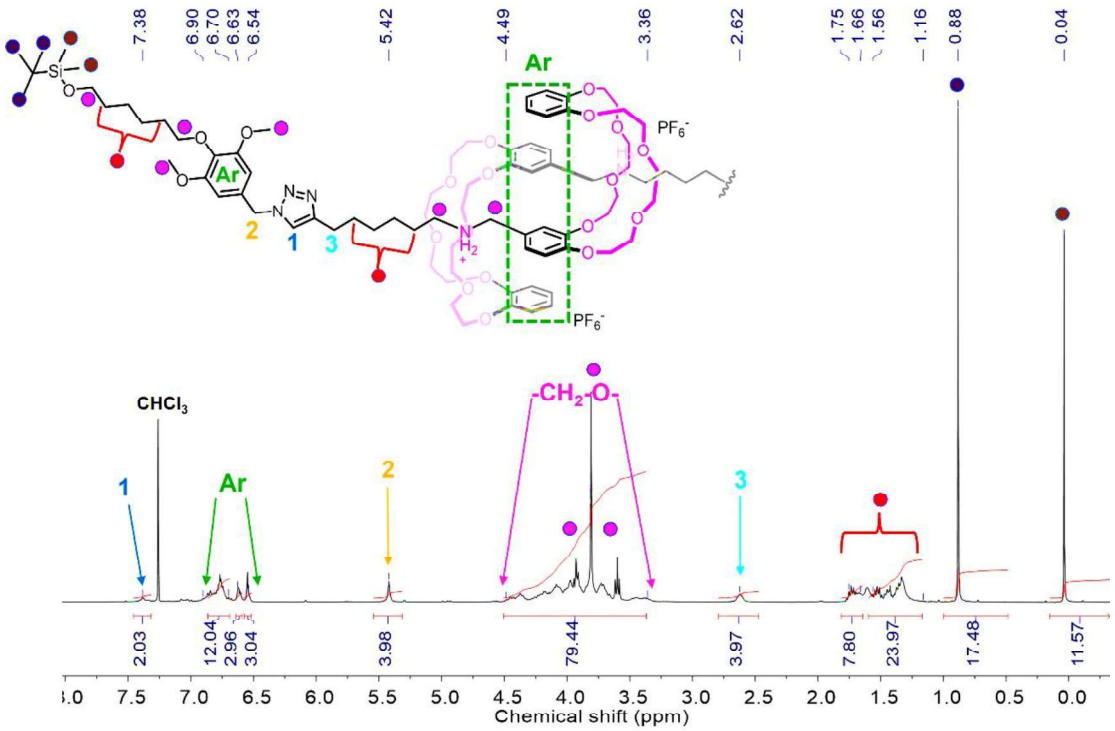

Figure 3.2. ^{1}H NMR spectrum of compound **32** in $CDCl_3$ at 25 °C (400 MHz).

Further methylation of the triazole rings was carried out using methyl iodide at 30 °C for 4 days to reach compound **33**, which contains a second station of molecular recognition for the macrocycles (Scheme 3.9).

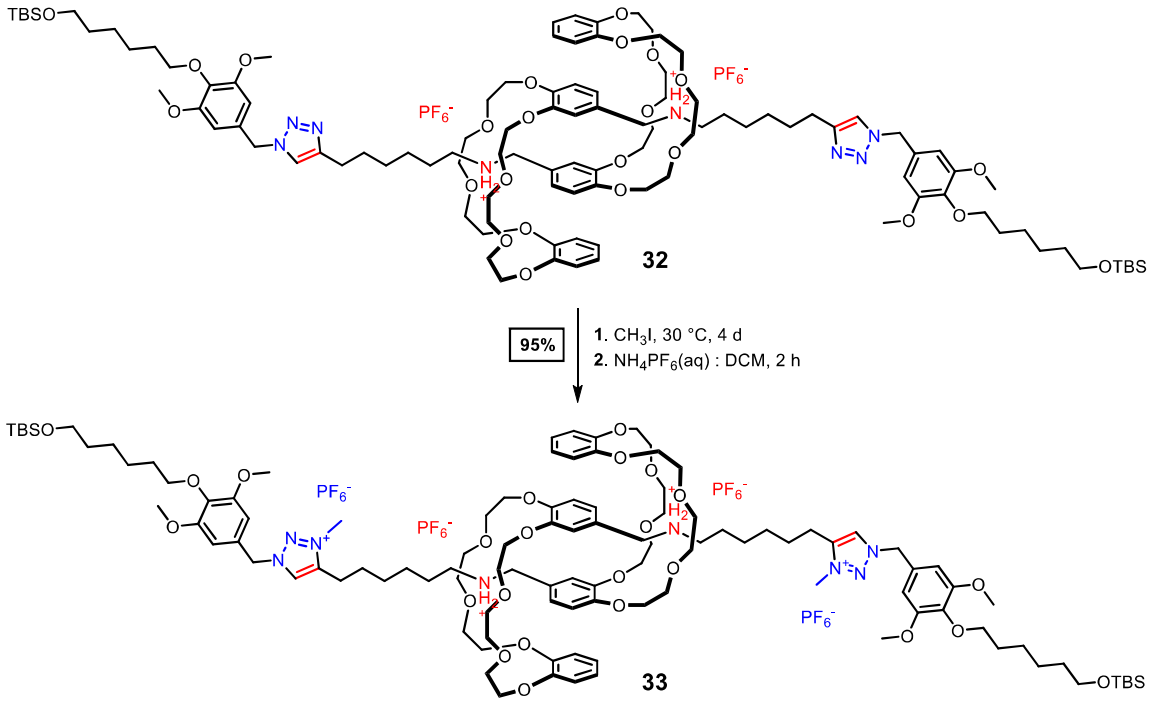

Scheme 3.9. Synthetic step to obtain compound **33**.

Finally, the hydroxyl groups were deprotected with a solution of HCl 1 M in THF, affording compound **34$_{Ext}$** as white solid in moderate yields (Scheme 3.10). The reaction times were around 30 minutes and the addition of ethyl acetate as cosolvent, helped to precipitate the desired product. The HR–MS spectrum of **34$_{Ext}$** shows a peak at m/z = 2256.9541 (Figure 3.3a) that corresponds to the molecular mass of $[M–(PF6)^-]^+$ with an error of 1.06 ppm when is compared with the theoretical value (Figure 3.3b).

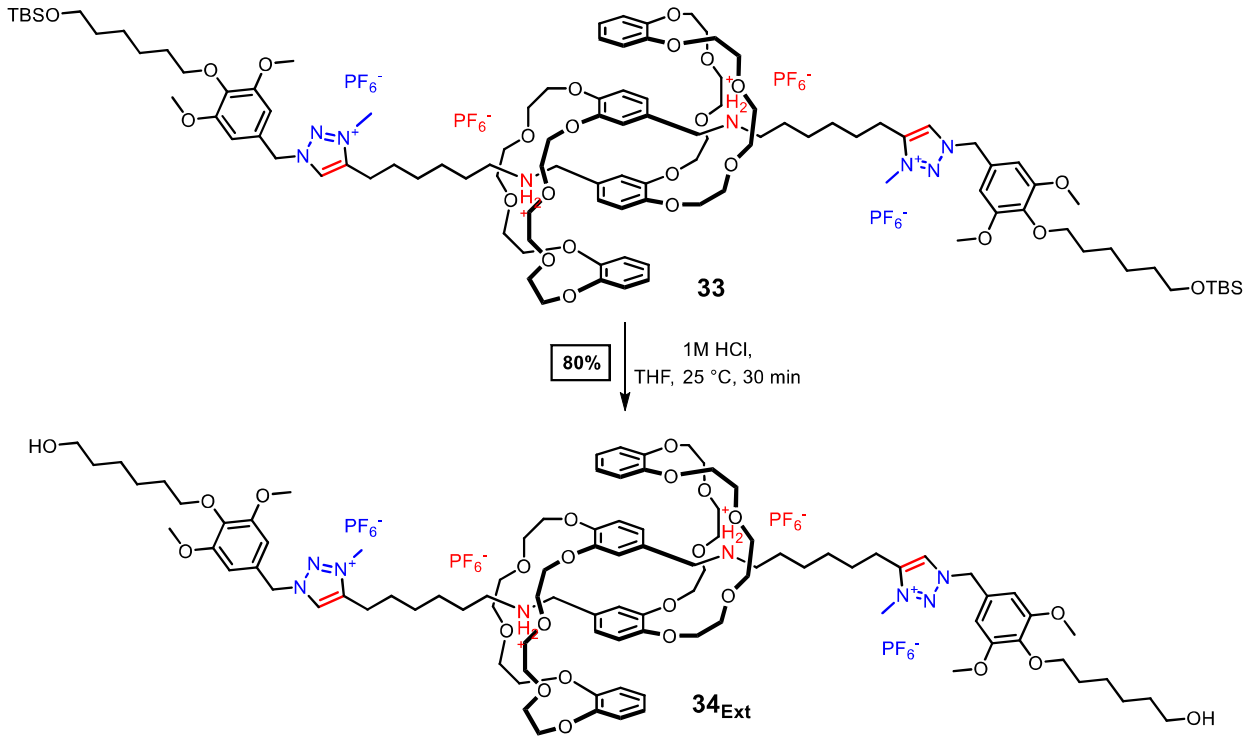

Scheme 3.10. Synthetic step to obtain compound **34$_{Ext}$**.

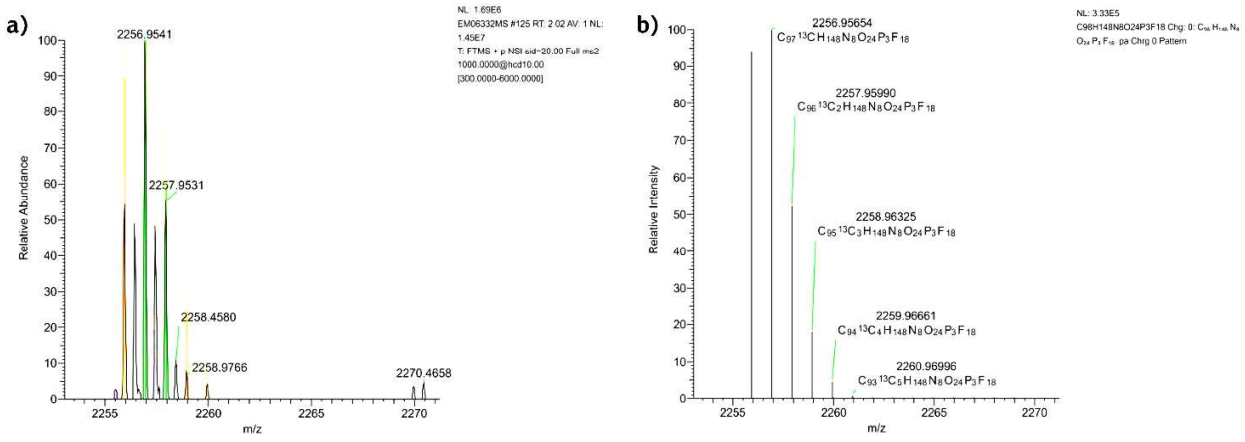

Figure 3.3. a) Experimental and **b)** theoretical high resolution mass spectra for **34$_{Ext}$**.

Having the [*c*2]daisy chain rotaxane **34**$_{Ext}$ in hands, we carried out the pH triggered contraction to form compound **34**$_{Cont}$ using a heterogeneous mixture of $CHCl_3$: NaOH 1 M (1:1). Deprotonation induces a move of the macrocyclic ring towards the triazolium ring, as observed by ^{1}H NMR spectroscopy (Figure 3.4). Such movement caused the flattering of the vinylic proton H_1 located at 8.05 ppm due to the interaction with the electronic density of the crown ether macrocycle. Additionally, benzylic protons H_2 that appears at 5.57 ppm in **34**$_{Ext}$ slightly move towards downfield for **34**$_{Cont}$, undergoing a broadening of the signal because of the proximity to the macrocycle. Signal at 2.63 ppm that correspond to protons H_3 for **34**$_{Ext}$ also are affected by the deprotonation, since they are sandwiched by the macrocycles in **34**$_{Cont}$. The signals corresponding to the CH_2 protons of the macrocycles in **34**$_{Cont}$ move towards upfield due to the weaker interaction with the triazolium station, compared to the strong interaction with the secondary ammonium group in **34**$_{Ext}$.

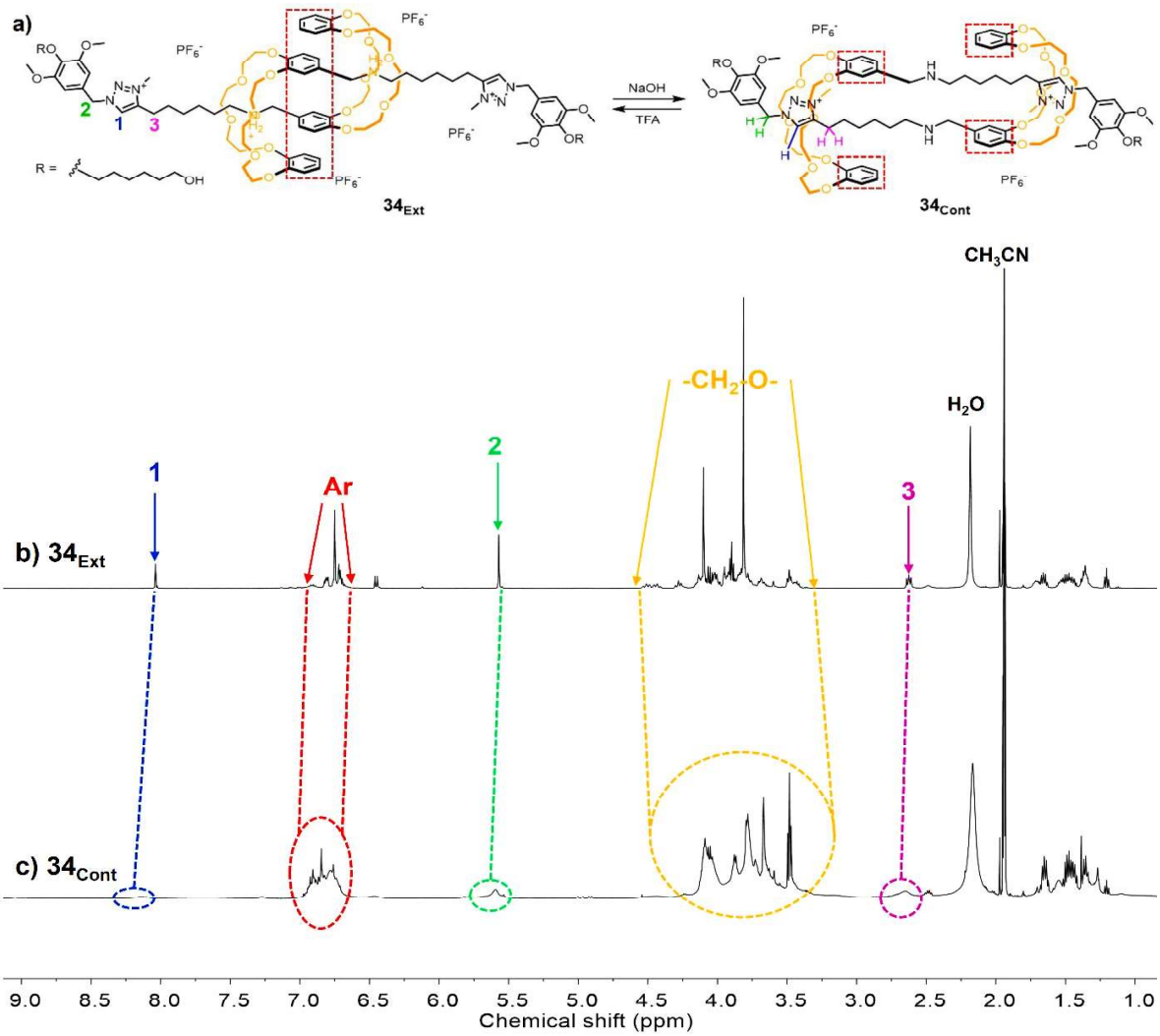

Figure 3.4. (**a**) pH-induced contraction and extension of compound **34**. ^{1}H NMR spectra (400 MHz, CD_3CN, 25 °C) of compounds (**b**) **34**$_{Ext}$ and (**c**) **34**$_{Cont}$ showing different chemical shifts between the extended and contracted states.

3.5. Synthesis of polyurethanes based on [*c*2]daisy chain rotaxane 34_{Ext}

Once the molecular actuation of compound **34** was proved by NMR spectroscopy, this monomer was used for the synthesis of polyurethanes with different diisocyanates, namely isophorone diisocyanate (IPDI), hexamethylene diisocyanate (HDI), and 4,4'-methylene diphenyl diisocyanate (MDI) (Scheme 3.11). The monomers were mixed in dry *N*,*N*-dimethylformamide, using dibutyltin dilaurate as catalyst, but unfortunately, the resulting products were not soluble enough to be analysed by Size Exclusion Chromatography (SEC), precluding the determination of the molecular weight.

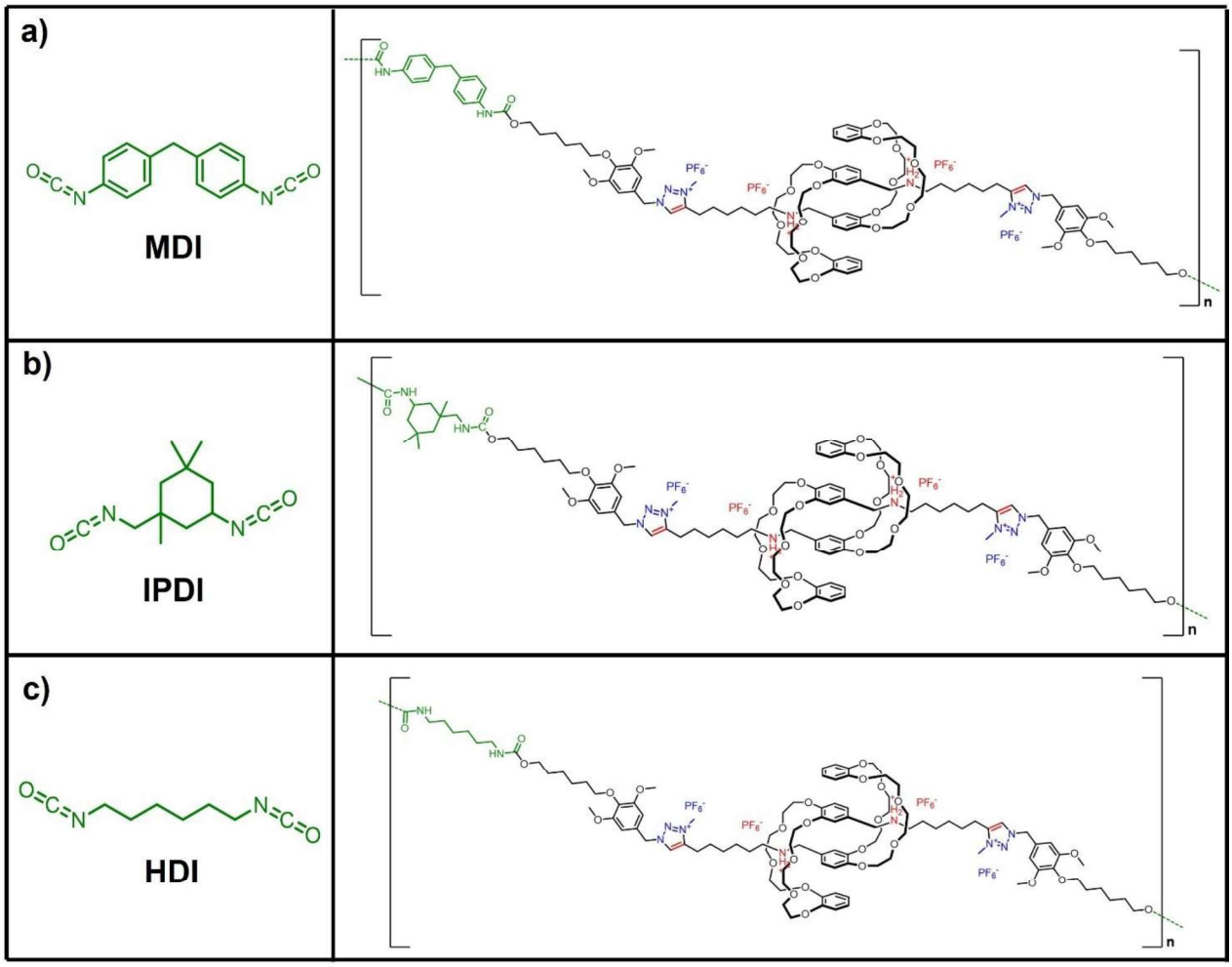

Scheme 3.11. Chemical structures of the employed diisocyanates and their respective expected polymer structures.

In addition, the poor yields and the lack of reproducibility to obtain intermediate **30** encourage us to propose an alternative route in which the reaction yields were reproducible (Scheme 3.12), and without increasing the length of the [*c*2]daisy chain rotaxane with respect to the size of $\mathbf{34}_{Ext}$.

3.6. Synthesis of the [*c*2]daisy chain rotaxane 41_{Ext}

The main step towards 41_{Ext} consists of a Copper(I)-catalysed Azide-Alkyne Cycloaddition (CuAAC) between pseudo[*c*2]daisy chain rotaxane **9** and the *O*-protected azide derivative **38** (Scheme 3.12). The two substrates are unravelled by doubly cutting the C-N bonds of the triazole rings formed. The synthesis of compound **9** was already described in section 2.1, then, we focus on the synthesis of azide derivative **38**.

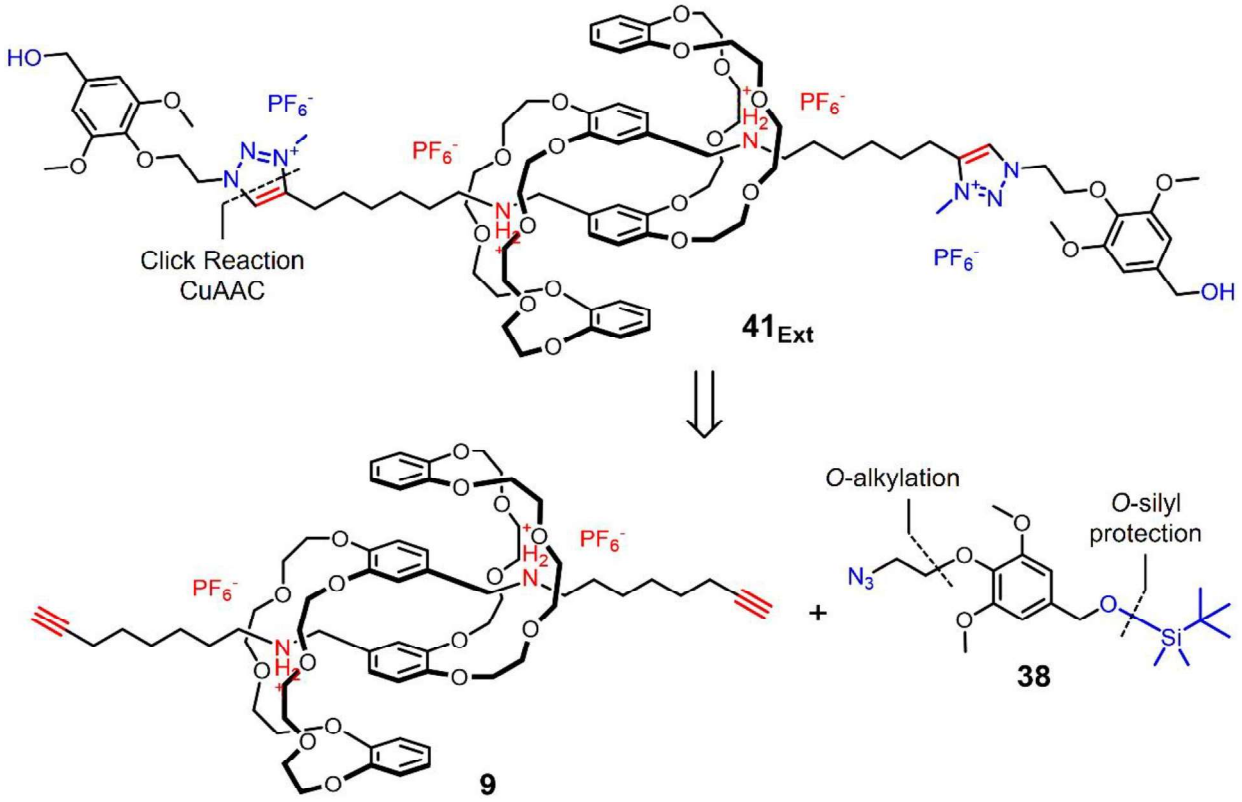

Scheme 3.12. Key retrosynthetic steps towards 41_{Ext}.

Building block **38** was obtained in four synthetic steps as following: the commercially available syringaldehyde was *O*-alkylated using anhydrous potassium carbonate as a base for the Williamson ether synthesis, using dry DMF as solvent and an excess of 1,2-dibromoethane to afford compound **35** in 80% yield.[18] Compound **35** was dissolved in a mixture of THF/MeOH (9:1) at low temperature under inert atmosphere and sodium borohydride was used as mild reducing agent[19] to yield alcohol **36** in 90% yield (Scheme 3.13). Subsequently, the bromine atom of compound **36** was substituted by an azide group through a bimolecular nucleophilic substitution reaction with sodium azide, leading to compound **37** in good yield. Finally, the benzylic alcohol derivate was protected with *tert*-butyldimethylsilyl chloride under standard conditions[20], producing *O*-silyl protected compound **38** in good yield as a colourless oil (Scheme 3.13).

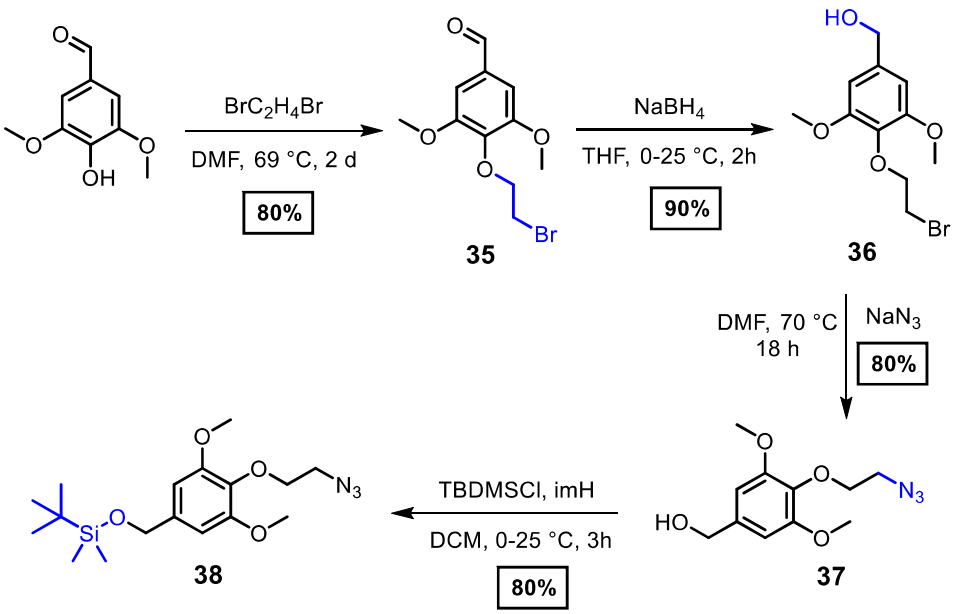

Scheme 3.13. Synthetic route to obtain compound **38**.

The *O*-silyl protected azide derivative **38** and the pseudo[*c*2]daisy chain rotaxane **9** were coupled by the CuAAC "click reaction" using the same procedure as described previously (Scheme 3.14).

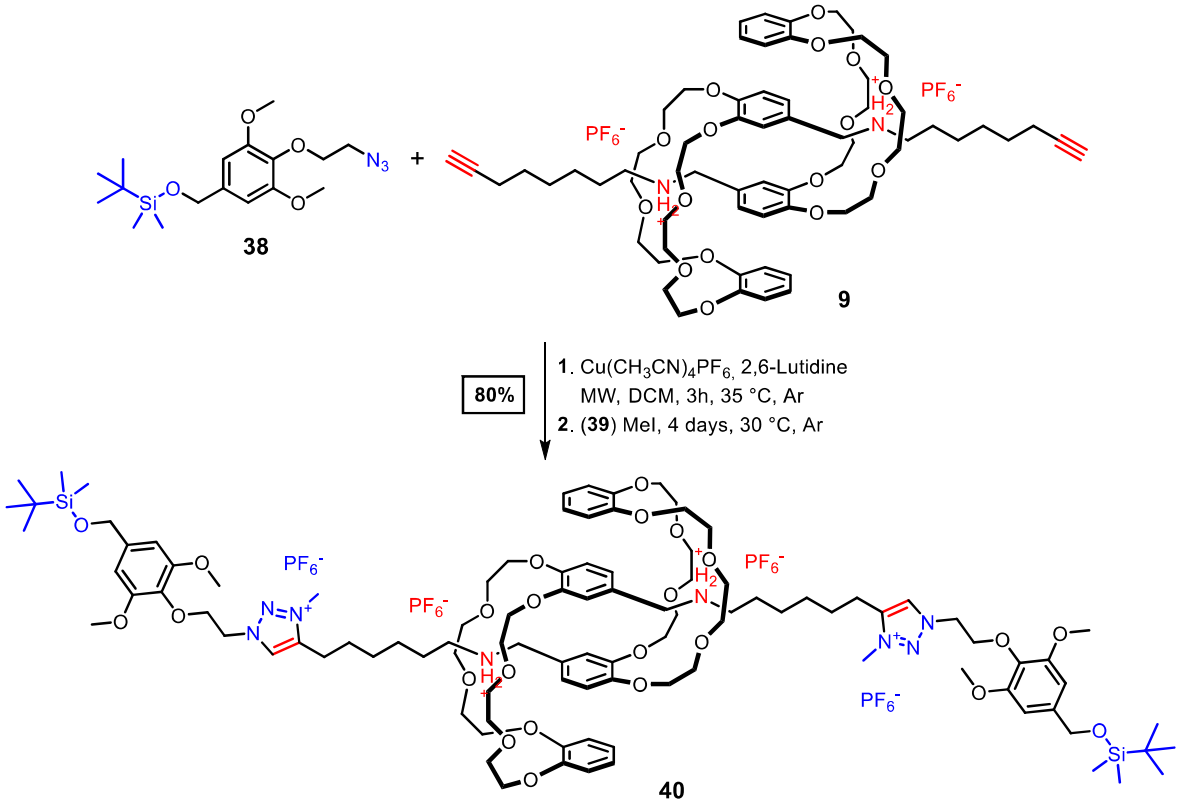

Scheme 3.14. Synthesis of [*c*2]daisy chain rotaxane **40**.

Pure compound **39** was obtained in 70% yield after column chromatography purification, and then triazole rings were quantitatively methylated using a large excess of methyl iodide at 25 °C, over four days to yield compound **40** in 90% yield (Scheme 3.14). The ^{1}H NMR spectrum of **40** shows all the expected proton signals, in particular the signal at 8.45 ppm that corresponds to the vinylic proton H_1 of the triazolium ring. The multiplets that appear between 6.90 and 6.40 ppm correspond to the aromatic protons H_{Ar} and the singlet at 6.54 ppm corresponds to aromatic protons H_2. Two triplets at 4.79 ppm and 4.41 correspond to protons H_3 and H_5 respectively. In the middle of these signals appear one singlet at 4.66 ppm that corresponds to the benzylic protons H_4. In the region between 4.35 and 3.35 ppm appear the broad multiplets for the methylene groups of the crown ether macrocycle, as well as the methoxy groups next to protons H_2 and the methyl group of the triazolium ring. Towards the upfield region of the spectrum, there is a triplet located at 2.76 ppm that corresponds to protons H_6, and two sets of multiplets between 1.75 and 1.35 ppm that correspond to the aliphatic protons (cyan colour). Finally, the *tert*-butyl and dimethyl groups attached to the silyl protecting group at 0.94 ppm and 0.10 ppm are observed at high field of the spectrum (Figure 3.5).

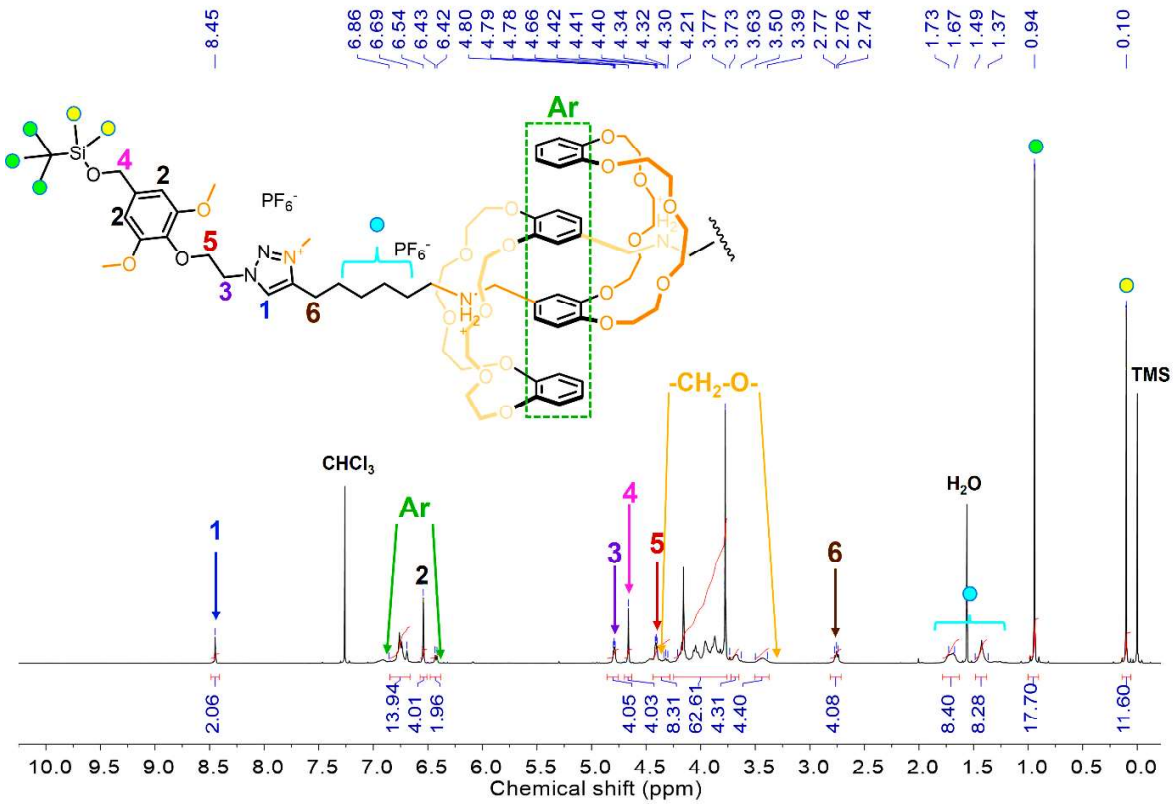

Figure 3.5. ^{1}H NMR spectrum of compound **40** in $CDCl_3$ at 25 °C (400 MHz).

[*c*2]Daisy chain rotaxane **40** was dissolved in a 2:1 mixture of THF/HCl 1 M for thirty minutes leading to a white precipitate, which corresponds to [*c*2]daisy chain **41**$_{Ext}$ having OH ending groups (Scheme 3.15).

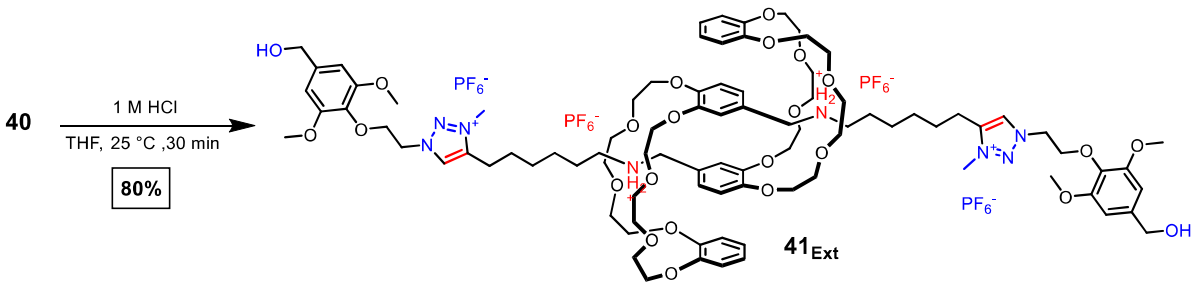

Scheme 3.15. Synthetic step to obtain **41**$_{Ext}$.

The pH-induced actuation was carried out in a mixture of $CHCl_3/CH_3CN$/NaOH 1 M (2:1:2) in order to obtain **41**$_{Cont}$ (Figure 3.6a). Such molecular movement was observed by ^{1}H NMR, with a behaviour similar to the one observed for **34**$_{Cont}$ (Figure 3.6b). Differences raised mainly from the broadening and low field shifting for signals corresponding to protons H_3 and H_5. In addition, the aliphatic protons shifted towards high field since they are sandwiched by the aromatic rings of the macrocycle.

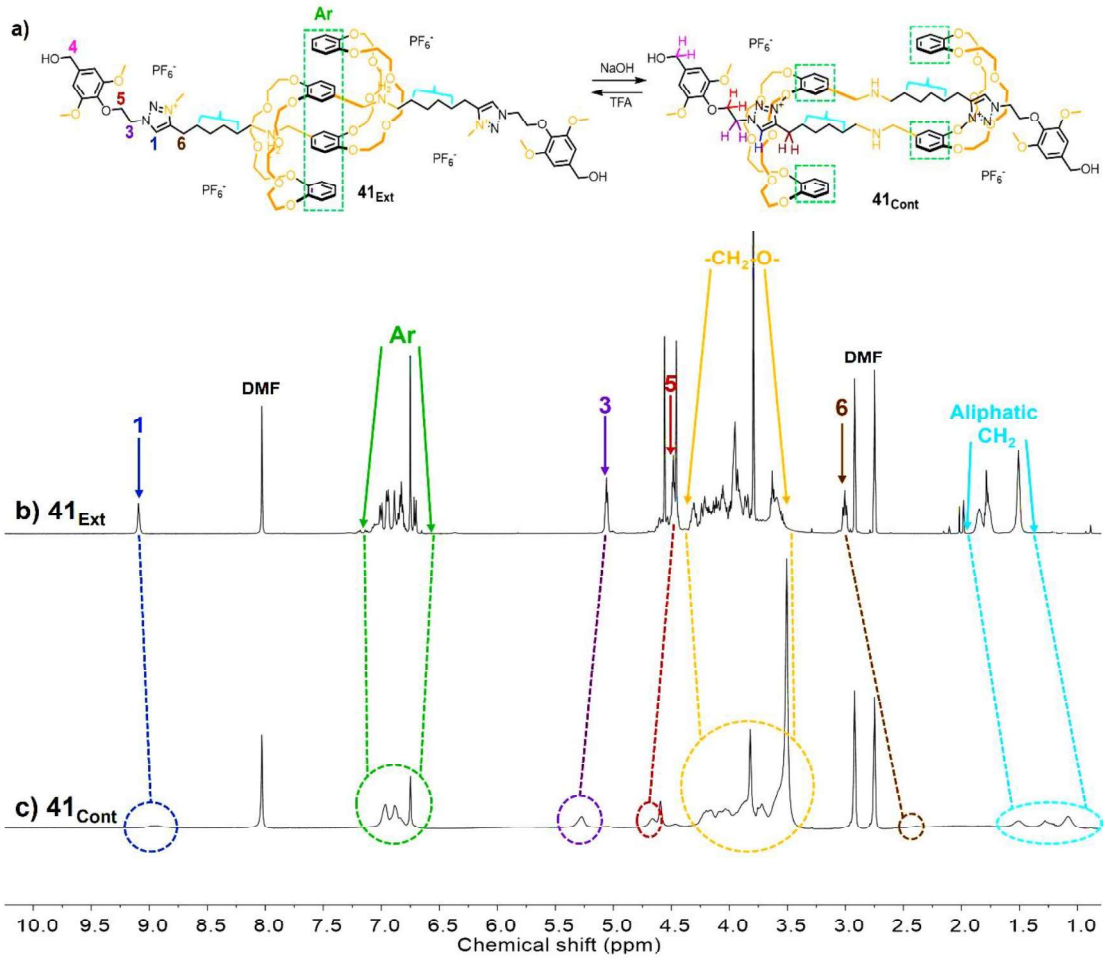

Figure 3.6. (**a**) pH-induced contraction and extension of compound **41**. ^{1}H NMR spectra (400 MHz, DMF-d_7, 25 °C) of compounds (**b**) **41**$_{Ext}$ and (**c**) **41**$_{Cont}$ showing different chemical shifts between the extended and contracted states.

3.7. Synthesis of polyurethanes based on [*c*2]daisy chain rotaxane 41_{Ext}

Once the molecular actuation of **41** was proved by NMR means, it was used as monomer in the synthesis of polyurethanes testing some diisocyanates. Isophorone diisocyanate, hexamethylene diisocyanate and 4,4'-methylene diphenyl diisocyanate were mixed separately with $\mathbf{41_{Ext}}$, using dry *N*,*N*-dimethylformamide as solvent and dibutyltin dilaurate as catalyst. Unfortunately, for the second time, the products obtained from the subsequent attempts of polymerisation were not soluble enough to be analysed by Size Exclusion Chromatography (SEC), precluding the determination of the molecular weight.

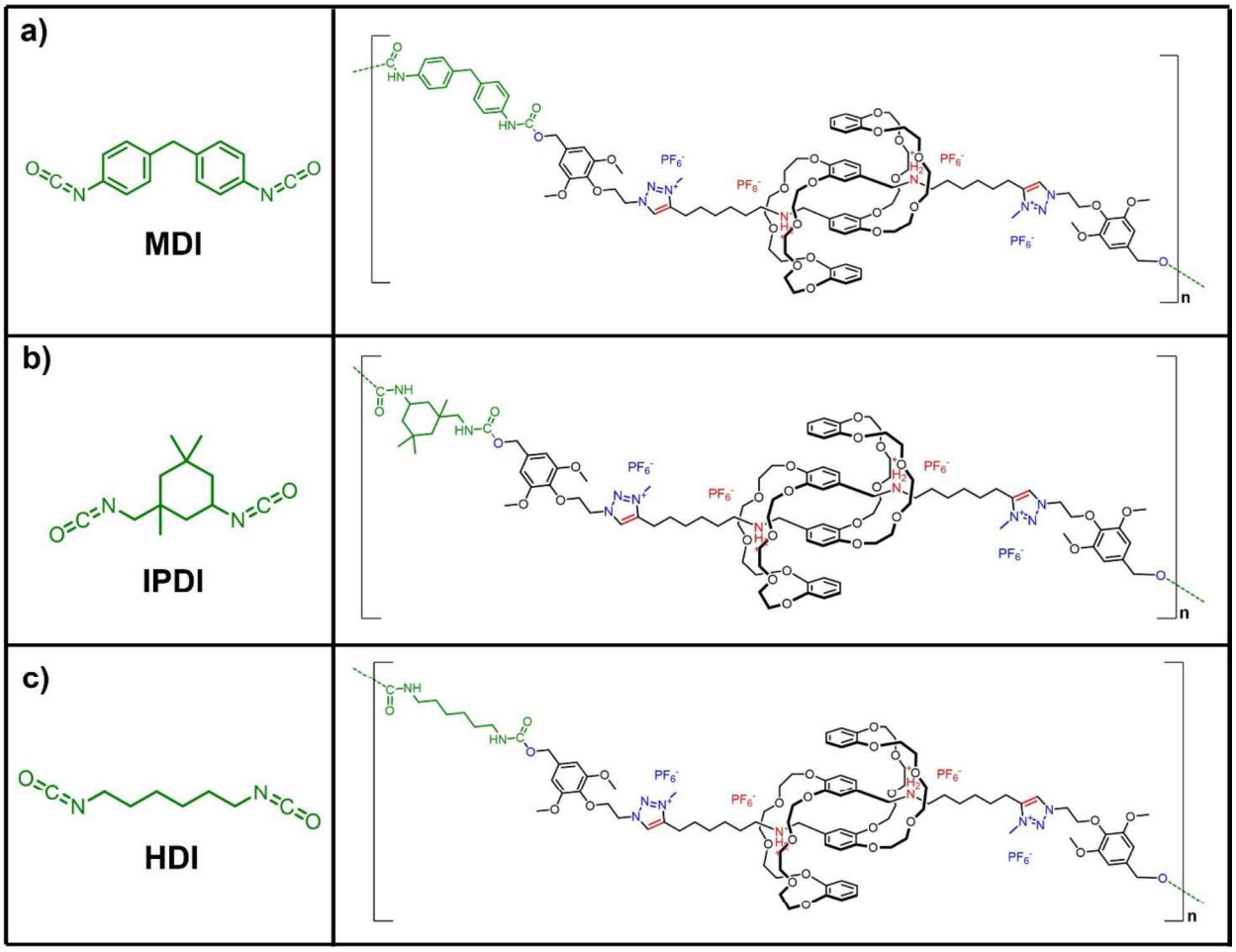

Scheme 3.16. Chemical structures of the employed diisocyanates and their respective expected polymer structures.

3.8. Conclusions

Four synthetic strategies were tested to obtain [*c*2]daisy chain rotaxanes for polymerisation with diisocyanates. From the first strategy, we can conclude that fluoride ions promote the unthreading process of rotaxanes, at least when the source of fluoride ions is tetrabutylammonium fluoride. We have to mention that other sources of fluoride were not tested since it was not the main purpose of this project.

The second strategy could not be carried out because we did not succeed to obtain the *O*-alkylated aldehyde **26** neither in a reproducible manner, nor in high yields. The last two synthetic routes allowed us to obtain [*c*2]daisy chain monomers, in spite of the synthesis of intermediate **30** presented low yields and reproducibility. However, the investigation about the polymerisation of pH-switchable [*c*2]daisy chain rotaxanes was limited due to solubility issues found with the obtained products. In all the cases, it was not possible to form a soluble material to be studied and characterised.

As perspective of this chapter, we propose the use of spacers between [*c*2]daisy chain monomers and the diisocyanates. This will probably allow to obtain materials soluble in common organic solvents and with flexible properties, depending on the nature of the chain extender.

References

[1] J. O. Akindoyo, M. D. H. Beg, S. Ghazali, M. R. Islam, N. Jeyaratnam, A. R. Yuvaraj, *RSC Adv.* **2016**, *6*, 114453.

[2] O. Bayer, *Angew. Chem.* **1947**, *59*, 257.

[3] H. Engels, H. Pirkl, R. Albers, R. W. Albach, J. Krause, A. Hoffmann, H. Casselmann, J. Dormish, *Angew. Chem. Int. Ed.* **2013**, *52*, 9422.

[4] Z. S. Petrovic, J. Ferguson, *Prog. Polym. Sci.* **1992**, *16*, 695.

[5] K. M. Zia, H. N. Bhatti, I. A. Bhatti, *React. Funct. Polym.* **2007**, *67*, 675.

[6] A. V. Menon, G. Madras, S. Bose, *Polym. Chem.* **2019**, *10*, 4370.

[7] T. J. Wallin, J. Pikul, R. F. Shepherd, *Nat. Rev. Mater.* **2018**, *3*, 84.

[8] R. Mutlu, G. Alici, M. in het Panhuis, G. M. Spinks, *Soft Robot.* **2016**, *3*, 120.

[9] A. Harynska, I. Gubanska, J. Kucinska-Lipka, H. Janik, *Polymers (Basel).* **2018**, *10*, 1304.

[10] J. Sawada, H. Sogawa, H. Marubayashi, S. Nojima, H. Otsuka, K. Nakajima, Y. Akae, T. Takata,

Polymer (Guildf). **2020**, *193*, 122358.

[11] S. D. Schnell, A. Linden, K. Gademann, *Org. Lett.* **2019**, *21*, 1144.

[12] H. Y. Zhou, Y. Han, Q. Shi, C. F. Chen, *J. Org. Chem.* **2019**, *84*, 5872.

[13] H. Y. Zhou, Y. Han, Q. Shi, C. F. Chen, *European J. Org. Chem.* **2019**, *2019*, 3406.

[14] D. Aoki, S. Uchida, T. Takata, *Angew Chem Int Ed* **2015**, *54*, 6770.

[15] Y. Gu, Y. Han, C. Chen, *Supramol. Chem.* **2015**, *27*, 357.

[16] E. J. Corey, A. Venkateswarlu, *J. Am. Chem. Soc.* **1972**, *94*, 6190.

[17] P. Patschinski, C. Zhang, H. Zipse, *J. Org. Chem.* **2014**, *79*, 8348.

[18] E. N. Guidry, J. Li, J. F. Stoddart, R. H. Grubbs, *J. Am. Chem. Soc.* **2007**, *129*, 8944.

[19] H. C. Brown, S. Krishnamurthy, *Tetrahedron* **1979**, *35*, 567.

[20] Y. Arakawa, S. Nakajima, S. Kang, G. I. Konishi, J. Watanabe, *J. Mater. Chem.* **2012**, *22*, 14346.

Chapter 4
Rational design of electrochemically active poly[*c*2]daisy chain rotaxanes for potential applications in soft robotics

Special thanks to Dr. Damien Dattler for his intellectual contributions and fruitful synthetic discussions, as well as the PhD candidate Leonardo Andreoni for carrying out the electrochemical measurements of both the monomers and the poly[c2]daisy chain rotaxanes, and Dr. Carlo Gotti for the fabrication and micrographs of polymer fibres. Also, I thank Prof. Eric Buhler for his help in the interpretation of the data obtained by neutron and light scattering techniques.

4.1. Artificial muscles for soft robotics: A brief introduction

Systems constructed from bioinspired compliant materials with mechanical properties similar to those found in living organisms are the core of the soft robotics field. These materials are designed and manufactured in a way that can bring man-made machines closer to the natural capabilities of biological systems,[1] rather than artificially assembled rigid robots that have elementary blocks and flexible joints connected by stiff links.[2] The latter are usually made from metallic parts, ceramics and other hard materials, which can represent a risk for safety, especially when they are used to carry out tasks at the human-robot interface. For example, in manufacturing processes at factories, normally, human, and robotic workspaces are separated to mitigate such safety concerns, owing to the lack of flexibility in the conventional actuation mechanisms of rigid robots.

In contrast to rigid-bodied robots, soft robots can be useful to carry out delicate tasks in unstructured and congested environments, since they possess deformable structures made of soft and extensible materials like silicone rubbers, which for example, upon a crash or a collision can absorb much of the energy.[3] The mimicking of biological functions such as the muscle-like actuation allows various applications for these systems. For instance, soft manipulators can be developed from elastomeric materials being able to bend with high curvatures,[4] to adapt their shape to the environment and perform a crawling movement based on an octopus-bioinspired silicon arm[5]; or even to carry out displacements on surfaces under rough conditions with high resilience.[6]

On the other side, skeletal muscles have been considered as one of the best actuators in Nature,[7] because of the features already mentioned in Chapter 1 (Section 1.1). Nowadays, aiming to mimic them is one of the most ambitious challenges for soft robotics. In that direction, some artificial soft actuators have been proposed based on hydrogel composites,[8] smart textiles[9] and origami structures consisting of two-dimensional layered materials.[10] In addition, other materials such as dielectric elastomers made of electroactive polymers like poly(*tert*-butyl acrylate) (PTBA)[11] are capable of producing strains of about 300% upon application of an electric field, and exhibit a temperature dependent bistability.

On the other hand, pneumatic artificial muscles use the pressurisation of a fluid to stimulate an expandable chamber made of a deformable material, with strains of about 15% and peak actuation speeds of about 350 mm s^{-1}.[12] They can produce linear motions along their axial directions when pressurised, being intrinsically compliant owing to the compressibility of the fluid. However, some of the drawbacks of this approach are the need for pressurised air and the slow depressurisation of the muscle.[13]

Some generic requirements for a muscle-inspired soft actuator are high work density, resulting in lighter and more agile devices.[14] Rapid responsiveness and high efficiencies in the contraction are also desired, as well as, high reversibility and controllability with the hand of durability.[15] Therefore, taking inspiration from Nature, a fibrillar approach is needed in order to reproduce the hierarchical organisation of the muscles, and the bundling of the fibres to generate a linear actuation of the contractile units. Actuating fibres can be obtained from different materials including carbon nanotubes and graphene,[16] as well as polymers.[17]

Focarete and co-workers reported a step forward artificial muscles based on hierarchically arranged electrospun polyurethane nanofibers.[18] They demonstrated the possibility to build materials capable to mimic the micrometric arrangements of myofibrils, with performance comparable to our muscles (Figure 4.1). Such bioinspired approach can be envisioned for the construction of engineered soft actuators based on artificial muscles made from polymer–based actuating fibres, which are characterised by flexibility and anisotropy. Therefore, stimuli-responsive polymers are one of the best candidates to provide a straightforward approach to produce synthetic fibrous actuators, since polymers can be easily treated, handled, and transformed into fibres by melting, solvent extruding, or electrospinning processes.

We considered this possibility within the framework of a European collaborative project H2020-FET-OPEN, in order to develop new materials for robotics involving the collective motion of molecular machines. In the MAGNIFY project, we set to the task of designing and obtaining electrochemically stimulable poly[*c*2]daisy chain rotaxanes, capable of changing their length at the nanometre scale upon electrical stimulation, in order to develop controlled molecular contraction and extension at the macroscopic scale.

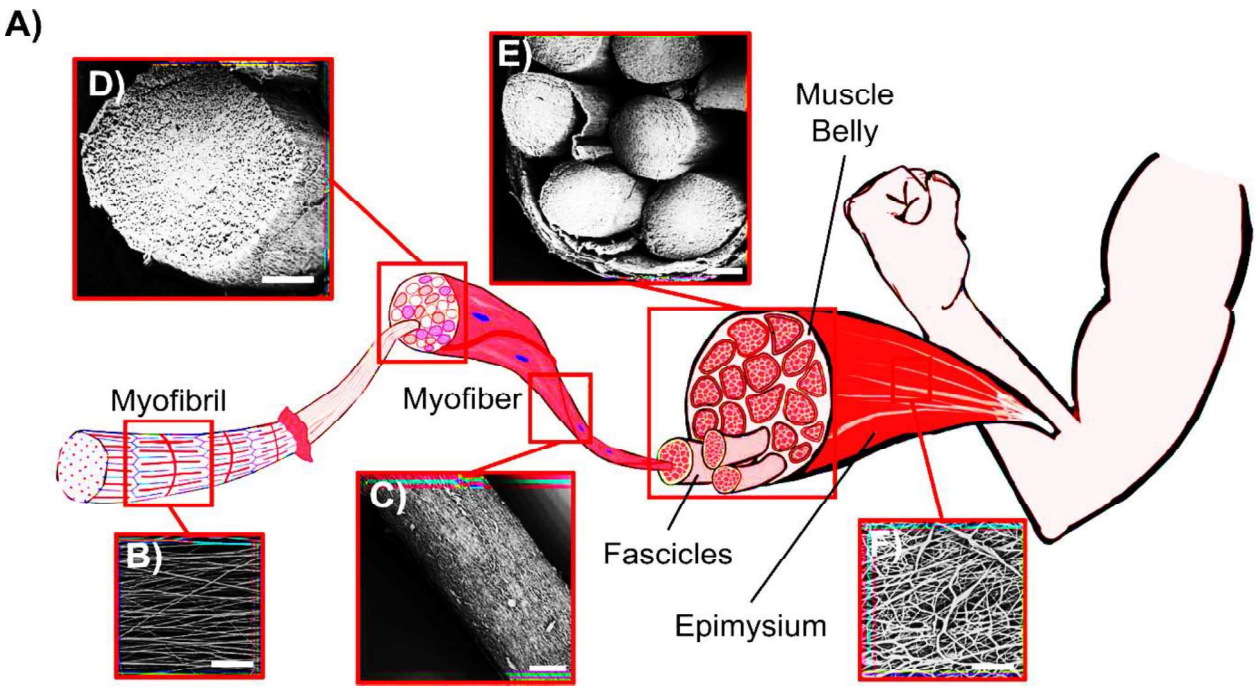

Figure 4.1. a) Representation of the skeletal muscle and the hierarchical organisation of its internal structure. **b)** Set of aligned nanofibers in which a single nanofiber corresponds to a myofibril (scale bar = 20 μm). **c)** Bundling of aligned fibres (scale bar = 100 μm). **d)** Cross-section micrograph displaying the parallel arrangement of the inner nanofibers (scale bar = 100 μm). **e)** Comparison of the cross-section of a biological muscle belly with the one of hierarchically nanofibrous electrospun structures (HNES). **f)** Membrane made of HNES similar to the epimysium membrane that surrounds the muscle belly (scale bar = 100 μm). Adapted from reference[18].

The polymers containing mechanically active interlocked units were designed to form bundles of fibres, as it occurs in natural muscle tissues. In order to actuate this system, electrochemical means were preferred over pH changes in order to avoid the production of chemical waste, to locally stimulate the actuator and to facilitate the potential applications of the obtained material in redox-responsive soft robotics.

Our work consisted mostly in the synthesis and characterisation of the monomer precursors and the corresponding polymers, while their implementation to lead to new materials for robotics has been carried out by our collaborators at the universities of Bologna and Groningen. One part of the synthetic work of this project, as well as the electrochemical characterisation of the monomers and the corresponding polymers were carried out in close collaboration with the research group of Prof. Credi at the Consiglio Nazionale delle Ricerche (CNR) and University of Bologna (UNIBO), specifically with Dr. Jessica Groppi and the current PhD candidate Leonardo Andreoni respectively.

4.2. Design of the poly[*c*2]daisy chains and the corresponding synthetic strategies

The controllable extension/contraction of the [*c*2]daisy chain rotaxane monomer is based upon the design of controllable molecular shuttles, which is widely documented in the literature (Figure 4.2).[19–22] The primary recognition site (blue) can then be modified (e.g., chemically, or electrochemically) such that the non-covalent interactions are weakened or turned off. As a result, the ring moves towards the secondary site (green). The reversibility of the switching reaction enables the reset of the initial state and the subsequent return of the ring onto the original position.

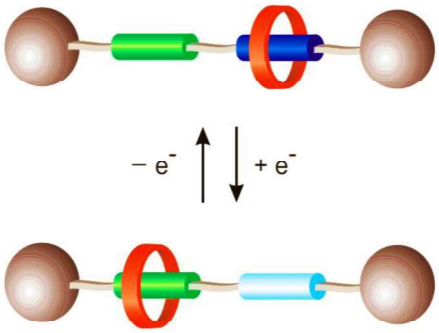

Figure 4.2. Schematic operation of a redox-controllable molecular shuttle based on a [2]rotaxane. The primary and secondary recognition sites are depicted in blue and green, respectively.

The molecular shuttling illustrated in Figure 4.2 can be combined with [*c2*]daisy chain topologies to yield "molecular muscles", that is cyclic rotaxane dimers in which the simultaneous stimuli-induced reversible shuttling of the two rings results into a contraction and extension of the molecule (Figure 4.3a).[23,24] As shown in Figure 4.3b, the serial connection (by covalent or supramolecular bonds) of many units of this kind would afford a linear polymer in which the synchronous activation of the molecular machine "monomers" can lead to mechanical actuation on higher length scales.[25–30]

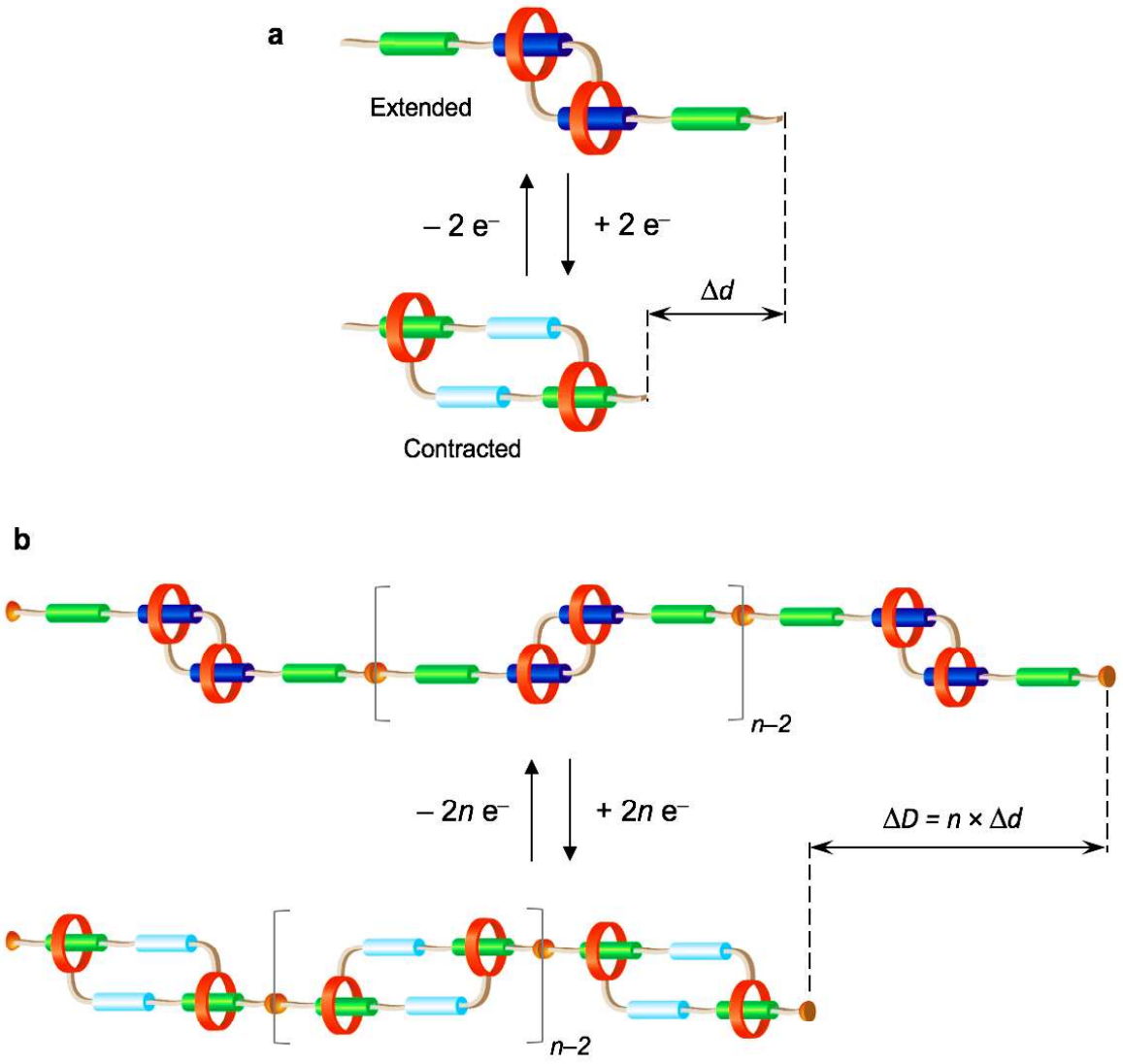

Figure 4.3. a) Electrochemically driven extension-contraction of a [*c2*]daisy chain rotaxane. **b)** If appropriately functionalized at its extremities, a [*c*2]daisy chain rotaxane "muscle" can undergo covalent or supramolecular polymerization to yield a molecular chain in which the collective motion of the individual monomers (Δ*d*) leads to extension-contraction of the chain on a larger scale (Δ*D*).

Until now, however, only bistable daisy chain molecular muscle monomers and polymers that use chemical (pH changes)[31–34] or photochemical (UV light irradiation)[35,36] activation have been extensively developed. Conversely, the molecular muscles needed by MAGNIFY must respond to electrical stimulation.[37,38] We therefore envisioned a first supramolecular polymerization approach using the monomer design shown in Scheme 4.1.

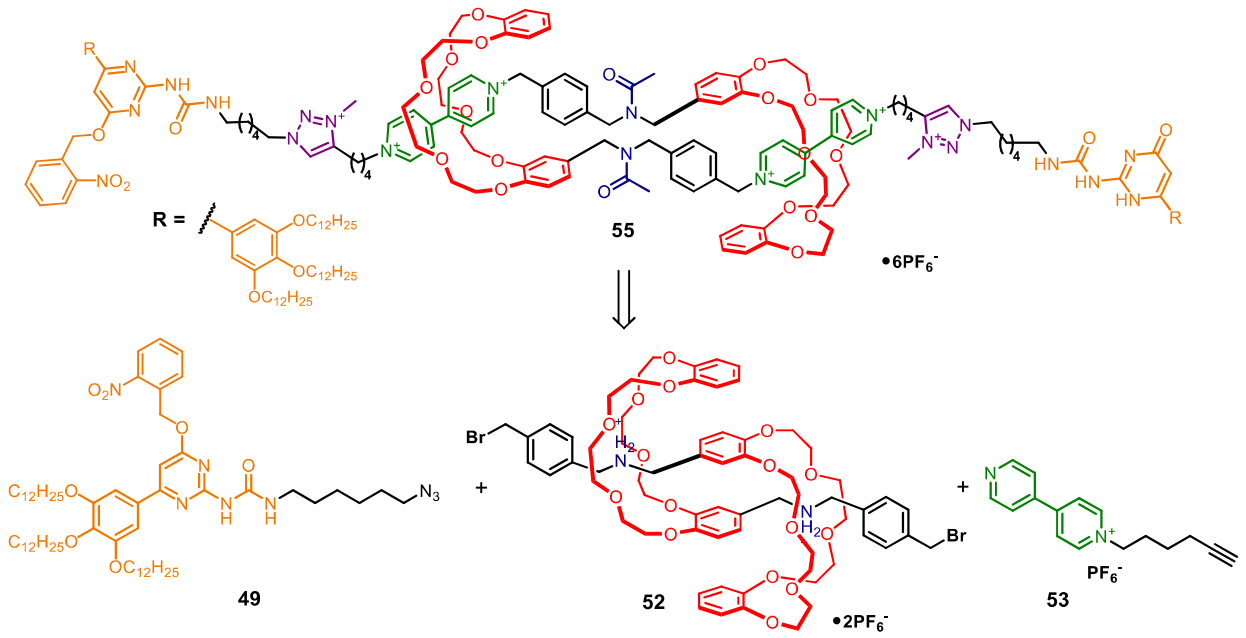

Scheme 4.1. Key intermediates **49**, **52** and **53** for the synthesis of **55**.

The general strategy to afford the [*c2*]daisy chain interlocking motif relies on the well-known self-assembling architecture encompassing [24]crown-8 ethers and the dibenzylammonium group. Once the pseudo[*c*2]daisy chain dimer is assembled, a bipyridinium equipped with an alkyne-terminated arm is attached to each dibenzylammonium moiety. The triazolium is introduced upon Cu-catalysed Alkyne-Azide Cycloaddition (CuAAC) between the alkyne-terminated pseudo[*c*2]daisy chain and an azide derivative containing a Upy-functionalised moiety. The unit R covalently attached to the Upy fragment play the role of stopper for the macrocycles, and also enable the formation of hydrogen-bonding supramolecular polymers upon photo-deprotection of the Upy units under UV irradiation.[39]

4.2.1. Strategy 1: Synthesis of compound 55 by CuAAC reaction

Compound **49** was synthesized following the synthetic route shown in Scheme 4.2. Fully *O*-alkylation of the gallic methyl ester was carried out with 1-bromododecane, followed by saponification reaction to obtain compound **42**. This compound is converted to the acyl chloride derivative in situ by reaction with oxalyl chloride in dry dichloromethane, and subsequently used to carry out the *C*-acylation of ethyl potassium malonate in presence of magnesium chloride and triethylamine,[40] leading to compound **43** (Scheme 4.2).

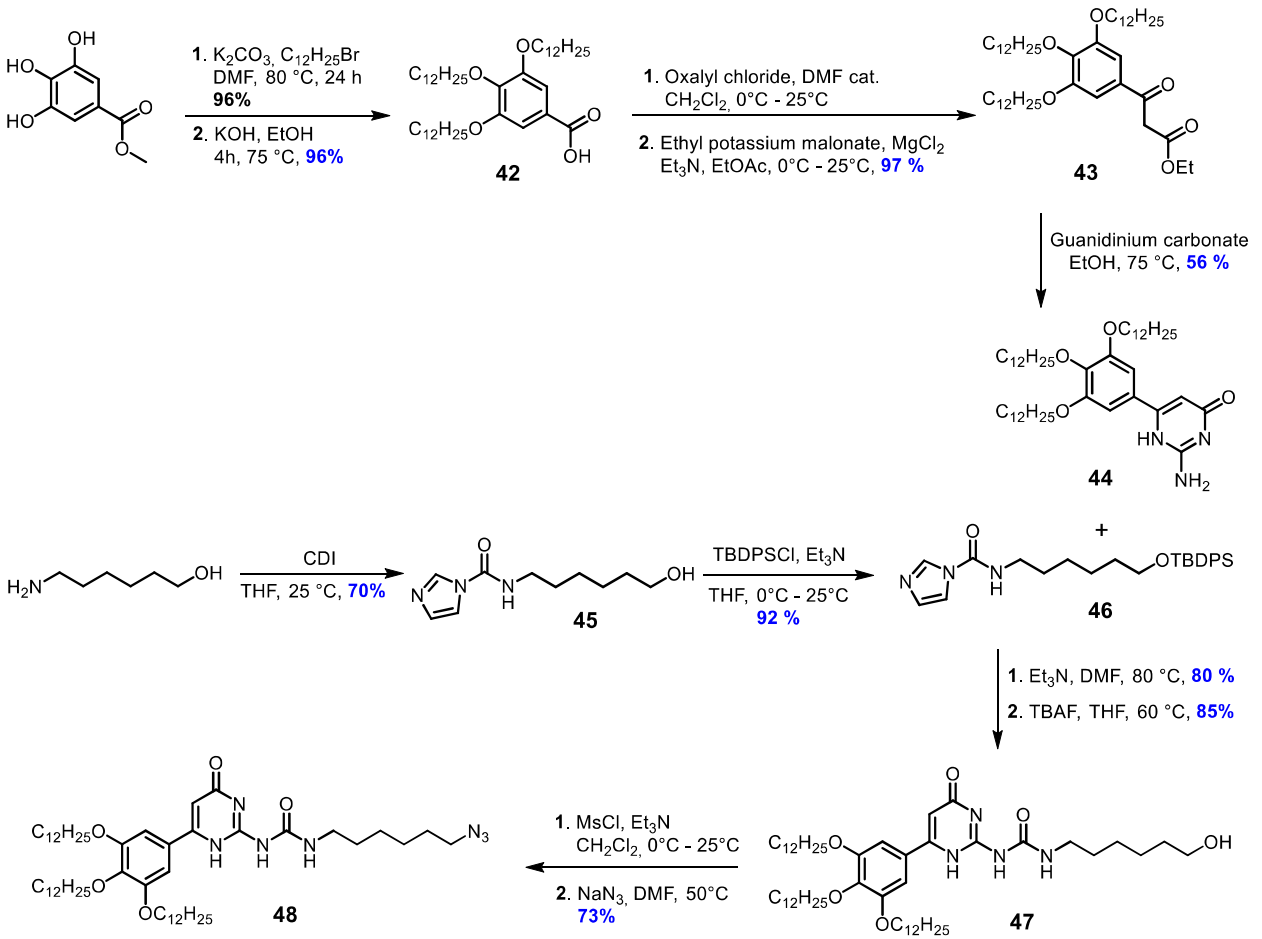

Scheme 4.2. Synthesis of compound **48**. This compound was prepared by Dr. Lara Faour as part of her postdoctoral work.

The interaction of guanidine carbonate with compound **43** in reflux ethanol led to the formation of the pyrimidine derivative **44**. This compound reacted with the carbonyldiimidazole (CDI) derivative **46**, previously obtained by mono-substitution of CDI and *O*-silyl protection with TBDPSCl. As result, compound **47** was obtained and then, transformed to the azide derivative in two steps: first, a mesylation reaction took place under standard conditions, followed by reaction with the azide group, leading to compound **48**. The introduction of the photolabile group *o*-nitrobenzyl can be performed by a reaction between the enol form of the Upy **48** with 1-(chloromethyl)-2-nitrobenzene under basic conditions, providing compound **49** in good yield (Scheme 4.3).

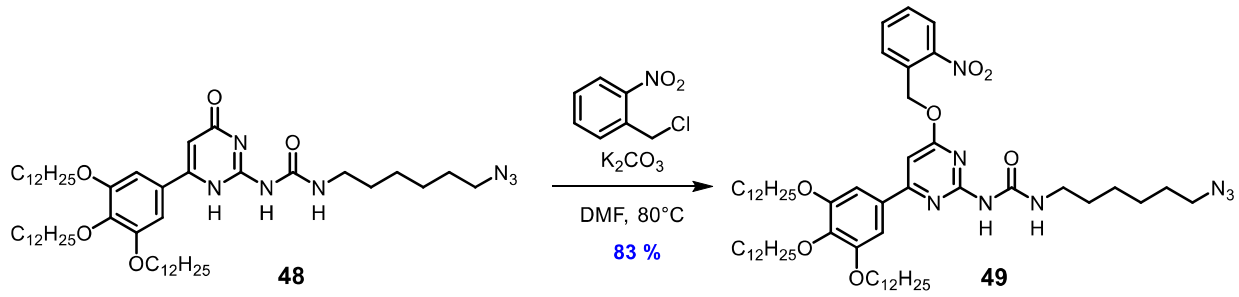

Scheme 4.3. Synthesis of compound **49**. This compound was prepared by Dr. Lara Faour as part of her postdoctoral work.

Compound **6** was put to react with commercially available methyl 4-(aminomethyl)benzoate in boiling toluene overnight. Reduction of the formed imine and the ester group with lithium aluminium hydride in boiling tetrahydrofuran led to secondary benzylamine derivative **50**. The hydroxyl group was replaced by the bromine atom using phosphorus tribromide in dry dichloromethane at low temperature, leading to the brominated compound **51**. This compound was protonated using an aqueous solution of hydrobromic acid, and after anion exchange with a saturated aqueous solution of ammonium hexafluorophosphate, dimer **52** was obtained (Scheme 4.4).

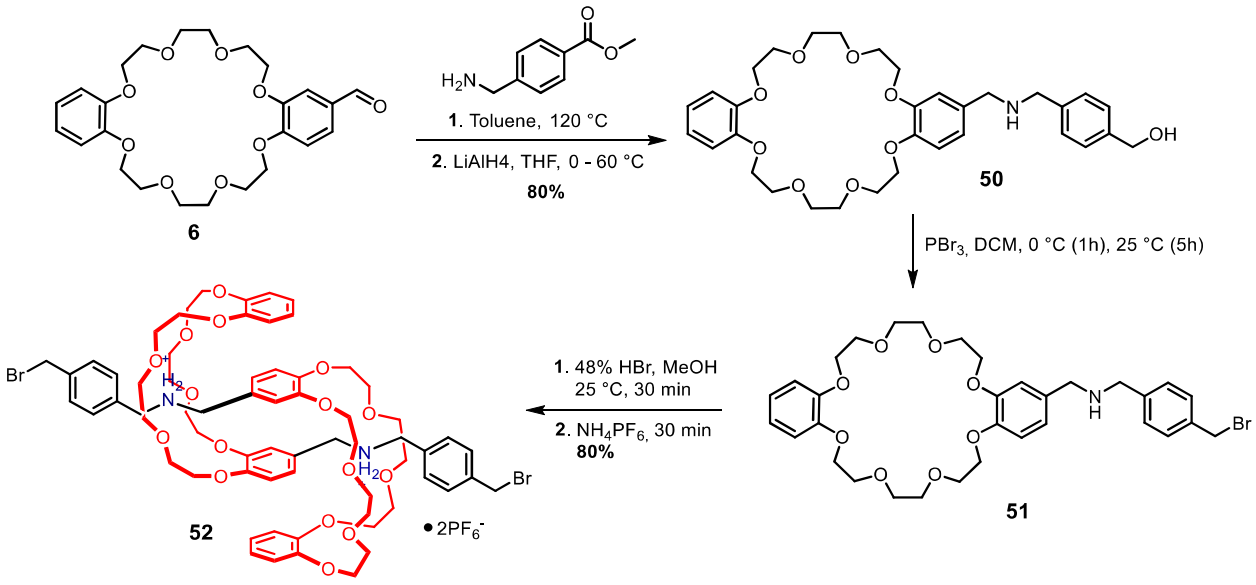

Scheme 4.4. Synthesis of compound **52**.

On the other side, commercially available 4,4'-dipyridyl and 6-chlorohex-1-yne were mixed in dry DMF for two days at 70 °C, leading to compound **53** (Scheme 4.5).

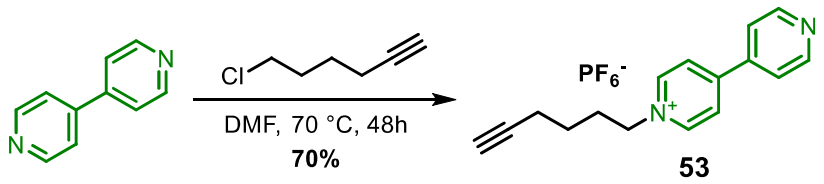

Scheme 4.5. Synthesis of compound **53**.

Pseudo[*c*2]daisy chain rotaxane **52** and bipyridinium **53** were dissolved in a 2:1 mixture of $CHCl_3/CH_3CN$ and heated at 60 °C for four days, leading to the disubstituted compound **54** (Scheme 4.6). Importantly, compounds **52**, **53** and **54** were provided by Dr. Jessica Groppi from the research group of Prof. Credi at CNR.

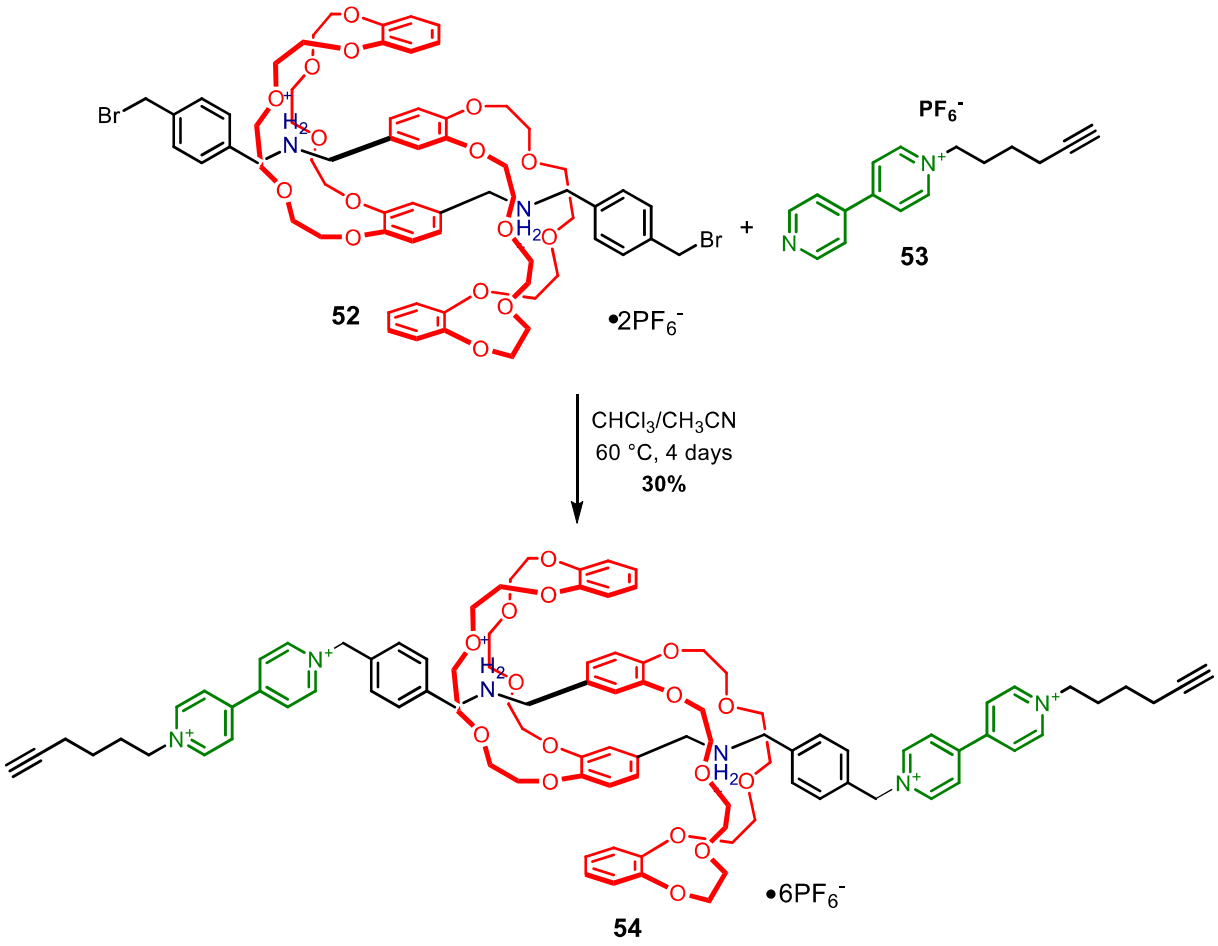

Scheme 4.6. Synthesis of compound **54**.

Compounds **54** and **49** were subjected to CuAAC reaction conditions envisioning the formation of compound **55** (Scheme 4.7), however, after many attempts, this compound was not obtained.

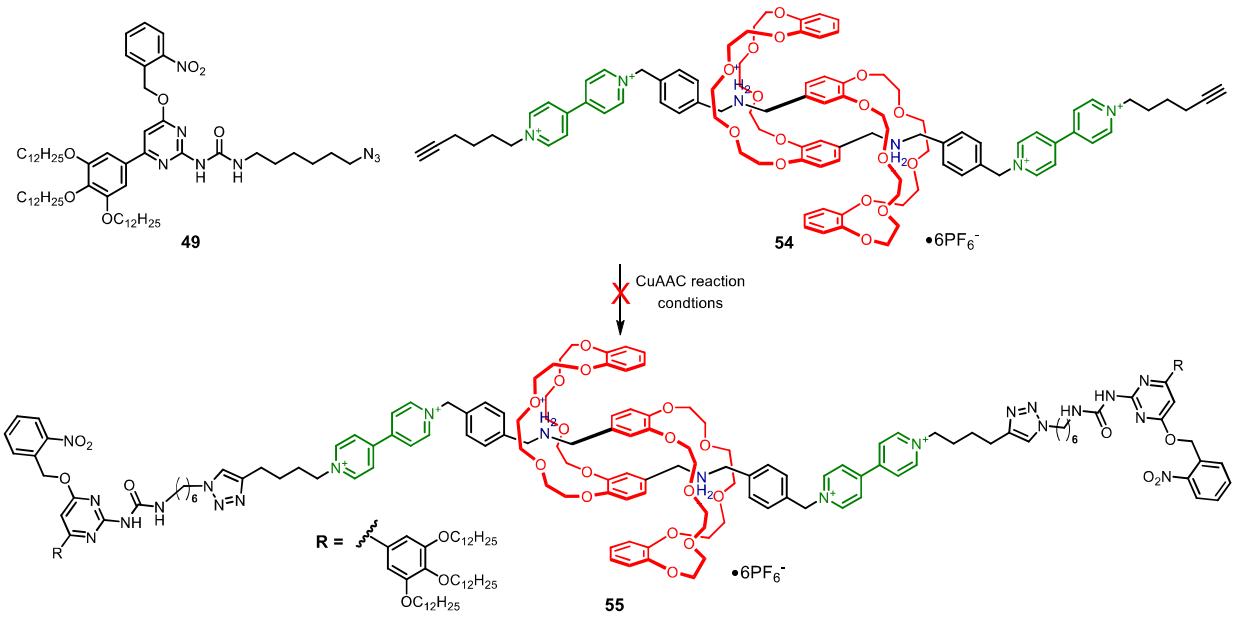

Scheme 4.7. Synthesis of compound **55**.

Monitoring of the reactions tested in order to obtain compound **55** showed in most of the cases, no consumption of the staring materials **49** and **54**. In addition, when dry DMF was tested as reaction solvent, dethreading of compound **54** was observed. After facing many problems while planning to introduce the UPy-protected side chain by click reaction on the corresponding bis-alkyne pseudo[*c*2]daisy chain rotaxane **54**, we envisioned a more convergent pathway with a nucleophilic substitution between bis-benzyl bromide pseudo[*c*2]daisy chain rotaxane **52** (provided by Dr. Groppi from CNR) and the protected-Upy-Bipy moiety **56** as key step (Scheme 4.8).

4.2.2. Strategy 2: Synthesis of compound 55 by S_{N2} nucleophilic substitution

Initially, compound **49** was coupled with compound **53** using copper(I) bromide as catalyst and PMDTEA as stabiliser in dry DMF to obtain compound **56** (Scheme 4.8a). This compound was subjected to reaction with pseudo[*c*2]daisy chain rotaxane **52** in a 2:1 mixture of $CHCl_3/CH_3CN$ for seven days at 65 °C, leading to compound **55** (Scheme 4.8b). However, after several attempts of purification by column chromatography with silica and alumina (neutral), and different mixtures of eluents, compound **55** was always obtained contaminated with the excess of compound **56**.

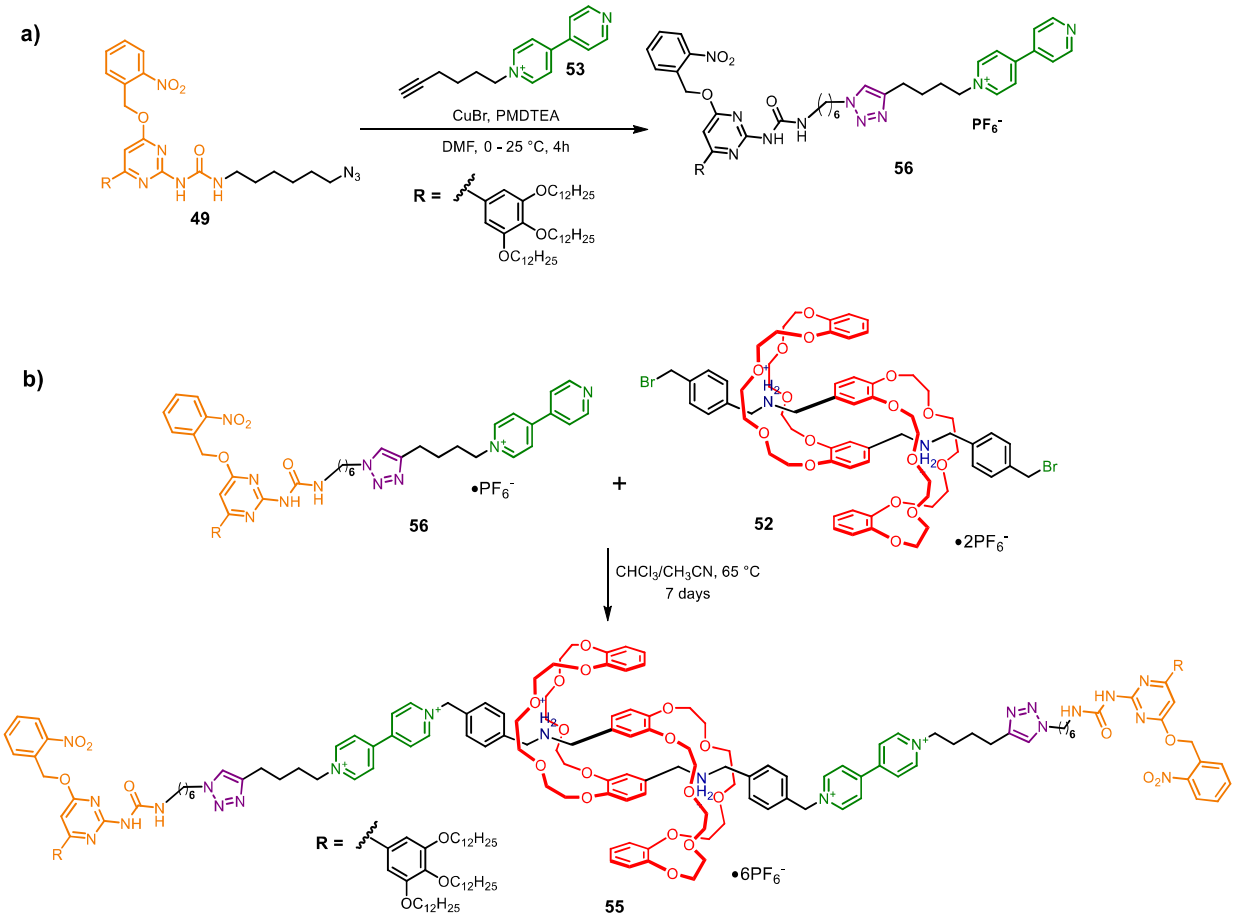

Scheme 4. 8. **a)** Synthesis of compound **56** by CuAAC reaction between compounds **49** and **53**. **b)** Synthesis of compound **55** by nucleophilic substitution of compound **56** over brominated pseudo[*c*2]daisy chain rotaxane **52**.

It is important to mention that an equimolar reaction was carried out to avoid such issue, but instead, the mixture of monosubstituted and disubstituted products was obtained. Thus, these results forced us to propose an alternative route to obtain compound **55**. So far, the assessed synthetic strategies described can be classified as convergent. However, a more linear approach was considered as an alternative to obtain the desired redox-active [*c*2]daisy chain rotaxane (Figure 4.4). Nevertheless, before putting aside definitely the convergent pathways, we decided to change the gallic residue by a *tert*-butyl unit (Scheme 4.9).

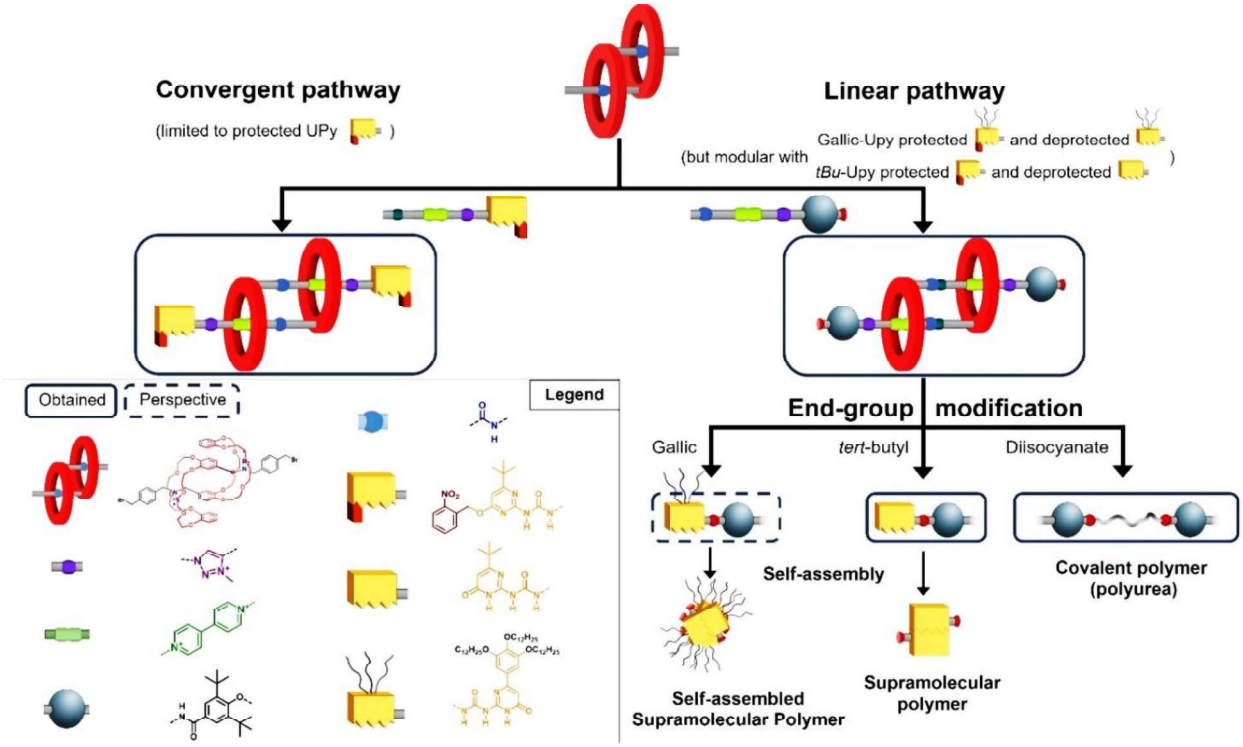

Figure 4.4. Convergent and linear synthetic strategies to obtain redox-active [*c*2]daisy chain rotaxane polymers.

The gallic acid derivative substituent on the Upy fragment precludes the purification of the desired [*c*2]daisy chain, probably by the formation of aggregates between the residues from the starting material and the obtained [*c*2]daisy chain rotaxane. The covalently attached long alkyl chains can interact between them *via* van der Waals forces, as well as the aromatic ring can do by π-π stacking interactions in a spontaneous way. In fact, this molecular association was observed in a previous work published by our research group, in which such molecular association plus the hydrogen bonding interaction between the Upy units, led to the formation of physically crosslinked supramolecular polymers.[39] Thus, replacing the fully *O*-alkylated gallic acid derivative substituent by a *tert*-butyl group was envisioned in order to avoid aggregation (Scheme 4.9).

4.2.3. Strategy 3: Synthesis of [*c*2]daisy chain rotaxane 61

Commercially available ethyl pivaloylacetate in presence of potassium *tert*-butoxide and guanidine carbonate reacted, leading to pyrimidinone **57** that was subjected to reaction with compound **46**, to produce compound **58**, after removing the *tert*-butyldiphenylsilyl group with tetrabutylammonium fluoride. This compound was subject to mesylation reaction under standard conditions, followed by nucleophilic substitution with sodium azide, leading to compound **59**. Finally, this compound reacted with compound **53** under CuAAC conditions to obtain compound **60**.

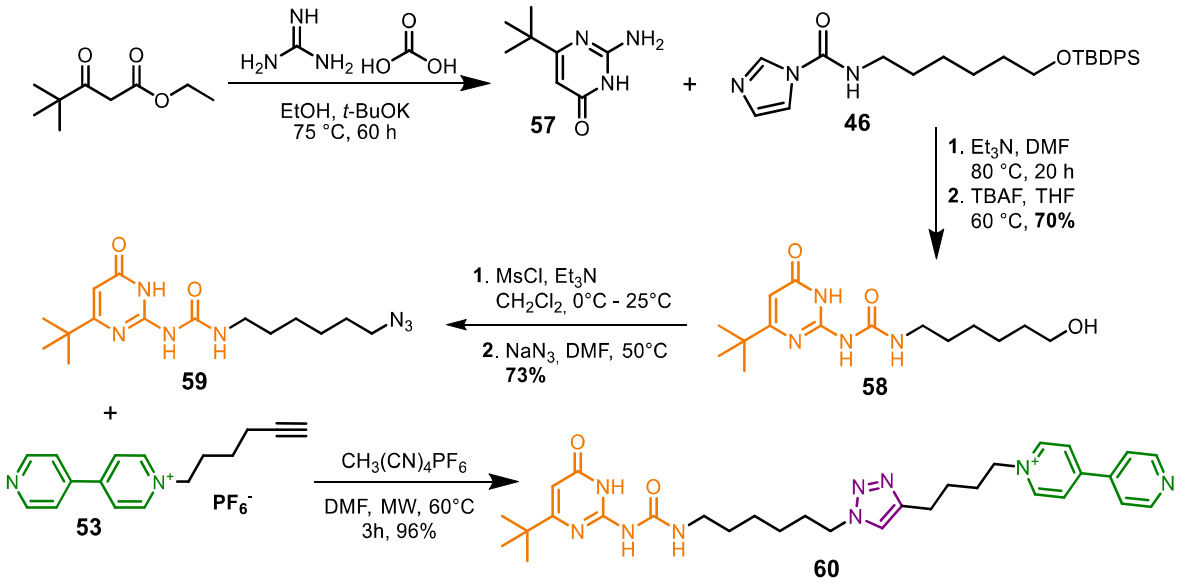

Scheme 4.9. Synthesis of compound **60**.

Subsequently, compound **60** was reacted with pseudo[*c*2]daisy chain rotaxane **52** via a double nucleophilic substitution to form the [*c*2]daisy chain rotaxane **61** as described in Scheme 4.10.

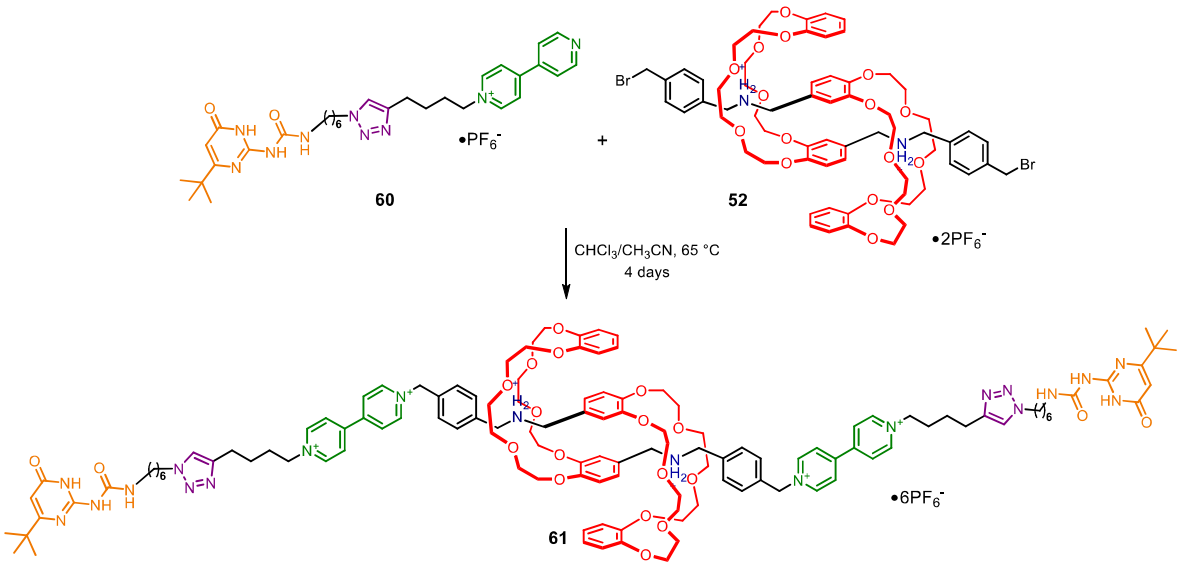

Scheme 4.10. Synthesis of [*c*2]daisy chain rotaxane **61**.

Purification of the crude mixture was performed by silica gel column chromatography using a ternary mixture of $CH_3OH/NH_4Cl/CH_3NO_2$ as eluent. However, although some remaining starting material **60** could be recovered, the [*c*2]daisy chain rotaxane **61** was stuck on the top of the column and could not be eluted. This may be due to the formation of supramolecular polymers since the Upy units were not protected.

4.2.4. Strategy 4: Synthesis of [*c*2]daisy chain rotaxane 64

To circumvent this problem, the *tert*-butyl-Upy-azide **59** was protected with the photolabile *o*-nitrobenzyl group to suppress any spontaneous supramolecular polymerisation. The resulting *tert*-butyl-protected-Upy-azide **62** was engaged in a CuAAC reaction with **53** to afford **63** in quantitative yield (Scheme 4.11).

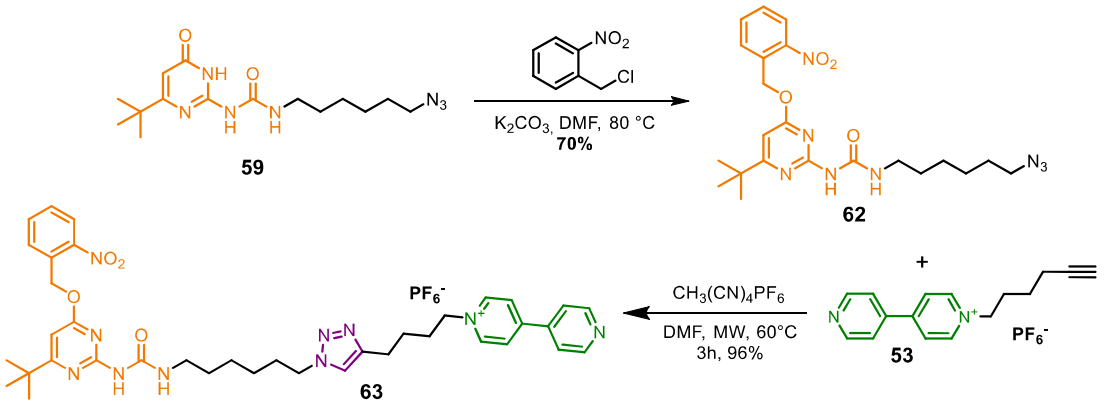

Scheme 4.11. Synthesis of compound **63**.

As described, the *tert*-butyl-protected-Upy-bipy **63** reacted with compound **52** to form the [*c2*]daisy chain **64** (Scheme 4.12).

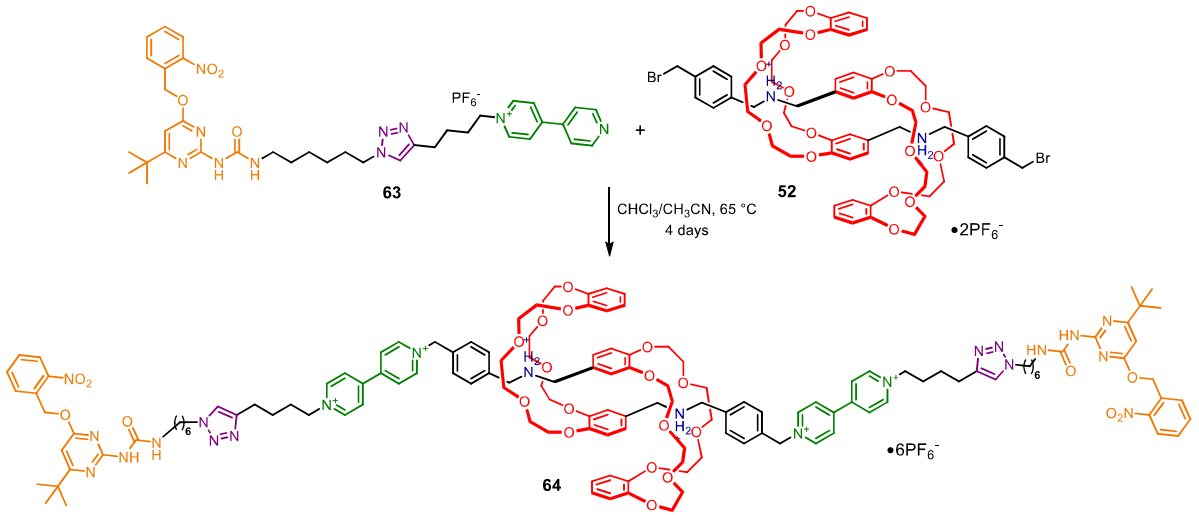

Scheme 4.12. Synthesis of [*c*2]daisy chain **64**.

The reaction was followed-up by UPLC-MS confirming the formation of compound **64** after four days of reaction. The crude mixture was then purified by column chromatography on silica gel (eluent MeOH, MeOH/NH_4Cl/CH_3NO_2 9/1/1 to 7/3/1). Starting material **63** was recovered, then two fractions F1 and F2 were collected and analyzed by UPLC and ^{1}H NMR (Figure 4.5).

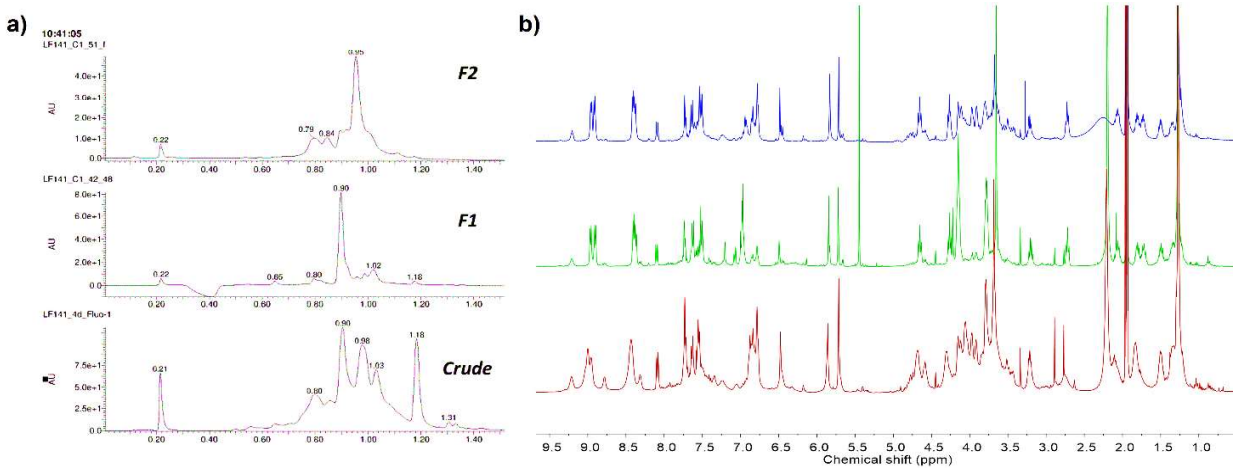

Figure 4.5. **a)** UPLC chromatograms and **b)** ^{1}H NMR spectra for the reaction crude and fractions F1 and F2 from the purification of [*c*2]daisy chain rotaxane **64**.

UPLC-MS analysis proved very informative as the m/z values with z = 2 and 3 for fraction 2 corresponding to [*c2*]daisy chain rotaxane **64**, while fraction 1 showed only M/2 and M/4 indicating the isolation of the unthreaded compound. Additionally, the ^{1}H NMR spectra confirmed the isolation of two different compounds, which differ mainly in the aromatic region around 7.00 ppm and in the region between 3.50 and 5.0 ppm. Subsequent acylation of the ammonium station was conducted on compound **14** in acetonitrile at 0°C using an excess of acetic anhydride in the presence of *N,N*-diisopropylethylamine (DIPEA) (Scheme 4.13).

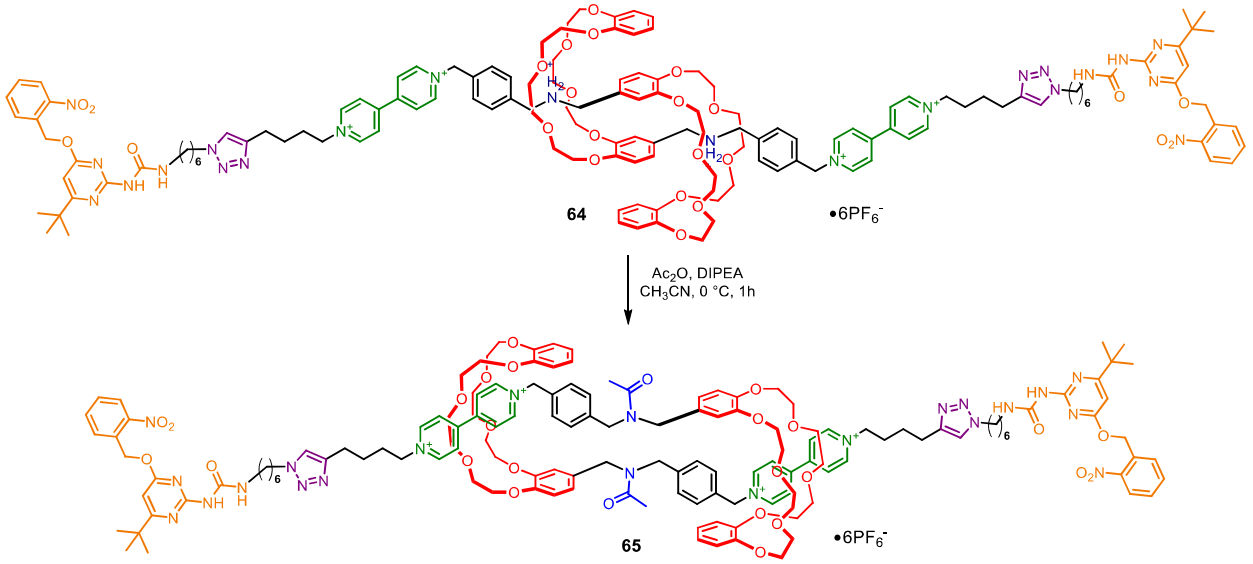

Scheme 4.13. Synthesis of acetylated [*c*2]daisy chain rotaxane **65**.

Full conversion to the desired product was monitored by UPLC-MS confirming the formation of compound **65** after one hour. Finally, *N*-methylation in acetonitrile using methyl iodide followed by precipitation using a solution of ammonium hexafluorophosphate afforded compound **66** with quantitative conversion over one night (Scheme 4.14).

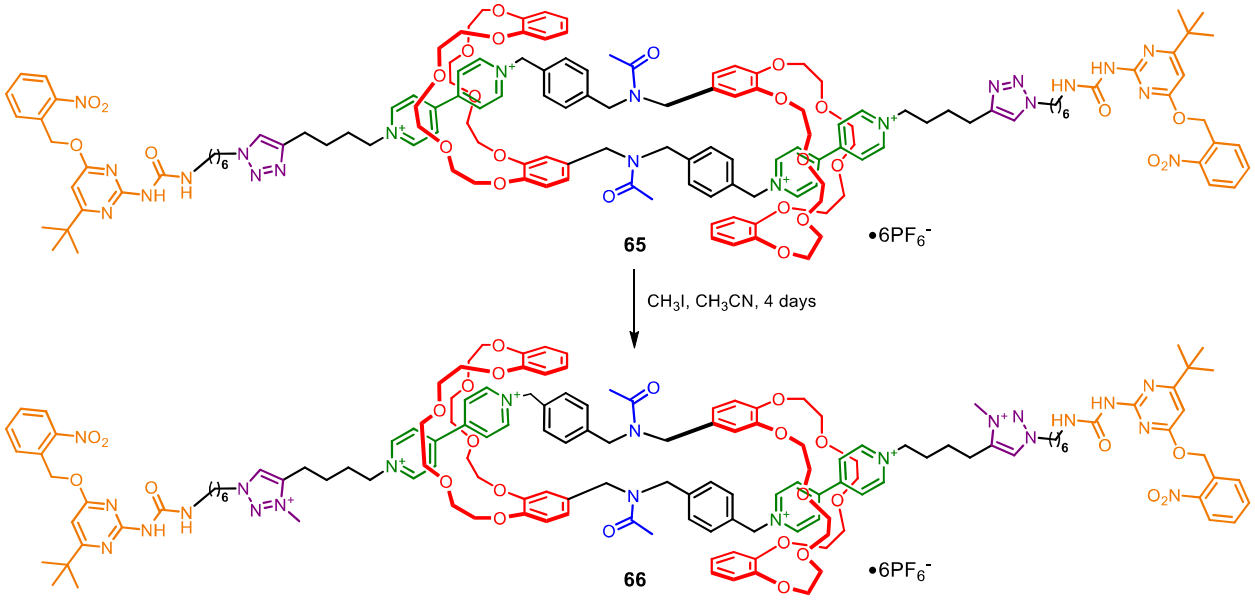

Scheme 4.14. Synthesis of the *N*-methylated compound **66**.

^{1}H NMR spectroscopy (Figure 4.6) and mass spectrometry (Figure 4.7) confirmed the isolation of compound **66** as a single compound.

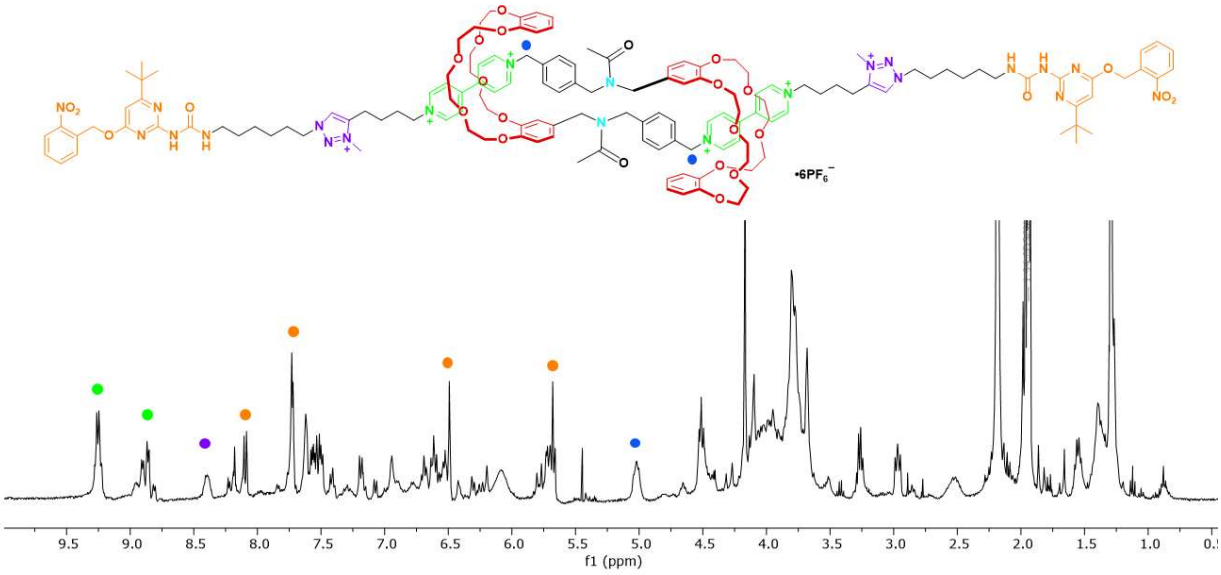

Figure 4.6. ^{1}H NMR spectrum of compound **66** in CD_3CN at 25 °C (400 MHz).

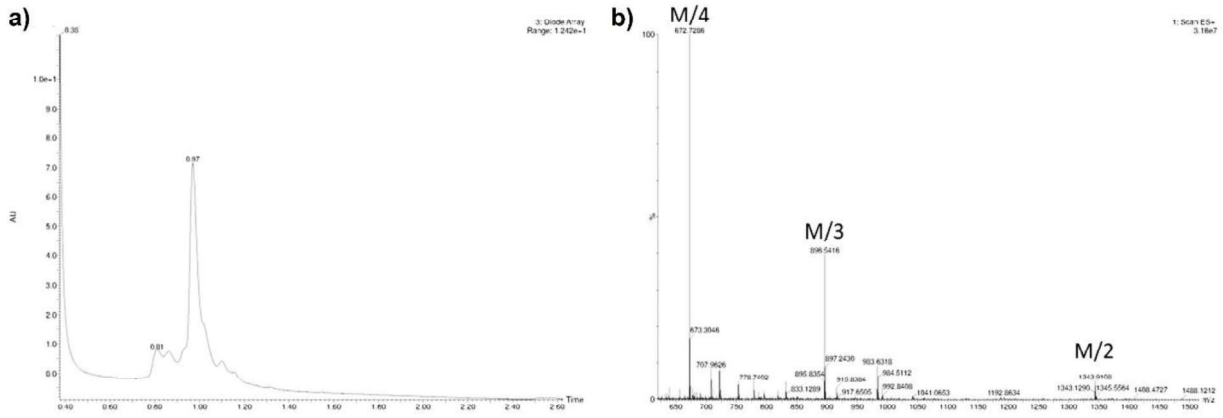

Figure 4.7. a) UPLC chromatogram and **b)** ESI mass spectrum of compound **66**.

Further deprotection of the *o*-nitrobenzyl group on the UPy units leads to the formation of the main chain supramolecular polymer with electrochemically active stations. However, the insolubility of this compound in hydrogen-bonding promoting solvents did not allow the photochemical deprotection and therefore, it was not possible to obtain the deprotected Upy-based [*c*2]daisy chain rotaxane. This results demonstrated the possibility of using a tert-butyl modified Upy fragment to obtain pure [*c*2]daisy chain rotaxanes, however, the convergent strategy was not the best approach to achieve our goals. Thus, we decided to focus on the alternative linear synthetic pathway.

4.3. Strategy 5: Synthesis of [*c*2]daisy chain rotaxane 75a-b

In parallel to the synthetic design following a convergent pathway, we designed another synthetic approach which allows to tune the polymerisation units at a later stage of the synthetic route. This strategy requires the synthesis of [*c2*]daisy chain rotaxane **75**, which can be easily modified on its end chain by different chemistries (urethane formation, amide coupling…) after protecting group removal (Scheme 4.15). This [*c*2]daisy chain rotaxane is synthesized according to the same key double nucleophilic substitution between the already used bis-benzyl bromide pseudo[*c*2]daisy chain rotaxane **52** (sometimes made in our laboratory and sometimes provided by CNR) and a new bipyridinium compound **74** incorporating already the methylated triazole unit. Importantly, one main objective during the development of the synthesis was oriented towards the scalability of all synthetic steps at the gram scale, as sufficient amounts of [*c*2]daisy chain rotaxane are required to reach the ambitious objectives of the MAGNIFY project.

The synthesis of compounds **75a-b** can be divided in two main parts as it was shown in Scheme 4.15: The double charged stopper **74a-b** and the pseudo[*c*2]daisy chain rotaxane **52**.

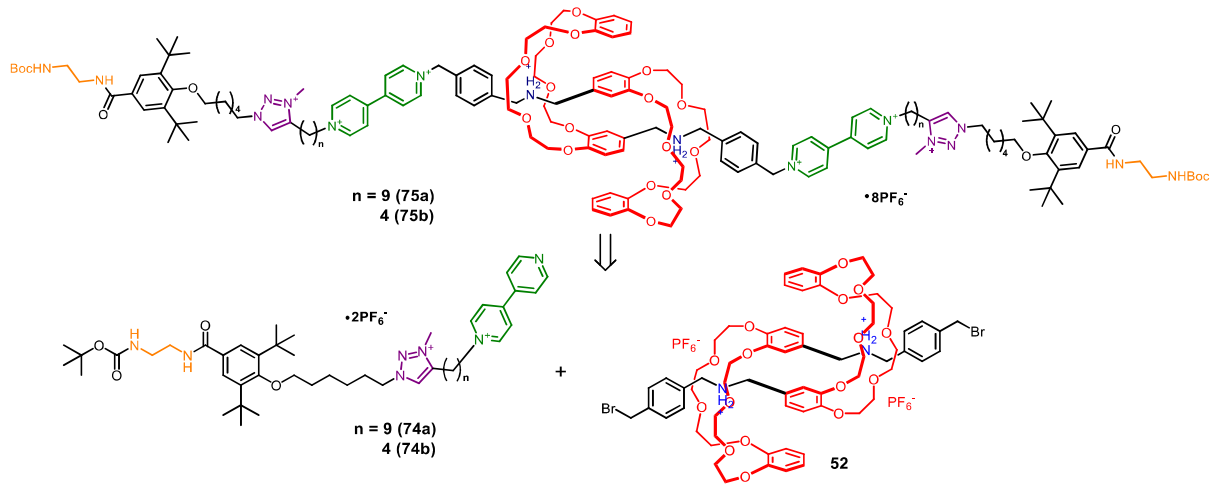

Scheme 4.15. Key steps for intermediate **75a-b.**

The synthesis of compound **52** was already described in Section 4.2. The synthetic route towards stoppers **74a-b** starts with commercially available 3,5-di-*tert*-butyl-4-hydroxybenzoate methyl ester. This compound was subjected to a *O*-alkylation reaction under high concentration conditions, using DMF as solvent and in presence of potassium carbonate as base to form the phenolate ion. This nucleophile poorly reacted with the 1,6-dibromohexane in excess even after one week of reaction. However, once the solvent was changed to methyl ethyl ketone, or 2-butanone, the reaction was completed in four days, forming the *O*-alkylated compound **67** (Scheme 4.16) in moderate yields.

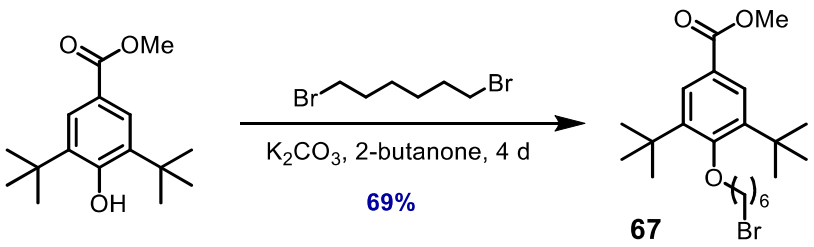

Scheme 4.16. Synthesis of compound **67**.

UPLC analysis of the reaction crude revealed the presence of four peaks (Figure 4.8a). The most intense one corresponds to the desired product **67**, which was confirmed by mass spectrometry analysis. In Figure 4.8b, we can observe the peaks [M+1] and [M+2] for **67** with m/z = 427.45 and 429.45 respectively. Moreover, the peaks with m/z = 371.41 and 373.41 correspond to the peaks [M+1] and [M+2] of a molecular fragment generated by a homolytic cleavage of the C–Br bond of the alkyl chain, and transposition of the bromine atom enabled by a 1,5-rearrangement, forming the brominated compound with two carbon atoms shown in Scheme 4.17.

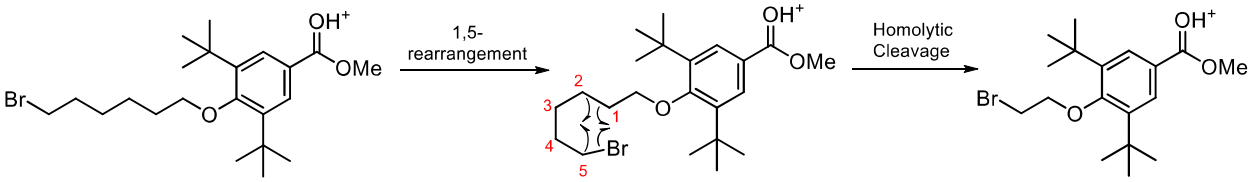

Scheme 4. 17. Proposed mechanism of molecular fragmentation of the molecular ion of compound **67**.

In addition, the peak at 2.78 min corresponds to an impurity very difficult to eliminate by column chromatography, which is reflected in a lower reaction yield. Analysing the mass spectrum (Figure 4.8c), we observed again the peaks [M+1] and [M+2] with the same values of m/z, which indicates that the impurity possesses whether a similar of the same structure to the molecular fragment that was detected in the ionization of compound **67**. This was a clear indication that the impurity came from the reaction between 3,5-di-*tert*-butyl-4-hydroxybenzoate methyl ester with 1,2-dibromoethane. Then, our hypothesis is that a certain percentage of 1,2-dibromoethane was present as contaminant in the commercial 1,6-dibromohexane. Furthermore, we can observe the peaks [M+1] and [M+2] with m/z = 339.37 and 341.47 respectively that corresponds to the molecular fragment formed by the heterolytic cleavage of the ester bond, and subsequent formation of the carbonyl cation, as it is presented in Figure 4.8c. Finally, another molecular fragment is observed, formed by the homolytic cleavage of one *tert*-butyl group at the meta position of the aromatic ring of the molecular ion.

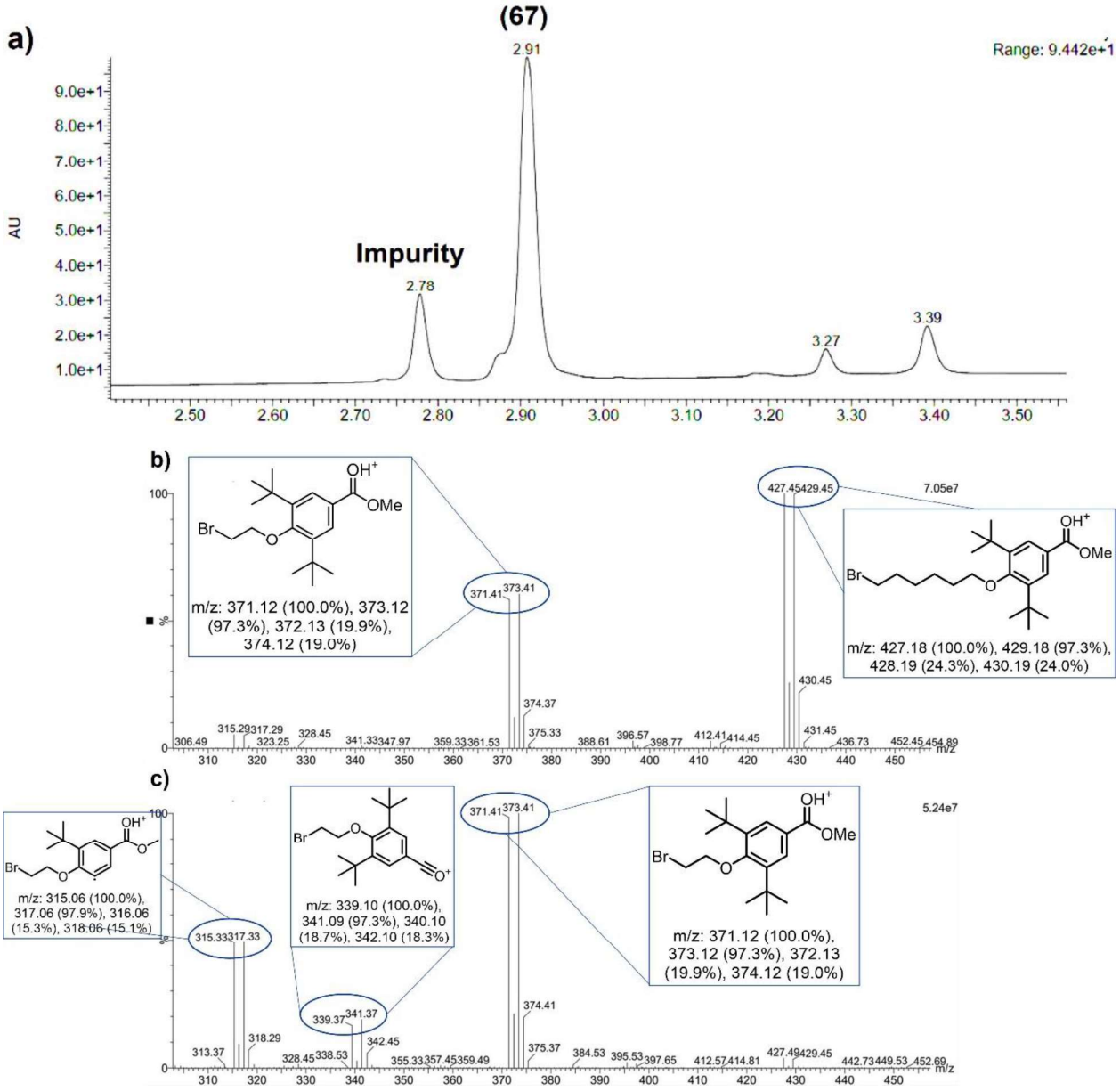

Figure 4.8. (**a**) Chromatogram of the reaction crude of **67**. (**b**) and (**c**) ESI-mass spectra of peaks at 2.91 and 2.78 minutes.

On the other side, the long reaction time (four days) can be attributed to the steric hindrance of the bulky *tert*-butyl groups that preclude the interaction of the phenolate ions with the carbon atom adjacent to the bromine of the alkyl halide, as well as a moderately deactivation of the aromatic ring due to the electron withdrawing effect of the ester group.

Subsequently, the terminal bromine atom of the alkyl tail was replaced by an azide group using sodium azide in DMF as solvent and under high concentration conditions, leading to compound **68** in an almost

quantitative yield (Scheme 4.18). Then, a saponification reaction was carried out to transform the ester group in a carboxylic acid one, using sodium hydroxide (in excess) as base and an aqueous mixture of THF/MeOH/H_2O, giving quantitative access to compound **69** (Scheme 4.18), which was pure enough to be used in the next synthetic steps without chromatographic purification.

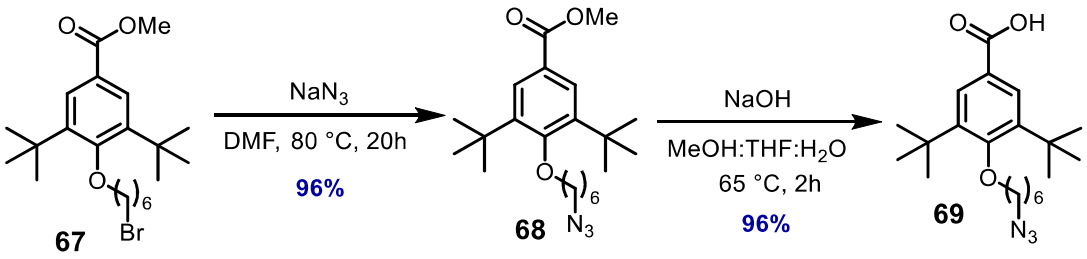

Scheme 4.18. Synthesis of compounds **68** and **69**.

Finally, **69** was involved in a peptide coupling reaction with one side Boc-protected ethylenediamine, using 1-Ethyl-3-(3-dimethylaminopropyl)carbodiimide (EDCI) as an activator of the carboxyl group to form amide **70** (Scheme 4.19). This carbodiimide was preferred over the classic 1,3-dicyclohexylcarbodiimide (DCC) because of its solubility in dichloromethane and of the solubility of the urea byproduct after the amide bond formation, in aqueous solvents and allowing its removal during the workup.[41]

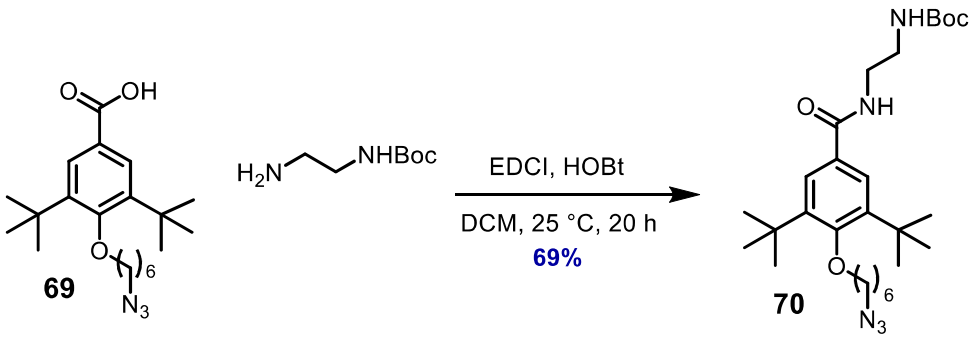

Scheme 4.19. Synthesis of compound **70**.

Despite the kinetics of the condensation is governed by the reaction between the carboxylic acid and the EDCI, *N*-hydroxybenzotriazole (HOBt) was involved. It is widely used for the generation of amide bonds with high yields, by the formation of an activated ester with the carboxylic acid derivative. The HOBt is a good leaving group, which favours the acylation reaction of the primary amine.[42] Figure 4.9 shows the ^{1}H NMR spectrum with all the expected signals for compound **70**.

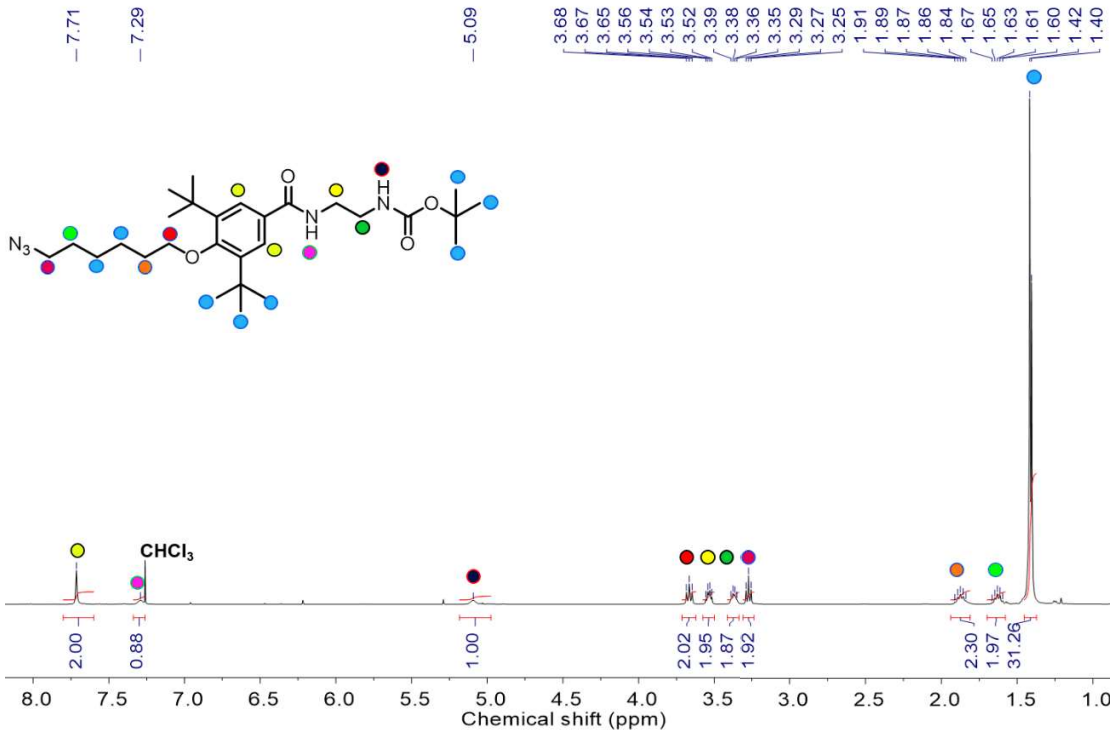

Figure 4.9. ^{1}H NMR spectrum of **70** in $CDCl_3$ at 25 °C (400 MHz).

One of the most important part of our [*c*2]daisy chain systems is the alkyl spacer that links the two redox-active recognition sites for the crown ether, the 4,4'-bipyridinium and the triazolium rings, as the distance between them determines the nanoscopic motion achieved by the mechanically interlocked molecules. Therefore, we carried out the synthesis of two alkyl spacers having different length, in order to study their influence on the kinetics of the molecular motion of the macrocycles once the molecule is actuated. The commercially available undec-10-yn-1-ol was converted into a primary alkyl bromide using the traditional conditions of the Appel's reaction,[43] employing carbon tetrabromide and triphenylphosphine, leading to the alkyl bromide **71a** as a colourless liquid with 80% yield after purification by column chromatography. The same procedure was carried out with the commercially available hex-5-yn-1-ol to obtain alkyl bromide **71b**, also as a colourless liquid but in lower yield (70%) due to its high volatility. (Scheme 4.20)

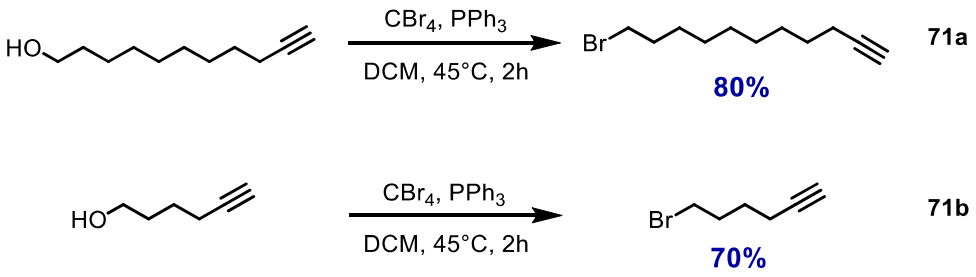

Scheme 4.20. Synthesis of the alkyl bromide spacers **71a** and **71b**.

Having compounds **70** and 7l**a-b** in hands, we carried out the construction of the *N*-methyltriazolium moiety, which acts as a molecular station for the macrocycle DB24C8 in rotaxane systems.[44] Thus, azide derivative **70** was coupled with haloalkynes **71a-b** separately through a Copper(I)-catalysed Azide-Alkyne Cycloaddition (CuAAC) "click reaction" leading to compound **72a-b** (Scheme 4.21).

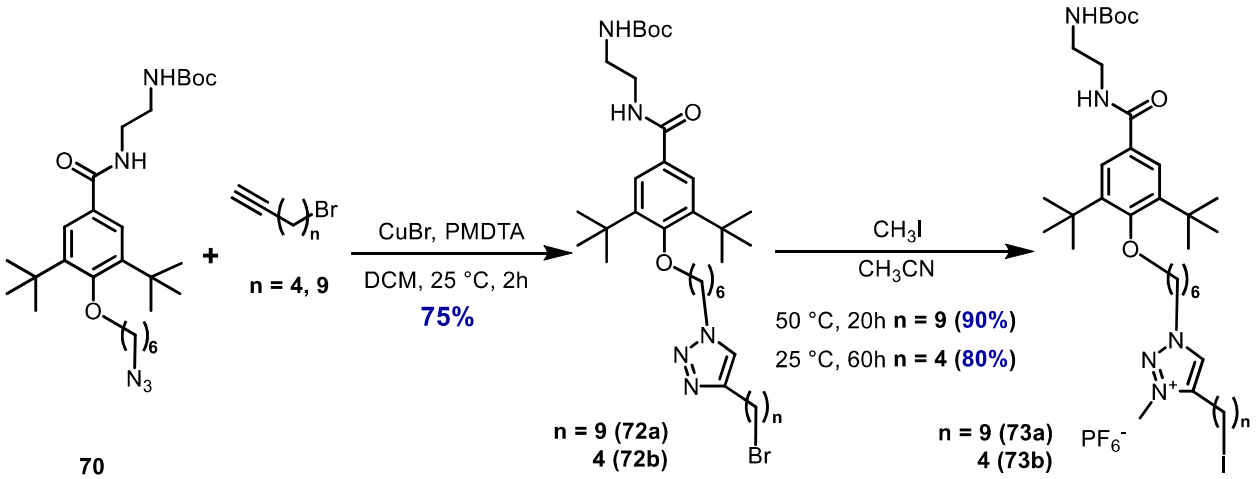

Scheme 4.21. Synthesis of compounds **72a-b** and **73a-b**.

The cycloaddition between these two functional groups in the presence of copper(I) species which accelerate the reaction with a high stereospecificity, leads to the formation of 1,4-disubstitued triazoles with high reaction yields. In our case, the copper source was copper bromide (CuBr) in combination with the nitrogen-based ligand *N*,*N*,*N*′,*N*″,*N*″-pentamethyldiethylenetriamine (PMDETA) that serves as stabiliser for the Cu(I) species, ameliorating the catalytic performance by protecting them from oxidation or disproportionation processes.[45]

N-methylation of the triazole rings was achieved using methyl iodide in excess and under mild heating yielding compound **73a** in 90% yield. For the *N*-methylation on the triazole ring of compound **72b**, the reaction was run at room temperature and for longer reaction times to avoid the intramolecular 6-Exo-Tet cyclization, favoured according to the Baldwin's rules[46] (Scheme 4.22), thus leading to compound **73b** in high yields. During the formation of compound **73b**, we observed by UPLC the presence of byproduct **73c** when the reaction was run at 50 °C. This cyclization did not occur with compound **72a** since it bears a longer alkyl chain and there is no proximity with the nitrogen atoms.

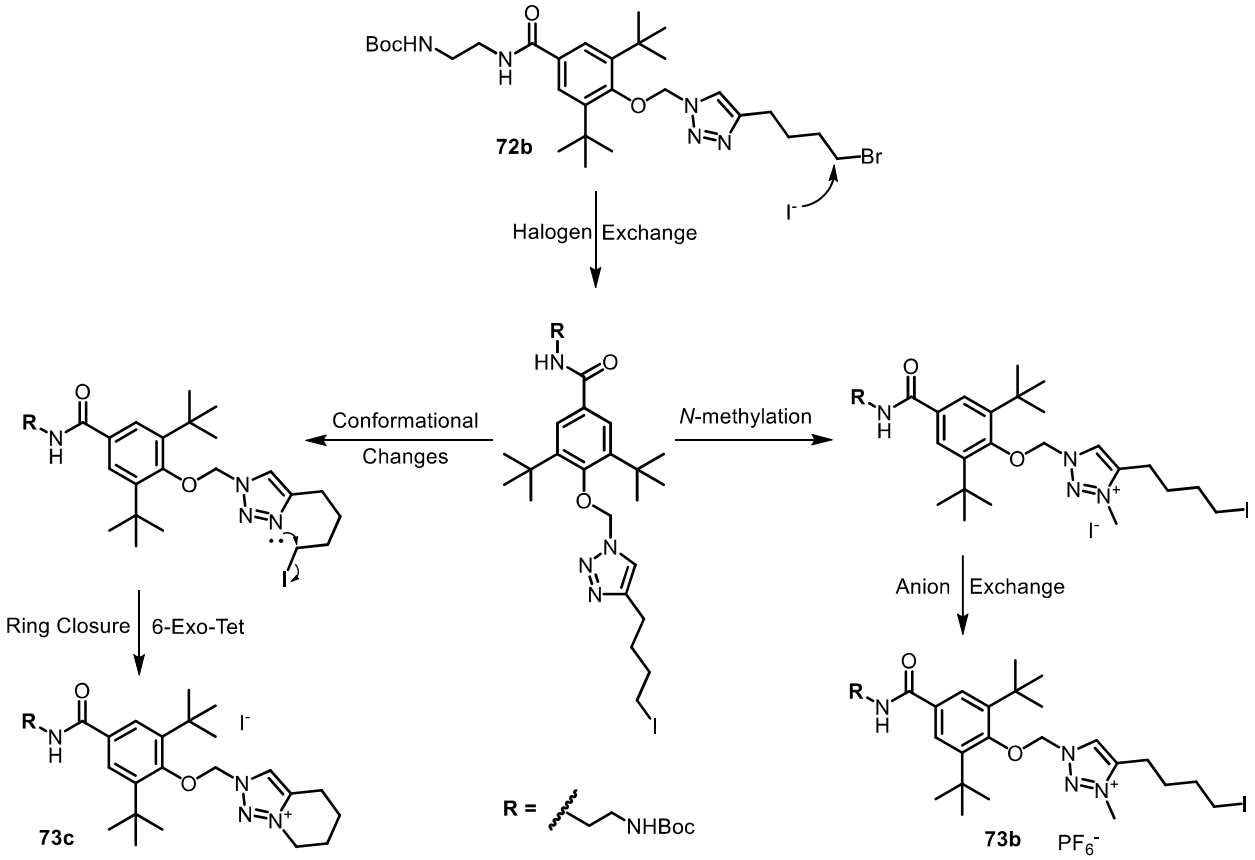

Scheme 4.22. Hypothetical mechanism for the formation of byproduct **73c**.

Compounds **73a-b** were subjected to nucleophilic substitution S_N2 with an excess of 4,4'-bipyridine, in order to avoid the bis-*N*-alkylation of the aromatic core, leading to compounds **74a-b** in good yields after purification by column chromatography (Scheme 4.23).

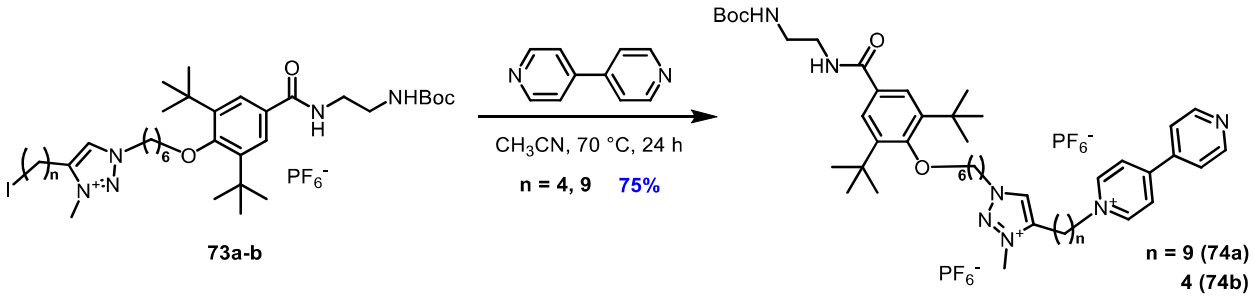

Scheme 4.23. Synthesis of the stoppers **74a-b**.

Figure 4.10 shows the ^{1}H NMR spectrum with all the expected signals for compound **74a**. In particular, we observe at downfield two doublets for the pyridinium ring at 8.78 and 8.33 ppm, as well as two doublets for the pyridine ring at 8.85 and 7.79 ppm. Additionally, the singlet at 8.10 ppm corresponds to the vinylic

proton of the triazolium ring due to the electron withdrawing effect of the aromatic system. This effect applies also for the proton signals of the CH_2 adjacent to the pyridinium ring and the nitrogen of the triazolium ring, which are displayed as triplets at 4.55 and 4.47 ppm respectively. For **74b**, the ^{1}H NMR spectrum is similar, but it displays a smaller number of protons in the aliphatic region.

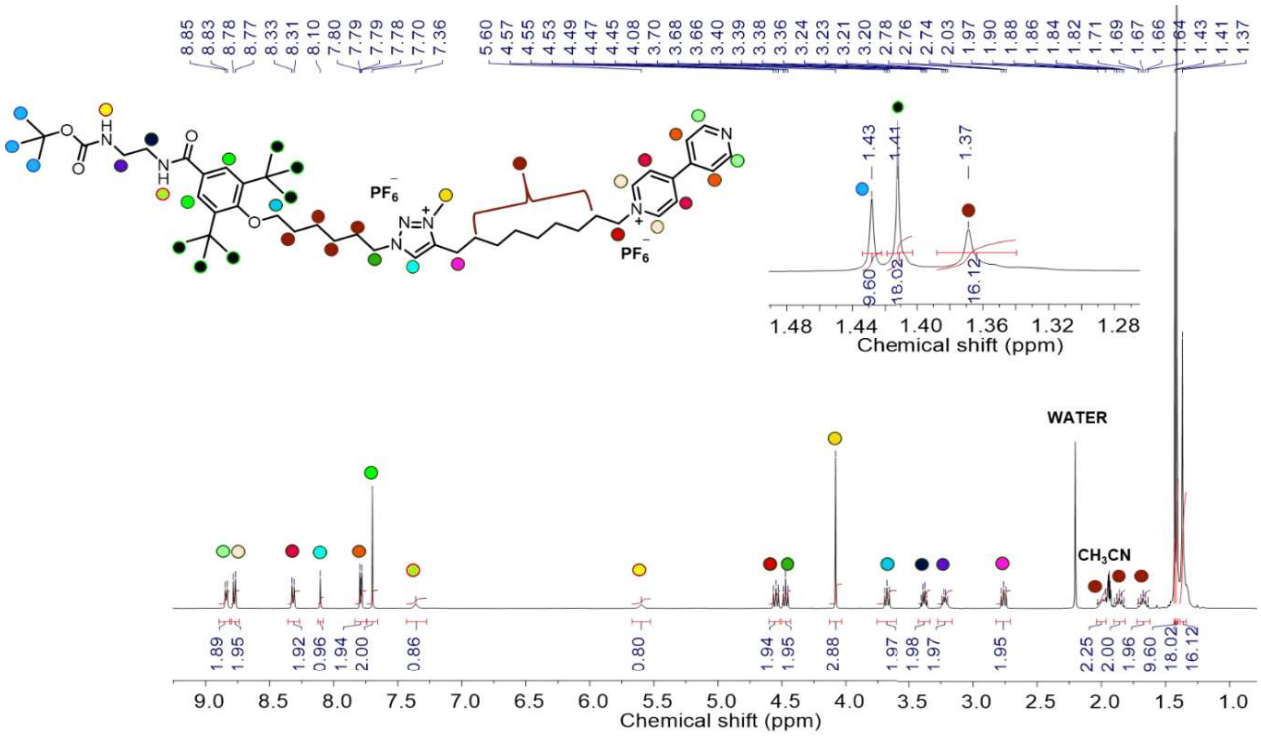

Figure 4.10. ^{1}H NMR spectrum of compound **74a** in CD_3CN at 25 °C (400 MHz).

Finally, the S_N2 alkylation on pseudo[*c*2]daisy chain **52** with stoppers **74a-b** led to the construction of the [*c*2]daisy chain topology and introduction of the redox active recognition sites simultaneously. Based on this strategy, two [*c*2]daisy chain rotaxane structures (**75a-b**) with different lengths of alkyl spacers between the redox-active stations were obtained (20–25% yield), after four days of reaction in a mixed solvent system (chloroform/acetonitrile, *v*/*v* = 2:1) at 60 °C under stirring (Scheme 4.24).

Along the course of the reaction, unthreaded products **75c** and **75d** were also obtained in similar yields to the threaded structures. This could be explained by the polarity of the solvent mixture, which can enable the disassembly of the pseudo[*c*2]daisy chain rotaxane, and subsequent formation of the unthreaded products. We tried to find a solvent mixture that could allow us to solubilise all the compounds, and at the same time to maintain a lower percentage of acetonitrile, but ratio chloroform/acetonitrile, *v*/*v* = 2:1 was our best. Decreasing the amount of acetonitrile in the reaction mixture did not allow the complete solubilisation of the

pseudo[*c*2]daisy chain rotaxane **52**, which was also reflected in lower reaction yields (~10%). Nevertheless, it was relevant to obtain such non-interlocked compounds **75c-d**, as it will be shown later in this chapter 4.

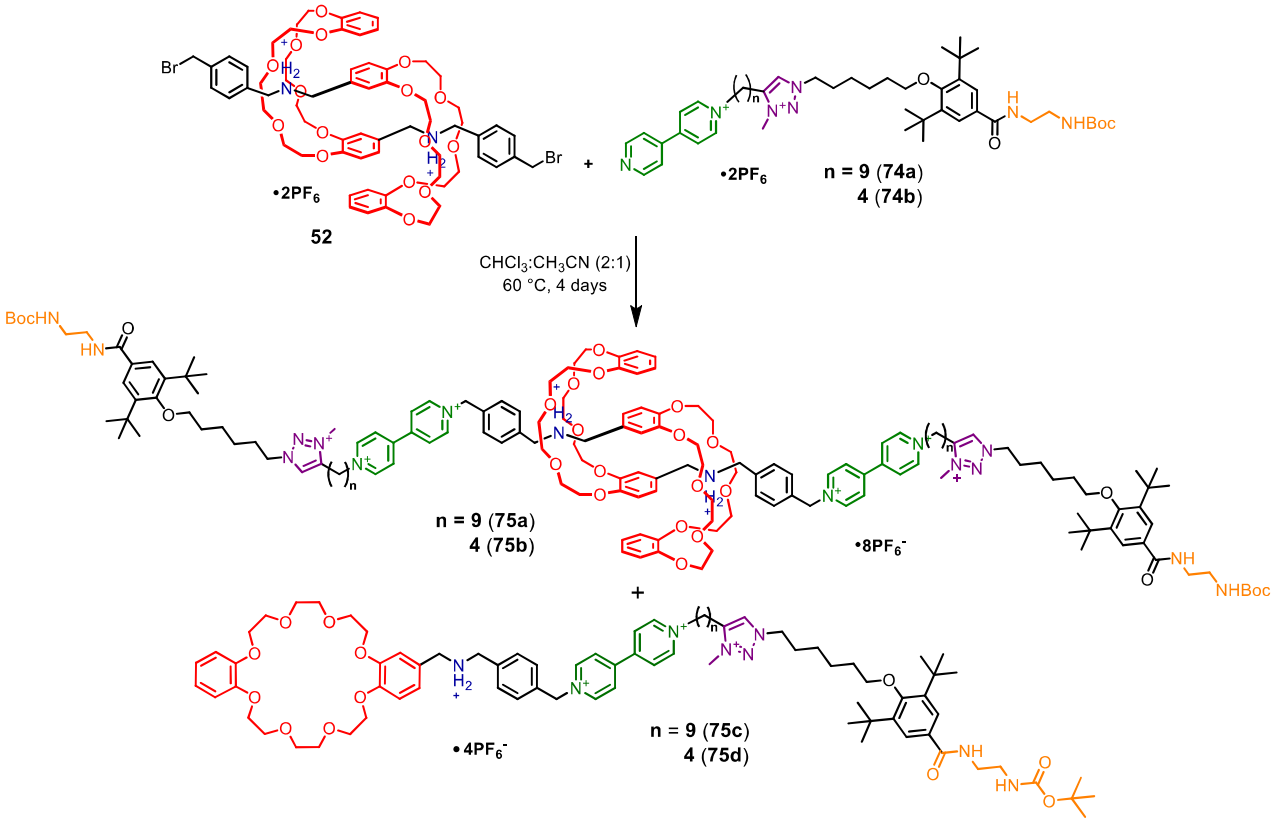

Scheme 4.24. Synthesis of the [*c*2]daisy chain compounds **75a-b** and their corresponding unthreaded compounds **75c-d**.

UPLC analysis of the reaction crude of **75a** revealed the presence of three peaks mainly (Figure 4.11a). The most intense one at 1.01 min corresponds to the starting material **74a**, which was confirmed by mass spectrometry. Figure 4.11b shows peaks with m/z = 838.84 and 419.84 which corresponds to the molecular mass of **74a** without one (Z=1) and two $(PF_6)^-$ counterions (Z=2). The peaks at 0.94 and 0.86 min in the chromatogram (Figure 4.11a) are attributed to the desired [*c*2]daisy chain product **75a** and its corresponding unthreaded product **75c** (Figure 4.11c-d). This was confirmed by ESI mass spectrometry, where we can observe a peak with m/z = 568.33 (Z=5) in the mass spectrum of **75a** (Figure 4.11c), while for **75c** this peak is not present, and it is possible just to observe the peak with m/z = 710.25 which corresponds to the mass of the unthreaded compound without two $(PF_6)^-$ counterions (Z=2).

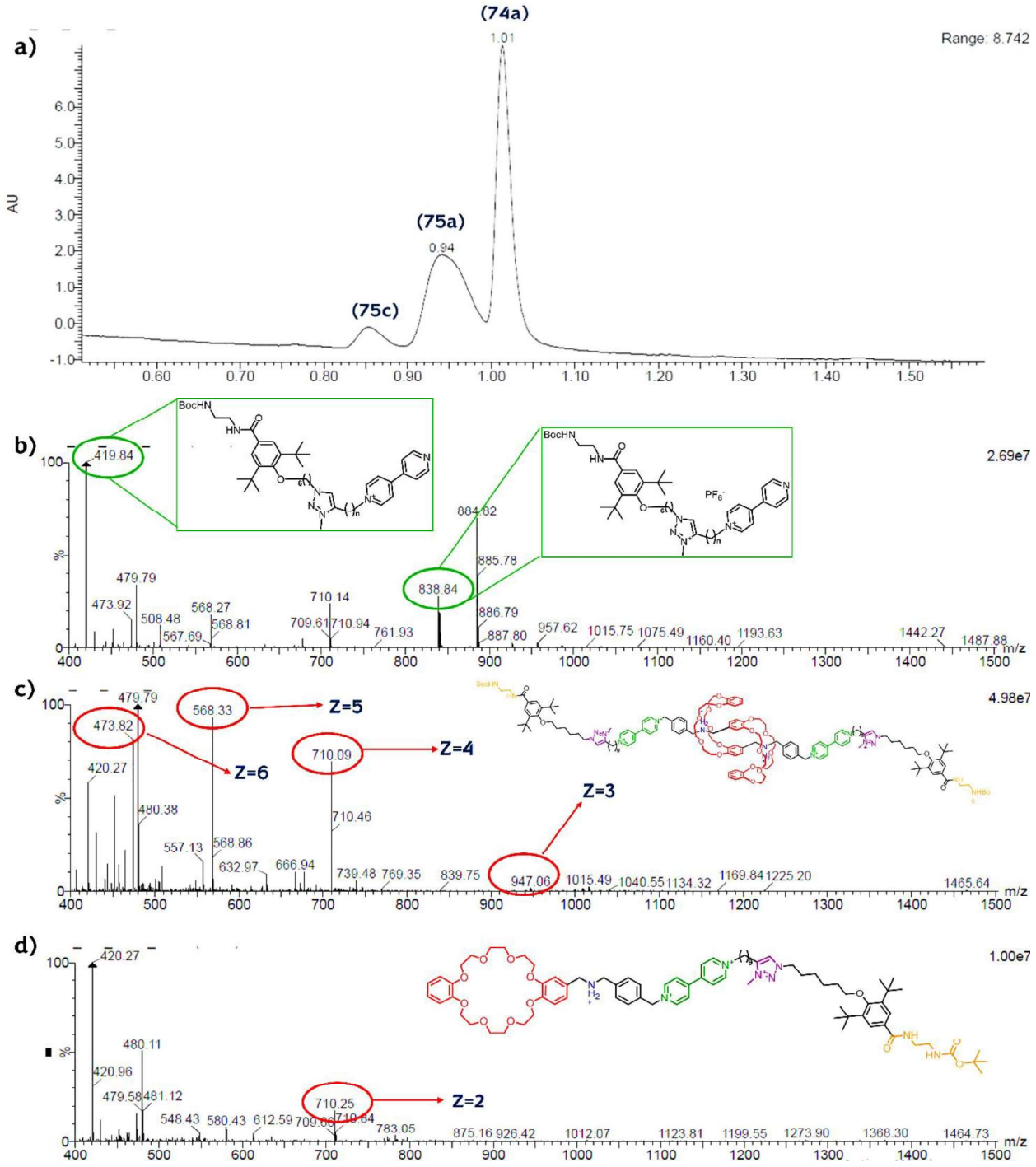

Figure 4.11. a) Chromatogram of the reaction crude for the synthesis of **75a**. ESI mass spectra of **b**) **74a**, **c**) **75a** and **d**) **75c**.

The reaction that led to **75b** showed the same behaviour as for **75a** (Figure 4.12a). The most intense one at 1.16 min corresponds to the starting material **74b**, and the peaks at 1.09 and 1.03 min in the chromatogram (Figure 4.12a) are attributed to the desired [*c*2]daisy chain product **75b** and its corresponding unthreaded product **75d** (Figure 4.12b-c). This was confirmed by ESI mass spectrometry, where we can observe a peak

with m/z = 540.48 (Z=5) in the mass spectrum of **75a** (Figure 4.11b), while for **75d** this peak is not present, and it is possible just to observe the peak with m/z = 675.00 which corresponds to the mass of the unthreaded compound without two $(PF_6)^-$ counterions (Z=2).

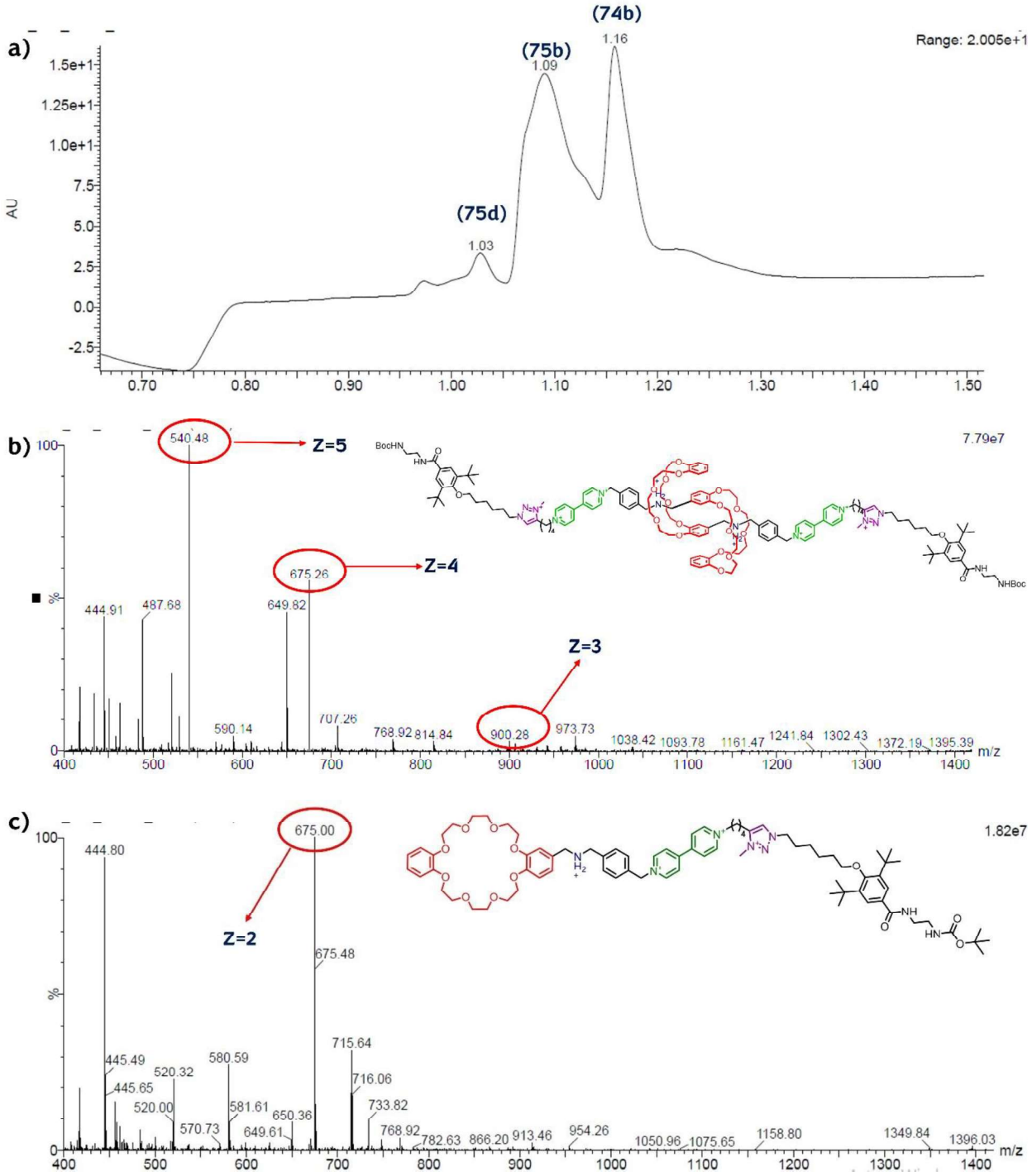

Figure 4.12. **a**) Chromatogram of the reaction crude for the synthesis of **75b**. ESI mass spectra of **b**) **75b**, **c**) **75d**.

The ^{1}H NMR spectrum of **75a** (Figure 4.13) showed all the expected and well-resolved set of signals, which were assigned with the help of 2D NMR experiments. The multiplets between 9.00 and 8.40 ppm correspond to protons A_1, B_1 and A_2, B_2 of the bipyridinium aromatic rings. The singlet at 8.10 ppm corresponds to the vinylic proton T_1 of the triazolium ring. Proton signal at 7.69 ppm corresponds to protons C_1 of the aromatic ring containing the bulky *tert*-butyl groups. Additionally, in the aromatic region we can observe two sets of doublets for protons D_1 and D_2 at 7.63 and 7.53 ppm respectively. The proton Nl that is located at 7.42 ppm corresponds to the NH of the aromatic amide and is shown as a broad and non-well defined triplet. In the region between 6.90 and 6.50 ppm are located the multiplets that correspond to the aromatic protons Ar of the crown ether macrocycles.

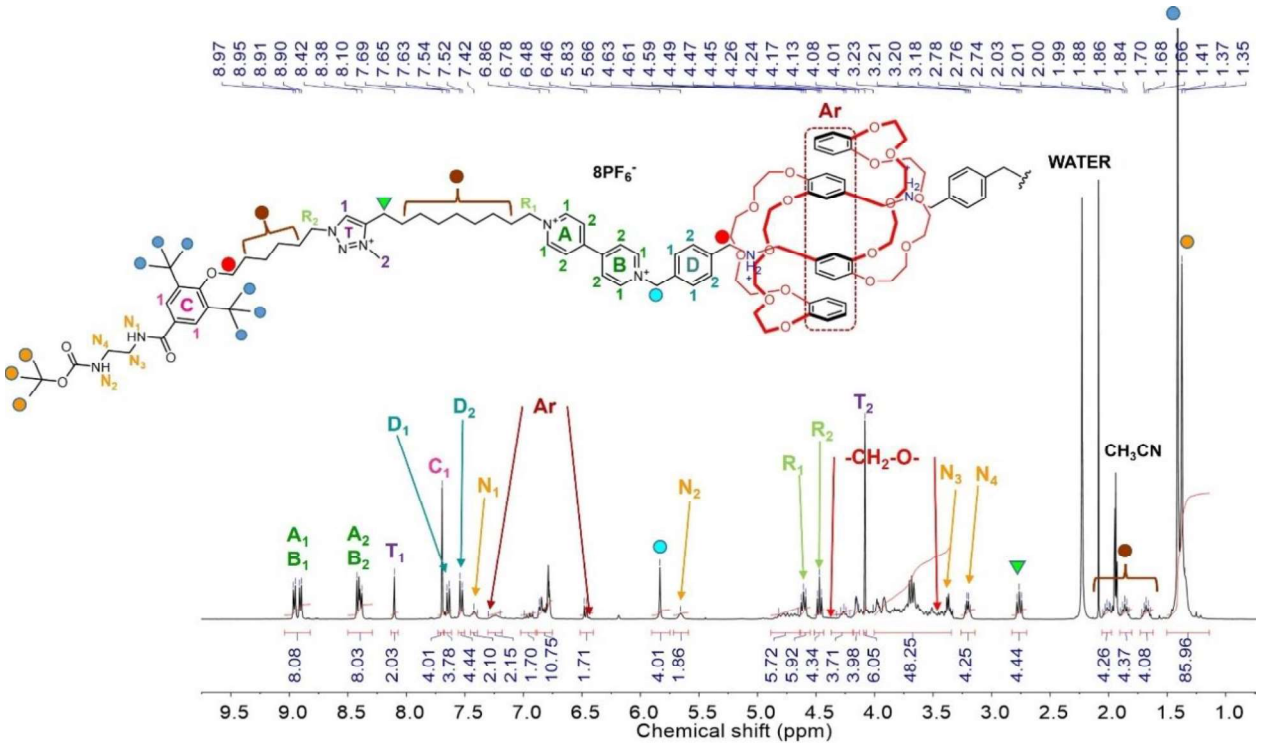

Figure 4.13. ^{1}H NMR spectrum of the [*c*2]daisy chain **75a** in CD_3CN at 25 °C (400 MHz).

Going towards upfield, we can observe a singlet at 5.83 ppm (cyan circle) that corresponds to the benzylic protons in α to the pyridinium ring B and aromatic ring D. Next to this singlet, we can observe another broad and non-well defined triplet that corresponds to the proton N2 of the Boc-protecting group. Additionally, a triplet at 4.61 ppm corresponds to protons R1 in α to the pyridinium ring A. Next to this signal appears a triplet at 4.47 ppm that corresponds to protons R2 in α to the triazolium ring T. Then, a complicated region of various overlapped multiplets between 4.30 and 3.30 ppm corresponds to the CH_2 protons of the crown ether macrocycles, as well as the CH_2 protons next to the phenolic oxygen of aromatic ring C and the protons

adjacent to the secondary ammonium station. In addition, the proton signals corresponding to the aliphatic CH_2 are located at upfield in the region between 2.00 and 1.50 ppm, as well as included in the intense peak at 1.41 ppm that correspond to the protons of the *tert*-butyl groups attached to the aromatic ring C.

Due to the interlocked nature of the molecule, signals corresponding to the -CH_2O- protons of the crown ethers are not well resolved and therefore, it is not possible to assign each of them. However, the integral value matches with the expected number of protons, like in the case of the aliphatic region in which there is overlapping of different set of signals. Finally, another important signal is the one that corresponds to the *tert*-butyl protons of the Boc protecting group, that is as a singlet at 1.35 ppm (in orange).

The interpretation of the ^{1}H NMR spectrum of **75b** is very similar to the one for **75a**, since they differentiate only in the number of carbons between the triazolium and bipyridinium station (Figure 4.14).

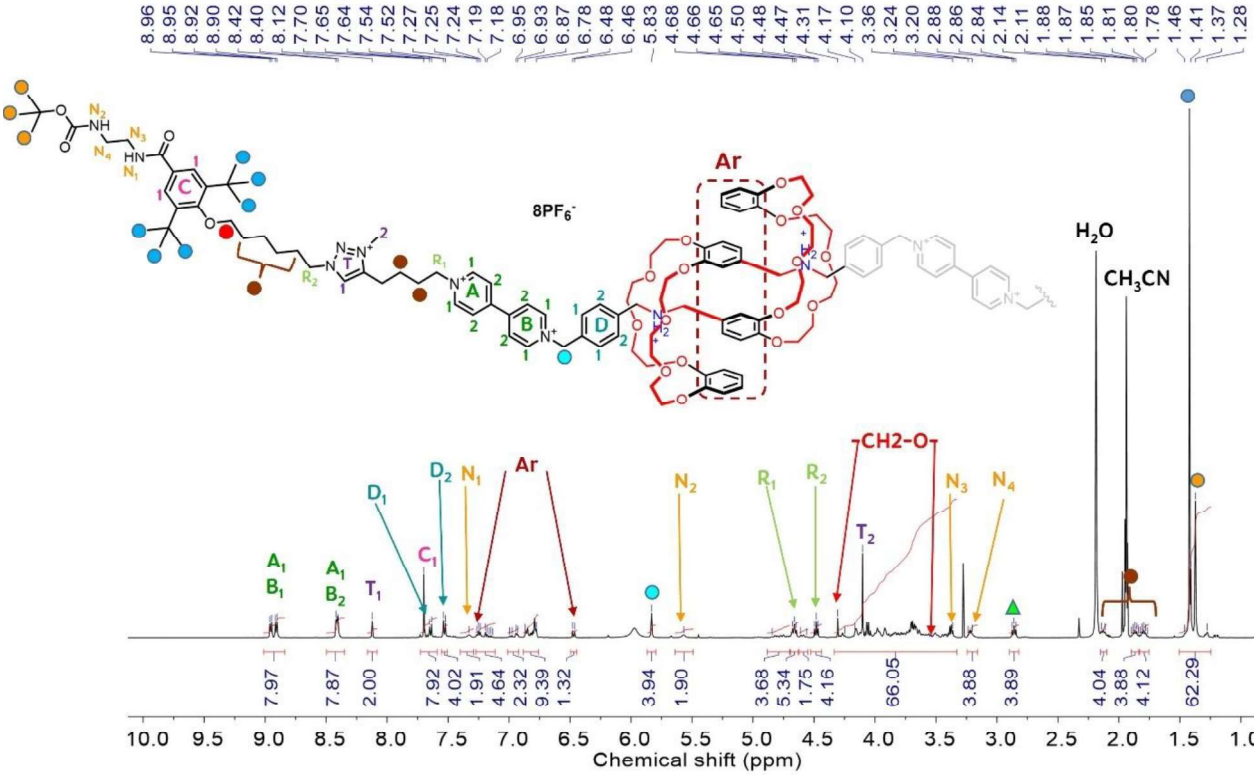

Figure 4.14. ^{1}H NMR spectrum of the [*c*2]daisy chain **75b** in CD_3CN at 25 °C (400 MHz).

As we mentioned, during the reaction course that leads to compound **75a-b**, we also obtained the unthreaded compounds **75c-d**. We chose the ^{1}H NMR of compound **75c** as an example to describe the most representative proton signals (Figure 4.15). At downfield, we can observe the signals corresponding to the protons $A_{1\text{-}2}$ and $B_{1\text{-}2}$ of the bipyridinium unit, as well as the vinylic proton T_1. In the aromatic region we can

observe a singlet at 7.76 ppm correspond to protons C_1, a set of double doublets at 7.56 and 7.49 ppm that corresponds to protons $D_{1\text{-}2}$, and between 7.10 and 6.90 ppm a pair of double doublets for protons $F_{1\text{-}2}$, where one of it is masked by the multiplet that is attributed for protons $E_{1\text{-}3}$. In the middle of the 1H NMR spectrum we can find three set of multiplets between 4.12-4.05 ppm and 3.87-3.78 ppm that are assigned to the CH_2 protons of the crown ether macrocycle. It is important to highlight that this region as well as the aromatic region are less complex to analyse and the spectrum contains sharper and more shaped defined signals with respect to the [*c*2]daisy chain threaded structure of compound **75a**.

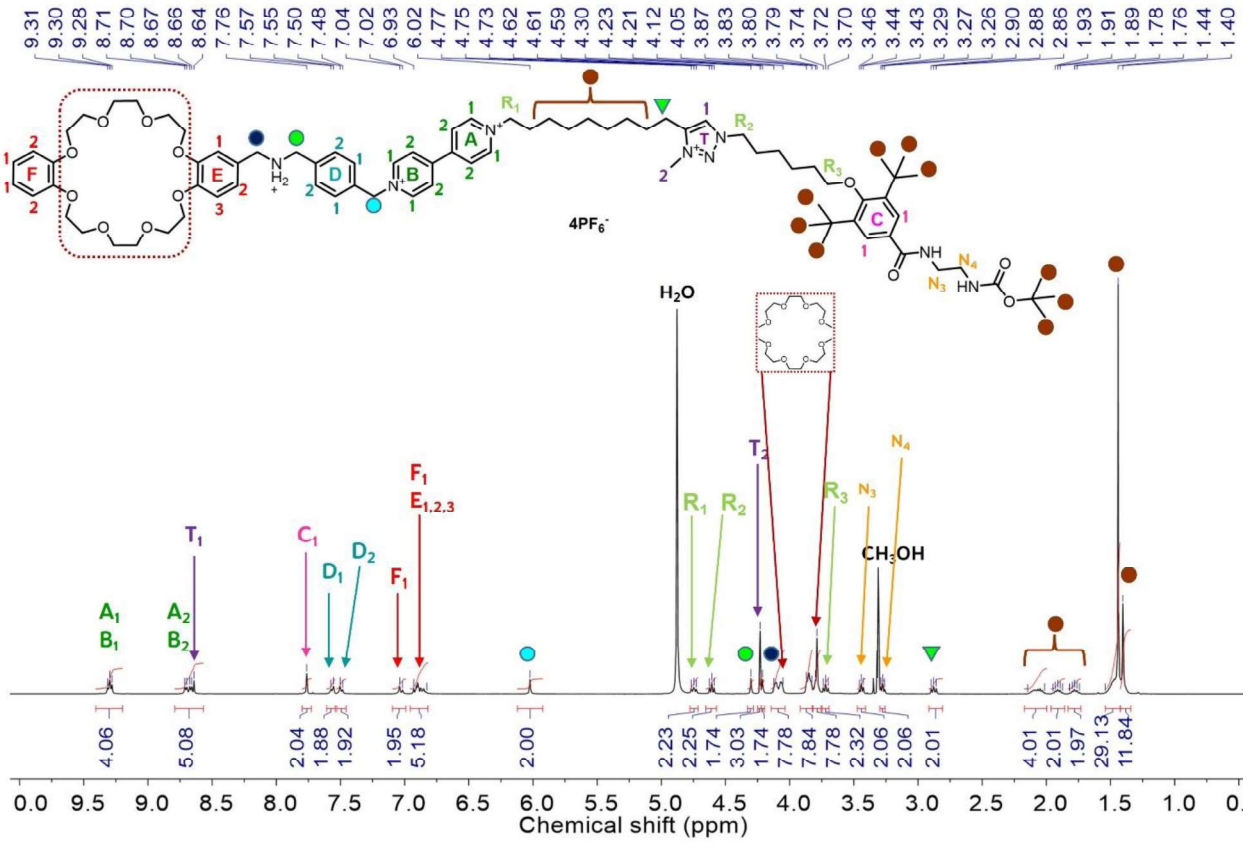

Figure 4. 15. ^{1}H NMR of unthreaded compound **75c** in CD_3OD at 25 °C (400 MHz).

4.4. Synthesis of [*c*2]daisy chain rotaxane monomers 77a-b

Since our goal involved the construction of a redox responsive [*c*2]daisy chain system, it was absolutely necessary to protect the secondary ammonium ($–NH_2^+–$) station to break the strong [N^+–H···O] intercomponent interactions with the crown ether, allowing it to move exclusively between the 4,4'-bipyridinium ($bipy^{2+}$) and the triazolium ring. Therefore, *N*-acylation reaction on the $–NH_2^+–$ centre was

carried out with an excess of acetic anhydride at low temperature, in presence of the non-nucleophilic base DIPEA (Scheme 4.25a), an ideal amine to deprotonate this systems.[47]

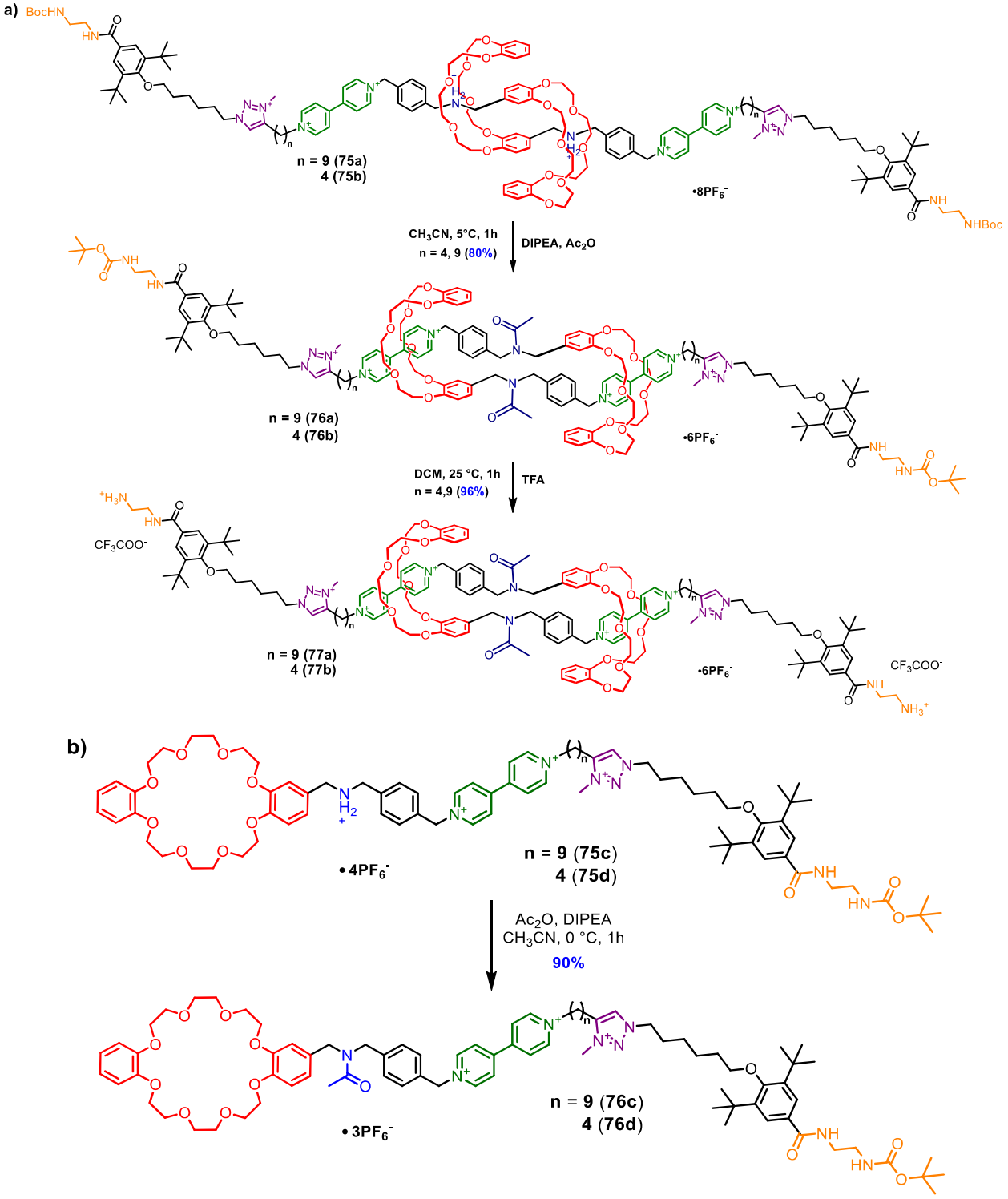

Scheme 4.25. **(a)** Synthesis of bis-ammonium [*c*2]daisy chain monomers **77a-b**. **(b)** Synthesis of the acetylated unthreaded compounds **76c-d**

In addition, the unthreaded products were subjected to the same acylation conditions, leading to compounds **76c-d** (Scheme 4.25b). Here, it is important to highlight the sensitivity of these molecules, threated and unthreaded, regarding to the type of base used. Upon addition of bases like sodium hydroxide and triethylamine, the solution turned deep green no matter the temperature, indicating decomposition of the benzyl viologen fragment.

The remaining synthetic step consisted in the Boc deprotection, using TFA in dichloromethane to yield free-bis(ammonium) [*c*2]daisy chain monomers **77a-b** in high yields (Scheme 4.25a). The ^{1}H NMR spectrum of **77a** shows all the expected signals (Figure 4.16), specially the disappearance of the singlet corresponding to the *tert*-butyl units of the Boc protecting group. In addition, UPLC analysis revealed the presence of one compound with the expected mass, a behaviour that was also observed for monomer **77b** containing a shorter alkyl linker.

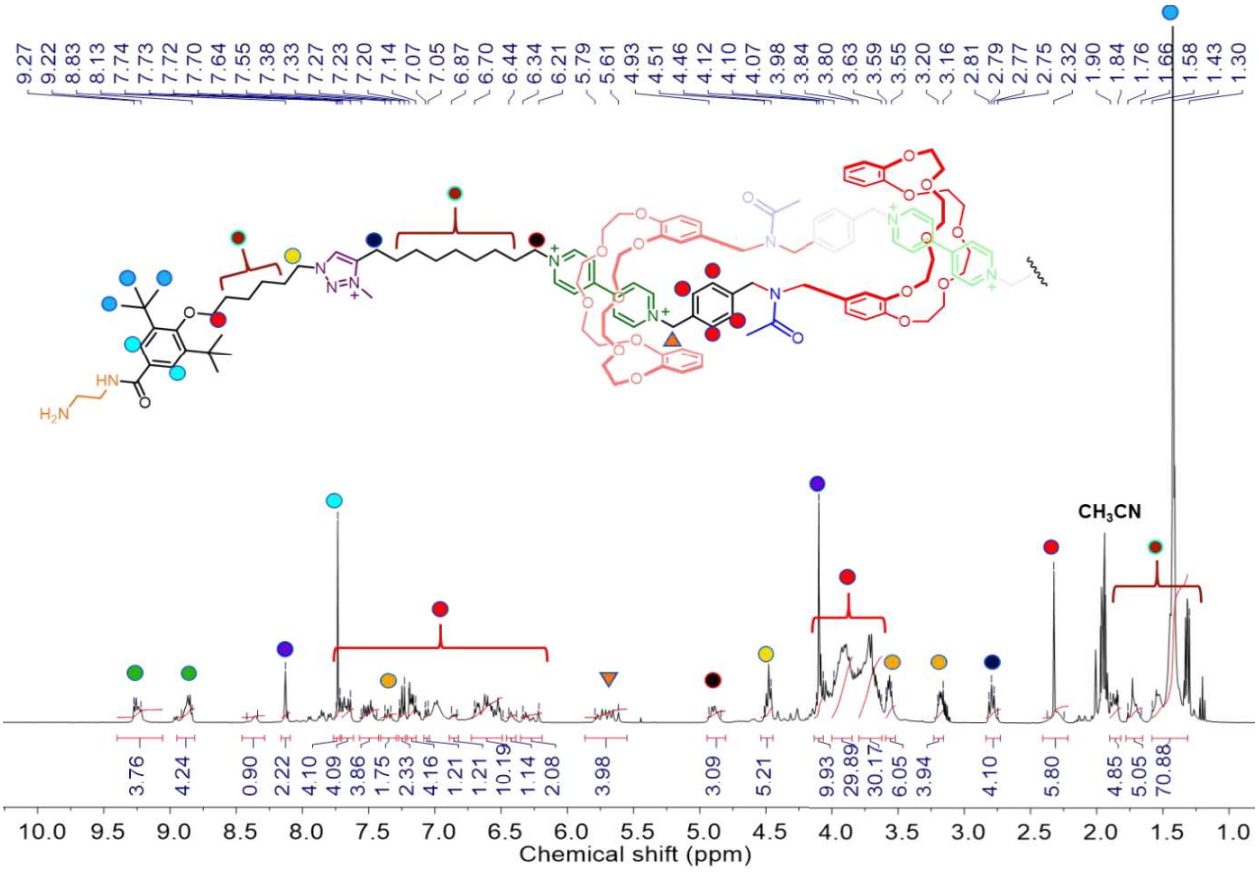

Figure 4.16. ^{1}H NMR spectrum of [*c*2]daisy chain **77a** in CH_3CN at 25 °C (400 MHz)

The deprotection reaction that led to compound **77a** was monitored by UPLC-MS (Figure 4.17a). The chromatogram shows only one peak that corresponds to the fully deprotection of NH groups, which was confirmed by ESI-MS (Figure 4.17b). The MS spectrum shows three peaks with m/z = 545.28, 681.29, and 908.18 that correspond to Z = 5, 4 and 3 respectively.

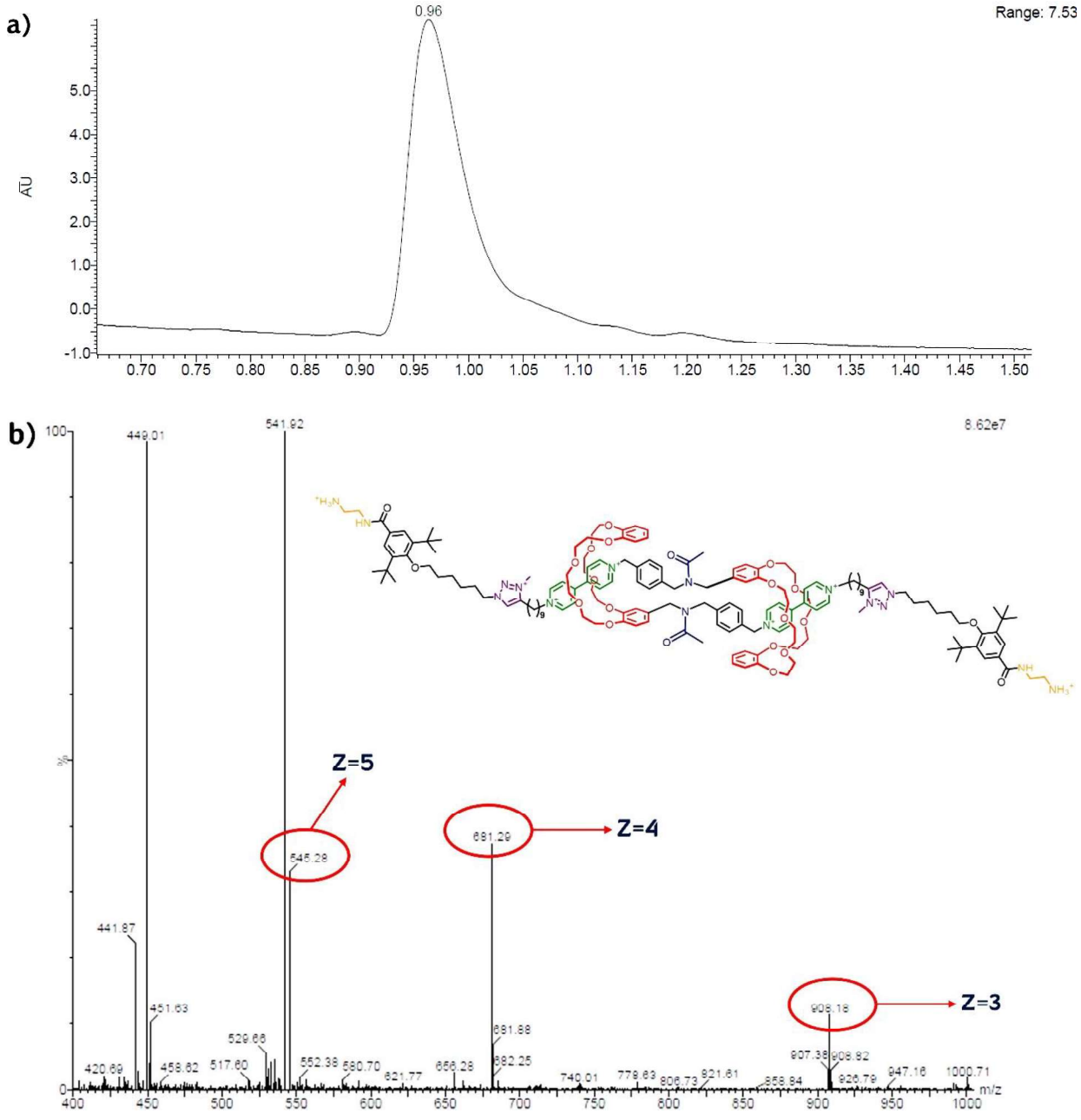

Figure 4.17. a) Chromatogram of the reaction crude for the synthesis of **77a**. **b)** ESI mass spectrum of **77a**.

As for **77a**, the deprotection reaction that led to compound **77b** was monitored by UPLC-MS (Figure 4.17a). The chromatogram shows only one peak that corresponds to the fully deprotection of NH groups, which was confirmed by ESI-MS (Figure 4.17b). The MS spectrum shows three peaks with m/z = 517.07, 646.03, and 861.08 that correspond to Z = 5, 4 and 3 respectively.

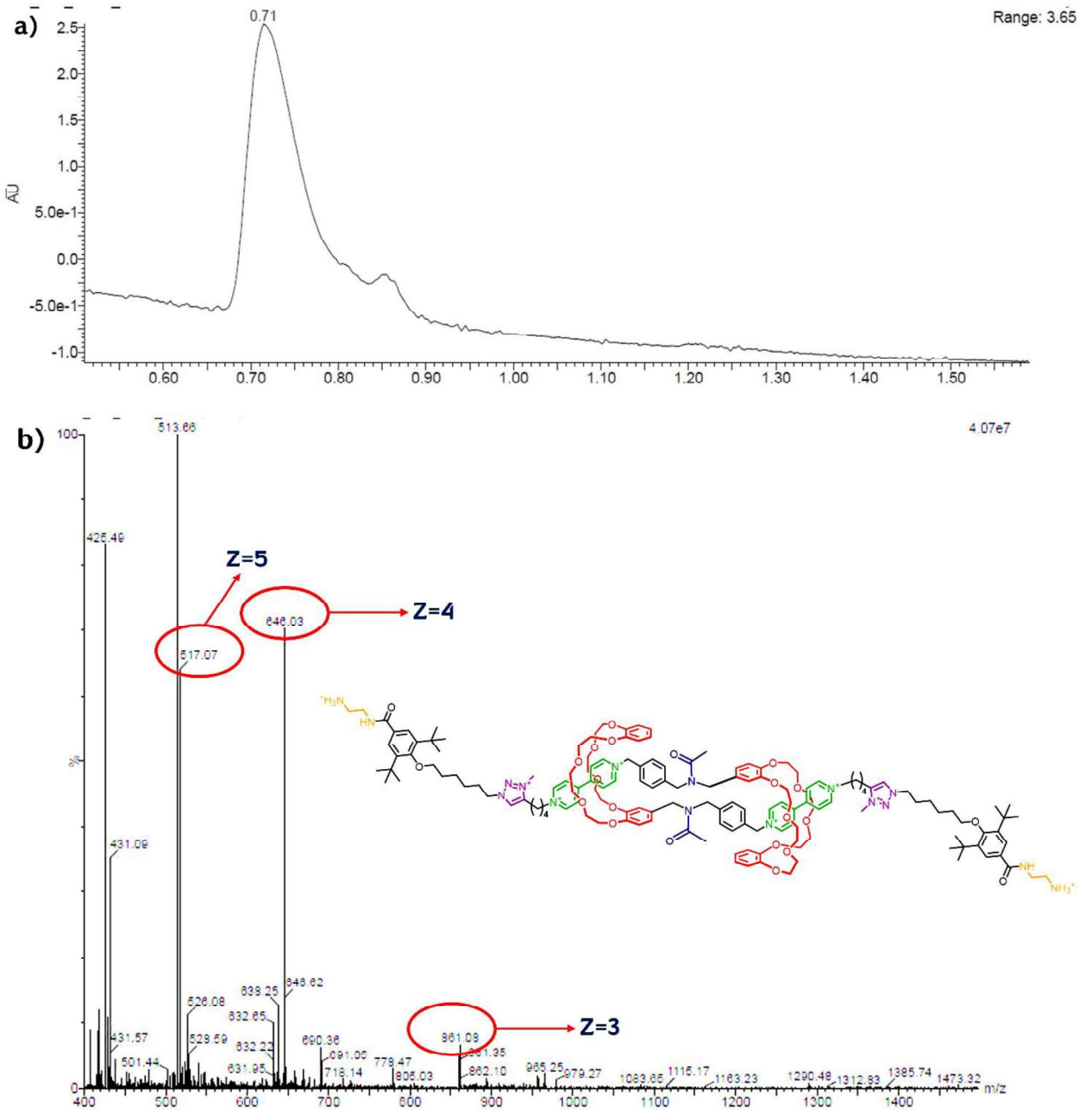

Figure 4. 18. a) Chromatogram of the reaction crude for the synthesis of **77b**. **b)** ESI mass spectrum of **77b**.

With these monomers in hands, the next step was to carry out the hydrogen bonding polymerisation using ureidopyrimidinone (Upy) groups, considering that they can serve as supramolecular connectors for

hydrogen-bonded poly[*c*2]daisy chains.[39] The selection of the R groups attached to the Upy moiety allow tuning the solubility of Upy groups and their ability to dimerize thanks lateral interaction (Scheme 4.26).[48,49]

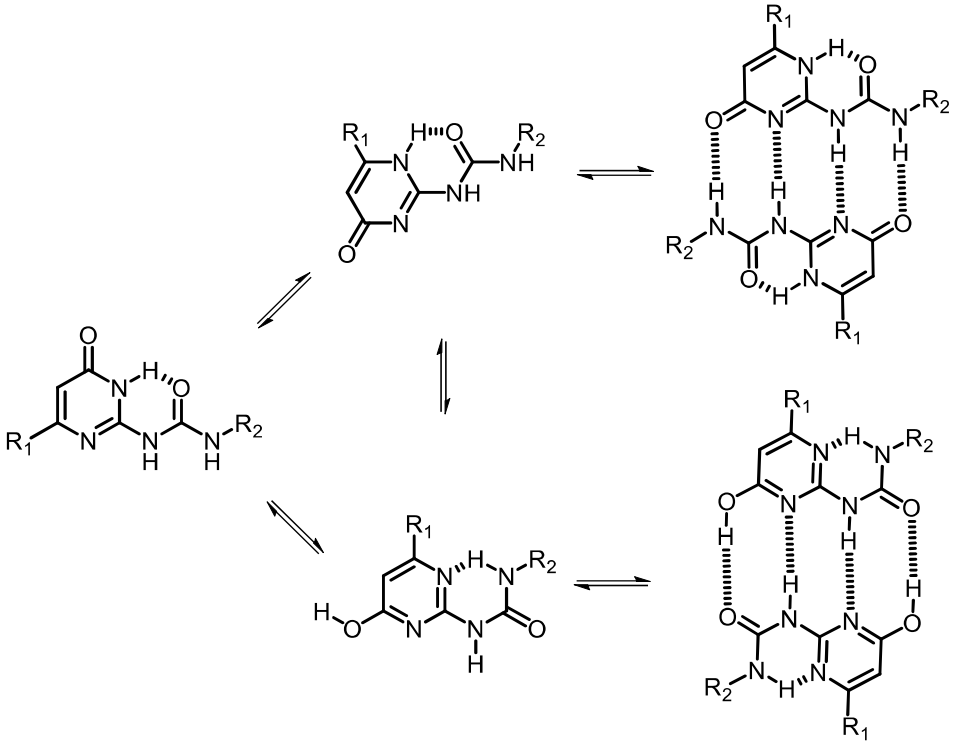

Scheme 4.26. Tautomeric equilibria of the Upy motif.

4.5. Synthesis of protected and free ureidopyrimidinone derivatives 81 and 82

Indeed, under specific conditions such as characteristics of the solvent and the nature of the R groups, the Upy dimers usually stack into helical columnar assembly, a phenomenon that induces physical crosslinking[50] of supramolecular polymers leading to the formation of a 3D network. In order to take advantage of the structure-property relationship of these systems and to form hydrogen bonded supramolecular polymer chains containing [*c*2]daisy chain rotaxanes, we carried out the synthesis of the *tert*-butyl ureidopyrimidinone (*t*-Bu-Upy) **79**. In the synthetic strategy 4 (section 4.2.3), we observed that the sterically demanding *tert*-butyl group grafted strategically at the R_1 position prevents the stacking of the Upy dimers,[51] that usually occurs in Upy systems bearing a methyl, or an aromatic group at this position.[39] It is worthy to recall that we initially planned to obtain [*c*2]daisy chain rotaxanes containing a Upy derivative functionalised in such position with a gallic acid derivative fully *O*-alkylated with C_{12} chains. However, such substitution did not allow to obtain pure [*c*2]daisy chain rotaxanes monomers.

Thus, the synthesis of Upy derivative **79** started from the previously synthesized pyrimidinone **57** that was subjected to reaction with carbonyldiimidazole (CDI) to obtain compound **78** in 70% yield. Since imidazole is a good leaving group, the reaction with β-alanine was straightforward to obtain ester derivative **79** (Scheme 4.27).

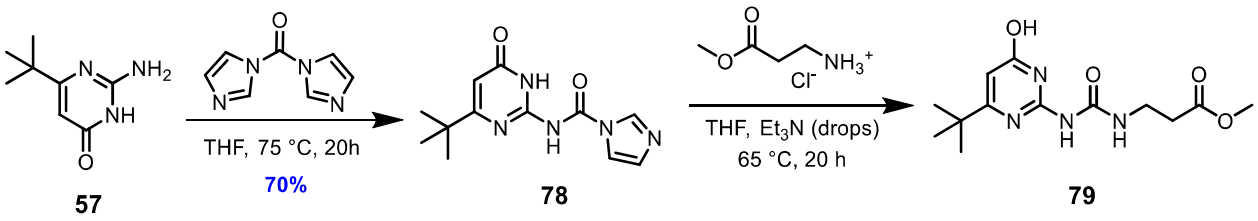

Scheme 4.27. Synthesis of compound **79**.

This compound was subjected to reaction with benzyl bromide in the presence of potassium carbonate and dry DMF at 80 °C, leading to the protected Upy derivative **80**. Under saponification conditions, both protected and non-protected Upy methyl esters **80** and **79** were transformed to the desired ureidopyrimidone derivatives **81** and **82** respectively, both having a carboxylic acid as end group (Scheme 4.28), crucial for functionalisation of [*c*2]daisy chain rotaxane systems.

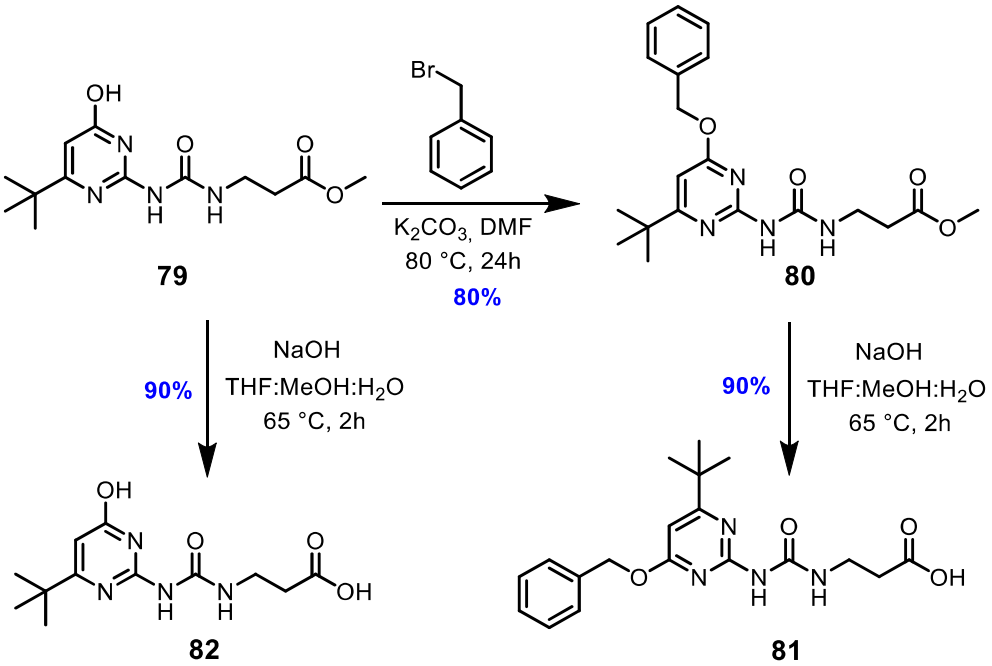

Scheme 4.28. Synthesis of protected and free Upy-carboxylic acid derivatives **81** and **82** respectively.

4.6. Synthesis of Upy-containing [*c*2]daisy chain rotaxanes 83a and 84b

Initially, compounds **81** and **82** were then reacted separately with bis(ammonium) [*c*2]daisy chain rotaxanes **77a** by amide coupling using EDCI, HOBt and dry DMF as solvent, allowing the formation of protected and non-protected Upy [*c*2]daisy chain rotaxanes **83a** and **84a-b** respectively, both in moderate yields (Scheme 4.29). Isolation of these molecules was confirmed by both ^{1}H NMR experiments and UPLC-MS analyses. This synthetic strategy allowed the obtaining of Upy-functionalised [*c*2]daisy chain rotaxanes after an optimised purification process. Firstly, liquid – liquid extractions with an HCl solution 1 M were needed to destroy the activated ester of the Upy-carboxylic acid in excess that was not consumed. Then, liquid-liquid extractions with an aqueous solution of $NaHCO_3$ allowed removing the excess of Upy-carboxylic acid by deprotonation. Finally, the organic phase was washed with HCl solution 1 M to avoid basic reminiscences that could decompose the [*c*2]daisy chain rotaxanes. This methodology of purification was enough to afford compounds **83a** and **84a-b** with moderate yields. However, these compounds were not soluble in common organic solvents and slightly soluble in methanol, DMF and DMSO, which inhibit the formation of Upy dimers and as consequence, the formation of hydrogen-bonded supramolecular polymers.

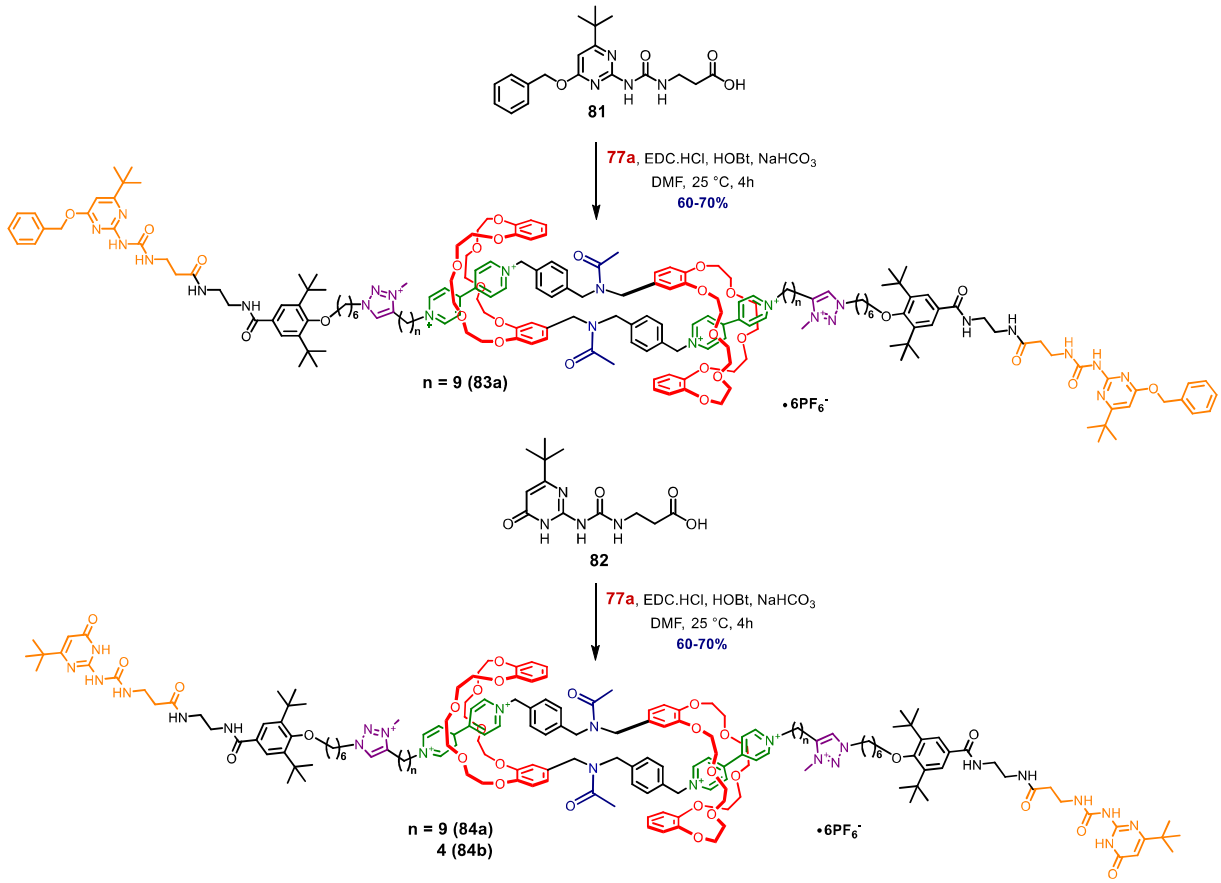

Scheme 4.29. Synthesis of [*c*2]daisy chain rotaxanes **83a** and **84a** containing the *tert*-butyl Upy fragment.

All the attempts to solubilise the Upy [*c*2]daisy chains in different solvent systems that promote hydrogen bonding were unsuccessful, therefore, we decided to stop investing efforts in a hydrogen bonding supramolecular approach, and we focused on a covalent polymerisation of our [*c*2]daisy chain monomers.

4.7. Synthesis and characterisation of polyureas based on [*c*2]daisy chain rotaxanes

The presence of free bis-amine functional groups at the extremities of the [*c*2]daisy chain rotaxanes **77a-b**, was used for the formation of polyureas by reaction with commercially available diisocyanate methylene diphenyl diisocyanate (MDI) (Scheme 4.30). The urea bond formation was carried out in the presence of sodium hydrogen carbonate in order to deprotonate the NH_3^+ ending groups of the starting material. Polymers **85a** and **85b** were obtained after precipitation from a solvent mixture of MeOH/HCl 1 M (1:5), in order to quench the unreacted MDI and to neutralise the base.

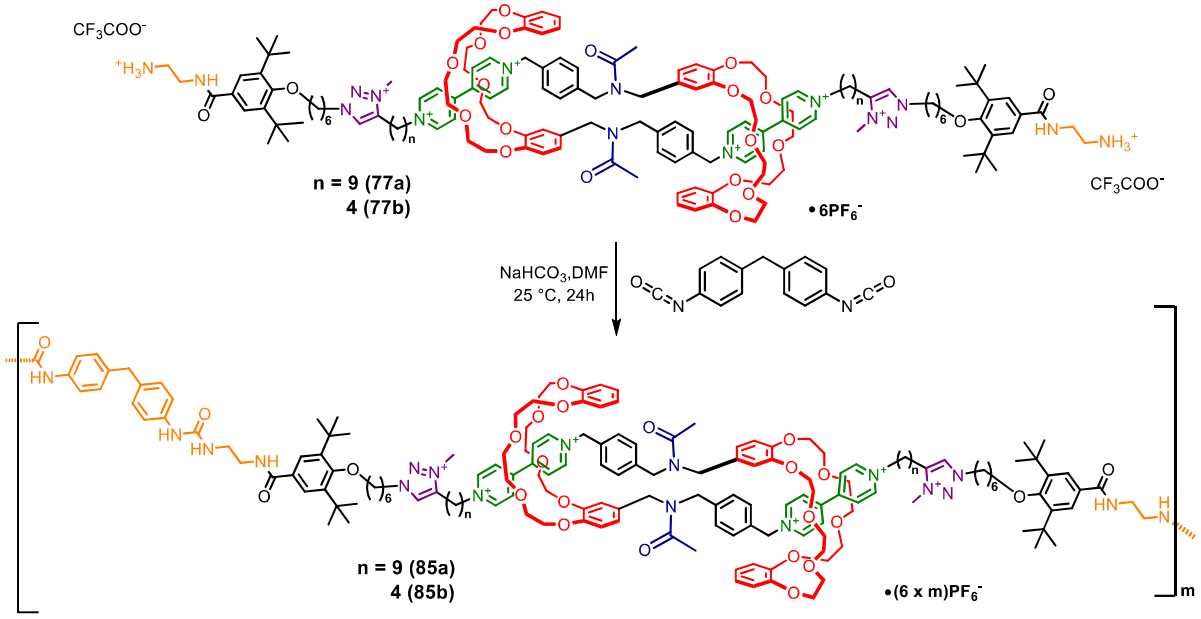

Scheme 4.30. Synthesis of [*c*2]daisy chain based polyureas **85a-b**.

The GPC analysis of polyurea **85a** was performed in a 0.1 M solution of $NaNO_3$ in DMF, indicating a molecular weight of 203.213 g/mol with a dispersity index of 1.9 (Figure 4.19a). Such molecular weight corresponds to a polymer with approximately 55 units. In the case of 85b, the GPC analysis showed a polymer with an estimated molecular weight of 30.694 g/mol with a dispersity index of 1.2 (Figure 4.19b), that corresponds to a polymer with approximately 9 units. However, this result is not completely reliable because the baseline of the curve overlaps with the one that corresponds to the solvent impurities due to low solubility of the product and apparent accumulation of it in the column.

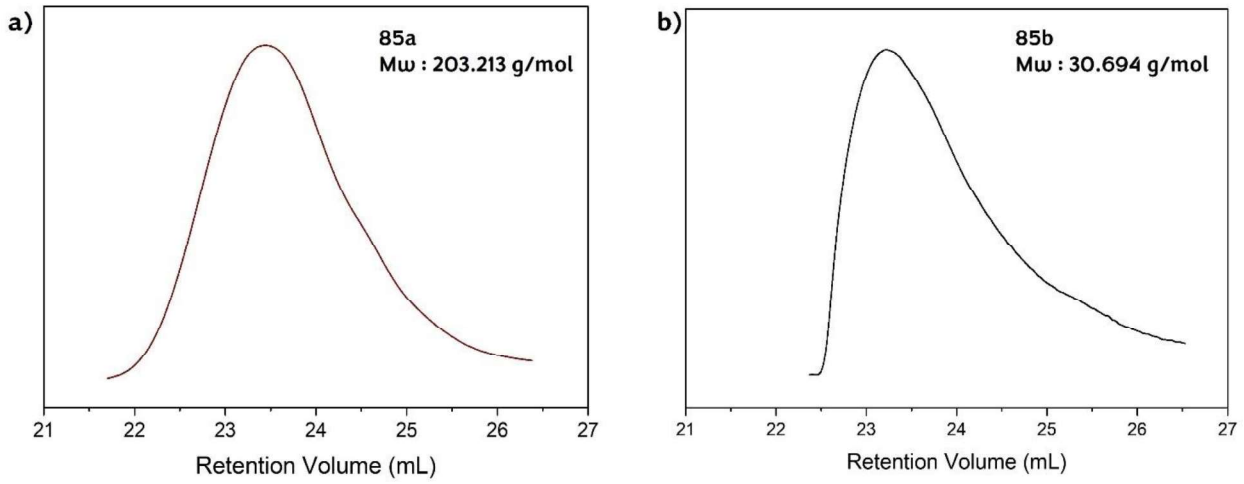

Figure 4. 19. GPC profiles of [c2]daisy chain rotaxane polyureas (**a**) **85a** and (**b**) 85b (eluent; DMF (0.1 M $NaNO_3$ solution); flow rate 1 mL/min; detected by RALS)

4.7.1. Electrochemical characterisation of [*c*2]daisy chain based polyureas

As mentioned in the introduction of this chapter (Section 4.1), the MAGNIFY concept relies on the use of molecular machines, capable of changing their length at the nanometre scale upon electrical stimulation, in order to develop controllable contractile materials at the macroscopic scale. In our system, [*c*2]daisy chain rotaxane-based polyureas are initially in an extended conformation, which means that the crown ether macrocycles surround the bipyridinium units (primary stations). Upon reduction of the bipyridinium, the macrocycles move away towards the triazolium moieties (secondary stations), leading to polymers in the contracted state. Subsequent reoxidation of the bipyridinium units resets the system to the extended conformation (Scheme 4.31).

The reversible large amplitude motion triggered by electrochemical stimulation gives also control over the conformations of the [*c*2]daisy chain rotaxanes. The structural rearrangements caused by the redox processes could be studied in detail by comparing the redox potentials of the polymers, with those ones of non-polymerised, acetylated [*c*2]daisy chains **76a-b**, and unthreaded redox-active molecules **76c-d** (Scheme 4.32). The electrochemical switching of polyureas **85a-b** was studied by cyclic voltammetry (CV) and differential pulse voltammetry (DPV). These techniques were used to determine the redox potentials of the investigated compounds, allowing the attribution of each electrochemical event to a specific electroactive unit.[52]

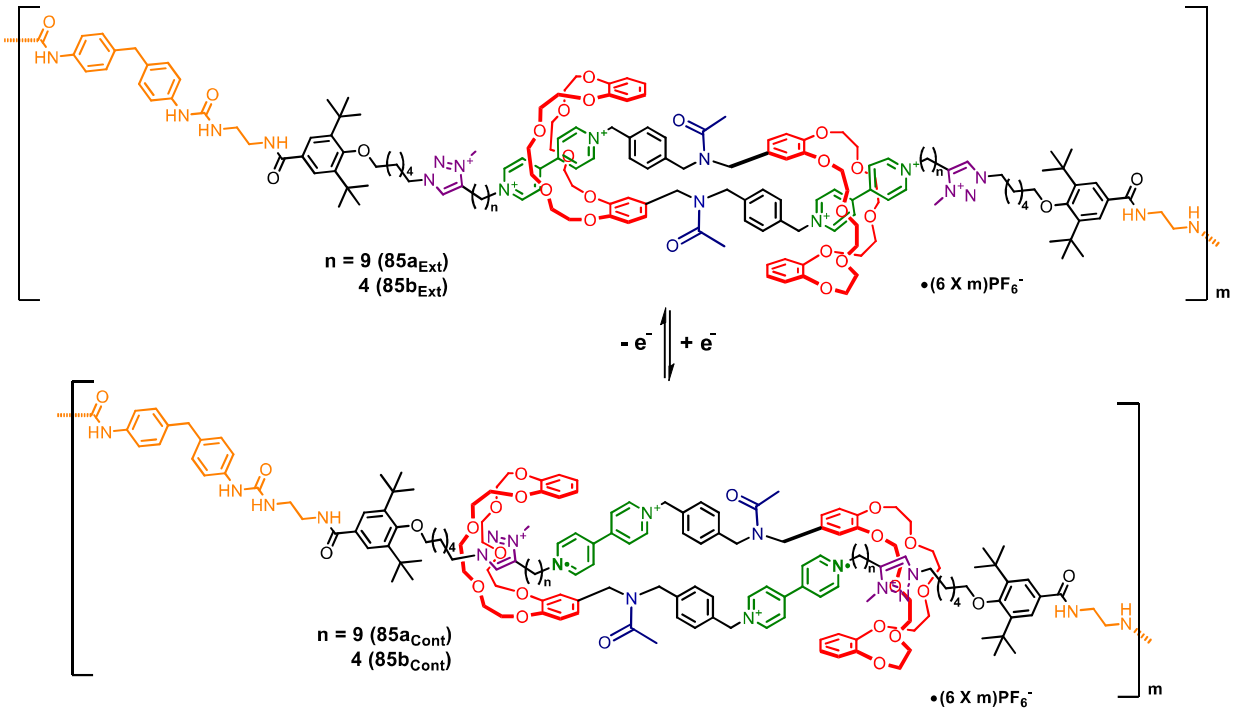

Scheme 4.31. Representation of the redox-induced contraction/extension of the poly[*c*2]daisy chain rotaxanes **85a-b**.

CV experiments are suited to evaluate the reversibility of the redox processes and the presence of subsequent chemical reactions, whereas DPV experiments allow to determine the redox potential of weak or poorly reversible processes, thanks to their higher sensitivity.[53]

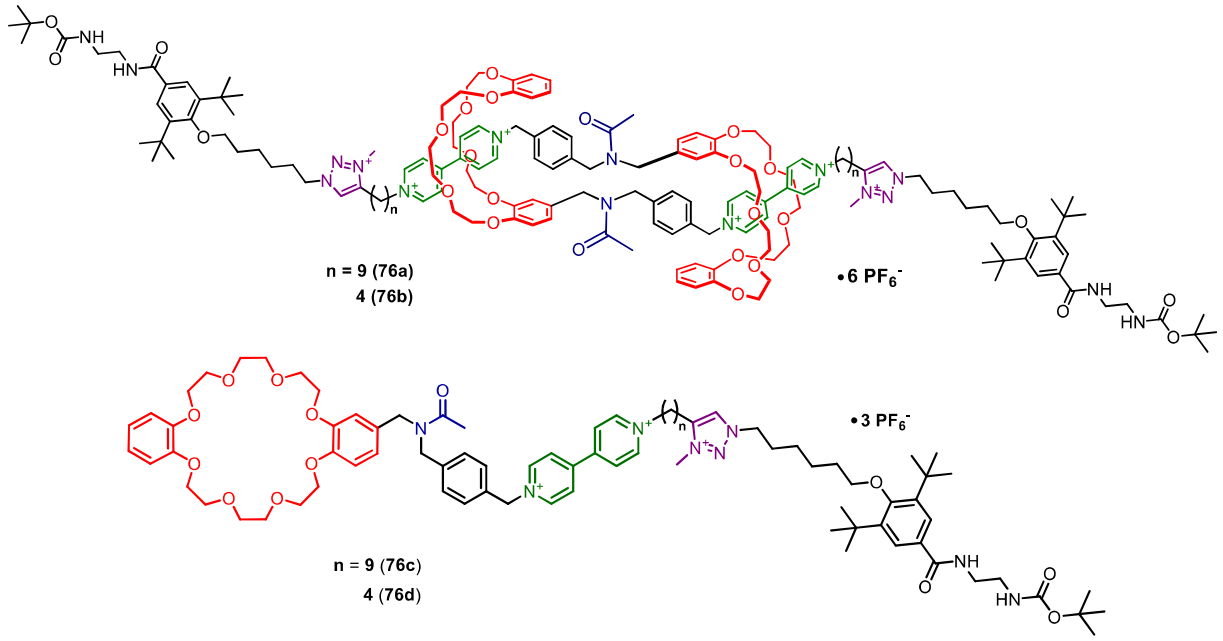

Scheme 4. 32. Chemical structures of acetylated [*c*2]daisy chain rotaxanes **76a-b** and non-interlocked derivatives **76a-b**.

The threaded models **76a** and **76b** allowed us to investigate the electrochemical properties of the monomers, and to verify their electromechanical switching. The unthreaded models gave access to the reduction potentials of the redox-active units (bipyridinium and triazolium) not surrounded by the crown ether ring. The CV pattern of unthreaded compound **76c** in dry *N*,*N*–dimethylformamide (Figure 4.20a) shows the two reversible single-electron reduction processes of the bipyridinium unit at –0.36 V and –0.75 V vs SCE, and a poorly reversible process at more negative potential values (–1.84 V vs SCE), which is ascribed to the reduction of the triazolium station.

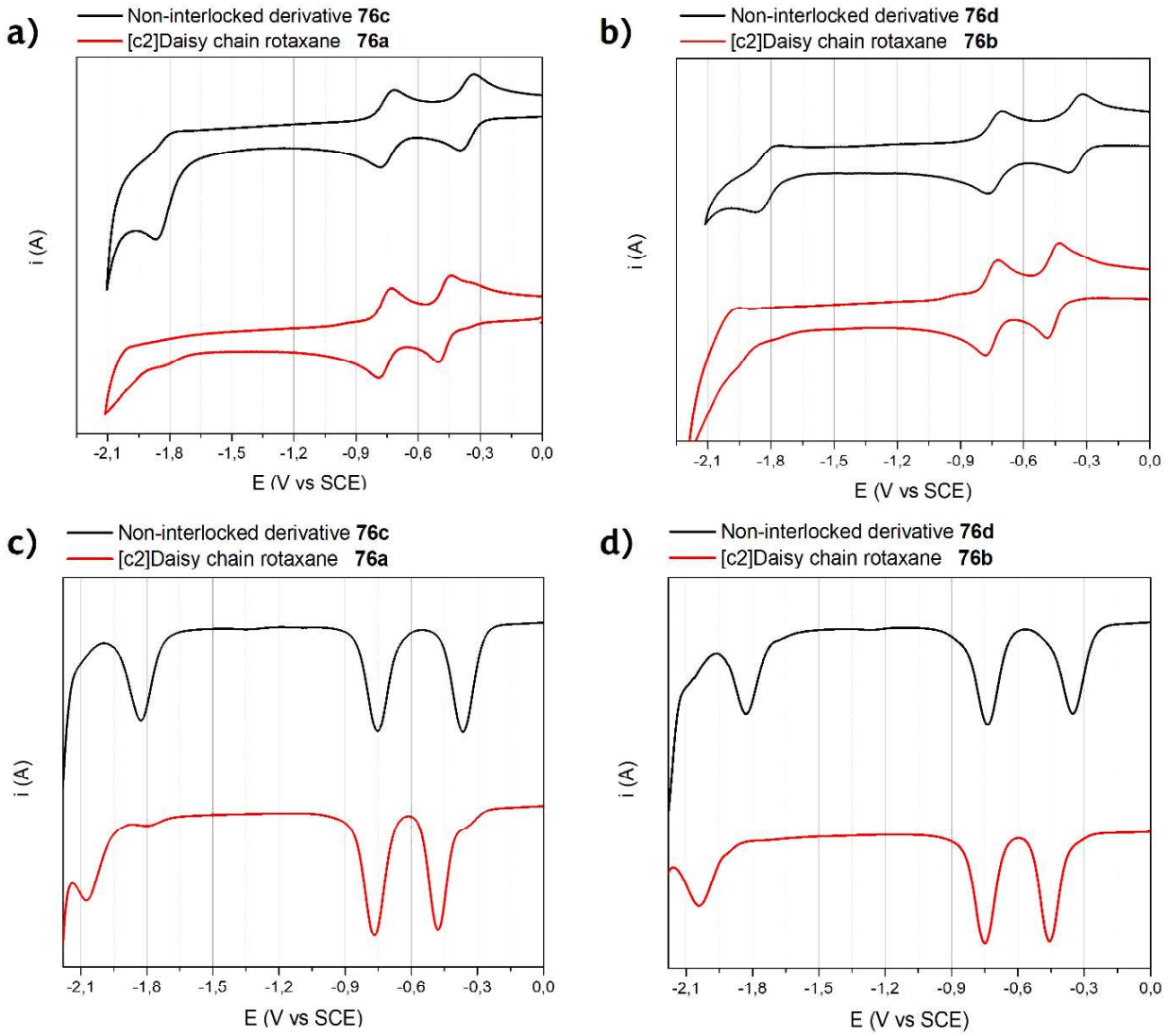

Figure 4. 20. CV curves (**a-b**) and DPV curves (**c-d**) obtained for the non-interlocked derivatives **76c** and **76d** and the [*c*2]daisy chain rotaxanes **76a** and **76b**. Conditions: deoxygenated dimethylformamide / tetraethylammonium perchlorate, 25 °C, glassy carbon working electrode, CV scan rate: 100 mV/s, DPV scan rate: 20 mV/s.

The two reversible reduction processes of the bipyridinium are also observed for the [*c*2]daisy chain rotaxane **76a** at–0.47 and –0.76 V vs SCE. The first process is negatively shifted with respect to the unthreaded compound **76c**, while the second one occurs at a very similar potential (Figure 4.20a). These results show that in the [*c*2]daisy chain rotaxane structure, the crown ether macrocycles initially surround the bipyridinium stations and then move away after their first reduction.

On the other hand, the triazolium reduction is negatively shifted in the [*c*2]daisy chain rotaxane **76a** with respect to compound **76c**: CV experiments it is not possible to distinguish this signal from the reduction of the solvent, but the process is visible at -2.06 V vs SCE in the DPV curves (Figure 4.20c). This shifted reduction indicates that the macrocycles encircle the triazolium sites, when the bipyridinium stations are reduced.

Voltammetry experiments performed on the non-interlocked derivative **76d** and the [*c*2]daisy chain rotaxane **76b** gave analogous results (Figure 4.20b). Only minor differences are observed passing from compounds containing a linker of 9 carbons between the triazolium and bipyridinium stations, to the ones with a shorter linker (4 carbons). Thus, it can be concluded that the length of the alkyl spacer does not have a strong influence on the electrochemical properties of the systems.

On the other side, the redox behaviour of polymers **85a** and **85b** (Scheme 4.31) was interpreted compared with the non-polymerized daisy chains **76a** and **76b** as models (Scheme 4.32). The two polymers showed similar cyclic voltammograms and differential pulse voltammograms in dry dimethylformamide (Figure 4.21). The two reduction processes of the bipyridinium are observed at around –0.48 and –0.76 V, in agreement with the processes observed in the model compounds. The first reduction of the bipyridinium is electrochemically poorly reversible, as denoted by the large peak-to-peak separation in the cyclic voltammetry curves. Owing to the poor reversibility of the first process, the reduction potentials of the bipyridinium units were evaluated from the DPV experiment. The second reduction is fully reversible, but a weak peak is present at slightly more negative potentials. This process could be assigned to the second reduction of the bipyridinium surrounded by the macrocycle.

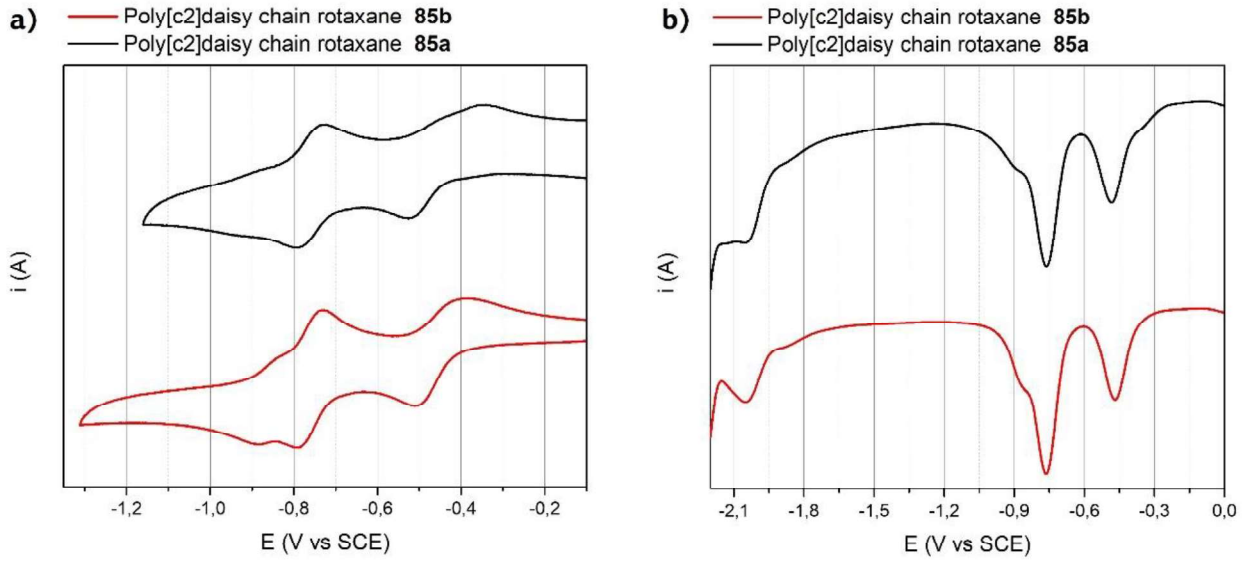

Figure 4.21. CV curves (**a**) and DPV curves (**b**) obtained for the polymers **85a** and **85b**. Conditions: deoxygenated DMF/tetraethylammonium perchlorate, 25 °C, glassy carbon working electrode, CV scan rate: 50 mV/s, DPV scan rate: 20 mV/s.

Regarding the reduction of the triazolium unit, it is shifted towards negative values, and it takes place in the proximity of the electrochemical window of the solvent, making it poorly visible in the CV experiment. This reduction process is observed at around -2.0 V vs SCE in the DPVs. As for model [*c*2]daisy chain rotaxanes, this shifted reduction is related to the presence of the macrocycles around the triazolium units, after the bipyridinium reduction. A very weak process is observed at around -1.8 V vs SCE in the DPV curves, and it could be related to a very small percentage of triazolium sites not surrounded by the macrocycle. The signal is close to the detection limit of the technique, and it is difficult to precisely evaluate its intensity. Thus, we reason that the switching process after the reduction of the bipyridinium may not be fully quantitative, but the portion of daisy chains still in the extended configuration is expected to be negligible.

Overall, these results show that in the [*c*2]daisy chain rotaxane-based polymers: i) the [*c*2]daisy chains are initially in the extended conformation, with the macrocycles surrounding the bipyridinium units; ii) when the latter are reduced, the daisy chains adopt a contracted conformation, with the macrocycles interacting with the triazolium stations; iii) the daisy chains return to their extended conformation upon re-oxidation of the bipyridinium units. The figure 4.22 displays the reduction potentials of all the models, alongside those of the polymers.

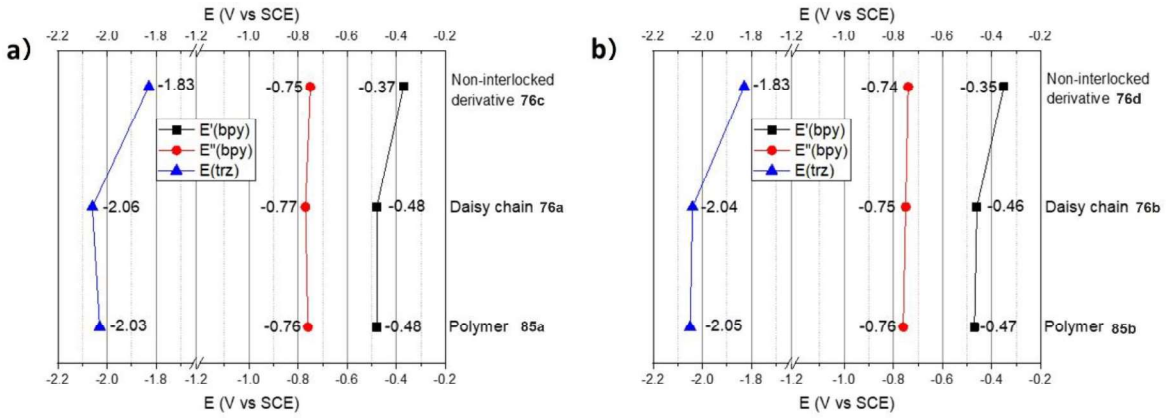

Figure 4.22. Reduction potential comparison diagrams obtained for: (**a**) the non-interlocked derivative **76c**, the daisy chain **76a**, and the polymer **85a**; (**b**) the non-interlocked derivative **76d**, the daisy chain **76b**, and the polymer **85b**. The reduction potentials are obtained from DPV experiments, and their values are reported in the diagrams.

The poor reversibility of the first process can be related to slower kinetics of the electromechanical switching; this feature is not present in the acetylated [*c*2]daisy chain rotaxanes **76a** and **76b**, and therefore it can be ascribed to the incorporation of the actuating unit in a polymeric chain. In fact, in the polymer, the contractile movement of one monomer is linked to the ones of the neighboring units and this factor can hamper the motion; this is further confirmed by the presence of voltammetric signals that would suggest that a small population of monomers persists in the extended conformation, even after reduction of the bipyridinium. Moreover, the conformational degrees of freedom in the polymer are higher than in the monomeric unit, possibly slowing down the kinetics of the switching.

In addition, the poor reversibility of the first reduction is less pronounced in polymer **85b** than in polymer **85a**. In the CV curves of **85b**, at slow scan rate (20 to 50 mV/s), the first process appears to be quasi-reversible, while, in the case of **85a**, this process shows poor reversibility even at slow scan rate. This different behavior could be related to the different length of the alkyl spacer between the two stations of the daisy chains (4 and 9 carbons, respectively), which could affect the kinetics of the electrochemical switching.

The fatigue resistance of polymers **85a** and **85b** was also investigated by repeating cyclic voltammetries without renewing the diffusion layer (Figure 4.23). The repetition of the measurement (up to 10 times) leads to only to minor changes in the voltammetric curves.

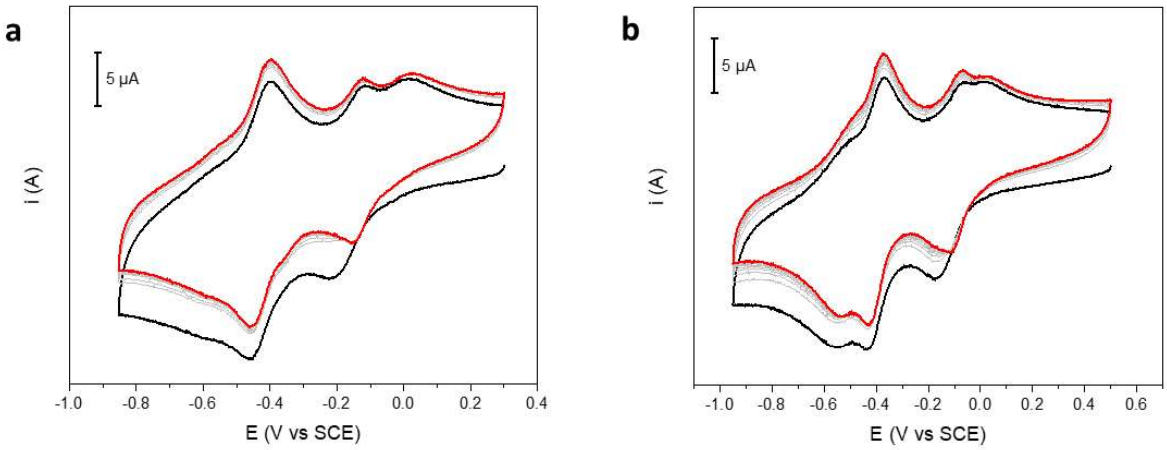

Figure 4. 23. Stack diagram of ten CV curves performed consecutively on polymers (**a**) **85a** and (**b**) **85b** without renewal of the diffusion layer. Scan 1 is shown in black, scan 10 (red), scans 2-9 (gray). Conditions: deoxygenated *N*,*N*-dimethylformamide / tetraethylammonium perchlorate, 25 °C, glassy carbon working electrode, scan rate: 1 V/s.

4.7.2. Electrospinning of the polyurea based on [*c*2]daisy chain rotaxane 85a

The central idea of the MAGNIFY project relies on the construction of an artificial myofibril based on molecular machines. In that sense, poly[*c*2]daisy chain rotaxane **85a** was electrospun pure and in blends with (poly[4,40-methylenebis(phenyl isocyanate)-alt-1,4-butanediol/di(propylene glycol)/polycaprolactone] (hence called PU), a polyurethane that is elastic enough to not hinder the contractile movement of the [*c*2]daisy chain units, and that serves as shell carrier polymer for the fibres containing molecular machines. In fact, polyurethane nanofibers are usually produced by electrospinning[54] and are good supports for the mechanical contraction/extension processes of materials.[55,56] Moreover, the MDI fragment of the isocyanate present in both polymers should favour the formation π-π and hydrogen bonding interactions between the two materials. Such intermolecular interactions were expected to enhance the alignment of the polymer chains during the electrospinning process.

Three blends of PU/**85a** were prepared by electrospinning containing the following proportions: 80/20, 70/30 and 50/50 w/w. In addition, pure polyurea **85a** in DMF was subjected to the electrospinning process. The obtained electrospun mats exhibited a pale yellow colour (Figure 4.24), containing uniform, smooth and free fibres. These fibres were observed by scanning electron microscopy (SEM) which shows highly orientated structures for polymer compositions from pure PU to the blends and pure polyurea nanofibers (Figure 4.25.)

Figure 4.24. Typical appearance of nanofibrous mats containing pure [*c*2]daisy chain rotaxane polyurea **85a**.

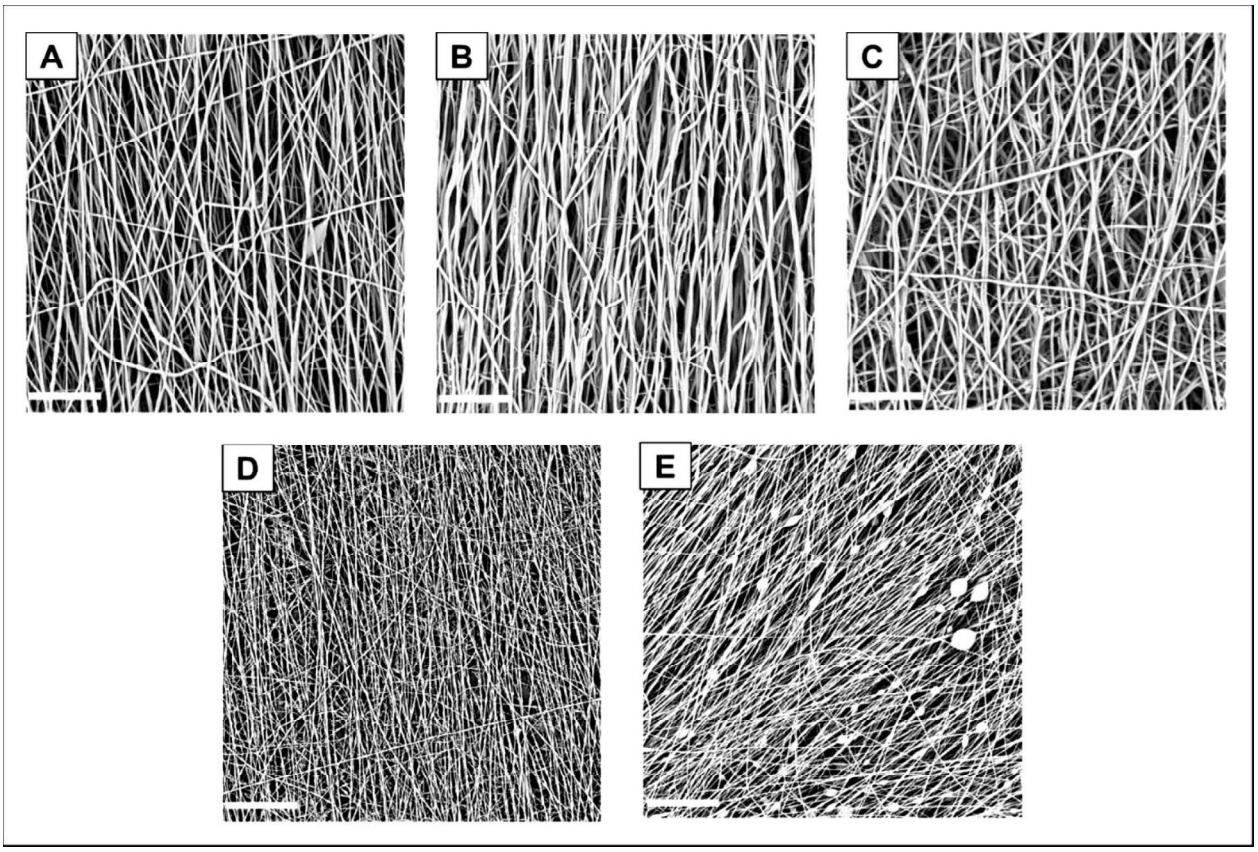

Figure 4.25. SEM images of (**A**) Pure PU nanofibers, (**B**) PU/**85a** 80:20; (**C**) PU/**85a** 70:30; (**D**) PU/**85a** 50:50; (**E**) Pure Polyurea **85a** nanofibers. Scale bar = 8 μm.

4.7.3. Small Angle Neutron Scattering (SANS) and Static Light Scattering (SLS)

SANS experiments are a powerful tool to investigate at the same time the local configuration and the shapes of objects in solution in the range of l–300 nm. We carried out the characterisation of polyurea **85a** by SANS in deuterated dimethyl sulfoxide in its extended (oxidized) and contracted (reduced) states on the Dll spectrometer at the Laue-Langevin Institute (Grenoble, France). The curves are displayed in Figure 4.26 and the data obtained for **85aExt** and **85aCont** indicate that the systems possess different organisations.

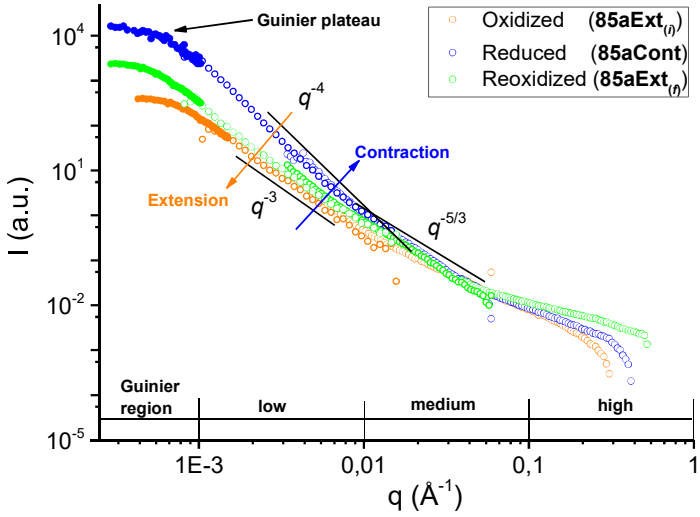

Figure 4. 26. Superimposition of the SANS spectra of a 0.5% (m/v) solution of polyurea **85aExt** in DMSO-d_6 in its initial oxidized state (empty orange circles), **85aCont** (reduced state, empty blue circles) and **85aExt** after reduction (reoxidized, empty green circles).

Large values of q give information on the local structure of the objects. In this region, we observe a continuous and non-reversible change in the curves along the molecular actuations. This behaviour is not in agreement with what we expected, nevertheless, we need further experiments to confirm and explain such behaviour. The curves are rather smooth, indicating that we do not a have a free polymer but a self-assemble of polymer chains in solution, however, further studies and complementary experiments are required to determine the supramolecular global structure of the polymer.

Additionally, in the mid-q range a slope with a decay $q^{-5/3}$ is observed for all the three curves, which indicates that polymer chains are solvated in a good solvent. At low values of q, slopes with a decay q^{-3} for **85aExt** and q^{-4} for **85aCont** were observed for the scattered intensities, indicating the presence of large assemblies. For **85aExt**, such assemblies present rough interfaces, while for **85aCont**, smooth larger aggregates are expected. Once the system is contracted, the rigidity increases, giving a better tendency to form bundles of chains, what could explain the aggregates in such state. Hydrogen bonding between the urea

units, as well as π-π stacking of the MDI aromatic units can contribute to the formation of well organised and compact bundles of chains in the contracted state. Importantly, this $q^{-3} \rightarrow q^{-4}$ transition is reversible as it can be observed in the curve for the reoxidized system (green empty circles).

Small angle neutron scattering (SANS) measurements provide structural information at the scale between 1 and 30 nm, but complementary Static Light Scattering (SLS) measurements allowed us to study our system between 20 and 300 nm. These results were overlapped and plotted in the same plot for the SANS curves, which allowed us to observe the Guinier plateau (filled coloured circles). The presence of this plateau gives an indication about the presence of finite objects in this range, and also allowed us to obtain the gyration radius R_g = 131 nm for the initial state. Complementary experiments are required to extract with the help of this data and a mathematical model, the size as well as the molecular mass of the polymer **85aExt**.

Additional experiments of SLS were carried out for a 0.5% m/v solution of polyurea **85aExt** containing 0.01 mol.L^{-1} of lithium bromide (Figure 4.27), in order to calculate the molecular weight of the polymer under the same conditions of the GPC measurements.

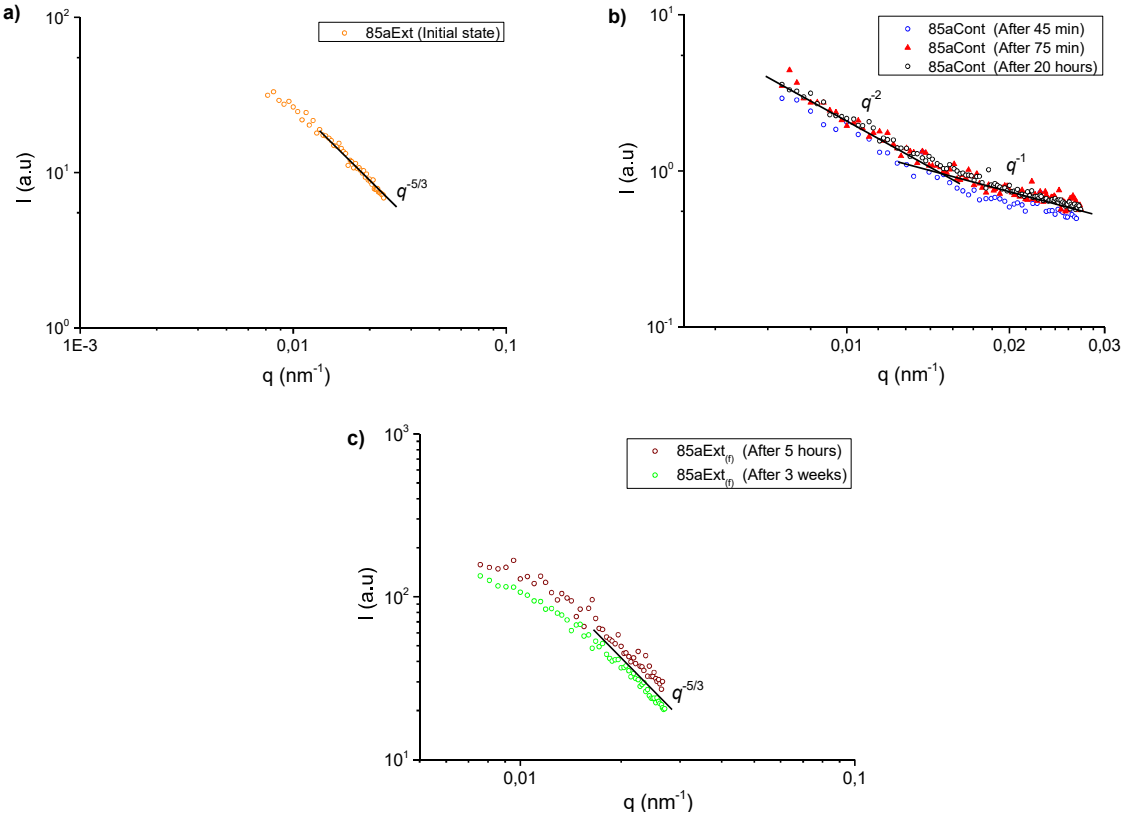

Figure 4. 27. Static Light Scattering curves for polyurea **85a** in (**a**) the extended state, (**b**) the contracted state after reduction with metallic zinc, and (**c**) the extended state after reoxidation of the system opened to the air.

For **85aExt** at the initial state, we observed a slope with a decay $q^{-5/3}$ typical of a polymer chain in a good solvent (Figure 4.27a). After reduction (**85aCont**), slopes with a decay q^{-2} and q^{-1} are observed, which corresponds to the presence of semiflexible fibres with a tendency towards rigidity (Figure 4.27b). Once the systems are reoxidized putting it contact to the opened air, we observed a slope with the same decay of $q^{-5/3}$ as for the initial state **85aExt** (Figure 4.27c), confirming the reversibility of the contraction/extension event.

Importantly, [*c*2]daisy chain rotaxane polyurea presents a good stability in the reduced state. Three measurements were carried out at different times after reduction of **85aExt** with metallic zinc (Figure 4.27b), observing that the curves remained unchanged along the time. The same behaviour was noticed for the reoxidation process of polyurea **85aExt** (Figure 4.27c). The SLS plot was the same after five hours of reoxidation and after three weeks, indicating a good stability of the polymer in solution. On the other hand, we found an increase on the gyration radius of **85aExt** (R_g = 153 nm) in presence of lithium bromide. This observation may correspond to either a counterion exchange of $(PF_6)^-$ by Br^-, or an increment of the ionic character of the solution that makes polymer chains to become more swollen, however, further studies have to be carried out to confirm our hypothesis.

4.8. Conclusions

The proposed linear synthetic strategy was successful in obtaining redox-responsive [*c*2]daisy chain rotaxane monomers in the gram scale (~3 to 4 g per batch). This pathway allows to obtain diverse electrochemically switchable polymers by late-stage functionalization of the [*c*2]daisy chain rotaxanes. Our initial approach to obtain hydrogen bonding polymers using a Upy fragment was not successful due to solubility issues. Therefore, we stand as perspective, the functionalization of the Upy fragment with groups that can provide a better solubility in common organic solvents to the final molecule.

However, although a supramolecular polymer was not obtained, our synthetic pathway allowed us to obtain covalent polymers of high molecular weights. We used MDI as diisocyanate due to its high reactivity and structural similarities with the polyurethane matrix used for blends in the electrospinning process carried out to form nanofibers. The possibility to form highly oriented fibers by electrospinning is a quite exceptional result regarding the complexity of the molecules synthesized, both in blends and in their pure form.

In addition, electrochemical studies demonstrate that [*c*2]daisy chains **77a** and **77b** monomers can be switched between the extended and contracted conformation upon reduction and re-oxidation of the bipyridinium sites. The switching appears to be fast and reversible, as denoted by the electrochemical reversibility of the bipyridinium reductions. They also show that polymers **85a** and **85b** can be switched

several times without major degradation of the systems. This achievement represents a fundamental milestone of the MAGNIFY project, giving a step further towards the amplification of the mechanical motion of the [*c*2]daisy chain units. In terms of kinetics, as expected, the polymer containing a shorter linker (**85b**) between the two redox-active station showed a faster motion that the one having a longer spacer of 9 carbons (**85a**). In comparison with non-polymerised molecules **76a** and **76b**, the contraction/extension event of the polymers is slightly slower, in agreement with the complex nature of these molecules.

We believe that altogether these results represent a huge step in the step of molecular machines and lay the foundations towards a better understanding about the behavior of molecular machines integrated in polymer systems, in order to obtain artificial molecular muscles based on the amplification of molecular motions. Currently, further studies are ongoing to accomplish the final milestone of the MAGNIFY project, which involves the actuation in the bulk of the artificial myofibrils, and which will open the door towards the use of these materials for soft robotics applications.

References

[1] C. D. Onal, D. Rus, *Bioinspiration and Biomimetics* **2013**, *026003*, 10.

[2] F. Schmitt, O. Piccin, L. Barbé, B. Bayle, *Front. Robot. AI* **2018**, *5*, 84.

[3] D. Rus, M. T. Tolley, *Nature* **2015**, *521*, 467.

[4] A. D. Marchese, R. Tedrake, D. Rus, *J. Robot. Res.* **2016**, *35*, 1000.

[5] M. Calisti, M. Giorelli, G. Levy, B. Mazzolai, B. Hochner, C. Laschi, P. Dario, *Bioinspiration and Biomimetics* **2011**, *6*, 10.

[6] M. T. Tolley, R. F. Shepherd, B. Mosadegh, K. C. Galloway, M. Wehner, R. J. Wood, G. M. Whitesides, *Soft Robot.* **2014**, *1*, 1.

[7] D. Yong, Y. Kim, S. Lee, M. Lee, J. Lee, B. Kim, N. Cho, *Mater. Sci. Eng. C* **2008**, *28*, 294.

[8] B. B. Salahuddin, H. Warren, G. M. Spinks, *Smart Mater. Struct.* **2020**, *29*, 055042.

[9] D. Kongahage, J. Foroughi, *Fibers* **2019**, *7*, 21.

[10] W. Xu, D. H. Gracias, *ACS Nano* **2019**, *13*, 4883.

[11] Z. Yu, W. Yuan, P. Brochu, B. Chen, Z. Liu, Q. Pei, *Appl. Phys. Lett.* **2009**, *95*, 1.

[12] M. De Volder, D. Reynaerts, *J. Micromechanics Microengineering* **2010**, *20*, DOI 10.1088/0960-

1317/20/4/043001.

[13] R. V. Ham, T. G. Sugar, B. Vanderborght, K. W. Hollander, D. Lefeber, *IEEE Robot. Autom. Mag.* **2009**, *16*, 81.

[14] J. D. Madden, *Science* **2007**, *318*, 1094.

[15] J. Deng, Y. Xu, S. He, P. Chen, L. Bao, Y. Hu, B. Wang, X. Sun, H. Peng, *Nat. Protoc.* **2017**, *12*, 1349.

[16] L. Kong, W. Chen, *Adv. Mater.* **2014**, *26*, 1025.

[17] T. Mirfakhrai, J. D. W. Madden, R. H. Baughman, *Mater. Today* **2007**, *10*, 30.

[18] C. Gotti, A. Sensini, G. Fornaia, C. Gualandi, A. Zucchelli, M. L. Focarete, *Front. Bioeng. Biotechnol.* **2020**, *8*, 767.

[19] C. J. Bruns, J. F. Stoddart, in *Nat. Mech. Bond*, **2016**, pp. 3–54.

[20] R. A. Bissell, E. Córdova, A. E. Kaifer, J. F. Stoddart, *Nature* **1994**, *369*, 133.

[21] P. R. Ashton, R. Ballardini, V. Balzani, I. Baxter, A. Credi, M. C. T. Fyfe, M. T. Gandolfi, M. Go, A. Piersanti, N. Spencer, J. F. Stoddart, M. Venturi, A. J. P. White, D. J. Williams, I. Frae-cnr, V. Gobetti, D. Chimica, G. Ciamician, V. Uni, V. Selmi, I. College, S. Kensington, L. Sw, *J. Am. Chem. Soc.* **1998**, *120*, 11932.

[22] G. Ragazzon, A. Credi, B. Colasson, *Chem. - A Eur. J.* **2017**, *23*, 2149.

[23] M. C. Jimenez, C. Dietrich-buchecker, J. Sauvage, *Angew Chem Int Ed* **2000**, *39*, 3284.

[24] C. J. Bruns, J. F. Stoddart, *Acc. Chem. Res.* **2014**, *47*, 2186.

[25] S. Silvi, M. Venturi, A. Credi, *J. Mater. Chem.* **2009**, *19*, 2279.

[26] F. Niess, V. Duplan, J. P. Sauvage, *Chem. Lett.* **2014**, *43*, 964.

[27] K. Fournel-Marotte, F. Coutrot, *Nat. Chem.* **2017**, *9*, 105.

[28] E. N. Guidry, J. Li, J. F. Stoddart, R. H. Grubbs, *J. Am. Chem. Soc.* **2007**, *129*, 8944.

[29] P. G. Clark, M. W. Day, R. H. Grubbs, *J. Am. Chem. Soc.* **2009**, *131*, 13631.

[30] A. Goujon, E. Moulin, G. Fuks, N. Giuseppone, *Chinese Chem. Soc.* **2019**, *1*, 83.

[31] J. Wu, K. C. F. Leung, D. Benítez, J. Y. Han, S. J. Cantrill, L. Fang, J. F. Stoddart, *Angew. Chemie - Int. Ed.* **2008**, *47*, 7470.

[32] G. Du, E. Moulin, N. Jouault, E. Buhler, N. Giuseppone, *Angew. Chemie - Int. Ed.* **2012**, *51*, 12504.

[33] A. Goujon, T. Lang, G. Mariani, E. Moulin, G. Fuks, J. Raya, E. Buhler, N. Giuseppone, *J. Am. Chem. Soc.* **2017**, *139*, 14825.

[34] J. Chang, S. Tseng, C. Lai, Y. Liu, S. Peng, S. Chiu, *Nat. Chem.* **2017**, *9*, 128.

[35] R. E. Dawson, S. F. Lincoln, C. J. Easton, *Chem. Commun.* **2008**, 3980.

[36] K. Iwaso, Y. Takashima, A. Harada, *Nat. Chem.* **2016**, *8*, 625.

[37] C. J. Bruns, J. Li, M. Frasconi, S. T. Schneebeli, J. Iehl, H. P. Jacquot De Rouville, S. I. Stupp, G. A. Voth, J. F. Stoddart, *Angew. Chemie - Int. Ed.* **2014**, *53*, 1953.

[38] C. J. Bruns, M. Frasconi, J. Iehl, K. J. Hartlieb, S. T. Schneebeli, C. Cheng, S. I. Stupp, J. F. Stoddart, *J. Am. Chem. Soc.* **2014**, *136*, 4714.

[39] A. Goujon, G. Mariani, T. Lang, E. Moulin, M. Rawiso, E. Buhler, N. Giuseppone, *J. Am. Chem. Soc.* **2017**, *139*, 4923.

[40] M. W. Rathke, P. J. Cowan, *J. Org. Chem.* **1985**, *50*, 2622.

[41] A. El-faham, F. Albericio, *Chem. Rev.* **2011**, *111*, 6557.

[42] L. C. Chan, B. G. Cox, A. Pr, S. Road, I. Park, C. Way, *J. Org. Chem.* **2007**, *72*, 8863.

[43] R. Appel, *Angew. Chem. Int. Ed.* **1975**, *14*, 801.

[44] F. Coutrot, E. Busseron, *Chem. - A Eur. J.* **2008**, *14*, 4784.

[45] V. D. Bock, H. Hiemstra, J. H. Van Maarseveen, *European J. Org. Chem.* **2006**, 51.

[46] J. E. Baldwin, *J. Chem. Soc. Chem. Commun.* **1976**, 734.

[47] M. V. Martínez-Díaz, N. Spencer, J. F. Stoddart, *Angew. Chemie (International Ed. English)* **1997**, *36*, 1904.

[48] F. H. Beijer, R. P. Sijbesma, H. Kooijman, A. L. Spek, E. W. Meijer, *J. Am. Chem. Soc.* **1998**, *120*, 6761.

[49] M. M. L. Nieuwenhuizen, T. F. A. de Greef, R. L. J. van der Bruggen, J. M. J. Paulusse, W. P. J. Appel, M. M. J. Smulders, R. P. Sijbesma, E. W. Meijer, *Chem. - A Eur. J.* **2010**, *16*, 1601.

[50] D. J. M. van Beek, A. J. H. Spiering, G. W. M. Peters, K. te Nijenhuis, R. P. Sijbesma, *Macromolecules* **2007**, *40*, 8464.

[51] J. Verjans, A. André, E. van Ruymbeke, R. Hoogenboom, *Macromolecules* **2022**, *55*, 928.

[52] H. V. Schroder, C. A. Schalley, *Chem. Sci.* **2019**, *10*, 9626.

[53] A. C. Fahrenbach, C. J. Bruns, H. Li, A. Trabolsi, A. Coskun, J. F. Stoddart, *Acc. Chem. Res.* **2014**, *47*, 482.

[54] H. Zhuo, J. Hu, S. Chen, L. Yeung, *J. Appl. Polym. Sci.* **2008**, *109*, 406.

[55] A. Pedicini, R. J. Farris, *Polymer (Guildf).* **2003**, *44*, 6857.

[56] B. K. Gu, Y. A. Ismail, G. M. Spinks, S. I. Kim, I. So, S. J. Kim, *Chem. Mater.* **2009**, *21*, 511.

[57] Y. Wei, M. J. A. Hore, *J. Appl. Phys.* **2021**, *129*, 171101.

General conclusion and perspectives

The induction of liquid crystallinity into mechanically interlocked molecules, by covalent attachment of mesogens to the dynamic molecular machine was used as synthetic approach to obtain a liquid crystalline [*c*2]daisy chain rotaxane. With our bistable LC [*c*2]daisy chain rotaxane in hands, the first objective of chapter 2 was accomplished. The second objective consisted in studying the impact of the pH-triggered sliding motion on the liquid crystalline properties of the obtained materials, where we found that both extended and contracted [*c*2]daisy chain rotaxanes exhibited SmA liquid crystalline phase. Remarkably, the compound in the extended fashion exhibited a more stable mesophase at high temperatures, than the one in the contracted state, probably due to a stronger affinity with the secondary ammonium station than with the triazolium ring. To finalize this work in the form of a publication of the first liquid crystalline [*c*2]daisy chain rotaxane, some refinements of the scattering data as well as more advanced molecular modelling are currently ongoing, in order to have a precise structural view relating the conformation of the molecular machine with the observed LC structure.

In chapter 3, we succeeded to obtain two pH-switchable [*c*2]daisy chain rotaxane monomers with free hydroxyl groups to form polyurethanes. However, we were not able to form a polymer that could be analysed or studied due to solubility issues. Additionally, along this chapter we found some lessons in terms of synthetic organic chemistry that are important to mention: The first one is to use acid-sensitive *O*-silyl protecting groups like *tert*-butyldimethylsilylchlorosilane to avoid using tetrabutylammonium fluoride as deprotecting agent in the presence of [*c*2]daisy chain rotaxanes. We observed that TBAF promoted the dethreading and in some cases the decomposition of the interlocked molecule. The second lesson learnt from this work is related to mesylation reaction. In our particular case, we observed the formation of the chlorinated product instead of the mesylated one even under standard conditions for mesylation reaction. Third, a sterically hindered phenolate containing an electron-withdrawing carbonyl group, which was the case of 3,5-di-*tert*-butyl-4-hydoxybenzaldehyde is very hard to functionalise. We emphasize in the electron withdrawing effect, since in chapter 4, we were able to functionalise the compound 3,5-di-*tert*-butyl-4-hydoxybenzene methyl ester.

Following with chapter 4, we carried out a multi-gram scale synthesis of redox-responsive [*c*2]daisy chain rotaxanes (up to 4 g) and their respective precursors (up to 40 g). The bistable molecular machines were

subjected to polymerisation reaction with MDI diisocyanate to obtain polyureas, which reversible molecular actuation was characterised in solution by electrochemistry and small angle scattering techniques (SANS, SLS). Additionally, mats made of electrospun fibres of this material were produced and analysed by SEM, revealing highly oriented polymeric fibres of [*c*2]daisy chain rotaxane polyureas. This is a milestone in the MAGNIFY project, and not only a big step for our research group but also for the field of molecular machine. It is clear that we did not arrive to this point in a straightforward manner, because before having an optimised synthetic pathway to put in operation, we planned, designed, and invested efforts in four different synthetic strategies. We overcome many challenges like common reactions that in principle should work and they did not, like the click chemistry in the first strategy, the purification of the final products, solubility issues, among others.

Currently, the next milestone will be to carry out the electrochemical actuation of the molecular machines in the material made of electrospun fibres either in the form of blend with a percentage of polyurethane, or with pure polyurea. Independently of the results obtained in such experiments, this thesis and the last chapter in particular let the road paved for our research group and for material scientists and synthetic chemist interested in pushing forward the development of stimuli-responsive materials based on the collective motion of [*c*2]daisy chain rotaxanes.

Chapter 5
Experimental part

5.1. General experimental methods and instruments

Solvents and chemical reagents. All reagents and solvents were purchased at the highest commercial quality and used without further purification unless otherwise noted. Dry solvents were obtained using a double column SolvTech purification system. Water was deionized by using a milli-gradient system (Millipore, Molsheim, France). Microwave reactions were carried out with a single mode cavity Discover SP Microwave (CEM Corporation, NC, USA), producing continuous irradiation at 2455 MHz and equipped with simultaneous external air-cooling system. Yields refer to spectroscopically purified (^{1}H Nuclear Magnetic Resonance) homogeneous materials.

Chromatographic methods. Thin Layer Chromatographies (TLC) were performed using silica on TLC Al foils (silica gel matrix with fluorescent indicator 254 nm, thickness: 500 µm, Sigma-Aldrich). In most cases, irradiation using a *Bioblock VL-4C* UV-Lamp (6 W, 254 nm and/or 365 nm) as well as potassium permanganate stain were used for visualization. Flash Column Chromatographies were performed using silica gel (60 Å, 230 - 400 mesh, 40 - 63 µm, Sigma-Aldrich). Ultra-Performance Liquid Chromatographies coupled to Mass Spectroscopy (UPLC-MS) were carried out on a *Waters Acquity UPLC-SQD* apparatus equipped with a PDA detector (190–500 nm, 80Hz and a SQD spectrometer), using a reverse phase column (Waters, BEH C18 1.7 µm, 2.1 × 50 mm or CSH Fluoro Phenyl Column, 130Å, 1.7 µm, 2.1 mm × 100 mm), the MassLynx 4.1 – XP software and a gradient (water-acetonitrile + 0.1% TFA) as eluent.

Nuclear Magnetic Resonance (NMR). ^{1}H NMR spectra were recorded on a *Bruker Avance 400* spectrometer at 400 MHz and ^{13}C NMR spectra at 100 MHz. The spectra were internally referenced to the residual solvent peaks ($CDCl_3$: 7.26 ppm, CD_3OD: 3.31 ppm, CD_3CN: 1.94 ppm, and DMSO-d_6: 2.50 ppm ^{1}H spectra, and $CDCl_3$: 77.16 ppm, CD_3OD: 49.00 ppm, CD_3CN: 118.26 and 1.32 ppm and DMSO-d_6: 39.52 ppm for ^{13}C spectra). For ^{1}H NMR assignments, the chemical shifts are given in ppm. Coupling constants *J* are given in Hz. Peaks are described as singlet (s), doublet (d), triplet (t), quartet (q), multiplet (m) and broad (b).

Mass spectrometry. Electron Spray Ionization (ESI) was recorded on a SQD mass spectrometer from Waters either by direct injection or after chromatography. High Resolution Mass Spectrometry (HR-MS) was performed on a micrOTOF-Q instrument from Bruker. Matrix-Assisted Laser Desorption/Ionization (MALDI) was performed on an Autoflex apparatus (Bruker). The sample matrix was dithranol dissolved in high purity dichloromethane and the sample solvent either in dichloromethane or *N*,*N*-dimethylformamide. Results were calibrated against a peptide calibration standard (Bruker) prepared in a mixture of acetonitrile and 0.1% TFA in ultrapure water in a volume ratio 1:2 and spotted with a 1,8- Diazabicyclo[5.4.0]undec-7ene (DBU) matrix in the same solvent system.

Gel Permeation Chromatography (GPC). GPC experiments were performed at the Institut Charles Sadron (ICS) at the Plateforme de caractérisation des polymères, on three PLgel-B columns (granulometry: 10 mm, length: 30 cm, internal diameter: 7.5 mm, separation in the $10^3 - 10^7$ g.mol^{-1}). A triple detector from Viscotek was used (light scattering, viscometer, and refractometer). A 0.1 M sodium nitrate solution of HPLC-grade dimethylformamide was used as solvent. Rate of flow: 1 mL/min. The samples were dissolved in the solvent 24 h prior to experiment and heated up to 50 °C before being filtered on a 0.45 µm PTFE filter and injected.

Differential Scanning Calorimetry (DSC). DSC experiments were performed on a Nano-DSC III from Setaram at the Institut Charles Sadron (ICS).

Small Angle Neutron Scattering (SANS). SANS data were recorded on the D11 spectrometer at the Laue-Langevin Institute (Grenoble, France). D11 is the archetype of a long, pinhole geometry instrument for small-angle neutron scattering (SANS), designed for the study of large scale structures in chemistry, biology, and solid state physics. The instrument receives neutrons from the vertical cold source of the ILL high flux reactor, which is situated about 100 m from the first part of the instrument (the selector) and about 140 m from the sample position. The detector is hence in a very low background environment.

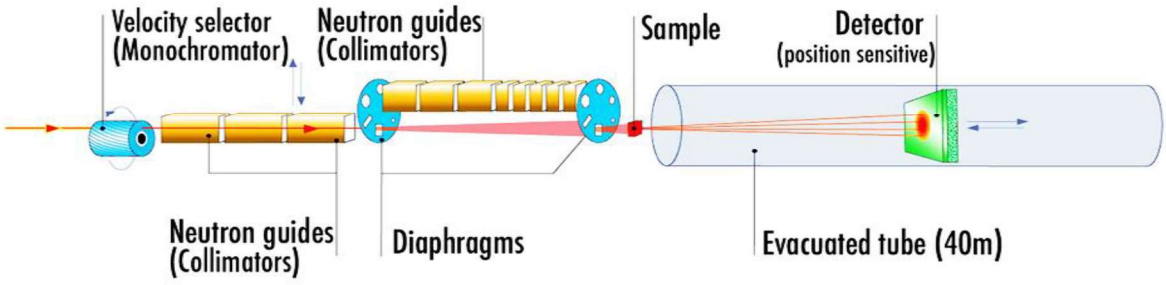

Figure 5.1. Principle of the neutron scattering method.

The polychromatic beam from the cold source is monochromated by a helical slot (ASTRIUM) velocity selector which selects neutrons of ±9 % about a mean wavelength determined by the rotation speed of the drum. The neutrons are then collimated by a series of moveable glass guides. Guide sections are inserted into or removed from the beam depending on the incident beam divergence required. The sample zone, situated 40 m down-stream from the velocity selector, may be equipped with various sample environments such as an automatic temperature controlled sample changer, cryostat, magnet, shearing cell, Bohlin rheometer, dilution refrigerator, horizontal sample-changer under vacuum, etc. Neutrons scattered from the sample are detected on a 96 x 96 cm^2 CERCA ^3He multi-detector mounted on a moveable trolley within the evacuated detector tube. The detector may be placed at any distance between 1.2 and 39 metres from the sample position, giving a total accessible momentum transfer range of 3 10^{-4} to 1 $Å^{-1}$.

Three sets of D and λ were chosen (D = 30 m and λ = 12 Å; D = 16.5 m and λ = 6 Å; D = 2.5 m and λ = 6 Å) allowing a total q-range from 0.0007 $Å^{-1}$ to 0.5 $Å^{-1}$. Data were corrected for empty cell scattering, electronic background, and detector uniformity, and then converted into absolute scale (cm^{-1}) using normalization by the attenuated direct beam classical method. The solvent was carefully subtracted, as well as the incoherent background using the infinite projection of the flat points methods. The scattering vector q is defined as:

$$q = \frac{4\pi}{\lambda}\sin\left(\frac{\theta}{2}\right) \tag{5.1}$$

where θ is the scattering angle. The absolute neutron scattering intensity I, in cm^{-1}, combines the form factor of the scattered objects $P(q)$ and the interparticle scattering factor $S_2(q)$:

$$I(q) = \frac{1}{V}\frac{d\sigma}{d\Omega} = (\Delta\rho)^2\left(V_{scattered\ objects}\ \phi_{Vol}\ P(q) + S_2(q)\right) \tag{5.2}$$

where Δρ is the contrast difference per unit volume between the scattered objects and the solvent, $V_{\text{scattered objects}} = N \times v \times m \times 1.66 \times 10^{-24}$ is the volume of the N monomers or unimers with mass m in an object, v their specific volume, and φVol their volume fraction. Δρ is defined as:

$$\Delta\rho = (\rho_{monomer} - \rho_{solvent}) \tag{5.3}$$

with ρ_{monomer} and ρ_{solvent} the scattering length densities of the monomer and the solvent, respectively, which can be calculated with their chemical compositions:

$$\rho = \sum \frac{n_i \, b_i}{N_A \, m \, v} \tag{5.4}$$

with b_i the scattering length of the n_i atom of the compound, m the molar mass of the molecule and ν its specific volume, and N_A is Avogadro's number.

Static Light Scattering (SLS). SLS data were recorded at the University Paris Diderot on the 3D DLS spectrometer (LS Instruments, Fribourg, Switzerland) equipped with a 25 mW HeNe laser (JDS uniphase) operating at λ = 632.8 nm, a two channel multiple tau correlator (1088 channels in autocorrelation), a variable-angle detection system, and a temperature-controlled index matching vat (LS Instruments). The scattering spectrum was measured using two single mode fibre detections and two high sensitivity APD detectors (Perkin Elmer, model SPCM-AQR-13-FC). Solutions were directly filtered through 0.22 μm Millipore filter into the scattering cell.

Electrochemical measurements. The electrochemical measurements were carried out in a potentiostat Autolab 30 multipurpose using glassy carbon as working electrode, platinum wire as counter electrode, Ag wire as quasi-reference electrode and ferrocene as internal standard for the potential.

5.2. Synthetic work

Oct-7-yn-1-ol (1)

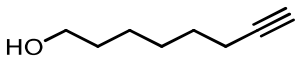

In a 500 mL two-neck round-bottom flask equipped with a stirring bar and a findenser containing fresh distilled and dried ethylene-1,2-diamine (150 mL) at 4 °C was added sodium hydride (60% suspension in oil, 7.0 g, 175 mmol). The grey cloudy mixture was allowed to warm to 65 °C under vigorous stirring for one hour to give a deep blue mixture. After cooling down the mixture to 45 °C, 3-octyn-1-ol (6.5 mL, 45 mmol) was added dropwise over fifteen minutes. The solution was stirred at 65 °C for one hour and then cooled to 4 °C using a cold bath containing a water: ice mixture. Water (100 mL) and diethyl ether (200 mL) were then added slowly to the reaction mixture, which was acidified using 12 M hydrochloric acid carefully until reaching pH 1. The aqueous layer was extracted with diethyl ether (3 x 200 mL) and the organic layers were combined, dried over sodium sulfate, and concentrated. The crude residue was purified by column chromatography (SiO_2 (200 g), *n*-pentane| EtOAc 10% → *n*-pentane | EtOAc 40%) to provide compound **1** (4.6 g, 80%) as a pale yellow liquid.

^{1}H NMR ($CDCl_3$, 400 MHz, 25 °C): δ = 3.63 (t, *J* = 6.7 Hz, 2H), 2.19 (td, *J* = 7.0, 2.7 Hz, 2H), 1.91 (t, *J* = 2.6 Hz, 1H), 1.61 – 1.51 (m, 4H), 1.49 – 1.33 (m, 4H).

^{13}C NMR ($CDCl_3$, 100 MHz, 25 °C): δ = 84.7, 68.3, 63.0, 32.7, 28.6, 28.5, 25.4, 18.5.

2-(oct-7-yn-1-yl)isoindoline-1,3-dione (2)

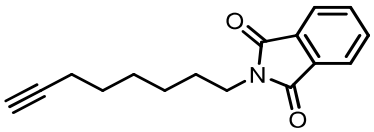

In a 100 mL one-neck round-bottom flask equipped with a stirring bar was prepared a mixture of alcohol **1** (0.50 g, 3.96 mmol), PPh_3 (1.1 g, 4.2 mmol), and phthalimide (0.61 g, 4.2 mmol) in anhydrous tetrahydrofuran (15 mL). Diisopropyl azodicarboxylate (DIAD; 0.8 mL, 4.2 mmol) was slowly added to the solution, and the reaction mixture was stirred for three hours at 0 °C and then during two days at 25 °C. Water (30 mL) was added and the aqueous phase was extracted with dichloromethane (2 x 30 mL). The organic layers were combined, dried over sodium sulfate, and evaporated. The crude residue was purified by column chromatography (SiO_2 (100 g), cyclohexane| EtOAc 10%) to afford compound **2** (0.7 g, 70%) as a white solid.

^{1}H NMR ($CDCl_3$, 400 MHz, 25 °C): δ = 7.90 – 7.80 (m, 2H), 7.76 – 7.67 (m, 2H), 3.68 (td, *J* = 7.5, 1.3 Hz, 2H), 2.18 (td, *J* = 7.0, 2.7 Hz, 2H), 1.91 (t, *J* = 2.6 Hz, 1H), 1.68 (p, *J* = 7.4, 6.8 Hz, 2H), 1.52 – 1.25 (m, 8H).

^{13}C NMR ($CDCl_3$, 100 MHz, 25 °C): δ = 169.1, 132.4, 132.0, 122.1, 84.5, 68.1, 41.9, 33.7, 28.6, 27.5, 27.4, 18.5.

ESI-MS: m/z calcd. For $C_{16}H_{18}NO_2$: 256.13 $[M+H]^+$, found: 256.26

Oct-7-yn-1-amine (3)

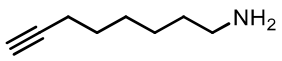

In a 250 mL one-neck round-bottom flask equipped with a stirring bar and a findenser was prepared a solution of compound **2** (3.0 g, 11.8 mmol) in methanol (100 mL). Hydrazine hydrate 25% (3 mL, 60 mmol) was added to the mixture, which was stirred at reflux for four hours and then cooled down to room temperature. After removing the solvent, the residue was taken back in a 2 M potassium hydroxide solution (50 mL). The solution was extracted three times with dichloromethane (3 x 50 mL) and then the organic layers were dried over sodium sulfate and concentrated to yield compound **3** (1.0 g, 69%) as a pale yellow liquid.

^{1}H NMR ($CDCl_3$, 400 MHz, 25 °C): δ = 2.69 (t, *J* = 6.7 Hz, 2H), 2.18 (td, *J* = 7.0, 2.7 Hz, 2H), 1.91 (t, *J* = 2.6 Hz, 1H), 1.59 – 1.42 (m, 2H), 1.40 – 1.23 (m, 6H).

^{13}C NMR ($CDCl_3$, 100 MHz, 25 °C): δ = 84.5, 68.1, 41.9, 33.7, 28.6, 27.5, 27.4, 18.5.

1,2-bis(2-(2-(2-hydroxyethoxy)ethoxy)ethoxy)benzene (4)

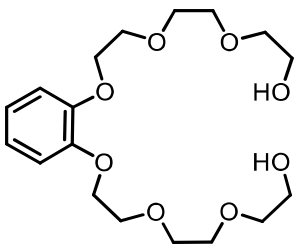

A 250 mL two-neck round-bottom flask equipped with a stirring bar and a findenser was charged with catechol (2.7 g, 24.5 mmol), potassium carbonate (8.4 g, 61.5 mmol), and lithium bromide (2.2 g, 25 mmol) suspended in dry *N*,*N*–dimethylformamide (120 mL). 2-[2-(2-chloroethoxy]ethanol (7.5 mL, 52 mmol) was added dropwise under argon and the reaction mixture was stirred at 96 °C during three days. Then, the solvent was evaporated, the residue dissolved in CH_2Cl_2 (120 mL) and washed with 10% K_2CO_3 solution (3

x 100 mL). The organic layers were combined, dried over sodium sulfate, and concentrated under reduced pressure to yield compound **4** (8.80 g, 96%) as a brown oil, which was pure enough to be used in the next step.

^{1}H NMR ($CDCl_3$, 400 MHz, 25 °C): δ = 6.91 (s, 4H), 4.19 – 4.17 (m, 4H), 3.90 – 3.87 (m, 4H), 3.77 – 3.68 (m, 12H), 3.62 – 3.60 (m, 4H).

^{13}C NMR ($CDCl_3$, 100 MHz, 25 °C): δ = 148.4, 121.6, 113.6, 72.9, 70.8, 70.2, 69.6, 68.2, 61.7.

ESI-MS: m/z calcd. For $C_{18}H_{31}O_8$: 375.20 $[M+H]^+$, found: 375.69

1,2-bis(2-{2-[2-(*p*-toluenesulfonoyloxy)ethoxy]ethoxy}ethoxy)benzene (5)

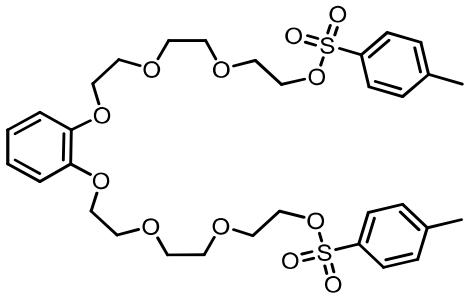

A 500 mL two-neck round-bottom flask equipped with a stirring bar was charged with compound **4** (8,8 g, 23.5 mmol), triethylamine (12 mL, 90 mmol) and 4-(dimethylamino)pyridine (0.3 g, 2.5 mmol) dissolved in dry dichloromethane (50 mL) and the solution was cooled down to 4 °C using a water: ice bath. A solution of *p*-toluenesulfonylchloride (12.5 g, 65 mmol) in dichloromethane (150 mL) was then added dropwise over a period of 30 minutes at 4 °C. The reaction mixture was stirred overnight at room temperature. Then, it was acidified with a 1 M HCl solution (100 mL), and the organic phase was washed with brine (100 mL) and dried over sodium sulfate. The solvent was then removed, and the residue was purified by column chromatography (SiO_2 (300 g), Cyclohexane: EtOAc 30% →60% →90%) to yield compound **5** (12 g, 75%) as a light orange oil.

^{1}H NMR ($CDCl_3$, 400 MHz, 25 °C): δ = 7.78 (d, *J* = 8.3 Hz, 4H), 7.32 (d, *J* = 8.0 Hz, 4H), 6.90 (s, 4H), 4.12 – 4.16 (m, 8H), 3.83 – 3.80 (m, 4H), 3.70 – 3.66 (m, 8H), 3.62 – 3.58 (m, 4H), 2.42 (s, 6H).

^{13}C NMR ($CDCl_3$, 100 MHz, 25 °C): δ = 149.0, 144.9, 133.1, 129.9, 128.1, 121.8, 114.9, 70.9, 70.8, 69.9, 69.4, 68.9, 68.8, 21.8.

ESI-MS: m/z calcd. for $C_{32}H_{44}O_{13}S_2$: 700.22 $[M+H_2O]^+$, found: 700.78

(2-formyl)dibenzo[24]crown-8 (6)

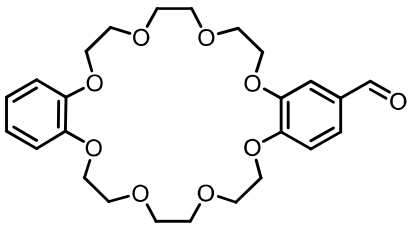

A 1 L two-neck round-bottom flask equipped with a stirring bar, a findenser and a dropping funnel was charged with caesium carbonate (22.0 g, 67.5 mmol) and 4-formylcatechol (2.2 g, 16 mmol) dissolved in dry tetrahydrofuran (200 mL). The bistosylate **5** (12.0 g, 17.5 mmol) was dissolved in dry tetrahydrofuran (100 mL) and charged in the dropping funnel, while the suspension was maintained under stirring at 65 °C during thirty minutes. The bistosylate solution was added dropwise over ninety minutes and the reaction mixture was stirred at 65 °C for three days. Then, the solvent was removed, and the residue was taken back in chloroform (200 mL) and washed with 10% potassium carbonate (200 mL). The organic phase was dried over sodium sulfate, the solvent evaporated and the crude residue was purified by column chromatography (SiO_2 (200 g), EtOAc → EtOAc: MeOH 2%) to yield compound **6** (4.5 g, 59%) as a white solid.

^{1}H NMR ($CDCl_3$, 400 MHz, 25 °C): δ = 9.81 (s, 1H), 7.41 (dd, *J* = 8.1, 1.9 Hz, 2H), 7.37 (d, *J* = 8.2 Hz, 1H), 6.94 (d, *J* = 8.2 Hz, 1H), 6.89-6.86 (m, 4H), 4.22-4.18 (m, 8H), 3.96 – 3.92 (m, 8H), 3.84 – 3.82 (m, 8H).

^{13}C NMR ($CDCl_3$, 100 MHz, 25 °C): δ = 190.9, 154.4, 149.3, 149.0, 130.3, 126.9, 121.5, 114.2, 112.0, 111.2, 71.7, 71.5, 71.4, 70.1, 69.7, 69.8.

ESI-MS: m/z calcd. for $C_{25}H_{34}O_{10}$: 494.20 $[M+H_2O]^+$, found: 494.16

Compound 8

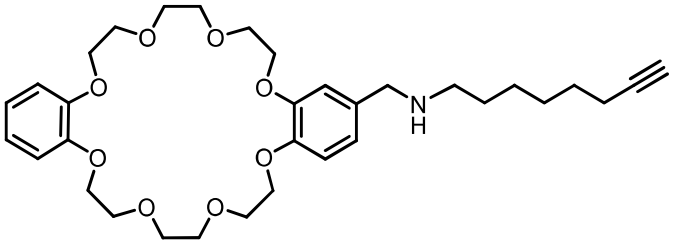

A 500 mL two-neck round-bottom flask equipped with a stirring bar and a findenser was charged with compound **6** (2.0 g, 4.2 mmol) and oct-7-yn-1-amine (0.53 g, 4.3 mmol) in dry toluene (100 mL). The solution was heated during 15h at reflux using a Dean-Stark apparatus. The solvent was then evaporated under reduced pressure providing the imine derivative as a yellow oil (compound **7**). This oil was dissolved in

anhydrous methanol (100 mL), and then, sodium borohydride (0.8 g, 21 mmol) was added portionwise at 0 °C. The solution was then stirred at room temperature during four hours, then a 1 M aqueous solution of HCl (100 mL) was added to the mixture. The solvent was evaporated, and the residue was taken back in dichloromethane (150 mL) and the organic phase was washed with a 2 M aqueous solution of NaOH (100 mL), dried over sodium sulfate and concentrated under reduced pressure. The crude was purified by column chromatography (SiO_2 (100 g), CH_2Cl_2|MeOH|NH4OH 85|10|5) to yield compound **8** (1.8 g, 69%) as a pale yellow oil.

^{1}H NMR ($CDCl_3$, 400 MHz, 25 °C): δ = 6.96 – 6.76 (m, 7H), 4.18 – 4.11 (m, 8H), 3.92 – 3.82 (m, 16H), 3.69 (s, 2H), 2.59 (t, *J* = 7.3 Hz, 2H), 2.17 (td, *J* = 7.0, 2.6 Hz, 2H), 1.93 (t, *J* = 2.6 Hz, 1H), 1.55 – 1.25 (m, 8H).

^{13}C NMR ($CDCl_3$, 100 MHz, 25 °C): δ = 149.0, 148.9, 147.9, 133.9, 121.5, 120.9, 114.2, 114.0, 84.7, 71.3, 70.7, 69.6, 69.5, 68.3, 53.8, 49.4, 30.0, 28.7, 28.4, 26.9, 18.4.

ESI-MS: m/z calcd. for $C_{33}H_{48}NO_8$: 586.34 $[M+H]^+$, found: 586.43

Pseudo[*c*2]daisy chain rotaxane (9)

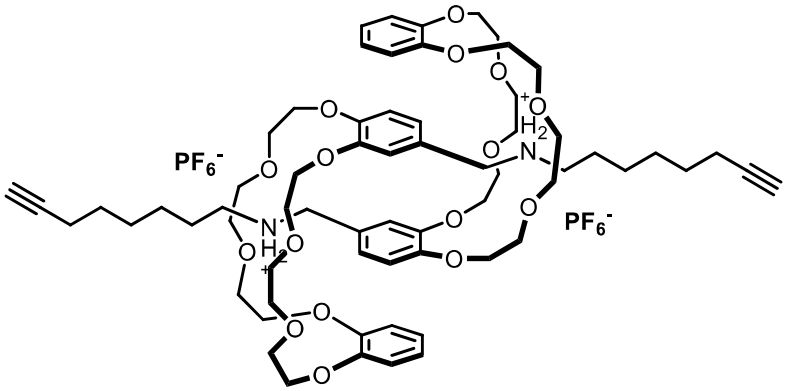

In a 100 mL one-neck round-bottom flask equipped with a stirring bar was prepared a solution of amine **8** (1.8g, 5.7 mmol) in diethyl ether (30 mL). A 2 M HCl solution in diethyl ether (10 mL) was slowly added to the suspension, which was stirred for one hour at room temperature. The solvent was evaporated and the solid taken back in a biphasic mixture of an aqueous solution of NH_4PF_6 (2.0 g in 20 mL of H_2O) and dichloromethane (20 mL). The mixture was vigorously stirred for two hours, then the organic phase was extracted with CH_2Cl_2 (2 x 10 mL), dried over sodium sulfate, and concentrated under reduced pressure to yield compound **9** (2.0 g, 92%) as a beige solid.

^{1}H NMR ($CDCl_3$, 400 MHz, 25 °C): δ = 6.91 (d, *J* = 8.3 Hz, 2H) 6.85-6.70 (m, 10H), 6.57 (s, 2H), 4.44-4.38 (m, 2H), 4.35 – 4.29 (m, 2H), 4.23 – 3.63 (m, 48H), 3.56 – 3.36 (m, 4H), 2.09 (td, *J* = 6.9, 1.8 Hz, 4H), 1.92 (brs, 2H), 1.48 – 1.14 (m, 16H).

^{13}C NMR ($CDCl_3$, 100 MHz, 25 °C): δ = 147.9, 147.8, 147.0, 146.5, 146.3, 124.8, 123.2, 121.4, 121.2, 113.4, 112.7, 112.0, 84.4, 72.6, 72.0, 71.3, 71.0, 70.6, 69.6, 68.8, 67.8, 67.2, 67.0, 66.9, 52.4, 49.0, 28.2, 26.8, 26.4, 18.0.

ESI-MS: m/z calcd. for $C_{66}H_{96}N_2O_{16}P_2F_{12}$: 586.84 $[M\text{-}2PF_6]^{2+}$, found: 586.45

4-ethoxy-2,3-difluoro-4'-(4-pentylcyclohexyl)-1,1'-biphenyl (12)

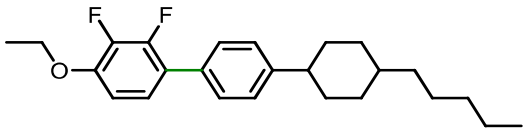

A 50 mL two-neck round-bottom flask equipped with a stirring bar and a findenser was charged with (4-ethoxy-2,3-difluorophenyl)boronic acid (2.0 g, 9.90 mmol), potassium carbonate (1.65 g, 11.94 mmol) and 1-iodo-4-(4-pentylcyclohexyl)benzene (3.6 g, 10.10 mmol) dissolved in a mixture of water (6 mL), toluene (13 mL) and ethanol (6 mL). The resulting mixture was degassed with argon at room temperature during five minutes under vigorously stirring. Then, the palladium catalyst $Pd(PPh_3)_4$ (0.12 g, 0.104 mmol) was added leading to a colour change from white to dark brown. The reaction mixture was heated up to 80 °C under continuous stirring for twenty hours and then, cooled at room temperature. The mixture was poured in water (10 mL) and the aqueous phase was extracted with dichloromethane (3 x 10mL). The organic phases were washed with water (10 mL), dried over sodium sulfate, evaporated under reduced pressure and the crude residue was purified by silica column chromatography using cyclohexane to yield compound **12** as a white solid (3.46 g, 90%).

^{1}H NMR ($CDCl_3$, 400 MHz, 25 °C): δ = 7.43 (d, *J* = 8.1 Hz, 2H), 7.28 (d, *J* = 8.1 Hz, 2H), 7.09 (td, *J* = 8.4, 2.1 Hz, 1H), 6.99–6.94 (m, 1H,), 4.13 (q, 2H), 2.51 (t, *J* = 12.1 Hz, 1H), 1.91 (t, *J* = 14.1 Hz, 2H), 1.49-1.44 (m, 8H), 1.36-1.21 (m, 8H), 1.11 – 1.02 (m, 2H), 0.91 (t, *J* = 6.5 Hz, 3H).

^{13}C NMR ($CDCl_3$, 100 MHz, 25 °C): δ = 149.6, 147.7, 147.1, 144.0, 141.7, 139.3, 132.3, 128.7, 127.2, 124.5, 123.1, 112.3, 64.6, 44.5, 37.5, 37.4, 34.4, 33.7, 32.4, 31.0, 29.6, 26.9, 22.2, 14.8, 14.3.

2,3-difluoro-4'-(4-pentylcyclohexyl)-[1,1'-biphenyl]-4-ol (13)

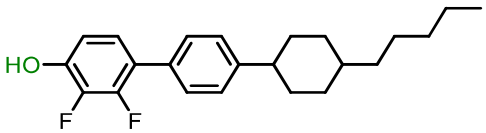

In a 100 mL one-neck round-bottom flask equipped with a stirring bar was dissolved compound **12** (3.46 g, 8.96 mmol) in dried dichloromethane (20 mL). The solution was cooled down at -70 °C using a dry ice: acetone cool bath and boron tribromide (1.15 mL, 12.2 mmol) was slowly added under argon atmosphere. The mixture was stirred during one hour at -70 °C and then, the mixture was allowed to reach room temperature under continuous stirring for 20 hours. Water (10 mL) was added dropwise to avoid exothermic reactions and the aqueous phase was extracted with dichloromethane (2 x 20 mL). The organic phases were dried over sodium sulfate and evaporated under reduced to yield compound **13** (3.13 g, 96%) as a white solid. The product was used for the next steps without any further purification process.

^{1}H NMR ($CDCl_3$, 400 MHz, 25 °C): δ = 7.42 (dd, *J* = 8.3, 1.6 Hz, 2H), 7.28 (d, *J* = 8.1 Hz, 2H), 7.08 (td, *J* = 8.3, 2.3 Hz, 1H), 6.84 (ddd, *J* = 8.7, 8.0, 2.0 Hz, 1H), 5.19 (d, *J* = 3.7 Hz, 1H), 2.50 (tt, *J* = 12.3, 3.1 Hz, 1H), 1.95–1.86 (m, 4H), 1.48 (qd, *J* = 13.9, 13.4, 3.6 Hz, 2H), 1.35-1.20 (m, 9H), 1.12–1.02 (m, 2H), 0.90 (t, *J* = 7.0 Hz, 3H).

^{13}C NMR ($CDCl_3$, 100 MHz, 25 °C): δ = 149.6, 147.7, 147.1, 144.0, 141.7, 139.3, 132.3, 128.7, 127.2, 124.5, 123.1, 112.3, 44.5, 37.5, 37.4, 34.4, 33.7, 32.4, 26.8, 22.9, 14.3.

ESI-MS: m/z calcd. for $C_{23}H_{28}F_2O$: 380.19 $[M\text{-}H + Na]^{+\cdot}$, found: 380.33

Compound 14

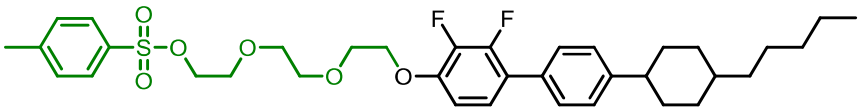

In a 100 mL one-neck round-bottom flask equipped with a stirring bar and a findenser was charged with the phenolic derivative **13** (2.75 g, 7.7 mmol), triethylene glycol di(*p*-toluenesulfonate) (10.5 g, 23 mmol), anhydrous potassium carbonate (1.59 g, 11.5 mmol) and potassium iodide (0.13 g, 0.77 mmol). Dry acetone (50 mL) was added and the solution was refluxed under argon atmosphere during 24 hours. The reaction was cooled down to room temperature, the solvent was removed under reduced pressure and the crude residue was purified by column chromatography (SiO2, Cyclohexane/Ethyl Acetate 20%) yielding compound **14** as a white solid (3.0 g, 60%).

^{1}H NMR (CDCl$_3$, 400 MHz, 25 °C): δ = 7.79 (d, *J* = 8.3 Hz, 2H), 7.42 (d, *J* = 8.2 Hz, 2H), 7.33 (d, *J* = 8.6 Hz, 2H), 7.28 (d, *J* = 8.5 Hz, 2H), 7.09 (td, *J* = 8.4, 2.3 Hz, 1H), 6.81 (ddd, *J* = 8.9, 7.7, 1.9 Hz, 1H), 4.24 – 4.19 (m, 2H), 4.18 – 4.15 (m, 2H), 3.89 – 3.85 (m, 2H), 3.73 – 3.66 (m, 4H), 3.64 – 3.60 (m, 2H), 2.51 (tt, *J* = 12.3, 3.4 Hz, 1H), 2.43 (s, 3H), 1.90 (td, *J* = 16.2, 15.1, 2.1 Hz, 4H), 1.48 (dd, *J* = 12.7, 2.8 Hz, 2H), 1.33-1.23 (m, 9H), 1.06 (qd, *J* = 12.3, 11.6, 3.1 Hz, 2H), 0.91 (t, *J* = 6.5 Hz, 3H).

^{13}C NMR (CDCl$_3$, 125 MHz, 25 °C): δ = 150.1, 147.6, 147.4, 144.9, 140.9, 133.1, 132.3, 129.9, 128.7, 128.1, 127.2, 123.7, 123.6, 110.1, 71.0, 70.9, 69.7, 69.6, 69.4, 68.9, 44.5, 37.5, 37.4, 34.4, 33.7, 32.3, 26.8, 22.9, 21.7, 14.2.

ESI-MS: m/z calcd. for $C_{36}H_{48}F_2O_7S$: 662.31 $[M+H_2O]^+$, found: 662.54

Compound 15

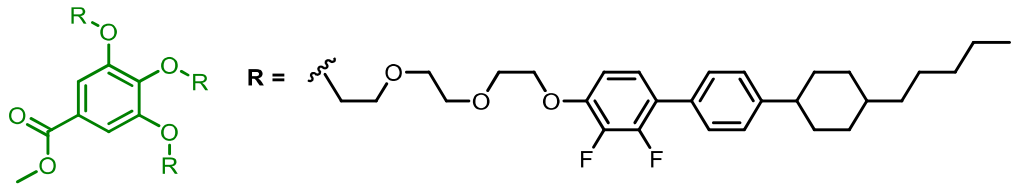

In a 100 mL one-neck round-bottom flask equipped with a stirring bar and a findenser was dissolved compound **14** (1.4 g, 2.2 mmol), methyl gallate (0.10 g, 0.55 mmol), and potassium carbonate anhydrous (0.45 g, 3.2 mmol) in dried methyl ethyl ketone (5 mL). The reaction mixture was stirred for 24 h at 70 °C under argon atmosphere. After cooling to room temperature, water (10 mL) was added and the product was extracted with ethyl acetate (3 x 10 mL). The organic layers were washed with brine (2 x 5 mL), dried over sodium sulfate and the solvent was evaporated under reduced pressure. The crude residue was purified by column chromatography (SiO_2, Cyclohexane/Ethyl acetate 20%→50%→70%) yielding compound **15** (0.4 g, 50%).as a waxy solid.

^{1}H NMR (CDCl$_3$, 400 MHz, 25 °C): δ = 7.44-7.38 (m, 6H), 7.31 (s, 2H) 7.29-7.24 (m, 6H), 7.10-7.02 (m, 3H), 6.84-6.75 (m, 3H), 4.26-4.18 (m, 12H), 3.89-3.81 (m, 15H), 3.75-3.73 (m, 12H), 2.49 (t, *J* = 12.1 Hz, 3H), 1.90 (t, *J* = 12.8 Hz, 9H), 1.47 (qd, *J* = 14.2, 13.5, 3.5 Hz, 6H), 1.36-1.20 (m, 30H), 1.12 – 1.00 (m, 6H), 0.91 (t, *J* = 6.5 Hz, 9H).

^{13}C NMR (CDCl$_3$, 100 MHz, 25 °C): δ = 166.1, 152.9, 150.1, 147.6, 147.4, 137.8, 136.7, 132.4, 128.7, 127.2, 123.7, 123.6, 110.1, 110.0, 106.4, 72.5, 71.2, 70.7, 69.9, 69.6, 68.9, 65.4, 44.5, 37.5, 37.4, 34.4, 33.7, 32.4, 26.8, 22.9, 14.3.

Compound 16

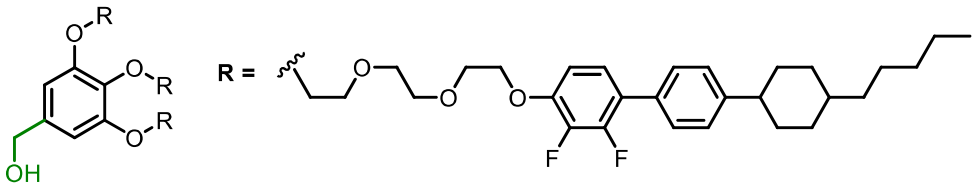

In a 25 mL one-neck round bottom flask equipped with a stirring bar was prepared a solution of ester **15** (0.20 g, 0.12 mmol) in dry tetrahydrofuran (10 mL). The solution was cooled down to 4 °C and lithium aluminium hydride (0.175 g, 0.44 mmol) was added under argon atmosphere. The reaction mixture was stirred at 25 °C for six hours and monitored by thin layer chromatography. When no remaining started material was observed, a 1 M HCl solution (10 mL) was added at 4 °C and the aqueous phase was extracted with dichloromethane (2 x 20 mL). The combined organic layers were dried over sodium sulfate and evaporated under reduced pressure to yield alcohol **16** (0.18 g, 92%) as a waxy white solid.

^{1}H NMR (CDCl$_3$, 400 MHz, 25 °C): δ = 7.42-7.38 (m, 6H), 7.27-7.24 (m, 6H), 7.09-7.02 (m, 3H), 6.81-6.76 (m, 3H), 6.60 (s, 2H), 4.55 (s, 2H) 4.22-4.14 (m, 12H), 3.90-3.80 (m, 12H), 3.74 (s, 12H), 2.50 (t, *J* = 12.0 Hz, 3H), 1.90 (t, *J* = 12.8 Hz, 12H), 1.47 (qd, *J* = 13.9, 13.3, 3.2 Hz, 6H), 1.36-1.16 (m, 27H), 1.11-1.01 (m, 6H), 0.90 (t, *J* = 7.0 Hz, 9H).

^{13}C NMR (CDCl$_3$, 125 MHz, 25 °C): δ = 152.9, 150.1, 147.6, 147.4, 137.8, 136.7, 132.4, 128.7, 127.2, 123.7, 123.6, 110.1, 110.0, 106.4, 72.5, 71.2, 70.8, 70.7, 69.9, 69.6, 68.9, 65.4, 44.5, 37.5, 37.4, 34.4, 33.7, 32.4, 26.8, 22.9, 14.3.

HR-MS: m/z calcd. for $C_{94}H_{122}F_6O_{13}$: 1596.8716 $[M + Na]^+$, found: 1596.8723

Compound 17

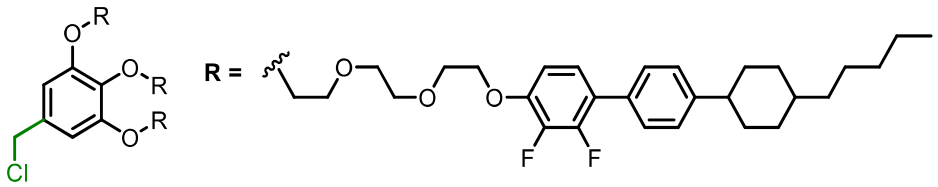

A 25 mL one-neck round bottom flask equipped with a stirring bar was charged with aryl alcohol **16** (0.18 g, 0.11 mmol) and a catalytic amount of dry *N*,*N*-dimethylformamide (one drop). Dry dichloromethane (2 mL) was added and thionyl chloride (0.019 g, 12 µL, 0.16 mmol) was added carefully to the reaction mixture. After continuous stirring for two hours, the volatile compounds were removed and the residual mixture was dissolved in dichloromethane (10 mL) and washed with water (2 x 5 mL). The solvent was

evaporated under reduced pressure yielding compound **17** which was pure enough to be used in the next step without further purification.

^{1}H NMR ($CDCl_3$, 400 MHz, 25 °C): δ = 7.42-7.38 (m, 6H), 7.27-7.24 (m, 6H), 7.08-7.02 (m, 3H), 6.79 (ddd, *J* = 9.0, 5.7, 1.9 Hz, 3H), 6.61 (s, 2H), 4.45 (s, 2H) 4.22-4.14 (m, 12H), 3.90-3.85 (m, 10H), 3.82 – 3.79 (m, 2H), 3.75-3.70 (m, 12H), 2.49 (t, *J* = 12.0 Hz, 3H), 1.90 (t, *J* = 12.9 Hz, 12H), 1.47 (qd, *J* = 13.9, 13.4, 3.4 Hz, 6H), 1.40-1.20 (m, 27H), 1.11-1.01 (m, 6H), 0.90 (t, *J* = 7.0 Hz, 9H).

^{13}C NMR ($CDCl_3$, 125 MHz, 25 °C): δ = 152.9, 150.1, 147.6, 147.4, 143.3, 140.8, 138.6, 132.9, 132.4, 128.8, 128.7, 127.2, 123.7, 123.6, 110.1, 108.3, 72.5, 71.2,70.7, 69.9, 69.6, 69.1, 53.6, 46.8, 44.5, 37.5, 37.4, 34.4, 33.7, 32.4, 26.8, 22.9, 14.3.

HR-MS: m/z calcd. for $C_{94}H_{121}ClF_6O_{12}$: 1614.8377 $[M+Na]^+$, found: 1614.8375

Compound 18

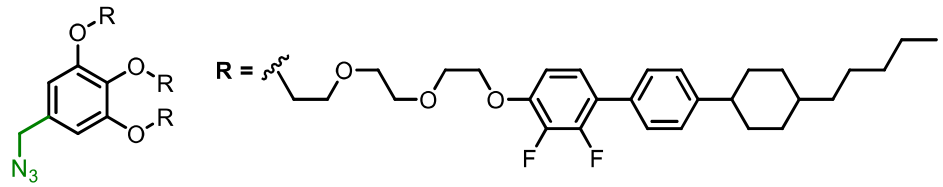

In a 25 mL one-neck round bottom flask equipped with a stirring bar was dissolved the aryl chloride **17** (0.69 g, 0.43 mmol) in dry *N*,*N*-dimethylformamide (5 mL). Sodium azide (0.11 g, 1.73 mmol) was added and the solution was stirred for twenty hours at 80 °C. Water (15 mL) was added and the aqueous phase was extracted with dichloromethane (2 x 20 mL). The organic phase was dried over sodium sulfate, the solvent evaporated under reduced pressure and the crude residue purified by column chromatography (SiO2, Cyclohexane: Ethyl acetate 30% → 50%) to yield compound **18** (0.55 g, 80%) as a white waxy solid.

^{1}H NMR ($CDCl_3$, 400 MHz, 25 °C): δ = 7.42-7.38 (m, 6H), 7.27-7.24 (m, 6H), 7.08-7.02 (m, 3H), 6.81-6.76 (m, 3H), 6.53 (s, 2H), 4.23-4.15 (m, 14H), 3.90-3.85 (m, 10H), 3.83 – 3.80 (m, 2H), 3.76-3.74 (m, 12H), 2.52 - 2.46 (m, 3H), 1.93-1.86 (m, 12H), 1.52-1.42 (m, 6H), 1.37-1.20 (m, 27H), 1.11-1.01 (m, 6H), 0,90 (t, *J* = 7.0 Hz, 9H).

^{13}C NMR ($CDCl_3$, 125 MHz, 25 °C): δ = 153.0, 150.1, 147.6, 147.4, 138.5, 132.4, 130.9, 128.7, 128.7, 127.2, 123.7, 110.0, 107.8, 72.5, 71.2, 71.0, 70.8, 70.7, 69.9, 69.6, 69.1, 55.0, 44.5, 37.5, 37.4, 34.4, 33.7, 32.7, 26.8, 22.9, 14.3.

HR-MS: m/z calcd. for $C_{94}H_{121}F_6N_3O_{12}$: 1621.8781 $[M + Na]^+$, found: 1621.8779

Compound 19

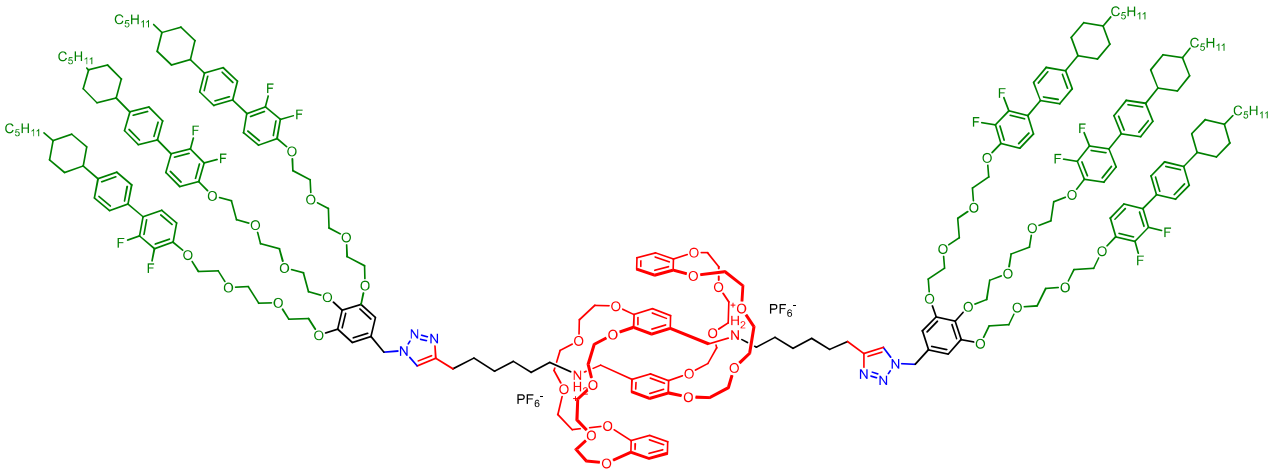

In a microwave tube equipped with a stirring bar were dissolved pseudo[*c*2]daisy chain rotaxane **9** (0.15 g, 0.10 mmol) and benzyl azide **18** (0.35 g, 0.22 mmol) in dry dichloromethane (3 mL). $Cu(CH_3CN)_4PF_6$ (0.076 g, 0.20 mmol) and 2,6-lutidine (0.016 g, 18 µL, 0.15 mmol) were added and the solution was purged with argon. The reaction was stirred for three hours at 35°C under MW radiation (dynamic mode, 40W), and then it was stirred overnight at 25 °C without MW irradiation. Ethylenediaminetetraacetic acid (2 mL) was added to the reaction mixture which was stirred for 30 minutes. The aqueous phase was extracted with dichloromethane (2 x 10 mL), the solvent was evaporated under reduced pressure and the product was purified by column chromatography (SiO_2, dichloromethane: methanol 1% → 2%) to yield obtain [*c*2]daisy chain rotaxane **19** as a waxy solid (0.135 g, 60%).

^{1}H NMR ($CDCl_3$, 400 MHz, 25 °C): δ = 7.38 (d, *J* = 8.1 Hz, 12H), 7.29 (bs, 2H), 7.24 (s, 6H), 7.05 (td, *J* = 8.6, 2.1 Hz, 7H), 6.90 – 6.50 (m, 29H), 5.34 (s, 4H), 4.50 – 3.50 (m, 128H), 3.48 – 3.28 (m, 4H), 2.59 (t, *J* = 7.6 Hz, 4H), 2.49 (tt, *J* = 12.3, 3.0 Hz, 6H), 1.89 (t, *J* = 12.0 Hz, 24H), 1.72 – 1.65 (m, 4H), 1.60 – 1.54 (m, 4H), 1.46 (qd, *J* = 13.7, 13.2, 3.4 Hz, 12H), 1.36 – 1.16 (m, 62H), 1.10 – 1.00 (m, 12H), 0.90 (t, *J* = 7.0 Hz, 18H).

^{13}C NMR ($CDCl_3$, 125 MHz, 25 °C): δ = 152.7, 150.2, 150.0, 148.5, 147.7, 147.2, 147.1, 146.4, 146.2, 132.2, 128.7, 128.6, 127.2, 124.8, 123.8, 123.7, 123.6, 121.1, 113.0, 111.9, 110.2, 110.1, 109.9, 107.7, 72.3, 71.9, 70.9, 70.4, 70.3, 69.6, 69.5, 69.4, 69.3, 54.1, 53.6, 48.9, 44.5, 37.5, 37.4, 34.4, 33.7, 32.4, 29.0, 26.8, 25.6, 22.9, 14.3.

HR-MS: m/z calcd. for $C_{254}H_{338}F_{12}N_8O_{40}$: 2185.2263 $[M-2PF_6]^{2+}$, found: 2185.2241

Compound 20$_{Ext}$

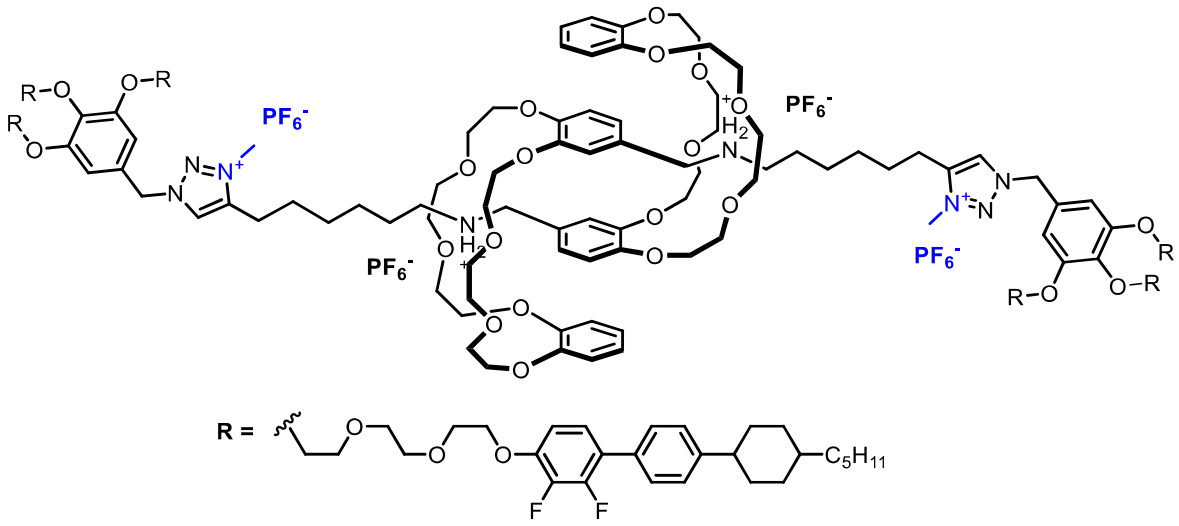

In a 10 mL one-neck round-bottom flask equipped with a stirring bar was dissolved [*c*2]daisy chain rotaxane **19** (0.10 g, 0.022 mmol) in methyl iodide (2 mL) and dry chloroform (1 mL). The mixture was stirred during four days under inert atmosphere at 30 °C. The solvent was evaporated to remove methyl iodide, then a 1:1 solution of CH_2Cl_2: $NH_4PF_{6\,(aq)}$ (6 mL) was added and the solution was stirred for two hours. The aqueous phase was extracted with dichloromethane (2 x 10 mL), the organic layer was dried over sodium sulfate and the solvent was evaporated under reduced pressure affording compound 20Ext (0.11 g, 96%) as a pale yellow solid.

^{1}H NMR ($CDCl_3$, 400 MHz, 25 °C): δ = 8.16 (s, 2H), 7.45 – 7.35 (m, 12H), 7.25 – 7.23 (m, 12H), 7.05 (ddt, *J* = 8.3, 5.9, 2.3 Hz, 6H), 6.85 – 6.75 (m, 24H), 6.37 (d, *J* = 8.5 Hz, 2H), 5.47 (s, 4H), 4.50 – 3.20 (m, 134H), 2.70 – 2.60 (m, 4H), 2.48 (tt, *J* = 12.0, 2.8 Hz, 6H), 1.89 (t, *J* = 11.7 Hz, 22H), 1.75 – 1.65 (m, 8H), 1.46 (qd, *J* = 14.4, 13.5, 3.8 Hz, 14H), 1.36 – 1.16 (m, 62H), 1.10 – 1.01 (m, 12H), 0.89 (t, *J* = 7.0 Hz, 18H).

^{13}C NMR ($CDCl_3$, 125 MHz, 25 °C): δ = 152.5, 150.2, 150.0, 148.5, 147.7, 146.9, 145.1, 143.0, 132.1, 128.7, 128.6, 127.2, 126.2, 124.2, 123.9, 121.5, 121.1, 112.0, 110.2, 109.9, 108.1, 72.3, 71.9, 70.9, 70.6, 69.6, 69.3, 69.2, 69.1, 69.0, 54.1, 53.6, 52.1, 48.9, 44.4, 37.5, 37.4, 37.3, 34.4, 33.7, 32.4, 31.1, 26.8, 25.6, 22.9, 16.1, 14.3.

HR-MS: m/z calcd. for $C_{256}H_{342}F_{18}N_8O_{40}P$: 4543.4486 $[M\text{-}3PF_6\text{-}2H]^+$, found: 4543.4433

Compound 20$_{Cont}$

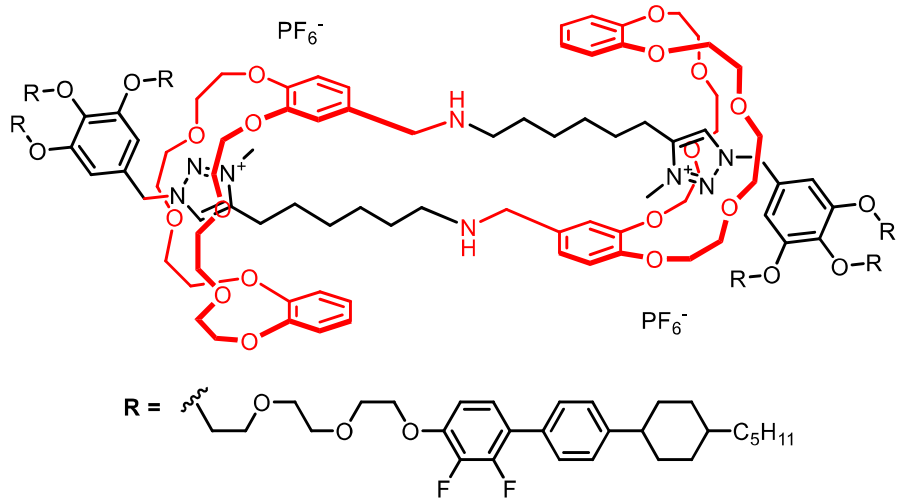

In a 10 mL one-neck round-bottom flask equipped with a stirring bar was dissolved compound **20$_{Ext}$** in chloroform (5 mL). Then, a 1 M NaOH solution (1 mL) was added, and the solution was stirred vigorously for two minutes. The aqueous phase was extracted with chloroform (2 x 5 mL) and washed with water (1 x 5 mL). The combined organic layers were dried over sodium sulfate and the solvent was evaporated under reduced pressure to yield contracted [*c*2]daisy chain **20$_{Cont}$** quantitatively as a beige solid.

^{1}H NMR ($CDCl_3$, 400 MHz, 25 °C): δ = 9.02 (s, 2H), 7.40 – 7.35 (m, 12H), 7.27 – 7.24 (m, 6H), 7.10 – 7.00 (m, 8H), 6.95 – 6.56 (m, 22H), 4.60 – 2.90 (m, 132H), 2.53 – 2.35 (m, 10H), 1.89 (t, *J* = 12.4 Hz, 24H), 1.46 (qd, *J* = 13.7, 13.3, 3.2 Hz, 16H), 1.40 – 1.20 (m, 68H), 1.10 – 1.00 (m, 16H), 0.90 (t, *J* = 7.0 Hz, 18H).

^{13}C NMR ($CDCl_3$, 125 MHz, 25 °C): δ = 152.6, 150.2, 150.1, 147.7, 147.6, 147.4, 147.3, 146.4, 140.7, 132.3, 128.7, 127.2, 126.2, 124.2, 123.8, 123.7, 123.6, 123.5, 121.5, 121.4, 121.1, 112.1, 109.9, 72.5, 71.2, 71.1, 70.8, 70.7, 70.6, 69.9, 69.6, 69.5, 69.1, 68.4, 44.5, 37.5, 37.4, 34.4, 33.7, 32.4, 26.8, 22.9, 14.3.

HR-MS: m/z calcd. for $C_{256}H_{342}F_{12}N_8O_{40}$: 2199.2419 $[M\text{-}2PF_6]^{2+}$, found: 2199.2453

4-((6-hydroxyhexyl)oxy)-3,5-dimethoxybenzaldehyde (27)

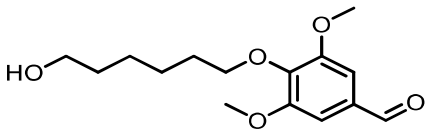

In a 250 mL two-neck round bottom flask equipped with a stirring bar and a findenser was dissolved syringaldehyde (3.0 g, 16.8 mmol) in dry DMF (50 mL). Potassium carbonate (4.1 g, 30 mmol) was added and the suspension was stirred at 70 °C during 30 min. Then, 6-bromohexanol (2.5 mL, 18.6 mmol) was added in one portion and the reaction was maintained under stirring at 70 °C during two days. Water (100 mL) was added to the reaction mixture and the aqueous phase was extracted with ethyl acetate (2 x 100 mL). The combined organic layers were washed with brine (50 mL), dried over sodium sulfate and the solvent was evaporated under reduced pressure. The product was purified by column chromatography (SiO_2 (200 g), Cyclohexane | EtOAc 20% → Cyclohexane |EtOAc 40%) to yield compound **27** (4.2 g, 90%) as a transparent and viscous liquid.

^{1}H NMR ($CDCl_3$, 400 MHz, 25 °C): δ = 9.85 (s, 1H) 7.11 (s, 2H), 4.06 (t, *J* = 6.7 Hz, 2H), 3.90 (s, 6H), 3.64 (t, *J* = 6.6 Hz, 2H), 1.76 (q, *J* = 6.7 Hz, 2H), 1.62 – 1.55 (m, 2H), 1.53 – 1.46 (m, 3H), 1.44 – 1.34 (m, 2H).

^{13}C NMR ($CDCl_3$, 100 MHz, 25 °C): δ = 191.3, 154.0, 143.1, 131.7, 106.8, 73.6, 63.0, 56.4, 32.8, 30.2, 25.7, 25.6.

ESI-MS: m/z calcd. for $C_{15}H_{22}O_5$: 283.15 $[M+H]^+$, found: 283.65

4-((6-((*tert*-butyldimethylsilyl)oxy)hexyl)oxy)-3,5-dimethoxybenzaldehyde (28)

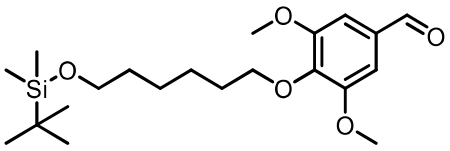

In a 250 mL one-neck round bottom flask equipped with a stirring bar and a septum was dissolved compound **27** (4.2 g, 15 mmol) in dry dichloromethane (40 mL). Imidazole (1.3 g, 19.5 mmol) was added to the solution, and which was stirred at 4 °C under inert atmosphere. TBDMSCl (2.5 g, 16.6 mmol) was added in one portion, leading to the formation of a white precipitate and the reaction mixture was stirred at 25 °C for four hours. Water (50 mL) was added to the mixture and the organic phases were extracted with dichloromethane (2 x 50 mL). The organic phase was dried over sodium sulfate and the solvent was

evaporated under reduced pressure to yield compound **28** (1.3 g, 77%) as a liquid after purification by column chromatography (SiO_2 (200 g), *n*-pentane | EtOAc 5% → *n*-pentane |EtOAc 20%).

^{1}H NMR ($CDCl_3$, 400 MHz, 25 °C): δ = 9.85 (s, 1H), 7.11 (s, 2H), 4.06 (t, *J* = 6.8 Hz, 2H), 3.90 (s, 6H), 3.60 (t, *J* = 6.6 Hz, 2H), 1.79 -1.72 (m, 2H), 1.57 – 1.43 (m, 4H), 1.41 – 1.34 (m, 2H), 0.88 (s, 9H), 0.03 (s, 6H).

^{13}C NMR ($CDCl_3$, 100 MHz, 25 °C): δ = 191.3, 154.0, 143.2, 131.7, 106.9, 73.8, 63.4, 56.4, 33.0, 30.2, 26.1, 25.7, 25.7, 18.5, -5.1.

ESI-MS: m/z calcd. for $C_{21}H_{36}O_5Si$: 397.24 $[M+H]^+$, found: 397.73

(4-((6-((*tert*-butyldimethylsilyl)oxy)hexyl)oxy)-3,5-dimethoxyphenyl)methanol (29)

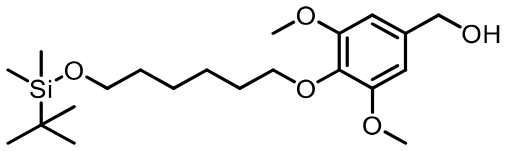

In a 100 mL one-neck round bottom flask equipped with a stirring bar and a septum was dissolved aldehyde **28** (1.25 g, 3.15 mmol) in dry tetrahydrofuran (10 mL). Under vigorous stirring at 4 °C was added sodium borohydride (0.25 g, 6.6 mmol) and the suspension was stirred at room temperature during two hours. Water (20 mL) was added to the reaction mixture and the aqueous phase was extracted with dichloromethane (2 x 20 mL). The organic phase was dried over sodium sulfate and the solvent was evaporated under reduced pressure, to yield compound **29** (1.2 g, 96%) as a transparent liquid, which was pure enough to be used in the next step.

^{1}H NMR ($CDCl_3$, 400 MHz, 25 °C): δ = 6.58 (s, 2H), 4.61 (s, 2H), 3.94 (t, *J* = 6.8 Hz, 2H), 3.83 (s, 6H), 3.60 (t, *J* = 6.6 Hz, 2H), 1.88 (bs, 1H), 1.78–1.71 (m, 2H), 1.57–1.42 (m, 4H), 1.39–1.34 (m, 2H), 0.88 (s, 9H), 0.04 (s, 6H).

^{13}C NMR ($CDCl_3$, 100 MHz, 25 °C): δ = 153.6, 136.6, 136.4, 103.9, 73.4, 65.6, 63.3, 56.1, 32.9, 30.1, 26.0, 25.7, 25.6, 18.4, -5.3.

ESI-MS: m/z calcd. for $C_{21}H_{38}O_5Si$: 382.25 $[M-OH]^+$, found: 382.82

***tert*-butyl((6-(4-(chloromethyl)-2,6-dimethoxyphenoxy)hexyl)oxy)dimethylsilane (30)**

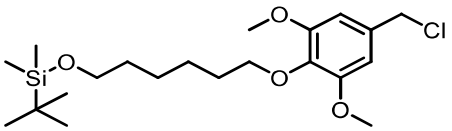

In a 100 mL one-neck round bottom flask equipped with a stirring bar and a septum was dissolved alcohol **29** (1.2 g, 3 mmol) and triethylamine (0.6 mL, 4.4 mmol) in dry dichloromethane (20 mL). Under stirring at 4 °C was added mesyl chloride (0.28 mL, 3.6 mmol) in a dropwise manner for 10 minutes. The solution was allowed to reach room temperature under continuous stirring during 4 hours. Water (20 mL) was added to the reaction mixture at low temperature and the aqueous phase was extracted with dichloromethane (2 x 20 mL). The combined organic phase was dried over sodium sulfate, the solvent was evaporated under reduced pressure and the reaction crude was purified by column chromatography (SiO_2 (50 g), Cyclohexane: EtOAc 10%), to afford compound **30** (0.8 g, 25%) as a transparent liquid.

^{1}H NMR ($CDCl_3$, 400 MHz, 25 °C): δ = 6.60 (s, 2H) 4.54 (s, 2H), 3.95 (t, *J* = 6.7 Hz, 2H), 3.85 (s, 6H), 3.61 (t, *J* = 6.6 Hz, 2H), 1.76 (q, *J* = 6.7 Hz, 2H), 1.57 – 1.33 (m, 6H), 0.89 (s, 9H), 0.04 (s, 6H).

^{13}C NMR ($CDCl_3$, 100 MHz, 25 °C): δ = 153.9, 138.6, 131.4, 104.6, 73.4, 62.6, 56.1, 46.4, 33.0, 30.9, 26.0, 25.7, 25.6, 18.4, -5.3.

HR-MS: m/z calcd. for $C_{21}H_{37}ClO_4Si$: 439.2042 $[M+Na]^+$, found: 439.2036

((6-(4-(azidomethyl)-2,6-dimethoxyphenoxy)hexyl)oxy)(*tert*-butyl)dimethylsilane (31)

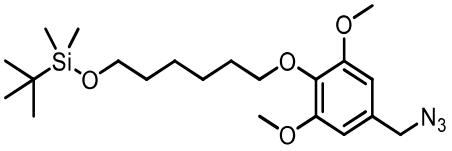

In a 100 mL one-neck round bottom flask equipped with a stirring bar and a findenser was dissolved compound **30** (0.8 g, 1.92 mmol) in dry DMF (10 mL). Sodium azide (0.3 g, 4.8 mmol) was added and the suspension was stirred at 70 °C overnight. Water (30 mL) was added to the reaction mixture and the aqueous phase was extracted with dichloromethane (2 x 20 mL). The organic phase was dried over sodium sulfate and the solvent was evaporated under reduced pressure, to obtain compound **31** (0.65 g, 80%) as a transparent liquid after purification by column chromatography (SiO_2 (20 g) Cyclohexane: EtOAc 20%).

^{1}H NMR ($CDCl_3$, 400 MHz, 25 °C): δ = 6.51 (s, 2H) 4.28 (s, 2H), 3.96 (t, *J* = 6.7 Hz, 2H), 3.85 (s, 6H), 3.61 (t, *J* = 6.6 Hz, 2H), 1.76 (q, *J* = 6.7 Hz, 2H), 1.57 – 1.33 (m, 6H), 0.89 (s, 9H), 0.04 (s, 6H).

^{13}C NMR (CDCl$_3$, 100 MHz, 25 °C): δ = 155.1, 134.5, 131.5, 106.4, 73.7, 62.6, 56.1, 53.5, 33.0, 30.9, 26.0, 25.7, 25.6, 18.4, -5.3.

HR-MS: m/z calcd. for $C_{21}H_{37}N_3O_4Si$: 446.2446 $[M+Na]^+$, found: 446.2438

***Bis-O*-protected [*c*2]daisy chain (32)**

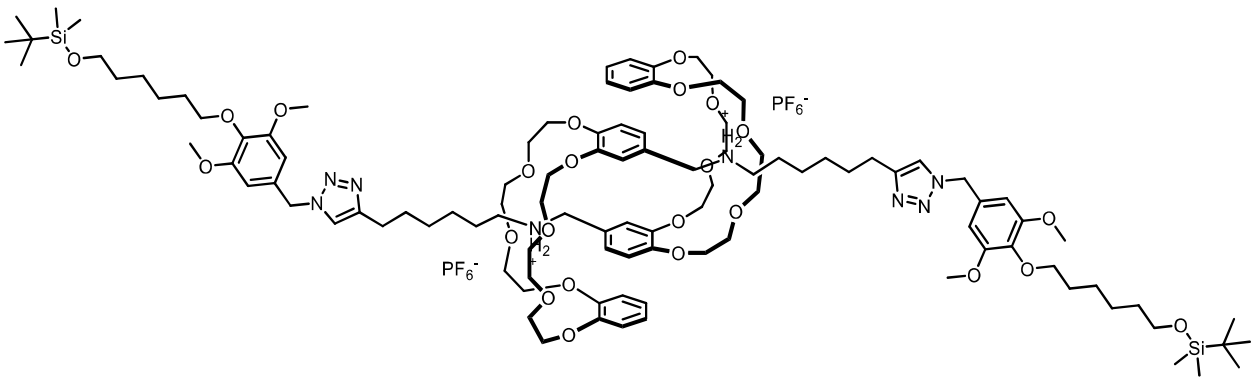

In a microwave tube was dissolved azide derivative **31** (0.48 g, 1.15 mmol) and pseudo[*c*2]daisy chain rotaxane **9** (0.72 g, 0.5 mmol) in dry and degassed dichloromethane (5 mL). Tetrakis(acetonitrile)copper(I) hexafluorophosphate (0.38 g, 1.04 mmol) and 2,6-lutidine (0.07 mL, 0.6 mmol) were added and the reaction mixture was stirred for five minutes. Then, the reaction mixture was heated by microwave irradiation (40 W) during three hours at 35 °C and finally, stirred with an aqueous EDTA solution (5 mL) adjusted to basic pH (~9). The aqueous phase was extracted with dichloromethane (2 x 10 mL), the combined organic layers were dried over sodium sulfate and the solvent was evaporated under reduced pressure. Further purification by column chromatography (SiO_2 (40 g), CH_2Cl_2: MeOH 1% → CH_2Cl_2: MeOH 3%) yielded compound **32** (0.73 g, 69%) as a white solid.

^{1}H NMR (CDCl$_3$, 400 MHz, 25 °C): δ = 7.22 (s, 2H) 6.89 (d, *J* = 9.5 Hz, 2H), 6.81 – 6.71 (m, 12H), 6.50 (s, 2H), 6.51 (s, 4H), 5.41 (s, 4H), 4.50 – 4.25 (m, 10H), 4.21 – 3.67 (m, 60H), 3.60 (t, *J* = 6.6 Hz, 4H), 3.53 – 3.35 (m, 4H), 2.61 (t, *J* = 7.6 Hz, 4H), 1.74 (dt, *J* = 14.6, 6.9 Hz, 4H), 1.60 – 1.50 (m, 8H), 1.47 – 1.24 (m, 20H), 0.89 (bs, 18H), 0.04 (s, 12H).

^{13}C NMR (CDCl$_3$, 100 MHz, 25 °C): δ = 154.5, 147.8, 147.1, 146.7, 146.1, 144.9, 138.5, 127.2, 125.0, 122.1, 121.2, 120.1, 115.5, 111.6, 111.1, 106.7, 73.6, 72.1, 70.7, 70.4, 70.3, 67.0, 66.7, 63.3, 57.7, 56.3, 48.8, 37.4, 30.1, 28.1, 26.1, 27.1, 26.9, 26.3, 26.2, 26.0, 23.8, 21.1, 14.3.

ESI-MS: m/z calcd. for $C_{108}H_{170}F_{12}N_8O_{24}P_2Si_2$: 1010.09 $[M-2(PF_6)^-]^{2+}$, found: 1010.63

***Bis-O*-protected methylated [*c*2]daisy chain (33)**

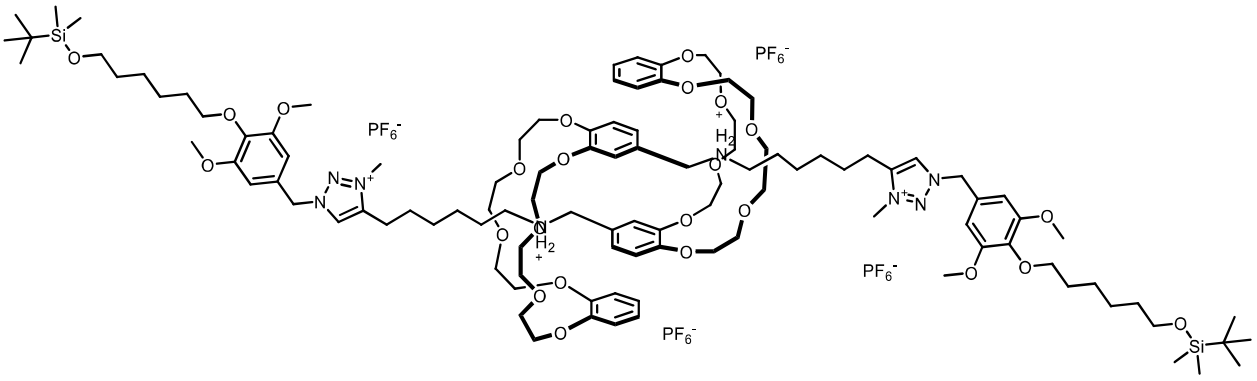

In a 100 mL one-neck round bottom flask equipped with a stirring bar and a septum was dissolved [*c*2]daisy chain rotaxane **32** (0.72 g, 0.31 mmol) in a mixture 10% CH_3CN: CH_3I 90% (10 mL). The mixture was stirred during four days at room temperature and then, solvents were evaporated. The resulting solid was washed with diethyl ether (5 mL) to give a yellow solid. The residue was dissolved in a biphasic mixture of 10:1 dichloromethane: acetonitrile (10 mL) and a saturated aqueous NH_4PF_6 solution (10 mL). The resulting solution was stirred during two hours at room temperature. Then, the aqueous phase was extracted with dichloromethane (2 x 10 mL) and the organic layers were dried over sodium sulfate and concentrated under reduced pressure to give compound **33** (0.76 g, 96%) as a slightly yellow solid.

^{1}H NMR ($CDCl_3$, 400 MHz, 25 °C): δ = 8.17 (s, 2H), 7.00 – 6.60 (m, 18H), 5.52 (s, 4H), 4.50 – 4.30 (m, 7H), 4.20 – 3.60 (m, 73H), 3.40 (bs, 4H), 2.68 – 2.64 (m, 4H), 1.75 – 1.65 (m, 9H) 1.52 (dt, *J* = 14.0, 6.7 Hz, 5H), 1.47 – 1.25 (m, 18H), 0.88 (bs, 18H), 0.03 (s, 12H).

^{13}C NMR ($CDCl_3$, 100 MHz, 25 °C): δ = 154.1, 147.6, 147.5, 146.4, 146.2, 144.9, 138.3, 127.5, 126.2, 125.0, 122.6, 121.1, 120.9, 111.9, 111.7, 106.7, 73.5, 72.0, 70.7, 70.4, 70.3, 67.0, 66.7, 63.3, 57.7, 56.3, 48.8, 37.4, 32.9, 30.1, 28.1, 26.1, 27.1, 26.9, 26.4, 26.3, 26.0, 23.6, 21.1, 14.4.

MALDI-MS: m/z calcd. for $C_{110}H_{176}F_{24}N_8O_{24}P_4Si_2$: 2484.125$[M\text{-}PF_6]^+$, found: 2484.534

***Bis-O*-deprotected methylated [*c*2]daisy chain (34_{Ext})**

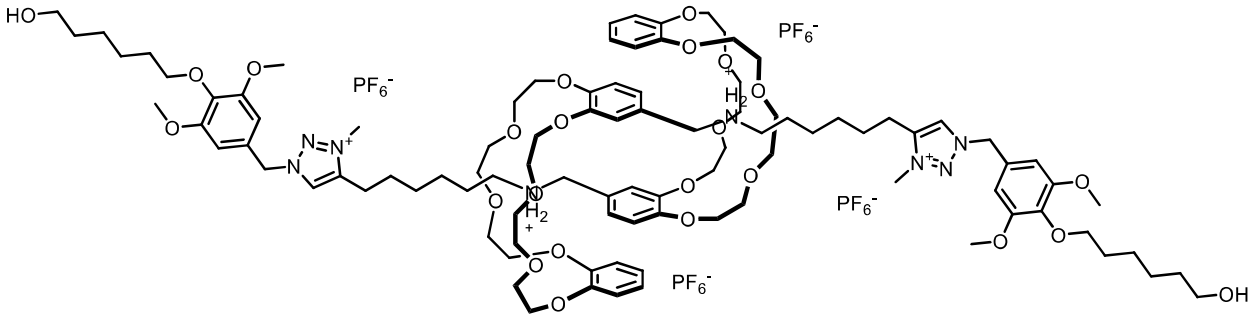

In a 50 mL one-neck round bottom flask equipped with a stirring bar and a septum was dissolved the [*c*2]daisy chain **33** (0.75g, 0.29 mmol) in THF (5 mL). Then, a 1 M HCl (2 mL) was added under vigorous stirring at 25 °C. After forty minutes, ethyl acetate (10 mL) was added to the reaction mixture and the obtained white precipitate was filtrated from the reaction mixture. The solid was washed with ethyl acetate and dried under vacuum to yield compound $\mathbf{25_{Ext}}$ (0.55, 80%) as a white solid.

^{1}H NMR (CD_3CN, 500 MHz, 25 °C): δ = 8.04 (s, 2H), 6.85 – 6.80 (m, 4H), 6.76 – 6.67 (m, 12H), 6.45 (d, *J* = 8.4 Hz, 2H), 5.57 (s, 4H), 4.54 – 4.45 (m, 4H), 4.30 – 4.25, 4.28 (t, *J* = 9.7 Hz, 2H), 4.20 – 4.00 (m, 24H), 3.93 - 3.74 (m, 42 H), 3.70 – 3.60 (m, 6H), 3.50 – 3.40 (m, 8H), 2.63 (t, *J* = 7.8 Hz, 4H), 2.49 (bs, 2H), 1.73 – 1.63 (m, 9H), 1.60 – 1.30 (m, 23H).

^{13}C NMR (CD_3CN, 125 MHz, 25 °C): δ = 154.9, 148.7, 147.1, 146.9, 145.9, 139.1, 128.2, 128.0, 126.2, 123.6, 121.6, 114.1, 113.0, 112.8, 112.7, 107.7, 73.8, 72.9, 71.4, 71.3, 71.2, 71.0, 68.5, 68.2, 68.0, 67.9, 62.5, 58.0, 56.8, 52.8, 49.6, 38.3, 33.5, 30.8, 28.8, 27.3, 27.1, 26.9, 26.4, 26.3, 26.0, 23.6, 21.1, 14.4.

HR-MS: m/z calcd. for $C_{98}H_{148}F_{24}N_8O_{24}P_4$: 1055.9957 $[M\text{-}2PF_6]^{2+}$, found: 1055.9965

***Bis-O*-deprotected methylated [*c*2]daisy chain (34_{Ext})**

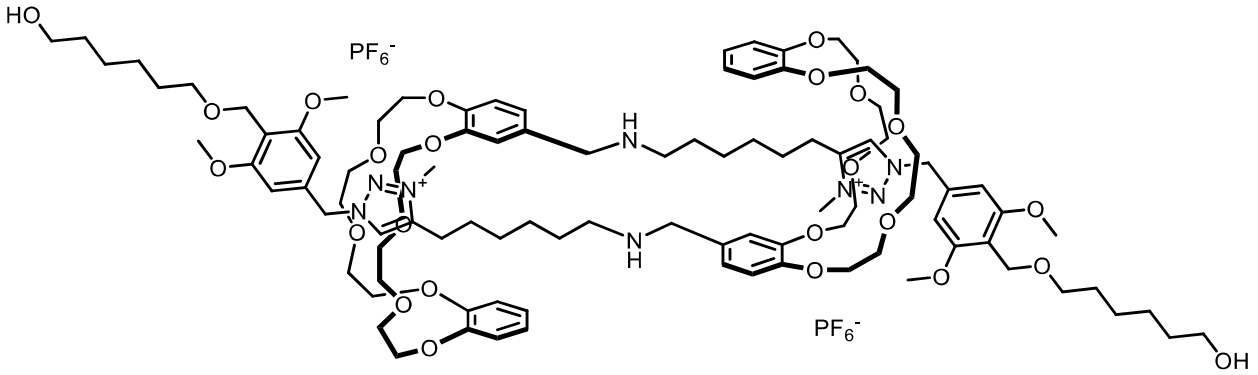

In a 10 mL one-neck round bottom flask equipped with a stirring bar was dissolved compound $\mathbf{34_{Ext}}$ (0.11 g, 0.048 mmol) in a mixture of CH_2Cl_2 80%: CH_3CN 20% (5 mL) and the organic phase was washed with a 1 M aqueous solution of sodium hydroxide (5 mL). The organic phase was dried over sodium sulfate and then evaporated to give compound $\mathbf{34_{Cont}}$ (0.092 g, 96%) as a white solid.

^{1}H NMR (CD_3CN, 500 MHz, 25 °C): δ = 7.59 (s, 2H) 6.97 – 6.71 (m, 18H), 5.59 (s, 4H), 4.23 – 3.33 (m, 92H), 2.65 (bs, 4H), 2.49 (dt, *J* = 14.3, 7.1 Hz, 2H), 1.65 (dt, *J* = 14.3, 6.6 Hz, 4H), 1.55 – 1.32 (m, 24H).

^{13}C NMR (CD_3CN, 125 MHz, 25 °C): δ = 154.8, 149.7, 148.7, 148.5, 147.1, 139.1, 128.5, 128.2, 122.3, 121.7, 115.1, 112.8, 79.1, 73.8, 71.6, 71.4, 71.1, 70.7, 70.6, 70.4, 70.3, 70.1, 69.9, 69.8, 69.7, 69.5, 62.5, 58.0, 56.8, 49.6, 33.5, 30.8, 26.4, 26.3, 26.0, 23.8, 23.7, 23.6.

4-(2-bromoethoxy)-3,5-dimethoxybenzaldehyde (**35**)

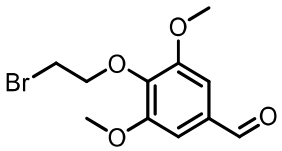

In a 100 mL two-neck round bottom flask equipped with a stirring bar and a findenser was dissolved syringaldehyde (1.2 g, 6.6 mmol) in dry *N*,*N*-dimethylformamide (40 mL). Then was added potassium carbonate (1.8 g, 13.1 mmol), 1,2-dibromoethane (2.5 mL, 29.62 mmol) and the mixture was stirred at 70 °C during two days. Water (50 mL) was added to the reaction mixture and the aqueous layer was extracted with dichloromethane (2 x 40 mL). The organic phase was washed with brine (20 mL), dried over sodium sulfate and the solvent was evaporated under reduced pressure. The crude product was purified by column chromatography (SiO_2 (50 g), Cyclohexane | EtOAc 5% → Cyclohexane |EtOAc 25%) to yield compound **35** (1.31 g, 69%) as a white solid.

^{1}H NMR ($CDCl_3$, 400 MHz, 25 °C): δ = 9.88 (s, 1H); 7.13 (s, 2H), 4.37 – 4.34 (m, 2H), 3.93 (s, 6H), 3.63 – 3.60 (m, 2H).

^{13}C NMR ($CDCl_3$, 100 MHz, 25 °C): δ = 191.2, 153.8, 141.9, 132.3, 106.7, 72.8, 56.4, 29.6.

ESI-MS: m/z calcd. for $C_{11}H_{13}BrO_4$: 289.01 $[M+H]^+$, found: 289.23

(4-(2-bromoethoxy)-3,5-dimethoxyphenyl)methanol (36)

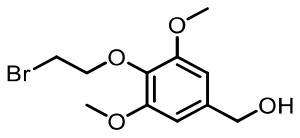

In a 100 mL two-neck round bottom flask equipped with a stirring bar and septa was dissolved aldehyde **35** (4.4 g, 15.15 mmol) in dry tetrahydrofuran (100 mL). Under inert atmosphere and continuous stirring at 4 °C was added sodium borohydride (1.3 g, 34.83 mmol) in portions. The suspension was stirred at 25 °C during two hours and then water (50 mL) was added to the reaction mixture. The aqueous phase was extracted with dichloromethane (2 x 100 mL) and the combined organic phase was dried over sodium sulfate and concentrated under reduced pressure to yield compound **36** (4.30 g, 96%) as a transparent liquid, which was pure enough to be used as such in the next step.

^{1}H NMR ($CDCl_3$, 400 MHz, 25 °C): δ = 6.57 (s, 2H), 4.61 (s, 2H), 4.24 – 4.21 (m, 2H), 3.84 (s, 6H), 3.60 – 3.56 (m, 2H), 1.98 (bs, 1H).

^{13}C NMR ($CDCl_3$, 100 MHz, 25 °C): δ = 153.4, 137.3, 135.2, 103.7, 72.7, 65.5, 56.2, 29.7.

HR-MS: m/z calcd. for $C_{11}H_{15}BrO_4$: 297.0309 $[M+Li]^+$, found: 297.0312

(4-(2-azidoethoxy)-3,5-dimethoxyphenyl)methanol (37)

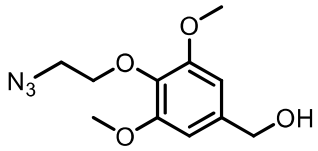

In a 250 mL two-neck round bottom flask equipped with a stirring bar and a findenser was added a solution of compound **36** (4.3 g, 14.77 mmol) in dry *N*,*N*-dimethylformamide (60 mL). Sodium azide (2.0 g, 31 mmol) was added and the suspension was stirred at 70 °C during six hours. After cooling down to room temperature, water (40 mL) was added to the reaction mixture and the aqueous phase was extracted with dichloromethane (2 x 100 mL). The organic phase was dried over sodium sulfate and the solvent was

evaporated under reduced pressure yielding compound **37** (3.0 g, 80%) pure enough as a transparent liquid, which was pure enough to be used as such in the next step.

^{1}H NMR ($CDCl_3$, 400 MHz, 25 °C): δ = 6.60 (s, 2H), 4.64 (d, *J* = 5.4 Hz, 2H), 4.14 – 4.11 (m, 2H), 3.87 (s, 6H), 3.55 – 3.53 (m, 2H).

^{13}C NMR ($CDCl_3$, 100 MHz, 25 °C): δ = 153.4, 137.1, 135.7, 103.7, 71.5, 65.5, 56.1, 51.1.

((4-(2-azidoethoxy)-3,5-dimethoxybenzyl)oxy)(*tert*-butyl)dimethylsilane (38)

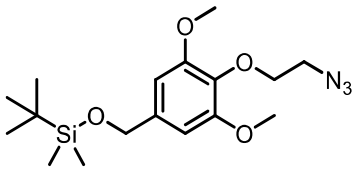

In a 250 mL two-neck round bottom flask equipped with a stirring bar was dissolved compound **37** (2.4 g, 9.5 mmol) in dry dichloromethane (50 mL) followed by addition of imidazole (1.0 g, 14 mmol). The solution was cooled down to 4 °C under inert atmosphere and continuous stirring, and TBDMSCl (2.0 g, 13 mmol) was added portionwise. A white precipitate was observed and the suspension was stirred at room temperature during four hours. Water (40 mL) was added to the reaction mixture and the aqueous phase was extracted with dichloromethane (2 x 100 mL). The organic phase was dried over sodium sulfate and the solvent was evaporated under reduced pressure, yielding compound **38** (2.42 g, 69%) as a transparent liquid after column chromatography (SiO_2 (100 g), Cyclohexane | EtOAc 5% → Cyclohexane |EtOAc 30%).

^{1}H NMR ($CDCl_3$, 400 MHz, 25 °C): δ = 6.62 (s, 2H), 4.54 (d, *J* = 5.4 Hz, 2H), 4.14 – 4.11 (m, 2H), 3.89 (s, 6H), 3.55 – 3.53 (m, 2H), 0.89 (s, 9H), 0.04 (s, 6H).

^{13}C NMR ($CDCl_3$, 100 MHz, 25 °C): δ = 153.4, 137.2, 135.3, 104.0, 71.5, 67.8, 56.1, 51.5, 30.3, 18.3, -5.10.

HR-MS: m/z calcd. for $C_{17}H_{29}N_3O_4Si$: 375.2116 $[M+Li]^+$, found: 374.2126

***Bis-O*-protected [*c*2]daisy chain (39)**

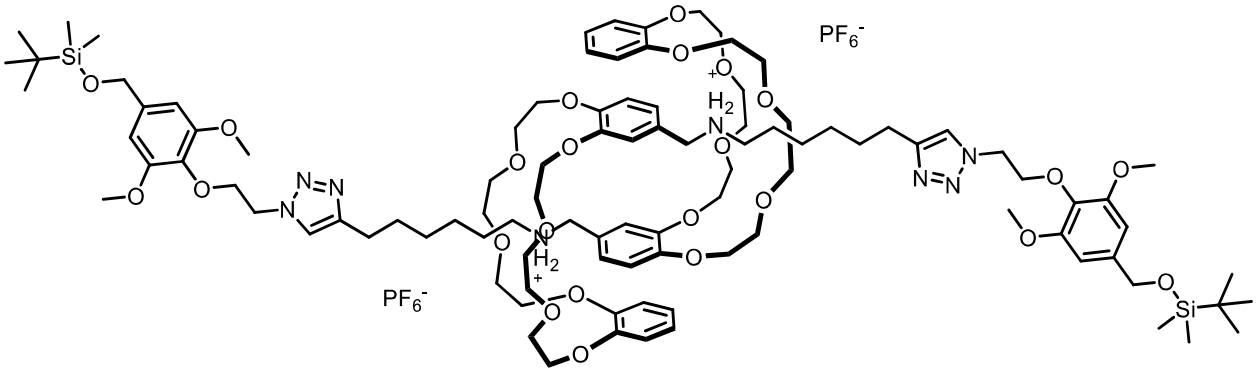

In a microwave tube was dissolved azide **38** (0.54 g, 1.5 mmol) and pseudo[*c*2]daisy chain rotaxane **9** (0.96 g, 0.69 mmol) in dry and degassed dichloromethane (20 mL). Tetrakis(acetonitrile)copper(I) hexafluorophosphate (0.53 g, 1.4 mmol) and 2,6-lutidine (0.12 mL, 0.96 mmol) were added to the reaction mixture and the solution was stirred for five minutes. The reaction mixture was heated using microwave irradiation (40 W) during three hours at 35 °C and finally, stirred with an aqueous EDTA solution (20 mL) adjusted to basic pH (~9). The aqueous phase was extracted with dichloromethane (2 x 20 mL), the organic phases were dried over sodium sulfate and the solvent evaporated under reduced pressure. Purification was carried out by column chromatography (SiO_2 (80 g), CH_2Cl_2: MeOH 1% → CH_2Cl_2: MeOH 3%) leading to compound **39** (1.0 g, 69 %) as a white solid.

^{1}H NMR ($CDCl_3$, 500 MHz, 25 °C): δ = 7.80 (s, 2H) 6.91 (d, *J* = 9.9 Hz, 2H), 6.82 – 6.71 (m, 12H), 6.58 – 6.56 (m, 6H), 4.68 – 4.64 (m, 8H), 4.47 – 3.66 (m, 78H), 2.65 (t, *J* = 7.6 Hz, 4H), 1.68 – 1.62 (m, 8H), 1.39 – 1.30 (m, 8H), 0.95 (s, 18H), 0.11 (s, 12H).

^{13}C NMR ($CDCl_3$, 100 MHz, 25 °C): δ = 153.1, 147.8, 147.7, 147.6, 146.4, 146.2, 138.3, 134.8, 124.8, 123.1, 122.4, 121.3, 121.1, 113.3 112.6, 112.0, 111.8, 102.6, 72.5, 71.9, 71.5, 71.2, 71.0, 70.9, 70.9, 70.5, 70.4, 67.7, 67.1, 67.0, 66.8, 64.9, 56.0, 53.6, 52.3, 50.6, 48.9, 29.4, 28.7, 26.7, 26.6, 26.0, 25.6, 18.5, 0.13, -5.10.

ESI-MS: m/z calcd. for $C_{100}H_{154}F_{12}N_8O_{24}P_2Si_2$: 953.53 $[M\text{-}2(PF_6)^-]^{2+}$, found: 953.91

***Bis-O*-protected methylated [*c*2]daisy chain (40)**

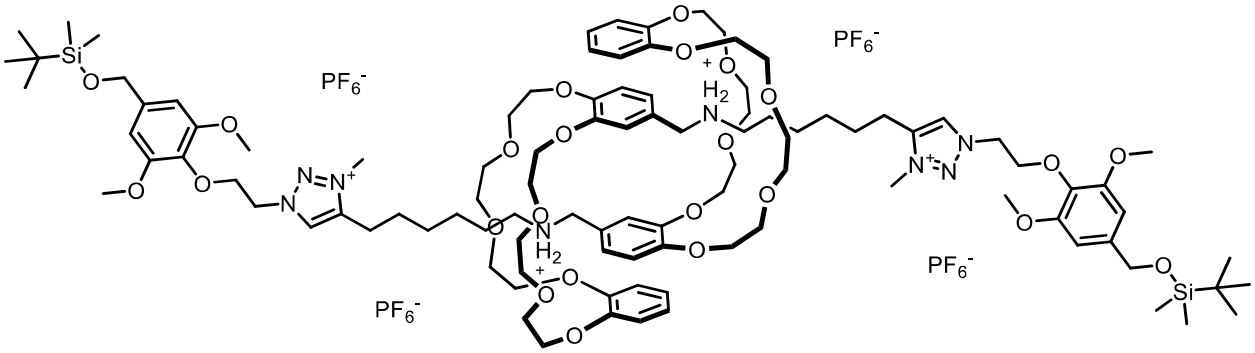

In a 50 mL one-neck round bottom flask equipped with a stirring bar was dissolved [*c*2]daisy chain rotaxane **39** (0.96 g, 0.44 mmol) in a mixture CH_3CN 10%: CH_3I 90% (10 mL). The mixture was stirred for four days at 30 °C and then, solvents were evaporated. The resulting solid was washed with diethyl ether (5 mL) to give a yellow solid. The residue was dissolved in a 10:1 mixture of CH_2Cl_2: CH_3CN (10 mL) and a saturated aqueous NH_4PF_6 solution (10 mL). The resulting solution was stirred during one hour at room temperature. Then, the aqueous phase was extracted with CH_2Cl_2 (2 x 10 mL) and the organic layers were dried over sodium sulfate and concentrated under reduced pressure to give compound **40** (1.0 g, 96%) as a pale yellow solid.

^{1}H NMR ($CDCl_3$, 500 MHz, 25 °C): δ = 8.45 (s, 2H), 6.96 – 6.69 (m, 14H), 6.54 (s, 2H), 6.42 (d, *J* = 8.4 Hz, 2H), 4.80 – 4.78 (m, 4H), 4.66 (s, 4H), 4.49 – 3.39 (m, 82H), 2.76 (t, *J* = 7.6 Hz, 4H), 1.76 – 1.67 (m, 8H), 1.49 – 1.39 (m, 8H), 0.94 (s, 18H), 0.10 (s, 12H).

^{13}C NMR ($CDCl_3$, 100 MHz, 25 °C): δ = 153.0, 147.8, 147.7, 146.5, 146.3, 144.6, 138.8, 134.0, 128.5, 125.1, 121.2, 121.0, 113.5, 112.2 112.1, 111.9, 102.6, 72.2, 72.1, 70.9, 70.8, 70.7, 70.6, 70.5, 69.5, 67.3, 67.2, 66.8, 64.9, 56.0, 54.2, 52.2, 48.9, 37.4, 28.3, 26.7, 26.3, 26.1, 23.0, 18.5, 0.14, -5.10.

ESI-MS: m/z calcd. for $C_{102}H_{160}F_{24}N_8O_{24}P_4Si_2$: 968.05 $[M–2H–(PF_6)^-]^{2+}$, found: 968.11

***Bis-O*-deprotected methylated [*c*2]daisy chain (41$_{Ext}$)**

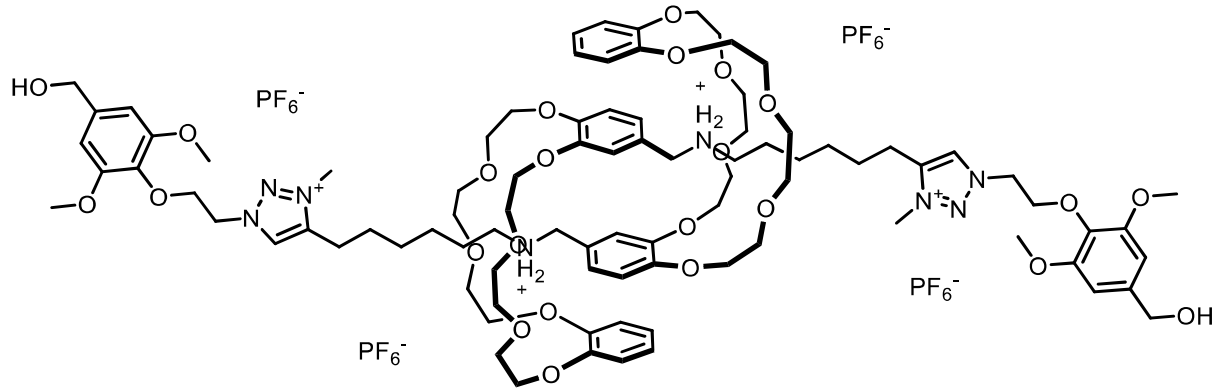

In a 50 mL one-neck round bottom flask equipped with a stirring bar was dissolved [*c*2]daisy chain rotaxane **40** (1.73g, 0.69 mmol) in tetrahydrofuran (10 mL). Then a solution 1 M HCl (5.0 mL) was added under vigorous stirring at room temperature. After 40 minutes, ethyl acetate (10 mL) was added to the reaction mixture and the obtained white precipitate was filtrated from the reaction mixture. The solid was washed with ethyl acetate and dried under vacuum to yield compound **41$_{Ext}$** (1.42g, 90%) as a white solid.

^{1}H NMR (DMF-*d*$_7$, 500 MHz, 25 °C): δ = 9.09 (s, 2H), 7.14 – 6.79 (m, 14H), 6.75 (s, 4H), 6.71 (d, *J* = 8.4 Hz, 2H), 5.06 (s, 4H), 4.63 – 3.76 (m, 76H), 3.64 – 3.54 (m, 10H), 3.01 (t, *J* = 7.8 Hz, 4H), 1.85 – 1.75 (m, 8H), 1.51 (bs, 8H).

^{13}C NMR (DMF-*d*$_7$, 100 MHz, 25 °C): δ = 154.2, 149.3, 147.7, 147.5, 145.6, 141.1, 135.5, 130.4, 126.5, 123.9, 122.0, 114.5, 113.7, 113.3, 104.6, 73.3, 72.0, 71.9, 71.8, 71.7, 71.6, 71.0, 69.0, 68.7, 68.6, 68.5, 68.4, 64.7, 57.0, 55.3, 53.2, 49.9, 38.6, 29.5, 28.0, 27.6, 27.4, 26.6, 24.0.

HR-MS m/z calcd. for $C_{90}H_{132}F_{24}N_8O_{24}P_4$: 2143.8275 $[M–(PF_6)^-]^+$, found: 2143.8307

***Bis-O*-deprotected methylated [*c*2]daisy chain (41$_{Cont}$)**

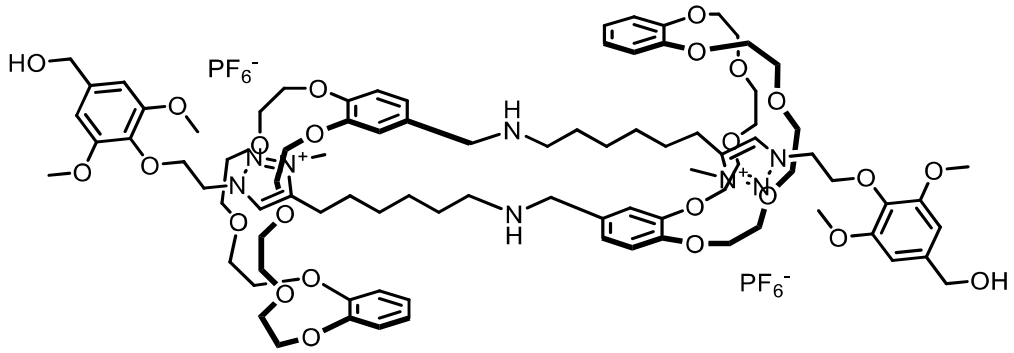

In a 50 mL one-neck round bottom flask equipped with a stirring bar was dissolved compound **41$_{Ext}$** (0.11 g, 0.048 mmol) in a mixture CH_2Cl_2 80%:CH_3CN 20% (5 mL) and washed with a 1 M aqueous solution of sodium hydroxide (5 mL). The organic phase was dried over sodium sulfate and the solvent evaporated under reduced pressure to give compound **41$_{Cont}$** (0.092 g, 96%) as a white solid.

^{1}H NMR (CD3CN, 500 MHz, 25 °C): δ = 6.96 – 6.69 (m, 18H), 5.59 (s, 2H), 4.60–3.00 (m, 76H), 2.65 (bs, 2H), 2.49 (dt, *J* = 14.3, 7.1 Hz, 2H), 1.75 – 1.05 (m, 32H).

^{13}C NMR (DMF-*d*$_7$, 100 MHz, 25 °C): δ = 154.9, 149.7, 148.7, 148.5, 147.2, 140.3, 139.1, 130.4, 128.5, 128.2, 122.3, 121.7, 115.1, 112.8, 79.1, 73.8, 71.6, 71.4, 71.1, 70.7, 70.3, 70.1, 69.8, 69.6, 62.5, 58.0, 56.8, 49.6, 33.5, 30.8, 26.4, 26.3, 23.7.

ESI-MS m/z calcd. for $C_{90}H_{130}F_{12}N_8O_{24}P_2$: 853.46[M–2$(PF_6)^-$]$^{2+}$, found: 853.32

Methyl 4-((6-bromohexyl)oxy)-3,5-di-*tert*-butylbenzoate (67)

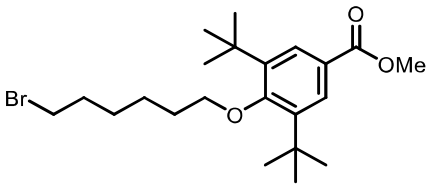

In a 500 mL two-neck round-bottom flask equipped with a stirring bar and a findenser was prepared a solution of methyl 3,5-di-*tert*-butyl-4-hydroxybenzoate (10 g, 38.0 mmol) in methyl ethyl ketone (180 mL) (previously dried with potassium carbonate). Then, potassium carbonate (15 g, 113 mmol) was added and the mixture was heated at 80 °C during 30 minutes. Subsequently, 1,6-dibromohexane (22 mL, 143 mmol) was added and the suspension was continuously stirred at 80 °C for four days. After that, water (200 mL) was added to the reaction mixture and the aqueous phase was extracted with ethyl acetate (2 x 200 mL). The organic phase was dried over sodium sulfate, the solvent was evaporated under reduced pressure and the crude was purified by column chromatography (SiO_2 (500 g), *n*-pentane → *n*-pentane |EtOAc 1%) to yield compound **67** (9.6 g, 59%) as a pale yellow liquid.

^{1}H NMR ($CDCl_3$, 400 MHz, 25 °C): δ = 7.94 (s, 2H) 3.88 (s, 3H), 3.69 (t, *J* = 6.8 Hz, 2H), 3.42 (t, *J* = 6.8 Hz, 2H), 1.90 (p, *J* = 6.9 Hz, 4H), 1.55 – 1.43 (m, 22H).

^{13}C NMR ($CDCl_3$, 100 MHz, 25 °C): δ = 167.6, 162.6, 144.1, 128.5, 124.4, 52.1, 36.1, 33.9, 32.8, 32.0, 29.5, 25.9.

ESI-MS: m/z calcd. for $C_{22}H_{35}BrO_3$: 427.18 $[M+H]^+$, found: 427.45

Methyl 4-((6-azidohexyl)oxy)-3,5-di-*tert*-butylbenzoate (68)

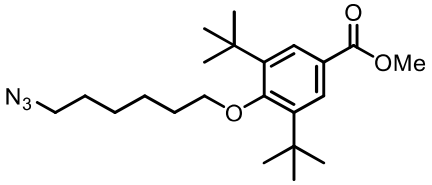

In a 250 mL one-neck round-bottom flask equipped with a stirring bar and a findenser was prepared a solution of compound **67** (9.6 g, 22 mmol) in dry *N*,*N*-dimethylformamide (100 mL). Then, sodium azide (3.0 g, 45 mmol) was added and the suspension was stirred at 80 °C during six hours. After that, water (150 mL) was added to the reaction mixture and the aqueous phase was extracted with diethyl ether (2 x 100 mL). The organic phase was washed with water (2 x 100 mL), dried over sodium sulfate and the solvent was

evaporated under reduced pressure to yield compound **68** (7.0 g, 80%) as a transparent liquid, which was pure enough to be used as such in the next step.

^{1}H NMR ($CDCl_3$, 400 MHz, 25 °C): δ = 7.94 (s, 2H) 3.88 (s, 3H), 3.70 (t, *J* = 6.8 Hz, 2H), 3.28 (t, *J* = 6.9 Hz, 2H), 1.90 (p, *J* = 7.5 Hz, 2H), 1.63 (q, *J* = 8.6, 7.8 Hz, 2H), 1.43 (m, 22H).

^{13}C NMR ($CDCl_3$, 100 MHz, 25 °C): δ = 167.6. 162.5, 144.1, 128.5, 124.4, 52.1, 51.5, 36.0, 32.0, 29.5, 26.5, 25.5.

ESI-MS: m/z calcd. for $C_{22}H_{35}N_3O_3$: 358.25 $[M\text{-}CH_3O]^+$, found: 358.45

4-((6-azidohexyl)oxy)-3,5-di-*tert*-butylbenzoic acid (69)

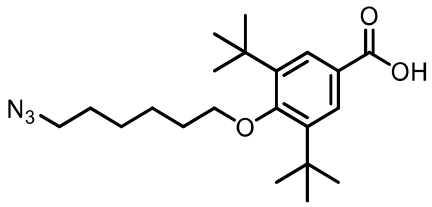

In a 250 mL one-neck round–bottom flask equipped with a stirring bar and a findenser was prepared a solution of ester **68** (7.0 g, 18 mmol) in a mixture of tetrahydrofuran (45 mL), methanol (15 mL) and water (5 mL). Then sodium hydroxide (3.6 g, 90 mmol) was added, and the reaction mixture was stirred at 65 °C for four hours. After that, the reaction was cooled down to room temperature and a 1 M HCl solution (50 mL) was added and the aqueous phase was extracted with dichloromethane (2 x 100 mL) The organic phase was dried over sodium sulfate and the solvent was evaporated under reduced pressure to give compound **69** (6.0 g, 90%) as transparent liquid that turns into a solid.

^{1}H NMR ($CDCl_3$, 400 MHz, 25 °C): δ = 8.03 (s, 2H), 3.72 (t, *J* = 7.5 Hz, 2H), 3.29 (t, *J* = 7.0 Hz, 2H), 1.91 (p, *J* = 7.4 Hz, 2H), 1.68 – 1.62 (m, 2H), 1.49 – 1.40 (m, 22H).

^{13}C NMR ($CDCl_3$, 100 MHz, 25 °C): δ = 163.4, 144.3, 135.8, 129.2, 123.4, 51.5, 36.1, 32.0, 30.5, 29.6, 26.9, 25.5.

ESI-MS: m/z calcd. for $C_{21}H_{33}N_3O_3$: 375.25 $[M]^+$, found: 375.31

***tert*-Butyl (2-(4-((6-azidohexyl)oxy)-3,5-di-*tert*-butylbenzamido)ethyl)carbamate (70)**

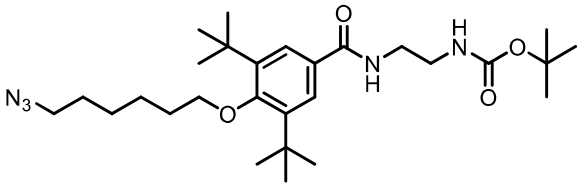

In a 250 mL one-neck round–bottom flask equipped with a stirring bar was prepared a solution of carboxylic acid derivative **69** (6.0 g, 16 mmol) in dry dichloromethane (100 mL). Then *N*-hydroxybenzotriazole (4.5 g, 33.5 mmol), 1-ethyl-3-(3-dimethylaminopropyl)carbodiimide (EDCI) (9.0 g, 48 mmol) and *N*-Boc-ethylenediamine (4.5 mL, 28 mmol) were added. The reaction was stirred at room temperature for 18 hours, and then, water (100 mL) was added. The aqueous phase was extracted with dichloromethane (2 x 100 mL) and the organic phase was dried over sodium sulfate, the solvent was evaporated under reduced pressure. The reaction crude was purified by column chromatography (SiO_2 (200 g), DCM | MeOH 1% → DCM |MeOH 4%) to yield compound **70** (5.95 g, 72%) as a pale yellow solid.

^{1}H NMR ($CDCl_3$, 400 MHz, 25 °C): δ = 7.71 (s, 2H), 7.29 (bs, 1H), 5.09 (bs, 1H), 3.67 (t, *J* = 7.5 Hz, 2H), 3.54 (q, *J* = 5.1 Hz, 2H), 3.37 (q, *J* = 5.5 Hz, 2H), 3.27 (t, *J* = 6.9 Hz, 2H), 1.87 (p, *J* = 7.5 Hz, 2H), 1.63 (p, *J* = 6.9 Hz, 2H), 1.42 (bs, 22H), 1.40 (s, 9H).

^{13}C NMR ($CDCl_3$, 100 MHz, 25 °C): δ = 168.3, 161.1, 157.6, 143.9, 128.3, 125.8, 79.9, 76.6, 51.5, 42.2, 40.5, 36.0, 32.0, 29.5, 28.9, 28.5, 26.9, 25.5.

HR-MS: m/z calcd. for $C_{28}H_{48}N_5O_4$: 518.3701 $[M+H]^+$, found: 518.3697

11-bromoundec-1-yne (71a)

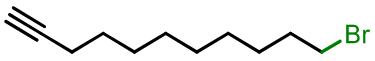

In a 250 mL two-neck round–bottom flask equipped with a stirring bar and a findenser was prepared a solution of undec-10-yn-1-ol (5.0 g, 16 mmol) and carbon tetrabromide (12 g, 37 mmol) in dry dichloromethane (100 mL) at 4 °C. Then, triphenylphosphine (TPP) (10 g, 38 mmol) was added portionwise to the reaction mixture, allowing it to reach 25 °C. Once the addition of TPP finished, the solution was stirred during two hours at 45 °C under argon atmosphere. After that, the dichloromethane was evaporated under vacuum to half of its volume and the reaction mixture was cooled down using a water: ice bath followed by addition of diethyl ether (150 mL). A white precipitate was obtained as side product, which was filtered and washed twice with *n*-pentane. The filtrate was evaporated under reduced pressure and the crude residue

purified by column chromatography (SiO_2 (150 g), *n*-pentane → *n*-pentane |DCM 1%) to yield compound **71a** (5.0 g, 73%) as a transparent liquid.

^{1}H NMR ($CDCl_3$, 400 MHz, 25 °C): δ= 3.39 (t, *J* = 6.9 Hz, 2H), 2.17 (td, *J* = 7.1, 2.7 Hz, 2H), 1.93 (t, *J* = 2.7 Hz, 1H), 1.89 – 1.80 (m, 2H), 1.51 (dt, *J* = 14.5, 6.7 Hz, 2H), 1.40 (tt, *J* = 12.6, 7.3 Hz, 4H), 1.30 (bs, 6H).

^{13}C NMR ($CDCl_3$, 100 MHz, 25 °C): δ = 83.8, 68.9, 33.3, 32.3, 29.6, 28.8, 28.4, 28.2, 28.0, 18.1.

6-bromohex-1-yne (71b)

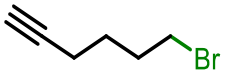

In a 250 mL two-neck round–bottom flask equipped with a stirring bar and a findenser was prepared a solution of hex-5-yn-1-ol (4.0 g, 40 mmol) and carbon tetrabromide (17 g, 53 mmol) in dry dichloromethane (100 mL) at 4 °C. Then, triphenylphosphine (14 g, 53 mmol) was added portionwise to the reaction mixture, allowing to reach 25 °C. Once the addition of TPP finished, the solution was stirred during two hours at 40 °C under argon atmosphere. After that, the solvent was evaporated under vacuum to half of its volume and the reaction mixture was cooled down using a water: ice bath followed by addition of diethyl ether (150 mL). A white precipitate was obtained as side product, which was filtered and washed twice with *n*-pentane. The filtrate was evaporated and the crude residue purified by column chromatography (SiO_2 (120 g), *n*-pentane) to yield compound **71b** (4.0 g, 60%) as a transparent liquid.

^{1}H NMR ($CDCl_3$, 400 MHz, 25 °C): δ= 3.43 (t, *J* = 6.9 Hz, 2H), 2.22 (td, *J* = 7.1, 2.7 Hz, 2H), 1.91 (t, *J* = 2.7 Hz, 1H), 1.51 - 1.40 (m, 4H).

^{13}C NMR ($CDCl_3$, 100 MHz, 25 °C): δ = 83.8, 68.6, 32.3, 31.3, 27.4, 17.1.

Compound 72a

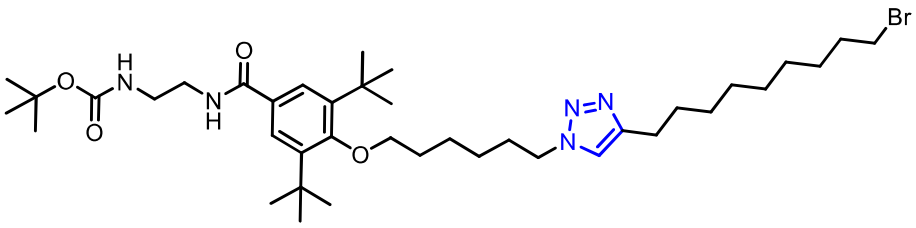

In a 500 mL one-neck round–bottom flask equipped with a stirring bar was prepared a solution of azide **70** (9.0 g, 17 mmol) and haloalkyne **71a** (5.0 g, 22 mmol) in dry dichloromethane (200 mL). Copper bromide

(CuBr) (2.7 g, 19 mmol) was added under inert atmosphere, and the reaction mixture was cooled down to 4 °C. *N*,*N*,*N*′,*N*″,*N*″-pentamethyldiethylenetriamine (PMDETA) (4 mL, 20 mmol) was added dropwise and the reaction mixture was allowed to reach room temperature. After continuous stirring during two hours, the reaction was finished as monitored by UPLC and a (10:1) mixture of water: methanol (100 mL) was added. The organic phase was washed with water until there was no blue coloration in the aqueous phase. The solvent was evaporated and the crude was purified by column chromatography (SiO_2 (300 g), DCM → DCM |MeOH 3%) to yield compound **72a** (9.0 g, 69%), as a pale yellow solid.

^{1}H NMR ($CDCl_3$, 400 MHz, 25 °C): δ = 7.70 (s, 2H), 7.32 (m, 1H), 7.24 (s, 1H), 5.12 (m, 1H), 4.30 (t, *J* = 7.2 Hz, 2H), 3.64 (t, *J* = 7.4 Hz, 2H), 3.54 – 3.51 (m, 2H), 3.40 – 3.35 (m, 4H), 2.68 (t, *J* = 7.2 Hz, 2H), 1.94 – 1.89 (m, 2H), 1.86 – 1.79 (m, 4H), 1.64 (q, *J* = 7.7 Hz, 2H), 1.50 – 1.20 (m, 41H).

^{13}C NMR ($CDCl_3$, 100 MHz, 25 °C): δ = 168.2, 161.0, 157.6, 148.5, 143.9, 128.3, 125.8, 120.5, 79.9, 77.3, 76.4, 50.1, 42.1, 40.5, 36.0, 34.2, 32.9, 32.0, 30.4, 29.6, 29.5, 29.4, 29.3, 29.3, 28.8, 28.4, 28.2, 26.7, 25.8, 25.4.

HR-MS: m/z calcd. for $C_{39}H_{66}BrN_5O_4$: 748.4371 $[M+H]^+$, found: 748.4356

Compound 72b

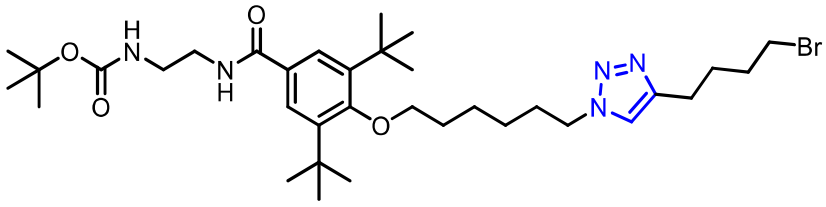

In a 250 mL one-neck round–bottom flask equipped with a stirring bar was prepared a solution of azide **70** (10.0 g, 19 mmol) and haloalkyne **71b** (4.0 g, 24 mmol) in dried dichloromethane (150 mL). CuBr (3.0 g, 21 mmol) was added under inert atmosphere and the reaction mixture was cooled down using a water: ice bath. PMDETA (5 mL, 24 mmol) was added dropwise and the reaction mixture was allowed to reach room temperature under stirring during two hours. Once the reaction was finished, a (10:1) mixture of water: methanol was added. The aqueous phase was extracted with dichloromethane (2 x 150 mL) and the organic layers were mixed and washed with water until there was no more blue coloration in the aqueous phase. The organic layers were dried over sodium sulfate, the solvent was evaporated under reduced pressure and the crude material was purified by column chromatography (SiO_2 (350 g), DCM → DCM |MeOH 4%) to yield compound **72b** (9.0 g, 69%) as a pale orange solid.

^{1}H NMR ($CDCl_3$, 400 MHz, 25 °C): δ = 7.70 (s, 2H), 7.31 (m, 1H), 5.10 (m, 1H), 4.31 (t, *J* = 7.2 Hz, 2H), 3.68 – 3.62 (t, *J* = 7.4 Hz, 4H), 3.60 – 3.50 (m, 2H), 3.40 – 3.35 (m, 2H), 2.74 (t, *J* = 7.2 Hz, 2H), 1.97 – 1.80 (m, 4H), 1.79 – 1.70 (m, 2H), 1.67 - 1.58 (m, 2H), 1.50 – 1.20 (m, 31H).

^{13}C NMR ($CDCl_3$, 100 MHz, 25 °C): δ = 168.3, 161.1, 157.7, 148.1, 143.9, 128.4, 125.8, 120.6, 79.9, 69.6, 52.4, 42.1, 40.5, 36.0, 32.3, 30.4, 30.0, 29.6, 29.4, 28.5, 26.7, 25.7.

ESI-MS: m/z calcd. for $C_{34}H_{56}BrN_5O_4$: 678.36 $[M+H]^+$, found: 678.70

Compound 73a

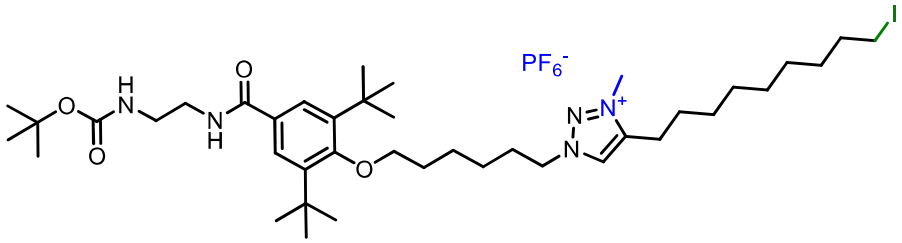

In a 100 mL one-neck round–bottom flask equipped with a stirring bar and a findenser was prepared a solution of compound **72a** (9.0 g, 12 mmol) in methyl iodide (20 mL) and dried acetonitrile (20 mL) under argon atmosphere. After stirring the solution at 50 °C for 30 hours, the solvents were evaporated under reduced pressure and the residue was washed with cyclohexane. A solution of this compound in dichloromethane (20 mL) was stirred with a saturated aqueous solution of NH_4PF_6 (20 mL) during two hours. After a liquid-liquid extraction and evaporation, compound **73a** was obtained (10.1 g, 90% yield) as an orange solid, which was pure enough to be used as such in the next step.

^{1}H NMR ($CDCl_3$, 400 MHz, 25 °C): δ = 8.16 (s, 1H), 7.70 (s, 2H), 7.38 (m, 1H), 5.15 (m, 1H), 4.50 (t, *J* = 7.2 Hz, 2H), 4.15 (s, 3H), 3.64 (t, *J* = 7.4 Hz, 2H), 3.55 – 3.51 (m, 2H), 3.40 – 3.36 (m, 2H), 3.18 (t, *J* = 6.9 Hz, 2H), 2.78 (t, *J* = 7.2 Hz, 2H), 2.05 – 2.00 (m, 2H), 1.88 – 1.68 (m, 6H), 1.50 – 1.20 (m, 41H).

^{13}C NMR ($CDCl_3$, 100 MHz, 25 °C): δ = 168.3, 161.0, 157.6, 145.1, 143.9, 128.4, 127.9, 125.8, 79.9, 76.4, 54.0, 42.1, 40.5, 37.4, 36.0, 33.5, 32.0, 30.5, 29.4, 29.3, 29.2, 29.0, 28.9, 28.4, 26.8, 26.3, 25.2, 23.3, 7.7.

HR-MS: m/z calcd. for $C_{40}H_{69}F_6IN_5O_4P$: 810.4389 $[M-PF_6]^+$, found: 810.4379

Compound 73b

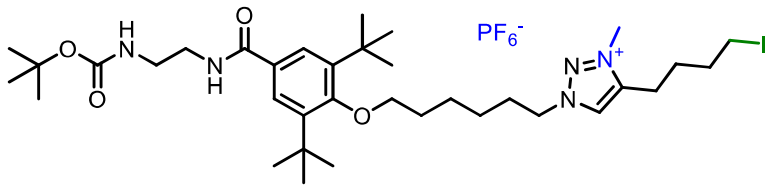

In a 100 mL one-neck round–bottom flask equipped with a stirring bar and a findenser was prepared a solution of compound **72b** (9.0 g, 13 mmol) in methyl iodide (20 mL) and dried acetonitrile (20 mL) under argon atmosphere. After stirring the solution at 25 °C for three days, the solvents were evaporated under reduced pressure and the residue was washed with cyclohexane. A solution of this compound in dichloromethane (50 mL) was vigorously stirred with a saturated aqueous solution of NH_4PF_6 (50 mL) for two hours. After a liquid-liquid extraction and evaporation, compound **73b** was obtained (10 g, 87%) as an orange solid, which was pure enough to be used as such in the next step.

^{1}H NMR ($CDCl_3$, 400 MHz, 25 °C): δ = 8.81 (d, *J* = 6.5 Hz, 2H), 8.74 – 8.71 (m, 2H), 8.21 (s, 1H), 8.17 – 8.14 (m, 2H), 7.68 (s, 2H), 7.62 (d, *J* = 5.9 Hz, 2H), 7.55 (bs, 1H), 4.64 – 4.62 (m, 2H), 4.43 – 438 (m, 2H), 4.11 (s, 3H), 3.59 (t, *J* = 6.6 Hz, 2H), 3.54 – 3.52 (m, 2H), 3.37 – 3.35 (m, 2H), 2.88 (t, *J* = 6.4 Hz, 2H), 2.17 – 2.10 (m, 2H), 2.00 – 1.96 (m, 2H), 1.82 (bs, 6H), 1.38 (bs, 11H), 1.34 (s, 18H).

^{13}C NMR ($CDCl_3$, 100 MHz, 25 °C): δ = 168.4, 161.0, 157.6, 154.3, 151.3, 145.0, 143.9, 141.4, 128.4, 128.2, 126.2, 125.8, 121.8, 79.8, 61.3, 53.9, 53.6, 41.9, 40.6, 37.4, 36.0, 32.0, 30.0, 29.4, 29.1, 28.5, 26.3, 25.2, 23.0, 22.4.

ESI-MS: m/z calcd. for $C_{35}H_{59}F_6IN_5O_4P$: 740.36 $[M–(PF_6)^-]^+$, found: 740.94

Compound 74a

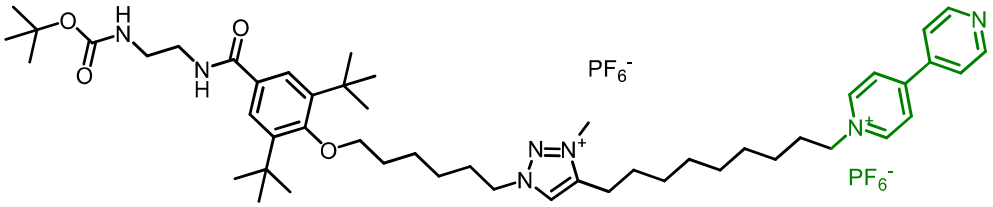

In a 500 mL one-neck round–bottom flask equipped with a stirring bar and a findenser was prepared a solution of compound **73a** (10 g, 10.6 mmol) in dried acetonitrile (200 mL). Then, 4,4'-dipyridyl (6.0 g, 38 mmol) was added and the solution was stirred at 75 °C during one day under inert atmosphere. Afterwards, the solvent was evaporated under reduced pressure and the crude residue was purified by column

chromatography (SiO_2 (300 g), DCM| MeOH 8%). The resulting compound was dissolved in a (9:1) mixture of dichloromethane/acetonitrile (50 mL) and stirred vigorously with an aqueous solution of NH_4PF_6 (50 mL) for two hours. Then, the organic phase was separated, dried over sodium sulfate and the solvent evaporated under reduced pressure to yield compound **74a** (9.0 g, 75%).as an orange powder.

^{1}H NMR (CD_3CN, 400 MHz, 25 °C): δ = 8.84 (d, *J*=6.1 Hz, 2H), 8.78 (d, *J* = 7.0 Hz, 2H), 8.32 (d, *J* = 6.9 Hz, 2H), 8.10 (s, 1H), 7.81 – 7.77 (m, 2H), 7.70 (s, 2H), 7.36 (bs, 1H), 5.60 (bs, 1H), 4.55 (t, *J* = 7.1 Hz, 2H), 4.47 (t, *J* = 7.1 Hz, 2H), 4.08 (s, 3H), 3.68 (t, *J* = 7.6 Hz, 2H), 3.38 (q, *J* = 5.7 Hz, 2H), 3.22 (q, *J* = 5.8 Hz, 2H), 2.76 (t, *J* = 7.6 Hz, 2H), 2.03 – 1.97 (m, 2H), 1.86 (p, *J* = 7.5 Hz, 2H), 1.67 (p, *J* = 7.9 Hz, 2H), 1.43 (s, 9H), 1.41 (s, 18H), 1.37 (bs, 16H).

^{13}C NMR (CD_3CN, 100 MHz, 25 °C): δ = 168.2, 161.6, 157.6, 155.0, 152.1, 145.8, 145.7, 144.7, 142.2, 129.8, 128.5, 127.0, 126.7, 122.8, 79.4, 77.4, 62.5, 54.5, 41.3, 41.1, 38.2, 36.6, 32.3, 31.9, 30.0, 29.9, 29.8, 29.7, 29.6, 29.5, 28.6, 27.6, 27.5, 26.6, 25. 7, 23.7.

HR-MS: m/z calcd. for $C_{50}H_{77}N_7O_4PF_6$: 984.5674 $[M\text{-}PF_6]^+$, found: 984.5670

Compound 74b

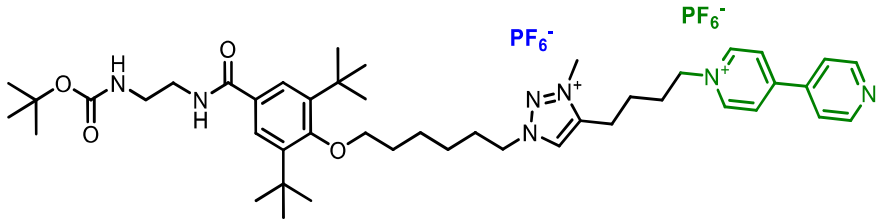

In a 500 mL one-neck round–bottom flask equipped with a stirring bar and a findenser was prepared a solution of compound **73b** (10 g, 11.5 mmol) in dried acetonitrile (200 mL). 4,4'-dipyridyl (6.0 g, 38 mmol) was added and the solution was stirred at 75 °C during one day under inert atmosphere. Then, the solvent was evaporated under reduced pressure and the crude product was purified by column chromatography (SiO_2 (300 g), DCM| MeOH 4% → DCM |MeOH 10%). The resulting compound was dissolved in a (9:1) mixture of dichloromethane/acetonitrile (50 mL) and vigorously stirred with an aqueous solution of NH_4PF_6 (50 mL) during two hours. Then, the organic phase was separated, dried and the solvent evaporated to yield compound **74b** (8.0 g, 65%) as an orange powder.

^{1}H NMR (CD_3CN, 400 MHz, 25 °C): δ = 8.81 (d, *J* = 6.5 Hz, 2H), 8.74 – 8.71 (m, 2H), 8.21 (s, 1H), 8.17 – 8.14 (m, 2H), 7.68 (s, 2H), 7.62 (d, *J* = 5.9 Hz, 2H), 7.55 (bs, 1H), 4.65 – 4.62 (m, 2H), 4.43 – 4.38 (m,

2H), 4.11 (s, 3H), 3.59 (t, J = 6.6 Hz, 2H), 3.53 – 3.51 (m, 2H), 3.37 – 3.35 (m, 2H), 2.88 (t, J = 6.4 Hz, 2H), 2.18 – 2.10 (m, 2H), 2.00 – 1.94 (m, 2H), 1.82 (bs, 6H), 1.38 (s, 11H), 1.34 (bs, 18H).

^{13}C NMR (CD_3CN, 100 MHz, 25 °C): δ = 168.4, 161.0, 157.6, 154.3, 151.3, 145.0, 144.0, 143.9, 141.4, 128.4, 128.2, 126.2, 125.8, 121.8, 79.8, 61.3, 54.0, 53.6, 41.9, 40.6, 37.4, 36.0, 32.0, 30.0, 29.4, 29.1, 28.5, 26.3, 25.2, 23.0, 22.4.

HR-MS: m/z calcd. for $C_{45}H_{67}F_6N_7O_4P$: 914.4891 $[M\text{-}PF_6]^+$, found: 914.4883

Compound 75a

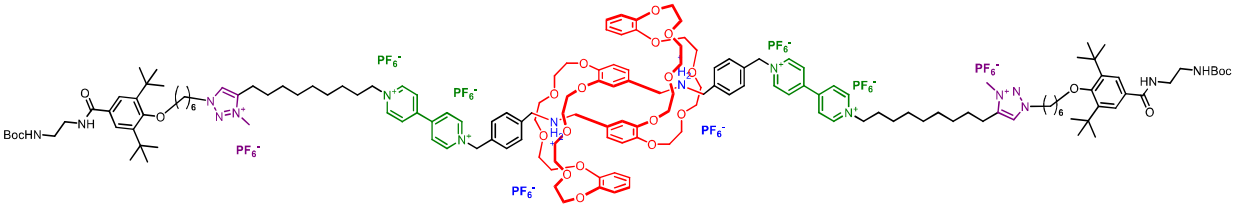

In a 100 mL one-neck round–bottom flask equipped with a stirring bar and a findenser was prepared a mixture of bipyridinium derivative **74a** (2.3 g, 2 mmol) and pseudo[*c*2]daisy chain rotaxane **52** (1.5 g, 0.9 mmol) in a (3:1) mixture of chloroform/acetonitrile (40 mL). The reaction mixture was stirred at 65 °C during four days under argon atmosphere. Afterwards, the solvents were evaporated under reduced pressure and the crude was purified by column chromatography (SiO_2 (120 g), dichloromethane: methanol 10% → dichloromethane: methanol 50% → methanol 100% → methanol: 2 M ammonium chloride 10% → methanol: 2 M ammonium chloride 20%: nitromethane 10%). Solid ammonium hexafluorophosphate was added to the combined fractions containing compound **75a**, leading to a yellow precipitate that was filtrated, washed with water, and dried under vacuum, affording compound **75a** (0.9 g, 24%) as a yellow solid.

^{1}H NMR (CD_3CN, 400 MHz, 25 °C): δ = 8.96 (d, J = 7.1 Hz, 4H), 8.91 (d, J = 7.0 Hz, 4H), 8.42 – 8.38 (m, 8H), 8.10 (s, 2H), 7.69 (s, 4H), 7.64 (d, J = 8.2 Hz, 4H), 7.53 (d, J = 8.3 Hz, 4H), 7.42 (bs, 2H), 7.30 – 7.20 (m, 2H), 6.99 – 6.92 (m, 2H), 6.87 – 6.78 (m, 10H), 6.47 (d, J = 8.4 Hz, 2H), 5.83 (s, 4H), 5.66 (bs, 2H), 4.86 – 4.68 (m, 6H), 4.65 – 4.56 (m, 6H), 4.47 (t, J = 7.1 Hz, 4H), 4.32 – 4.23 (m, 4H), 4.17 – 4.13 (m, 4H), 4.08 (s, 6H), 4.01 – 3.30 (m, 48H), 3.23 – 3.18 (m, 4H), 2.76 (t, J = 7.1 Hz, 4H), 2.05 – 2.00 (m, 4H), 1.86 (p, J = 7.6 Hz, 4H), 1.68 (p, J = 7.9 Hz, 4H), 1.51 – 1.15 (m, 86H).

^{13}C NMR (CD_3CN, 100 MHz, 25 °C): δ = 168.4, 161.7, 157.7, 151.5, 150.6, 148.7, 148.6, 147.3, 147.0, 146.6, 146.5, 146.4, 145.7, 144.7, 135.3, 134.5, 130.8, 130.7, 128.5, 128.4, 128.1, 126.7, 125.6, 123.8, 121.8, 112.9, 77.4, 72.7, 72.5, 71.5, 71.3, 71.2, 68.7, 68.3, 65.0, 63.0, 54.4, 38.1, 36.6, 32.2, 31.9, 30.8, 29.9, 29.8, 29.7, 29.6, 29.5, 29.4, 28.5, 27.5, 27.4, 26.5, 26.4, 25.5, 23.6.

ESI-MS: m/z calcd. for $C_{166}H_{240}F_{48}N_{16}O_{24}P_8$: 946.93 $[M\text{-}2H^+\text{-}8(PF_6)^-]^{3+}$, found: 946.50

Compound 75c

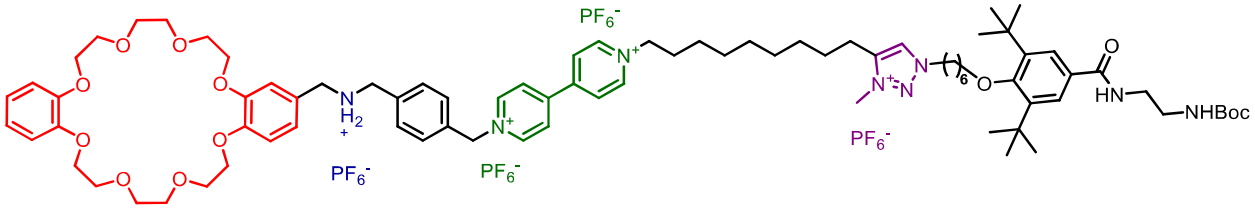

This unthreaded compound was obtained as a yellow solid during the reaction course that led to compound **75a**.

^{1}H NMR (CD_3OD, 400 MHz, 25 °C): δ = 9.30 (t, *J* = 6.8 Hz, 4H), 8.69 (dd, *J* = 15.3, 6.5 Hz, 4H), 8.64, (s, 1H), 7.76 (s, 2H), 7.56 (d, *J* = 8.0 Hz, 2H), 7.49 (d, *J* = 8.0 Hz, 2H), 7.03 (d, *J* = 8.6 Hz, 2H), 6.93 – 6.83 (m, 5H), 6.02 (s, 2H), 4.75 (t, *J* = 7.6 Hz, 2H), 4.61 (t, *J* = 7.2 Hz, 2H), 4.30 (s, 2H), 4.23 (s, 3H), 4.21 (s, 2H), 4.12–4.05 (m, 8H), 3.93 – 3.83 (m, 8H), 3.80 – 3.75 (m, 8H), 3.72 (t, *J* = 7.4 Hz, 2H), 3.44 (t, *J* = 6.0 Hz, 2H), 3.27 (t, *J* = 6.0 Hz, 2H), 2.88 (t, *J* = 7.4 Hz, 2H), 2.15 – 2.01 (m, 4H), 1.91 (p, *J* = 7.4 Hz, 2H), 1.78 (p, *J* = 8.0 Hz, 2H), 1.54 - 1.44 (m, 29H), 1.40 (bs, 12H).

^{13}C NMR (CD_3OD, 100 MHz, 25 °C): δ = 170.6, 162.3, 158.9, 151.2, 150.7, 150.1, 149.9, 147.3, 147.0, 146.3, 144.9, 135.7, 134.5, 132.3, 130.3, 129.5, 129.1, 128.6, 128.3, 127.2, 125.7, 124.8, 123.3, 123.1, 117.0, 117.0, 116.4, 115.8, 80.1, 77.7, 71.7, 71.5, 70.8, 70.7, 70.7, 70.6, 70.2, 69.9, 65.1, 63.2, 54.7, 52.1, 51.4, 41.7, 40.9, 37.9, 36.9, 32.6, 32.5, 30.5, 30.4, 30.3, 30.2, 30.1, 28.7, 27.9, 27.3, 27.3, 26.3, 24.2.

HR–MS: m/z calcd. for $C_{83}H_{120}N_8O_{12}Cl_4$: 1563.7824 $[M+H]^+$, found: 1563.8500

Compound 75b

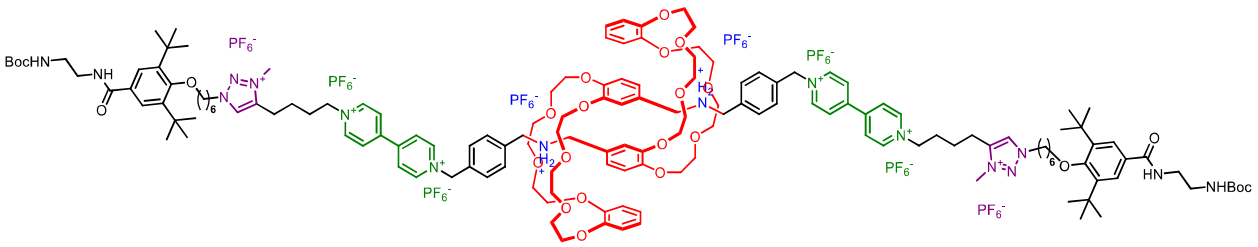

In a 100 mL one-neck round–bottom flask equipped with a stirring bar and a findenser was prepared a mixture of bipyridinium derivative **74b** (4.0 g, 3.8 mmol) and pseudo[*c*2]daisy chain rotaxane **52** (2.9 g, 1.8 mmol) in a mixture of chloroform/acetonitrile (60 mL). The mixture was vigorously stirred at 65 °C during four days under argon atmosphere. Afterwards, the solvents were evaporated under reduced pressure and the

crude residue was purified by column chromatography (SiO_2 (120 g), dichloromethane: methanol 10% → dichloromethane: methanol 50% → methanol 100% → methanol: 2 M ammonium chloride 10% → methanol: 2 M ammonium chloride 20%: nitromethane 10%). Solid ammonium hexafluorophosphate was added to the combined fractions containing compound **75b**, leading to a yellow precipitate that was filtrated, washed with water, and dried under vacuum, affording compound **75b** (1.6 g, 23%) as a yellow solid.

^{1}H NMR (CD_3CN, 500 MHz, 25 °C): δ = 8.94 (dd, *J* = 17.7, 6.9 Hz, 4H), 8.42 – 8.38 (m, 8H), 8.13 (s, 2H), 7.70 (s, 4H), 7.64 (d, *J* = 8.2 Hz, 4H), 7.53 (d, *J* = 8.3 Hz, 4H), 7.33 (bs, 2H), 7.27 – 7.16 (m, 2H), 7.00 – 6.78 (m, 12H), 6.47 (d, *J* = 8.4 Hz, 2H), 5.83 (s, 4H), 5.57 (bs, 2H), 4.85 – 4.71 (m, 3H), 4.66 (t, *J* = 7.6 Hz, 6H), 4.61-4.56 (m, 2H), 4.48 (t, *J* = 7.2 Hz, 4H), 4.31 – 4.25 (m, 2H), 4.20– 3.35 (m, 60H), 3.24 – 3.15 (m, 4H), 2.86 (t, *J* = 7.1 Hz, 4H), 2.15 – 2.10 (m, 4H), 1.99 – 1.96 (m, 4H), 1.91 – 1.76 (m, 8H), 1.50 – 1.25 (m, 62H).

^{13}C NMR (CD_3CN, 125 MHz, 25 °C): δ = 168.1, 161.5, 157.5, 151.5, 150.8, 148.7, 148.6, 147.4, 147.1, 146.6, 146.5, 144.7, 144.6, 135.4, 134.5, 130.8, 130.7, 129.7, 128.7, 128.4, 128.3, 126.7, 125.6, 123.8, 121.8, 114.4, 112.9, 79.4, 77.4, 72.7, 72.5, 71.5, 71.3, 71.2, 71.2, 70.7, 70.6, 68.8, 68.3, 67.9, 65.0, 62.3, 54.5, 53.3, 52.5, 41.2, 41.0, 38.2, 36.6, 32.2, 30.8, 29.9, 29.7, 28.5, 26.5, 25.6, 23.9, 23.0.

ESI-MS: m/z calcd. for $C_{156}H_{220}F_{48}N_{16}O_{24}P_8$: 899.88 $[M\text{-}2H^+\text{-}8(PF_6)^-]^{3+}$, found: 899.88

Compound 76a

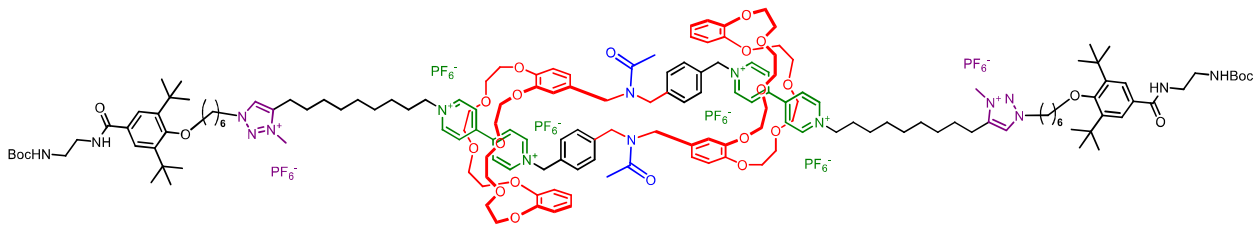

In a 50 mL one-neck round–bottom flask equipped with a stirring bar was prepared a solution of [*c*2]daisy chain **75a** (0.9 g, 0.22 mmol) in acetonitrile (14 mL). Acetic anhydride (2.0 mL, 21.5 mmol) was added and the solution was cooled down in a water/ice bath. Then, a 10% *N*,*N*,*N*–diisopropylethylamine solution in acetonitrile (4 mL) was added dropwise under stirring at 0 °C. After one hour, a 1 M HCl solution (10 mL) was added and the product was extracted with dichloromethane (2 x 40 mL), the organic phase was dried over sodium sulfate and the solvent evaporated under reduced pressure. The residue was dissolved in a small amount of dichloromethane and ethyl acetate (10 times the volume of DCM) was added to precipitate and wash the desired product. The solvents were removed under reduced pressure and the procedure was repeated twice. Finally, the product was washed with toluene and dried under reduced pressure affording

acetylated compound **76a** (0.75 g, 88%) as an orange powder which was pure enough to be used as such for the next step.

^{1}H NMR (CD_3CN, 400 MHz, 25 °C): δ = 9.34 – 9.21 (m, 3H), 8.95 – 8.82 (m, 4H), 8.12 (s, 2H), 7.94 – 7.73 (m, 3H), 7.70 (s, 4H), 7.66 – 7.62 (m, 2H), 7.54 – 7.45 (m, 4H), 7.40 – 7.30 (m, 3H), 7.27 – 7.13 (m, 13H), 7.08 – 6.98 (m, 1H), 6.88 – 6.78 (m, 1H), 6.75 – 6.15 (m, 14H), 5.80 – 5.50 (m, 5H), 4.93 – 4.84 (m, 3H), 4.48 (t, *J* = 7.1 Hz, 4H), 4.20 – 3.50 (m, 62H), 3.38 (q, *J* = 5.7 Hz, 4H), 3.22 (q, *J* = 5.4 Hz, 4H), 2.79 (t, *J* = 7.7 Hz, 4H), 2.32 (s, 6H), 1.90 – 1.80 (m, 6H), 1.75 – 1.65 (m, 4H), 1.60 – 1.30 (m, 88H).

^{13}C NMR (CD_3CN, 100 MHz, 25 °C): δ = 172.1, 168.1, 161.5, 157.5, 148.0, 147.9, 147.8, 147.7, 146.8, 146.0, 145.9, 145.7, 144.6, 138.8, 132.3, 131.2, 130.5, 129.8, 129.7, 129.1, 128.4, 128.0, 127.9, 127.2, 126.6, 126.2, 113.0, 112.9, 79.3, 77.4, 71.5, 71.4, 71.3, 70.7, 70.6, 70.5, 69.1, 69.0, 68.9, 65.0, 60.9, 55.9, 54.4, 43.9, 41.2, 41.0, 38.1, 36.7, 32.2, 30.5, 30.4, 30.3, 30.2, 30.1, 30.0, 29.9, 29.8, 29.7, 29.5, 28.5, 27.5, 26.5, 25.6, 23.7, 21.7, 18.6, 17.2, 14.4, 12.9.

HR-MS: m/z calcd. for $C_{170}H_{242}F_{24}N_{16}O_{26}P_4$: 1752.8365 $[M-2PF_6]^{2+}$, found: 1752.8262

Compound 76b

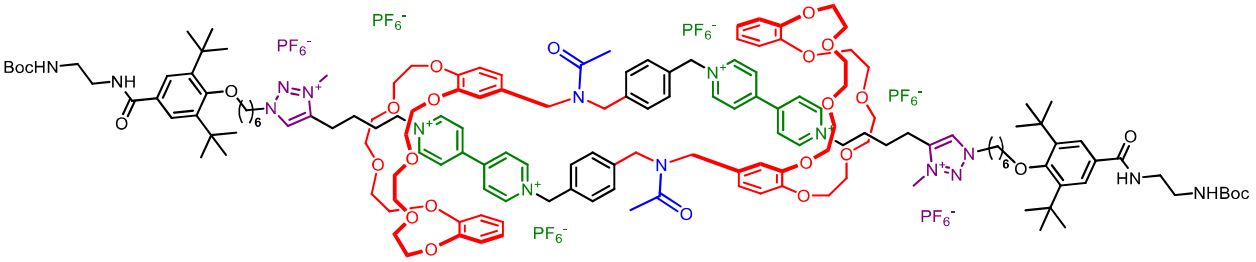

In a 50 mL one-neck round–bottom flask equipped with a stirring bar was prepared a solution of [*c*2]daisy chain **75b** (1.6 g, 0.22 mmol) in acetonitrile (20 mL). Acetic anhydride (2.0 mL, 21.5 mmol) was added to the solution which was cooled down in a water/ice bath. Then, a 10% *N*,*N*,*N*–diisopropylethylamine solution in acetonitrile (4 mL) was added dropwise under stirring at 0 °C. After one hour, a 1 M HCl solution (10 mL) was added and the product was extracted with dichloromethane (2 x 50 mL). The organic phase was dried over sodium sulfate, the solvents were evaporated under reduced pressure and the crude residue was dissolved in a small amount of dichloromethane and ethyl acetate (10 times the volume of dichloromethane) was added to precipitate and wash the desired product. The solvents were removed under reduced pressure and the procedure was repeated twice. Finally, the product was washed with toluene and dried under reduced pressure affording acetylated compound **76b** (1.3 g, 86%) as an orange solid pure enough to be used as such in the next step.

^{1}H NMR (CD$_3$CN, 400 MHz, 25 °C): δ = 9.27 – 9.23 (m, 4H), 8.89 (qd, *J* = 18.9, 17.6, 6.8 Hz, 5H), 8.39 – 8.29 (m, 1H), 8.21 – 8.16 (m, 2H), 7.77 – 7.70 (m, 6H), 7.63 (d, *J* = 10.6 Hz, 2H), 7.51 (dd, *J* = 10.9, 7.5 Hz, 4H), 7.43 – 7.40 (m, 1H), 7.34 – 7.32 (m, 2H), 7.24 (d, *J* = 7.3 Hz, 1H), 7.19 (d, *J* = 8.2 Hz, 3H), 7.08 (d, *J* = 8.1 Hz, 1H), 6.92 – 6.82 (m, 1H), 6.72 – 6.49 (m, 10H), 6.42 (t, *J* = 5.7 Hz, 1H), 6.31 (d, *J* = 8.1 Hz, 1H), 6.21 (d, *J* = 13.4 Hz, 1H), 5.74 (dt, *J* = 26.2, 14.4 Hz, 1H), 5.59 – 5.56 (m, 2H), 5.04 – 5.00 (m, 4H), 4.51 (q, *J* = 7.3 Hz, 5H), 4.20 – 3.60 (m, 64H), 3.38 (q, *J* = 5.7 Hz, 4H), 3.22 (q, *J* = 5.7 Hz, 4H), 2.99 – 2.94 (m, 4H), 2.62 – 2.44 (m, 3H), 1.99 – 1.96 (m, 6H), 1.90 – 1.82 (m, 6H), 1.47 – 1.27 (m, 70H).

^{13}C NMR (CD$_3$CN, 100 MHz, 25 °C): δ = 172.4, 172.2, 168.1, 161.6, 150.6, 148.1, 148.0, 147.9, 147.8, 146.8, 146.2, 145.6, 145.1, 144.7, 140.3, 138.9, 132.4, 131.2, 130.5, 129.9, 129.8, 129.2, 128.5, 127.9, 127.3, 127.1, 126.7, 126.2, 124.0, 121.9, 113.0, 79.4, 77.4, 71.6, 71.5, 70.7, 70.6, 69.0, 68.9, 68.6, 65.0, 61.4, 60.9, 55.9, 55.3, 54.6, 51.7, 48.6, 43.9, 41.3, 41.1, 38.3, 36.7, 36.6, 32.3, 32.2, 30.0, 29.8, 29.8, 28.6, 26.6, 25.7, 25.0, 23.9, 21.8, 21.7, 21.4, 21.1, 20.6, 18.6, 17.3, 14.5, 12.9.

HR-MS: m/z calcd. for $C_{160}H_{222}F_{24}N_{16}O_{26}P_4$: 1682.2566 $[M\text{-}2PF_6]^{2+}$, found: 1682.2539

Compound 77a

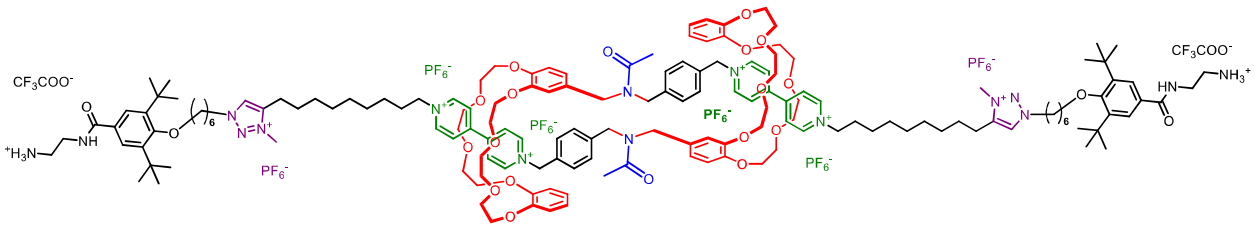

In a 50 mL one-neck round–bottom flask equipped with a stirring bar was prepared a solution of [*c*2]daisy chain rotaxane **76a** (0.75 g, 0.22 mmol) in dichloromethane (5 mL). Trifluoroacetic acid (3 mL, 40 mmol) was added and the solution was stirred at 25 °C for two hours. Once the solvent was evaporated, the residue was dissolved in a small amount of dichloromethane and ethyl acetate (10 times the volume of dichloromethane) was added to precipitate and wash the desired product. The solvents were removed under reduced pressure and the procedure was repeated two times. Finally, the product was washed with toluene and dried under vacuum affording the free bis-amine [*c*2]daisy chain **77a** (0.6 g, 84%) as an orange powder which was pure enough to be used as such in the next step.

^{1}H NMR (CD$_3$CN, 400 MHz, 25 °C): δ = 9.27 – 9.22 (m, 4H), 8.93 – 8.83 (m, 4H), 8.42 – 8.34 (m, 1H), 8.13 (s, 2H), 7.74 – 7.72 (m, 4H), 7.70 – 7.64 (m, 4H), 7.55 – 7.44 (m, 4H), 7.55 – 7.44 (m, 3H), 7.38 – 7.33 (m, 2H), 7.27 – 7.23 (m, 2H), 7.20 – 7.12 (m, 4H), 7.07 – 7.05 (m, 1H), 6.86 – 6.83 (m, 1H), 6.70 – 6.50 (m, 10H), 6.44 – 6.38 (m, 1H), 6.34 – 6.21 (m, 2H), 5.80 – 5.60 (m, 4H), 4.94 – 4.84 (m, 3H), 4.51 – 4.46 (m,

5H), 4.12 – 4.07 (m, 10H), 3.98 – 3.84 (m, 10H), 3.80 - 3.63 (m, 30H), 3.59 – 3.55 (m, 6H), 3.20 – 3.16 (m, 4H), 2.81 – 2.75 (m, 4H), 2.35 – 2.25 (m, 6H), 1.90 – 1.84 (m, 5H), 1.76 – 1.66 (m, 5H), 1.60 – 1.30 (m, 70H).

^{13}C NMR ($CDCl_3$, 100 MHz, 25 °C): δ = 173.1, 172.4, 172.3, 170.6, 162.3, 160.3, 159.9, 147.9, 146.1, 145.8, 145.0, 140.2, 138.9, 132.5, 131.2, 129.9, 129.4, 129.2, 128.5, 128.0, 127.3, 127.1, 126.3, 124.1, 121.9, 113.0, 111.7, 77.6, 71.5, 70.7, 69.0, 65.0, 62.5, 61.0, 55.9, 54.5, 43.9, 42.5, 38.8, 38.2, 36.7, 32.3, 30.5, 30.1, 29.8, 29.6, 27.6, 26.6, 25.7, 23.8, 21.5, 21.2, 18.7, 17.3, 14.5, 12.9.

HR-MS: m/z calcd. for $C_{160}H_{226}F_{24}N_{16}O_{22}P_4$: 1652.2824 $[M-2PF_6]^{2+}$, found: 1652.2665

Compound 77b

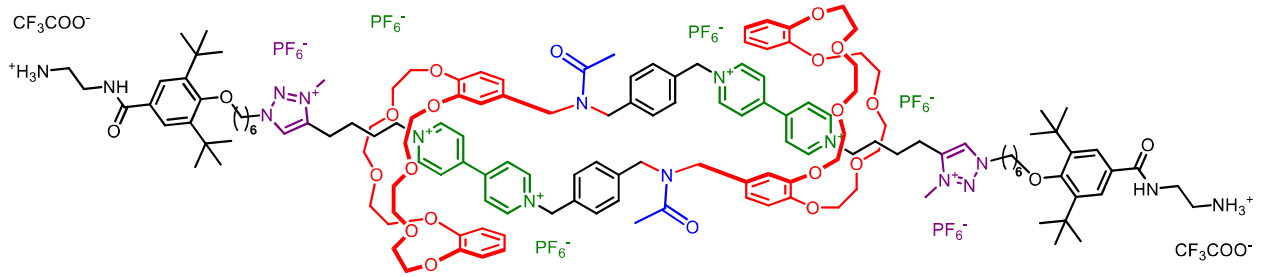

In a 50 mL one-neck round–bottom flask equipped with a stirring bar was prepared a solution of [*c*2]daisy chain rotaxane **76b** (1.24 g, 0.34 mmol) in dichloromethane (10 mL). Trifluoroacetic acid (5 mL, 40 mmol) was added and the solution was stirred at room temperature for four hours. Once the solvent was evaporated under reduced pressure, the residue was dissolved in a minimum amount of dichloromethane and ethyl acetate (10 times the volume of dichloromethane) was added to precipitate and wash the desired product. The solvents were removed under reduced pressure and the procedure was repeated twice. Finally, the product was washed with toluene and dried under vacuum affording the free bis-amine [*c*2]daisy chain rotaxane **77b** (1.05 g, 85%) as an orange powder, which was pure enough to be used as such for the next step.

^{1}H NMR (CD_3CN, 400 MHz, 25 °C): δ = 9.26 (d, *J* = 21.1 Hz, 4H), 8.98 – 8.68 (m, 5H), 8.23 (d, *J* = 2.7 Hz, 1H), 8.18 (s, 1H), 7.80 – 7.60 (m, 10H), 7.52 (d, *J* = 7.2 Hz, 4H), 7.42 (bs, 2H), 7.18 (d, *J* = 7.7 Hz, 2H), 7.10 – 7.90 (m, 6H), 6.72 – 6.42 (m, 12H), 6.33 (d, *J* = 8.3 Hz, 1H), 6.22 (bs, 1H), 5.83 – 5.63 (m, 4H), 5.05 – 5.00 (m, 5H), 4.60 – 4.50 (m, 5H), 4.20 – 3.50 (m, 64H), 3.17 (bs, 4H), 3.00 – 2.95 (m, 4H), 2.63 – 2.43 (m, 4H), 2.06 – 1.96 (m, 8H), 1.92 – 1.82 (m, 6H), 1.46 – 1.36 (m, 40H), 1.35 – 1.25 (m, 12H).

^{13}C NMR (CD_3CN, 100 MHz, 25 °C): δ = 170.5, 162.2, 160.1, 159.7, 148.1, 147.9, 147.7, 146.2, 144.9, 131.3, 130.5, 130.2, 129.4, 128.5, 128.4, 127.1, 115.1, 112.9, 77.5, 71.5, 71.4, 70.7, 70.6, 70.5, 69.0, 68.8, 55.8, 54.6, 42.4, 38.7, 38.3, 36.6, 32.2, 30.0, 29.8, 29.2, 28.6, 26.6, 25.6, 25.0, 23.9, 23.4, 21.6, 18.6, 17.2, 12.9.

HR-MS: m/z calcd. for $C_{150}H_{206}F_{24}N_{16}O_{22}P_4$: 1582.2041 $[M-2PF_6]^{2+}$, found: 1582.1998

2-amino-6-(*tert*-butyl)pyrimidin-4(3*H*)-one (57)

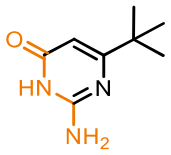

A 500 mL one-neck round–bottom flask equipped with a stirring bar and a findenser was charged with the commercially available ethyl pivaloylacetate (12.08 g, 70.3 mmol), guanidine carbonate (11 g, 91.3 mmol) and potassium *tert*-butoxide (10.43 g, 93.1 mmol) dissolved in dry ethanol (250 mL) and the solution stirred at reflux for three days. The solvent was removed and a 1 M HCl aqueous solution was added to adjust the pH about 5. The precipitate was filtered and washed with diluted 1 M HCl solution and deionized water until the pH of the filtrate was about 7. The precipitate was collected and dried under vacuum to provide compound **54** (9.86 g, 84% yield) as a pale yellow powder which was pure enough to be used as such in the next step.

^{1}H NMR (DMSO-d_6, 400 MHz, 25 °C): δ = 6.46 (bs, 2H), 5.45 (s, 1H), 1.11 (s, 9H).

^{13}C NMR (DMSO-d_6, 100 MHz, 25 °C): δ = 164.8, 155.1, 96.9, 36.3, 28.9, 27.3.

***N*-(4-(*tert*-butyl)-6-hydroxypyrimidin-2-yl)-1*H*-imidazole-2-carboxamide (78)**

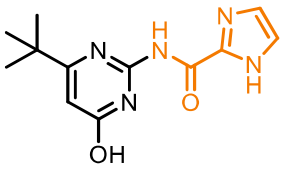

A 500 mL one-neck round–bottom flask equipped with a stirring bar and a findenser was charged with 6-*tert*-butylisocytosine **54** (2.5 g, 14.97 mmol) and 1,1–carbonyldiimidazole (3.16 g, 19.46 mmol) dissolved in dry tetrahydrofuran (15 mL) and triethylamine. This solution was heated at reflux under continuous stirring for six hours under argon atmosphere. The reaction mixture was concentrated under reduced pressure

acetone was added. The resulting precipitate was washed thoroughly with acetone, filtered off and dried, providing compound **55** (88 %) as a pale yellow powder.

^{1}H NMR (DMSO-*d*$_6$, 400 MHz, 25 °C): δ = 12.30 (s, 1H), 8.18 (s, 1H), 7.58 – 7.57 (m, 1H), 6.90 – 6.88 (m, 1H), 5.65 (s, 1H), 1.17 (s, 9H).

^{13}C NMR (DMSO-*d*$_6$, 100 MHz, 25 °C): δ = 177.0, 163.2, 159.3, 156.2, 136.7, 136.1, 128.4, 117.1, 98.9, 36.8, 29.0.

Methyl 3-(3-(4-(benzyloxy)-6-(*tert*-butyl)pyrimidin-2-yl)ureido)propanoate (80)

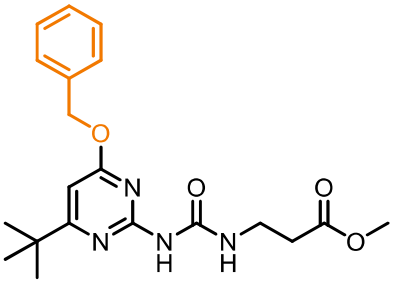

In a 100 mL one-neck round–bottom flask equipped with a stirring bar was dissolved compound **56** (1.0 g, 4.0 mmol) in dry *N*,*N*-dimethylformamide (20 mL) and potassium carbonate (1.0 g, 8.0 mmol) under argon atmosphere. Benzyl bromide (0.7 mL, 6.0 mmol) was added and the mixture was stirred at room temperature overnight. Water (40 mL) was added and dichloromethane (2 x 40 mL) was used for liquid-liquid extraction. The solvent was removed under reduced pressure and the crude residue was purified by silica column chromatography to yield compound **57** (1.0 g, 69%) as a pale yellow solid.

^{1}H NMR (DMSO-*d*$_6$, 400 MHz, 25 °C): δ = 9.61 (s, 1H), 9.38 (t, *J* = 5.7 Hz, 1H), 7.52 (dd, *J* = 8.0, 1.5 Hz, 2H), 7.41 – 7.31 (m, 3H), 6.42 (s, 1H), 5.36 (s, 2H), 3.58 (s, 3H), 3.47 (q, *J* = 6.1 Hz, 2H), 2.57 (t, *J* = 6.2 Hz, 2H), 1.23 (s, 9H).

^{13}C NMR (DMSO-*d*$_6$, 100 MHz, 25 °C): δ = 178.1, 172.1, 169.9, 157.3, 154.1, 136.1, 128.9, 128.4, 128.2, 96.1, 67.5, 51.4, 36.9, 35.2, 34.1, 28.9.

HR–MS: m/z calcd. for $C_{20}H_{26}N_4O_4$: 387.2027 $[M+H]^+$, found: 387.2018

3-(3-(4-(benzyloxy)-6-(*tert*-butyl)pyrimidin-2-yl)ureido)propanoic acid (81)

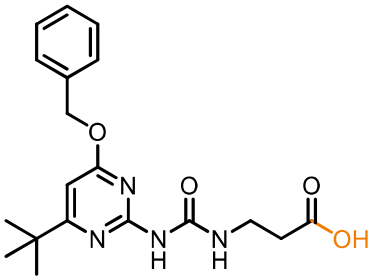

In a 100 mL one-neck round–bottom flask equipped with a stirring bar and a findenser was dissolved compound **57** (1.0 g, 2.6 mmol) in a mixture of tetrahydrofuran (45 mL), methanol (15 mL) and water (5 mL). Then sodium hydroxide (0.4 g, 10.4 mmol) was added, and the reaction mixture was stirred at 65 °C for four hours. After that time, the reaction mixture was cooled down and a 1 M HCl solution (50 mL) was added and the aqueous phase was extracted with dichloromethane (2 x 100 mL) The organic phase was dried over sodium sulfate and the solvent was evaporated under reduced pressure to yield compound **58** (0.86 g, 90%) as transparent liquid that turns into a solid.

^{1}H NMR (DMSO-d_6, 400 MHz, 25 °C): δ = 12.31 (s, 1H), 9.58 (s, 1H), 9.38 (t, *J* = 5.7 Hz, 1H), 7.51 (dd, *J* = 8.0, 1.4 Hz, 2H), 7.41 – 7.31 (m, 3H), 6.42 (s, 1H), 5.37 (s, 2H), 3.43 (q, *J* = 6.1 Hz, 2H), 2.46 (t, 2H), 1.23 (s, 9H).

^{13}C NMR (DMSO-d_6, 100 MHz, 25 °C): δ = 178.2, 173.2, 169.9, 157.3, 154.1, 136.2, 128.8, 128.4, 128.2, 96.1, 67.4, 36.1, 35.3, 34.3, 28.9.

3-(3-(4-(tert-butyl)-6-oxo-1,6-dihydropyrimidin-2-yl)ureido)propanoic acid (82)

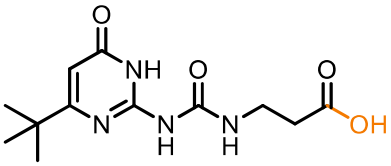

In a 100 mL one-neck round–bottom flask equipped with a stirring bar and a findenser was dissolved compound **56** (1.7 g, 5.7 mmol) in a mixture of tetrahydrofuran (45 mL), methanol (15 mL) and water (5 mL). Then, sodium hydroxide (1.0 g, 26 mmol) was added, and the reaction mixture was stirred at 65 °C during four hours. After that time, the reaction was cooled down and a 1 M HCl solution (50 mL) was added and the aqueous phase was extracted with dichloromethane (2 x 100 mL) The organic phase was dried over sodium sulfate and the solvent was evaporated under reduced pressure to yield compound **59** (1.45 g, 90%) as transparent liquid that turns into a solid.

^{1}H NMR (DMSO-d_6, 400 MHz, 25 °C): δ = 12.2 (s, 1H), 9.69 (s, 1H), 9.40 (t, *J* = 5.7 Hz, 1H), 6.55 (s, 1H), 3.43 (q, *J* = 6.1 Hz, 2H), 2.46 (t, 2H), 1.23 (s, 9H).

^{13}C NMR (DMSO-d_6, 100 MHz, 25 °C): δ = 178.5, 173.7, 169.9, 156.5, 149.1, 96.9, 36.1, 35.3, 34.3, 28.2.

Compound 83a

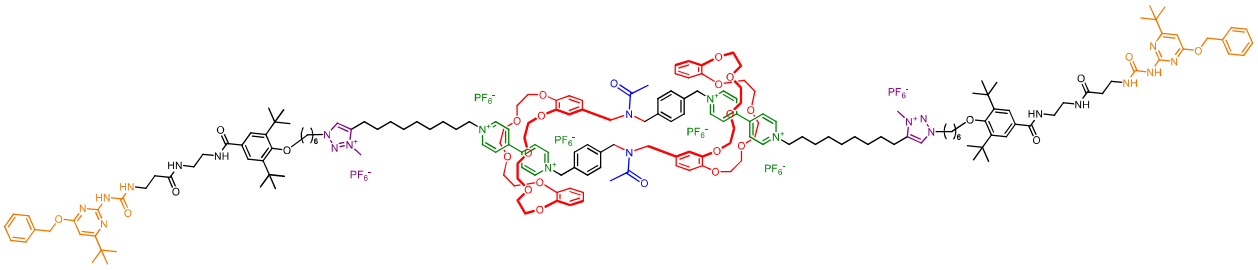

In a 10 mL one-neck round–bottom flask equipped with a stirring bar was prepared a solution of [*c*2]daisy chain **53a** (40 mg, 0.011 mmol) in dry *N*,*N*-dimethylformamide (2 mL). Then, sodium hydrogen carbonate (10 mg, 0.11 mmol), hydroxybenzotriazole (6.0 mg, 0.044 mmol), EDCI (9.6 mg, 0.05 mmol) and compound **58** (12 mg, 0.033 mmol) were added. The reaction mixture was stirred at 30 °C during six hours and the end of the reaction was confirmed by UPLC-MS. Then, a 1 M HCl solution (5 mL) was added maintaining the stirring for 30 minutes. Afterwards, a saturated solution of sodium hydrogen carbonate (5 mL) was added and the aqueous phase was extracted with dichloromethane (3 x 30 mL). Finally, the organic phase was washed a 1 M HCl solution (10 mL), dried over sodium sulfate and the solvent evaporated under reduced pressure affording compound **60a** (31.5 mg, 70%).as an orange solid.

ESI–MS: m/z calcd. for $C_{198}H_{270}F_{36}N_{24}O_{28}P_6$: 858.51 $[M\text{-}6(PF_6)^-]^{4+}$, found: 858.55

Compound 84a

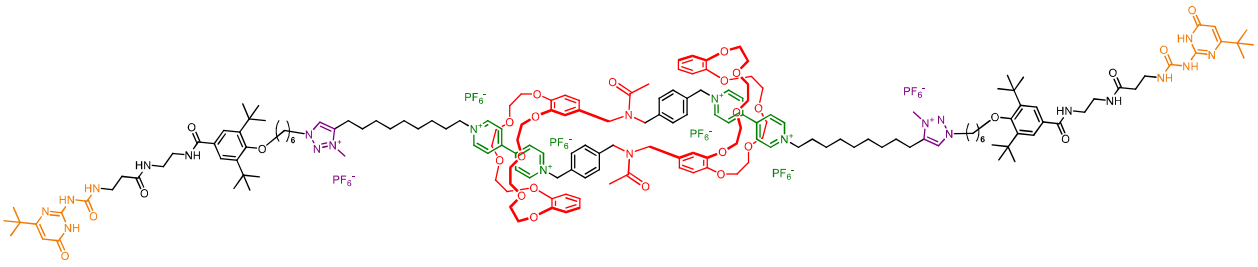

In a 10 mL one-neck round–bottom flask equipped with a stirring bar was prepared a solution of [*c*2]daisy chain **53a** (40 mg, 0.011 mmol) in dry *N*,*N*–dimethylformamide (2 mL). Then, sodium hydrogen carbonate (10 mg, 0.11 mmol), hydroxybenzotriazole (6.0 mg, 0.044 mmol), EDCI (9.6 mg, 0.05 mmol) and compound **59** (9 mg, 0.033 mmol) were added. The reaction mixture was stirred at 30 °C during six hours

and the end of the reaction was confirmed by UPLC-MS. Then, a 1 M HCl 1 solution (5 mL) was added maintaining the stirring for 30 minutes. Afterwards, a saturated solution of sodium hydrogen carbonate (5 mL) was added and the aqueous phase was extracted with dichloromethane (2 x 20 mL). Finally, the organic phase is washed with a 1 M HCl solution (20 mL), dried over sodium sulfate and the solvent evaporated under reduced pressure affording compound **61a** (32 mg, 70%) as an orange solid.

ESI–MS: m/z calcd. for $C_{184}H_{258}F_{36}N_{24}O_{28}P_6$: 812.98 $[M\text{-}2H\text{-}6(PF_6)^-]^{4+}$, found: 812.89

Compound 84b

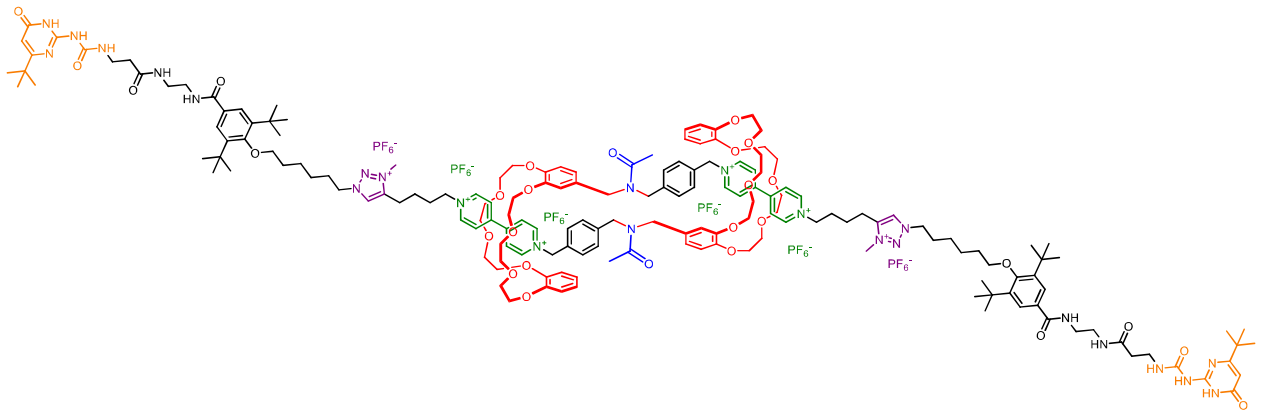

In a 10 mL one-neck round–bottom flask equipped with a stirring bar was prepared a solution of [*c*2]daisy chain **53b** (0.1 g, 0.027 mmol) in dry *N*,*N*–dimethylformamide (9 mL). Then, sodium hydrogen carbonate (0.022 g, 0.27 mmol), hydroxybenzotriazole (0.01 g, 0.078 mmol), EDCI (0.03 g, 0.15 mmol) and compound **59** (0.025 g, 0.087 mmol) were added. The reaction mixture was stirred at 30 °C during six hours and the end of the reaction was confirmed by UPLC-MS. Then, a 1M HCl solution (5 mL) was added maintaining the stirring for 30 minutes. Afterwards, a saturated solution of sodium hydrogen carbonate (5 mL) was added and the aqueous phase was extracted with dichloromethane: acetonitrile 10% (2 x 40 mL). Finally, the organic phase was washed with a 1 M HCl solution (30 mL), the product stuck on the walls of the separating funnel was dissolved in methanol, and the solvent evaporated giving an orange solid (0.07 g, 60%).

ESI–MS: m/z calcd. for $C_{174}H_{238}F_{36}N_{24}O_{28}P_6$: 777.94 $[M\text{-}2H\text{-}6(PF_6)^-]^{4+}$, found: 777.96

Compound 85a

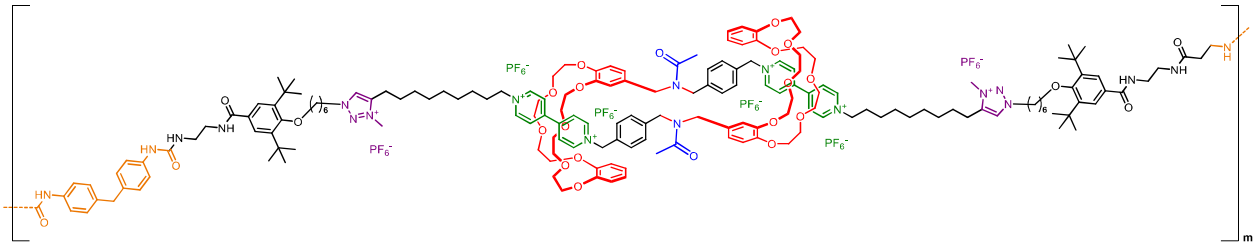

In a 100 mL one-neck round–bottom flask equipped with a stirring bar was prepared a mixture of [*c*2]daisy chain **53a** (2.0 g, 0.52 mmol) and sodium hydrogen carbonate (0.40 g, 5.2 mmol) in dry *N*,*N*-dimethylformamide (6 mL). Then, an aliquot (4 mL) of a 0.135 M MDI solution in dry *N*,*N*-dimethylformamide was added, followed by one drop of dibutyltin dilaurate (DBTDL) and the reaction mixture was vigorously stirred for 48h under argon atmosphere at 30 °C. After that time, a (8:2) solution of 1 M HCl/MeOH (20 mL) was added, and an orange precipitate was formed. The polymer was purified by centrifugation, washed twice with water, dissolved in acetonitrile and dried under reduced pressure to yield compound **62a** (1.6 g, 80%) as an orange solid.

Compound 85b

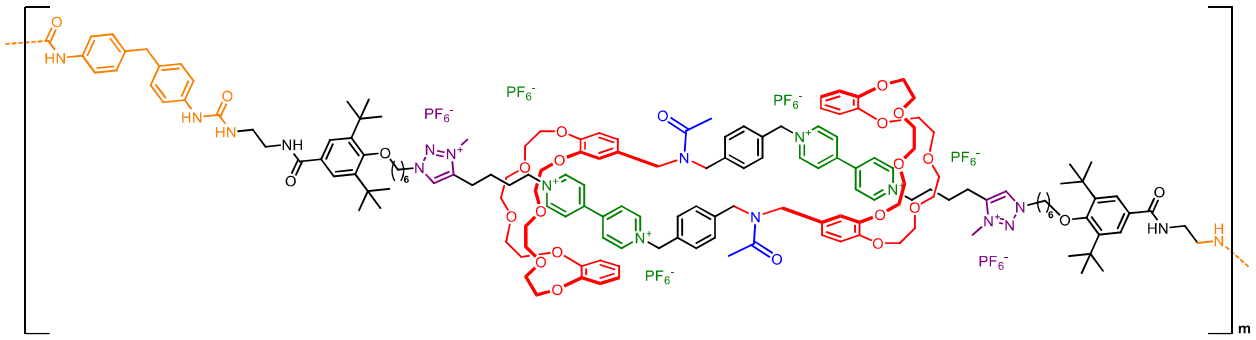

In a 100 mL one-neck round–bottom flask equipped with a stirring bar was prepared a mixture of [*c*2]daisy chain **53b** (0.50 g, 0.14 mmol) and sodium hydrogen carbonate (0.12 g, 1.44 mmol) in dry *N*,*N*-dimethylformamide (1 mL). Then, an aliquot (4 mL) of a 0.036 M MDI solution prepared in dry *N*,*N*-dimethylformamide was added, followed by one drop of dibutyltin dilaurate (DBTDL) and the reaction mixture was vigorously stirred for 48h under argon atmosphere at 30 °C. After that time, a (8:2) solution of 1 M HCl/MeOH (20 mL) was added, and an orange precipitate was formed. The polymer was purified by centrifugation, washed twice with water, dissolved in acetonitrile and dried under reduced pressure to yield compound **62b** (0.4 g, 75%) as an orange solid.

5.3. NMR and MS spectra

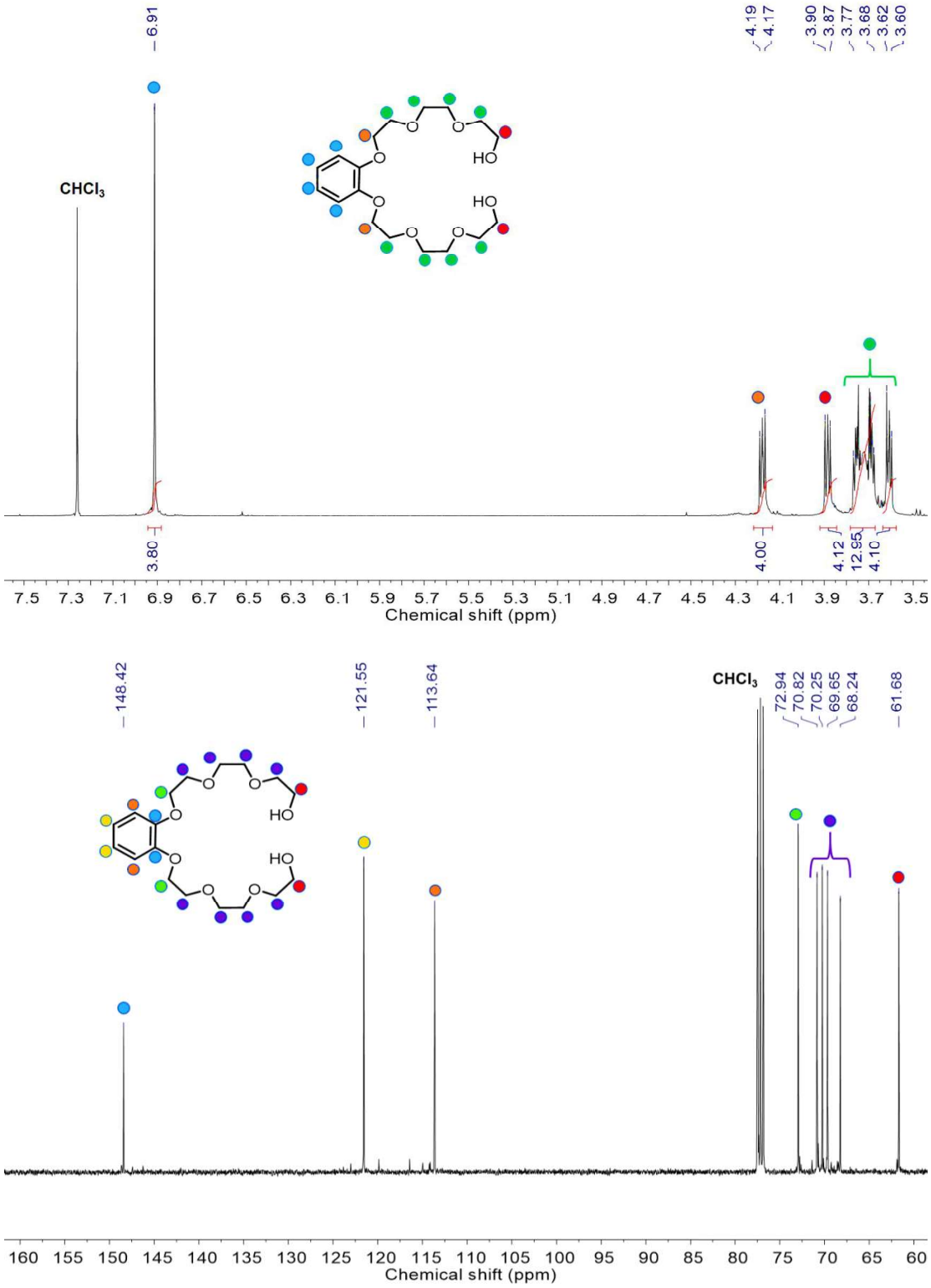

Figure 5.2. ^{1}H (top) and ^{13}C (bottom) NMR spectra of compound **4** in $CDCl_3$ at 25 °C.

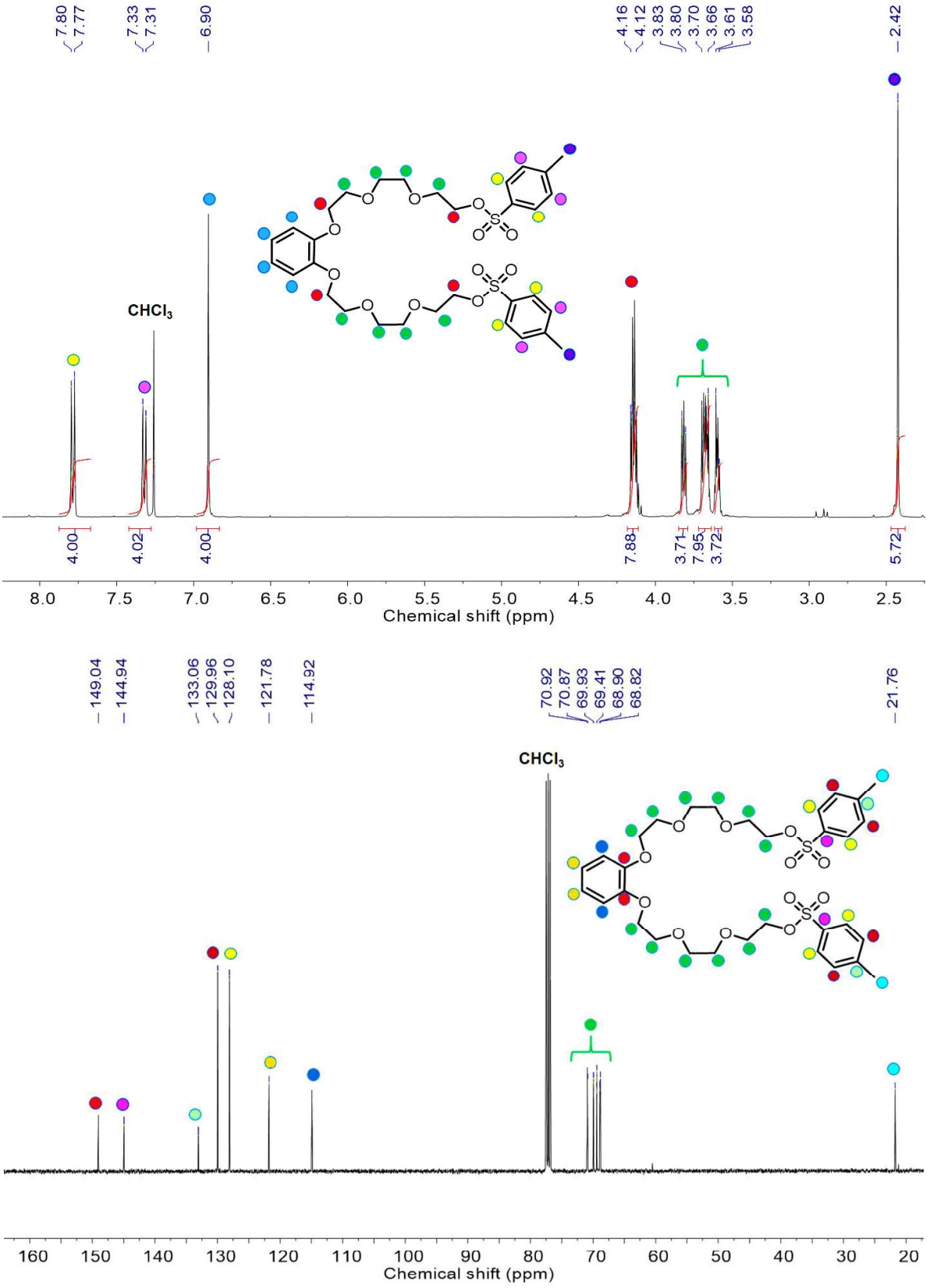

Figure 5.3. ^{1}H (top) and ^{13}C (bottom) NMR spectra of compound **5** in $CDCl_3$ at 25 °C.

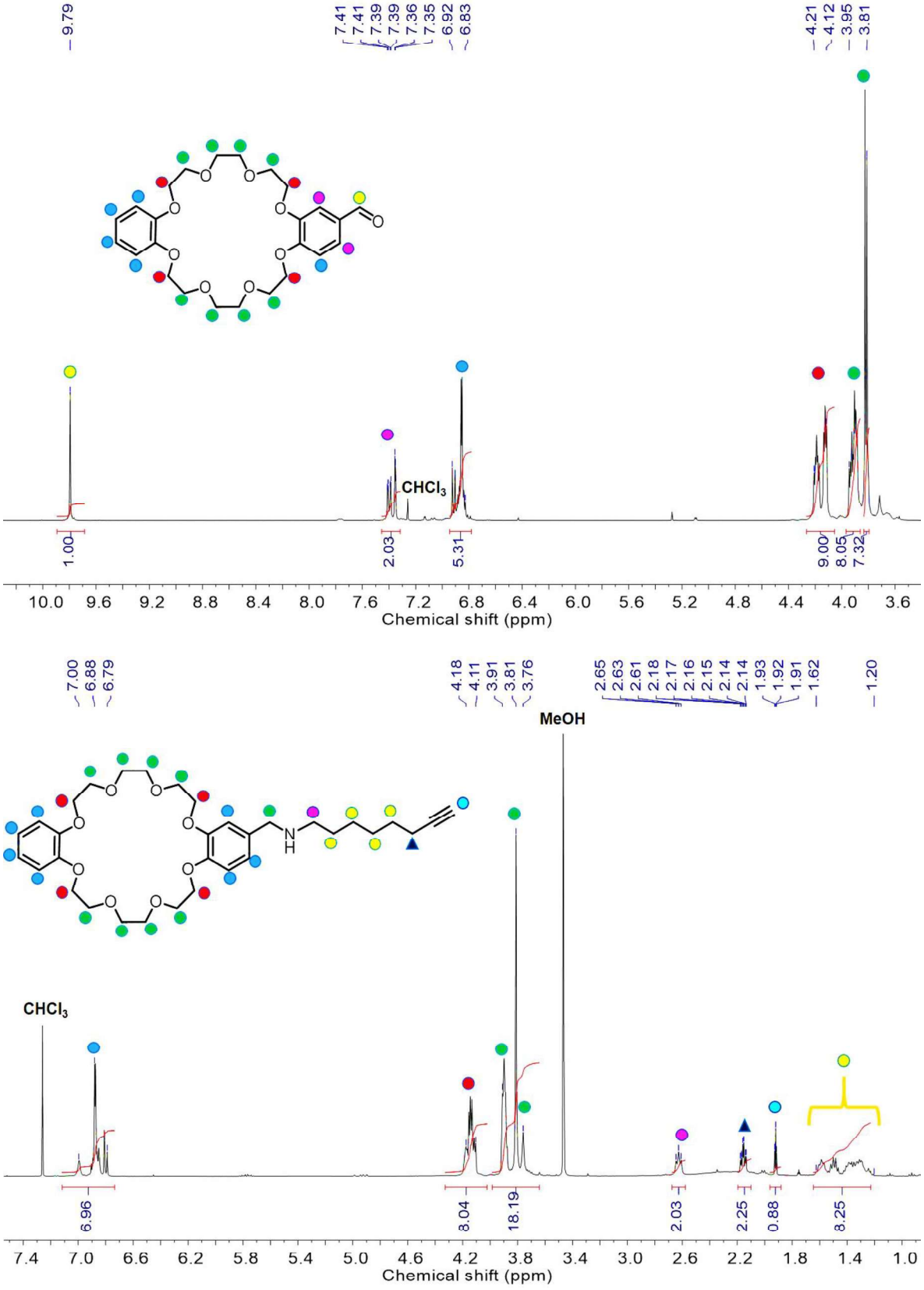

Figure 5.4. ^{1}H NMR spectra of compound **6** (top) and compound **8** (bottom) in $CDCl_3$ (**6**) and CD_3OD (**8**) at 25 °C.

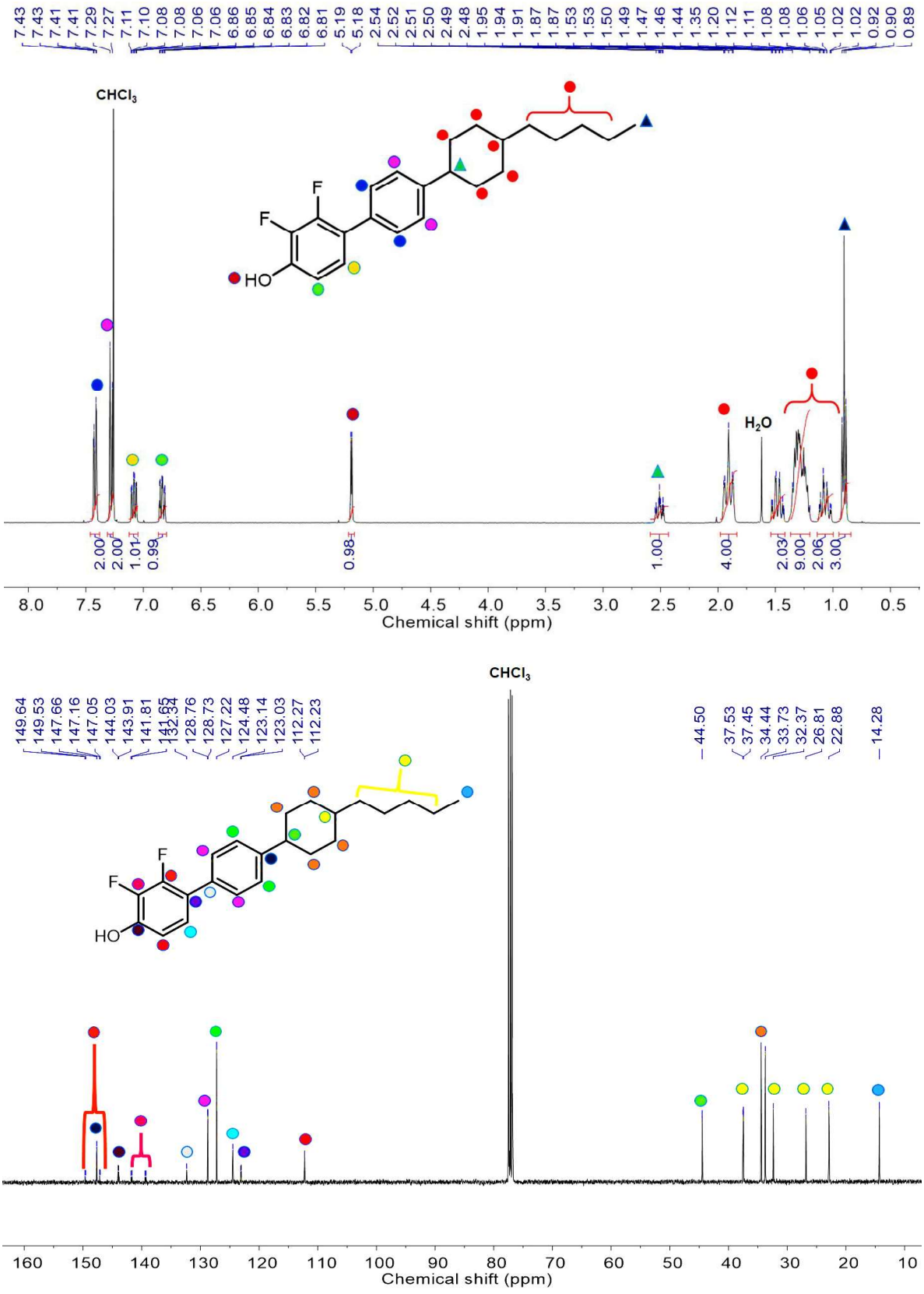

Figure 5.5. ^{1}H (top) and ^{13}C (bottom) NMR spectra of compound **13** in $CDCl_3$ at 25 °C.

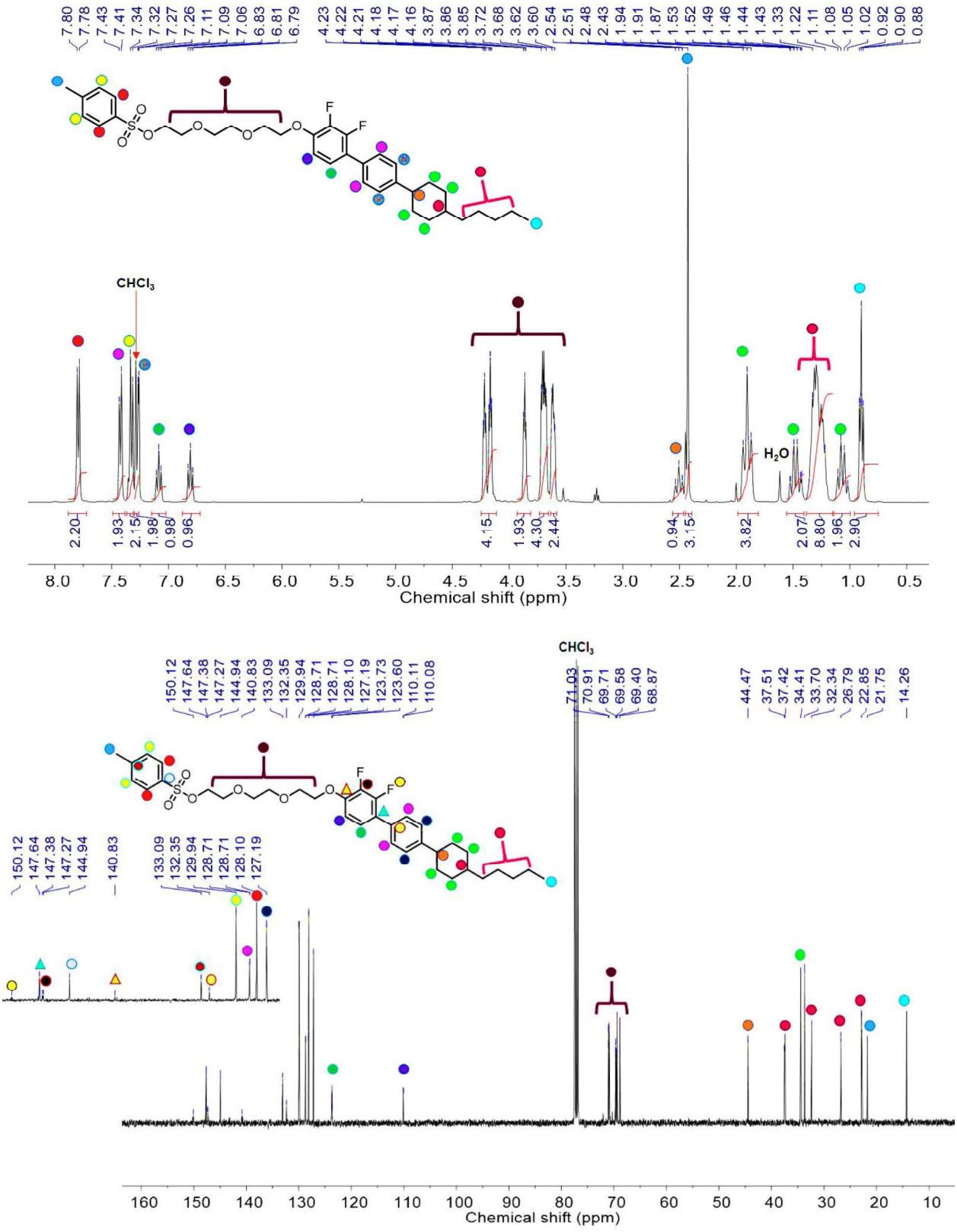

Figure 5.6. ^{1}H (top) and ^{13}C (bottom) NMR spectra of compound **14** in $CDCl_3$ at 25 °C.

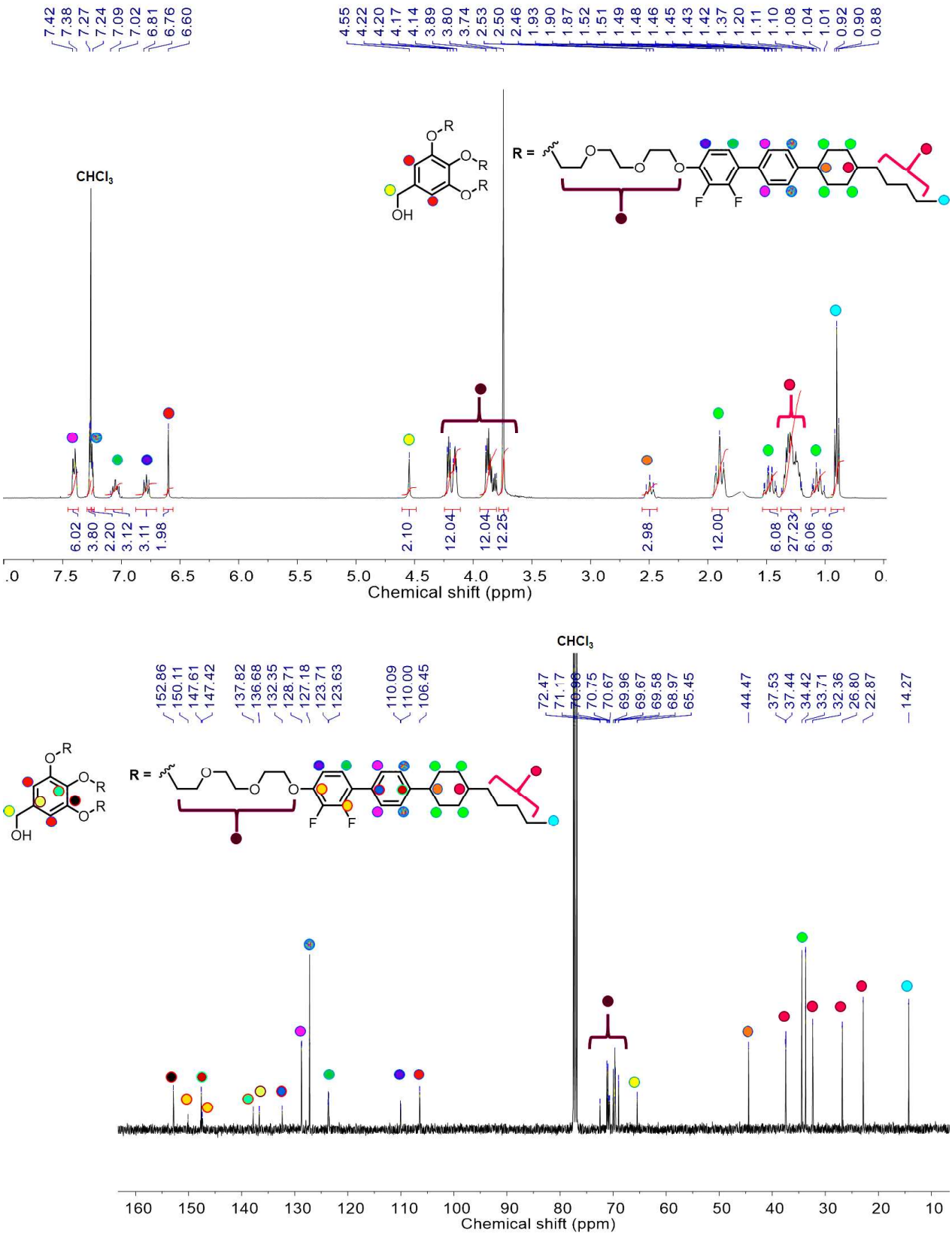

Figure 5.7. ^{1}H (top) and ^{13}C (bottom) NMR spectra of compound **16** in $CDCl_3$ at 25 °C.

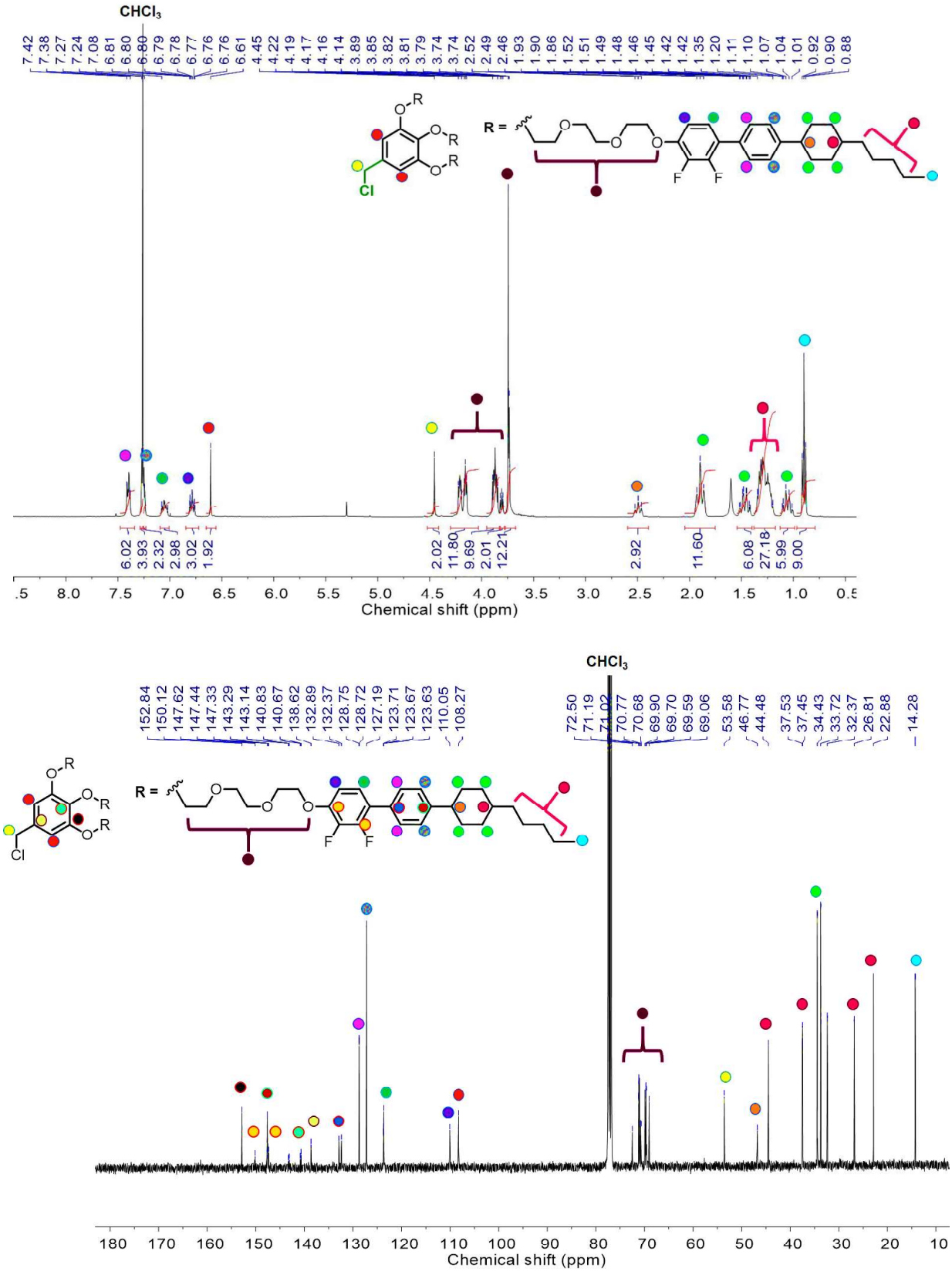

Figure 5.8. ^{1}H (top) and ^{13}C (bottom) NMR spectra of compound **17** in $CDCl_3$ at 25 °C.

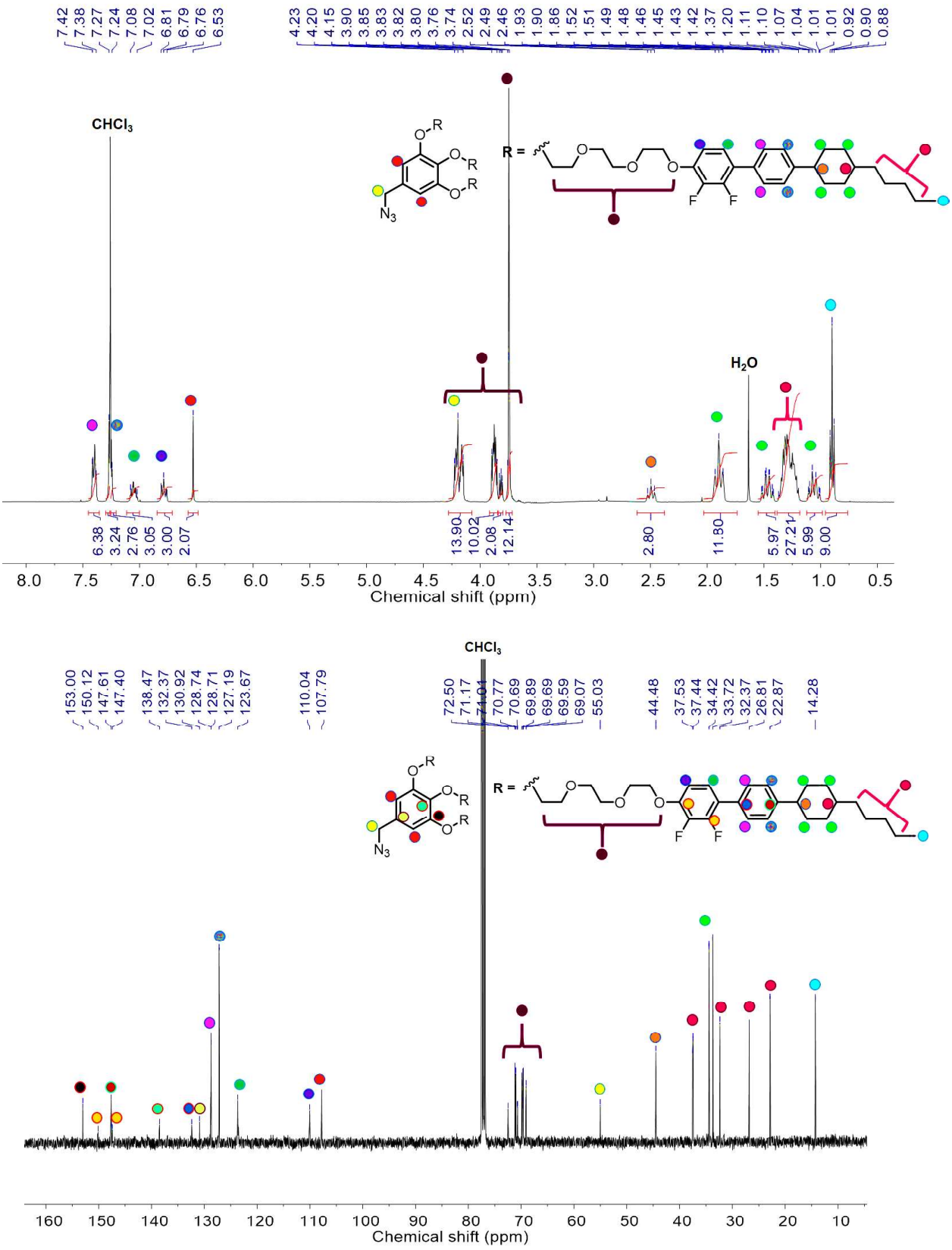

Figure 5.9. ^{1}H (top) and ^{13}C (bottom) NMR spectra of compound **18** in $CDCl_3$ at 25 °C.

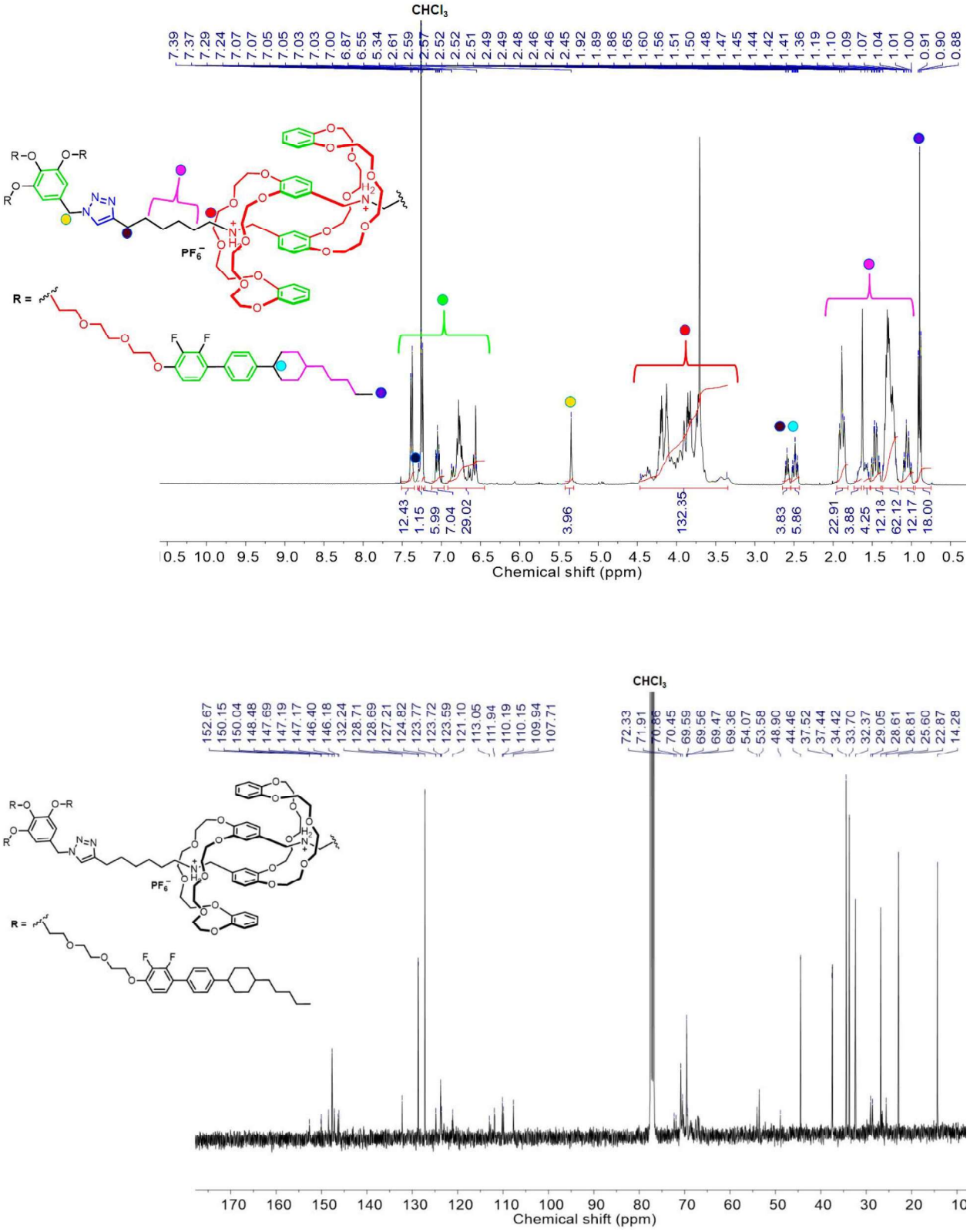

Figure 5.10. ^{1}H (top) and ^{13}C (bottom) NMR spectra of compound **19** in $CDCl_3$ at 25 °C.

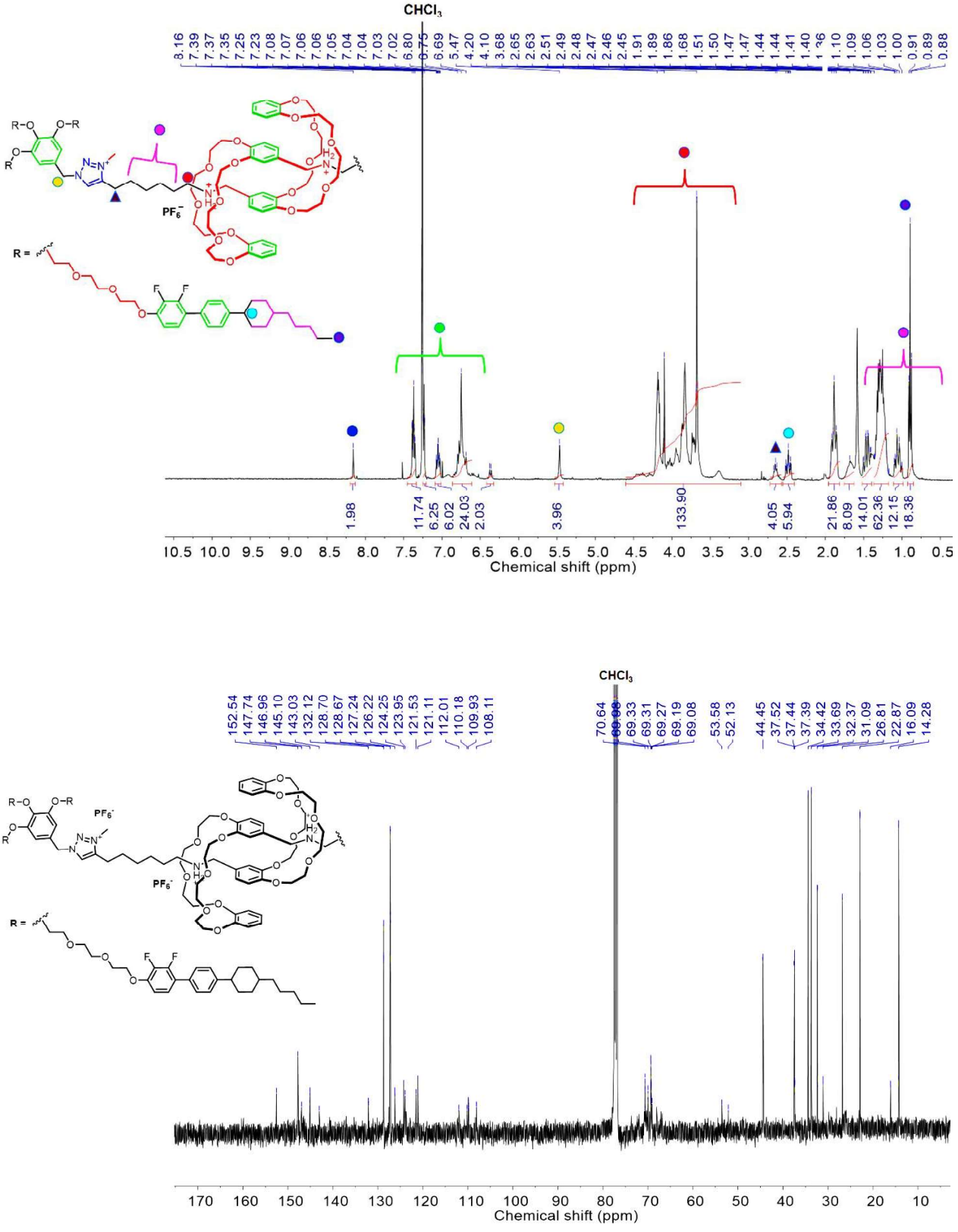

Figure 5.11. ^{1}H (top) and ^{13}C (bottom) NMR spectra of compound **20**$_{Ext}$ in $CDCl_3$ at 25 °C.

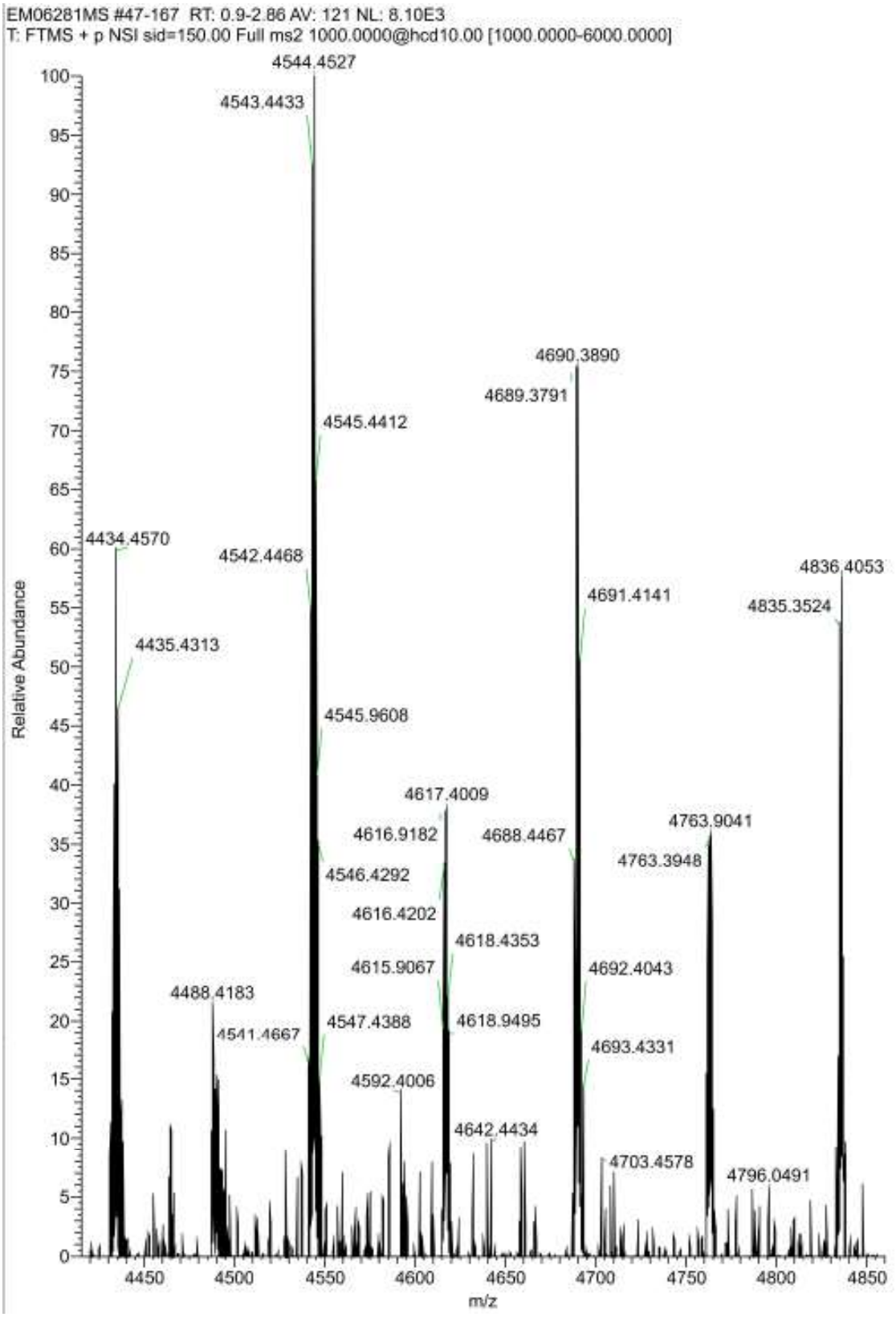

Figure 5.12. HR-MS spectrum of compound $\mathbf{20}_{\mathbf{Ext}}$.

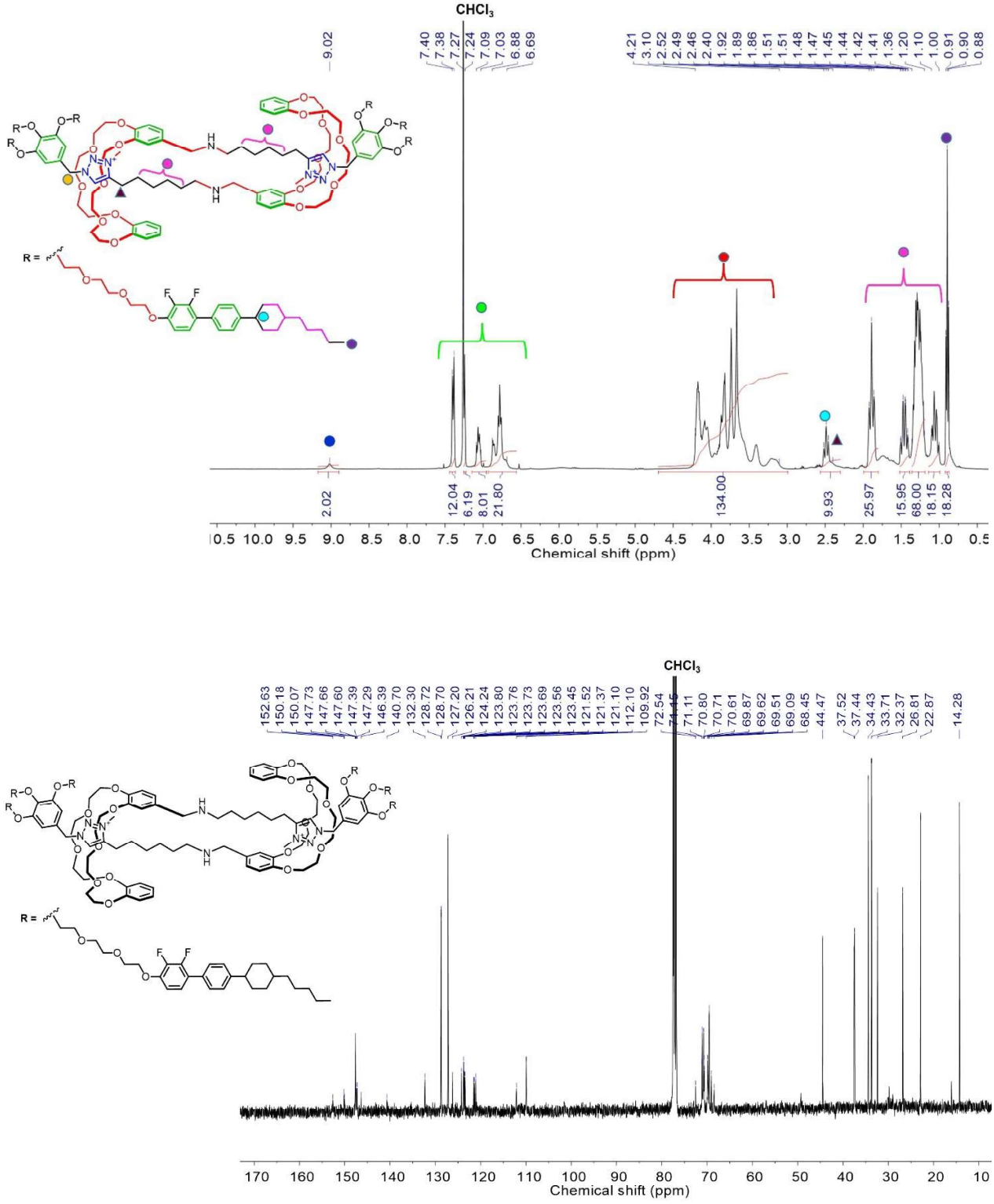

Figure 5.12. ^{1}H (top) and ^{13}C (bottom) NMR spectra of compound **20**$_{Cont}$ in $CDCl_3$ at 25 °C.

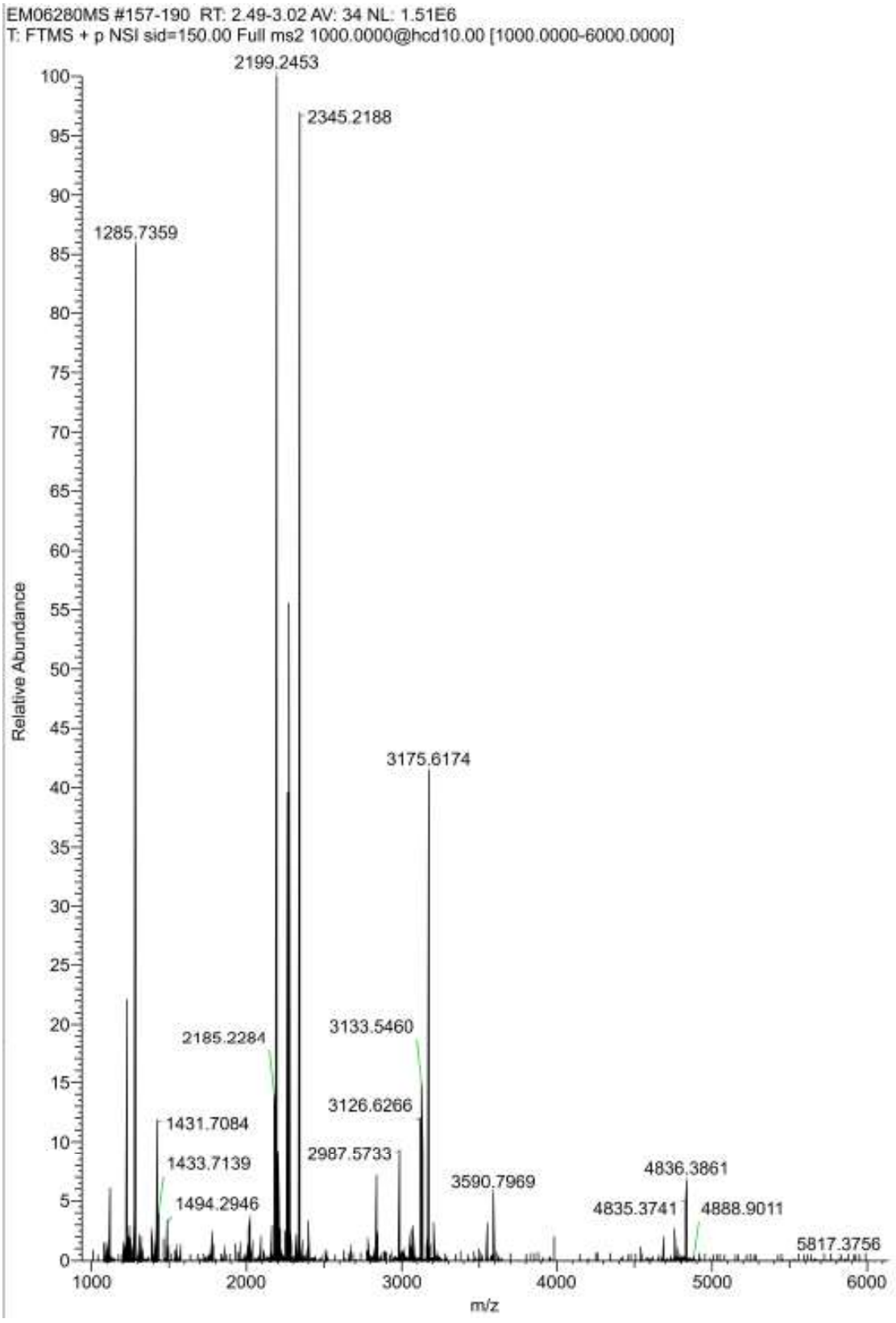

Figure 5.13. HR-MS spectrum of compound $\mathbf{20}_{\mathbf{Cont}}$.

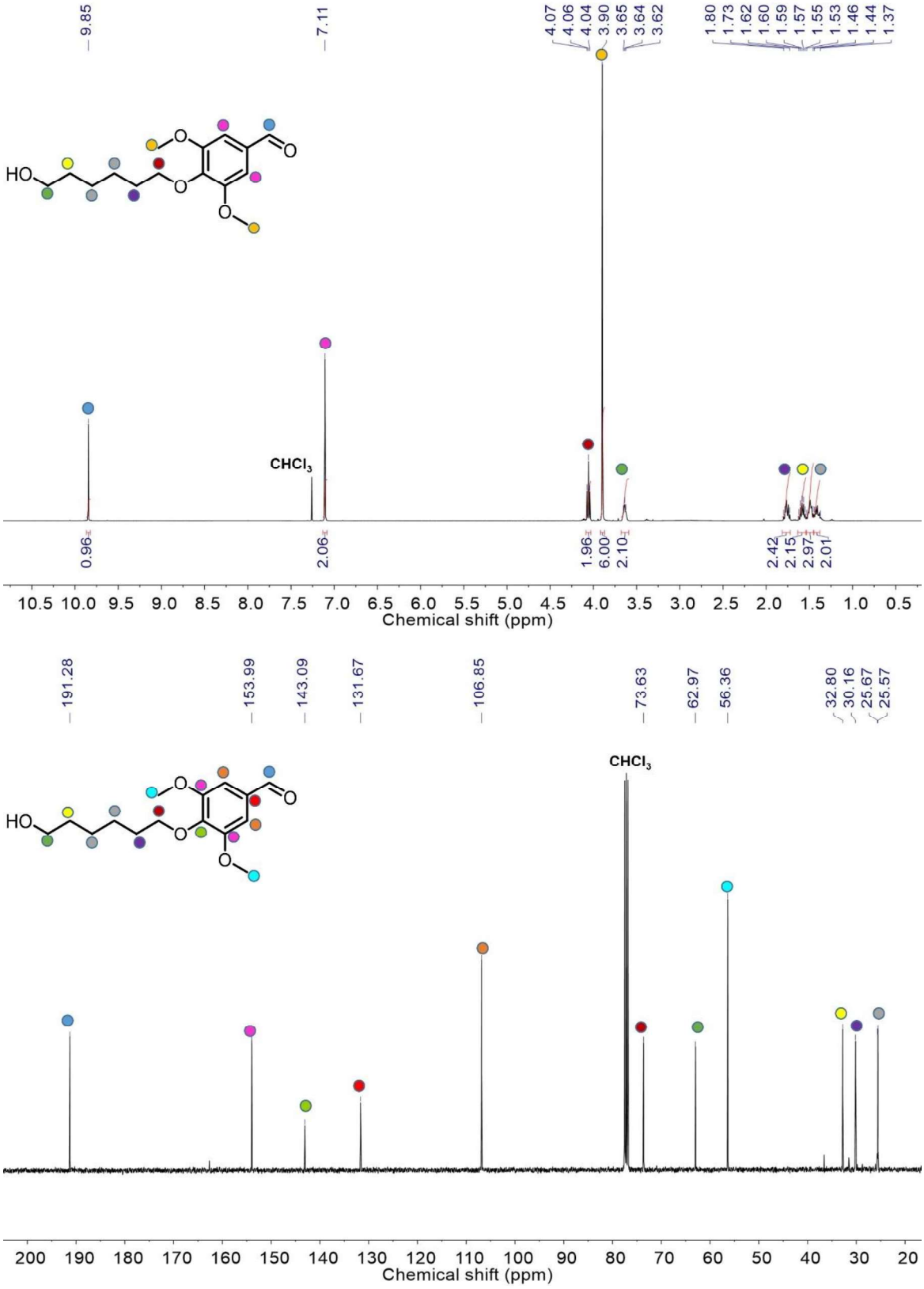

Figure 5.14. ^{1}H (top) and ^{13}C (bottom) NMR spectra of compound **27** in $CDCl_3$ at 25 °C.

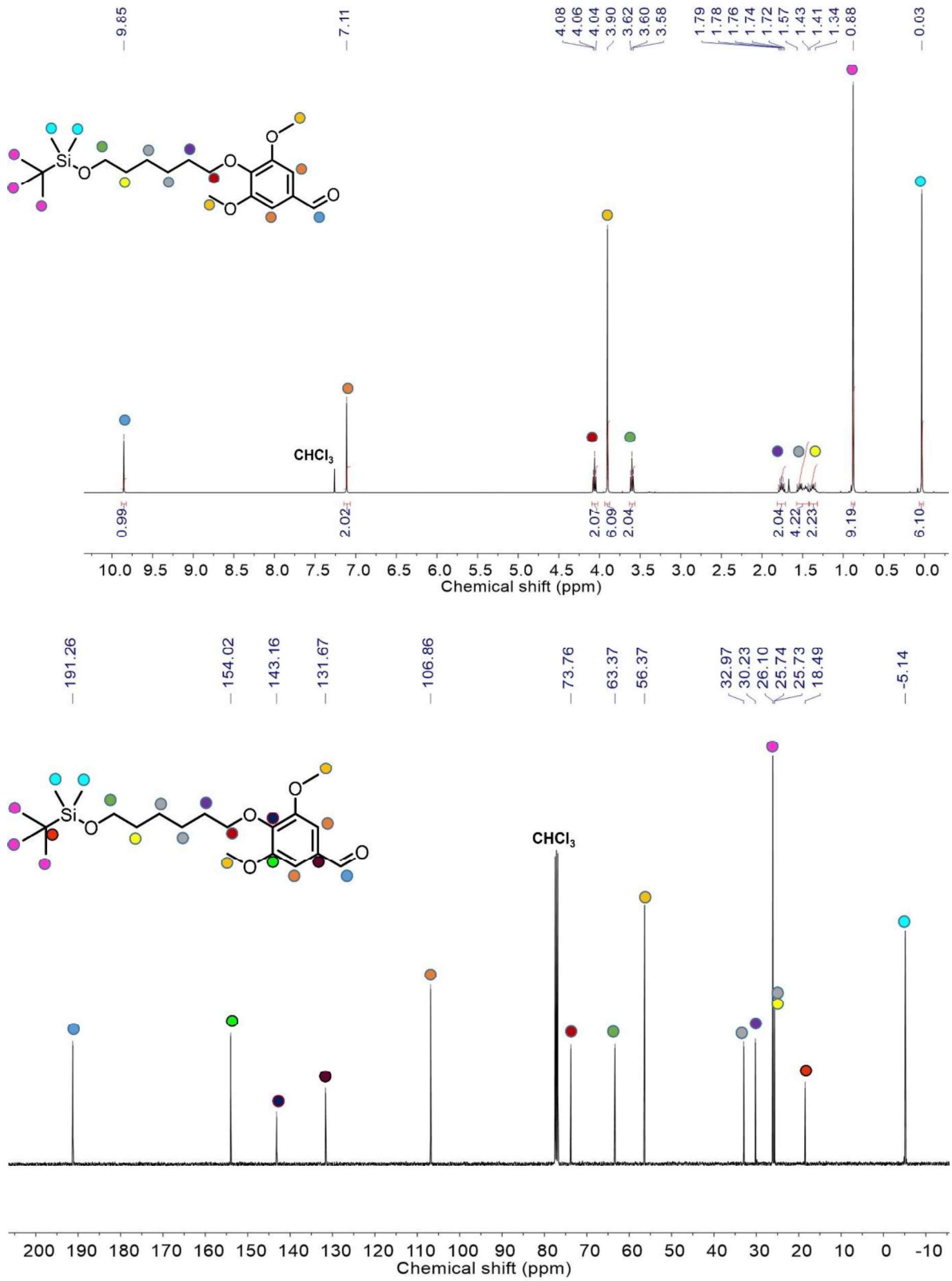

Figure 5.15. ^{1}H (top) and ^{13}C (bottom) NMR spectra of compound **28** in $CDCl_3$ at 25 °C.

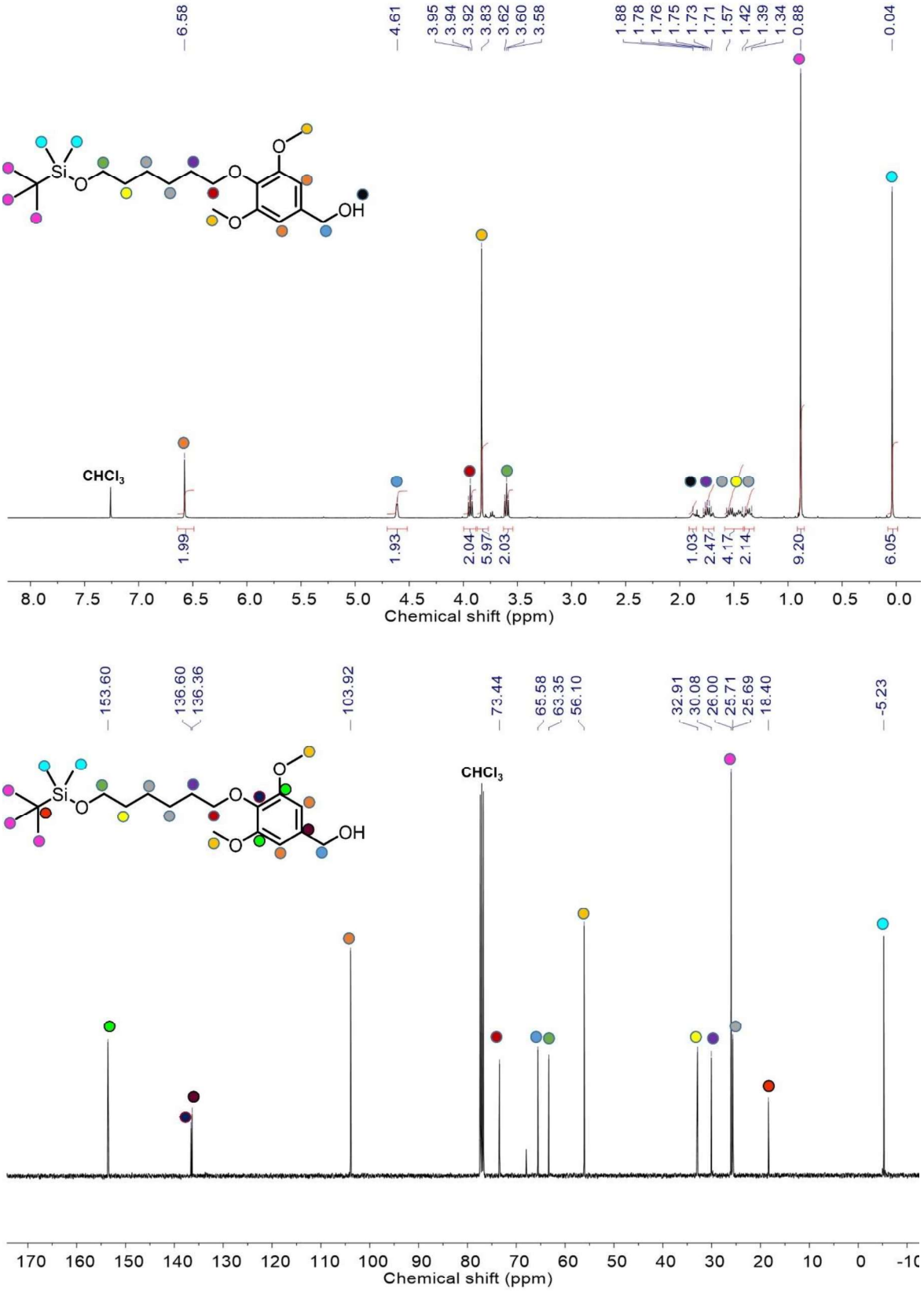

Figure 5.16. ^{1}H (top) and ^{13}C (bottom) NMR spectra of compound **29** in $CDCl_3$ at 25 °C.

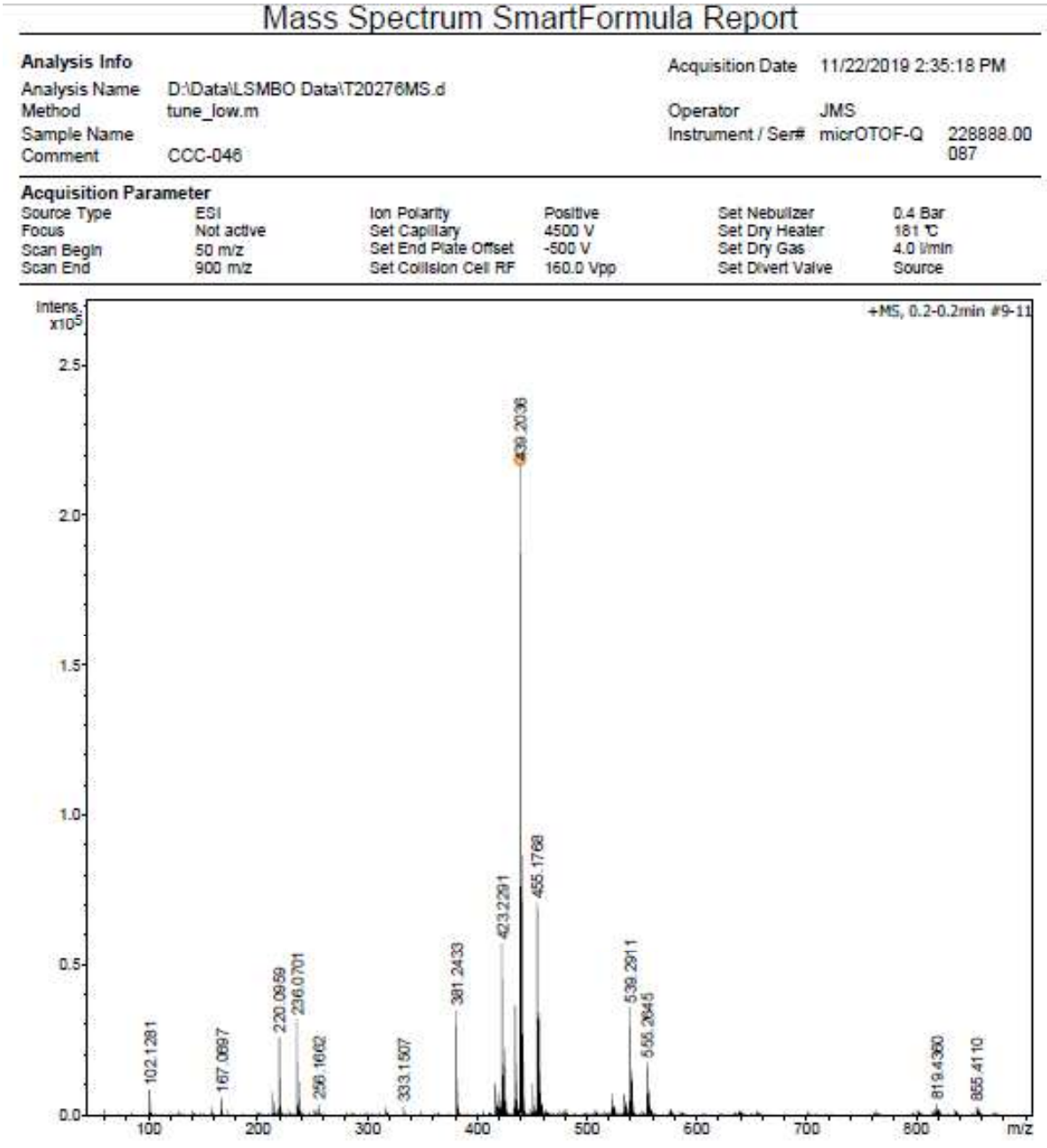

Figure 5.17. HR-MS spectrum of compound **30**.

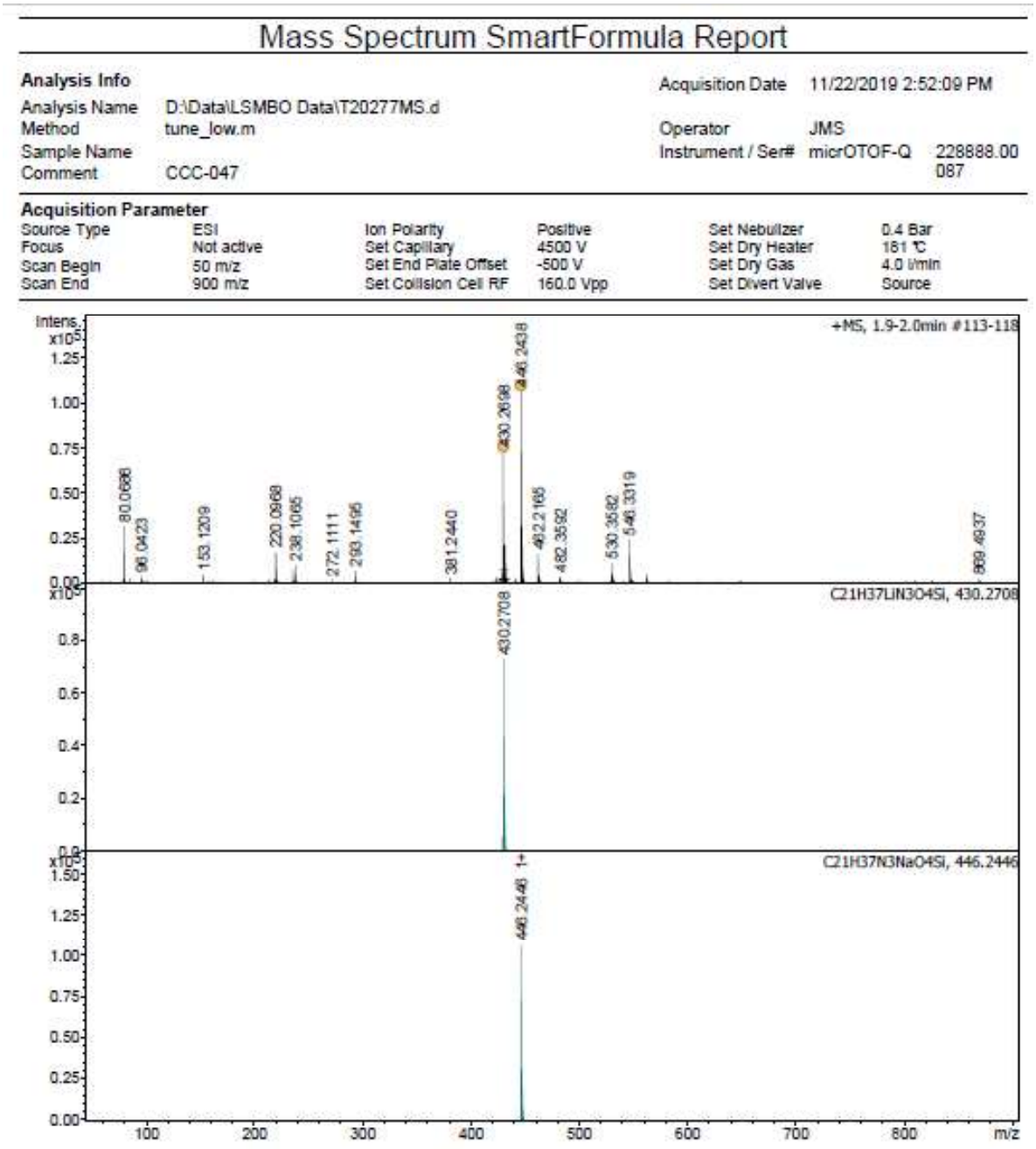

Figure 5.18. HR-MS spectrum of compound **31**.

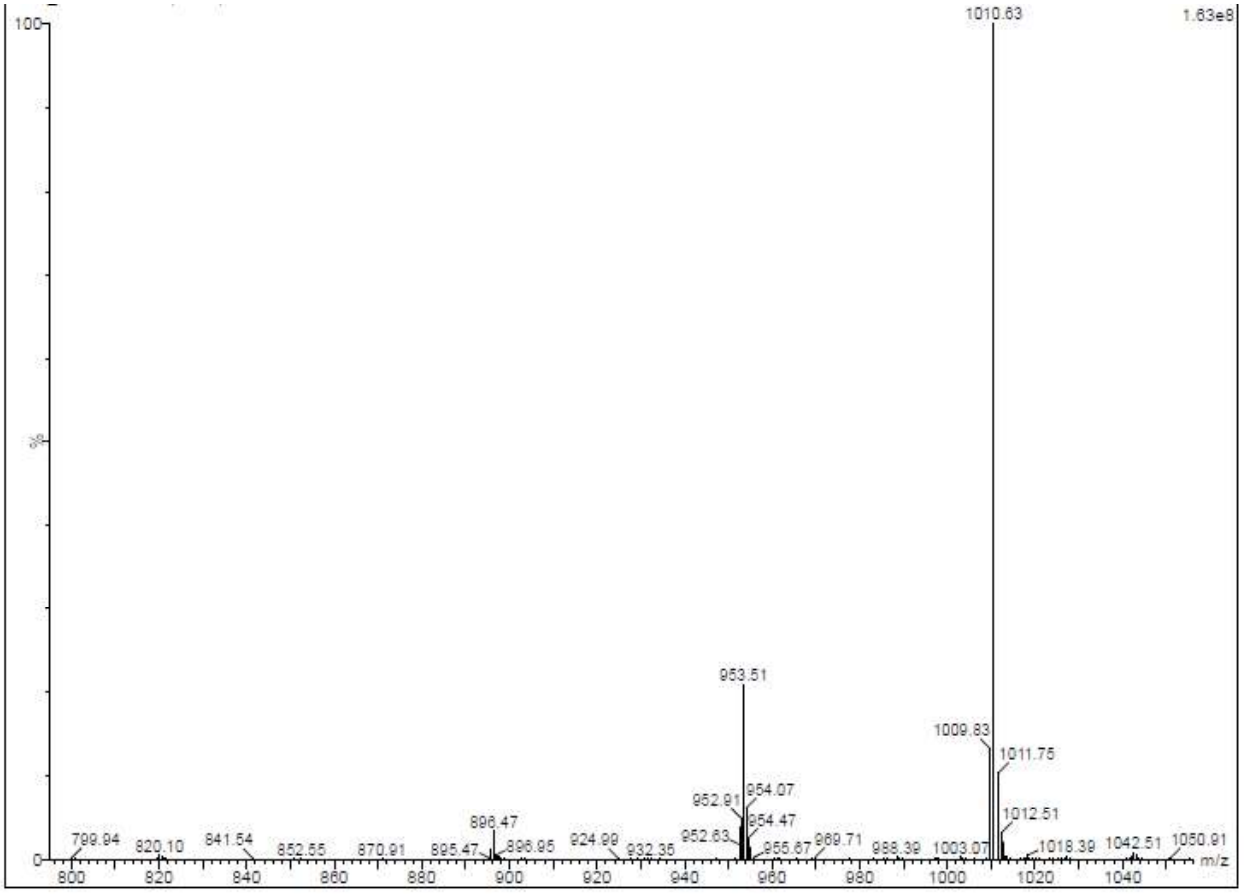

Figure 5.19. ESI-MS spectrum of compound **32**.

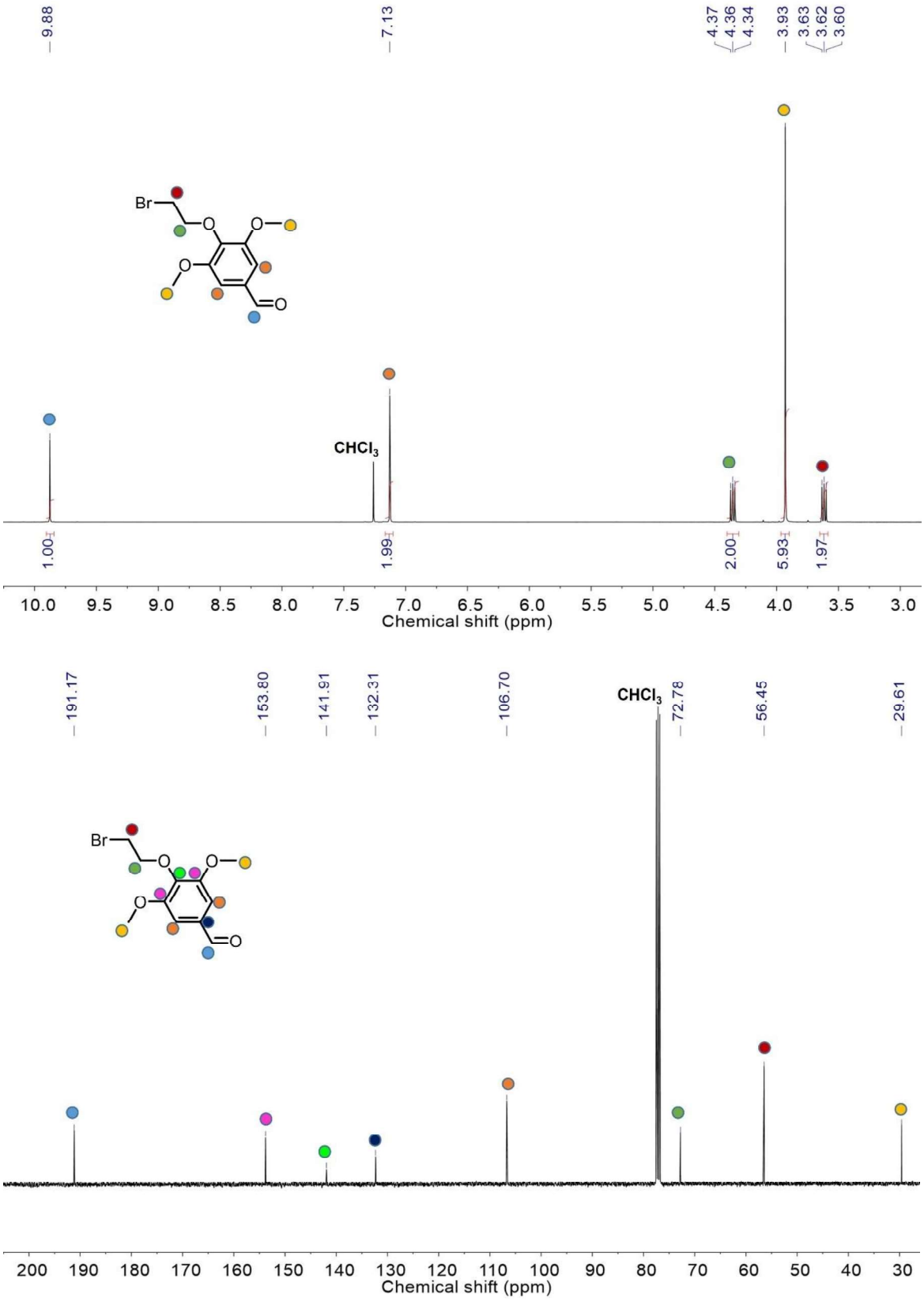

Figure 5.20. ^{1}H (top) and ^{13}C (bottom) NMR spectra of compound **35** in $CDCl_3$ at 25 °C.

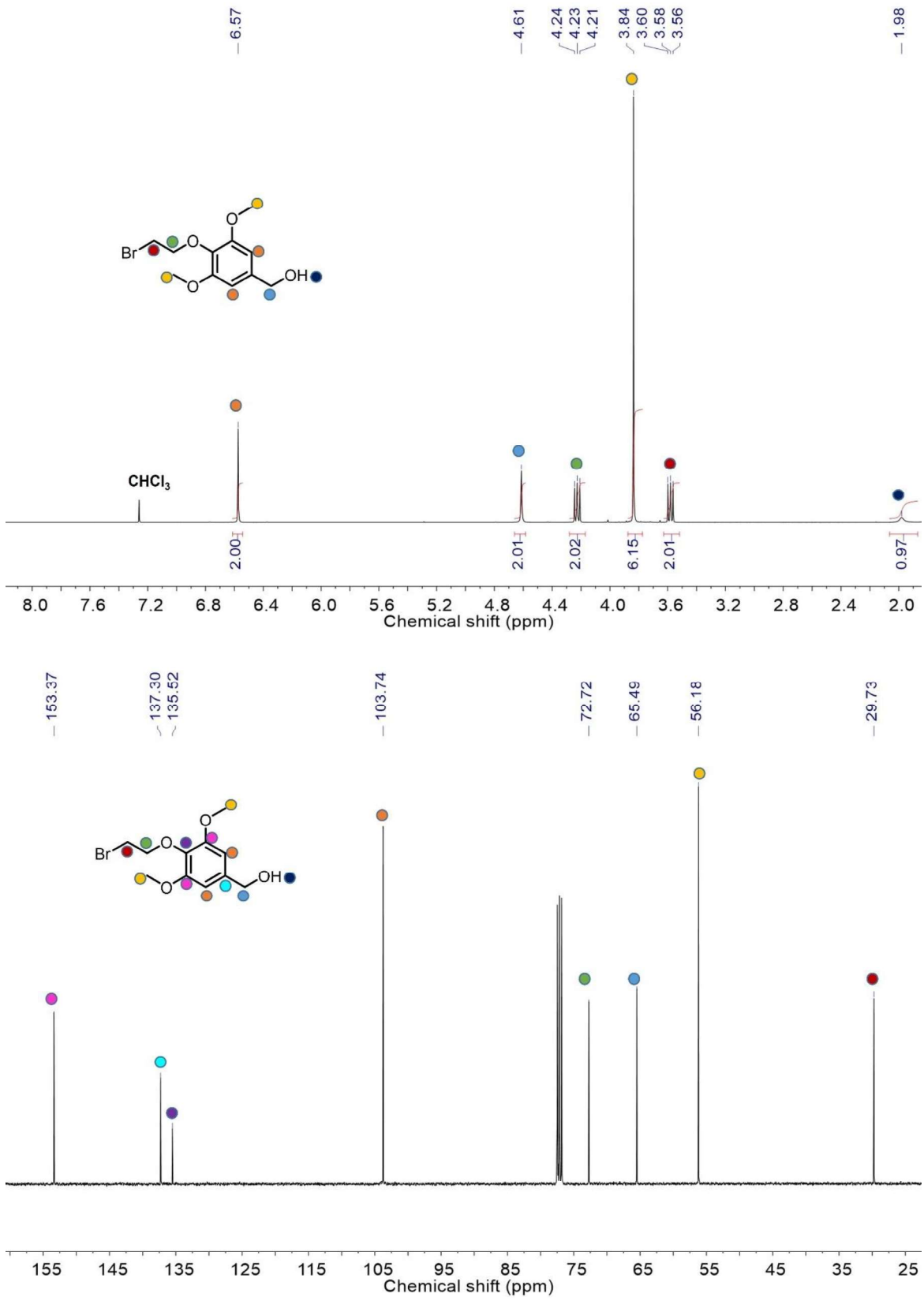

Figure 5.21. ^{1}H (top) and ^{13}C (bottom) NMR spectra of compound **36** in $CDCl_3$ at 25 °C.

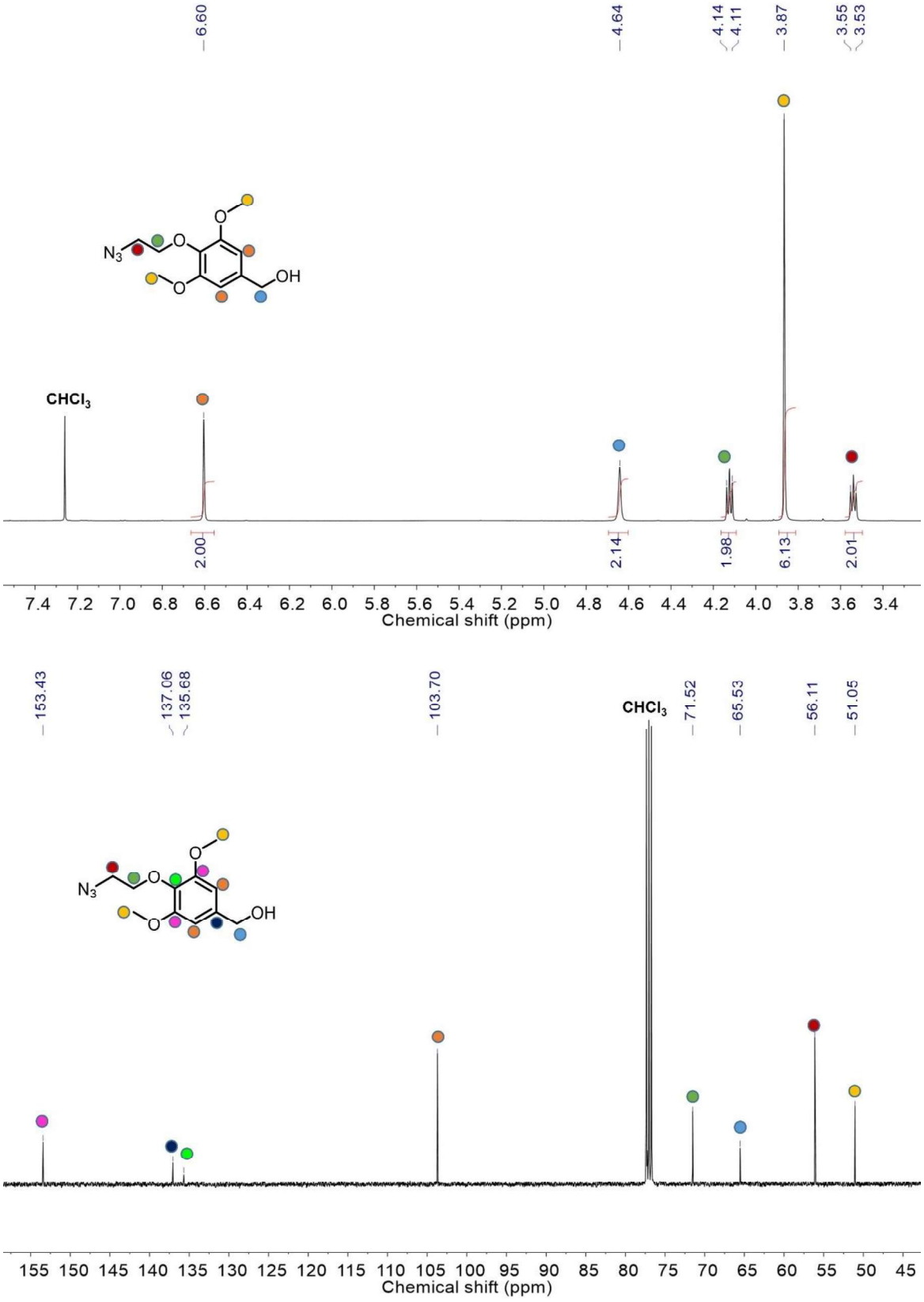

Figure 5.22. ^{1}H (top) and ^{13}C (bottom) NMR spectra of compound **37** in $CDCl_3$ at 25 °C.

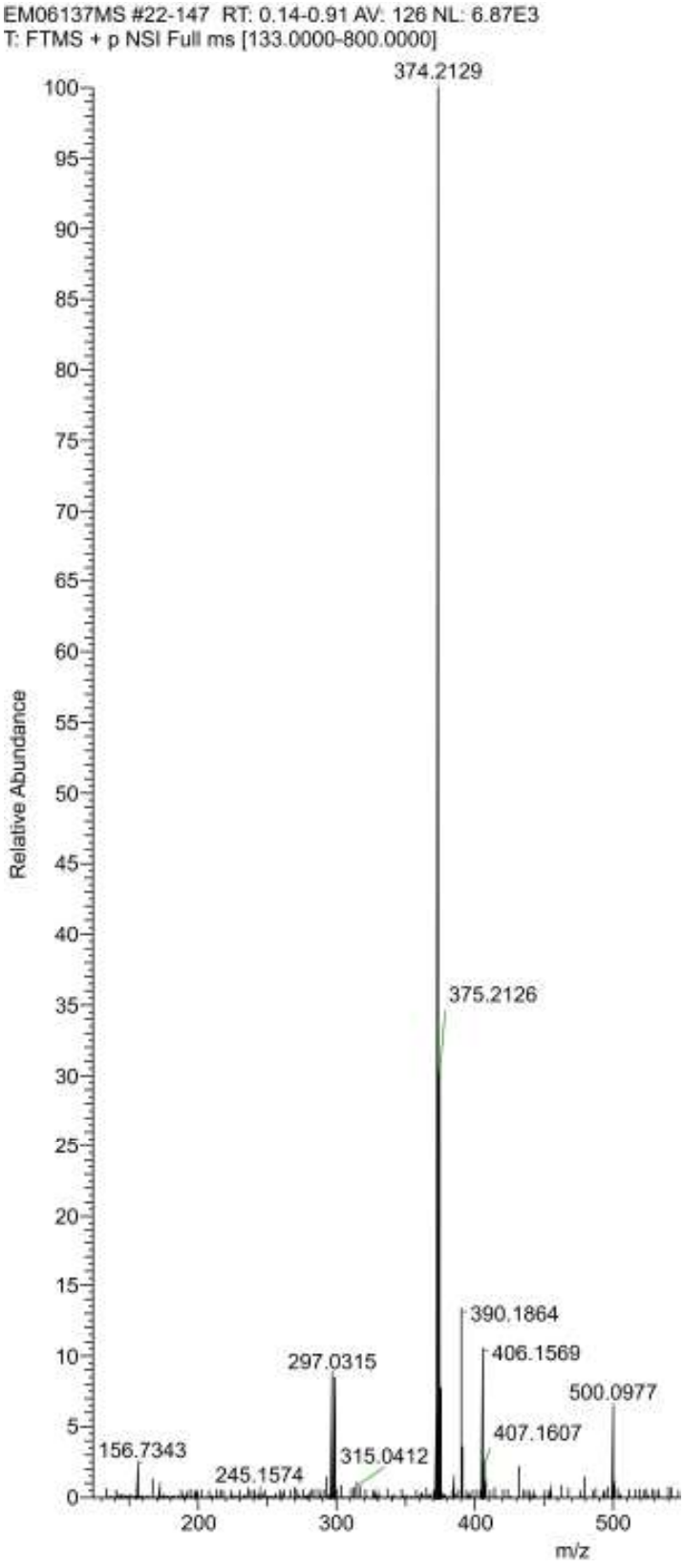

Figure 5.23. HR-MS spectrum of compound **38**.

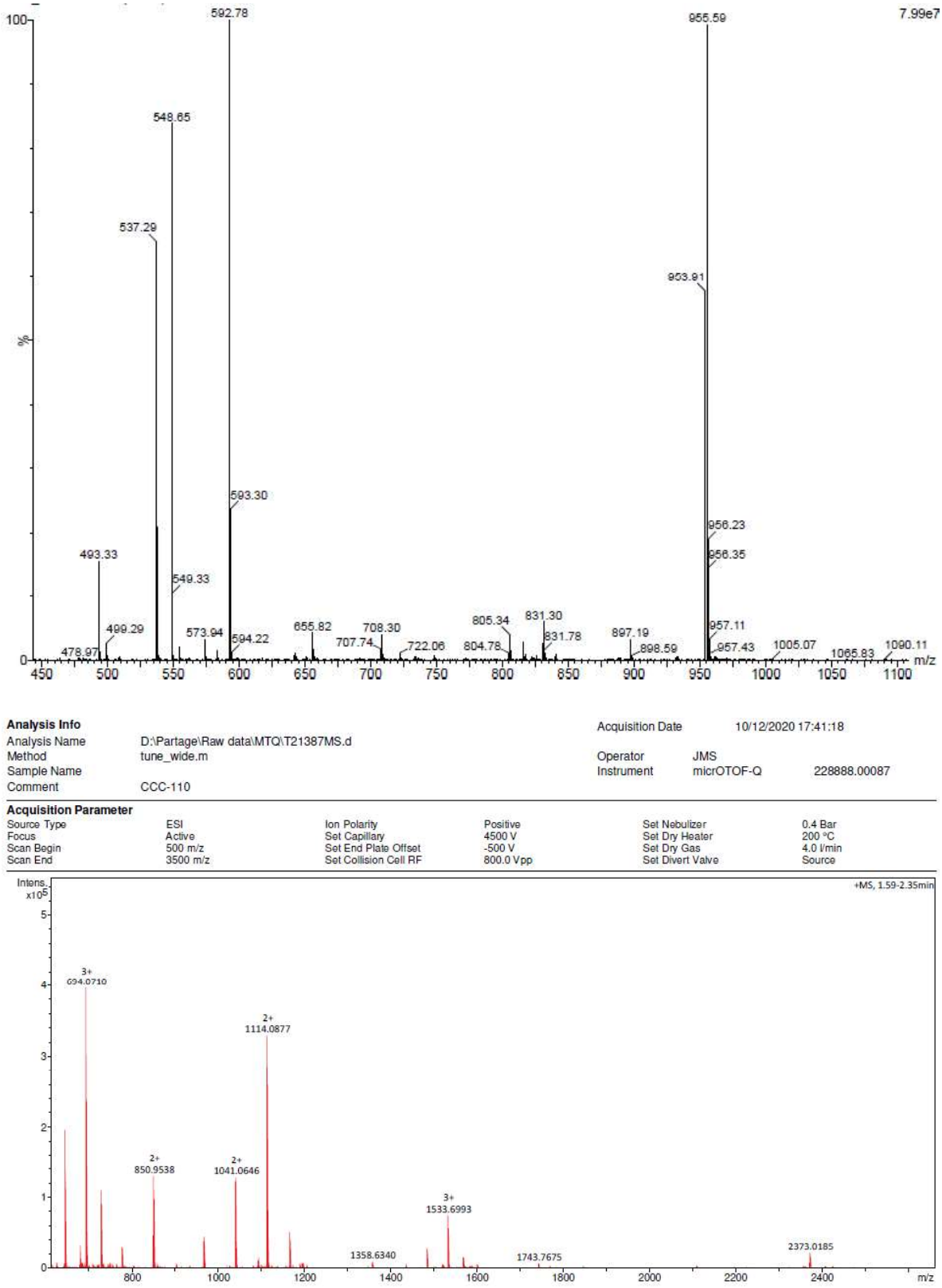

Figure 5.24. ESI-MS spectrum of compound **39** (top) and HR-MS spectrum of compound **40** (bottom).

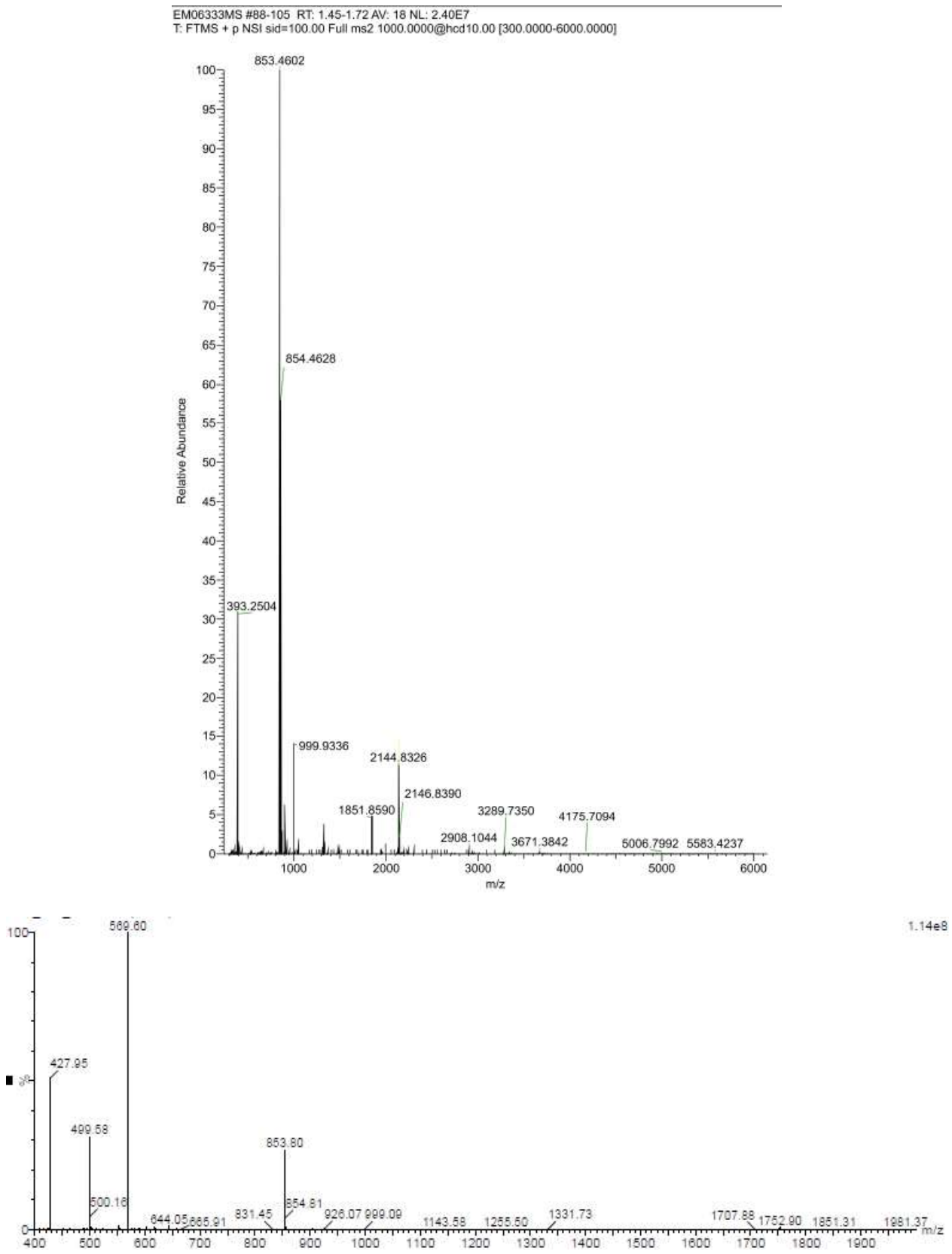

Figure 5.25. HR-MS spectrum of $\mathbf{41}_{\mathbf{Ext}}$ (top) and ESI-MS spectrum $\mathbf{41}_{\mathbf{Cont}}$ (bottom).

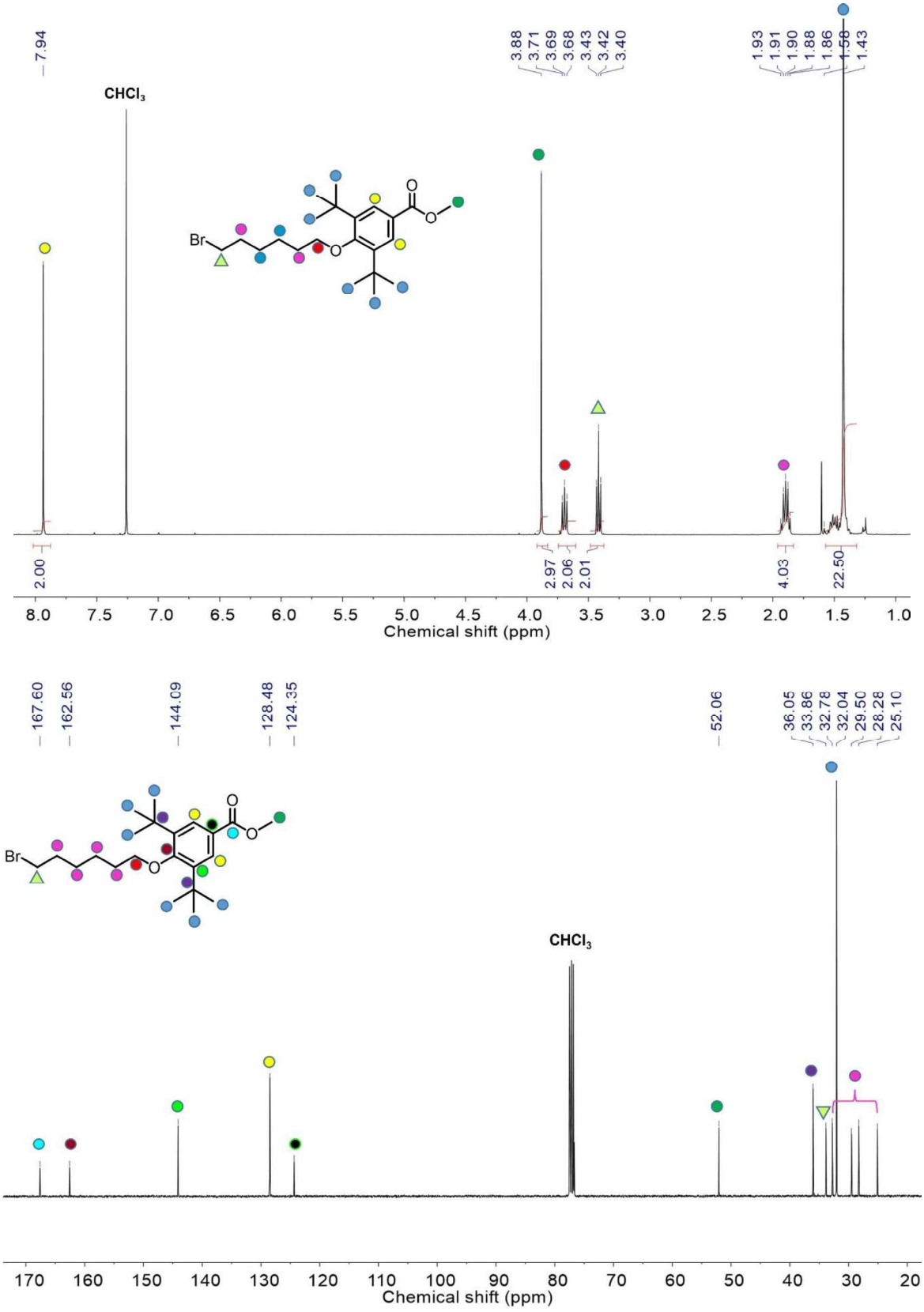

Figure 5.26. ^{1}H (top) and ^{13}C (bottom) NMR spectra of compound **67** in $CDCl_3$ at 25 °C.

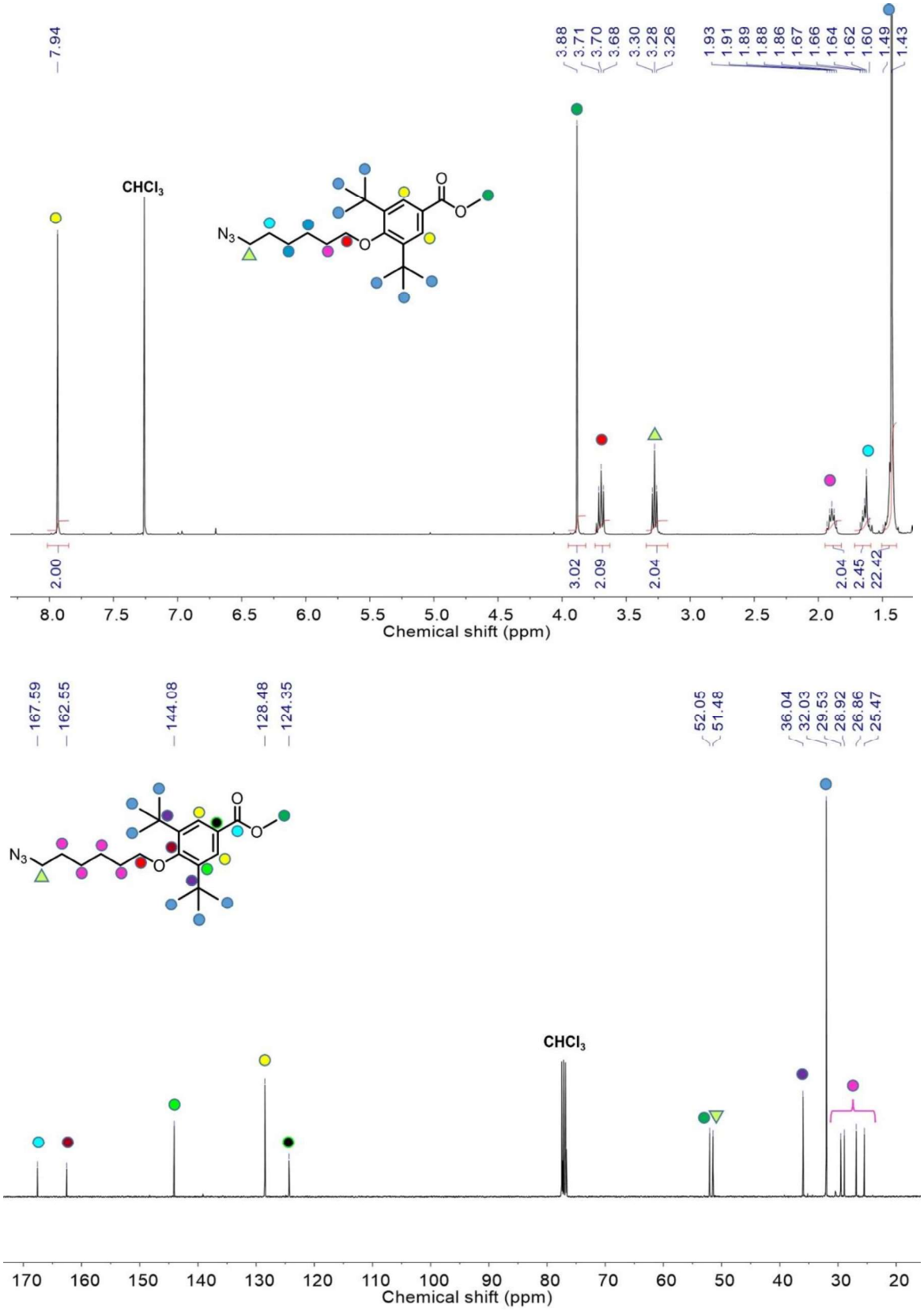

Figure 5.27. ^{1}H (top) and ^{13}C (bottom) NMR spectra of compound **68** in $CDCl_3$ at 25 °C.

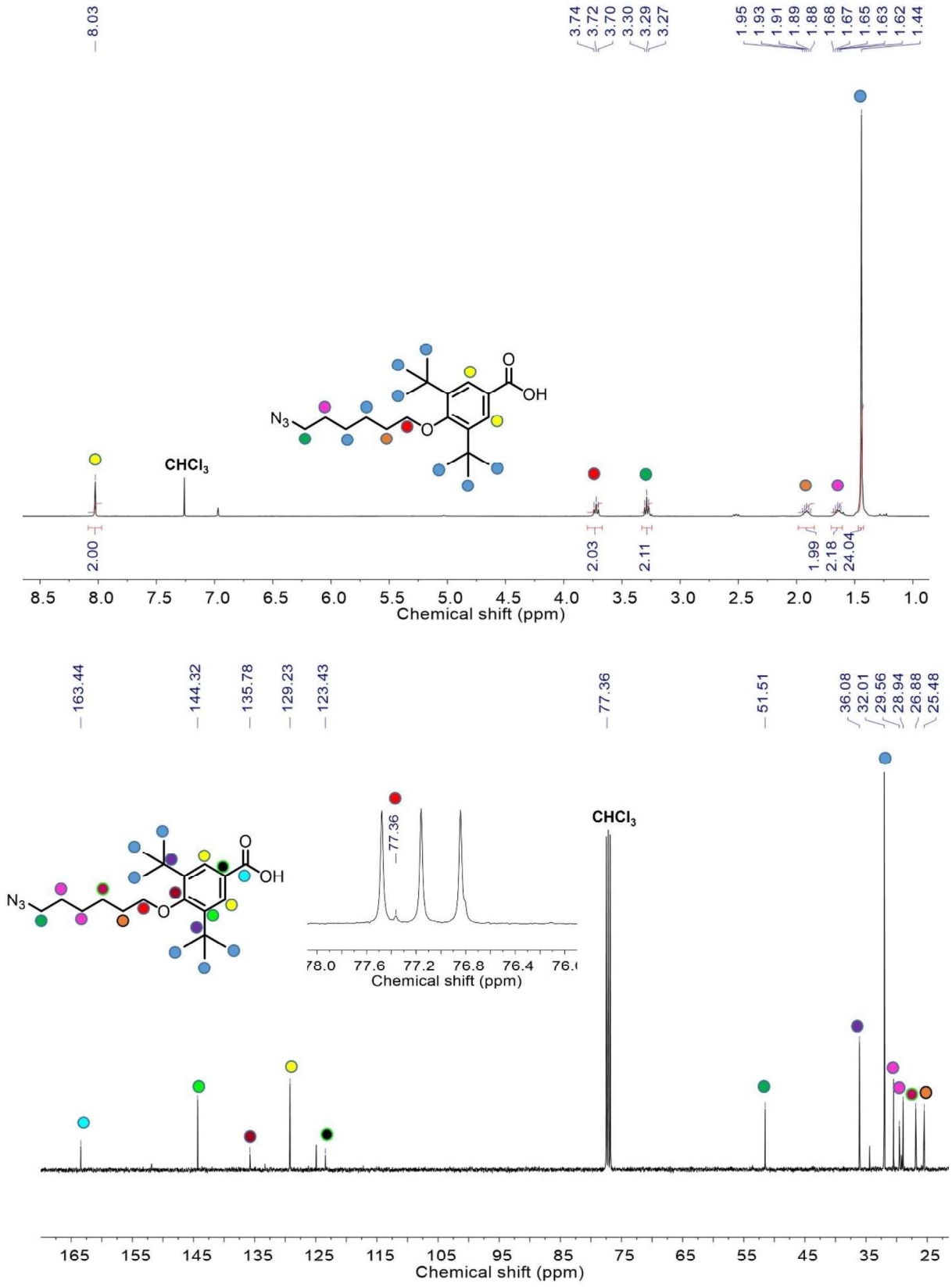

Figure 5.28. ^{1}H (top) and ^{13}C (bottom) NMR spectra of compound **69** in $CDCl_3$ at 25 °C.

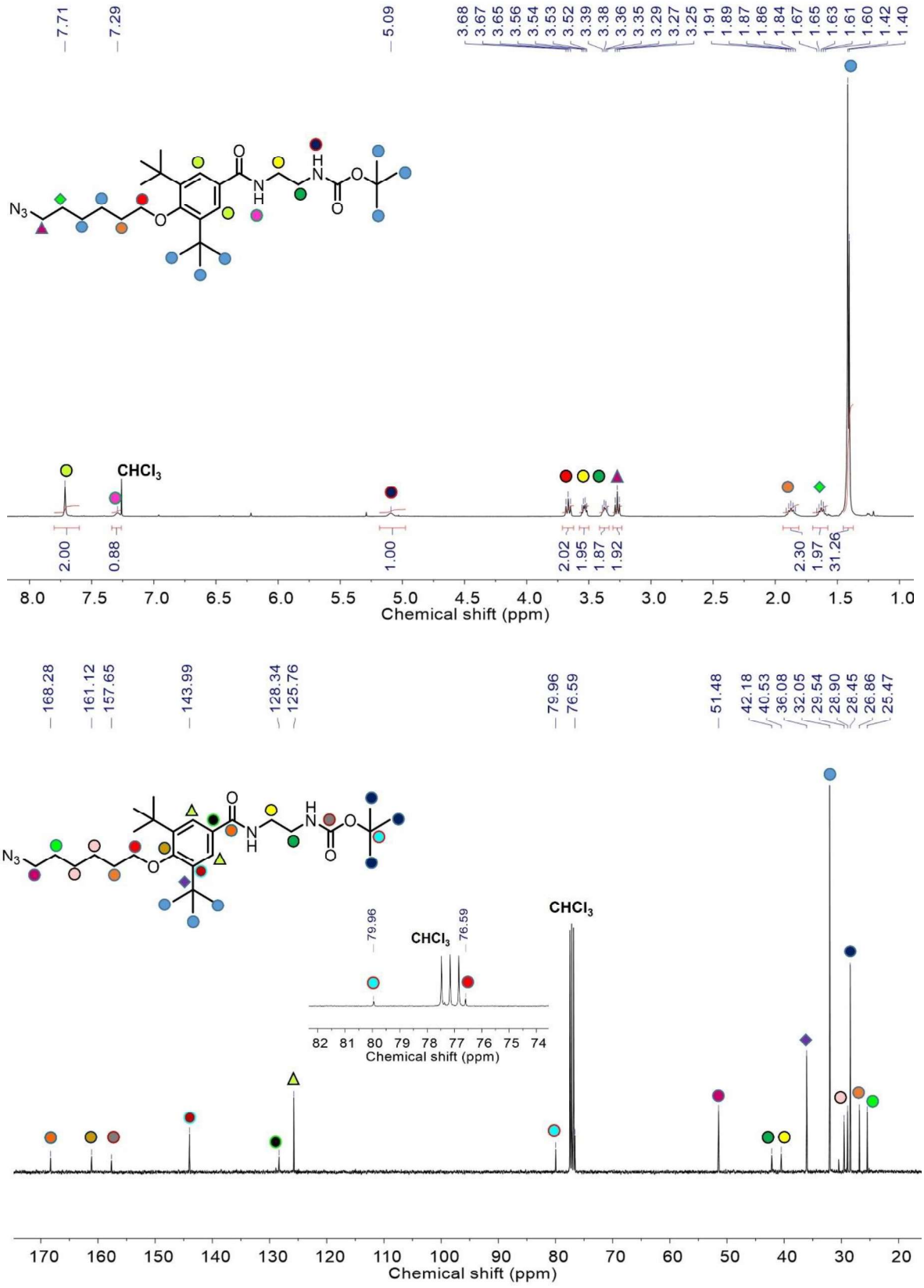

Figure 5.29. ^{1}H (top) and ^{13}C (bottom) NMR spectra of compound **70** in $CDCl_3$ at 25 °C.

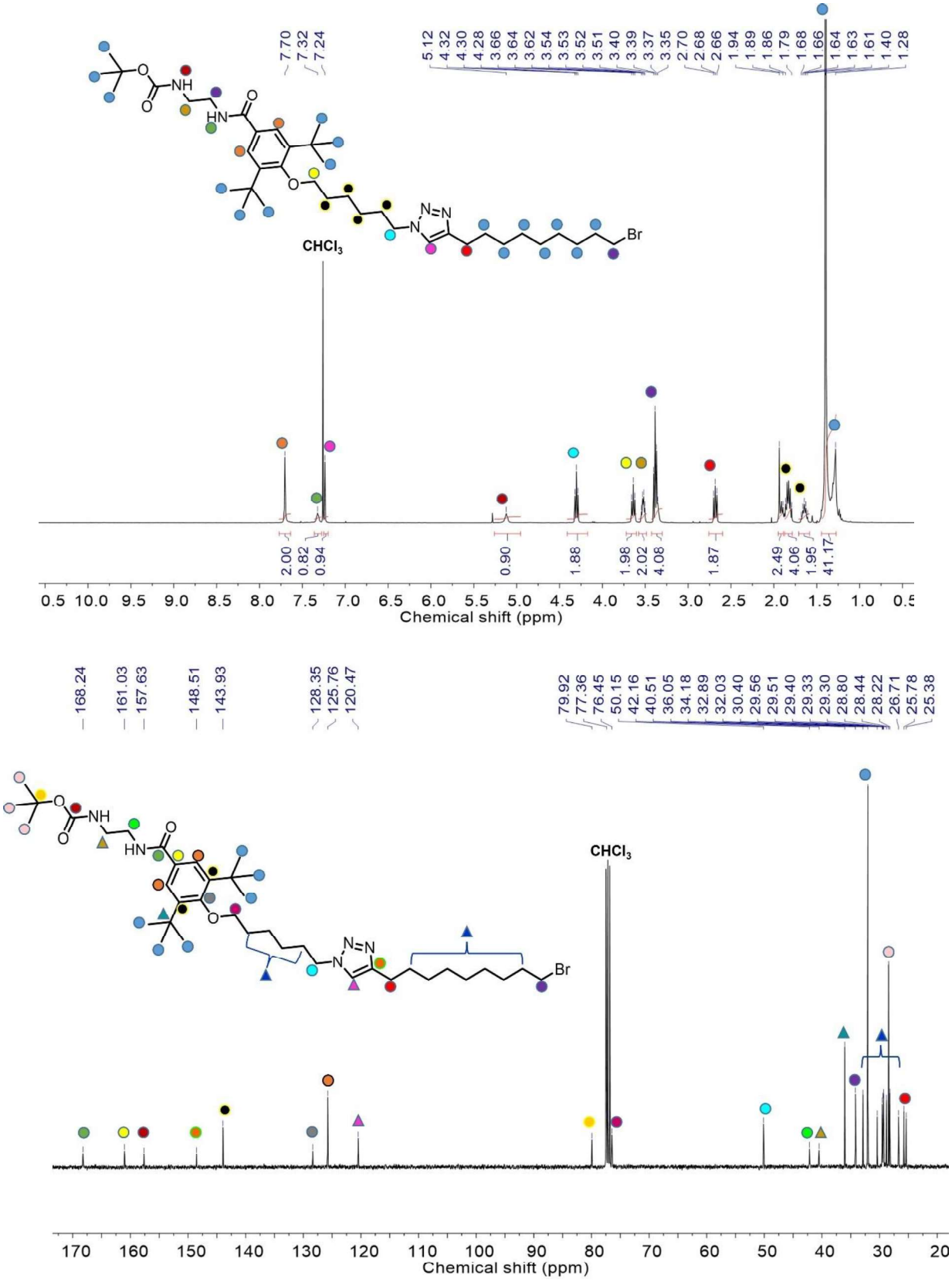

Figure 5.30. ^{1}H (top) and ^{13}C (bottom) NMR spectra of compound **72a** in $CDCl_3$ at 25 °C.

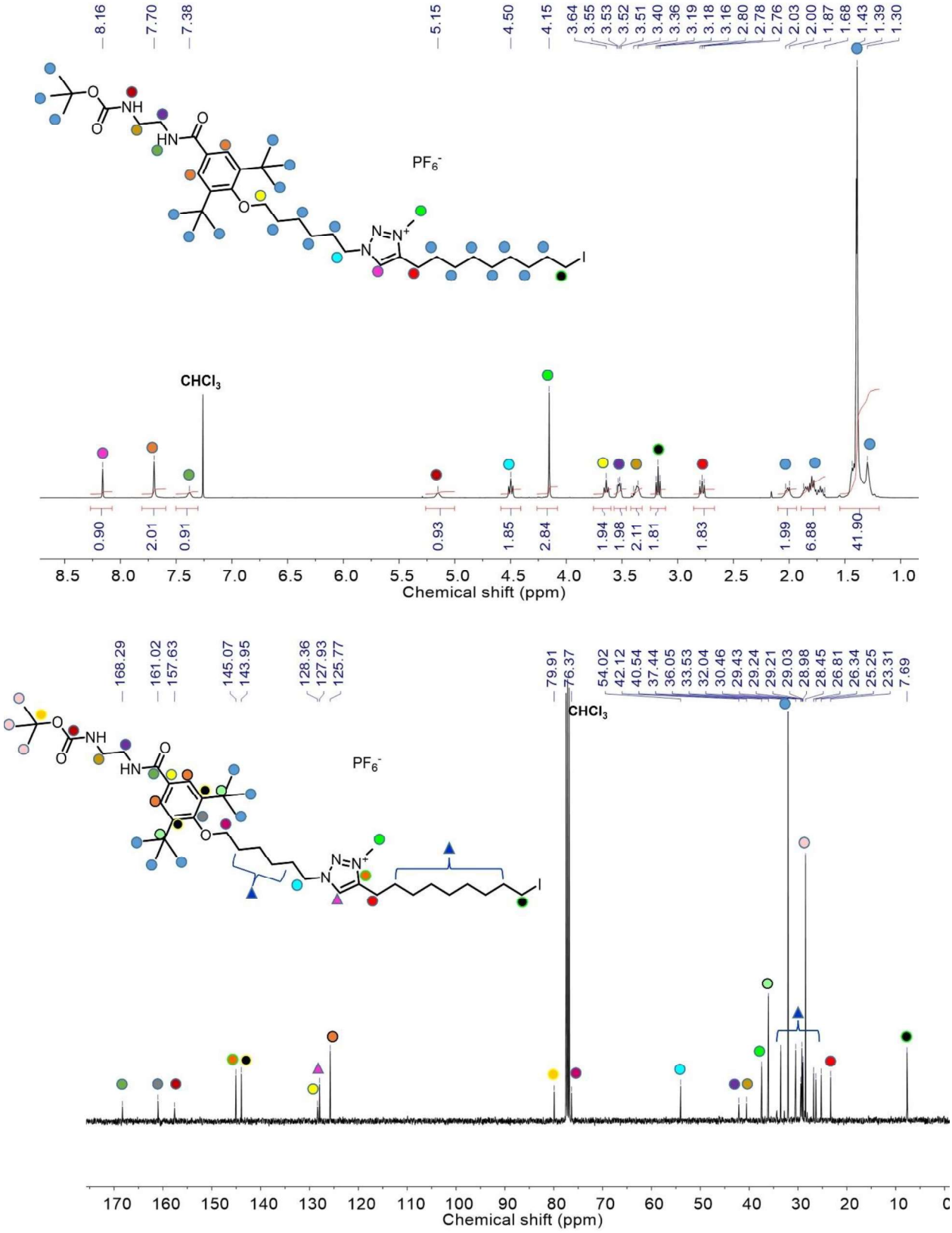

Figure 5.31. ^{1}H (top) and ^{13}C (bottom) NMR spectra of compound **73a** in $CDCl_3$ at 25 °C.

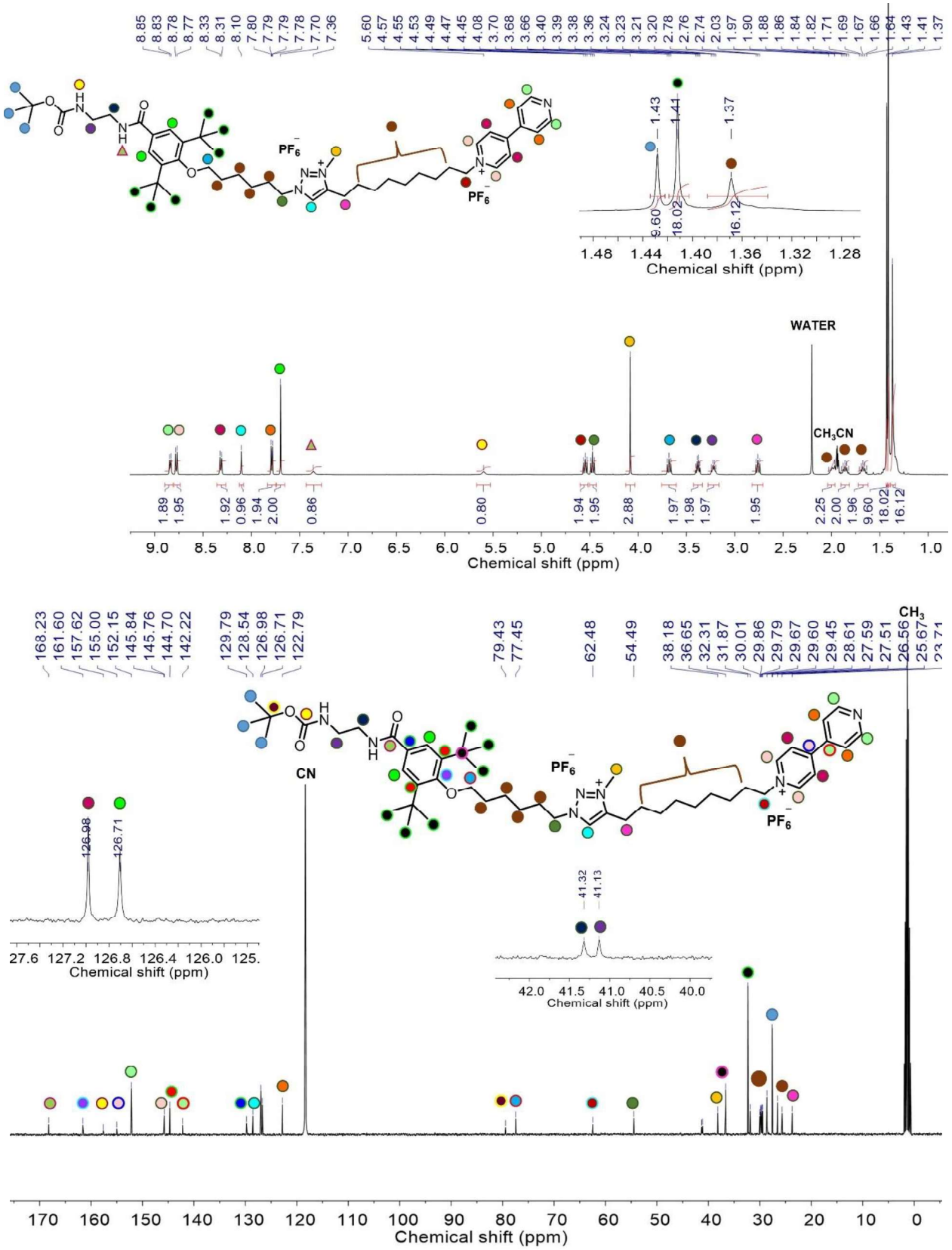

Figure 5.32. ^{1}H (top) and ^{13}C (bottom) NMR spectra of compound **74a** in CD_3CN at 25 °C.

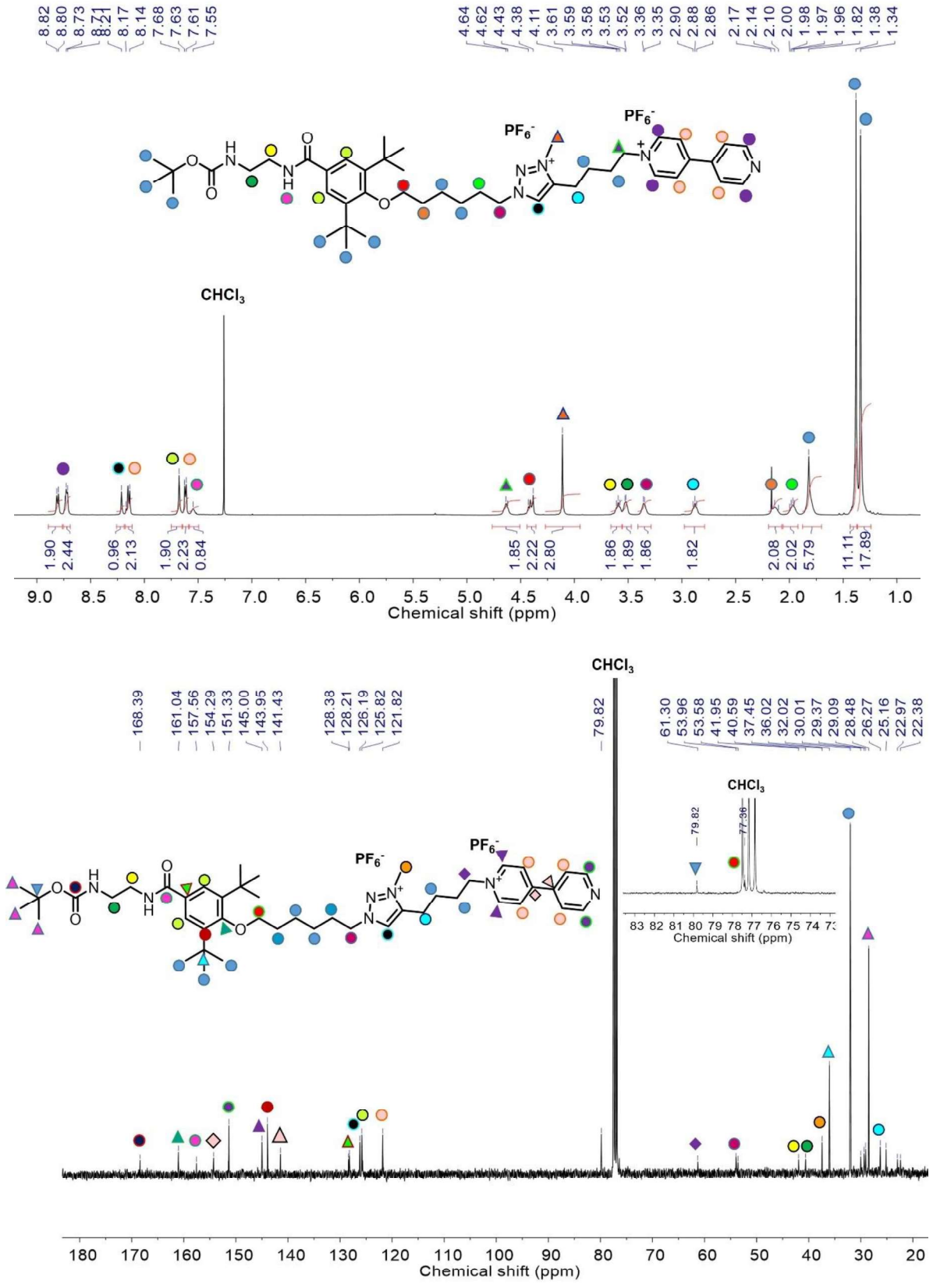

Figure 5.33. ^{1}H (top) and ^{13}C (bottom) NMR spectra of compound **74b** in $CDCl_3$ at 25 °C.

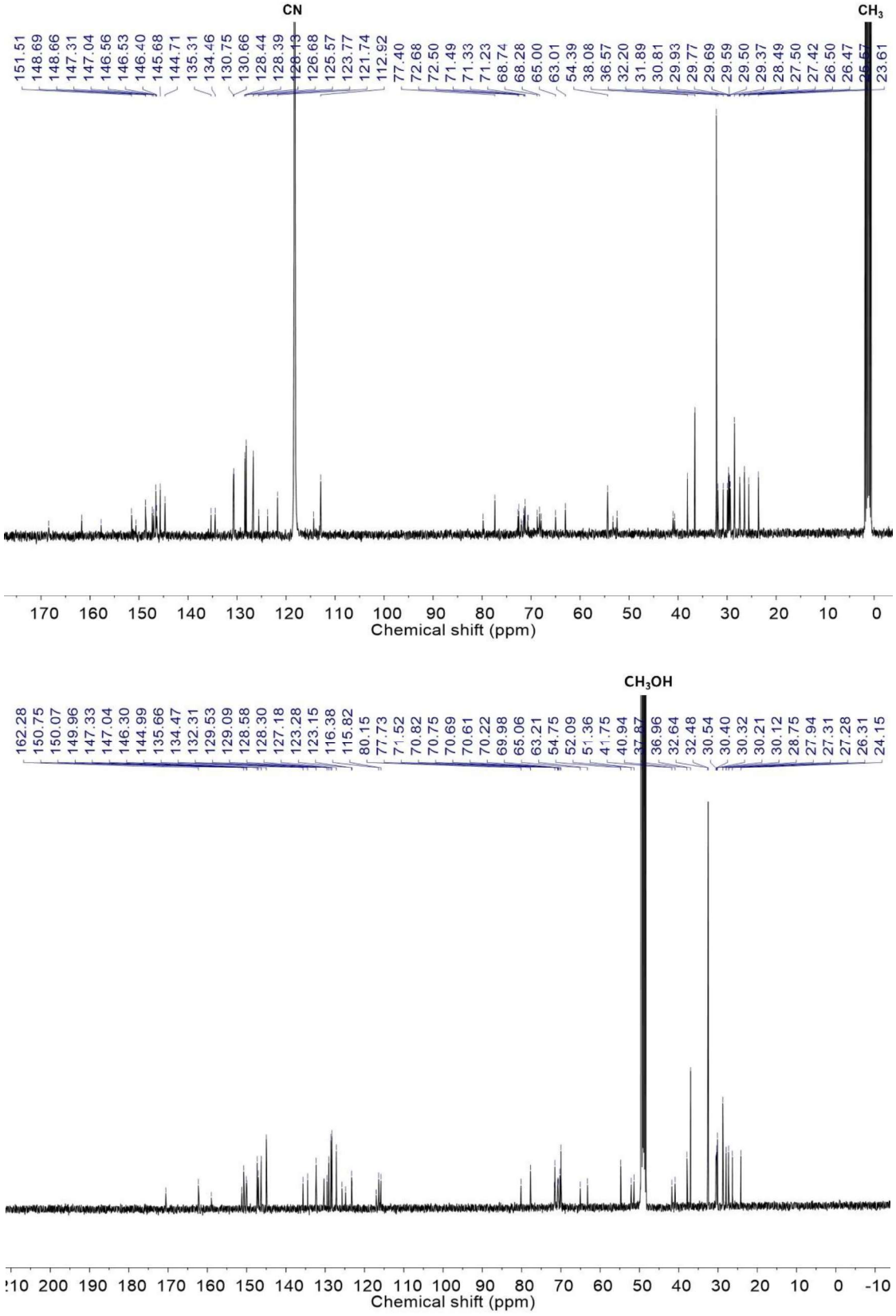

Figure 5.34. ^{13}C NMR spectra of compounds **75a** in CD_3CN and **75c** in CD_3OD at 25 °C.

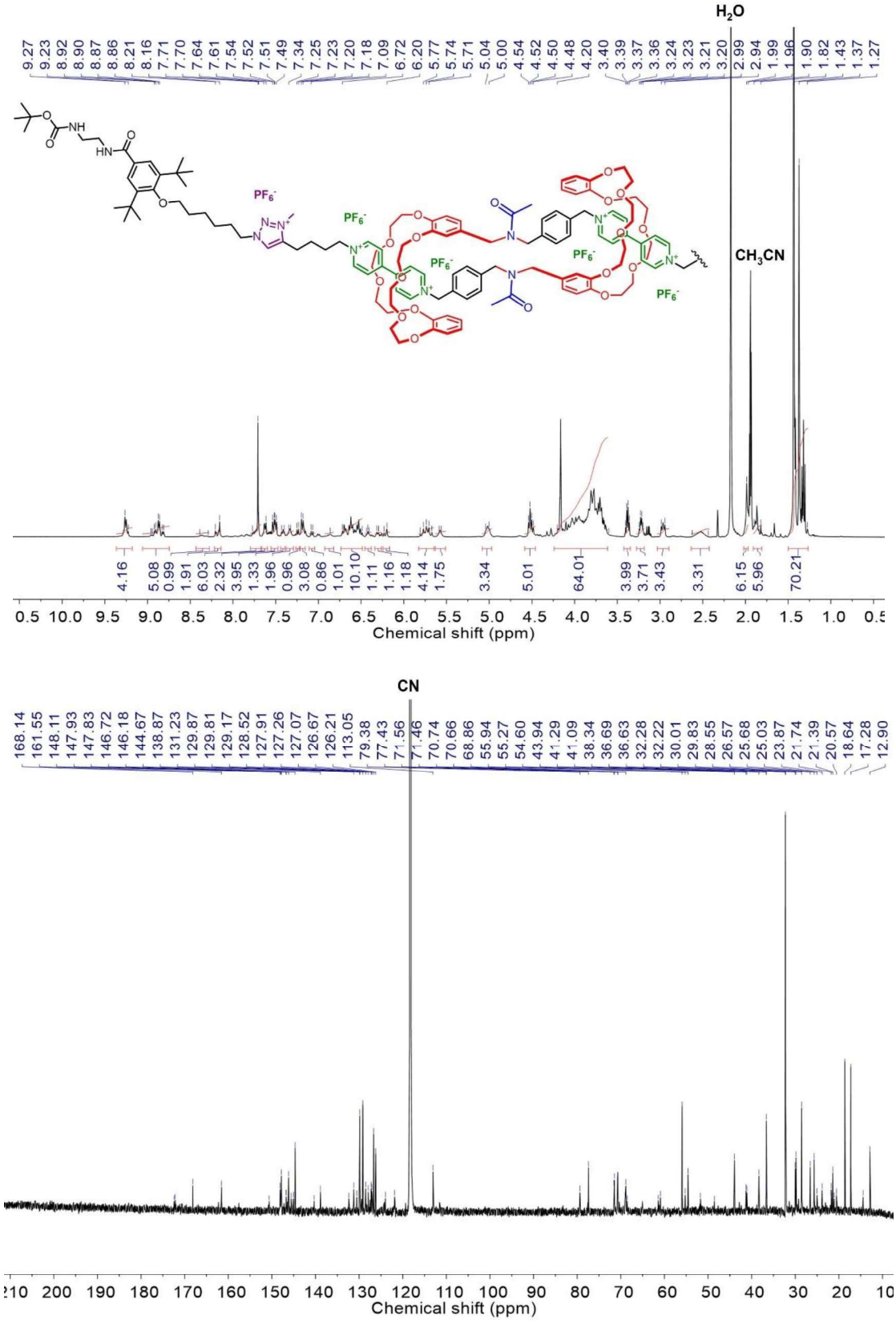

Figure 5.35. ^{1}H (top) and ^{13}C (bottom) NMR spectra of compound **76b** in CD_3CN at 25 °C.

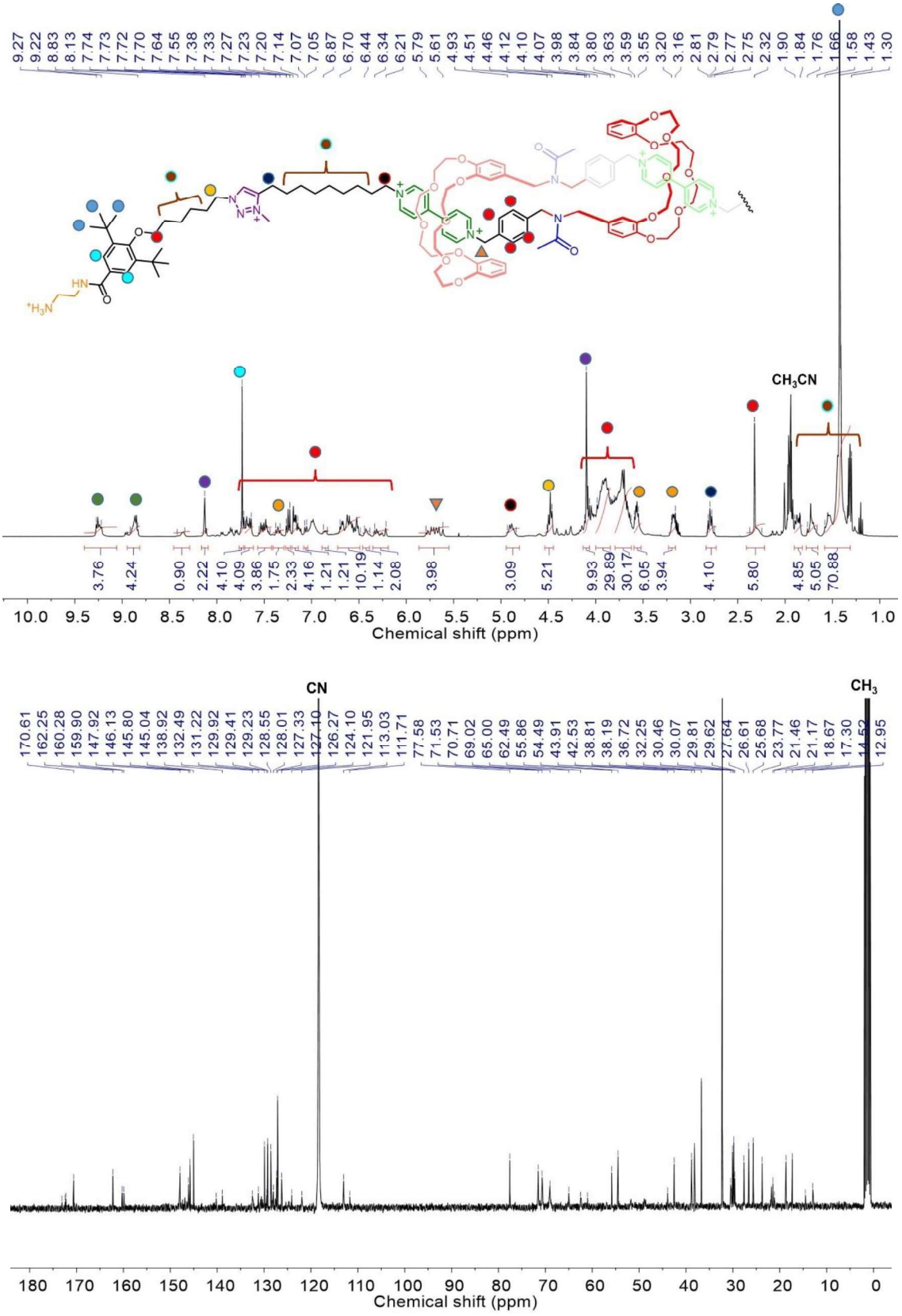

Figure 5.36. ^{1}H (top) and ^{13}C (bottom) NMR spectra of compound **77a** in CD_3CN at 25 °C.

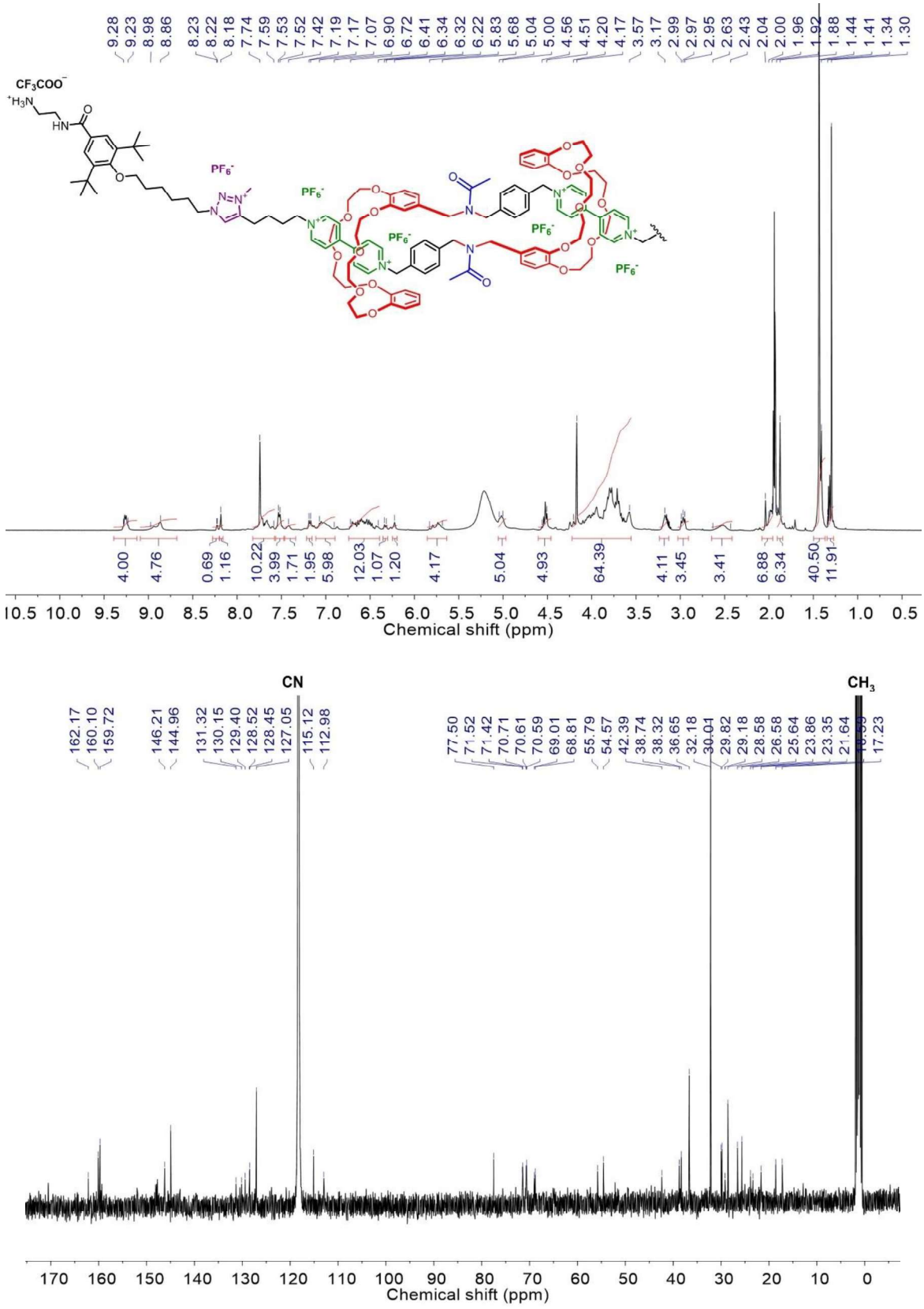

Figure 5.37. ^{1}H (top) and ^{13}C (bottom) NMR spectra of compound **77b** in CD_3CN at 25 °C.

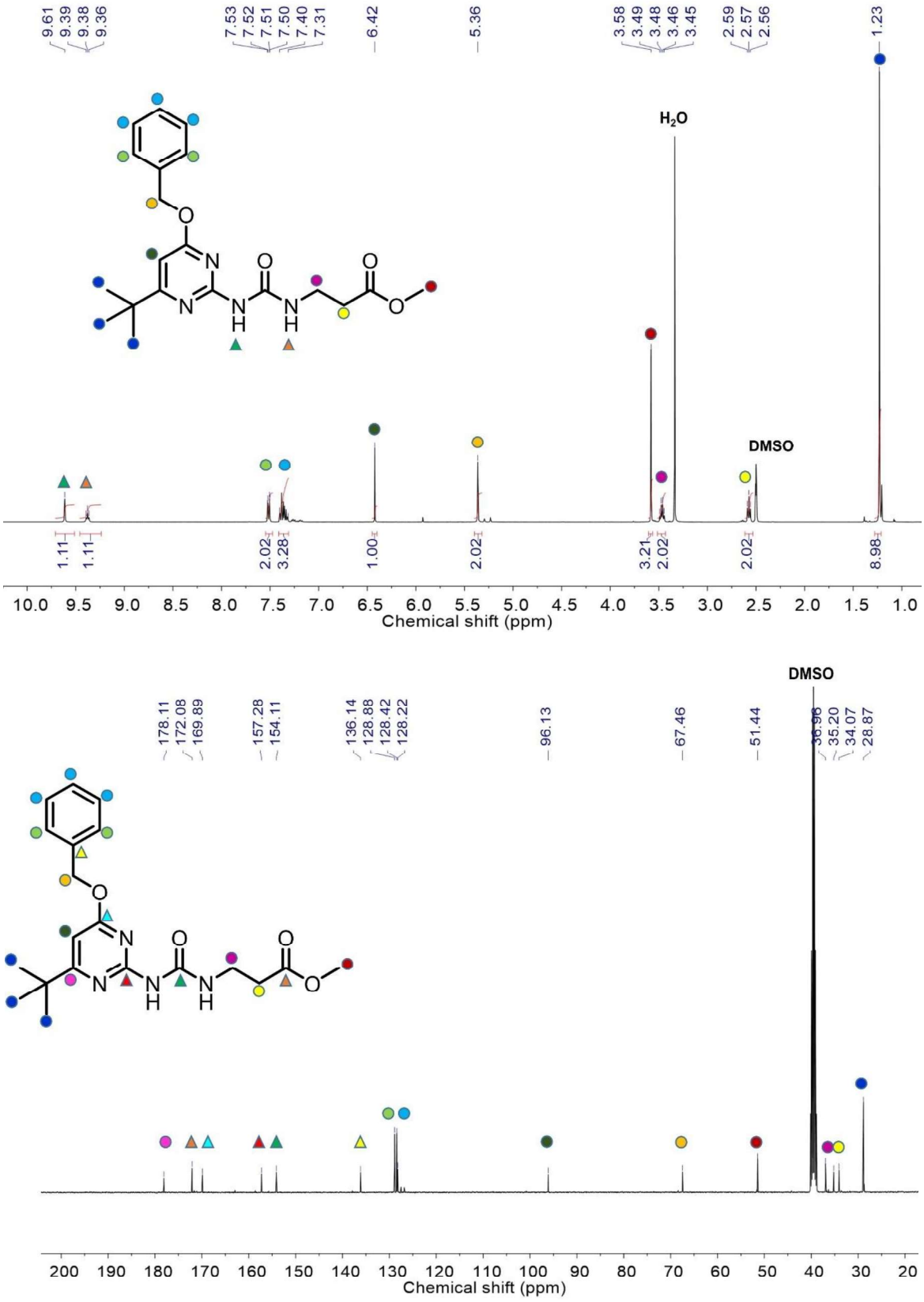

Figure 5.38. ^{1}H (top) and ^{13}C (bottom) NMR spectra of compound **80** in DMSO-d_6 25 °C.

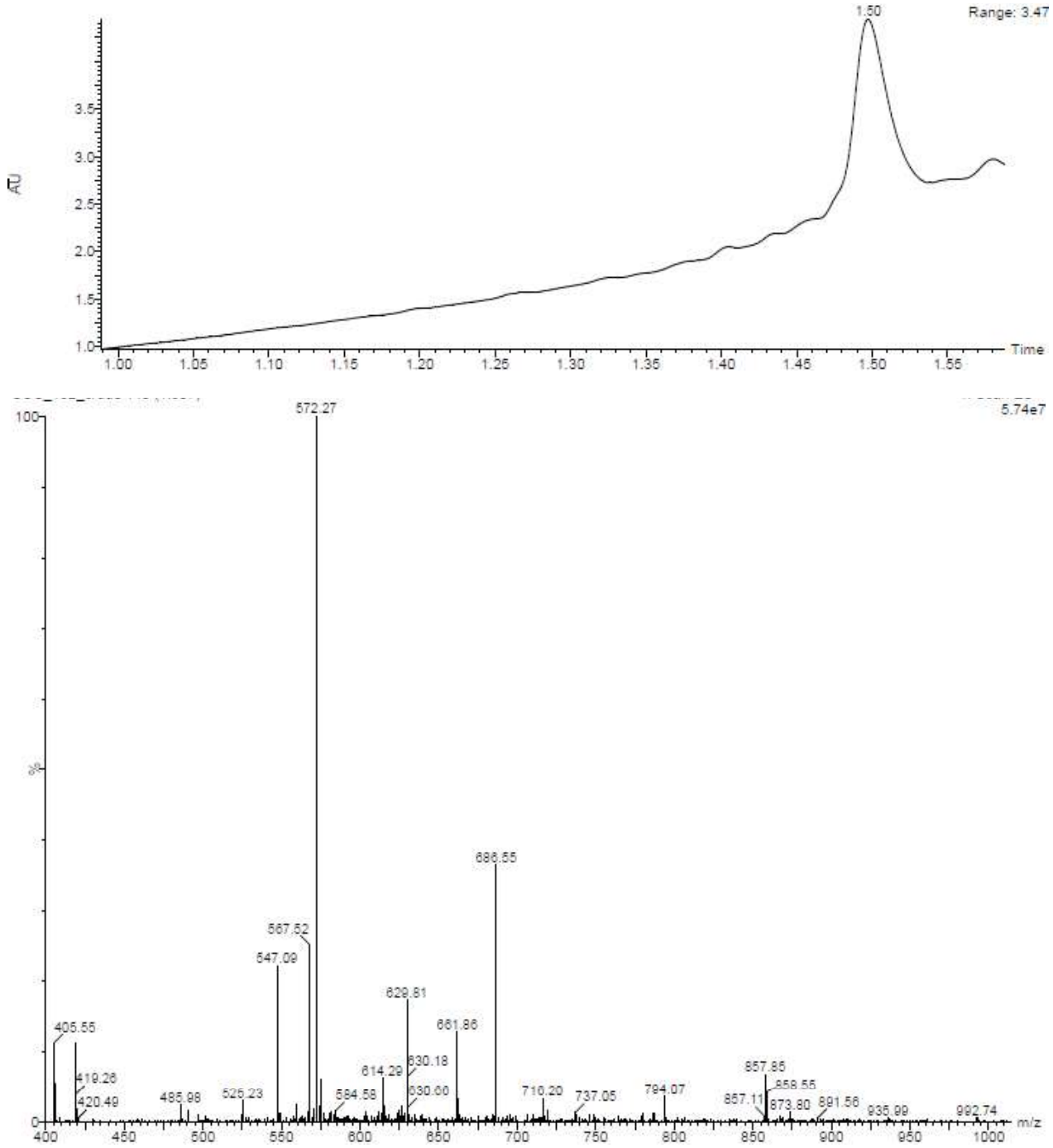

Figure 5.39. Chromatogram (top) and ESI-MS spectrum (bottom) of compound **83a.**

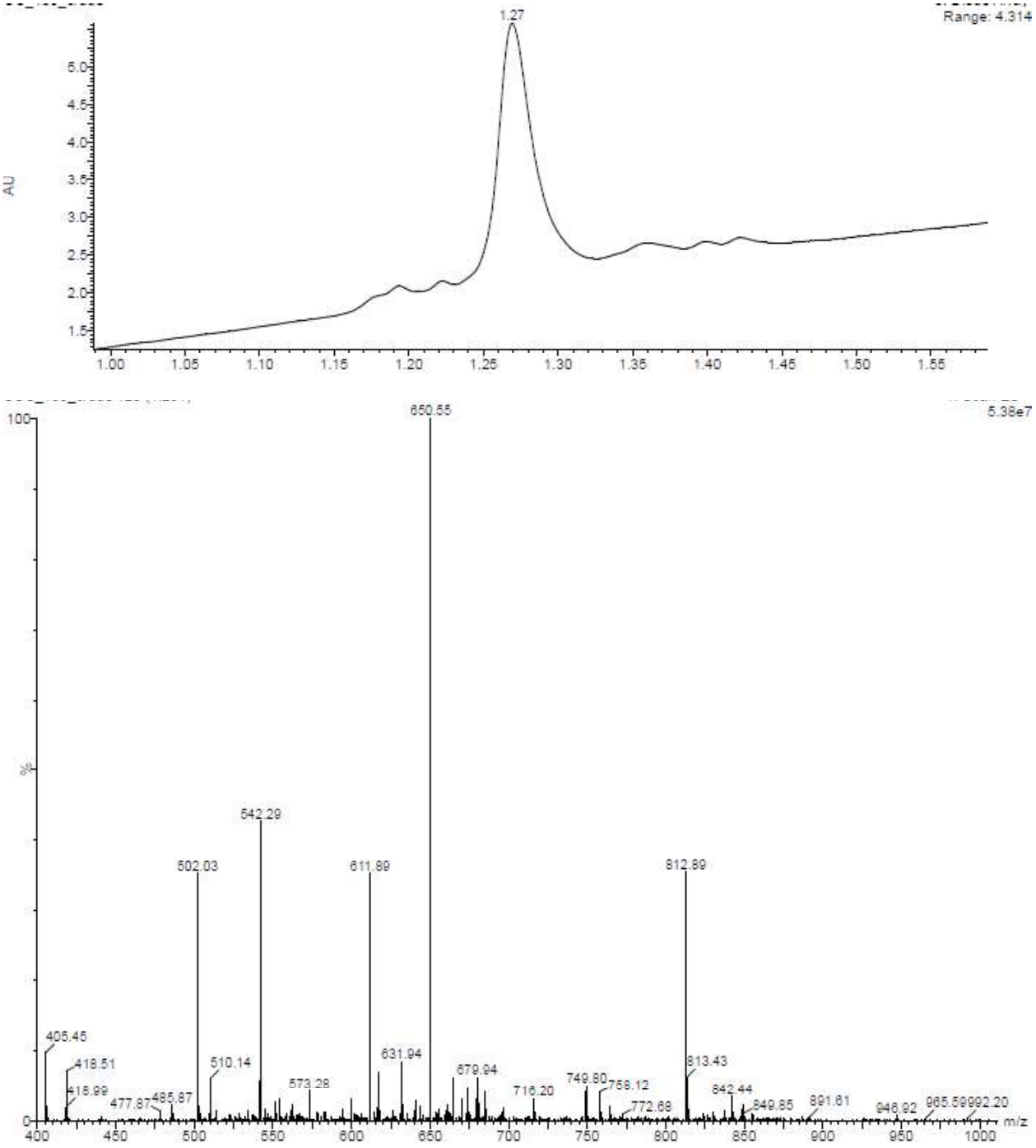

Figure 5.40. Chromatogram (top) and ESI-MS spectrum (bottom) of compound **84a.**

Université de Strasbourg

Christian Camilo CARMONA VARGAS

École doctorale
Sciences chimiques | ED 222
Université de Strasbourg

Synthèse et couplage de rotaxanes [c2] bistables pour la fabrication de matériaux stimulables.

Résumé

Les matériaux actionnables basés sur des machines moléculaires synthétiques ont un grand potentiel pour faire partie d'une révolution technologique permettant de relever certains défis en médecine régénérative, interfaces homme-machine, robotique, entre autres. Dans cette direction, plusieurs groupes de recherche ont investi de nombreux efforts pour coupler les machines moléculaires entre elles et avec leur environnement afin d'exploiter leur mouvement collectif (à l'échelle nanométrique) à des échelles de longueur plus élevées. Cependant, pour aller plus loin et obtenir des actions macroscopiques optimisées, il est nécessaire de contrôler précisément leur organisation spatiale en 3D sur de très longues distances. Ce travail décrit trois approches différentes pour la synthèse de matériaux qui traduisent le mouvement de leurs composants en une réponse macroscopique. Le chapitre 1 est consacré à l'état de l'art des rotaxanes bistables [*c*2] afin de contextualiser le lecteur. Le chapitre 2 décrit la voie de synthèse suivie pour obtenir des mésophases mécaniquement actives avec un rotaxane bistable [*c*2] à l'état cristallin liquide. Les chapitres 3 et 4 sont principalement consacrés à la conception et à la synthèse de monomères de rotaxanes bistables [*c*2] qui seront impliqués dans des polymérisations covalentes et supramoléculaires. En particulier, le chapitre 4 aborde la plupart des approches synthétiques qui ont été conçues pour obtenir des monomères de rotaxanes bistables [*c*2] sensibles à l'oxydoréduction, lesquels ont été utilisés pour la polymérisation et l'électrofilage de fibres. Ce dernier chapitre a été réalisé dans le cadre du projet collaboratif MAGNIFY FET-open, un consortium composé de l'Université de Groningen, de l'Université de Bologne, du Centre National de Recherche en Italie et de notre institution, le Centre National de la Recherche Scientifique.
Mots clés : machines moléculaires synthétiques, rotaxanes [*c*2]bistables, polymères, chimie supramoléculaire, chimie organique synthétique.

Abstract

Actuating soft materials based on synthetic molecular machines has great potential to be part of a technological revolution addressing challenges in regenerative medicine, human-machine interfaces, robotics, among others. In this direction, several research groups, including ours, have invested significant efforts in coupling molecular machines with each other and their environment to extract their collective (nanometric) motion at higher length scales. However, to further advance these molecular machines and extract optimized macroscopic actuations, precise control over their spatial 3D organization over very long distances is required. This work describes three different approaches for synthesizing materials that translate the motion of their components into a macroscopic response. Chapter 1 is dedicated to the state of the art of [*c*2]daisy chain rotaxanes to provide context for the reader. Chapter 2 describes the synthetic pathway followed to obtain mechanically active mesophases using a liquid-crystalline [*c*2]daisy chain rotaxane. Chapters 3 and 4 are primarily focused on the design and synthesis of [*c*2]daisy chain rotaxane monomers for involvement in covalent and supramolecular polymerizations. In particular, Chapter 4 addresses most of the synthetic approaches that were developed to obtain redox-responsive poly[c2]daisy chain rotaxane monomers, which were utilized for polymerization and subsequent electrospinning into fibres. The work presented in this final chapter was conducted within the framework of the MAGNIFY FET-open collaborative project, a consortium composed of the University of Groningen, the University of Bologna, the National Research Centre in Italy, and our institution, the Centre National de la Recherche Scientifique.

Keywords: synthetic molecular machines, [*c*2]daisy chain rotaxanes, polymers, supramolecular chemistry, synthetic organic chemistry.